Design and Characterisation of Fluidised Bed Cooling Towers

A thesis submitted to Middlesex University in partial fulfilment of the requirements for the degree of Doctor of Philosophy in Mechanical Engineering.

Louis Mbua Egbe

School of Engineering Systems

This work was carried out at the Energy Technology Centre, School of Engineering Systems, Middlesex University, Bounds Green Road, London N11 2NQ, UK.

March 2001

ABSTRACT

This thesis discusses the operating characteristics and design of fluidised bed cooling towers (FBCT), which may be used to cool hot water for industrial purposes. Limited data exist for such a three-phase fluidised bed acting as a cooling tower. This motivated some early workers to investigate its usefulness in cooling tower applications and they showed that the FBCT produces heat and mass transfer rates much higher than in conventional fixed-bed towers. Despite this advantage, the FBCT has not been commercially exploited to date. An extensive experimental study is presented using up-to-date instrumentation to determine the thermal and hydraulic characteristics with a view to establishing a design criteria for full-scale FBCTs. Experimental tests were performed to account for the effect of the plenum chamber and the spray zone region upon the thermal performance of the FBCT. Data analysis was performed so that the effect of the fluidised bed alone as well as the plenum chamber could be known. A prototype was designed and built incorporating nine calibrated Platinum Resistance Thermometers for fluid temperature measurements with one located just below the fluidised bed itself while another was positioned below the plenum chamber to measure outlet water temperatures. Two differential pressure transducers and an electronic water flowmeter were used to measure air pressures and water flow rates respectively. All instruments were connected to a data-logger linked to a personal computer. Two different software packages were written and installed on the computer, to automatically retrieve experimental data from the rig during test runs and to automatically process the retrieved variables for analysis. Nine independent variables were measured in order to determine the tower thermal-hydraulic performance. Water and air flow rates ranged from 0.5 - 5 and 0.5 - 4 kg/s m^2 respectively giving liquid/gas mass flux ratios that ranged from about 0.1 - 6. The inlet hot water temperature ranged from about 25 - 55°C while the inlet air wet-bulb temperature averaged about 18°C. Four different spherical packing arrangements were studied at static bed heights that ranged from about 25 to 400 mm. The spray nozzle height from the distributor grid ranged from 400 - 1500 mm. Data analysis was performed for thermal-hydraulic performance using both dimensional analysis and the Merkel approach. A least-square multiple regression analysis carried out on dimensionless and dimensional groups that resulted from this analysis showed that correlations derived are in good agreement with other experimental data. Correlations were derived for the prediction of the bed air pressure drop and hence the power requirement, the tower thermal performance, the minimum fluidisation velocity, and the expanded bed height. Correlations used to design a full-scale FBCT are presented. Novel work included measurements of local radial and axial temperature variations within the fluidised bed. Thermal performance decreased as the liquid/gas mass flux ratio was increased while it increased as the particle size was decreased. High density particles gave a higher bed air pressure, and hence a higher power requirement than low density ones. Minimum fluidisation gas velocity was independent of the static bed height. Expanded bed height increased as the liquid and gas mass fluxes were increased. Thermal performance was found to increase when the effect of the plenum chamber was included in the analysis as compared to the fluidised bed itself. Methodological criteria for the design of a full scale FBCT have been developed. Design analysis suggests that FBCTs can be several times smaller in size than conventional cooling towers, and that they may operate with a similar or lower power requirement than the latter.

ACKNOWLEDGMENTS

It was a pleasure undertaking this research work at the Energy Technology Centre at the School of Engineering Systems. In this instance, I will like to take this opportunity to thank my Director of Studies Professor Anthony White whose smooth but firm supervisory skills made this research programme possible. I am also indebted to my Supervisors, Mr. Peter Barham and Dr. John Lewis whose practical, academic and advisory roles were indispensable to the completion of this thesis.

I also thank Professor Jorge Kubie of Napier University who organised a partial funding from National Power Plc while he was present at Middlesex University. I would also like to thank Dr. Mark Biggs of Surrey University for his help at the preliminary stages of this work, Professor S.C. Kranc of University of South Florida USA for providing rare academic material. All other researchers and workers at the School of Engineering Systems who provided spiritual and physical support for this project must be commended especially Dr. Hassan Ipakchi, Olaf Schmidt, Dr. Jason Jones, J. Gopaul, David Farlie Mr. John Cranston and Stephen James Watt. I thank God, the ultimate Hope.

TABLE OF CONTENTS

LIST OF TABLES

LIST OF FIGURES

NOTATION

a	Interfacial area per unit static bed volume	[m^2/m^3]
a_t	Total surface area of particles	[m^2]
C_W	Specific heat capacity of water	[kJ/kg K]
C_V	Specific heat capacity of moist air	[kJ/kg K]
D_C	Column Diameter	[m]
D_L	Axial dispersion coefficient	[m^2/s]
D_{ZL}	Liquid Axial Dispersion Coefficient	[m^2/s]
D_{ZS}	Solid Axial Dispersion Coefficient	[m^2/s]
d_p	Packing diameter	[m]
d_S	Droplet median volume diameter	[m]
f	Grid percentage free open area	[-]
G	Gas mass flux	[kg/s m^2]
G_{mf}	Minimum fluidisation gas mass flux	[kg/s m^2]
g	Acceleration due to gravity, 9.81	[m/s^2]
H	Spray height of nozzle orifice from the distributor grid	[m]
HTU	Height of a gas-phase transfer unit	[m]
H_A	Bulk air enthalpy of dry air	[kJ/kg]
H_i	Saturated Enthalpy at the gas-liquid interphase	[kJ/kg]
H_W	Saturated air enthalpy at the water temperature	[kJ/kg]
h_{fg}	Latent heat of evaporation of water	[kJ/kg]
h_G	Gas-phase heat transfer coefficient	[kW/m^2 K]
h_W	Liquid-phase heat transfer coefficient	[kW/m^2 K]
h_L	Volume of liquid holdup per unit volume of static bed	[m^3/m^3]
Ka	Overall volumeric mass transfer coefficient	[kg/s m^3]
K_G	Overall Gas-phase mass transfer coefficient	[kg/s m^3]
k_G	Gas-phase mass transfer coefficient	[kg/s m^2]
L	Liquid mass flux	[kg/s m^2]
M	Mass	[kg]

NTU	Number of transfer units	[-]
ΔP	Bed air pressure drop	[Pa.]
r	Correlation Coefficient	[-]
S_P	Linear distance between two solid particles	[m]
T_{AMD}	Ambient dry bulb temperature	[°C]
T_{AMW}	Ambient wet bulb temperature	[°C]
T_{DB}	Inlet air dry bulb temperature	[°C]
T_{WB}	Inlet air wet-bulb temperature	[°C]
T_{ODB}	Outlet air dry bulb temperature	[°C]
T_{OWB}	Outlet air wet-bulb temperature	[°C]
T_{HW}	Inlet hot water temperature	[°C]
T_{CW}	Plenum outlet cooled water temperature	[°C]
T_{GCW}	Distributor grid outlet cooled water temperature	[°C]
T_i	Temperature at the air-water interface	[°C]
T_0	Reference temperature	[°C]
T_w	Water Temperature	[°C]
U_G	Superficial gas velocity	[m/s]
U_{GF}	Flooding gas velociy	[m/s]
U_{mf}	Minimum fluidisation gas velocity	[m/s]
U_{LF}	Flooding liquid velocity	[m/s]
U_L	Superficial liquid velocity	[m/s]
V_E	Expanded bed height	[m]
V	Static bed height	[m]
V_l	Volumetric liquid holdup	[m^3]

DIMENSIONLESS GROUPS

Fr_L	Liquid-particle Froude number	$[L^2/(d_p g \varrho_L^2]$
Fr_G	Gas-particle Froude number	$[G^2/(\rho^2 g d_p]$
Pe_c	Peclet number	$[V U_L/(\epsilon_L D_L]$

Re_L	Liquid-particle Reynolds number	$[d_pL/\mu_L]$
Re_G	Gas-particle Reynolds number	$[d_pG/\mu_G]$
We_G	Gas-particle Weber number	$[d_pG^2/\sigma_L\rho_G]$
We_L	Liquid-particle Weber number	$[d_pL^2/\sigma_L\rho_L]$

GREEK SYMBOLS

ϵ_0	Initial static bed porosity	[-]
ε	Total bed holdup of liquid and gas	[-]
ϵ_G	Gas holdup per unit volume of expanded bed height	[-]
ε_{GF}	Flooding gas holdup	[-]
$\varepsilon_{l,\,st}$	Static liquid holdup	[-]
ϵ_L	Liquid holdup per unit operational bed height	[-]
ϵ_P	Solid holdup per unit operational bed height	[-]
μ_L	Liquid viscosity	[kg/m s]
μ_G	Gas viscosity	[kg/m s]
ϱ_L	Density of liquid	[kg/m^3]
ρ_B	Bulk density of particles	[kg/m^3]
ϱ_P	Density of an individual particle	[kg/m^3]
ρ_G	Density of gas	[kg/m^3
σ_v	Surface tension of liquid	[N/m]
ϕ	Sphericity of particles ($\phi = 1$ for spheres)	[-]
(Q	Sphericity	[-]
ω_A	Specific humidity of bulk moist air	[kg/kg]
ω_i	Specific humidity of air at the air/water interface	[kg/kg]

CHAPTER I

INTRODUCTION

1.1 General Snrvey of Cooling Towers

Extremely large quantities of heat are often rejected in industrial processes. Steam power plant, for example, utilises heat for the generation of electricity. In this process, water is changed to steam in a boiler which is then converted to mechanical energy in a turbine and then to electrical energy. However, only about 25 to 35% of the heat input to the boiler is used to produce electricity, the remainder being rejected to the atmosphere, the largest portion of which is rejected in the steam condenser. Enormous quantities of water are used to condense the steam to water and at this low temperature water has to be rejected or cooled and recycled. According to data shown in Table 1.1 and released in 1994 by National Power Plc., UK, 6.6 m^3/s of cooling water is required for a 500 MW electric power station, while Jackson (1951) reports that a large chemical plant pumps cooling water at a rate of 9.6 m^3/s. Where low temperature hot water is to be rejected directly to the atmosphere, industrial plant must be sited near lakes, rivers or the sea. The direct rejection of hot water to these reservoirs could lead however to thermal pollution problems. Where location of industrial plant is such that cooling water in large quantities is scarce, then the water must be cooled and recycled.

Evaporative cooling of water is one of the most widely used methods of cooling large quantities of low temperature water. To this end, cooling towers have been developed. In 1983, Cheremisinoff *et al.* and Singham *et al.* published works that review the different types of cooling towers in use. The most common types being the forced or induced draught towers and the natural draught towers. The former is the most widely employed and uses fans to force air at the bottom or induce air at the top of the tower while hot water is sprayed downwards. In natural draught

towers, air is introduced at the bottom of the tower by natural draught and no fan is needed, thus eliminating the power cost. However, this advantage is counteracted because natural draught towers are far bigger in size than induced draught towers. They are huge hyperboloidal shaped structures with base diameter of up to 100 m and about 100 m in height. The enormous size grossly escalates the capital cost. On the other hand, hybrid towers combine the design features of natural and mechanical draught towers. The advantages and disadvantages of the different types of towers are well outlined by Cheremissinoff *et al.* (1983).

1.2 Operation and Construction

In conventional cooling towers, the air is forced into the bottom or induced at the top of the tower and drawn upwards while coming into direct contact with the hot water sprayed downwards in a generally counter-current or cross-flow action. However, the prevailing method is the counter-current method of cooling. The downward spray of water was introduced to achieve the optimum cooled water temperature since the effect of gravity on the droplets causes a better mixing and hence an increased heat transfer rate. The construction and operation of a conventional counterflow cooling tower is shown in Figure 1.1.

Although cooling of the water would occur in an empty tower, it is necessary to increase the residence time of droplets as they pass down the tower. A higher residence time ensures a more intimate mixing between air and water droplets and hence a better heat exchange between the two fluids. This is usually achieved by the inclusion of ***packings*** or ***fills***. Different types of packing arrangements achieve different cooling rates due to different surface areas and geometries that enhance heat transfer. This has been demonstrated by Kelly *et al.* (1956) and Lowe and Christie (1961) who tested different types of packing for conventional cooling towers.

The cooling of the water in cooling towers is as a result of both evaporative

cooling and sensible or convective heat exchange. The hot water from the plant is pumped to the top of the tower and sprayed over the packing. As it falls to the collecting basin at the bottom, it encounters a stream of cold ambient air moving in a counter-current direction as shown in Figure 1.1. The mixing of the two fluid streams at different temperatures causes a temperature gradient to be created. As the water evaporates from the surface of the droplets, latent heat of vaporisation is required thus producing a cooling effect to the warmer fluid. Convective heat is also lost from the water to the air thus causing an increased cooling rate. About 20-25 percent of the total cooling of the water in the tower is caused by convective heat transfer while the rest of the heat transfer is by evaporative cooling (Cheremisinoff *et al.*, 1983; Barile *et al.*, 1974). In these processes, the incoming moist air is unsaturated with water vapour. Evaporative cooling will continue as long as the air in the tower remains unsaturated with water vapour. Also, water with a higher temperature than ambient air will reject convective heat to the saturated air which would then cease to be saturated and further evaporative cooling would occur with the ultimate discharge of air into the atmosphere, which acts as a **"heat sink"**. During this process of simultaneous heat and mass transfer, water is lost from the main bulk of water to the moist air. Cooling tower water also often contains dissolved solids which are sometimes removed by the blowdown of the tower basin thus causing more water to be lost. Lost water is replaced by the addition of a water make-up device thus increasing both the operational and capital cost.

As air blows upwards, counter-currently to the hot water, water droplets will drift into the atmosphere when the air reaches a critical velocity. This drift may be prevented by the inclusion of a drift eliminator or demister. However, these devices are designed for particular air velocities and water drop sizes and droplets may therefore escape through them causing a further loss of cooling tower water. Cheremisinoff *et al.* (1983) estimate that in normal operation, water losses amount to about 0.2 percent of the total volume of water circulated for every 5-6 K ***range of cooling***. However, this may also depend on the tower design and type. Table

1.1 shows that water loss may approach as high as 4% for every 5 K range of water cooling. These are but some of the disadvantages of conventional cooling towers, the main advantages being:

(1) The fixed packing arrangement allows a good prediction of the required cooled water temperature.
(2) There is considerable literature relating to the design of conventional towers.
(3) The pressure drop through the packing is low giving rise to low operational cost.

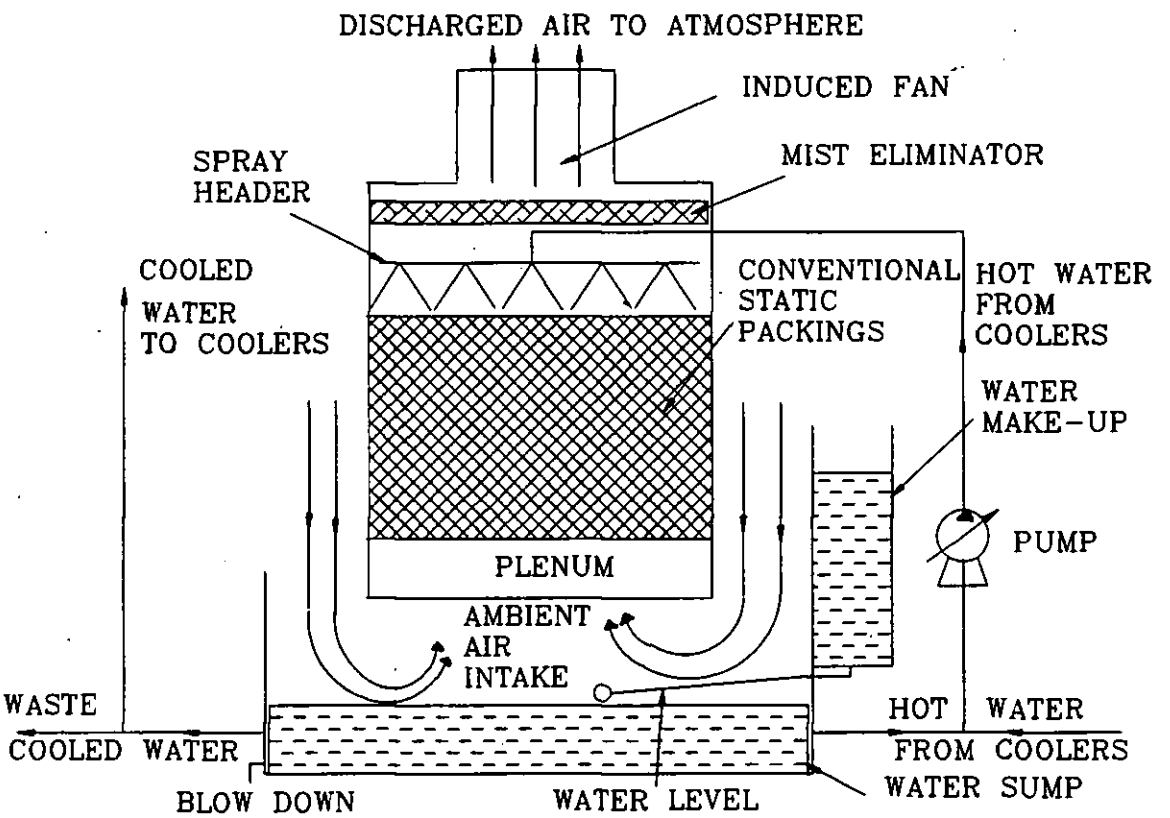

Figure 1.1 A diagram schematic of a conventional induced-draught cooling tower.

	Unit		
Tower Design	-	Hybrid	Hybrid
No. of Cells per Tower	-	8	14
Electrical Power	MW	50	500
Cell Height	m	18.2	15.9
Cell Width	m	17.2	19.1
Cell Length	m	11.68	15.6
Rated Water Flowrate	m^3/s	2.69	6.6
Total Air Flowrate	m^3/s	3954	9702
Exit air velocity	m/s	1.54	2.33
Wet Bulb Temperature	°C	7.9	8.8
Dry Bulb Temperature	°C	9.6	11.2
Tower Pumping Head	m	10	9.5
Make-up Flowrate	m^3/s	0.12	0.233
Evaporation Rate	m^3/s	0.04	0.077
Purge Flowrate	m^3/s	0.08	0.156
Total Fan Power	MW	0.96	1.764
Maximum Drift Loss	%	< 0.01	< 0.005

Table 1.1 Data of mechanical induced draught cooling towers showing the size and power requirements for 50 MW and 500 MW electricity plants (National Power Plc, 1994).

The disadvantages are:

(1) Poor heat transfer properties because of the static nature of packings.

(2) As seen in Table 1.1, conventional towers require a large land area to accommodate their size.

(3) Large capital investment is required.

(4) Static packing attracts microbes which may cause Legionaire Disease.

(5) Optimization is difficult because of differences in packing arrangements.

(6) The enormous height as in Table 1.1, calls for high pumping cost thus increasing the overall operating cost.

These disadvantages provide fresh opportunities for new and superior design methods of water cooling to be explored. In 1971, Professor Ronald Barile and co-workers, in their paper *The Turbulent Bed Cooling Tower*, published data that showed that fluidised bed cooling towers (FBCT) could replace conventional packed bed towers because of their superior heat and mass transfer characteristics and hence small size for a given cooling effect. The design involved the replacement of the conventional packing arrangement with low density spheres which undergo a process known as ***fluidisation*** as the air moves upwards and the water is sprayed downwards as shown in Figure 1.2 below. This design of cooling tower was further investigated experimentally in 1977, by Dengler who reported that a FBCT is a "novel gas-liquid contacting operation that holds huge potential for large flow volumes transfer". Although evaporative cooling within a fluidisation process is relatively new, the fluidisation phenomenon is well understood and a large body of experimental work has been reported. A description of fluidisation has been given by Zabrodsky (1966) who described fluidisation as a state where granular particles possess fluidity when an ascending fluid is passed through the bed at an increasing velocity so that at one instance, the force resisting the flow of fluid is equal to the bed weight after which there is no increase in hydraulic resistance of the bed. This results in the bed expanding and suspending beyond the stability limit of a fixed bed, the stability limit marking the transition point to the fluidised state.

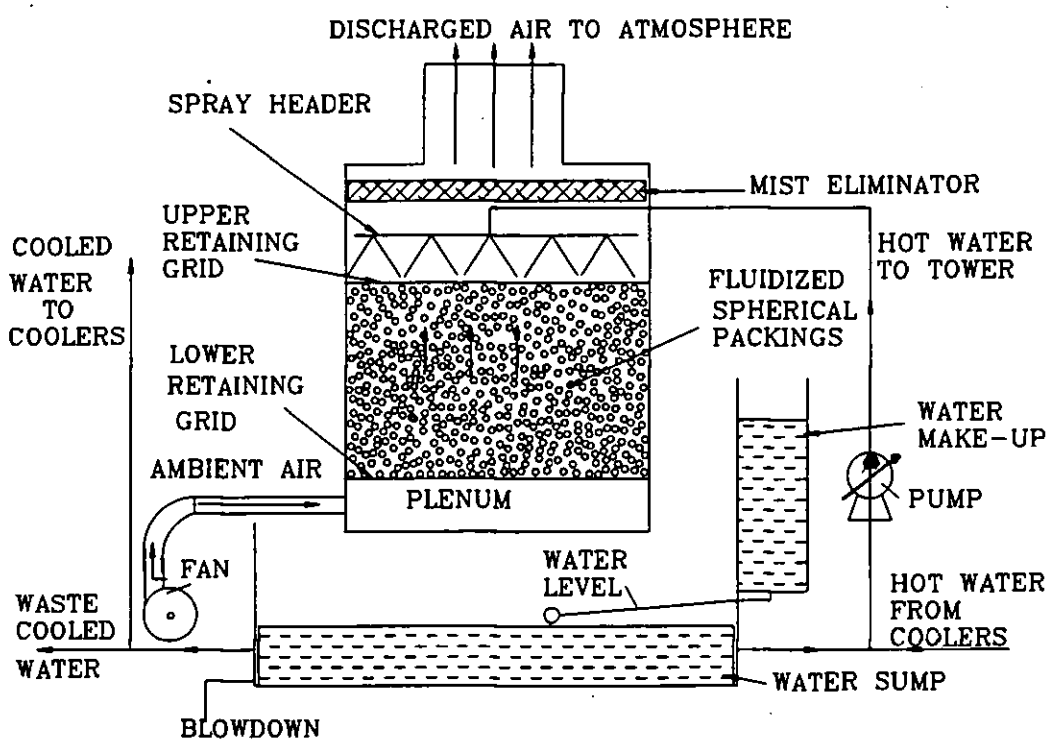

Figure 1.2 Schematic diagram of forced-draught FBCT.

At low fluid velocities or flow rates the solid particles lie on one another on a porous plate or retaining grid at bottom of the column as shown in Figure 1.3*a*. This is the ***fixed*** or ***static state.*** If the velocity of the upward flowing fluid is increased still further, fluidisation occurs, bubbles are formed and intensive mixing of the bed is realised with a turbulent action similar to a boiling fluid. This is the ***fluidised state***. Further increase of the fluid velocity, will eventually cause entrainment of the solid particles from the column into the upward moving fluid. The contact and close proximity of the particles to one another ceases as the solid particles become mobile. This is the ***pneumatic or hydraulic transport state.*** Figures 1.3 (*a, b c*) and 1.4 show the relationship between the upward gas and the

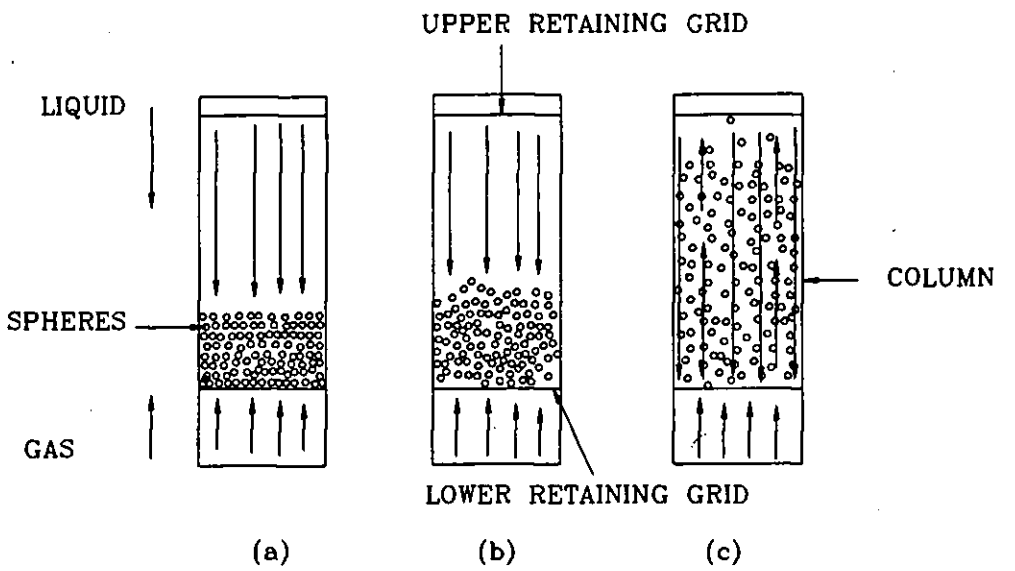

Figure 1.3 Shematic diagram of counter-current three-phase fluidised bed.

downward liquid throughputs and the behaviour of the whole bed of material. The quantity of material over the porous retaining grid remains constant. Figure 1.3*a* corresponds to a fixed bed of particles and pressure drop increases as velocity of the gas increases at a constant liquid flow rate. The gas velocity at which fluidisation begins is called the ***minimum*** or ***incipient fluidisation velocity*** as shown in Figure 1.3*b*. This is displayed as line MM in Figure 1.4. As the gas flow rate increases, the pressure drop over the whole of the bed remains constant and is equal to the total weights of the fluidised solid material and the bed fluids, the height of the bed on the other hand increases as displayed in Figure 1.3*c*. This is the ***expansion*** phenomenon characteristic of fluidised bed and corresponds to the

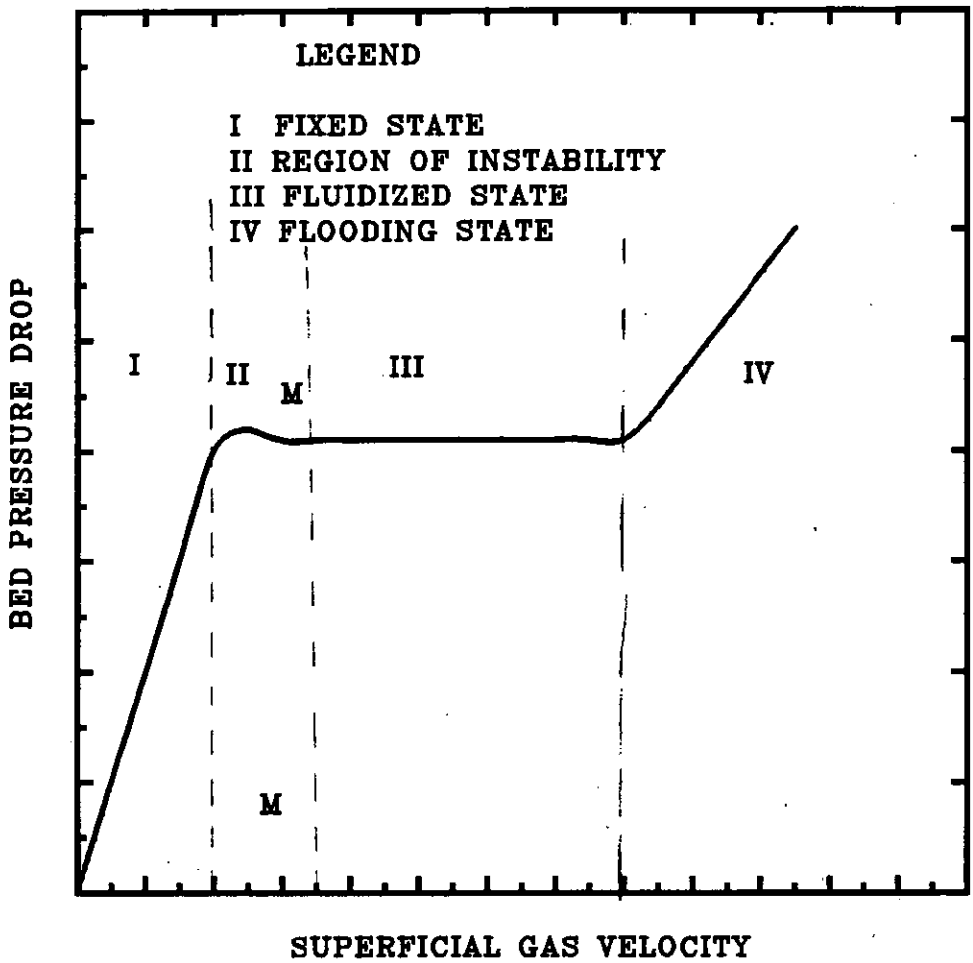

Figure 1.4 Schematic depiction of the fluidisation phenomenon.

limit of existence of the fluidised bed. At a particular gas flow rate, the liquid droplets together with the solid material are entrained out of the contacting zone. In an ideal case of uniform expansion the bed will cease to exist at this gas velocity. This is the ***flooding*** or ***maximum fluidisation*** state.

The advantages of the fluidised bed cooling technique are principally derived from the very large particle area exposed to the fluid, the ease with which solids can be handled in the fluidised state and the excellent heat and sometimes mass transfer transport due to the bubbling of the bed. Moreover, the constant agitation ensures self washing of spherical packing and hence reduction of the possibility

of the buildup of microbes. In addition, the operational cost may be reduced since untreated water may be used.

The disadvantages of fluidisation are that operating rates are limited to within the range over which the bed can exist and in addition, the cost of power required to fluidise the bed may be excessive especially with dense and deep beds. Also, there are limits of size and depth of particles that may be handled by the system. Moreover, it is difficult to characterise the particles themselves and there can be a wide range of behaviour in accordance to the conditions under which a particular fluidised bed is being operated. The most outstanding advantage of a fluidised bed cooling tower is its small size for a given cooling duty, due to its high heat transfer rate. Despite the advantages of this technology, it has not been commercially exploited to date. Although the fluidised bed cooling tower was recently demonstrated to be practical by Grandov *et al.* (1995), their work lacked generalisation as the correlations developed were specific to the cooling tower studied. The present work includes a more generalised dimensionless variables.

Egbe (1996a) also carried out an experimental investigation with a view to study the feasibility of utilizing the FBCT as a full-scale device and found that although this is possible, an advanced prototype model needs to be built. Additionally, Fan *et al.* (1989) commented on the uncertainties and incoherencies associated with available design data and noted that knowledge of heat and mass transfer relating to three-phase fluidised beds is minimal. Moreover, the analysis of Barile *et al.* (1974) showed that fundamental differences exist between conventional and fluidised bed cooling towers implying that a new design method needs to be created.

1.3 Aims and Objectives

The main aim and objectives of the present study, therefore, are to:

1 extend the range of performance data available relating to fluidised bed cooling towers (FBCT)

2 develop a computer-based design method for FBCT's based on performance correlations.

To accomplish these aims, the following objectives were identified:

1 to review the past work carried out relating to FBCT

2 to design and construct an experimental model fluidised bed cooling tower

3 to obtain experimental data covering a wide range of variables and to develop design correlations

4 to evolve a design method which will predict the optimum sizing and performance of full-scale FBCT

5 to write a computer program to facilitate the design of FBCT for engineers.

1.4 Outline of Thesis

This thesis contains ten chapters. In this introductory chapter, a general survey of conventional and fluidised bed cooling towers is made and the aims and objectives of this work are stated.

Chapter II outlines the theoretical frame work on which this thesis is based.

In Chapter III, a review is made of past and on-going thermal-hydraulic investigations on three-phase fluidised bed processes and fluidised bed cooling towers.

In chapter IV, the experimental model FBCT and its associated instrumentation are described. Experimental design, the dependent and independent variables were also defined.

Chapter V gives the experimental results relating to hydrodynamic performance

of the experimental FBCT in terms of the bed air pressure drop. Results relating to the bed air pressure drop, liquid and gas hold up, minimum and flooding gas velocities are also given in Chapter V.

Experimental results relating to bed expansion were given in Chapter VI.

Chapters VII and VIII contain the experimental results relating to the FBCT thermal performance. In all cases, a critical and rigorous qualitative analysis was made as the results are compared and contrasted with those of other investigators.

Chapter IX concerns general thermal-hydraulic discussions relating to the experimental results. Thermal-hydraulic correlations were developed to quantify the qualitative analysis done in chapters V to VIII, and to validate results using dimensional analysis performed in chapter II. The design methodology was also developed and a comparative design analysis was made between the FBCT and conventional towers.

The thesis concludes, together with recommendations for further work, in chapter X.

CHAPTER II

FLUIDISED BED COOLING TOWER THEORY

The design of the FBCT requires that experimental justification is provided in relation to its thermal and hydraulic performance in order to substantiate theoretica assumptions. With respect to the latter, several theories have been put forward. However, a generalised method that will encompass all the different hypothese is yet to be developed. Most investigators have resorted to empirical relationships. One of the reasons for this approach may be attributed to the complexity in the operation of the FBCT, possibly because its hydrodynamics consist of several different dependent and independent parameters with the bed displaying unpredictable fluidisation behaviour at certain experimental conditions. Moreover, the FBCT hydrodynamics directly influences the degree of fluidisation. Since this in turn affects the rate of heat and mass transfer, it follows that the thermal and hydraulic performance are interrelated. The completely general theory to determine the thermal performance of the FBCT is non-existent. However, the rate of heat and mass transfer may be calculated from the incomplete general conventional theories put forward by other investigators and then adapted for use in designing the FBCT. In this chapter, new methods that attempt to generalise the different theories relating to fluidised bed hydrodynamics and heat and mass transfer are put forward taking into account the work of other investigators. Additionally, new theoretical techniques are presented so as to justify the present experimental work on heat and mass transfer and hydrodynamics.

2.1 Hydrodynamics

The hydrodynamics of the FBCT consists basically of the bed air pressure drop, the gas and liquid holdups, the maximum and minimum fluidisation gas velocities and the bed expansion due to fluidisation. In countercurrent gas-liquid-solid flow with the gas as the continuous phase, the mode of transport is such that energy and momentum are expended by the upward flowing gas in order to overcome the

combined weight of the downward flowing liquid and the bed solid particles. The loss of power by the air is signified by the bed air pressure drop, ΔP.

2.2 Bed Air Pressure Drop

Most present day investigators including Forrester *et al.* (1997) base their hydrodynamic models for chemical reactors on Computational Fluid Dynamics (CFD). Although this method may achieve good results, it does not seem to dwell much on the fundamentals of three-phase beds. In addition, most CFD solutions seem to be geared towards particular solutions of three-phase fluidisation. Other researchers such as Xukun *et al.* (1997) have concentrated on quasi-theoretical analysis for two-phase liquid-solid flow. So far, the theoretical model of Epstein (1981) remains the most convincing because of its simplicity. In deriving his equations for the bed pressure drop, the following assumptions were used.

1. The buoyancy of the fluidised solid particles and the weight of the liquid is supported by the upward gas drag on the particles and liquid.
2. Frictional resistance due to the wall was neglected.
3. Only axial pressure gradients are considered. Radial pressure distribution is assumed to be uniform such that the pressure drop experienced by the air at any radial position at a particular bed level is unchanged.
4. Purely counter-current three-phase flow exists in the tower.

For three-phase gas-liquid-solid countercurrent flow, the total axial pressure gradient for a unit crossectional area at any level in the tower is the total bed weight per unit volume at that point. If an element in the bed shown in Figure 2.1 below is considered, the differential equation for the bed air pressure drop may therefore be written as:

$$-\frac{dP}{dV} = [\epsilon_P\rho_P+\epsilon_L\rho_L+\epsilon_G\rho_G]\,g \qquad (2.1)$$

The negative sign on the left-hand side in Equation 2.1 indicates that energy is expended by the gas as it passes along the bed. The total fractional volume balance of the individual phase holdups may be related by

$$\epsilon_P+\epsilon_L+\epsilon_G = 1 \qquad (2.2)$$

The total air pressure drop across the bed per unit static volume V, is then obtained by integrating Equation 2.1. Therefore,

$$-\int_{P_1}^{P_2} dP = -\Delta P = g\int_0^{V_E} [\epsilon_P\rho_P+\epsilon_L\rho_L+\epsilon_G\rho_G]\,dV \qquad (2.3)$$

So that

$$-\Delta P = V_E g\,[\epsilon_P\rho_P+\epsilon_L\rho_L+\epsilon_G\rho_G] \qquad (2.4)$$

where P_1 and P_2 are the static air pressures at the top and bottom of the tower respectively. The term $\epsilon_G\rho_G$, may be neglected since the weight of the air is small compared to the weight of the solid particles and water. Equation 2.4 then becomes

$$-\Delta P = V_E g\,[\epsilon_P\rho_P+\epsilon_L\rho_L] \qquad (2.5)$$

Since

$$\epsilon_P = 1-\epsilon_0 \qquad (2.6)$$

then substituting Equation 2.6 into Equation 2.5 gives:

$$-\Delta P = V_E g[(1-\epsilon_0)\rho_P+\epsilon_L\rho_L] \qquad (2.7)$$

The bed air pressure drop may be calculated if the liquid holdup ϵ_L, is known. Conversely, it can be measured by differential manometry. Measuring the liquid holdup and the bed air pressure drop will allow the verification of Equation 2.7 provided the expanded bed height is known.

2.3 Bed Expansion According to Vunjak-Novakovik *et al.* (1987)

In deriving the fundamental equations for the expanded bed height, it is important to bear in mind that the total material volume of an operating three-phase FBCT is made up of the fraction of gas, liquid and solids. The volume fraction is given in Equation 2.2. At any bed level, the solids fraction is that proportion that is occupied by the solid particles. Considering a bed element, the differential equation for mass balance indicating the rate of change of solid mass M, at a particular level of the FBCT with cross-section A, may therefore be written as:

$$\epsilon_P = \frac{dM}{dV}\cdot\frac{1}{\rho_P A} \qquad (2.8)$$

Rewriting Equation 2.8 yields:

$$\epsilon_p \rho_p A dV = dM \qquad (2.9)$$

Integrating Equation 2.9 from initial conditions gives:

$$\epsilon_p \rho_p A \int_0^{V_E} dV = \int_0^M dM \qquad (2.10)$$

Giving,

$$\epsilon_p \rho_p A V_E = M \qquad (2.11)$$

But the total mass and hence weight and density of the particles remain unchanged in the static and the fluidised states of the bed. So,

$$\epsilon_p A V_E = [1-\epsilon_0] AV \qquad (2.12)$$

Therefore,

$$\epsilon_p A V_E = [1-\epsilon_0] AV = [1-(\epsilon_L+\epsilon_G)] AV_E \qquad (2.13)$$

Substituting Equation 2.2 into 2.13 gives

$$\frac{V}{V_E} = \frac{1-(\epsilon_L+\epsilon_G)}{1-\epsilon_0} \qquad (2.14)$$

Equation 2.14 can be solved when the liquid holdup ϵ_L, and the gas holdup ϵ_G, are known.

The liquid holdup correlation has been given by Egbe (1996b). Since the total weight of liquid in the bed remains unchanged in the static and fluidised states of the bed, it follows that:

$$g\rho_L V_E \epsilon_L = g\rho_L V h_L \qquad (2.15)$$

Therefore,

$$\frac{\epsilon_L}{V} = \frac{h_L}{V_E} \qquad (2.16)$$

Since

$$\epsilon_G = 1-[\epsilon_L+(1-\epsilon_0)]\frac{V}{V_E} \qquad (2.17)$$

and

$$\epsilon_p = \frac{V}{V_E}(1-\epsilon_0) \qquad (2.18)$$

So

$$\epsilon_L = \frac{V}{V_E}h_L \qquad (2.19)$$

Substituting Equation 2.19 into 2.14 and then rearranging yields:

$$\frac{V_E}{V} = \frac{1-\epsilon_0+h_L}{1-\epsilon_G} \qquad (2.20)$$

The gas holdup ϵ_G, can be calculated from an equation developed empirically. Equation 2.20 has boundary conditions when $U_G \geq U_{mf}$ and $V_E/V \geq 1$ where $V_E/V=1$ at the minimum fluidisation gas velocity. Therefore the minimum fluidisation velocity may be calculated from Equation 2.20.

2.4 Maximum or Flooding Fluidisation Velocity

The maximum or flooding gas velocity is the upper limiting velocity of the FBCT. No theory is available at this stage to fully account for this parameter. However, an empirical method exists that has been developed by Sherwood *et al.* (1938) for fixed bed countercurrent three-phase flow. This method was successfully employed by Vunjak-Novakovic *et al.* (1980) and Uchida *et al.* (1980) to characterise the maximum gas velocity in a FBCT. It is dependent upon the fact that at flooding conditions, the group $[(U_G^2 a_t / g\varepsilon^3).(\rho_G / \rho_L).(\mu_L)^{0.2}]$ and $[L/G (\sqrt{(\rho_G / \rho_L)})]$ are related when the former is plotted as the ordinate against the latter as the abscissa. Under "true" flooding conditions, all the experimental points fall approximately on the correlated line.

Another method that can be applied to characterise the "true" flooding point is the method first put forward by Wallis (1969). He derived theoretical equations that characterise the maximum possible flow or flooding rates for a two phase system. In 1994, Soundarajan *et al.* attempted to adapt this method to characterise the maximum gas and liquid velocities in a three-phase FBCT. Moreover, they did not develop an all-encompassing correlation that comprehensively characterises the maximum flow rates. The equations of Wallis (1969) will be employed here but with the appropriate theoretical adaptation to take into consideration the expansion aspects and the presence of particles in the FBCT as opposed to two-phase or three-phase static flow.

Wallis (1969) derived the equation for horizontal two-phase flow to conclude:

$$j^{*0.5}_1 + j^{*0.5}_2 = 1 \qquad (2.21)$$

j^*_1 and j^*_2 are dimensionless groups that relate momentum fluxes to the

hydrodynamic forces. They can be represented as:

$$j^*_1 = \left[\frac{U_{Gf}}{(gD_C)^{0.5}}\right]\left[\frac{\rho_G}{\rho_L - \rho_G}\right]^{0.5} \qquad (2.22)$$

and

$$j^*_2 = \left[\frac{U_{Lf}}{(gD_C)^{0.5}}\right]\left[\frac{\rho_L}{\rho_L - \rho_G}\right]^{0.5} \qquad (2.23)$$

Equations 2.22 and 2.23 do not take into consideration the turbulent nature of the three-phase FBCT. Modifications are required so as to incorporate the effect upon flooding by three-phase fluidisation. The presence of the tower diameter D_C, in the two equations indicate that the flow is a two-phase gas-liquid flow which does not include the solid particles.

The bed under operation is maintained by the balance of the gas buoyancy and the gravitational forces acting on the particles and the liquid. Since the bed is at equilibrium just before the true flooding flow rates are achieved in a similar manner as a single phase flow that is described by Wallis, then Equations 2.23 and 2.24 may be used to characterise three-phase fluidised flow.

Bearing this in mind, therefore, the momentum fluxes and hydrostatic forces characterising the FBCT may therefore be resolved in three parts.

Taking into an analogical approach from Equations 2.22 and 2.23 and considering hydrostatic forces due to bed expansion in three-phase fluidised beds as opposed to an empty tower, we may thus replace the column diameter, D_C by the expanded bed height in equations 2.22 and 2.23 to yield:

$$j^*_3 = \left[\frac{U_{Gf}}{(V_E g)^{0.5}}\right]\left[\frac{\rho_G}{\rho_L - \rho_G}\right]^{0.5} \qquad (2.24a)$$

and

$$j^*_4 = \left[\frac{U_{LF}}{(V_E g)^{0.5}}\right]\left[\frac{\rho_L}{\rho_L - \rho_G}\right]^{0.5} \qquad (2.25a)$$

In Equations 2.24a and 2.25a, the expanded bed height V_E, is the bed expansion just before the spheres and droplets begin to accumulate at the top of the column so as to attain "true" flooding and hence the maximum fluidisation velocitiy. Making V_E the subject of Equation 2.20 and then substituting into Equations 2.24a and 2.25a yields:

$$j^*_3 = \left[\frac{U_{Gf}}{\left\{gV\left[\frac{1-\epsilon_0+h_L}{1-\epsilon_{Gf}}\right]\right\}^{0.5}}\right]\left[\frac{\rho_G}{\rho_L - \rho_G}\right]^{0.5} \qquad (2.24b)$$

and

$$j^*_4 = \left[\frac{U_{LF}}{\left\{gV\left[\frac{1-\epsilon_0+h_L}{1-\epsilon_{Gf}}\right]\right\}^{0.5}}\right]\left[\frac{\rho_L}{\rho_L - \rho_G}\right]^{0.5} \qquad (2.25b)$$

The hydrostatic and momentum fluxes that are due to the presence of spherical particles may therefore be written as:

$$j^*_5 = \left[\frac{U_{Gf}}{(gd_p)^{0.5}}\right]\left[\frac{\rho_G}{\rho_L - \rho_G}\right]^{0.5} \qquad (2.26a)$$

and

$$j^*_6 = \left[\frac{U_{LF}}{(gd_p)^{0.5}}\right]\left[\frac{\rho_L}{\rho_L - \rho_G}\right]^{0.5} \qquad (2.26b)$$

Analogical to Equation 2.21 and the fact that the total resolved forces and geometrical properties will remain unchanged in either a two or three dimensional model, then Equation 2.21 may be represented as the total of all the momentum and hydrostatic forces. So,

$$j^{*0.5}_1 + j^{*0.5}_2 + j^{*0.5}_3 + j^{*0.5}_4 + j^{*0.5}_5 + j^{*0.5}_6 = j_{Theory} = 1 \qquad (2.27)$$

Thus, for Equation 2.27 to be valid, substitution of experimental variables into the left hand side at the "true" flooding condition will yield unity. The liquid and gas flooding velocities may then be calculated when the gas holdup ε_G and the liquid holdup per unit static bed volume h_L, are known.

Having established the required hydraulic equations, it is now possible to establish the theory that is associated with the heat and mass transfer characteristics of the FBCT.

2.5 Heat and Mass Transfer

Several methods that provide an indication of a cooling tower thermal performance exist. The most common being the range of cooling. This is normally defined as the difference in temperature between the inlet hot water temperature and the and the outlet cooled water temperature. It may be represented as:

$$Range = T_{HW} - T_{CW} \qquad (2.28)$$

Another simple method of evaluating tower performance is called the ***approach***

to the wet-bulb temperature. This is the temperature attained by a small reservoir of water in contact with a large amount of air flowing past it. The approach may be defined as the difference in temperature between the outlet cooled water temperature and the inlet air ambient wet-bulb temperature ie

$$Approach = T_{CW} - T_{WB} \qquad (2.29)$$

The tower cooling effectiveness η, may be determined by how close it brings the cooled water temperature to the wet-bulb temperature of the entering air:

$$\eta = \frac{Range}{Total\ Tower\ Potential} = \frac{T_{HW} - T_{CW}}{T_{HW} - T_{WB}} \qquad (2.30)$$

2.6 Mathematical Modelling

The most widely used model in evaluating tower performance is commonly known as the "enthalpy potential" method developed by Merkel (1925) and by Harold Mickley (1949). This model is recognized as the most convenient and reliable way in determining the size of the equipment required for direct contact systems in general since its mathematical derivation is based on basic thermodynamic principles. The design of fluidised bed cooling towers (FBCT) also requires a similar procedure because it involves simultaneous heat and mass transfer which is fundamental in direct contact air-water systems with significant temperature and water vapour pressure gradients. Moreover, Barile *et al* (1974) and El-Dessouky (1993) have shown that this theory may be successively applied to design model FBCTs. Therefore, this theory will form the basis of a thermal design method for the sizing of a full-scale FBCT.

2.7 Direct Contact of Air and Water

Considering a differential height, dV, of a forced draft, adiabatic, countercurrent, constant cross-section fluidised bed cooling tower containing mobile spherical packing in which air and water are directly contacted. As shown in the control volume in Figure 2.1, ambient air enters the section at a mass rate of G kg/s m^2 of tower cross-section, at a bulk dry-bulb temperature T_{DB}, a specific humidity ω_A, and an enthalpy, H_A. The water enters the section at a mass rate of $L + dL$ kg/s m^2 of tower cross-section and a bulk temperature of $T_W + dT_W$. The water and air simultaneously exchange mass and heat and leaving at slightly different conditions. Assuming that the air is saturated at the air-water interface temperature T_i and at interface specific humidity ω_i, then the rate of phase exchange is:

$$G d\omega_A = dL = [\omega_i - \omega_A] k_G a_M dV \qquad (2.31)$$

Rearrangement of Equation 2.31 gives:

$$\frac{d\omega_A}{\omega_i - \omega_A} = \frac{k_G a_M}{G} dV \qquad (2.32)$$

This equation relates the change in humidity of the air to the height of the tower. However, except in the special case of constant water temperature ("a wet bulb run"), the relation between the humidity of the air ω_A and the humidity of saturated air at the temperature of the water-air interface ω_i is not known requiring that further equations be developed. The enthapy of the air is defined by the relation

$$H_A = C_V(T_{DB} - T_0) + h_{fg}\omega_A \qquad (2.33)$$

An enthalpy balance based on the first law of thermodynamics applied to the combined phases yields:

$$d[GH_A] = d[[L+dL]C_W(T_W - T_I)] \qquad (2.34)$$

Equation 2.34 relates the bulk enthalpy of the air, H_A to the bulk temperature of the liquid water. Therefore,

$$\frac{dH_A}{dT_W} = [L+dL]\frac{C_W}{G} \qquad (2.35b)$$

Integrating Equation 2.35 and neglecting the evaporated or condensed water gives the "operating line," the line that connects the bulk air enthalpy ω_{DI}, and bulk water temperature thus

$$(H_{A2}-H_{A1}) = \frac{LC_W}{G}(T_{HW}-T_{CW}) \qquad (2.36)$$

The rate of transfer of heat from the hot water at T_W through the liquid film to the liquid gas interface at T_i is given by:

$$LC_W dT_W = h_W a_H (T_W - T_I)\, dV \equiv G dH_A \qquad (2.37a)$$

Equation 2.37a relates the change in water temperature to the height of the tower.

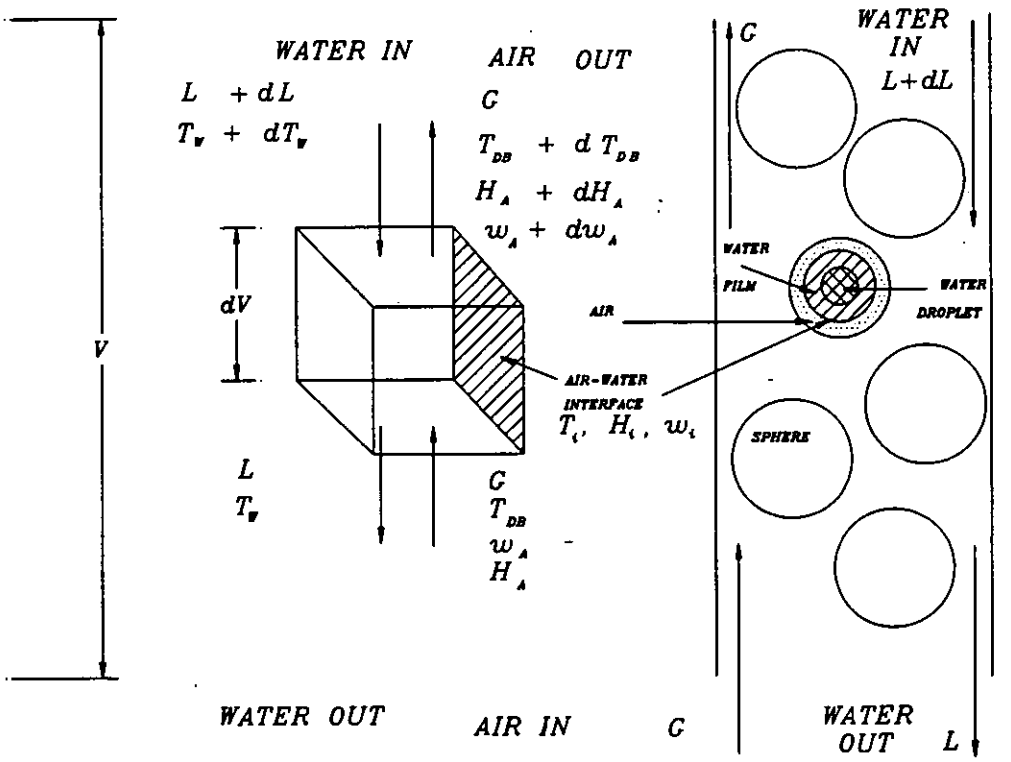

Figure 2.1 Control Volume of the interfacial element of the FBCT.

Rearrangement yields:

$$\frac{dT_W}{(T_W - T_i)} = \frac{h_W a_H}{LC_W} dV \qquad \textbf{(2.37b)}$$

The rate of transfer of sensible heat from the interface through the gas film to the gas stream at T_{DB} may be written

$$GC_V\, dT_D = h_G\, a_H\, (T_i - T_{DB})\, dV \qquad (2.38a)$$

Equation 2.38a relates the gas temperature and the tower height. It may be rearranged to give:

$$\frac{dT_{DB}}{T_i - T_{DB}} = \frac{h_G\, a_H}{GC_V} dV \qquad (2.38b)$$

These differential equations are sufficient to relate the bulk air temperature T_{DB}, air humidity ω_D, air enthalpy H_A, water temperature T_W, and static bed height, V. Simplification of these equations is required. Merkel (1925) first used the approximate air-water relation developed by Lewis (1922)

$$\frac{h_G}{k_G} = C_V \qquad (2.39)$$

to develop the enthalpy potential method. Introducing the Lewis relation into Equation 2.39, and assuming that the area of heat transfer, a_H equals the area of mass transfer, a_M, as a result of heat and mass transfer at the same gas-liquid interphase, gives:

$$GC_V dT_{DB} = k_G a_H (C_V T_i - C_V T_{DB})\, dV \qquad (2.40)$$

Multiplying both sides of Equation 2.31 by h_{fg}, and add to Equation 2.40:

$$G(C_V dT_{DB} + h_{fg} d\omega_D) = [(C_V T_i + h_{fg}\omega_i) - (C_V T_{DB} + h_{fg}\omega_B)]\, k_G a_M dV \qquad (2.41)$$

The specific heat capacity of moist air is basically constant and if most of the heat transferred is assumed to be by evaporation then one can safely neglect the

variation of sensible heat transfer. Introducing the air enthalpy H_A, Equation 2.41 may be written as:

$$GdH_A = k_G\, a_M (H_i - H_A)\, dV \qquad (2.42a)$$

or,

$$\frac{dH_A}{H_i - H_A} = \frac{k_G\, a_M}{G} dV \qquad (2.42b)$$

Equations 2.42a and 2.42b relate bulk air enthalpy and the tower height. Equation 2.42b may be integrated to obtain the tower height. Thus,

$$\int_{H_{A_1}}^{H_{A_2}} \frac{dH_A}{H_i - H_A} = \frac{k_G a_m V}{G} \qquad (2.43)$$

The integration may either be carried out graphically by plotting the reciprocal of the enthalpy driving force $1/(H_i - H_A)$ as a function of the corresponding bulk enthalpy or by any numerical approximation such as the Tchebycheff quadrature method (B.S. 4485, 1988). An appropriate substitution applied to Equation 2.43 and bearing in mind the energy balance yields:

$$C_W \int_{T_{cw}}^{T_w} \frac{dT_W}{H_i - H_A} = \frac{k_G\, aV}{L} \qquad (2.44)$$

Since the water interface temperature is not usually known, it must be assumed that all of the heat must pass from the main body of the water to the water side of the air water-interface to the bulk air, thus the thermal resistance of the water film is negligible. Also, since the introdution of the Lewis relation affects only the sensible heat transfer which constitutes about 20-25 % of total then:

$$\frac{H_W - H_A}{H_i - H_A} = \frac{k_G}{K_G} \qquad (2.45)$$

is constant as since the temperature at the air-water interface is at the temperature of the bulk water. The overall coefficient may then be introduced into equation 2.44 to give:

$$C_W \int_{T_{cw}}^{T_{hw}} \frac{dT_W}{H_W - H_A} = \int_{H_{cw}}^{H_{hw}} \frac{dH_W}{H_W - H_A} = \frac{KaV}{L} \qquad (2.46)$$

The left hand side of the Equation 2.46 is termed the required tower characteristic whilst the right hand side of the equation is termed the available tower characteristic and must be determined by experiment. At moderate inlet water temperatures, the available tower characteristic is dependent only on the nature of the packing and is characteristic only to a particular tower. The required tower characteristic is obtained by mathematical calculation of the left hand side of Equation 2.46, for a particular design liquid/gas mass flux ratio *L/G*, inlet hot water temperature, outlet cooled water temperature, average wet-bulb and dry-bulb temperatures. The left hand side increases as *L/G* increases whilst the right hand side has been experimentally shown to decrease with increases in *L/G*. The design point is the intersection of both the right side and left side of Equation 2.46. This method of analysis will form the basis of this work.

2.8 Dimensional Analysis

In gas-solid-liquid fluidisation relating to FBCTs, the individual inert particles are supported by the upward flowing air. Thus the resistance to the motion to the single sphere in the gas flowing upwards surrounded by water droplets, when both skin friction and form drag are significant in the FBCT can be represented as

$$\Delta P = f_1(\mu_L, \mu_G, \varphi, \rho_L, \rho_S, \rho_G, \sigma_G, \sigma_L, d_p, d_S, K_G, L, G, D_c, V, H, S_p) \quad (2.47)$$

If the spheres form part of a uniform suspension, the resistance force also depends on the presence of other particles since this affects the flow pattern. The presence of solid concentration causes a restriction of flow passages between particles. The air then moves in a tortuous path increasing the pressure drop and hence the shearing stresses which affect the flow pattern. Therefore it can be safely assumed that the nature of flow is related to the ratio of particle diameter d_p to the distance between the particles S_p. Richardson and Zaki (1954) state: "For a uniformly dispersed suspension, d_p/S_p is a function of the porosity $(\epsilon_G+\epsilon_L)$ only." Dimensionality, therefore, permits us to write the Equation of the bed pressure drop in terms of the properties of the fluid and tower and assuming that the controlling factor for mass transfer is the gas-side mass transfer coefficient:

$$\Delta P = f_2(\mu_L, \mu_G, \varphi, \rho_G, \rho_L, \rho_S, d_p, d_S, K_G, \varepsilon_G, \varepsilon_L, L, G, V, D_C) \quad (2.48)$$

Tabei *et al.* (1989) have empirically shown that the gas-liquid interfacial area is a function of only the gas and liquid holdups in a three-phase countercurrent gas-solid-liquid fluidised bed. Therefore, considering a unit cross-section of column, and a sphericity of 1 for the particles the dimensional equation can be written as:

$$R_t = f_3(\mu_L, \mu_G, a, \rho_L, \rho_S, \rho_G, \sigma_G, \sigma_L, d_p, d_S, K_G, L, G, V, H) \quad (2.49)$$

Barile *et al.* (1971, 1974) carried out dimensional analysis in order to relate the liquid holdup to other dimensionless groups and found that the resistance to the flow of air as well as the heat and mass transfer rate between air and water, in a three-phase counter-current FBCT, are proportional to the measure of the number expansion and contraction cycles V/d_p, the spheres must undergo to attain full

fluidisation. Also, the dimensions relating to the cross-sectional area of the FBCT may be eliminated because the experimentally dimensioned variables are based on their individual liquid and gas mass fluxes. So,

$$\Delta P = f_4(\mu_L, \mu_G, a, \rho_L, \rho_S, \rho_G, \sigma_G, \sigma_L, d_p, d_s, K_G, L, G, V, \frac{V}{d_p}, H) \quad (2.50)$$

Rearrangement of Equation 2.50 gives:

$$K_G = f_5\left[\Delta P, g, \mu_L, \mu_G, \rho_L, \rho_S, \rho_G, \sigma_G, \sigma_L, d_p, d_s, K_G, L, G, \frac{V}{d_p}, V, H\right] \quad (2.51)$$

One possible dimensionless combination relating ΔP, the liquid mass flux L, the gas mass flux G, and the particle diameter d_P and the fundamental properties of the fluids is:

$$\frac{\Delta P^2 L G d_p^6 \rho_L \rho_G}{\mu_G^3 \mu_L^3} \quad \textbf{(n2.1)}$$

If we consider the fluids individually, we may then write:

$$\frac{\Delta P L d_p^3 \rho_L}{\mu_L^3} \quad \textbf{(n2.2)}$$

and,

$$\frac{\Delta P G d_p^3 \rho_G}{\mu_G^3} \quad \textbf{(n2.3)}$$

We have shown that the liquid/gas mass flux ratio L/G is an important independent variable in the thermal performance of the FBCT. Therefore, Now, the group $n2.1$ may be represented in:

$$K_G = f_6\left[\frac{\Delta P^2 L G d_P^6 \rho_L \rho_G}{\mu_L^3 \mu_G^3}, \rho_L, \rho_G, \rho_P, g, a, \sigma_G, \sigma_L, d_p, d_S, L, G, \frac{V}{d_p}, \frac{L}{G}, V, H\right] \quad (2.52)$$

$$\left[\frac{\Delta P^2 \rho_L \rho_G}{(LG)^2}\right]\left[\frac{LGd_P^2}{\mu_L \mu_G}\right]^3 \quad \textbf{(n2.4)}$$

The above group may be rewritten as:

$$\frac{LGd_P^2}{\mu_L \mu_G} = \left[\frac{Ld_p}{\mu_L}\right]\left[\frac{Gd_p}{\mu_G}\right] \quad \textbf{(n2.5)}$$

is the combined group, the liquid-gas-particle Reynolds number. The left side of the group *n2.4* is dimensionless due to the bed air pressure drop.

As the water is sprayed down into the tower, droplets are formed. The size of the droplets is dependent upon several factors such as the inlet water temperature, the water mass flow rate and the nozzle static pressure. However, the main factor that determines the average drop size is the manufacturer's specification. Droplet size enhances the heat transfer rate because the the gas-liquid interfacial area is dependent upon it. Normally, the smaller the droplets for any particular liquid/gas mass flux ratio, the greater the gas-liquid interfacial area since coalescence of the gas-liquid interfaces enhances the gas liquid interfacial area. The effect is a decrease in the resistance to heat and mass transfer from the water-side of the air water interface to the gas-side and into the bulk of the air. There is thus an increase in evaporation rate with a consequent increase in the transfer of mass and heat due to enhanced partial pressure gradients.

The performance and resistance to motion of a FBCT is also dependent upon the degree of wetness, d_p/d_S of the inert particle surface. In addition, it is shown that the heat transfer rate can be represented by the dimensionless group of the tower characteristic *KaV/L*. Both the resistance and the heat and overall mass transfer

rate of the FBCT are dependent upon the adhesive force between liquid, gas and the particles. Thus the surface tension of the gas in the liquid is also important in the working of the FBCT. These two factors may be represented by the liquid-particle Weber number We_L, and the gas-particle Weber number We_G. Now, the density of the particle is also important in the heat and mass transfer process because low density particles have lower gravitational resistance to gas flow due to their lower weight as compared to high density particles affecting the degree of turbulence and random movement of the particles and liquid droplet in all directions. The density of the gas is also important in the resistance and the heat and mass transfer rate. However, the weight of the gas is negligible as compared to the weight of the particles and the liquid. The only dimensionless group that may represent the density of the particles can, therefore, be assumed to be ρ_P/ρ_L.

The gravitational and frictional forces acting on the FBCT so as to enhance the evaporation rate of the hot water may be represented by Froude number F_L and Reynolds number Re_L respectively. The gas particle Reynolds number Re_G, appears in the dimensional analysis because the amount of resistance to fluid flow is dependent upon the superficial gas velocity which in turn affects the gas holdup within the tower. It has already been shown that the gas-liquid interfacial area is proportional to the gas holdup. Since the rate of heat and mass transfer is dependent upon the gas-liquid interfacial area, then the justificaton of its inclusion in the dimensional analysis is evident. Vunjak-Novakovic *at al.* (1987) and Barile *et al.* (1971) have all developed correlations relating to the liquid holdup with other appropriate dimensionless groups and found that the amount of liquid retained in a FBCT during a wide range of operation is almost independent of the superficial gas velocity. The amount of liquid retained in the bed, therefore, is dependent upon the liquid-particle Froude number Fr_L only and since the gas-liquid interfacial area is proportional to the liquid holdup, the gas particle Froude Number Fr_G, does not appear as one of the dimensionless groups.

The spray nozzle height from the bed distributor grid also affects the heat and

mass transfer rate since the bed expands during fluidisation. Moreover, the spray nozzle height takes into account the end effect of the FBCT freeboard in relation to the heat and mass transfer. A possible dimensionless combination may therefore be *H/V*. Moreover, Barile *et al.* (1971, 1974) have shown that the tower characteristics *KaV/L*, and the bed air pressure drop ΔP are dependent upon the liquid particle Froude and Reynolds numbers. Rearranging Equation 2.52 and considering groups n2.1 to n2.5 gives:

$$\frac{KaV}{L} = f_7\left[\frac{d_pL}{\mu_L}, \frac{d_pG}{\mu_G}, \frac{\rho_P}{\rho_L}, \frac{L^2}{\rho_L^2\, gd_p}, \frac{d_pL^2}{\rho_L\sigma_L}, \frac{d_pG^2}{\rho_G\sigma_G}, \frac{d_p}{d_s}, \frac{V}{d_p}, \frac{L}{G}, \frac{H}{V}, \frac{\Delta P^2\rho_L\rho_G}{L^2G^2}\right] \quad (2.53)$$

Since both the tower characteristic group and the pressure drop terms are dependent variables, they are to appear in the left hand side of Equation 2.53. Therefore Equation 2.53 ought to be rearranged to include both the heat transfer term and the power terms into the left side of the Equation. Simplifying the power term by assuming that its square root and the tower characteristic are similarly interdependent gives:

$$\left[\frac{KaVG}{\Delta P\rho_L^{0.5}\rho_G^{0.5}}\right] = f_8\left[\frac{d_pL}{\mu_L}, \frac{d_pG}{\mu_G}, \frac{\rho_P}{\rho_L}, \frac{L^2}{\rho_L^2\, gd_p}, \frac{d_pL^2}{\rho_L\sigma_L}, \frac{d_pG^2}{\rho_G\sigma_G}, \frac{d_p}{d_s}, \frac{V}{d_p}, \frac{L}{G}, \frac{H}{V}\right] \quad (2.54)$$

Equation 2.54 relates the rate of heat transfer per unit energy expended by the air for a particular liquid and solid particle in a three-phase counter-current FBCT system. Alternatively, each of the dependent tower cahracteristic and resistance groups may be considered as dependent upon the independent groups of Equation 2.54.

The gas-liquid interfacial area is an important parameter that directly affects the rate of heat transfer and therefore merits theoretical consideration. Tabei, Hasatani and Kuroda (1989) investigated the gas-liquid interfacial area in a mobile bed

contactor and derived an empirical relation, which is valid for gas velocities in the range of 1 to 20 m/s and liquid velocity of 0.01 to 0.2 m/s at gas and liquid temperatures of 20 deg C. The relationship may be written as:

$$a = 2100\epsilon_G^{1.25}\epsilon_L^{0.75} \qquad (2.55)$$

Equation 2.55 is valid because a logarithmic plot of the group a/ϵ_L against ϵ_G/ϵ_L gave a straight line with gradient 1.25 m^{-1} and intercept 2100 m^{-1} for a wide range of experimental conditions using a large body of data from the work of other researchers.

Having established the required theory for the FBCT, it is now necessary that the work of other investigators is reviewed so as to throw more light as to the novelty of the derived theories. The next chapter will be devoted to the background work relating to this thesis.

CHAPTER III

REVIEW OF EXPERIMENTAL WORK ON THREE-PHASE FLUIDISATION

The Fluidised Bed Cooling Tower (FBCT) is sometimes called a Mobile Bed Contactor [Kito *et al.*(1978); Rama *et al.* (1983); Rama *et al.* (1985); Tabei *et al.* (1989)]. The names Turbulent Contact Absorber (Vunjak-Novakovic *et al.* (1980); Douglas (1963)), Turbulent Bed Contactor [Chen *et al.* (1968); Chen *et al* (1969); Dengler (1977); Douglas (1964); Guerriere *et al.* (1995); Vunjak-Novakovic *et al.* (1987)], Floating or Fluidised Bed Scrubber [Kielback (1959); Visvanathan *et al.* (1985)] are also in use. The acronym Fluidised Bed Cooling Tower (FBCT) will be adopted in this work.

Fluidisation is normally two-phase liquid-solid or gas-solid. Theoretical work on three-phase fluidisation is uncommon, chiefly due to inherent difficulties encountered in its mathematical treatment [Ostergaard *et. al* (1969)] as different types of three-phase fluidisation exist as shown in Figure 3.1. However, quite a number of researchers have experimentally investigated various parameters linked to the concept.

Most of their findings are based on co-current gas-liquid-solid three-phase fluidisation. Ostergaad and Michelson (1970), Dhanukha and Stepnek (1978) did investigations on co-current three-phase fluidisation. However, the main interest in this work is centred on three-phase counter-current flow. To obtain an in-depth understanding of this phenomenon, its fundamental mode of operation must be clearly explained.

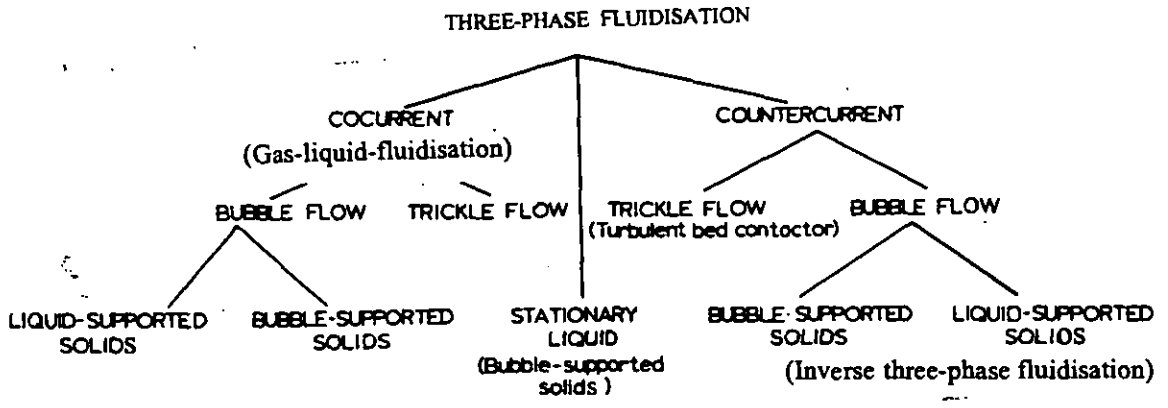

Figure 3.1 Different types of three-phase fluidised beds (Epstein, 1981).

3.1 Operating Regimes

Muroyama and Fan (1985) stated that three-phase fluidisation has only become the subject of scientific interest in the last three decades. The principles of fluidisation may apply to both three-phase and two-phase operations. Figure 3.2 below of the different regimes of three-phase counter-current gas-liquid-solid flow, shows the degree of complexity of three-phase operations.

Dengler (1977) reported that the Turbulent Bed Contactor may operate in a variety of distinct operating regimes of which fully developed fluidisation at minimum power consumption is most desirable for maximum transfer efficiency, the regime operation being dependent upon liquid and gas flow rates and fill size, density, and depth.

Balabekov *et al.* (1969), reported the existence of four hydrodynamic states of column operation in the range of gas velocities between 0.1 to 8 m/s, liquid mass flux of 0 to 35 kg/s m^2, static packing depth of 38 to 300 mm and packing

diameter of 6, 12, 16 and 22 mm in a 1.2 m long and 175 mm diameter column. The states were: packing in the stationary state, initial fluidisation of the packing, developed fluidisation and flooding of the column. They concluded that the optimal state for heat and mass transfer processes is when developed fluidisation is reached. FBCT Hydrodynamics was theoretically investigated by O'Neill *et al.* (1972). They claimed two subregimes within the developed fluidisation regime as illustrated in Figure 3.3 - fluidisation without incipient flooding (Type I) and fluidisation due to incipient flooding (Type II). Fluidisation without flooding is primarily noted among extremely low bulk density fills (ie less than 200 kg/m^3) and occurs when the particles fluidise much below its theoretical flooding point. Fluidisation due to incipient flooding occurs with heavier solid particles (ie $\rho_P \geq$ 300 kg/m^3 and $\leq$ 1329 kg/m^3) with the field being near or at its theoretical flooding point before fluidisation.

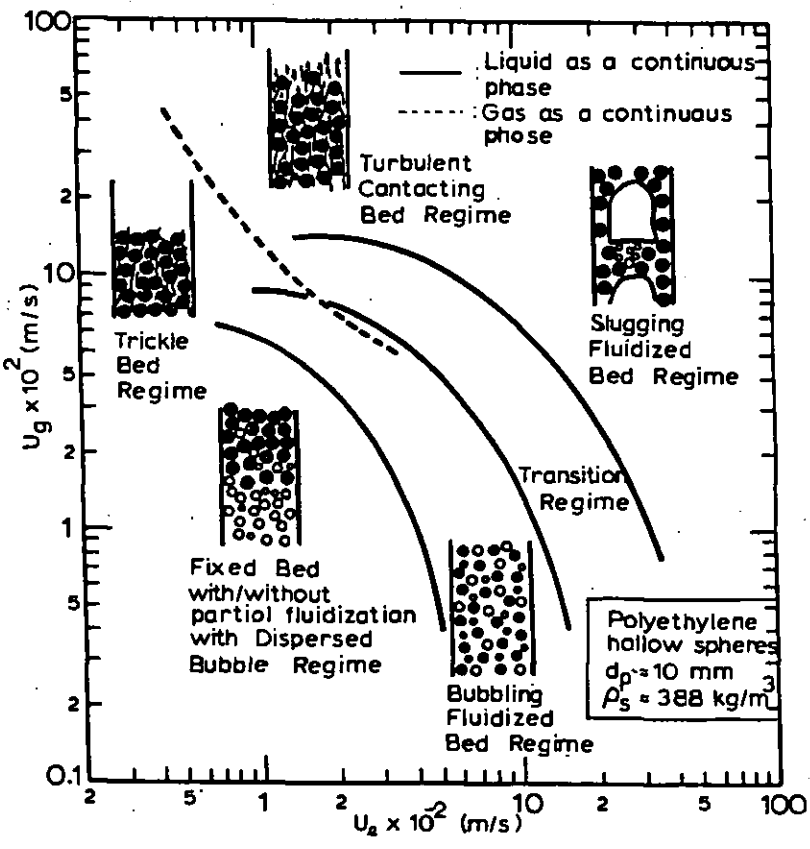

Figure 3.2 Flow regime of the counter-current gas-liquid-solid fluidization (Muruyama and Fan, 1985).

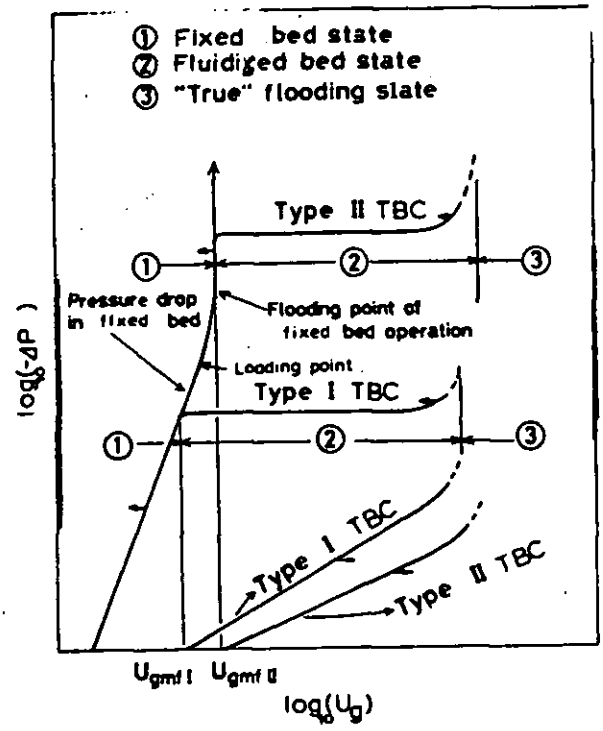

Figure 3.3 Operating regimes of the FBCT (Fan and Muruyama, 1989).

They reported that the better mode for contacting is fluidisation due to incipient flooding since more intense interfacial mixing is realised. They also concluded that increased fill density will generally increase fluidised mixing and transfer. On the other hand, Dengler (1977) stated that fill density is directly related to power cost and must, as a necessity be minimised for a cooling tower. The present study will dwell on both types I and II regimes of FBCT operation. The present work will cover both type I and II operating regimes with the maximum particle density for the type II operation limited to 325 kg/m^3 while the minimum particle density for the type I operation will be 69 kg/m^3.

Vunjak-Novakovic *et al.* (1980) studied the changeover from fixed to fluidised bed operation and to relate the corresponding hydrodynamic states. As mentioned in Chapter I, flooding sets an upper limit to counter-current operation in a bed of fixed packing. Their findings showed that in a bed of low density packing, the bed pressure drop equals the weight of both the packing and the liquid held up before flooding and, that further increase of the gas flowrate results in bed expansion, but

the values of the bed pressure drop and liquid hold-up remain unchanged and equal to those in a fixed bed at the minimum fluidisation velocity.

Vunjak-Novakovic *et al.* (1980) also stated that a packed bed with heavier packing (380-680 kg/m^3) cannot fluidise before the flooding point is reached because the bed pressure drop is insufficient to support the packing and the liquid hold-up. Also, the increase in liquid holdup and hence the increase in pressure drop cannot be attained until the interfacial activity which causes the flooding of a fixed bed reaches an advanced stage. Thus an increase in particle density requires a corresponding advance in flooding characterised by an increase in the liquid hold-up; the minimum fluidisation velocity remaining essentially independent of packing density since it equals the flooding velocity for the same liquid flowrate. They concluded that the optimal operating conditions are obtained where technical and economic requirements are balanced as shown in Figure 3.4.

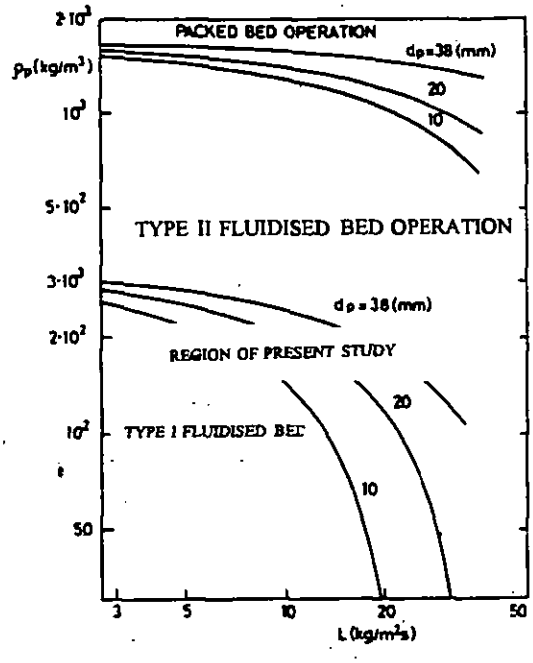

Figure 3.4 Phase diagram for counter-current flow of air and water in the FBCT with spherical particles (Vunjak-Novakovic *et al.*, 1987a).

3.2 Minimum Fluidisation Velocity

The minimum fluidisation velocity may be described as the flowrate at which a stationary bed transforms to a fluidised state. It represents the minimum fluidised state condition and is an important mark for design and operating conditions. As mentioned by Fan *et al.* (1989), Kito *et al.* (1976) expressed the U_{mf} as that velocity at which the rapid increase of bed air pressure drop through the fixed bed region levels off and approaches a constant value irrespective of changes in the gas flow rates. Kito *et al.* (1976) observed that the bed progressively expanded giving rise to a transition region before full fluidisation was realised. It follows that, the U_{mf} based on the pressure drop variation is always greater than that based on the initiation of bed expansion.

The U_{mf} generally decreases with increasing liquid flow rate and liquid viscosity and with decreasing particle diameter (Chen and Douglas, 1968; Kito *et al.*, 1976; Vunjak-Novakovik *et al,* 1980;) but is independent of static bed height (Balabekov *et al.*, 1969; Kito *et al.*, 1976; Egbe, 1996b). In addition, it increases with increasing particle density for both FBCT types when the calculated is based on the pressure drop variation method, when calculated based on initial bed expansion, it is independent of particle density for type II FBCTs. Gel'perin *et al.* (1968), Balabekov *et al.* (1969), showed that the U_{mf} increases with open area of supporting grid, but, as shown by Kito *et al.* (1976), but stated that it is independent of grid open area if the parameter fd_p/D_C is greater than 0.05.

A number of correlations for predicting U_{mf} are availaible in the excellent review of Fan and Muroyama (1989). The geometry of the experimental system, the operating conditions, and physical properties of liquid and gas, were considered in the development of these correlations (Muroyama and Fan, 1989). Most of the equations are empirical with no theoretical justification. Fan *et al.* (1989) predominantly attributed discrepancies in correlations to differences in methods of determining the minimum fluidisation gas velocity. They stated that some

models closely resemble those for two-phase fluidisation which are established on the equivalent relationship between dynamic pressure drop across the fixed bed and the effective weight of the solid particles in the fluidised condition and therefore consistent with the method of measurement of the U_{mf} based on pressure drop variations.

Over a range of packing densities from 365-1036 kg/m^3, Balabekov *et al* (1969), stated that for similar sphere diameters, the widest range of normal operation is obtained with spheres of density 600 kg/m^3 and the narrowest with spheres of density 365 kg/ m^3; the range of operation being that condition for developed fluidisation between initial fluidisation and "true" flooding.

3.3 Bed Pressure Drop and Liquid and Gas Holdups

The bed air pressure drop through the bed, is a very important dependent variable in FBCT operation and determines the energy consumption required during operation.

The pressure drop due to the weight of dry particles is always constant, while that due to liquid holdup depends strongly on the operating conditions and system geometry. Consequently, the variation in the bed air pressure drop in a FBCT mainly depends on the liquid holdup. The pressure drop through a bed with a grid open area greater than 70% is almost independent of gas velocity as suggested by Rama *et al.* (1983). Under these conditions, Tichy *et al.* (1972) found that the bed air pressure drop is almost independent of particle size and it increases as the liquid holdup increases. The bed pressure drop and the liquid holdup were also dependent upon the static bed height (Wonziak, 1977; Kito *et al.*,1976). For small grid open areas the bed air pressure drop sharply increases as the superficial gas velocity is increased (Blyakher *et al.*, 1967; and Balabekov *et al.*, 1969) due to increased liquid holdup in the column.

Experimental data on the bed air pressure drop in FBCTs have been reported by several investigators (Douglas *et al.*, 1963; Balabekov *et al.*,1969; Miconnet *et al.*, 1982). Dengler (1977) stated that the gas phase pressure drop across the column (ΔP) is the most important variable of fluidised bed contacting due to its direct bearing on operating power cost. Dengler (1977) also reported the validity of using an additive pressure drop model in which the total column pressure drop equals the sum of pressure drops due to individual resistances. This can be represented by the equation:

$$\Delta P = \Delta \Sigma P_i = \Delta P(\text{dry grid + empty column}) + \Delta P(\text{dry bed}) + \Delta P(\text{liquid holdup}) + \Delta P(\text{holdup on grid}) + \Delta P(\text{air/water interaction on grid}) \quad \textbf{(3.1)}$$

Liquid and gas flow rates, supporting grid open area, bulk density of the fill, and the shape, size, and surface characteristics of the individual fill particles all determine total pressure drop to some degree. Resistance due to mist eliminators, upper retaining grids, internal supports, and air/water disengaging sections are considered negligible. Although they contribute to the overall pressure loss their effect can be minimised by good design. Dengler (1977) used supporting grid which was 85 percent open. Therefore, the last two resistances, ΔP(holdup on grid) and ΔP(air/water interaction on grid) were neglected. The ΔP (dry grid +empty column) is a function only of gas flow rate and may also be minimized by good design. For that particular equipment the term rarely exceeded 2.5 mm of water column.

According to Dengler (1977), Liquid holdup ε_l, is that fraction of the expanded contacting zone which is liquid. The liquid holdup consists of an operational liquid holdup and a static liquid holdup. The operational liquid holdup can be measured by collecting the accumulated liquid upheld at the bottom of the bed after simultaneously shutting off the gas and liquid flows. The static holdup represents the liquid upheld by adhesive forces on the particles and can be measured by weighing the wetted and dry particles. Figure 3.5 below shows the

variation in the operational liquid holdup with the superficial gas velocity as measured by Vunjak-Novakovic *et al.* (1987). For a type I FBCT (ρ_s=156 kg/m^3), ε_l remains almost constant for gas velocities comprising both fixed and fluidized beds; for Type II FBCT, ε_l increases significantly after U_{mf} has been reached. The extent of the increase is dependent upon the static bed height and the liquid flowrate. The gas holdup can be determined when the expanded bed height and the liquid holdup are known. Investigation of the former have been conducted by Gel'perin

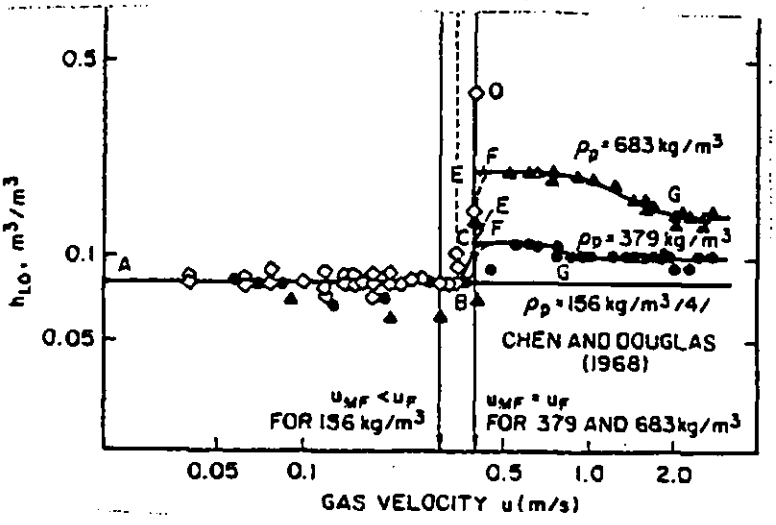

Figure 3.5 Liquid holdup dependence upon the superficial gas velocity for a type I and II FBCT subregimes (Vunjak-Novakovic *et al.*, 1987).

et al. (1968), Krainev *et al.* (1968), and Balabekov *et al.* (1969) using dense particles in columns with grids having small open areas. Balabekov *et al.* (1969) showed that gas holdup increased with increasing gas velocity, but was almost independent of liquid velocity at a constant gas velocity. They however, concluded that gas holdup is nearly independent of particle density, liquid viscosity, static bed height, and the open area and the orifice diameter of the of the supporting grid.

3.4 Expanded Bed Height

The dynamic or expanded bed height V_E is an essential design variable since the packing must be given adequate freeboard for uniform fluidisation. Knowledge of this factor would allow calculation of the expanded volume of the bed and provide a basis for the determination of liquid and gas holdups and pressure drop. According to Fan and Muruyama (1989), bed expansion can be determined visually by averaging the maximum and minimum heights between which the bed surface fluctuates or from the axial pressure distribution (Tichy *et al.*, 1972). Dengler (1977) reported that the expanded bed height has a strong, direct dependence on gas rate and a weak, direct dependence on liquid rate.

Bed expansion data were first reported for a grid of small open area by Gel'perin *et al.* (1966). Chen and Douglas (1968) showed that the bed height increased in proportion to increases in the superficial gas velocity in conformity with the findings of Dengler (1977). Tichy and Douglas (1972) reported that V_E/V is independent of both the static bed height and the particle density for low density particles. Rama *et al.* (1983) observed that a bed of cork particles with tapered cylindrical shape, expanded more than a bed of spherical or other irregularly shaped particles with similar densities. Experimental data on bed expansion for relatively high density particles ($470 < \rho_s < 2600$ kg/m^3) were obtained by Balabekov *et al.* (1969) and Strumillo *et al.* (1974). Tichy and Douglas (1973) have experimentally shown that sharp increases in the expanded bed height occur at superficial gas velocities approaching the "true" flooding point.

Levsh *et al.* (1968) has shown that the gas distributing grid strongly affects the bed expansion behaviour because in a grid of small open area a liquid layer builds up immediately above the grid, causing axial variations in liquid holdup. The behaviour of such beds is reminiscent of a bubble column with high gas holdup. A correlation of the height of the liquid holdup just above the gas distributor grid was established by Levsh *et al.* (1968). A list of empirical equations for the

expanded bed height developed by other researchers for particles similar to those employed industrially is well outlined in the excellent review of Fan and Muruyama (1989). However these equations must be applied with care because of the limited experimental conditions used for their development.

3.5 Axial Mixing

Axial backmixing is disadvantageous to three-phase contacting. It is normally categorised as fluid or solid-phase mixing. In both cases, complete backmixing leads to the limiting case of equilibrium stage operation, while the absence of backmixing is a requirement of counter-current (piston) flow. The FBCT as reported by Barile *et al.* (1971) operates between limits of true counter-current and equilibrium stage contacts, making analysis extremely difficult. Researchers have characterised the degree of axial mixing by means of an axial dispersion coefficient D_l (length^2/time). In the absence of backmixing, D_l equals zero and for complete backmixing D_l is infinite. Determination of the dispersion coefficient for a particular system may make the inclusion of second order axial mixing effects in analysis possible. Chen and Douglas (1969) state: "The backmixing in a turbulent contactor is brought about mainly via the turbulent eddies generated as a result of agitation of the liquid phase by the violent motion of the low density packing." However, some degree of mixing, will enhance the FBCT heat and mass transfer because of the high degree of turbulence involved in fully developed fluidisation.

Liquid phase axial mixing in a FBCT was first investigated by Chen and Douglas (1969) using a transient response technique. They measured the axial dispersion coefficient of liquid by introducing a step change in flow rate of an inert liquid to the flowing tracer liquid. They found that excess gas flow rate over that required for minimum fluidisation provides a measure of intensity of bed turbulence, and that the liquid axial dispersion coefficient for a particular solid particle increased as both the liquid flow rate and the factor G-G_{mf} were increased.

Koval *et al.* (1975) measured liquid axial dispersion coefficients in FBCTs of 100 and 200 mm internal diameter with grid having an open area of 46% with spherical particles having diameters of 9 and 19 mm and densities varying from 283 to 830 kg/m^3. Using the pulse response technique, Koval *et al.*(1975) evaluated the liquid axial dispersion coefficients from the first and second moments of the response curve and found that an increase in liquid flow rate resulted in a significant increase in D_{zL}. In addition, they indicated that the axial dispersion coefficient, or the column Peclet number ($Pe = V_L V_E / D_{zL}$), was virtually independent of particle density. The particle diameter had no effect upon the axial dispersion coefficient.

Rama *et al.* (1985) also measured D_{zl} in a FBCT using the step response method. They studied the behaviour of Pe_c and D_{zl} for low density particles and a grid with an opening of 70%. At low static bed heights ($V/D_C \leq 1.6$), Pe_c decreases with an increase in liquid velocity but remains independent of gas velocity in line with the observations of Chen and Douglas (1969) and Koval *et al* (1975). At higher static bed heights, ($V/D_C \geq 2.4$), Pe_c decreases with an increase in both gas and liquid velocities. High Pe_c were obtained where aggegation of particles occurred at the wall for low density, non-spherical particles, such as cork particles, in beds of high static bed height. In this instance, a large proportion of the liquid flowed down through the particle-free core giving rise to a small axial liquid phase dispersion coefficient. Rama *et al.* (1985) also found that particle shape affects the dependency of D_{zl} on U_G, i.e., $D_{zl} \propto U_G^{2.26}$ for spherical particles, $D_{zl} \propto U_g^{2.41}$ for irregular particles and $D_{zl} \propto U_G^{2.56}$ for tapered cylindrical particles. However, particle shape does not affect the dependency of D_{zl} on V_l ($=U_L / \epsilon_l$), ie., $D_{zl} \propto V_l^{2.92}$ for spherical and irregular shaped particles. They suggested the following empirical correlation for Pe_c:

$$Pe_c = 10^{4.5}\left[\frac{\phi d_p U_L \rho_L}{\mu_L}\right]^{-0.5}\left[\frac{\phi d_p u_G \rho_G}{\mu_G}\right]^{-0.3}\left[\frac{g[\phi d_p]^3 \rho_P^2}{\mu_L}\right]^{-0.2}\left[\frac{V}{d_p}\right]^{0.8}\left[\frac{d_p}{D_C}\right]^{1.5} \quad (3.2)$$

Equation 3.2 is based only on air-water-particle systems. The equation reasonably predicts the data of Chen and Douglas (1969) at gas velocities far removed from the U_{mf}. Fan *et al.* (1989) attributed this anomaly to the high bed expansion (for V_E/V up to 4) data used to develop the correlation by Rama *et al.* (1985). They pointed out that the values of Pe_c obtained by Koval *et al.* (1975) are significantly lower than those estimated from the equation 3.4. Fan *et al.* (1989) also attributed this behaviour to the small open area of the grid used by Koval *et al.* (1975) because the small area of the grid supports large amounts of liquid and the increased liquid holdup increases axial mixing and therefore reducing the value of Pe_c.

Muruyama and Fan (1989) mentioned that Tabei *et al.* (1988) studied the particle trajectories using cine photography and reported quantitatively an increase of the root mean square of the absolute axial particle velocities as the superficial gas velocity was increased. The behaviour of particle mixing was characterised by the solids axial dispersion coefficient D_{zs}, defined similarly to the fluid axial dispersion coefficient based on the dispersion model except that there was no convective solids transfer in the model when defining D_{zs}. Tabei *et al.* (1988) obtained D_{zs} by analysing the transient distribution of tracer particle concentrations in the bed where a layer of tracer particles was initially placed at the bottom of the bed. D_{zs} was found to increase with increasing U_G, U_L and D_C and was correlated by the following equation:

$$Pe_s \left[= \frac{d_p U_G}{\epsilon_G D_{zs}}\right] = 315\epsilon_p^{1.13}\epsilon_{l,st}^{-0.46}\left[\frac{d_p}{D_C}\right]^{0.7} \quad (3.3)$$

3.6 Heat and Mass Transfer

Studies of mass transfer are limited to gas-liquid interfacial phenomena. This is because FBCT operation usually involves inert plastic particles with no mass transfer through solid-liquid or solid-gas interfaces. In a FBCT, fluidised low density particles create a high specific interfacial area and a rapid renewal for gas-liquid interface through their violent, turbulent motion. Both of these phenomena greatly increase the contacting intimacy between the gas and liquid phases resulting in high volumetric gas-liquid mass transfer coefficient and a high heat transfer rate accompanied by vaporization or condensation of water, and a high particulate collection efficiency. These characteristics are desirable in applying FBCTs for absorbing or scrubbing of gaseous pollutants, cooling and dehumidification towers for saturated gases, and scrubbers to recover small particles, respectively.

The overall mass transfer coefficient and a height of transfer unit (HTU) are the primary parameters used to account for mass transfer performance. However, knowledge of both the gas-side and liquid-side mass transfer resistances and the specific interfacial area are essential to the characterization of mass transfer mechanisms.

Douglas *et al.* (1963) studied the FBCT in absorption of CO_2 and SO_2 from dust-laden gas by alkaline process liquid, and in condensation of steam from steam-air-H_2S mixtures coming out of batch pulp digesters. Mass transfer coefficients two orders of magnitude higher than in packed beds were reported in small diameter and shorter towers than would be possible with conventional packed beds. The reasons for these high transfer coefficients are that due to the vigorous movement of the bed, intimate mixing is initiated between the phases resulting in very high interfacial area. In addition, contacting between gas and liquid phases occurs at the wetted-sphere surfaces and at surfaces of liquid droplets which reside in the

large interstitial space. Thus in the fluidised state, spheres and droplets circulate violently throughout the column causing gas and liquid to take long and tortuous paths before leaving the bed. This combined with the liquid hold-up in the bed spaces causes a substantial increase in residence time. Moreover, the turbulent action of the solid spheres may be useful in breaking the droplets into smaller sizes and thus increase the effective bed interfacial area and subsequent heat and mass transfer coefficients.

W.J.M. Douglas (1964) studied the absorption of NH_3 in Boric acid solution and for dehumidification and cooling of hot air saturated with steam. HTU for NH_3 absorption was 0.5 to 0.33 of the HTU for packed beds resulting in a reduction in tower height. Similarly, low HTU values were obtained for air dehumidification and cooling. For the saturated air and water mixture, a column 254 mm high and 1 m in diameter and a spherical packing of 38 mm in diameter with a density of 537 kg/m^3 were used. The air flow rate ranged from 1.31 to 2.3 m/s and the water flow rate was 0.003-0.0203 m/s. Values for height of transfer unit were in the range of 0.2-0.63 m.

El-Dessouky Hisham (1993) published data on the thermal and hydraulic performance of a deep bed FBCT. Experiments were carried out in a packed column of 200 mm diameter and 2500 mm height. The packing used was spongy rubber spheres 12.7 mm in diameter and with density 375 kg/m^3. The air/water mass flux ratio L/G varied from 0.4 to 2.0 and bed height from 300 to 500 mm. In conclusion, El-Dessouky Hisham reported that the mass transfer coefficient is much higher in the FBCT than in conventional fixed bed towers with higher packing heights and that the tower characteristic strongly depends on the hot water inlet hot water temperature. However, his bed depth studied was very deep resulting in very high air pressure drop levels. In addition, the sphere bulk density was just above the threshold level of 300 kg/m^3 thus fluidisation occured in the flooding mode characterised by high liquid hold up and thus high bed air pressure drop values.

Guerriere *et al.* (1995) studied mass transfer in a turbulent bed contactor by dehumidification of saturated air by absorption using an aqueous solution of calcium chloride. Polypropylene spheres of 20 mm diameter, and sphere density of 315 kg/m^3 were fluidised by air in a column of 290 mm diameter and 1300mm high. They used static bed heights of 75 to 362 mm, liquid mass flux of 2.3 to 15 kg/s m^2 and superficial gas velocities ranging from 1 to 5 m/s. *Ka* based on the expanded bed height was found to; go through a maximum with increasing velocity; increase slightly with liquid flow rate and to decrease slightly with static bed height.

The liquid-side volumetric mass transfer coefficient, based on a unit cross section of the column was measured by Elenkov and Kossev (1970). They used the desorption of oxygen from a supersaturated water stream to air to measure the liquid-side volumetric coefficient in a FBCT with a grid opening of 41.7, 60, or 79%. The experiments used hollow polystyrene spheres 18 mm in diameter and 167 kg/m^3 in density, solid polystyrene spheres 17 mm in diameter and 930 kg/m^3 in density and solid spheres of rosin-paraffin mixture 17 mm in diameter and 1090 in kg/m^3 in density. The volumetric mass transfer coefficient increases with both increasing gas flow rate and increasing static bed height, but decreases as the open area of the supporting grid increases. At higher gas velocities, increasing the liquid rate generally causes an increase in the volumetric mass transfer coefficient, but at lower gas velocities it passes through a maximum in some cases. These authors suggested an empirical correlation.

Kossev and Elenkov (1973) used the evaporation of water to measure the gas-side volumetric mass transfer coefficient based on a unit column cross section. This is obtained using a gas phase concentration difference defined based on the relative mass fraction for absorbing species as the driving force instead of the partial pressure difference. The experiments were conducted under conditions similar to those in their previous study of the liquid-side mass transfer coefficient. The volumetric mass transfer coefficient increases significantly with increasing gas

velocity and increases moderately with increasing liquid velocity and static bed height and with decreasing grid opening. They developed a correlation for to calculate the gas-side volumetric mass transfer coefficient.

Only a handful of researchers have experimented on a fluidised bed cooling tower. Barile and Meyer (1971) first developed the FBCT and adapting it for use as a cooling tower using a cylindrical bed of low density polypropylene spheres in the range of 19 - 38 mm diameter. The bed air pressure drop and the liquid holdup were measured and correlations presented. Using gas flow rates of 0.51 to 5 m/s superficial gas velocity and 0.014 to 0.038 m/s liquid rates, they studied the FBCT flow regime as well as thermal performance and developed models for FBCT thermal performance to predict upper and lower bounds for outlet water temperature at various water/air ratios. Inlet water temperature was 41°C and a wet-bulb inlet air wet-bulb temperature of 21.7°C and dry-bulb of 28.3°C were used. They concluded that cooling performance, as measured by the outlet water temperature, improves as the value of the liquid/gas mass flux ratio *L/G*, is reduced and that a finite length of the actual tower would operate somewhere between the single equilibrium stage model and an infinite stage countercurrent model. They also arrived at the conclusion that hold-up and pressure drop were found to be functions of liquid-particle Reynolds number, Liquid Froude Number, packing depth and particle size and that the fluidised bed cooling tower offered an attractive alternative to conventional towers due to high performance levels and thus less capital investment although at a higher power cost than conventional cooling towers.

Barile, Hertwig and Dengler (1974) continued their work on the FBCT by extending their studies to include tower performance characteristics. Using hollow Polypropelene spheres of 31.75 mm diameter, bulk densities of between 108 to 160 kg/m^3 , water flow rates of between 2.5 to 11.9 kg/s m^2, air flow rates of 1.9 to 9 kg/s m^2, static bed depth of 0, 74.4, 305, 457 mm, inlet water temperature of 41°C and average wet-bulb temperature of 23 to 29°C as well as inlet dry-bulb

temperature of 34.4 to 40.6°C, they obtained an average cooling range of 11 °C. They stated that greater ranges would be obtained using a second stage. Using Merkel's 1925 equation, developed from sound thermodynamic theories, they developed correlations which agreed to the present work as in Chapter IX relating tower characteristic to Re, Fr, and the dimensionless static height to particle diameter ratio viz

$$\frac{KaV}{L} = 0.0819 Re_L^{0.025} Fr_L^{-0.169} \left(\frac{L}{G}\right)^{-0.248} \left[\frac{V}{d_p}\right]^{0.309} \quad (3.4)$$

They also developed a regression equation to predict the tower characteristic directly from dimensioned experimental variables for design purposes thus:

$$\frac{KaV}{L} = 12.39 \left(\frac{L}{G}\right)^{-0.404} (V)^{0.309} (d_p)^{-0.113} (L \times G)^{-0.156} \quad (3.5)$$

A data fit of the form of $C(L/G)^{-0.6}$ was performed and found that exponents of *L/G* differed appreciably but plots showed an apparently close agreement in relative effect of *L/G*. It was found, additionally, that above 305 mm static packing depth ($V/D_C \geq 1.1$), the static bed height had little cooling effect probably due to the unfavourable packing depth to column ratio. Overall transfer coefficients were an order of magnitude higher than those of conventional contactors. Also overall mass transfer coefficients were similar to those of ammonia absorption in magnitude and trend. Dengler (1977), in order to maximise performance studied liquid flow rate, static fill depth, hot water temperature, ambient wet-bulb temperature, and fill characteristics. Using factorial experiments, he studied the variable *L/G* in the range of 0.7 to 2.8, and liquid flow rates ranging from 0.84 kg/ sm^2. A decrease in tower characteristic with increasing *L/G* was observed with this effect being basically the same for both the conventional and fluidised bed cooling towers.

A study of the dependent variable *KaV/L* against the independent variable *L/G* with static fill depth as parameter resulted in "flattening of the tower characteristic curve". Dengler (1977) attributed this to axial mixing of the fill. Liquid rate had

little influence on the tower characteristic for small bed depths and for larger depths tower characteristic dropped drastically with increased liquid mass flux. Increased agitation enhanced axial mixing which reduced the performance of the FBCT. This effect was not observed for shallow depths. Dengler (1977) also observed that increased liquid increased the power ratio for all bed depths since this required larger pumping power at input and that there is larger liquid hold-up, which resulted in increased air pressure drop. Experimental inlet water temperatures of 34.4, 41, 48, 54.4 °C , were investigated. A 3 to 7 % decrease in tower characteristic was experienced per 5.5 K rise in hot water temperature. He attributed this to the effect of increased reject heat due to the larger temperature driving force between inlet water and the ambient air. Cooling effectiveness was independent of hot water temperature due to nearly constant proportionality of range of approach.

Dengler (1977) also studied the static fill depth and showed that it was as an important variable with respect to tower characteristic. Very large fill depths resulted in high pressure drop due to bed weight and increased water hold-up. Tower performance at large fill depths was observed to diminish at hot water temperature of 41°C, but had little significance at larger temperatures of between 48.0 and 54.4 °C.

Seetharamu and Swaroop (1982), using a 250 x 250 x 1200 mm rectangular section column, extended polystyrene spheres of diameter 25.4 mm and density 82.3 kg/m^3 as packing material, 75% free flow area grid, studied the effects of liquid flow rate, gas flow rate, static bed height and ambient conditions on the tower characteristics. Bed pressure drop and dynamic bed height were also under investigation. The pressure drop increased with gas flow rate with static bed height and liquid flow rate as parameters. The pressure drop was observed to be similar in trend and value with the data from conventional towers as reported by Kelly and Swenson (1956). They attributed this to a reduction in sphere bulk density density as compared to the work of Barile *et al.* (1974) and the type of

material used. The reduced pressure drop did not affect the performance of the tower. *KaV/L* increased with increased bed height and with lower *L/G* ratio. They used the well-known cooling tower correlation:

$$\frac{KaV}{L} = C\left(\frac{L}{G}\right)^n \qquad (3.6)$$

to interpret the results. Values of the exponent *n* varied from - 0.3678, - 0.4450, - 0.556 were obtained for static bed heights of 210, 260, 310 mm respectively. The dynamic bed height, an important parameter that fixes the height of the fluidised bed cooling tower was found to increase with an increase in liquid mass flux. This was attributed to the reduction in cross section to air flow. Turbulence and mixing were also found to be vigorous with an increase in liquid mass flux.

In a continuation paper, Seetharamu and Swaroop (1990) studied the effects of size on the performance of a FBCT. Using the previous tower and a larger one with dimensions 1100 mm x 1100 mm x 1200 mm but with percentage grid size open area of 82.5, air and water flow rates of between 1.4 to 1.6 kg/s m^2 and 0.6 to 1.1 kg/s m^2 respectively, they stated that the smaller tower exhibited more uniform fluidisation characteristics than the larger tower. This was, however, slightly obviated by using an induced fan for the larger tower which introduced air into the tower without significant non-uniformity. Cooled water temperature was found to increase with *L/G* ratio as well as the wet-bulb temperature increase for both small and large fluidised bed cooling towers. It was also observed that the steep increases in cold water temperature with *L/G* ratio stabilised to a constant value. The increase in cold water temperature diminished with the increase in static bed height of packing. These phenomena were explained by the driving force theory. The driving force in the cooling tower is the difference between the wet bulb of air and surrounding water film temperature. Theoretically the water from the FBCT can be cooled to the entering air wet bulb temperature. To cool the water to that temperature, practically the tower should have either an infinite bed height of packing or water flow tending to zero. For

both cases performance decreased with *L/G* ratio. As the water falls down on the packing to get cooled, the available thermal potential decreases as water begins to cool stage after stage during its descent. Also an increase in water flow at a particular height will have a slightly higher thermal potential to act as a driving force. This is applicable to both the large and small FBCTs. Cooling Tower effectiveness reduced as *L/G* ratio increased for same theoretical reason as aforementioned.

Seetharamu and Swaroop (1990) also stated that the packing height in fluidised bed cooling tower was several magnitudes lower than that required for splash type film arrangement as reported by Kelly and Swenson (1956). They reported a higher efficiency for film type fill than for splash. However, Seetharamu and Swaroop (1990) observed that for the same heat load the FBCT is smaller than both splash and film types thus reducing the capital investment. Concluding, they stated that FBCTs are capable of handling higher liquid mass flux and have a higher contact efficiency with heat and mass transfer coefficients of several orders higher than conventional fixed bed towers. Thus the FBCT could have less capital investment and same order of operating cost as that of conventional towers. Despite these important investigations, no detailed studies aimed at designing the FBCT exist. Furthermore, Seetharamu and Swaroop (1990) did not follow up the research so as to produce reliable data with an up to date equipment. More recent work by Egbe *et al.* (1999) demonstrated, as part of this thesis, that the thermal performance of a FBCT is dependent upon the particle size. Using particle size that ranged from 20 - 37.5 mm with densities ranging from 69 - 326 kg/m^3, they demonstrated that the height of the hot water spray nozzle influences the thermal performance, and that the volumeric mass transfer coefficient *Ka* as well as the tower characteristic *KaV/L* are in agreement with previous researchers. They employed a more sophisticated and robust equipment and instrumentation than has been previously employed on design and experimental methodology of the FBCT.

CHAPTER IV
EQUIPMENT, INSTRUMENTATION AND EXPERIMENTAL DESIGN

4.1 Equipment

Figures 4.1 to 4.6 in this chapter show the entire test equipment and the instrumentation used in this thesis. Calibration graphs for the water flow meters are also displayed.

Diagrams showing the experimental equipment itself are given in Figures 4.1 and 4.2. The FBCT equipment consisted of a 1500 mm long perspex column, 290 mm internal diameter, equipped with air and water flow systems. Ambient air is supplied by a centrifugal fan blower rated 0.87 m^3/s at 152.4 mm water gauge discharge pressure. The blower is driven by a three-phase 3 kW motor. Air flow rate is measured with an orifice plate of 108 mm orifice diameter in a 150 mm internal diameter duct before entering the plenum section of the column 700 mm long. Water is supplied from a 375 litre tank by a pump discharging a maximum of 8.5 m^3/min at 12 bar gauge discharge pressure. The water is sprayed into the top of the column via a 22 mm diameter copper pipe. The pipe was routed such that it enters the tower through a 25 mm diameter hole at a distance of about 1.35 m from the distributor grid of the 1.5 m working perpex section. The point at which the pipe meets the tower is re-enforced by a 12 mm thick 50 x 50 mm square perspex plate welded to the side of the column. This is done so as to prevent the generation and growth of cracks on the column due to excessive vibration at stress weak points as the water is pumped into the top. The pipe extends horizontally into the column and then vertically through a 90° elbow and located centrally in the tower. A 22 mm diameter copper pipe of a known length carried the spray nozzle head at the required height from the distributor grid. The water is sprayed down onto the packing by three different spray nozzle

arrangements while air/water separation is effected in the column plenum. To prevent water entrainment in this section it was necessary to route the air stream through a 150 mm perspex duct welded inside the horizontal run of the plenum section.

Perspex cylinder 5 mm thick, 700 mm long and 290 mm internal diameter is used as the plenum chamber. At the base of the plenum chamber, a perspex flange with 409 mm outside diameter is fastened to a piece of wood together with a gasket by stainless steel set screws and nuts. A centrally bored hole 25 mm diameter on the flange and gasket facilitated pipe connections to a water return pump. Similar perspex flanges 12 mm thick having outer diameters of 409 mm and centrally bored holes of 290 mm diameter are welded on both ends of all sections and fastened together by stainless steel set screws and nuts so as to keep the entire rig both water and air tight. At the top of the plenum chamber is fastened a 200 mm long and 290 mm diameter straightening section which ensures good air distribution as it enters the working section. A bed of hollow polypropylene spheres is supported in the column by a wire grid plate with mesh dimensions 10 mm x 10 mm. The total grid free open area is 82%.

Room air from the blower enters a rigid duct which reduces to 150 mm diameter. The air flow is controlled by a butterfly valve situated in this duct. A run of flexible 150 mm diameter ducting leads to another rigid duct connecting to the FBCT plenum chamber. Before entering the plenum chamber, the air initially moves horizontally through two ducts turning at each stage through 90° elbows for a distance of about 500 mm and then vertically downwards for 300 mm before entering the air measuring orifice plate connected to the plenum chamber horizontally through a galvanized steel duct 300 mm long and 150 mm internal diameter. The air entering the plenum chamber makes a 90° turn, straightened by a specially designed distributor and flows vertically upwards into the main column and, through the fluidised bed. This air is then discharged at the top through an upper grid having a 70% free open area and then through the zig-zag mist

eliminator or demister. At this point the air is almost saturated with water vapour and is carried into the atmosphere through a specially designed hood at the top of the tower which is connected to a flexible duct 150 mm diameter carrying the saturated air into the main ventilation duct and into the atmosphere. The rate of discharge of air is regulated by a butterfly damper in the main ventilation system. The hood is so designed that a manifold at its lower base acts as a collecting point for condensed vapour. Attached to this manifold, is a flexible plastic tube 10 mm in diameter and 4 m long that carries the collected water back to the tank so as to minimise evaporation and entrainment water losses.

Parts List of Figure 4.1

1. Blower
2. Motor
3. Butterfly damper
4. Wooden support
5. Flexible duct
6. Orifice device
7. Outlet air dry Bulb PRT
8. Outlet wet-bulb PRT
9. Inlet water PRT
10. Zig-zag mist eliminator
11. inlet air dry-bulb PRT
12. Inlet Air Wet-bulb PRT
13. Distributor grid FBCT outlet water PRT together with collector device
14. Air distributor
15. Outlet water PRT for the plenum chamber
17. Acrylic mist eliminator holder
18. Port cover
19. column clamp
20. Instrumentation panel
21. Condensed water collector

24. Orifice clamp
25. 50 mm x 50 mm mild steel square section
26. 50 mm x 100 mm x 1000 mm mild steel channel section
27. 50 mm x 100 mm x 900 mm mild steel channel section
28. Straightening section.
29. Plenum chamber
30. analogue to digital converter

B: Bed distributor grid
C: Thermostat
D: Discharge chute
F. Tower support frame
G: Bourdon gauge
H: Immersion heaters
M: U-Tube differential water manometer
N: Full cone nozzle
P: Differential pressure transducers
R: Return pump and rotameters
S: Polypropylene spheres
T: Tank
W: Water make-up column
CO: Tower working section

Indispensable for uniform fluidisation in a fluidised bed contactor, is a flat or smooth velocity profile over the entire column cross-section. In order to make a 90° turn and maintain a relatively smooth and uniform velocity profile in as short a distance as possible, a specially designed perspex distributor plate was fastened on top of the plenum chamber. The plate was 12 mm thick, 250 mm internal diameter (ID) and 409 mm outside diameter (OD). Equispaced holes, each 10 mm diameter, were drilled at a radial distance of 275 mm ensuring that almost all the sprayed water is returned to the tank. The distributor plate also acts as an air/water separator by providing a partial barrier for water carried over from the plenum by

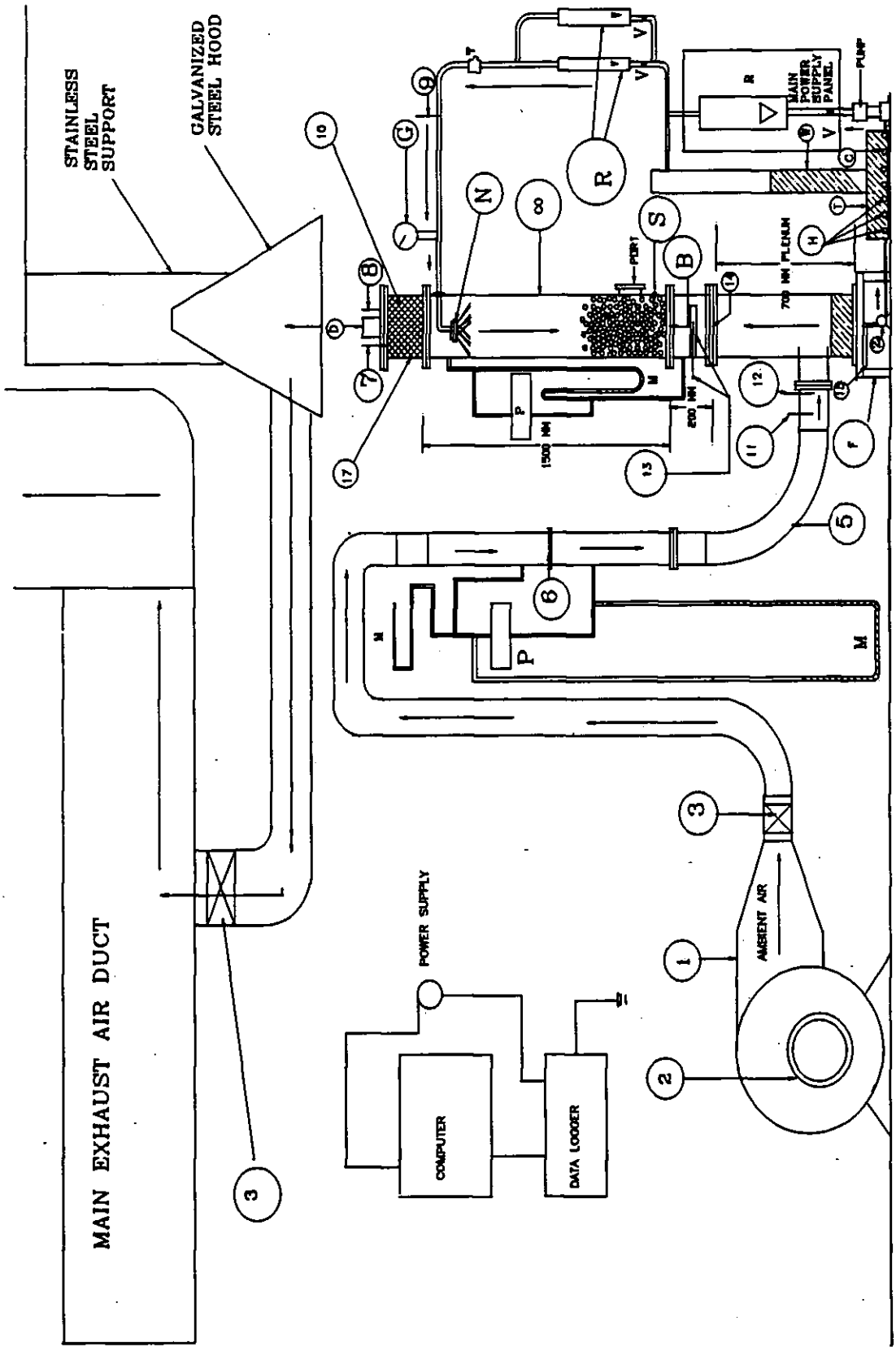

Figure 4.1 A schematic diagram of the prototype fluidised bed cooling tower.

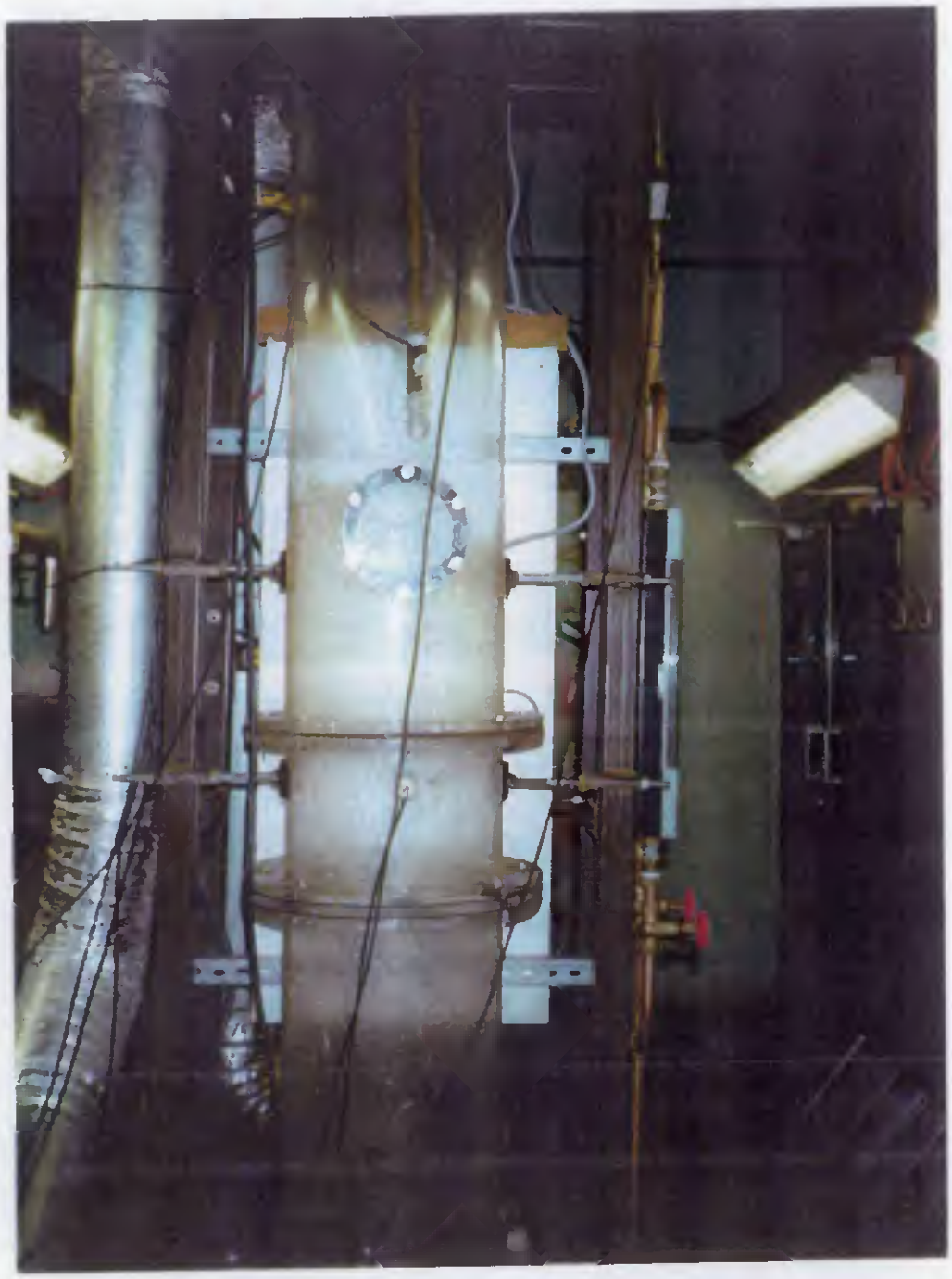

Figure 4.2 A picture of the prototype FBCT in fluidised operation.

by the upward moving air. The orifice on the distributor plate ensures turbulence in the straightening section thus creating a uniform profile in a short distance of 30 mm before reaching the grid distributor and the fluidised bed itself. This straightening section is an empty space consisting of a 200 mm long perspex cylindrical column at the base of the working section. It also allowed the air stream to uniformly fill the cross-section of the main column.

The water system is drawn from the 375 litres tank fitted with 5 water heaters each rated at 4 kW. The water temperature used ranges from 25 to 60°C and can be regulated by a thermostat. All heaters, together with the thermostat, are located at the base of the tank so as to improve temperature distribution. Mains water is used for all experimental runs. The water was recirculated from the bottom of the tower and back into the tank by a 0.75 kW mono-pump. A by-pass line and the return pump ensured that the recirculated water emerges with enough inertia that the contents of the tank are thoroughly mixed and, thus, provide a constant tank water temperature. However, it was often necessary to add cold mains water to maintain a steady tank and hence inlet hot water temperature. The basic method of heat and mass transfer is evaporation which causes loss of water. Make-up water is introduced by a valve that ensured that water levels are maintained. The height of the entire tower is about 3.5 m from ground level and the pressure pings were located approximately 30 mm below the bottom grid and 50 mm below the mist eliminator at the top of the tower.

4.1.1 Frame

The entire equipment is rigidly mounted on a frame which is a welded construction with a channel section at the base welded together to form a rectangle as in Figure C1 in the appendix. On top of the channel section is a welded 50 x 50 mm square mild steel construction about 3 m high. Mild steel clamps are welded to the main frame and are fastened to the working and distributor sections of the prototype tower so as to reduce vibration when the

equipment is in operation. Also mounted on the frame is the orifice device that is force-fitted vertically in place at the top and bottom by two specially designed stainless steel clamps with radial ends.

At the top of the frame, a rectangular device made up of square sections 50 x 50 mm welded construction is vertically force-fitted. At the top end of the device is fastened a trough that acts as a collecting basin for condensed water from the mainifold that results from the discharge of saturated air. This prevents water from interfering with electronic measurements because the rectangular device carried a rectangular wooden plate that holds the electronic instrumentation.

4.2 Air Flow Rate Measurement

The orifice plate pressure drop measuring the air flow rate and the bed air pressure drop were measured by two identical differential electro-pneumatic pressure transducers of type FCO34 from Furness Controls Ltd. These have a range of 0 to 1000 Pa at a signal output of 0 to 5 Volts with a supply voltage of 12 to 30V DC. Both instruments were mounted onto a metal bracket and onto the frame as shown in Figure C1 in the appendix. Both transducers were mounted vertically with the pressure ports facing downwards, at the top of the frame to ensure that the instruments were free from moisture during experimental test runs. They were fastened steadfastly onto the wooden plate by stainless steel winged nuts through two 6.3 mm holes in the bracket which are rigidly attached to the main frame so as to prevent excessive vibration. The pneumatic connectors are 6 mm OD, 4 mm ID and were connected to the pressure sample points by 3 mm ID, 6 mm OD plastic tubings. The hand pushed fit was secure enough to ensure that the whole pneumatic system was leak-free. These transducers were then connected in parallel to a single source power supply through a voltage divider. The input supply alternating voltage for the power source is 230V AC at frequencies of 50 to 60 Hz and a maximum supply output current of 4 mA. After installation, the pressure transducers were checked against standard manually read

U-tube differential water and paraffin manometers. Both tranducers agreed with the manual instruments to within ±0.13%. The differential pressure tranducers were calibrated by Furness Controls and Table C1 in the appendix shows the calibration figures for both transducers.

Instruments were calibrated using industrial transfer standards which are regularly checked against reference standards traceable to British National Standards. For differential pressure measurements, the accuracy is better than 1% in the range of differential pressure of between 10 to 20 kPa. History of traceability to National Standards and list of approved signatories are available from Furness Controls. The maximum working and storage temperatures of the transducers ranges from 10°C to 50°C and -20 to 70°C respectively. Care was taken during test runs so as not to exceed the working limits of both the differential pressure and the temperature specifications. Manual air flow instrumentation were also used in conjunction with the electro-pneumatic air flow sensors so as to improve measurement reliability. Therefore, the air flow rate was also measured by a differential paraffin manometer with the downstream and upstream tappings from the orifice plate meter connected to both the manometer and the differential pressure transducers. The orifice plate static pressure was measured by a differential paraffin manometer connected to the upstream tapping by plastic tubes and separated from the upstream differential connection by a Y-divider. The bed air pressure drop is measured by means of a differential water manometer. The upstream and downstream pressure tappings are all connected to both a differential water manometer and the pressure transducer. Bed air pressure pressure lines were constantly checked to ensure that they were moisture-free. Tappings for the air flow measurement were positioned in accordance to British Standard 1042 (1992). The downstream to upstream tapping distance ratio is 0.51. The upstream tapping distance for the bed air pressure drop measurement is placed at 30±1 mm from the gas distributor grid while the downstream tapping distance was located at 50±1 mm from the mist eliminator. All manual instrumentation for the air flow measurement was mounted onto the frame.

4.3 Water Flow Rate Measurement

Water flow rate was also measured manually and electronically to improve data reliability. The electronic water flow meter shown in Figure 4.1 is the FT2 model 200-030 designed by Titan Enterprises and it has a maximum working pressure of 10 bar water gauge and maximum temperature of 100°C. Flow ranges from 1.5 to 30 l/min at supply voltage of 4.5 to 15 Vdc. Average accuracy of the meter is ±0.25%. Using optical detection, and with the design material being polyphenylsufone, it has excellent chemical and temperature resistance. During operation, a stream of water is directed at a free running turbine in a specially shaped chamber. The rotating turbine blades interrupts a beam of infra-red light from a light emitting diode and converts it to a pulse output. The subsequent pulses of light are converted to a compatible square wave whose frequency output is directly proportional to the flow rate and the total number of pulses is proportional to the total volume of water passed. Greater accuracies were ensured by selecting a flow meter that has flow ranges that are similar to that required for test runs. The flow meter is factory calibrated at 1.01 bar pressure and at an average water temperature of 16.4°C against a volumetric flow rig, which had an uncertainty of 0.05% details of which is shown in Table 4.1. A calibration check on the flowmeter for a range of different waters temperatures similar to that employed for the tests was done by timing into a standard graduated measuring cylinder. As shown in Figure 4.3, the rate of water flow was independent of water temperature for the range of temperatures studied for water flow rates in the experimental test range of between 1 to about 20 l/min. The scatter of the results at water flow rates above 20 l/min may be attributed to instability of the electronic flowmeter at these ranges of operation. Observations indicated that there was a considerable degree of fluctuation of values as flow rates approached 20 l/min as seen in Figure 4.3. Therefore, measurements were in agreement and accurate to within limits of the manufacturers' recommendation in the region of operation of water flow rate of about 0.5 - 20 l/min.

Turbine Flowmeter Type: 200-030 Serial No: 20082			
Flowrate/l/min	Frequency/Hz	Meter K	Water
1.4745	29.266	1190.94	16.48
2.2979	46.014	1201.49	16.49
3.5029	72.759	1246.27	16.49
5.4146	113.922	1262.39	16.41
8.2470	171.954	1251.03	16.42
12.976	278.831	1289.29	16.36
19.422	418.092	1291.63	16.36
30.525	660.153	1297.59	16.17

Table 4.1 Calibration of the turbine optical flow meter (Titan Enterprises, 1997).

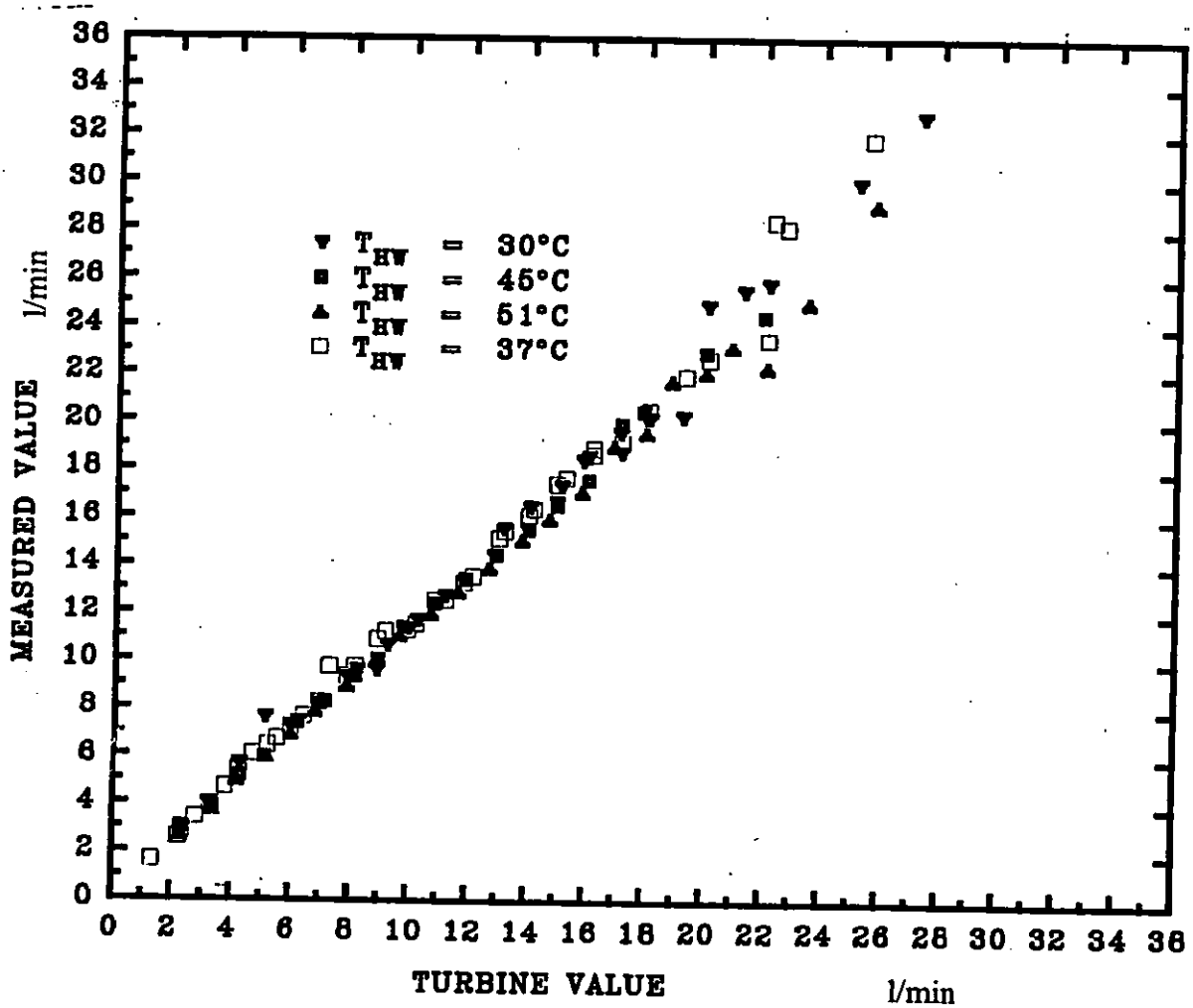

Figure 4.3 A calibration graph for the optical turbine flowmeter

The pulses were converted to voltage by a 0 to 10 V dc signal converter which provides an analogue output proportional to frequency input. A flash LED indicator is functional at both the minimum and the maximum flow rates. The visual measurement of the water flow rate is by three high and low rate rotameters calibrated in the temperature range of 25 to 60°C. The range of flow were 0.2 to 5 l/min, 2 to 20 l/min and 5 to 50 l/min. In all experimental runs, the appropriate rotameter reading was taken.

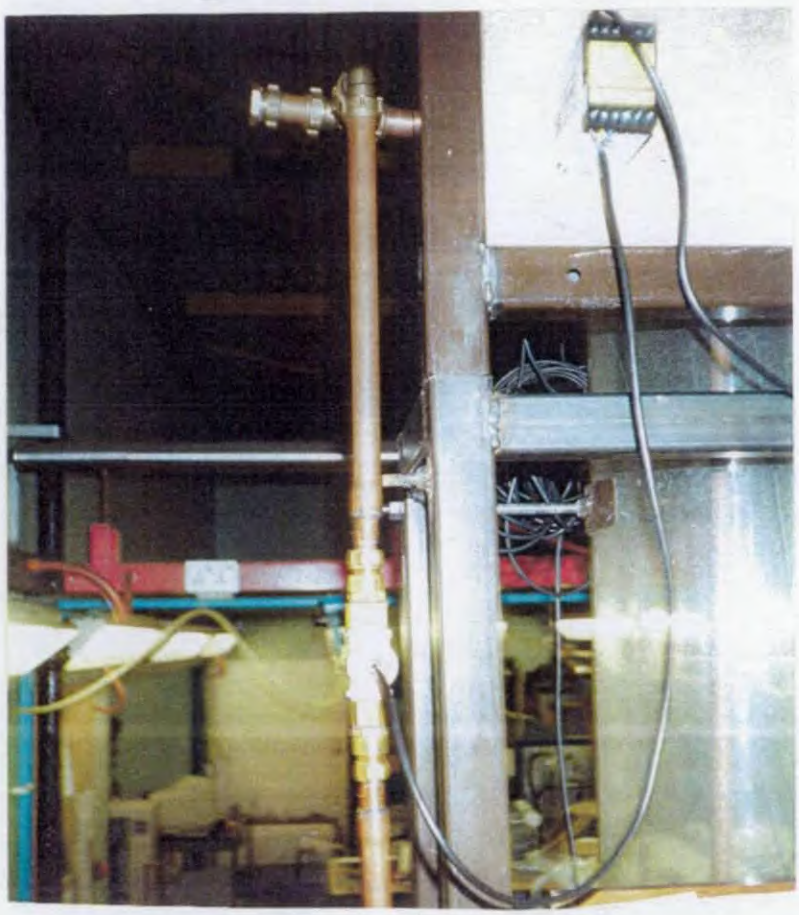

Figure 4.4 The optical flowmeter connected to the analogue to digital converter.

4.4 Temperature Measurement

Nine 100 Ω platinum resistance thermometers (PRT100) and two standard mercury-in-glass thermometers were employed for temperature measurements. The two mercury thermometers together with two PRTs were used to measure the inlet air wet and dry bulb temperatures so as to ensure reliability. Both sets of thermometers were inserted into the galvanized steel duct before the plenum chamber through four 25 mm holes at the surface. Thermometers were kept in place by rubber bungs which ensured that air leakage was minimised. Wet-bulb temperatures were measured by gauze-covered sensors wetted with distilled water from reservoirs attached to both the PRTs and the mercury thermometers.

Measurements recorded for each tests were: ambient dry-bulb temperature, T_{AMD}; ambient wet-bulb temperature, T_{AMW}; inlet air dry-bulb temperature, T_{DB}; inlet air wet-bulb temperature, T_{WB}; outlet air dry-bulb temperature, T_{ODB}; outlet air wet-bulb temperature, T_{OWB} ; inlet hot water temprature, T_{HW} ; cooled water temperature at the grid, T_{GCW}; outlet cooled water temperature, T_{CW}. To ensure accurate measurement of the inlet hot water temperature it was necessary that the inlet hot water PRT was placed about 50 mm from the nozzle spray orifice. The Platinum Resistance Thermometer (PRT) was inserted into a cast iron tee-Junction that connects the inlet water pipe to the spray nozzle. The grid water temperature was measured by a PRT in a specially designed acrylic equipment housing as shown in Figure 4.1. This was a 20 mm internal diameter x 200 mm long perspex tube. The tube was sealed by welding identical 25 mm x 25 mm square and 12 mm thick perspex plates at both ends of the tube. The PRT was horizontally secured inside the tube through an M10 threaded tapping through the surface of the distributor section and through an identical hole tapped through one of the 12 mm thick plates that sealed one end of the tube. Since the sensitive end of all PRTs carried an M10 threaded standard tapping, it was possible to fasten it through the holes. In all cases the taps were made water and air tight by appropriate compounds. The tube was horizontally orientated and placed inside

the distributor section with fifteen holes facing upwards each 8 mm diameter equispaced at 10 mm linear distance serve as openings for the cooled water at the grid. As the water flows downwards, the tube is filled with water covering the entire PRT. Only then was a test measurement taken. All PRTs were calibrated at the ice and boiling points of water against standard mercury-in-glass thermometers.

4.5 Data Acquisition

All measurements, save the orifice plate static pressure were logged into a calibrated 3530A Solartron Orion data logger having a display with front panel controls, a built-in automatic printer and a DC100 cartridge recorder and temperature compensation. The Orion can accommodate 500 channels with the shortest scanning time of 500 readings/second and the longest scanning time of 40 readings/second at an integration time of 80 ms. Operation can be manual or by remote control. Control and programming were manually achieved using front panel keys in conjunction with "prompt" messages, which appeared on the integral display. The soft key below the display facilitated the selection of squence menus.

The built-in magnetic cartridge recorder was used to store and retrieve setting-up routines. The printer with paper-strip printer gave an instant record of logged data and setting-up conditions. Processing and data reduction facilities provided automatic conversion of measurements to temperature, pressure and water flow rate. Engineering units and linear equations for the water flow rate, temperature and pressure were entered into the routine task.

Details of all channels were entered as "Channel definitions". All channels were allocated to logging tasks as "Task definitions". Test results were monitored automatically by an instantaneous display of current readings from any choosen channels and task output. Each input for the turbine flow meter, two differential pressure transducers and the nine PRTs were connected to the measuring circuit

by means of switches on two selector cards as in Table 4.2. One of the cards carried the PRT inputs while another carried inputs for the two differential pressure transducers and the optical turbine flow meter. Nine out of the ten channels available for the 6-pole connections were occupied by the PRTs as shown in Figures C2, C3 and C4 in the appendix.

On the other hand, three out of ten channels available for 6-pole connections were occupied by the two pressure transducers and the optical turbine flowmeter in the second connector. Odd number channels were used in accordance with the manual for 6-pole connections.

The wiring from the instruments were taken to screw terminals located within the plug-in input connectors fitted to each selector. In the case of the PRTs, the connector was not totally enclosed due to the large number, size and length of lead wires. All wires were securely held together by clamps that are incorporated in the connectors. Current energisation for all inputs was provided internally and automatically by the Orion via connector switches and were outputed to the instruments.

Outputs were either digital or analogue. Analogue outputs from all instruments were scaled using manufacturers' data. All the data was then down loaded into a spreadsheet. The results were then analysed for heat and mass balances and hydraulic losses.

4.6 Experimental Technique

Before all experimental runs, the atmospheric pressure was measured by means of a mercury barometer. All air pressure lines for the measurement of the bed air pressure drop, orifice plate static pressure and pressure drop were checked for water. All manometers were levelled with their appropriate fluids. The working section of the prototype FBCT was then filled to a predetermined height with

Platinum Resistance Thermometer card			
Channel No.	Description	Text No.	Position
21	Ambient Dry-bulb Temperature	3	1
23	Ambient Wet-bulb Temperature	4	2
25	Inlet Dry-bulb Temperature	5	3
27	Inlet Wet-bulb Temperature	6	4
29	Outlet-dry bulb Temperature	7	5
31	Outlet-wet bulb Temperature	8	6
33	Exit Water Temperature	9	7
35	Inlet Water Temperature	10	8
37	Grid Water Temperature	11	9
Pressure Transducers and Optical Turbine Flowmeter Card			
41	Bed Pressure Drop (Pa)	2	1
45	Orifice Diff. Pressure (Pa)	1	5
49	Water Flow Rate (l/min)	13	9

Table 4.2 Electronic temperature instrumentation on the data logger.

particles to be studied of known density and diameter. All four reservoirs housing the wet-bulb mercury-in-glass and PRTs were filled with distilled water. The tank was 3/4 filled with mains water so that the heater elements were completely covered with water. This prevents the burn-out of the thermostat. The thermostat was set to a value that is close to the water temperature to be studied for steady state temperature purposes. The mains power supply for the heater and main pump was set to "on". The mains power supply that served the return pump, Orion data logger, pressure transducers, optical turbine flowmeter were then set to "on" and the programme routine that controlled the electronic sensors was loaded by means of the magnetic cartridge and the monitor facility was recalled so as to monitor any choosen channels. After rebooting the Personal Computer, a 3.5" floppy disc was inserted in the A-drive and the programme PCPLUS that captures all the logged data on the display screen was recalled. In order to obtain stability as well as establish an initial check, the Orion was run at ambient conditions after which the ambient air conditions displayed by the computer monitor was compared to the manual readings taken from the mercury in-glass thermometers.

The tank water temperature was constantly monitored by means of a thermocouple connected to an interface that carried a digital display in the control panel. As the temperature of the tank water approached the required inlet hot temperature, the fan power supply was set to "on" and the motor started. The air control damper was then set to a differential pressure that corresponded approximately to the air mass flux. At this stage the Orion monitor was set to display the orifice differential pressure and the inlet hot water temperature channels. This, together with the manual differential paraffin manometer facilitated quick adjustment of the air mass flow rate.

High or low rate rotameter valves were opened depending on the liquid rate required. The valve that controlled the particular rotameter in use was then gradually opened until the desired liquid rate was attained. Since two of the rotameters were in parallel it was necessary to fully close the valve associated

with the rotameter not in use. This improved measurement reliability. Having obtained the correct water flow rate, the air control damper was again adjusted to give the correct orifice pressure drop corresponding to the required air flow rate. The test rig was then allowed to run for about 5 minutes so as to achieve steady state in accordance with BS 4485 Part I (1988). Meanwhile the Orion integral display was continuously monitored. The steady state was reached when the inlet hot water temperature and the orifice pressure drop was constant for a particular test run while the steady state of water was monitored by continual observation of the rotameter in operation. This took between 2 to 10 minutes. Since the entire test equipment was transparent, it was possible to observe sphere and droplet movement in all sections of the test rig.

The specially designed catchment that housed the PRT used to measure the cooled water temperature at the grid was monitored to ensure that the PRT was fully submerged in cooled water. Satisfying this condition, the computer menu for log data was called and a log file was created and opened. As soon as steady state was realised, the expanded bed height was measured by means of a metre rule. All manually and visually read values, including air and water flow rates, spray nozzle type and height, inlet wet and dry-bulb temperatures, column pressure drop and orifice differential and static pressures were recorded and the nature of the turbulence of the fill was noted. At the same time, the Orion was activated to run and the output from all probes were sampled and automatically read and recorded onto a floppy disc. Critical measurements were displayed on the computer screen as experiments and scanning progressed. Twenty scans were recorded at 5 second intervals. Total scanning time for each test run was 100 seconds. The twenty recorded measurements were statistically processed by the automatic in-built processing facility of the Orion so that the mean and standard deviation were displayed on the computer screen. These values formed the basis for validation of test runs. Manual and processed logged data were also compared for discrepancies. Logged data was automatically downloaded into the spredsheet and an energy balance calculation performed. Test runs were repeated if the manual, and

electronic values deviated by more than ±15% while an energy balance error of not more than ±25% was allowed.

Expanded bed height, despite its measurement difficulties, was estimated for each cooling run. The continually fluctuating height for developed fluidisation was visually estimated after observation for about 5 minutes and the maximum value were recorded. Comments on operating regimes, degree of agitation and flow anomalies were reported together with the complete range of regimes from fixed bed to flooding. Response time to step changes in flow was about 5 minutes.

4.7 Measurement Errors and Uncertainty Analysis

Temperature measurement PRTs were calibrated at the ice and boiling points of water and then compared with standard mercury-in-glass thermometers in conformity with BS 4485 Part I (1988) as shown in Table 4.4. Assuming that the standard points are 0°C (273.15 K absolute zero) and 100°C (373.15 K), then the average PRT had a precision of 0.26 K at the ice point and -1.62 K at the boiling point of water. The standard mercury thermometers had an average precision of 0.38 K at the ice point and 0.29 K at the boiling point of water. The average error of the PRT in relation to standard points was -0.43% while an estimated error of 0.09% was estimated for the standard mercury thermometers. An average absolute difference of 0.34% existed between the standard mercury thermometers and the PRTs. Similar errors were obtained with probes with wetted cloth for the wet-bulb temperatures.

Generally, the uncertainty associated with the PRT is estimated to be less than ±0.5°C. Calibration data and manufacturers' specification indicate that, apart from at the lowest and the highest end of the test ranges, the air flow rate and water flow rate measurements are accurate to ±5%.

The ambient air specific humidity was found not to be equal to that of the inlet air. One of the reasons may have been due to the differences in the quality of manufacture of PRTs as seen in Table 4.3. The BS 4485 Part I (1988) for water cooling towers stipulates an inlet air velocity of at least 3 m/s over the wet-bulb thermometers during test runs. While all test runs were close to this value as the moist air passed the inlet wet-bulb PRT and entered the plenum chamber, the same conditions were not likely to be met as the air passed the ambient wet-bulb PRT. This was because, whereas the inlet air wet-bulb thermometers were located inside the 150 mm diameter galvanized steel duct at about 80 mm from the plenum chamber entrance, that measuring the ambient wet-bulb thermometer was located just outside the blower entrance where air velocities were not likely to meet the BS 4485 (1988) requirements. This may have accounted for differences in the air specific humidities. Moreover, there was bound to be recirculated air in the room and this may have had dissimilar effects upon each of ambient and inlet air thermometers as they were at different locations. In addition, as the air travelled turbulently along the air line and into the tower, there is complete mixing between the recirculated air and the fresh room air entering the tower at a uniform temperature. This was not the case for the wet-bulb PRT located in the vicinity of the fan since little mixing of air occurs at this point and, thus, only local air conditions were sampled.

Another point of contention rested on the fact that PRTs were calibrated at the Triple and boiling points of water. The triple point of water is the temperature of water at which ice, water and water vapour are in equilibrium. The pressure of the mixture is assumped to be the vapour pressure of water at 0°C. Now, assuming ideal conditions, the higher the pressure, the lower the temperature. On the other hand, ice point water pressure is basically atmospheric. Calibration of the PRTs used for experimental tests were done at ice point conditions. Thus the ice point conditions were expected to be lower than the standard condition of 0.01°C. This was shown to be the case on two of the PRTs as shown in Table 4.4. However, majority of the PRTs gave higher temperatures than 0.01°C. This may have been

due to lack of lagging of the hypsometer and subsequent gain of heat from the surrounding causing slight rises in PRT temperatures. Moreover, there were possibilities of impurities in the ice.

It was assumed during calibration at the boiling point of water that there was no change in pressure between the atmosphere and pressure conditions in the hysometer. This was also bound to cause discrepancies between PRT values and the expected standard temperaure of 100°C. The use of high and low rate rotameters allowed for greater accuracies at the appropriate water flow rates. Each rotameter has its own hand controlled valve to which was set and watched and reset whenever necessary so that steady flow rates could be attained. Air bubbles in the water pipes caused fluctuations in both the rotameter and the turbine flowmeter. These cause pulsations in flow making manual and electronic logging of the water flow rate difficult. Moreover, changes in the speed of water as it travels through bends, Tee junctions, valves and other fittings introduced errors in the measurement of the water flow rate. In addition, changes in the inlet hot water temperature cause changes in the viscous drag which affects the resistance of the turbine to rotate and, therefore, changes the liquid flow rate. Measurement errors could then be introduced.

Similarly, changes in viscosity affects the rotameter reading. The maximum dynamic viscosity recommended for the turbine flowmeter is 3.5×10^{-3} kg/m s. Water viscosity for typical tests ranged from 4.83×10^{-3} at 60°C to 8.9×10^{-3} kg/m s at 25°C. Although these values are above the recommended maximum, the flowmeter was designed to run at up to 50% overange provided lubrication of turbine blades occurred during operation. Uniform fluidisation gave consistent pressure drop readings on the differential pressure transducers with an accuracy of 1.3 Pa or better. However, there were fluctuations in the bed air pressure drop measurements due to changes in flow patterns of the spheres and droplets during fluidisation. Air velocity measurements were also affected by bends in the airflow lines. Air flow velocities were calculated on the basis of the British Standard 1042

(1992) which stipulated conditions for air line lengths and bends. Not all conditions were fully met. Accuracies of instrumentation are given in Table 4.4.

4.8 Experimental Design

Due to the relatively large number of variables that were studied, there was no single all-encompassing experimental design. However, simple factorial experiments were designed to check interactions between independent variables so as to test theories. The variable based on the liquid/gas mass flux ratio *L/G*

Platinum Resistance Thermometer without Wetted Mesh				
Channel No.	Melting Point (°C)	STDV (°C)	Vapour Point (°C)	STDV (°C)
21	0.76	0.026	99.88	0.007
23	0.11	0.036	99.81	0.003
25	-0.08	0	99.86	0.02
27	0.35	0.036	99.86	0.002
29	0.07	0.026	100.04	0.005
31	0.57	0.026	100.01	0.003
33	0.46	0	100.10	0.009
35	-0.63	0.0266	86.52	0.062
37	0.17	0.0267	99.30	0
Average	0.260	0.023	98.38	0.012

Table 4.3 Calibration of Platinum Resistance Thermometers.

Parameter	Instrument	No. off	Range	Accuracy	Remarks
Temperature (°C)	PRT	9	-100-800°C	±0.2 K	Elect.
Temperature (°C)	Thermometer	2	0-100°C	±0.1 K	Manual
Logger	Orion 3530A	1	-200 to 300°C	<0.2 K	PRT
Logger	Orion 3530A	1	10mV-10V	<±1μV	DCV
Pressure Drop (Pa)	Diff. Pressure Transducer	2	0-1000 Pa	-1.3 Pa	Elect.
Static/Diff. Pressure (mm fluid)	Diff. Fluid Manometer	3	0-100 mm	±1 mm	Manual water/ Paraff.
Length (mm)	Metre Rule	1	0-100mm	±1 mm	Manual
Diameter (mm)	Micrometer	1	0-75mm	±0.10 mm	Manual
Water Flow Rate (l/min)	Optical Turbine Flowmeter	1	1.5-30	0.05%	Elect.
Water Flow Rate (l/min)	Rotameters	3	0.5-5 2-20 5-50	±0.1 ±0.1 ±0.1	Manual

Table 4.4 Accuracy of instruments.

was common in most tests. The variable, liquid mass flux L ranged from 0.3 to about 5 kg/s m^2 and the gas mass flux, G that ranged from about 0.3 to 4.0 kg/sm^2. These two variables defined the liquid mass flux ratio L/G which ranged from 0.1 to about 6. Static bed heights ranged from 0 to 400 mm. Inlet water temperatures ranged from 30 to 60°C. Particle densities ranged from 69 to 326 kg/m^3 while sphere particle diameters ranged from 20 to 37.5 mm (see Figure 4.6). Three different spray nozzle configurations were used. The vital data of two of them is shown in Table 4.5 and and the other, the gravity spray that operates at near atmospheric pressure, is shown in Figure 4.5. Spray nozzle heights ranged from 400 to 1500 mm. The variation of all these parameters were studied to determine the effects of these independent variables on the thermal and hydraulic performance and hence establish design correlations. The important variables were identified and a rough quantitative knowledge of their effect was established. This knowledge was required for design optimization. Insights into the fundamental mechanisms within the FBCT was also possible as a result of the parameter study which consisted of more than 1300 test runs. The development of tower characteristic was fundamentally important in selecting L/G as an independent variable. This parameter is useful for both crossflow and counter-flow configurations although it is strictly applicable to counterflow situations.

Design characteristics	3/4 FF - SS 4.8	3/4 G - SS 3050
Nominal orifice diameter (mm)	NA	4.4
Number of orifices	12	1
Nominal drop size (microns)	700 - 900	1240 - 3160
Spray angle	25°	26 - 31°
Spray coverage diameter (m)	0.6	NA
Spray height (m)	1	NA
Spray cone characteristics	Fine, Full	Coarse, Full
Nozzle static pressure (bar)	1-10	1 - 20
Capacity at design (l/min)	10.9 - 35	11.4 - 51

Table 4.5 Characteristics of the fine and coarse spray nozzles.

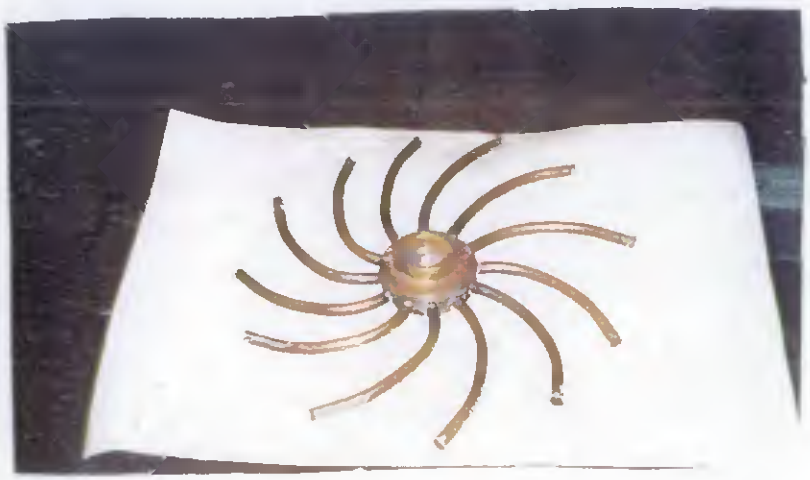

Figure 4.5 A photograph of the gravity or shower spray distributor.

Diameter (mm)	Average weight of sphere (g)	Average Number per m^2	Nominal Number per m^3	Particle Density kg/m^3	Particle Bulk Density kg/m^3	Specific Surface Area m^2/m^3
20	1.0	2900	165000	239	165	207
25.4	2.9	1850	79600	326	231	156
25	2.0	1850	79600	245	159	156
37.5	1.9	800	22600	69	43	100

Table 4.6 Packing Characteristics of the polypropylene particles (Euromatics Ltd.).

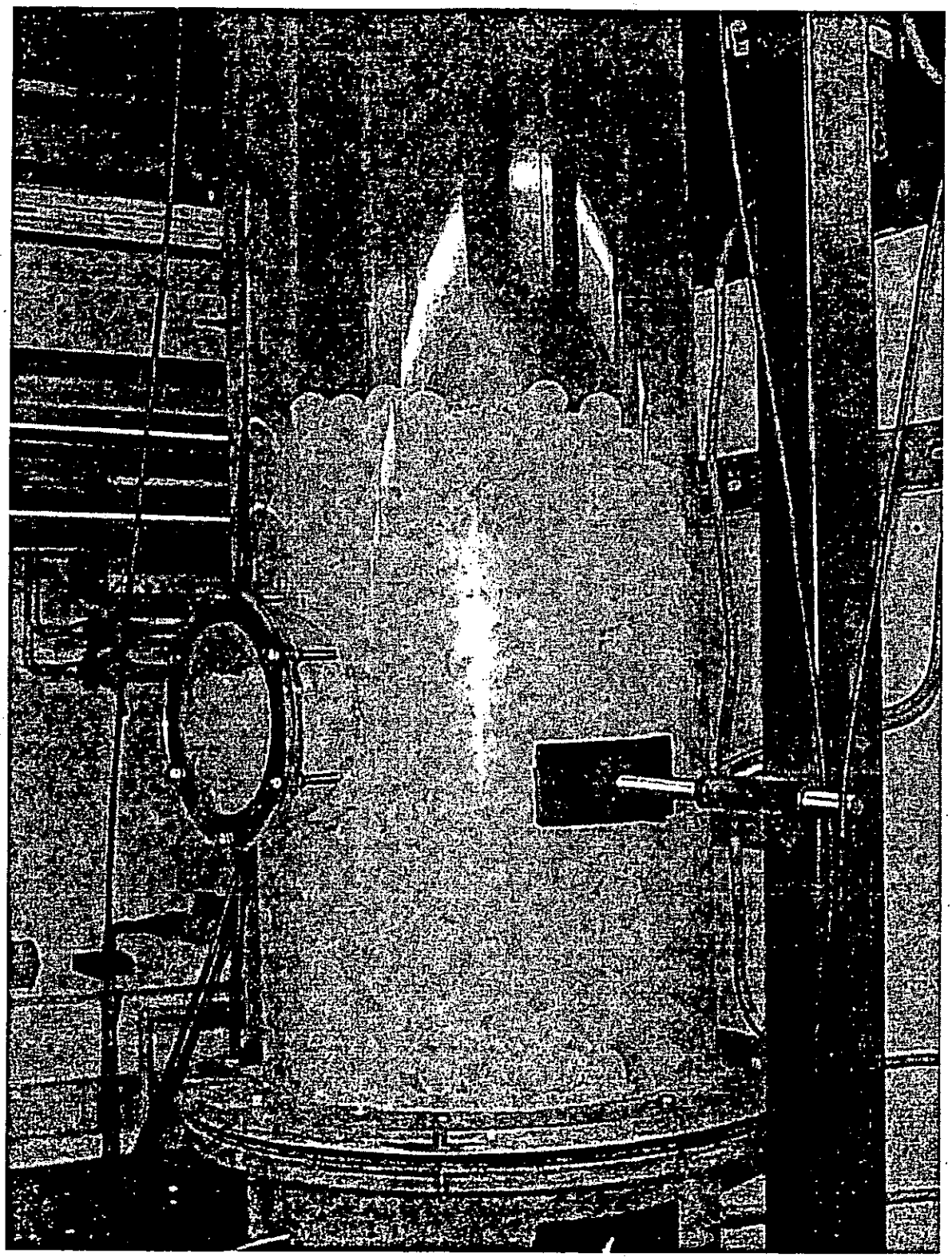

Figure 4.6 25.4 mm spherical packing arrangement.

Factor	No. of Levels	Levels	Units	Notation
Liquid Mass Flux	30	0.5 to 5.0	kg/sm^2	L
Gas Mass Flux	30	0.3 to 4.0	kg/sm^2	G
Particle Diameter	3	20 to 37.5	mm	d_P
Static Packing Height	14	0 to 400	mm	V
Spray Nozzle Height	5	400 to 1500	mm	H
Spray Nozzle Type	3	Coarse, Fine, Gravity		N
Inlet Hot Water Temp	7	30 to 60	°C	T_{HW}
Inlet Wet-bulb Temp	Ambient	11 to 30	°C	T_{WB}
Particle Density	4	69 to 326	kg/m^3	ρ_P
L/G Mass Flux Ratio	-	0.1 to 6	-	L/G
Factorial Combination	1.5876×10^7			

Table 4.7 Experimental Design.

In the experimental design, each of the independent variable was considered a factor as shown in Table 4.7. The response of the dependent variables, *KaV/L*, bed air pressure drop, bed expansion and minimum fluidisation gas velocity to a factor-factor combination with another factor as parameter, was observed and the results recorded.

Although these experiments were designed so that we have a total in the form of factor-level x factor-level x total number of experiments arrangement, performing 1.5876×10^7 x total number of experimental test runs was not possible. Consequently, some factors such as the liquid and gas mass fluxes, *L/G*, *V*, and

d_P were studied much more extensively than others.

An advantage of the factorial experiment was the possibility of allocating different treatments to each independent variable. This is the process of blocking. Randomising the order of experiments and the different effects upon the different thermal-hydraulic independent variables was also carried out. Both randomisation and blocking ensured the validity of the results. Experiments were also replicated to ensure repeatability of results. Repeatability of results ensured validity of experimental data.

All graphical display relating to experimental and analytical findings were made using the Sigma-Plot graphical and statistical application programme package with curve-fitting facilities up to about the seventh order polynomial.

CHAPTER V

EXPERIMENTAL RESULTS: BED AIR PRESSURE DROP

5.1 Introduction

The purpose of this chapter is to present and define the parameters, which were used to measure and analyse the hydraulic performance of a FBCT. The hydrodynamics of the FBCT was established by experiment conducted by the variation of all independent variables. The bed pressure drop was found to be dependent upon independent variables studied. The gas and liquid holdups were dependent upon the static bed height, the liquid and gas flow rates and sphere particle diameter and density. The expanded bed height was dependent upon seven of the eight independent variables studied. The minimum fluidisation gas velocity was found to be dependent upon the liquid flow rate, the size and density of the particles but independent of the static bed height. The gas maximum or flooding velocity was investigated as a dependent variable with the liquid rate as the independent variable. All dependent hydrodynamic variables were compared with the work of other investigators. Flow regimes were also established and a clear understanding of the mechanisms that influence the simultaneous heat and mass transfer phenomenon of the FBCT was attained.

5.2 Effect of the Gas Flow Rate on the Bed Air Pressure Drop

Figures 5.1 and 5.2 show the effects of the air mass flux on the bed air pressure drop for type I FBCT operation. They indicate three hydrodynamic states. In the first state, the bed was stationary with the spheres being very close to each other. The bed height and hence volume remained constant as the air flow rate is

increased keeping the liquid flow rate constant. The first state has a narrow range of operation. The bed air pressure drop increases slowly until the minimum fluidisation velocity is reached. For a particular water flow rate and set of hydrodynamic conditions, the intersticial spaces of the spheres are filled with water. Therefore, as the air mass flow rate is increased, the resistance to air flow as a result of this liquid film increases due to increases in interfacial shear stresses as the bed porosity decreases. This effect becomes much more significant as the gas flow rate increases since this is followed by an increase in the force required to destabilise the bed. Figures 5.1 and 5.2 also show that the bed air pressure drop increases as the water mass flow rate increases and that trends of operation are

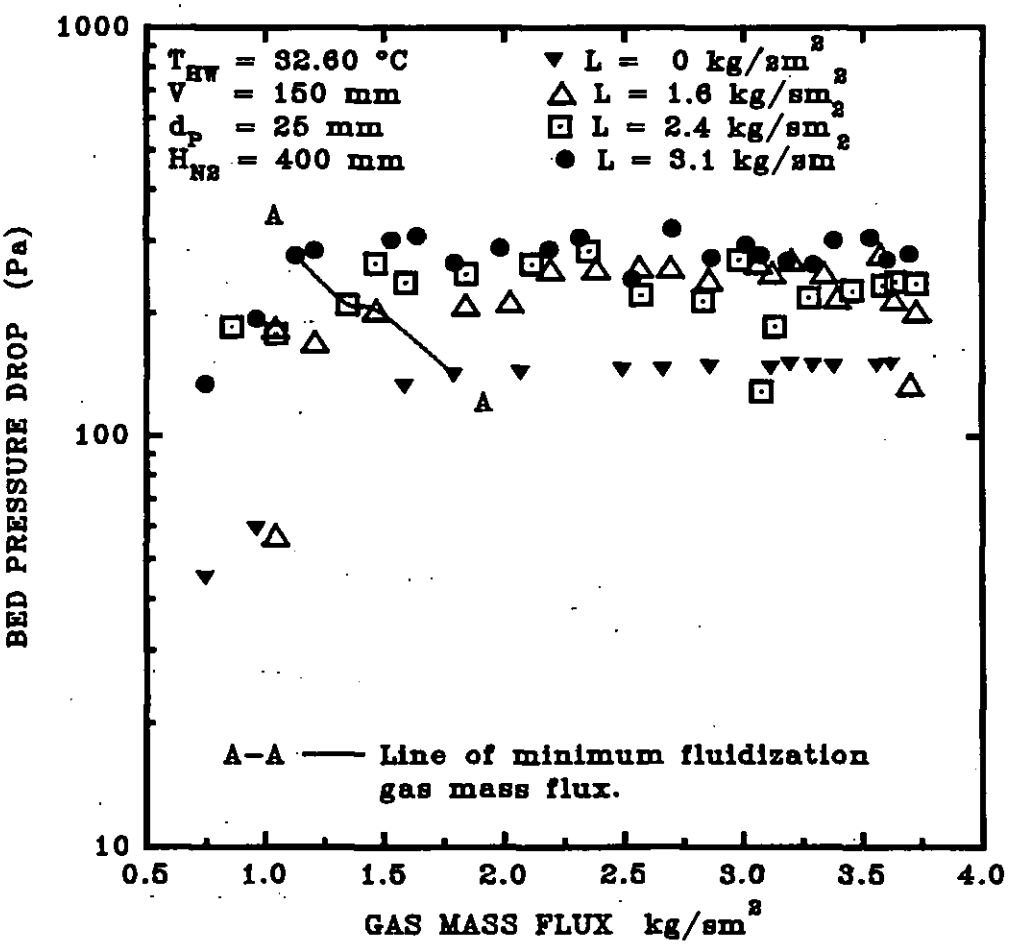

Figure 5.1 Variation of the bed air pressure drop with the gas mass flux. Type I. Shallow bed. ρ_P = 245 kg/m³. Fine droplet spray nozzle type 3/4 FF - SS 4.8.

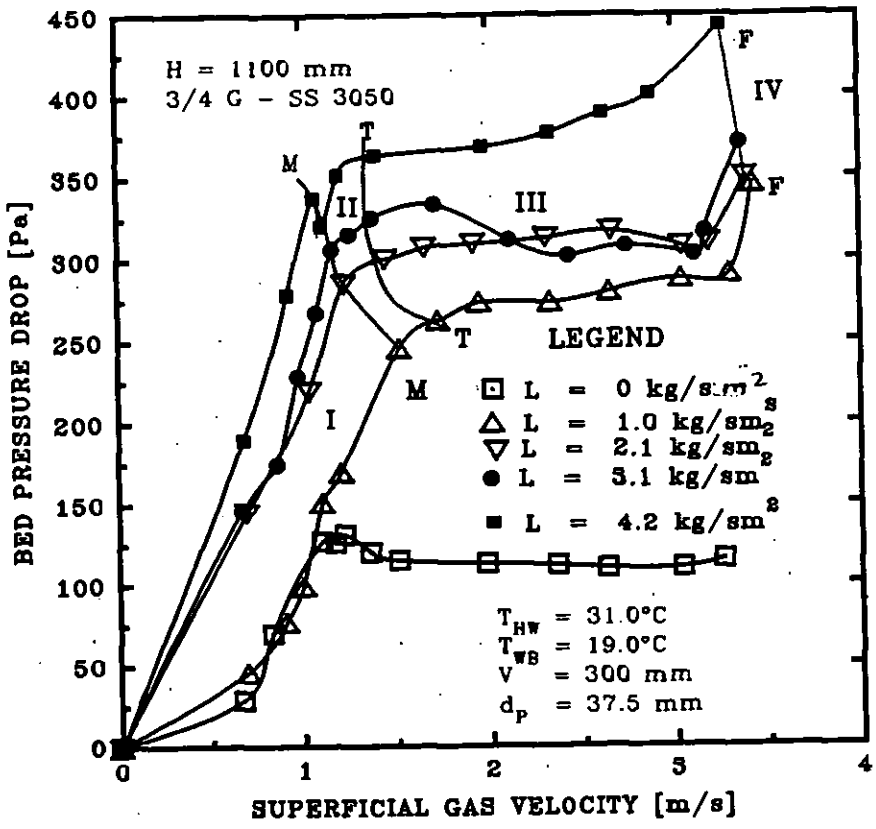

Figure 5.2 Effect of the superficial gas velocity and the liquid mass flux on the bed air pressure drop. Type I. ρ_P = 69 kg/m^3. MM is the line of minimum fluidisation velocity. TT is the transition line. FF is the line of flooding velocity. L = 0 kg/s m^2 indicates a two-phase liquid-gas flow in an empty tower.
------ Transition Lines
—— Pressure Drop

to a dry tower packed with spheres, indicating that the type I FBCT behaves like a two-phase aggregative fluidised bed.

For the type I FBCT, the first state ends when the minimum fluidisation velocity is reached as depicted by the line A-A shown in Figure 5.1. The second state is the state of incipient minimum fluidisation. Just before the minimum fluidisation velocity or gas mass flux is reached, the spheres began to expand in an almost imperceptible manner. This occurred beyond the line A-A and M-M in Figures 5.1 and 5.2. The movement started from the top of the bed with the uppermost spheres agitating without any significant motion. The range of existence of the gas mass flow at this state is dependent upon the density, the liquid mass flow rate,

particle density and diameter. It can be seen that the bed air pressure drop remained constant in the region of minimum fluidisation velocity. As the gas mass velocity is increased, the total number of agitating spheres increased since there is momentum transfer from the air to the spheres through the liquid. The subsequent effect is an increase in the free flowing area of the bed resulting in the decrease in the amount of energy lost by the air as the air flow resistance by the liquid film decreases. However, the entire bed is not fluidised and therefore most of the liquid film flows down through the column wall accounting for the levelling off of the bed air pressure drop as the minimum fluidisation gas velocity is attained. This bed behaviour is in good agreement with the theoretical analysis of type I FBCT by O'Neill *et al.* (1972). They showed that the bed air pressure drop remains constant after the minimum fluidisation velocity is attained because the bed air pressure drop reached the weight of the packing and the liquid holdup in the interstitial spaces of the spheres and that, the liquid holdup remains constant. This characteristic differentiates a three-phase fluidised bed from a conventional packed bed tower.

Further increases of the gas mass flow rate results in the bed attaining developed fluidisation that is characterised by initial fluidisation and visible bed expansion and hence volume but the bed pressure drop remains constant and equal to the bed pressure drop at the stationary and the minimum fluidisation states. As the gas mass flow rate is increased further, fully developed fluidisation is observed in all cases of study. The spheres and the liquid droplets begin to move in all directions in the tower in a vigorous, turbulent and random manner accompanied by fluctuations of the bed height from a minimum to a maximum level. This action causes instability of the liquid and gas phases at the gas liquid interface and the creation of vortices in both the liquid and gas phases. The turbulent and random motion causes the vortices of each of the phases mixing within the interstitial spaces of the bed and, therefore increasing the gas and liquid interstitial velocities. causing the creation of bubbles that move upwards at different velocities resulting in intimate mixing of the fluid streams. In addition, the turbulent action of the bed

increases the kinetic energy of the spheres, the energy being dissipated by transfer of momentum from the spheres to the droplets and particles, causing the droplets to break into smaller sizes. This behaviour increases the gas liquid interfacial activity since interfacial tension increases as a result of increases in shear stress levels in the bed.

Type I FBCT operation has also been investigated by Tichy and Douglas (1972) with similar results. However, differences exist between their investigation and the present work. In their resarch, they had a higher spray nozzle height from the distributor grid. Thus although the dimensions of their equipment were similar to the present design, they observed congregation of the particles on the wall of the column. This phenomenon usually occurs in type I FBCT operations. However, this was not observed in Figures 5.1 and 5.2. The reason for these differences may be that, at relatively low spray nozzle height from the bottom retaining screen, the fluid activity is concentrated in a smaller volume thus causing the bed to be supercharged and therefore the turbulence and hence kinetic energy levels of the bed increases causing the spheres to be knocked off the wall of the column where adhesive force is created between the spheres and the column wall with the liquid film acting as a bridge. Rama *et al.* (1983) also observed congregation of particles at the wall of the tower in type I operations possibly due to the unfavourably long distance of 1200 mm between the spray nozzle and the distributor screen as well as the low density of the particles.

Critical observation of Figures 5.1 and 5.2 reveals that the bed air pressure drop decreases slightly as the gas mass flow rate is increased in contrast to two-phase gas-solid dry bed. One of the reasons for this behaviour may be attributed to the increase in evaporation of the liquid as the gas mass fow rate is increased which decreases the actual amount of liquid that is involved in gas-liquid interfacial activity. Moreover, the amount of liquid entrained into the mist eliminator as drift increases as the gas flow rate increases thus decreasing the amount of liquid held up within the bed. This phenomenon was first observed by Uchida *et al.*(1980).

On the other hand, Soundarajan *et al.* (1994) reported increases in the bed air pressure drop after full fluidisation has been attained in disagreement with the present study. The reason for this ambiguity may lie in differences of opinion in connection with the criteria that distinguish type I from type II FBCT operations. Soundarajan *et al.* (1994) used a free open area of 34.9% in their measurement of the bed air pressure drop with the resultant effect that the amount of liquid retained in the distributor grid increases. The effect of this is to increase the drag force on the gas as it passes through the limited grid opening spaces. On this premise, their conjecture that, increases in the air bed pressure drop as the gas mass mass velocity increases after the minimum fluidisation has been attained may be due to a high liquid mass flux, may prove to be anomalous. Meanwhile, Uchida *et al.* (1980) and Tichy *et al.* (April, 1972) obtained similar results to the present study using free open areas of 72.4 and 78 % respectively and similar liquid mass flux to Soundarajan *et al.* (1994).

Figure 5.3 below displays the effect of the gas mass flux and the inlet hot water temperature on the bed air pressure drop using a coarse droplet spray configuration for a type II FBCT operation. The droplet median volume diameter is relatively larger than that used in Figure 5.1 and 5.2. As before, the regime consists of three states. In the first state of operation, liquid bubbles were seen above the bed before minimum fluidisation velocity was attained. This was one of the criteria for fluidisation with incipient flooding reported by by O'Neill *et al.* (1972) with fluidisation occuring after the flooding point is reached in contrast to type I operation. Observations relating to this operation noted severe congregation of the spheres at the wall in the second state of operation. Slugging and recirculation was also observed at this regime of operation. This anomaly tended to be concentrated at the top of the bed and was probably caused by the relatively low density of the 20 mm particles at the low gas mass flux levels, the relatively large static packing height and by the concentration of the narrow angle full cone coarse droplet spray at the centre of the bed at the relatively high liquid mass flux of 4.1 kg/s m^2. The high momentum of the spray is transferred to the particles

at the centre of the bed causing them to be pushed aside and align at the column wall. This created a free flowing area in the middle of the bed. As full fluidization is attained with increases in the gas mass flux, the bed movement became very turbulent with bed height fluctuations. At this gas mass flux, there was no evidence of congregation of particles at the wall or slugging but a free flowing area continued to exist in the middle of the bed while bed pulsations continued. In the first state of operation, when the bed was static, the bed air pressure drop increases rapidly as the gas mass flux increases before the minimum fluidisation velocity is reached. This behaviour is peculiar to three-phase counter-current FBCT since the bed particle density of 239 kg/m^3 is less than the threshold of 300 kg/m^3 required for type II FBCT operation as stipulated by O'Neill *et al.* (1972). Similar results were obtained by Balebakov *et al.* (July 1969), Gel'perin *et al.* (1972), Levsh *et al.* (1968b), Vunjak-Novakovic *et al.* (1987), Soundarajan *et al.* (1994) as shown in Figure 5.4 which was fundamentally so as to provide a comparison of the present work to those of other investigators. Other variables and operating ranges that are novel to this thesis will be provided in later sections. This is not surprising since their particle density was beyond the threshold value of 300 kg/m^3 in accordance to the theoretical analysis of O'Neill *et al.* (1972). Moreover, they used distributor grids of between 30 and 60%, which is less than the maximum threshhold of 70% free open area required so as to neglect the amount of liquid helup in the grid. However, O'Neill *et al.* (1972) had no experimental evidence to support their hypothesis. Thus, this characteristic may be attributed to the large single cone coarse droplets produced by the single orifice nozzle as well as the distance between the spray nozzle and the distributor grid. The large median volume droplet diameter of 2200 microns quickly fills the particle voids causing the bed flooded with liquid. This is enhanced by the short distance of the nozzle from the distributor grid which in turn causes the bed to become supercharged thus increasing the bed interfacial activity. The narrow angle of the spray also ensures that the wall effect is obviated and, therefore, almost all of the liquid flows through the bed. These factors, together with the fact that the static bed height is deep, increases the liquid residence time in the bed. Thus, as

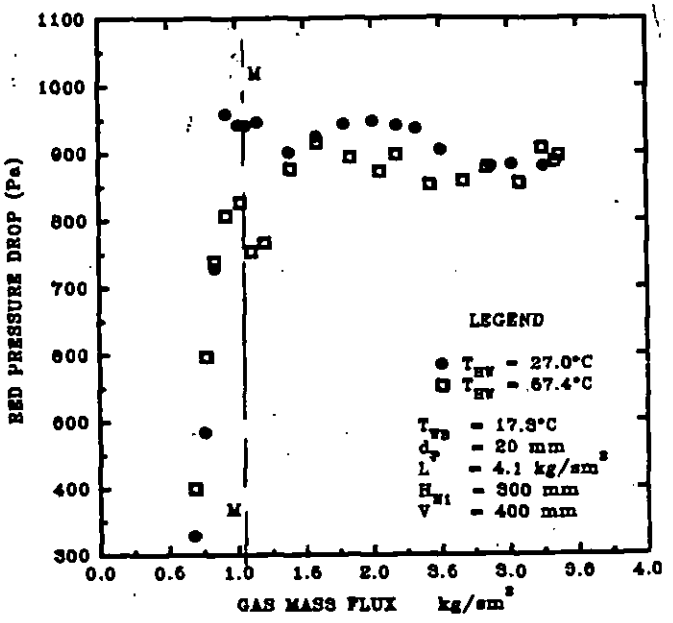

Figure 5.3 Variation of the bed air pressure drop with the gas mass flux and the inlet hot water temperature. Type II. $\rho_P = 239$ kg/m^3 for fine droplet spray nozzle type 3/4 FF - SS 4.8. Deep bed.

is increased further, and approaching the minimum fluidisation velocity, the bed air pressure drop increases much more rapidly as the drag force between the gas and the liquid film increases. The gas then transfers momentum to the liquid thus increasing interfacial shear stress. The resultant effect is bed instability causing the static bed to collapse and expand. Figure 5.3 shows that after the minimum fluidisation velocity, the bed pressure drop decreases steeply partly due to the increase in the free flowing area as the bed expands in line with increases in the gas mass flux, and partly due to the free flowing area in the middle of the bed caused by concentration of bed density. However, the range of gas mass flow in this state is small since the bed air pressure drop quicky increases as the gas mass flow is increased. The reason for this behaviour is that, the bed tries to achieve stability with the liquid redistributing itself within the newly found free space thus filling the voids. The effect is a rapid increase of the bed air pressure drop as the gas mass flux is increased further and bed the expands and achieve equilibrium with the pressure drop remaining relatively constant.

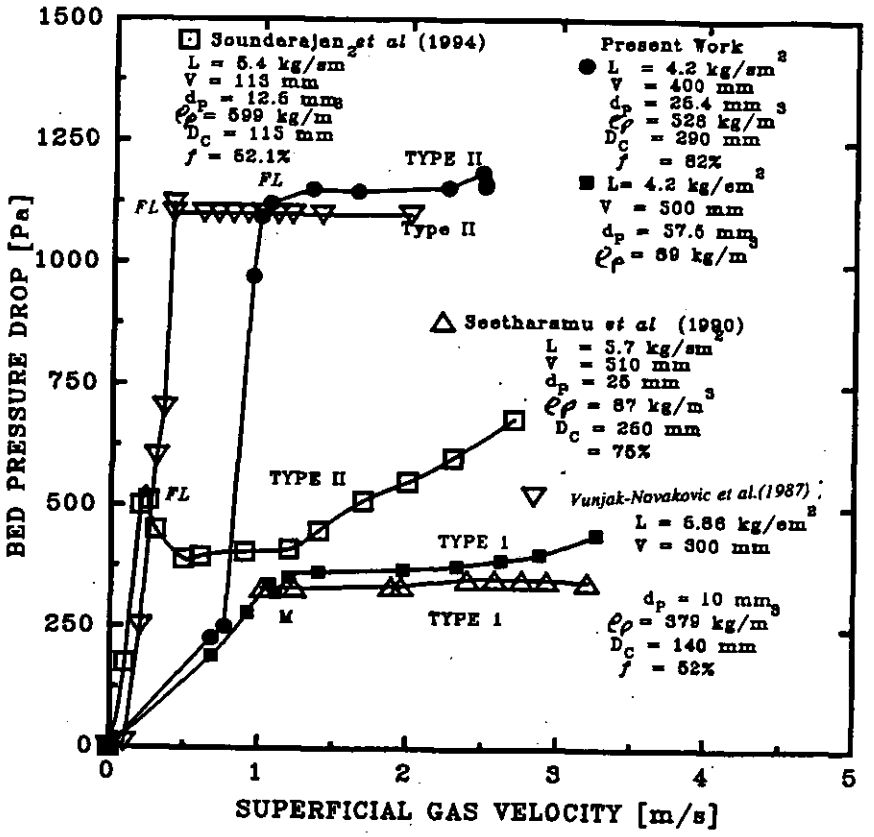

Figure 5.4 Comparison of the present work on bed air pressure drop with those of other investigators for both type I and II FBCT operations.

Similarly, as in type I FBCT operation, there is a slight decrease in the bed air pressure drop as the gas mass flux increases due to increased evaporation and liquid entrainment. However, the effect is much more noticeable in the type II operation. It can also be seen that the bed air pressure drop decreases as the inlet inlet hot water temperature is increased. As the inlet hot water temperature increases, the liquid molecules receive heat energy. The effect is unlockng of the potential energy within intermolecular bonds. The liquid molecules then become mobile with increased kinetic energy. The result is a reduction in liquid density and viscosity. Thus, as the gas mass flux is increased, the drag force between the gas and the liquid film decreases as the inlet hot water temperature increases. This hypothesis also supports the sharper fall in the bed air pressure drop in the transition region at higher inlet hot water temperature. Another possible explanation is that evaporation rate increases as the inlet water hot temperature

increases, the result being less liquid reaching the bed than at a lower inlet hot water temperature. Interestingly, the bed air pressure drop is independent of the inlet hot water temperature in the first state of the FBCT operation. This may be due to negligible effect of the liquid viscosity when the bed voids are completely filled by liquid as the gas mass flux is increased in the stable state. This is a novel and important finding as the FBCT can be operated at lower cost at higher inlet hot water temperature.

Earlier in this section, we have shown that, so far, there is no clear criteria that distinguish "fluidisation without incipient flooding" (type I) and "fluidisation due to incipient flooding" (type II). O'Neill *et al.* (1972), theoretically formulated a method to distinguish the two regimes. However, consideration was given only to the sphere particle diameter, density and the static bed height. The spray nozzle height, spray droplet size and configuration and fundamental parameters such as the inlet hot water temperature were largely ignored in the formulation of their theoretical model. Furthermore, their theoretical analysis had no practical justification. In the development of the maximum permissible density for type II regime of the FBCT, they included the correlation of Chen *et al.* (1968) for the liquid holdup. However, this correlation is in contradiction to their premise that a type II FBCT operation is only possible for particles with a density of about 300 kg/m^3 since Chen and Douglas (1968) experimented with spheres having an average density of 155 kg/m^3. Additionally, two cases of study so far have shown that operations with similar particle densities as seen in Figures 5.1 to 5.4 are capable of producing different results due to the differences in operating and experimental conditions. Figures on detailed hydraulic analysis of type I and II regimes will be given in later chapters of this thesis.

5.3 Effect of the Liquid Mass Flux on The Bed Air Pressure Drop

Figures 5.5 to 5.9 show the effect of the liquid mass flux on the bed air pressure drop for type I operation. Generally, the bed air pressure drop increases almost linealy as the liquid mass flux is increased keeping the gas mass flux constant.

However, the uniformity of fluidisation as the liquid flow rate increases is dependent upon several other factors. Figures 5.5 and 5.6 show the variation of the bed air pressure drop with both the static bed height and the liquid mass flux at constant gas mass flux of about three times the minimum fluidisation gas mass flux using two different nozzle configurations located at different heights from the supporting or distributor grid. It can be seen that the bed air pressure drop increasses gradually and then sharply as the static bed height is increased. In fact, the pressure drop is almost proportional to the static bed height. This is not surprising as the drag force between the upward flowing gas and the liquid film in the bed increases due to increases in the actual liquid holdup in the bed as the static bed height is increased. Visual observation of the bed as displayed in Figures 5.5 and 5.6 indicated that at high static bed height/diameter ratio ($V/D_C \geq 1$, V = 320 mm), fluctuation of the bed height occured but there was no evidence of congregation of spheres at the tower wall. The operation was vigorous and almost counter-current with excellent fluid-particle mixing as the liquid mass flow increased and no slugging was observed. These observations are peculiar to three-phase counter-current fluidised beds with air as the continuous phase as Gelr'perin *et al.* (1966), Tichy *et al.* (1972), Barile *et al.* (1971), Vunjak-Novakovic *et al.* (1987) have all confirmed that a type I FBCT behaves like a conventional aggregative fluidised bed with severe slugging and very large bubbles. Moreover, the theoretical findings of O'Neill *et al.* (1972) prohibit the operation of deep beds with $V/D_C \geq 1$ for this type of operation if the particle diameter is greater than 6.35 mm.

Several reasons may be responsible for this conflict of evidence. In the present study, the spray nozzle height from the supporting grid was smaller than those of previous investigators. With the gas mass flux being about three times that at the minimum fluidisation condition, the bed expands such that for deep beds, the ratio of the spray nozzle height to the expanded bed height is averagely equal to unity at relatively large liquid mass flux levels. Since the spray cone angle is narrow (25°), the droplets make direct contact with the uppermost centrally located

particles. The narrow spray angle also means that only a negligible amount of liquid runs down the side of the column wall. As the spray travels axially through the length of the bed, it also spreads radially within the interstitial spaces within increasing the liquid holdup therefore. The high kinetic energy generated in the bed by this action, together with the high superficial gas mass velocity stimulates high interstitial gas velocity which increases the interstitial gas momentum generating high interfacial tension between the liquid film and the gas. The effect is an increase in the drag force as the liquid mass flux is increased with a resultant loss of energy of the air and bence high bed air pressure drop as well as intense and extremely turbulent motion of the spheres. Uniform countercurrent flow is then attained. At static bed to column diameter ratio less than one, there was intermittent congregation of the particles at the column wall. However, this non-uniformity occured only at low liquid mass flux levels and there was a tendency

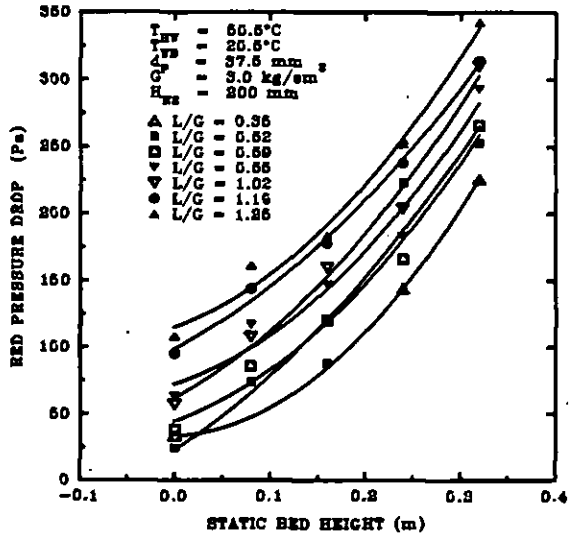

Figure 5.5 Effect of the static bed height and the liquid/gas mass flux ratio upon the bed air pressure drop. ρ_p = 69 kg/m^3 for fine droplet spray nozzle.

for the mono-layer to break on its own at about 5 seconds interval. This behaviour may be attributed to the fact that the ratio of spray nozzle distance above the distributor grid to the static packing height is relatively high (H/V ≥ 3) and, that the bed does not expand enough to make direct contact with the droplets in the immediate vicinity of the nozzle orifice. Moreover, the long tower freeboard

means that the residence time of the droplets in the bed is high increasing the kinetic energy lost by the downward flowing droplets due to deceleration by the air moving upwards at a relatively high velocity.

Furthermore, as the spray diameter increases as the spray nozzle height is increased, so does the ratio of the spray diameter/column diameter (D_S/D_C). Therefore, a portion of the liquid by-passes the bed and runs on the column wall. This action together with the low density of the particles causes the interfacial tension between the liquid film on the surface of the spheres and the column wall to increase. This may have caused the intermittent congregation of particles on the wall at low liquid mass flux levels. The breakup of the mono-layer can be explained by the residence time theory as reported by Rama *et al.* (1983) who carried out theoretical and experimental analysis on the residence time of liquid on the bed of FBCTs with low density particles and found that the average residence time was 2 to 7 seconds in line with the present observation. Thus as the liquid accumulates at the column wall, the total weight of the liquid at the column wall increases with time thus increasing the total weight of the bed. When the total weight of the bed becomes greater than the interfacial force between the liquid film on the particle surface and the column wall, the monolayer collapses downwards and the process is repeated. The wall effect becomes permanent at (V/D_C = 0.6, V = 160 mm). This again is due to the unfavourable H/V ratio causing most of the liquid to run on the column wall and therefore reducing the intimacy of three-phase gas-solid liquid contact in the fluidised bed itself with the result that the degree of turbulence decreases. The effect is a reduction in the amount of liquid retained in the bed leaving a larger free flowing area for the gas to flow and therefore a decrease in the bed air pressure drop. As the static bed height is decreased further (H/V = 10, V = 80 mm), the bed becomes restrained with very low turbulence and mixing. There was no evidence of congregation at the wall in this regime. The shallow bed height means that the actual amount of liquid holdup in the bed is small causing a decrease in the bed air pressure drop.

Figure 5.6 shows the effect of the liquid mass flux on the bed air pressure drop with the static packing depth as parameter for the large sized coarse droplets spray. This result, similar to Figures 5.1 and 5.5 confirms that the bed pressure drop increases almost linearly as the the static bed height and the liquid rate. Interestingly and in contrast to Figure 5.5, fluidisation was uniform. Additionally, the ratio of the spray nozzle height to the static bed height is relatively higher than in Figure 5.6. The cone angle for Figure 5.7 is similar to Figure 5.6. This predictable result may be attributed the large coarse droplets and the single orifice as well as the high gas mass flux. The large droplets generate a high degree of turbulence as a result of their weight and therefore high momentum which enhances mixing and hence uniform flow in comparison with small fine droplets. Figure 5.6, therefore, is in good agreement with the theoretical analysis of O'Neill *et al.* (1972) that uniform fluidisation and hence true counter-current FBCT operation only exist if $V/D_C \leq 1$. Their analysis is fully supported by the experimental findings of Gel'perin *et al.* (1966). Additionally they proposed an empirical rule which stipulates that, true counter-current FBCT flow may only be achieved if the ratio $D_C/d_P \geq 1$ in good agreement with the findings of Figure 5.6.

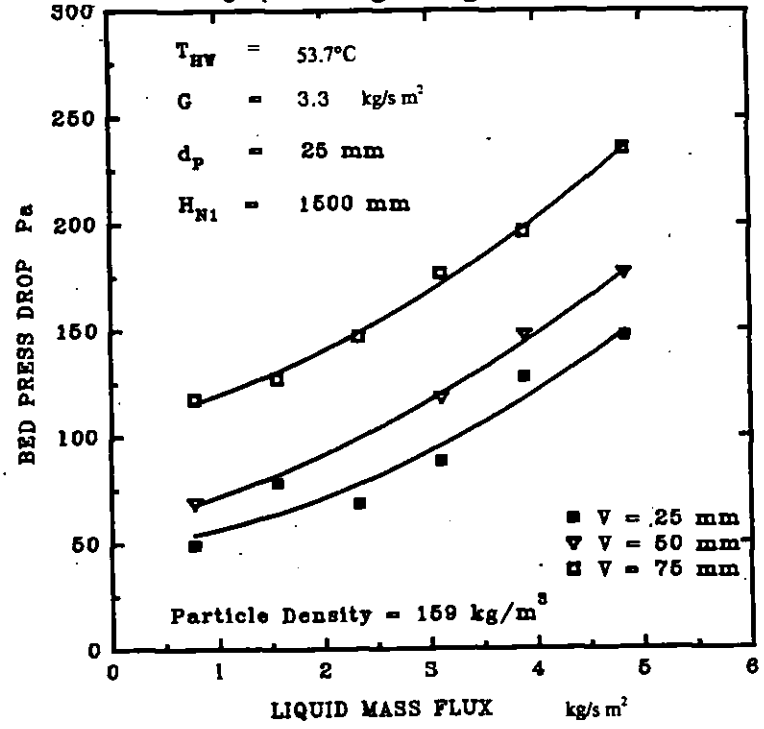

Figure 5.6 Effect of the static bed height and the liquid mass flux on the bed air pressure drop. ρ_P = 245 kg/m³. Coarse droplet spray nozzle.

Figures 5.7 and 5.8 display the effect the liquid mass flux on the bed air pressure drop for low density particles at relatively low gas mas flux levels (about twice the minimum fluidisation gas mass flux) using two different nozzle configurations and relatively large spray nozzle heights of 800 and 1500 mm. The bed air pressure drop generally increases as the static packing height is increased for all liquid mass flux studied. Also, the bed air pressure drop increases with the liquid flow rate with the static packing height as parameter. This experimental result is similar in trend to Figures 5.5 and 5.6. However, there is a clear case of scatter of results in Figures 5.7 and 5.8. In Figure 5.7, congregation of the particles at the column wall was severe for shallow static bed heights of between 80 and 160 mm at the moderate liquid mass flux of about 1 to 3 kg/s m^2. Rama *et al.* (1983) and Egbe (1996b), using particles and fluid mass fluxes with similar characteristics, reported similar observations. Rama *et al.* (1983) reported that the mono-layer could be broken by suddenly increasing the liquid mass flux before restoring operations to the required hydrodynamic conditions. However, this action may have an effect on the bed pressure drop values since different values may be obtained by variably increasing and decreasing liquid mass flux. The most effective method used to obviate the mono-layer condition was by completely cutting off the liquid flow at the particular fluidisation gas mass flux for about two minutes as reported by Egbe (1996b). This action helps to decrease the amount of liquid holdup at the column wall and the bed as well as decreasing the bed wettability. The effect is a reduction in surface tension between the liquid film at the column wall and the particles. Moreover, when the operation is restarted and restored to its original liquid flow rate with the bed in a state of agitation, turbulence continues to exist. At bed heights of 240 and 320 mm, the mono-layer effects becomes less significant. A better turbulence and interfacial activity level was observed due to increased expanded bed height and total weight of the bed especially at high liquid mass flux levels as well as lower H/V values. This hydrodynamic conditions were better and may have accounted for the smoother trend of results at this range of operation of the FBCT. Figure 5.8 shows that better prediction of the bed air pressure drop values could be obtained at a

slightly higher gas mass flux and H/V ratio than is possible in Figure 5.7. This may have been due to the increased turbulence obtained by increased gas mass flux in contact with the larger sized droplets. Thus although there were fluidisation anomalies, uniform counter-current flow continued to dominate.

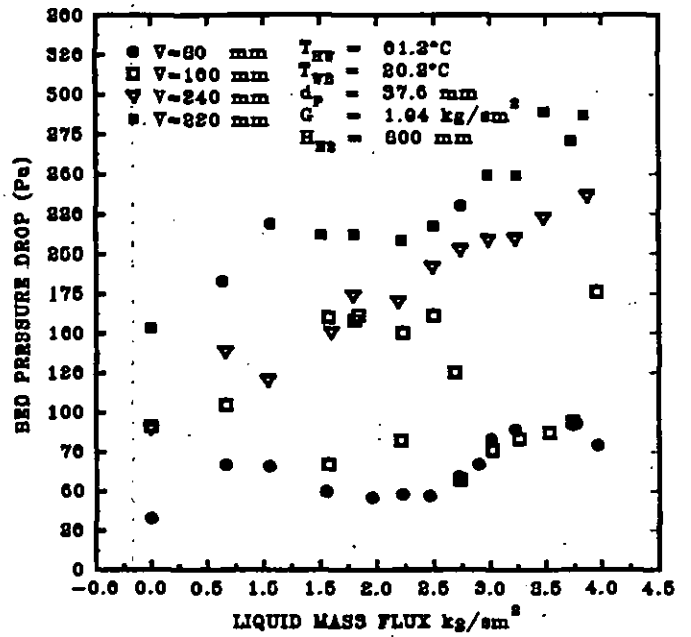

Figure 5.7 Effect of the liquid mass flux on the bed air pressure drop at low gas mass flux. ρ_P = 69 kg/m^3. Fine droplet spray nozzle.

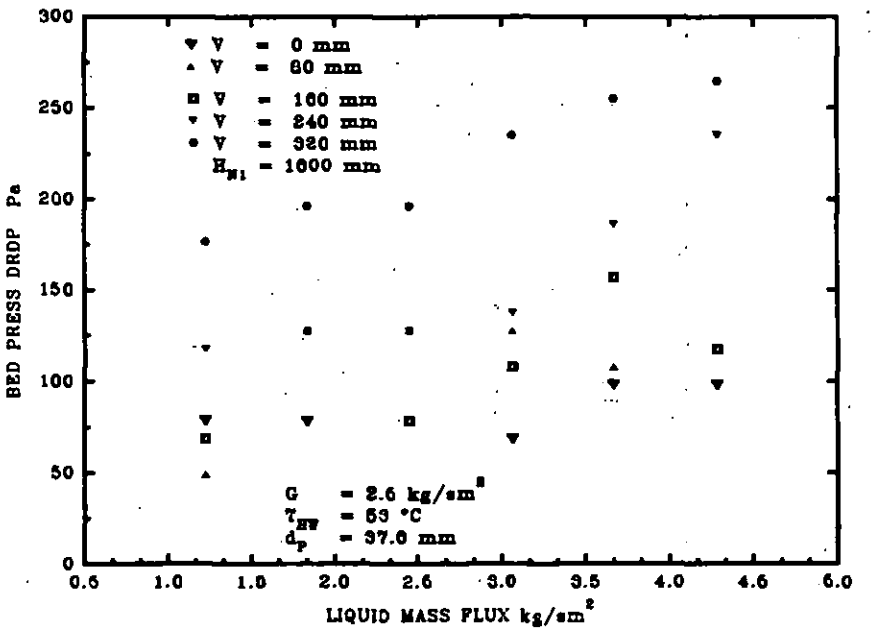

Figure 5.8 Effect of the liquid mass flux upon the bed air pressure drop. ρ_P= 69 kg/m^3. Coarse droplet spray nozzle.

Seetharamu *et al.* (1990) were the first investigators to report the similarity of their results on the FBCT with those of conventional fixed bed cooling towers. However, they did not directly compare their results with those of other investigators. In 1996 Egbe, in his paper for National Power Plc., *"Fluidised Bed Cooling Tower Studies"* also showed that the FBCT is capable of operating at a similar or lower bed pressure drop than conventional fixed bed towers. Figure 5.9 illustrates a comparison between the bed pressure drop values obtained in the present study with the result of Kelly and Swenson (1956) who experimented with a conventional fixed bed wet cooling tower. The approximately proportional increase in the bed air pressure drop with increases in the liquid mass flux for the FBCT is similar in trend to their result. For shallow static bed heights, typical bed air pressure drop levels are similar for both types towers. However, the bed air pressure drop per unit static packing height of tower is extremely higher for the FBCT than for conventional cooling towers. The reason for this difference may due to the larger porosity and hence lower liquid holdup in fixed bed towers than for FBCTs. In addition, the bed air pressure drop increased as the gas mass flux is increased for conventional static bed towers similarly to the initial static state of FBCTs as discussed in section 5.1.

5.4 Effect of the Particle Size and Density

Figures 5.10 and 5.11 show the effect of the density of the particles on the bed pressure drop. It can be seen that the bed air pressure drop increases with increases in the density of the particles at high operating gas mass fluxes as displayed in Figure 5.10 and at minimum fluidisation velocity conditions as in Figure 5.11. It was shown in Figures 5.1 to 5.4 in section 5.1 that, for a set of experimental conditions, the bed air pressure drop remains almost constant as the gas mass flux is increased after minimum fluidisation conditions are reached. Therefore, the close similarity of Figures 5.10 and 5.11 in trends and values confirms our earlier findings. The increase in the bed air pressure drop as the bed particle density increases for similar operating conditions is due to the increased

height of the bed. The increase in bed weight increases the possibility of a transition from "fluidisation without incipent flooding" to "fluidisation with incipient flooding" that is characterised by very high bed air pressure drop values, in line with the theory of O'Neill *et al.* (1972).

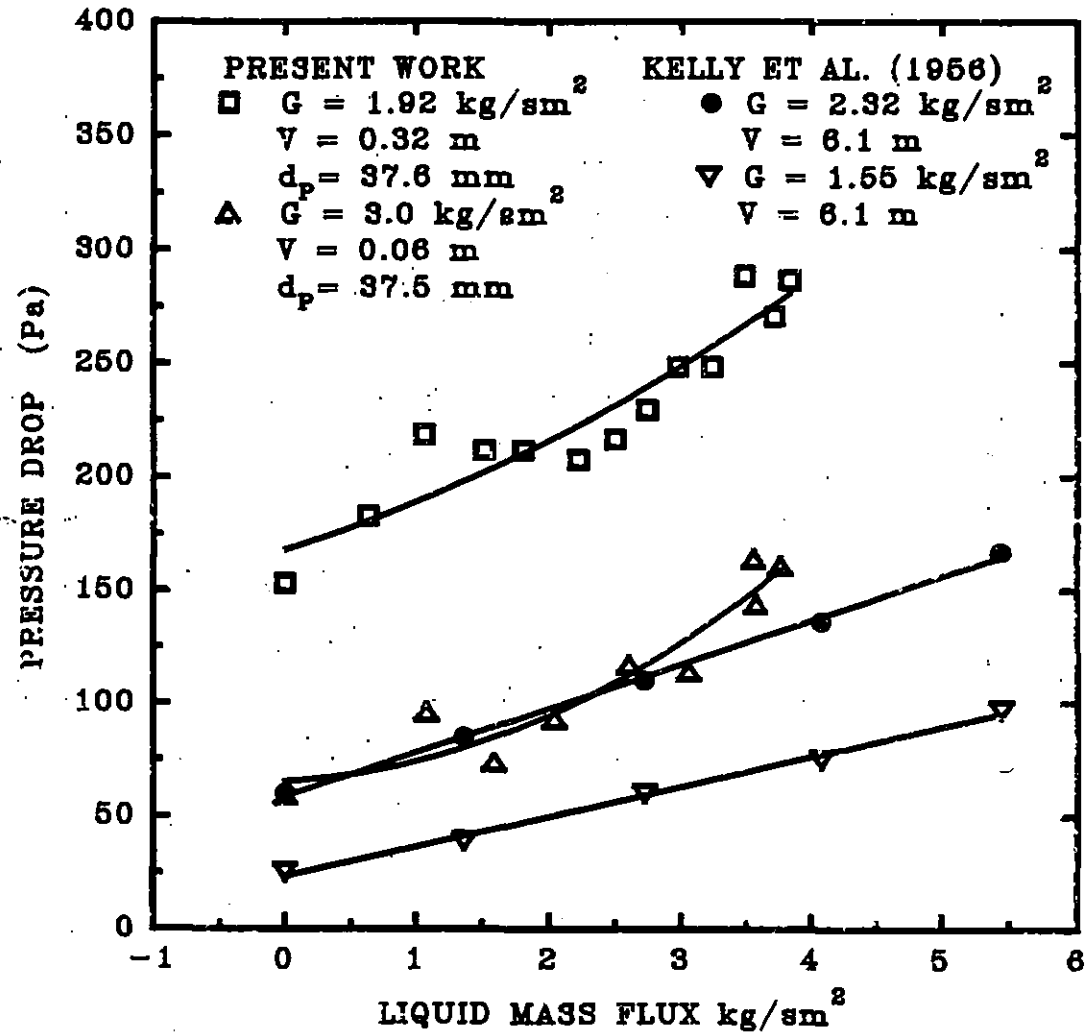

Figure 5.9 Comparison of the present data on the FBCT bed air pressure drop with that of conventional towers.

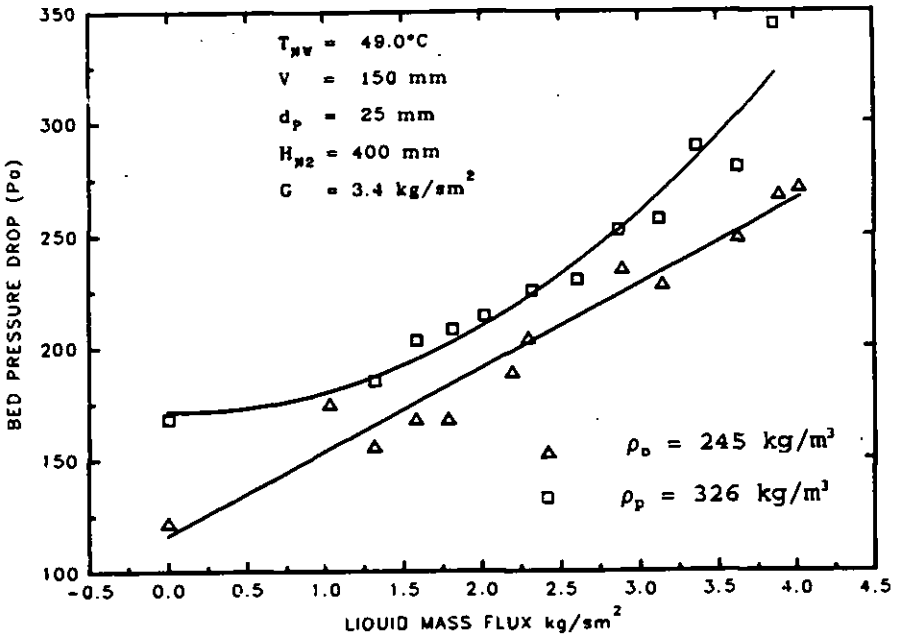

Figure 5.10 Developed fluidisation condition.

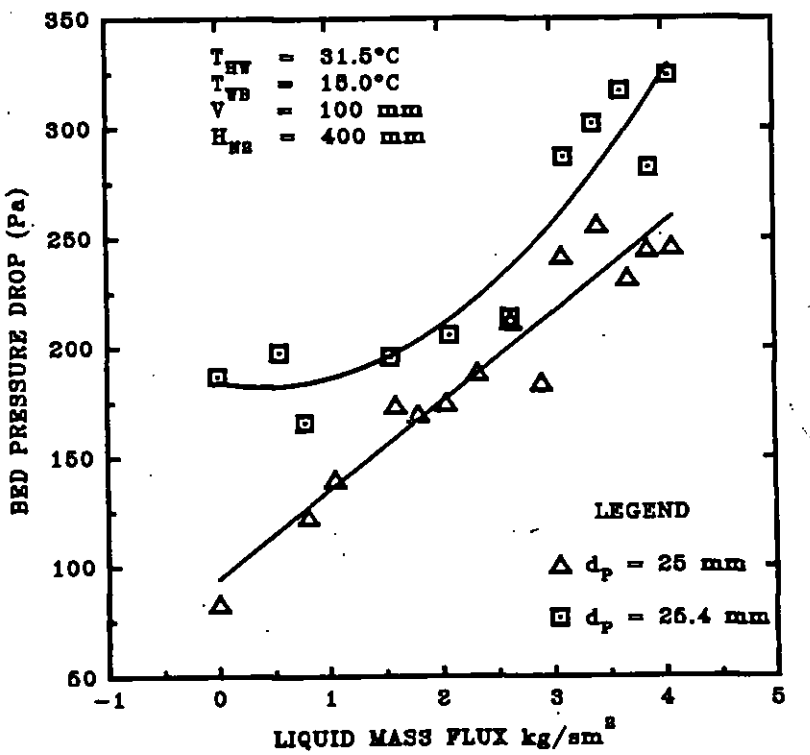

Figure 5.11 Minimum fluidisation condition. Effect of the liquid mass flux and the density of the particles on the bed air pressure drop. d_p = 25 mm, ρ_p = 245 kg/m³. d_p = 25.4 mm, ρ_p = 326 kg/m³. Fine droplet spray nozzle.

The bed particle density is an important parameter in the thermal and hydraulic design of a fluidised bed cooling tower because it strongly influences the cost and interfacial activity of the device. Therefore more detailed studies on the influence of the bed particle density on the bed air pressure drop were caried out.

Figures 5.12 and 5.13 show a comparison of bed air pressure drop data between the 20, 25.4 and 37.5 mm particles keeping the gas mass flux constant for two different nozzle configurations and spray nozzle height to static bed ratios *H/V*. Figure 5.12 shows that for each of the experimental investigation, the bed air pressure drop increases sharply from 0 to 1 kg/s m^2, and then slowly as the liquid flow rate increases followed by an unpredictable fall and scatter of results as the liquid flow rate is increased further, and then a gradual and smooth increase in the bed air pressure drop. This trend of behaviour of the bed may be due to a sharp increase in the bed expansion at relatively large liquid mass flux values. Higher bed expansion means increased free space for air to pass as compared to a smaller increase in the expanded bed height at relatively low liquid mass flux. Moreover, the large H/V ratio means that the falling spray droplets loose kinetic energy by the counteraction effect of the upward flowing air. Since the spray angle is relatively narrow, the high momentum of the spray is concentrated in the middle of the bed creates a hollow free flowing area in the centre of the bed. The effect is a slower increase in the bed pressure drop as the liquid mass flux is increased. As the liquid mass flux is increased further, the free flow area increases and at a particular liquid mass flux range, the rate of bed expansion and the rate of increase of the free flowing area in the bed in relation to increases in the liquid mass flux becomes greater than the rate at which the liquid droplets fill the voids of the bed. The result is a decrease in the residence time of the liquid in the bed hence the loss of energy by the upward flowing air is lower at this range of liquid mass flux. This may have accounted for the sudden break points and scatter in trend for each of the different particles. It is apparent from Figure 5.12 that the point at which this break occurs is dependent upon the diameter of the particles and independent of the density and that there is an optimum particle diameter at

which this phenomenon similarly affects the particles irrespective of the particle density. This is because the break point occurs at a similar range of operation of

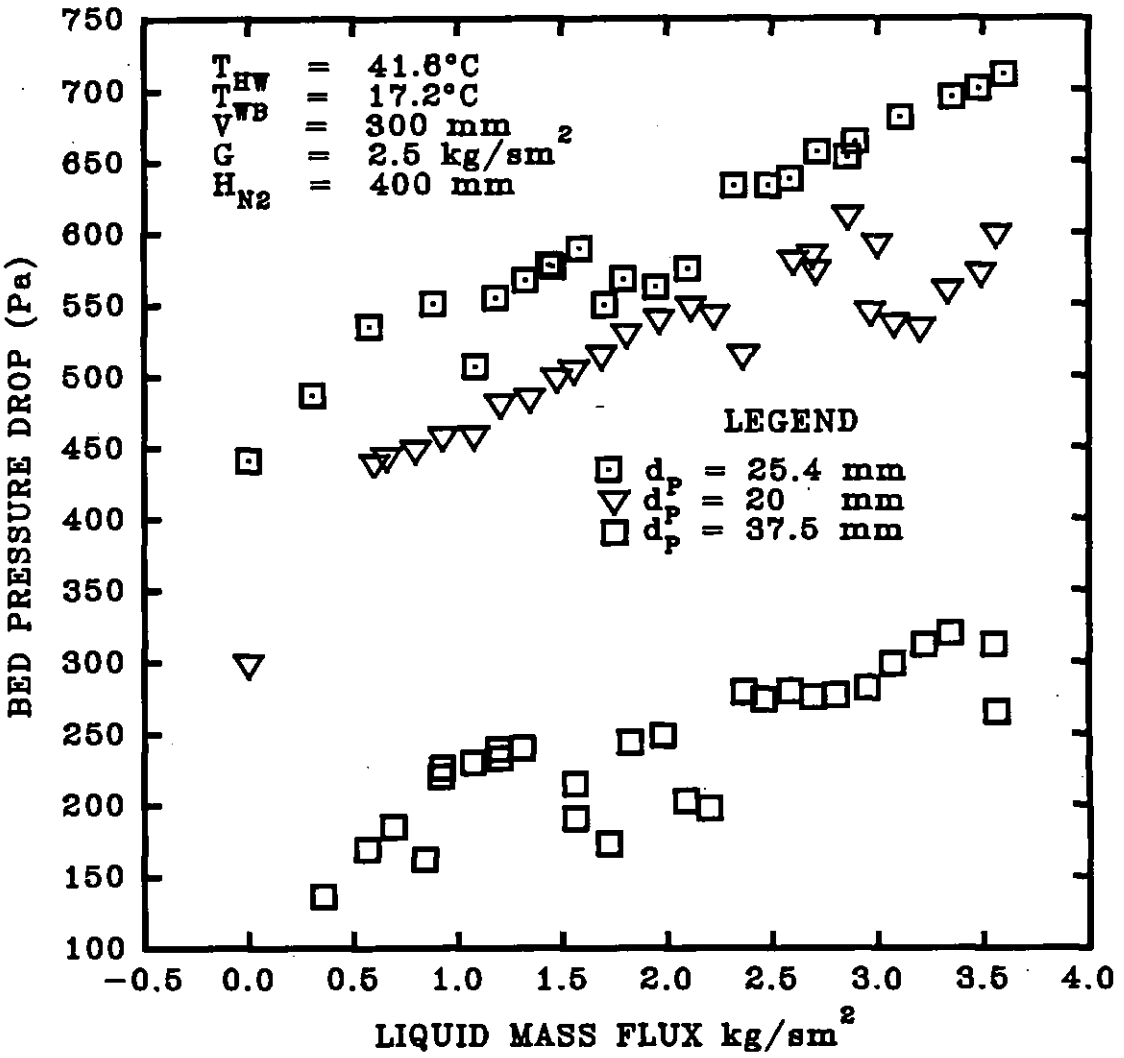

Figure 5.12 Effect of the particle size and the liquid mass flux upon the bed air pressure drop. ρ_P = 326 kg/m^3, d_p = 25.4mm; ρ_P = 239 kg/m^3, d_p = 20 mm; ρ_P = 69 kg/m^3, d_p = 37.5 mm. Fine droplet spray nozzle.

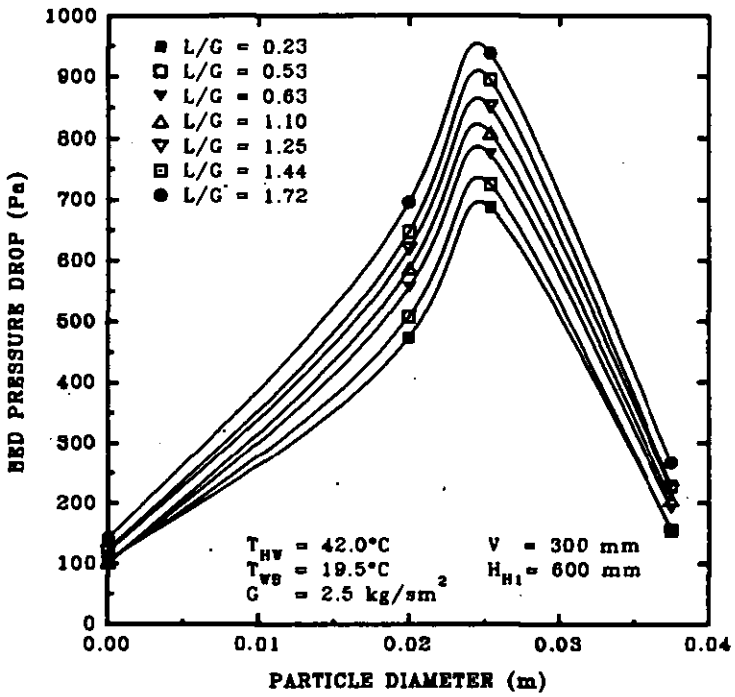

Figure 5.13 Effect of the particle diameter, and the liquid/gas mass flux ratio upon the bed air pressure drop. Fine droplet spray nozzle. Particle characteristics as in Figure 5.12.

between 1.5 to 2 kg/s m^2 liquid mass velocity for the 25.4 mm particle and the 37.5 mm particles while the break point occurs between about 2.3 to 3 kg/s m^2 liquid mass velocity for the 20 mm particle. As the liquid flow rate is increased, the interfacial activity increases as this action stimulates turbulence and randomisation of droplet and particle positions thereby facilitating uniform counter-current gas-liquid-solid fluidisation. At a certain point of operation, the rate at which the bed expands in relation to increases in the liquid mass flux becomes less than that at which the voids of the bed are being filled with the liquid droplets with resultant increases in the residence time of liquid in the bed causing the bed air pressure drop to increase.

Figure 5.12 shows that the loss of air power as it passes through the bed and counter-currently encountering the liquid, is dependent upon both the density and the size of the particles for similar sets of experimental conditions. Figure 5.13

shows the effect of bed particle characteristics on the bed air pressure drop leaving the gas mass flux, the static bed height and the bed particle characteristic at the same level as in Figure 5.12 with *L/G* as parameter and using a different H/V ratio and different nozzle configuration. The results represented in Figure 5.13 confirms the findings in Figure 5.12. Since the particles have different densities and diameters, it is difficult to draw a vivid conclusion as to the reasons for differences in bed air pressure drop values. Thus, a further test was done so as to logically explain responses of the bed pressure drop as the bed particle characteristics are varied. We have explained earlier in section 3.1 (see Figure 5.1) that the pressure drop at minimum fluidisation velocity remains constant as the gas mass flux increases as long as the flooding or maximum gas mass flux is not surpassed.

Figure 5.14 shows the effect of the particle diameter on the bed air pressure drop at the minimum fluidisation velocity for two particles with similar densities that averages 242 kg/m^3. The bed pressure drop increases as the particle diameter decreases. On the other hand, Figures 5.12 and 5.13 indicate that bed air pressure drop levels are higher for the 25.4 mm particles as compared to the 20 mm particles. Therefore, although the bed particle diameter is a factor influencing the bed air pressure drop, the density of the particles has a more dominant influence. Again, this is substantiated in Figure 5.13 where the bed air pressure drop obtained for an empty tower is similar to values obtained with a bed filled with the very low density particles with diameter 37.5 mm. The sharp increase and fall of bed air pressure drop values in Figures 5.13 and 5.14 may therefore be dominantly due to differences in the densities of the particles diameter effecting a smaller change. The increase in the bed air pressure drop due to a decrease in the bed particle diameter for particles with similar densities may be attributed to increases the bed liquid holdup as a result of the smaller static and expanded bed porosity and an increase in solid contact area for the gas. Present studies are in good agreement with the data of Vunjak-Novakovic *et al.* (1987b) who found that the liquid holdup increases as the bed particle diameter decreases. On the other

hand, the findings of Tichy *et al.* (1972) indicate that the bed air pressure drop is independent of the bed particle diameter. This is peculiar to the FBCT because their bed particle diameters were similar to those of Vunjak-Novakovic *et al.* (1987a).

Several reasons may serve to explain these discrepancies. Differences in the densities of the particles may account for these ambiguities because the average density of the particles used by Tichy *et al.* (1972); Vunjak- Novakovic *et al.* (1987a) and the present study was 155, 400, and 239 kg/m^3 respectively. It was previously shown in section 5.1 that there is no clear criteria by which a particular FBCT operation may be described as type I or II. Several factors come to play in determining this particular criterion notably the H/V ratio, the spray nozzle type and the spray water droplet size and that, a bed with particle density considerable less than the threshhold value of about 300 kg/m^3 may operate as a type II FBCT in a similar manner as a bed of particles with a density equal to or greater than the threshold value. This may partly have accounted for the agreement in the findings of the present study and those of Vunjak-Novakovic *et al.* (1987) where FBCT operations were "fluidisation due to incipent flooding" while operations due to Tichy *et al.* (1972) were not due incipient flooding. Another plausible explanation for these discrepancies may be due to differences of the intrumentation used to measure the bed air pressure drop. Tichy *et al.* (1972) used an auxillary vessel to separate the gas from the liquid before passing the gas through a differential pressure transducer for bed air pressure drop measurements. This may have rendered the detection of very small changes in hydrodynamic conditions difficult. Furthermore, Tichy *et al.* (1972) reported the presence of a monolayer of particles at the column wall which may have been very significant as their column diameter was about twice smaller than that used for the present study. This fluidisation anomaly may have counteracted any effect of the bed particle diameter upon the bed air pressure drop. Figure 5.14 is the bed air pressure drop response to changes in the liquid mass flux and the particle size at minimum fluidisation conditions and no mono-layer was observed during these

tests. Similarly, Vunjak-Novakic *et al.* (1987) did not report any fluidisation anomaly in his work.

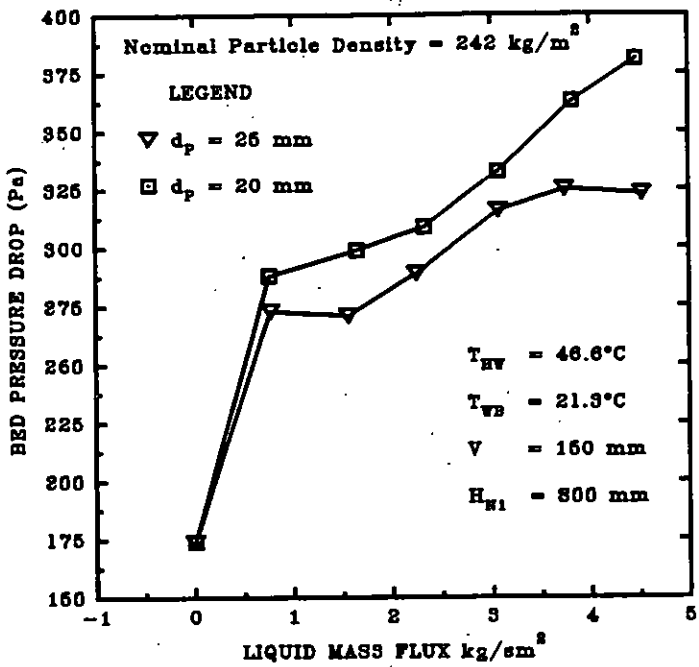

Figure 5.14 Effect of the particle size on the bed air pressure drop at the minimum fluidisation condition. ρ_P = 245 kg/m^3, d_P = 25 mm; ρ_P = 239 kg/m^3, d_p = 20 mm. Coarse spray nozzle.

5.4 Effect of the Spray Nozzle Configuration

It has already been shown in section 5.3 that the spray nozzle configuration and drop size may affect the bed air pressure drop. Figure 5.15 displays the effect of nozzle configuration, the median volume diameter and the liquid mass flux on the bed air pressure drop at a typical cooling tower inlet hot water temperature. For the same bed particle density and diameter, the bed air pressure drop increases as the droplet size increases. It also increases as the liquid mass flux is increased. The reason for the increase in the bed air pressure drop as the droplet diameter increases may partly be attributed to the high density of the particles. With a density of 326 kg/m^3, the bed fluidises after the flooding point is reached, which is the type II regime [O'Neill *et al.*(1972); Vunjak-Novakovic *et al.* (1980)]. This was experimentally substantiated in this work because liquid droplets and bubbles

were observed at the top of the bed before the minimum fluidisation velocity was reached. Moreover, it was shown in Figure 5.3 that type II regime may occur in deep beds having relatively low spray nozzle height/static bed height ratio H/V ie ($V/D_C \geq 1, H/V \leq 2$) although the particle density may not satisfy the theoretical conditions attributable to O'Neill *et al.* (1972).

Large water droplets means that the voids are easily filled with water as the bed expands during developed fluidisation and, therefore, increasing the liquid holdup and hence the drag force of the air passing through the gas liquid interface. The fine smaller droplets also fill the voids of the bed but their smaller size means that more droplets are required as compared to larger ones and, thus the drag force of the air through the bed is lower when smaller droplets are in use. As a large water droplet has a higher weight than a smaller one, droplet entrainment as drift may be less prevalent when large droplets are in use than for smaller ones at the same gas and liquid mass fluxes and similar experimental conditions. Higher water droplet entrainment for the fine spray droplets at high gas mass fluxes decreases the liquid holdup and hence the total weight of the bed with the effect that the bed pressure drop decreases. Large droplets may act as spheres in the fluidised bed in addition to the solid particles especially in the freeboard section. This may have increased the drag force between the air and the droplets thus increasing the bed air pressure drop. Additionally, the evaporation rate of the liquid may be enhanced by smaller droplets for a particlular liquid and gas mass flux and similar hydrodynamic conditions than for large water droplets especially at the relatively high superficial gas velocity of 2.5 m/s which is about more than twice the typical average minimum fluidisation velocity of about 1 m/s. Higher evaporation rate ensures mass transfer from the hot water to the moist air thus reducing the liquid and hence the total bed weight giving rise to a decrease in the bed air presssure drop. The bed air pressure drop response to the different nozzle configuration and spray droplet types as well as the different liquid mass flux levels in Figure 5.15 may not be due to fluidisation inconsistencies because similar fluidisation anomalies of recirculation, slugging and bed fluctuation were observed for both

nozzle types. These anomalies may have been the cause the scatter of results since the congregation of particles at the wall of the column was absent in both cases. The absence of this phenomenon may have been due to the high density of the particles. Higher particle density means that the interfacial tension force between the circumference of the wetted particles and the column wall is effectively counteracted by total weight of the bed and the kinetic energy of the turbulent

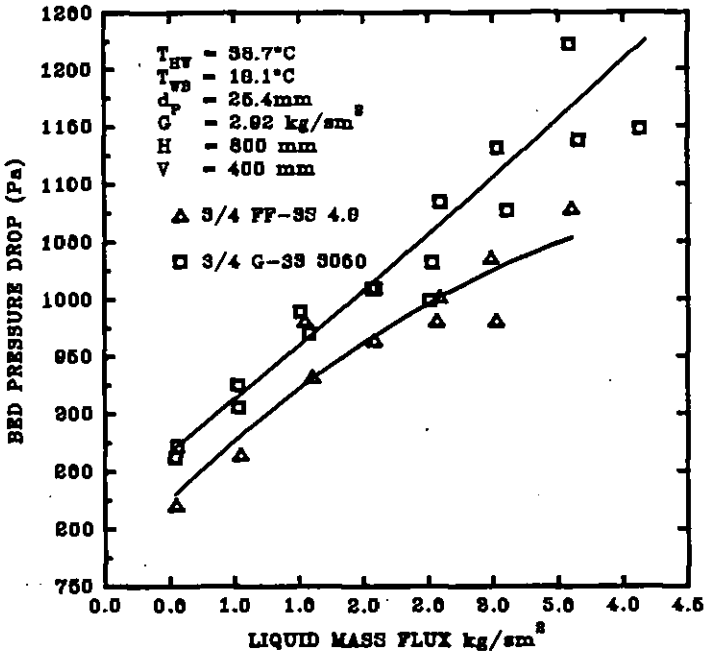

Figure 5.15 Effect of the spray nozzle configuration on the bed air pressure drop. ρ_P = 326 kg/m^3.

spheres and fluids during at developed fluidisation. Visual observation also indicated that bed turbulence levels were very high especially at relatively high liquid mass flux levels. Increased agitation and bed expansion due to increases in the liquid mass flux at a constant gas mass velocity may have created a higher free space for the gas to flow than otherwise would be possible. Thus, athough the amount of liquid in the bed increases as the liquid mass flux is increased, the rate at which water droplets fill the voids of the bed may have been partially counteracted by the rate at which the liquid droplets leave the bed especially with

a supporting grid with a relatively large free flowing area of 82%. This may be the reason for the exponential flattening of the curves at higher liquid mass flux levels. Justification of the above argument may in part be seen in Figure 5.16 which displays a similar result but with slightly different experimental conditions. The ratio of the spray nozzle height from the supporting grid/the static packing height H/V, remains the same as in Figure 5.15, while conditions for uniform and true countercurrent flow of fluids approximates the theoretical conditions of O'Neille *et al.* (1972). The smooth straight lines in Figure 5.16 indicate that the bed air pressure drop is directly proportional to the liquid mass flux and increases as the number of liquid droplets increase. Although Figure 5.16 is similar in trend to Figure 5.15, fundamental differences exist between the two studies. Bed air pressure drop values are reasonably higher in Figure 5.15 than in Figure 5.16. This may have been partly due to the decrease of the static bed height from 400 to 300 mm, and partly due to the decrease in the spray nozzle height from the supporting grid. Another reason for higher bed pressure drop values may be due to a higher superficial gas velocity in Figure 5.15 as compared to Figure 5.17.

Since Figure 5.15 and 5.16 are essentially type II regimes, the latter premise may not apply in this case as we have shown in section 5.1 that, the bed air pressure drop remains basically constant or slightly decreases as the gas mass flux increases for a constant liquid mass flux. However, the lower gas mass velocity in Figure 5.16 may serve to explain the better predictions of the bed air pressure drop in Figure 5.15 with a higher and constant gas mass flux in terms of scatter in trend and flattening of curves at higher liquid mass flux levels. At a relatively lower gas mass flux, turbulence levels were lower in Figure 5.16 than in Figure 5.15. High turbulence levels mean that the cyclical fluctuations in the bed height increases, the result being increased experimental unpredictability and uncertainty. Another explanation that may account for better predictions in Figure 5.16 of the bed air pressure drop values may found in the theory attributable to O'Neille *et al.* (1972) who reported that uniform fluidisation only occurs when $V/D_C \geq 1$, and the empirical suggestion by Gel'perin *et al.* (1966) that $D_C/d_P \geq 10$.

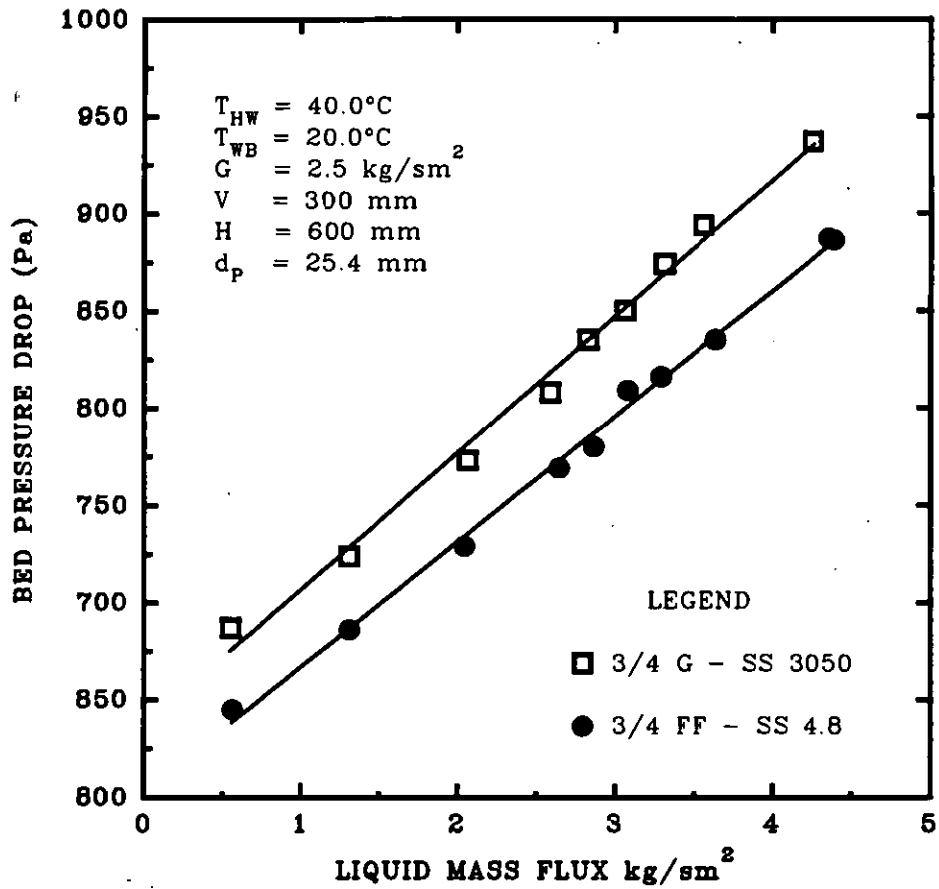

Figure 5.16 Effect of the spray nozzle configuration on the bed air pressure drop. ρ_P = 326 kg/m^3

Visual observation relating to Figure 5.16 indicates that uniform fluidisation occurs at relatively high liquid mass flux levels in the range of about 3 to 4.5 kg/s m^2 when large coarse droplets are in use. However, only slight slugging was observed at a liquid mass flux less than 3 kg/s m^2. The near absence of fluidisation inconsistencies may be due to the the shorter bed height of 300 mm as compared to the deep bed as in Figure 5.15. However, the degree of turbulence observed was less for shallow than for deep bed heights. This may have been due to the lower gas mass flux of 2.5 kg/s m^2 as compared to about 3 kg/s m^2 gas mass flux in Figure 5.15. Similar tests as in Figures 5.15 and 5.16 were done in Fig 5.17. In order to obtain the response of the bed air pressure drop with respect

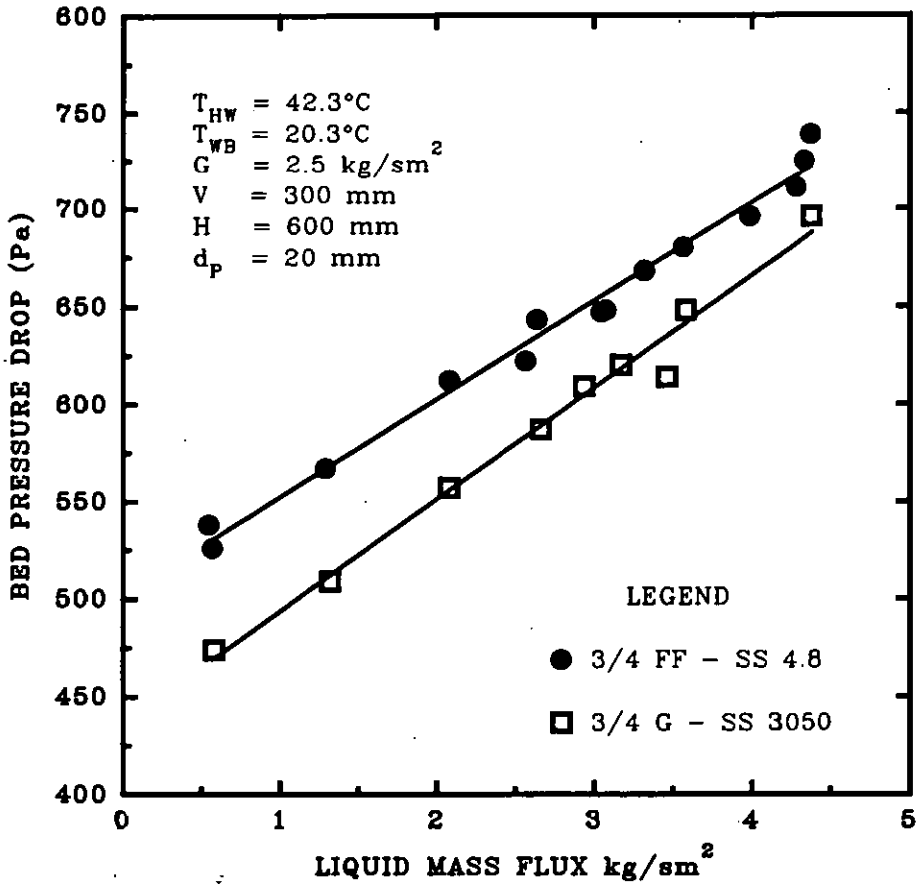

Figure 5.17 Effect of the nozzle configuration on the bed air pressure drop. ρ_P = 239 kg/m^3

to the spray droplet type for the relatively lower particle density. Figures 5.17 to 5.19 below confirms that the bed air pressure drop is almost directly proportional to the liquid mass flux keeping the gas mass flux constant and in line with Figures 5.15 and 5.16. However, the bed air pressure drop decreases as the droplet diameter increases in complete contrast to Figures 5.15 and 5.16. The reason for the differences in response may be due to differences in particle densities. In Figure 5.17, the droplets are concentrated in the centre of the bed without any significant spread to other sections. The low particle density means that the expanded bed height is sensitive to changes in fluid flow levels. Increased bed

expansion is followed by increases in air free flow area within the fluidised bed causing the residence time of liquid inthe bed to decrease. Due to the poor liquid

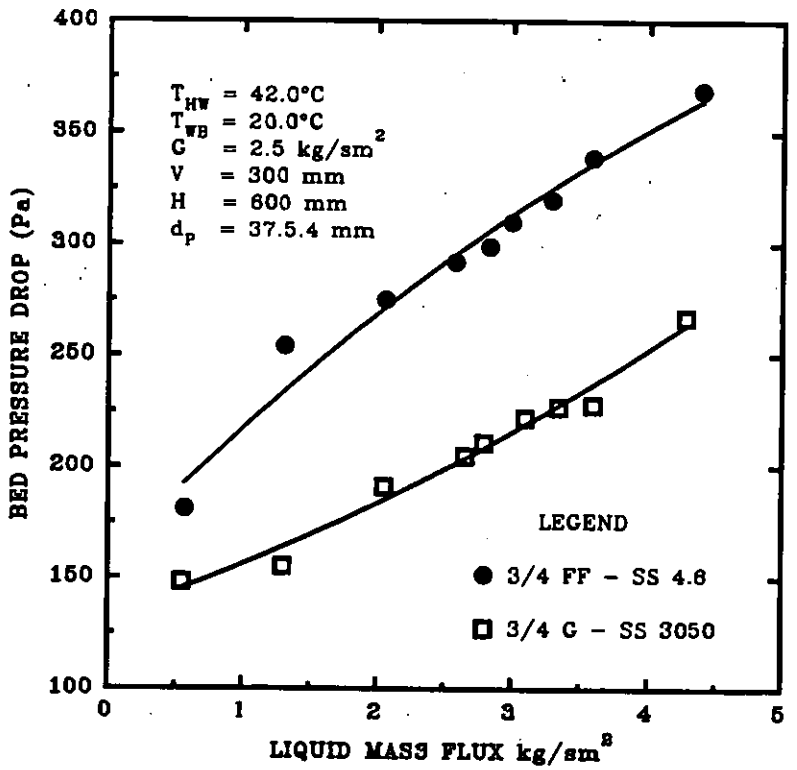

Figure 5.18 Effect of the nozzle configuration upon the bed air pressure drop. ρ_p = 69 kg/m^3.

distribution in the bed, air passes through the partially wet bed at a decreased drag force and hence decreased bed air pressure drop. As the liquid mass flux is increased further, the liquid holdup increases because of increased bed mixing and hence increased residence time but the particles at the centre of the bed are pushed towards the column wall thus creating a hollow free flowing area at the centre of the bed effecting is a reduction in the liquid residence time and a reduced drag force between the liquid film and the upward flowing gas, causing the bed air pressure drop to decrease. This phenomenon is apparent only for particles with relatively low densities and when large spray droplets are used for fluidisation but it was found to be absent when small droplet spray was in use. This may have been due to the fact that the small fine spray nozzle produced many more droplets

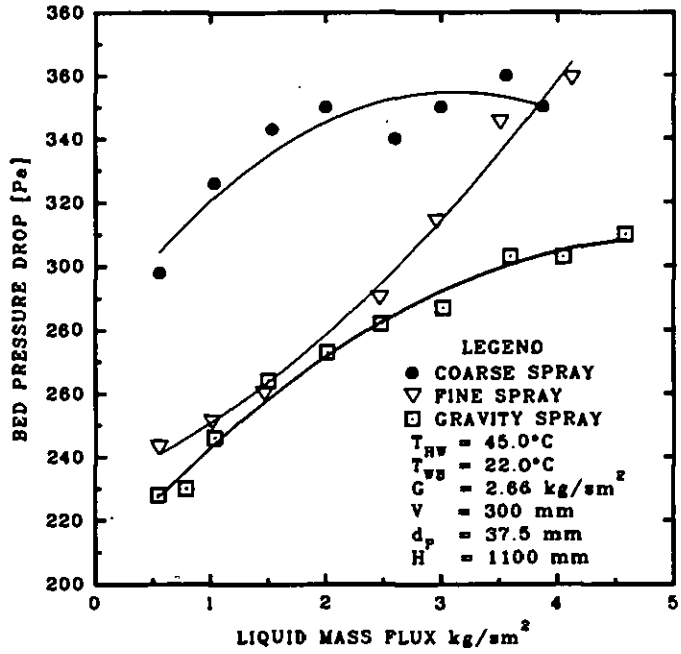

Figure 5.19 Effect of the nozzle configuration on the bed air pressure drop for all three spray types. ρ_P = 69 kg/m^3

for a particular liquid mass flux at similar hydrodynamic and experimental conditions than the large coarse spray nozzle. The result is that the wettability of the bed particles is better and the entire droplet penetration into the entire bed section is enhanced thus inducing a better liquid distribution and holdup than when large coarse spray is in use. Although both spray nozzles have similar cone characteristics, the design configuration to produce small sprays was induced by twelve similar equispaced orifices resulting in a better radial, axial and uniform distribution of droplets at the top and within the bed. This may have accounted for the absence of a hollow free flowing area in the middle with a resultant higher pressure drop than when large coarse droplets are in use.

A similar hypothesis may be applied to Figure 5.18 since bed air pressure drop responses to changes in spray types is similar to those in Figure 5.17. However, the bed pressure drop is more dependent upon the spray nozzle configuration. Again this may have been due to a lower density of the particles and partly due to the larger sphere particle diameter of 37.5 mm that ensures a larger static and expanded bed porosity. Fluidisation of particles was generally uniform. However, the degree of turbulence was higher as th density of the particles decreases. Tests on an empty tower showed similar results to 5.17 and 5.18 thus substantiating our explanations. Differences in bed air pressure drops in the latter Figures may have been caused by the presence of the pipe and nozzle inside the column and the bed air pressure drop due to dry empty tower. However, tests show that within the range of working gas mass flux, the bed pressure drop was negligible and, that there is no significant difference in the bed pressure drop when any of the different nozzles was in use. These findings are in good agreement with those of Rama *et al.* (1983) and Balabekov *et al.* (1969) who reported negligible bed air pressure drop in the range of velocity of 1 to 5 m/s, for tests done on a tower with a supporting grid similar to the present work. No correction of the bed pressure drop was made for the contribution of the empty tower.

5.6 Effect of The Spray Nozzle Height

Figure 5.20 shows the effect the spray nozzle height from the distributor grid and the liquid mass flux upon the bed air pressure drop keeping the gas mass flux constant for the low density particles. The bed air presure drop increases as the spray nozzle height and the liquid flow rate are increased. However, at relatively low liquid flow rates, the bed air pressure drop increases slowly and almost linearly as the spray nozzle height is increased while at relaively high liquid flow rates, it increases exponentially as the spray nozzle height is increased. The reason for this behaviour may be attributed to differences in the residence time of the liquid in the tower. As the spray nozzle height increases, the freeboard increases causing a larger bed working volume. The result is an increase in the liquid

holdup and, therefore, th bed air pressure drop. However, as the liquid mass flux is increased to a threshhold value level, the interstitial spaces of the bed are rapidly filled, resulting in a rapid increase of the interfacial drag force between the air and the liquid film and, causing the bed air pressure drop to increase. Furthermore, the interfacial activity of the bed increases as the spray nozzle height increases because the tower working volume is increased. For low density particles, the expanded bed height increases as the liquid flow rate is increased [Chen and Douglas, 1968]. Increased bed height and interfacial activity means that the free flowing area of air increases. Increases in the free flowing area decreases the residence time of the liquid in the bed since the rate at which the liquid leaves the tower is enhanced. In addition, there is a limit of liquid that can reside in the intersticial voids of the bed. Therefore, the bed air pressure drop evens out as the spay nozzle height increases for a particular liquid mass flux. Figure 5.21 is a cross-plot of Figure 5.20. It confirms earlier findings in section 5.2 that the bed air pressure drop varies almost linearly with the liquid mass flux.

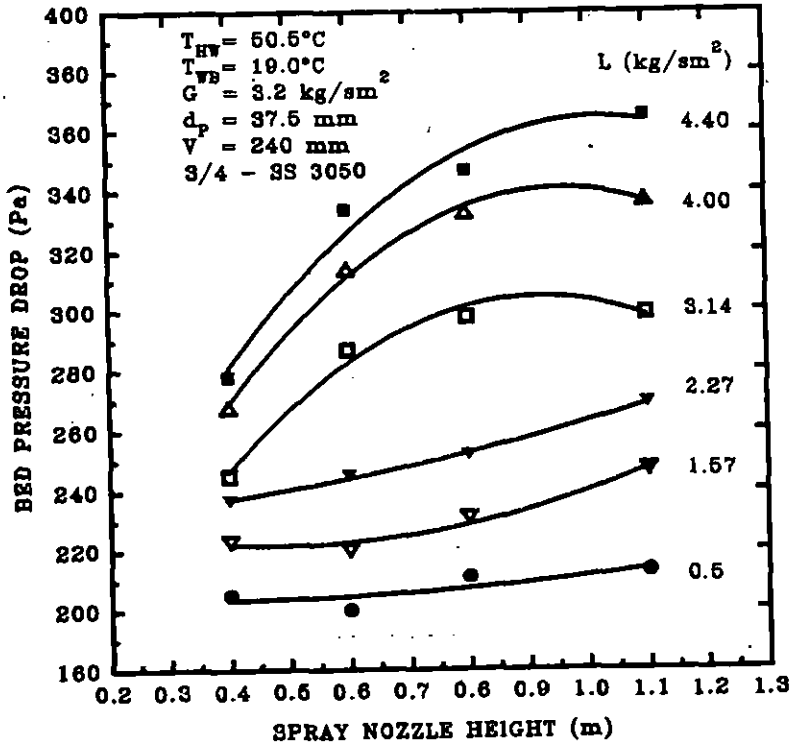

Figure 5.20 Effect of the spray nozzle height on the bed air pressure drop. ρ_p = 69 kg/m^3. Coarse droplet spray nozzle. Type I.

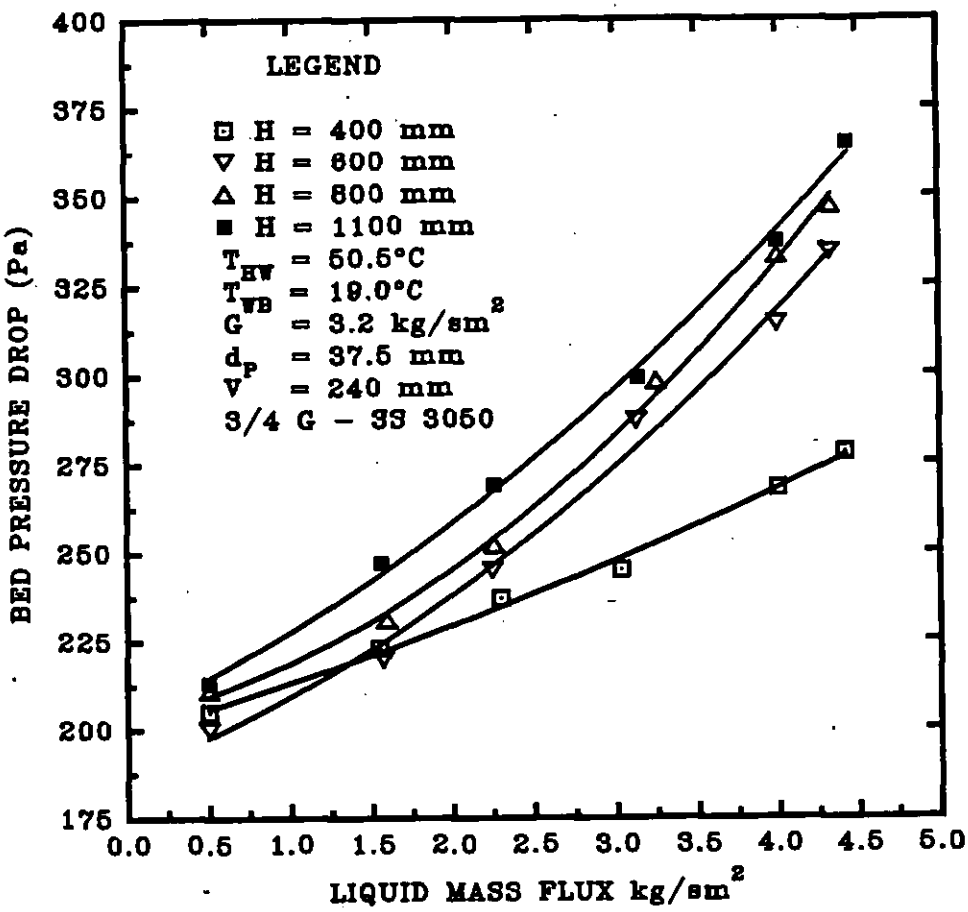

Figure 5.21 Cross-plot of Figure 5.20.

Figure 5.22 shows the effect of the spray nozzle height from the distributor grid and the static bed height upon the bed air pressure drop at typical liquid/gas mass flux ratio *L/G*, of 0.74 for a type II regime of the FBCT. The bed pressure drop increases as the static packing height is increased in line with the type I regime depicted in Figure 5.5. This may be attributed to increases in the actual liquid holdup as the static bed height increases. Between bed heights of 100 to 250 mm, the bed air pressure drop decreases as the spray nozzle height increases, passes through a minimum value and then increases sharply and then flattens out as in Figure 5.20. This peculiar behaviour may be attributed to the relatively high

density of the particles and the low *H/V* ratio. The closeness of the nozzle to the bed means that the droplet potential is fully utilised because fluidisation occurs after the flooding point is reached in accordance with the findings of O'Neill *et al.* (1972). Since the spray cone angle is narrow, and the spray droplet diameter is large, the liquid directly penetrates the bed and filling the voids. This action increases the tortuousity of the path of the liquid thus increasing the residence time and hence the liquid holdup. As the liquid holdup increases, the bed turbulence increases with the result that many more voids are filled and, therefore, increasing the liquid holdup and the bed air pressure drop further.

This premise is supported by visual observation. Intense and intimate motion of all three phases as well as uniformity were observed in the bed at H/V = 1.6 to 4. As the spray nozzle height is increased further, agitation became less intense and slugging of the bed was observed. Lower turbulence levels at relatively high gas mass fluxes as well as non-uniformity of fluidisation causes the bed to become unstable and the possibility of all bed voids being filled with liquid is decreased. Therefore, the gas passes through free spaces not filled with liquid at a lower drag force and bed air pressure drop. This action is counteracted as the spray nozzle height is increased further because of an increase in the tower working volume for similar hydrodynamic and experimental conditions. An increase in bed working volume is accompanied by an increase in the residence time of the liquid in the bed due to an increased droplet falling path. The flattening of the curves at the relatively large spray nozzle height of 1100 mm may have been partly due to wall effect as the spray diameter increases and partly due to increased interfacial activity which counteracts the decrease in the bed air pressure drop as the spray nozzle height is increased from 600 mm to 1100 mm.

At the low static packing height of 50 mm, fluidisation becomes uniform but the bed is restrained with low turbulence levels. Therefore, the dominant factors that affect the bed air pressure drop as the spray nozzle height is increasd is the residence time of the liquid in the bed and effect of an increased spray diameter.

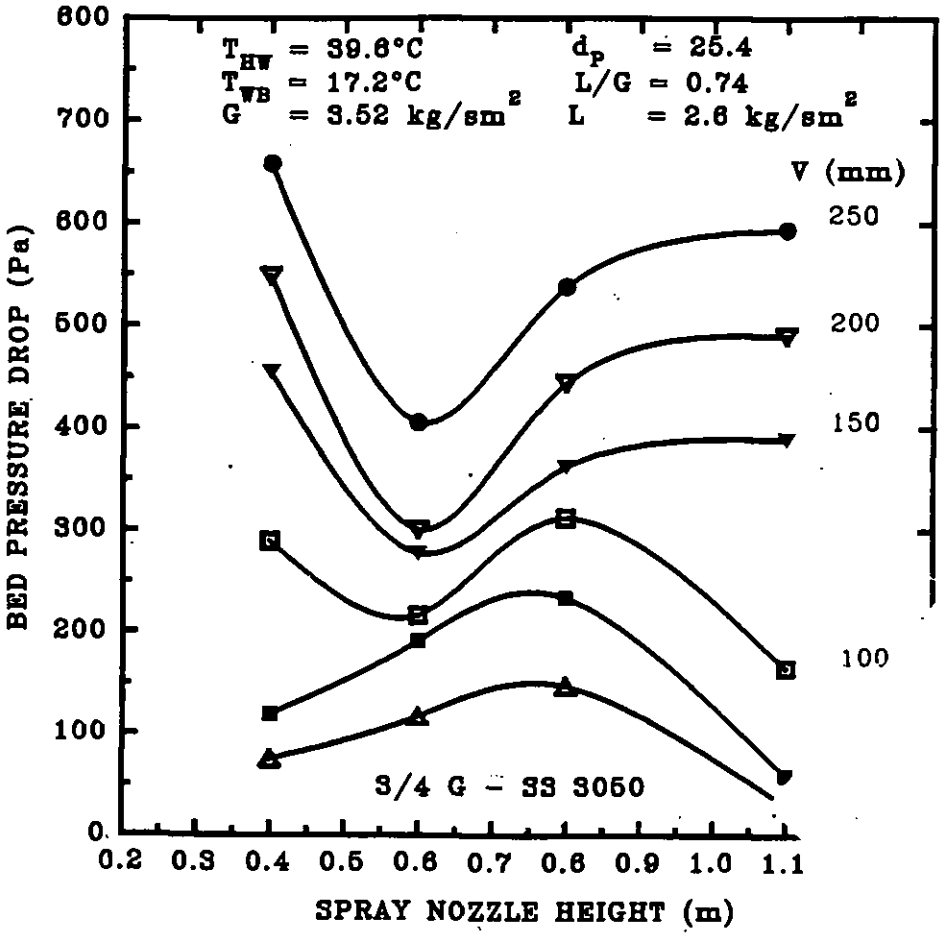

Figure 5.22 Effect of the spray nozzle height and the static bed height upon the bed air pressure drop. ρ_P = 326 kg/m^3. Coarse droplet spray nozzle. Type II.

Thus, the bed pressure drop increases as the spray nozzle height is increased until a point where the wall effect becomes dominant as the spray nozzle height becomes dominant and the pressure drop begins to fall since most of the liquid flows down the colum wall without any significant contact with the air and the particles.

5.6 Simultaneous Variation of Liquid and Gas Mass Flow Rates

The effect of of the simultaneous variation of the liquid and the gas mass fluxes with the bed air pressure drop at constant *L/G* ratios of 1.0 and 1.5 is shown in

Figures 5.23 to 5.25. Figure 5.23 shows that the bed air pressure drop is almost independent of both the liquid and gas mass fluxes. However, at relatively high fluid rates, it increases slowly as the fluid mass flux was increased. This may be due to increases in the liquid holdup in the bed. The bed air pressure drop is higher for the 25 mm than the 37.5 mm particles due to the higher density of the former compared to the latter. Additionally, the 25 mm particles have a lower initial and expanded bed porosity than the 37.5 mm particles. Therefore, the residence time of the liquid in the bed is longer in the former thus increasing the liquid holdup and the bed air pressure drop for the same set of hydrodynamic and experimental conditions as the 37.5 mm particles. A similar trend of result at similar conditions with an *L/G* ratio of 1.50 is displayed in Figure 5.24. The constancy of bed air pressure drop as the fluid mass rates are increased may be attributed to the fact that, the rate of liquid leaving the bed equals the rate at which voids are created as the bed expands. The rapid increase in the bed air pressure drop as the liquid and gas mass fluxes are increased may be due to the smaller *H/V* ratio as compared to Figure 5.23. It has already been shown in section 5.1 that, turbulence levels increase as the liquid and gas mass fluxes are increased at low *H/V* ratios. Therefore, the rapid increase in bed air pressure drop as the fluid rates are increased is expected.

Figure 5.25 also shows that the bed air pressure drop increases as the the static bed height is increased in conformity with the findings in section 5.2. The rapid increase in the bed air pressure may be due to the fact that the bed transforms from the static to fluidised state as the gas mass flux is increased. The break point may be accounted for by the bed expansion phenomenon which means that the free flowing area of the bed increases. However, the bed voids are quickly filled by the simultaneous increase in the liquid mass flux. The low *H/V* ratio of 2 means high turbulent levels are achieved and hence increased liquid holdups as the liquid mass flux is increased further. Figure 5.24 is similar in trend to Figure 5.25 and it also shows that the bed pressure drop increases as the static bed height and the liquid and gas mass flux was increased.

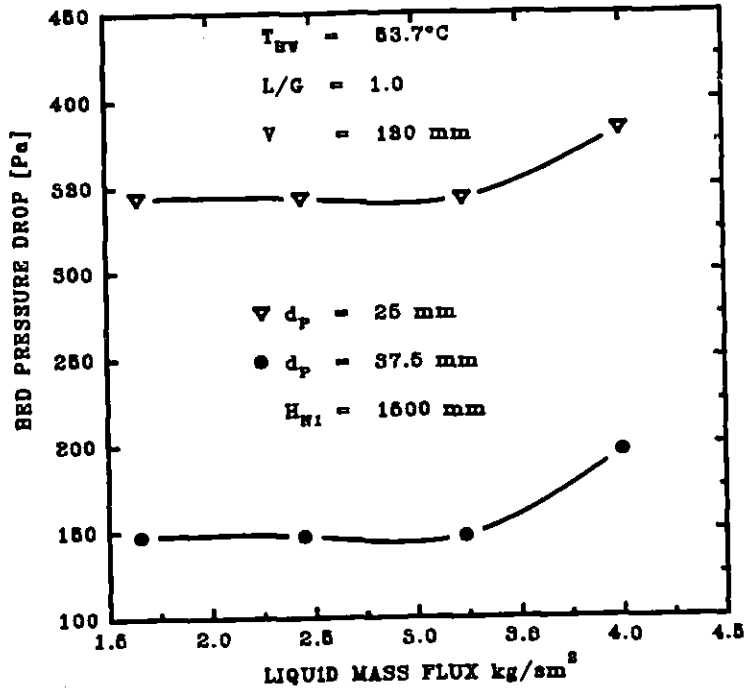

Figure 5.23 Effect of the simultaneous variation of the gas and the liquid mass fluxes on the bed air pressure drop. ρ_P = 69 kg/m^3, d_p = 37.5 mm; ρ_P = 245 kg/m^3, d_p = 25 mm. Coarse droplet spray nozzle.

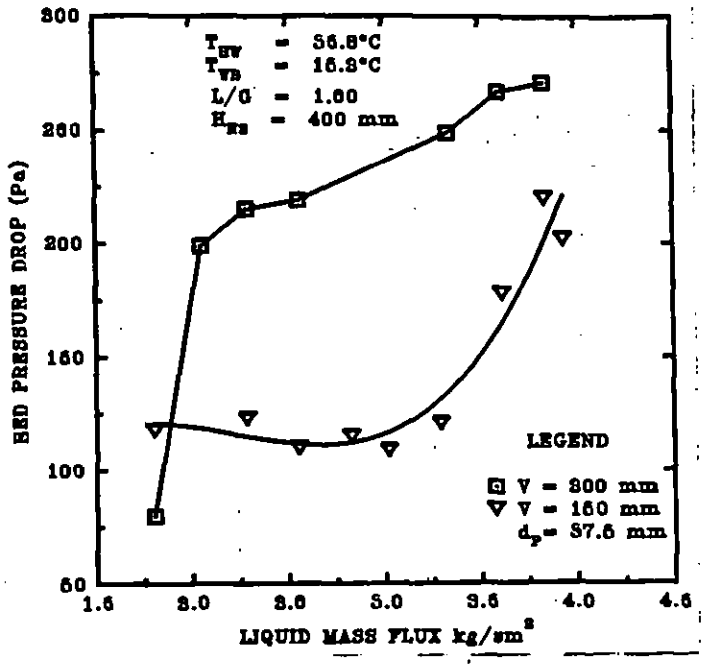

Figure 5.24 Effect of the simultaneous variation of the liquid and the gas mass fluxes and the static bed height on the bed air pressure drop. ρ_P = 69 kg/m^3. Fine droplet spray nozzle.

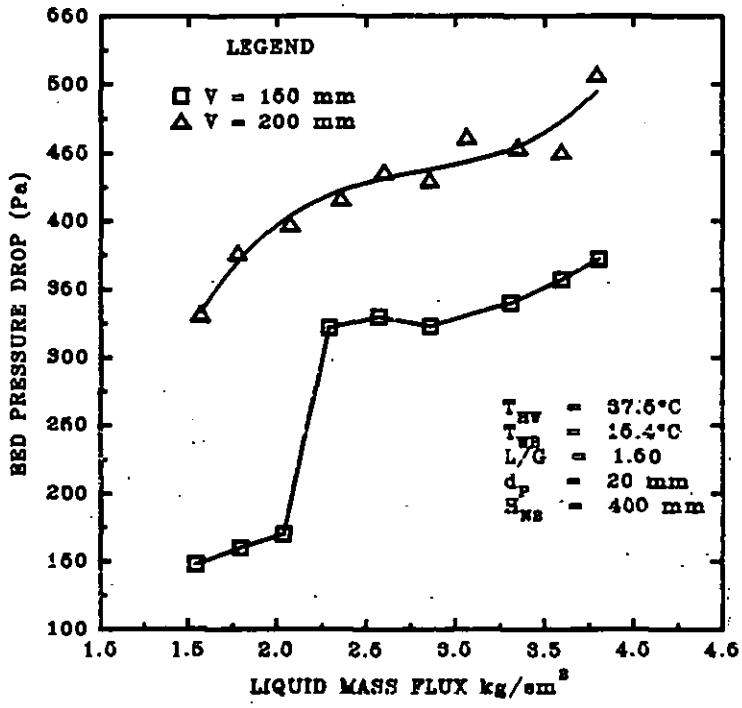

Figure 5.25 Effect of the simultaneous variation of the liquid and the gas mass fluxes upon the bed air pressure drop. $\rho_P = 239$ kg/m^3. Fine droplet spray nozzle.

We have shown that the bed air pressure drop is dependent upon the static bed height, the liquid and the gas mass fluxes, the liquid/gas mass flux ratio *L/G*, the bed particle diameter and density, the inlet hot water temperature, the spray nozzle height from the distributor grid and the spray nozzle configuration and droplet diameter. Uniform three-phase counter-current fluidisation in the FBCT for low density particles could be obtained for boundary conditions $V/D_C \geq 1$ and $G/G_{mf} \geq 2$. If $V/D_C \leq 1$, uniform fluidisation occurs when $G/G_{mf} \geq 3$ and $H/V \leq 2$. For high density particles, uniform fluidisation prevails when the theoretical conditions of O'Neill *et al.* (1972) are met.

5.7 Liquid and Gas Holdup

The liquid and gas holdups are important in the design of the FBCT because they give an indication of the hydrodynamic characteristics of the equipment. The hydrodynamics also determines the rate of heat and mass transfer and hence the

size of the equipment. The liquid holdup was calculated from the bed air pressure drop measurement using the equation of Egbe (1996b) while the gas holdup was calculated from the liquid holdup and the expanded bed heights. The result was compared with other data from the literature.

Figure 5.26 shows the variation of the liquid holdup, calculated from the data of Figure 5.23 , with the size and density of the particles when the liquid and gas mass fluxes are simultaneously varied keeping the liquid/gas mass flux ratio *L/G,* constant. The higher liquid holdup obtained for the 25 mm particle with density 245 kg/m^3 as compared to the 37.5 mm particle with density 69 kg/m^3 is expected. The reason for this difference in liquid holdup values may be attributed to the fact that smaller spheres have a lower static and dynamic porosity and many more spheres per unit area of tower than larger spheres for the same static bed height. As the gas and liquid mass fluxes are increased, the bed expands. However, the lower density relatively large particles achieve a higher bed expansion with a resultant higher porosity than the heavier particles. Therefore, an increase in the liquid flow rate results in a higher water retention rate in the interstices of the smaller particles because the longer flowing path giving rise to a higher liquid residence time and due to the higher number of particles and interstitial tortuosity. Moreover, a density of 245 kg/m^3 is closer to the threshhold value of 300 kg/m^3 for fluidisation in the "incipient flooding" mode that is characterised by high liquid holdup as recommended by O'Neill *et al.* (1972). This finding is in line with the findings of Vunjak-Novakovic *et al.* (1987) who reported that the liquid hold up increases as the liquid mass flux is increased and as the bed particle diameter is decreased. Present findings also agree in trend with pressure drop levels obtained in Figure 5.23. Figure 5.27 displays the effect of the liquid mass flux and the static bed height on the liquid holdup calculated from pressure drop values of Figure 5.8 and using the empirical Equation of Egbe (1996b):

$$Log\left(\frac{\Delta P}{V}\right) = 3.56\left[\frac{V}{d_p}\right]^{-0.02}\left[\frac{\rho_p}{\rho_L}\right]^{0.18} Re_L^{0.04} Fr_L^{-0.01} \qquad (5.1)$$

and the theoretical Equation discussed in chapter II:

$$\left(\frac{\Delta P}{V}\right) = g\left([1-\epsilon_0]\rho_p + h_L\rho_L\right) \qquad (5.2)$$

For a particular set of hydrodynamic and experimental conditions, the liquid holdup increases almost linearly as the liquid mass flux is increased because Increases in the liquid flow rate is accompanied by increases in the number of liquid droplets. An increased number of liquid droplets means that the level of turbulence increases and therefore enhances the chances of the interstitial voids

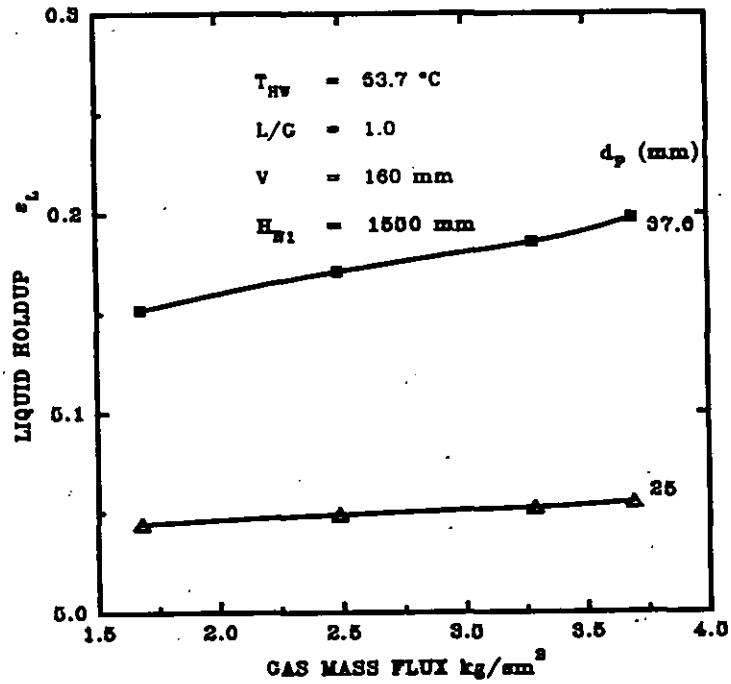

Figure 5.26 Effect of the simultaneous variation of the liquid and gas mass fluxes upon the volume of liquid holdup per unit volume of static bed height calculated from the Equation of Egbe (1996b). ρ_P = 69 kg/m^3, d_P = 37.5 mm; ρ_P = 245 kg/m^3, d_P = 25 mm. Coarse droplet spray nozzle.

being filled. Thus, for a particular gas mass flux, the residence time and the liquid holdup increases. The total volume of liquid in the fluidised bed increases as the static bed height increases as seen in Figure 5.27, but the rate of increase

per unit sataic bed volume is negative as seen in Figure 5.28 and 5.29 in agreement with the findings of Vunjak-Novakovic *et al.* (1987); Barile *et al.* (1971) and Gel'perin *et al.* (1968) as seen in Figures 5.30, 5.31 and Table 5.1. There is, therefore, an optimum packing volume for an FBCT to attain optimum liquid holdup. The correlations of Barile *et al.* (1971) and Gel'perin *et al.* (1968) given by Fan and Muruyama (1989).

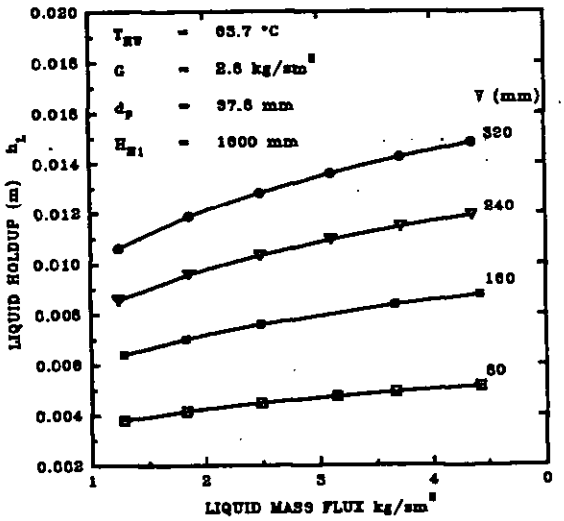

Figure 5.27 Effect of the liquid mass flux and the static bed height upon the actual liquid holdup. ρ_P = 69 kg/m^3. Coarse droplet spray nozzle.

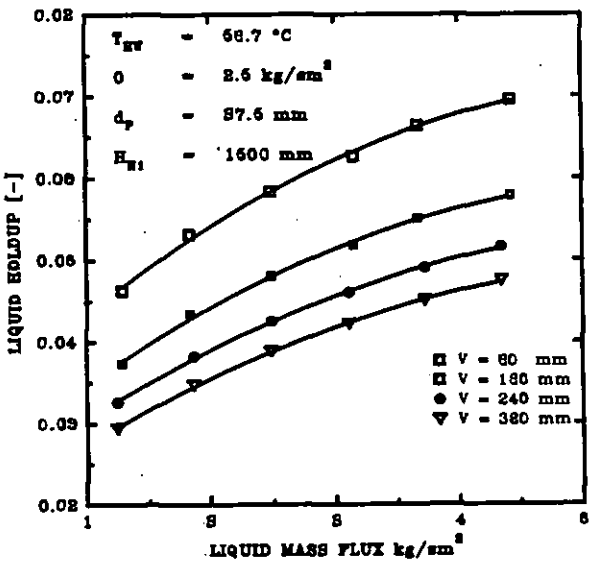

Figure 5.28 Effect of the liquid mass flux and the static bed height upon the volume of liquid holdup per unit volume of static bed height calculated from the Equation of Egbe (1996b) using the experimental data of Figure 5.8.

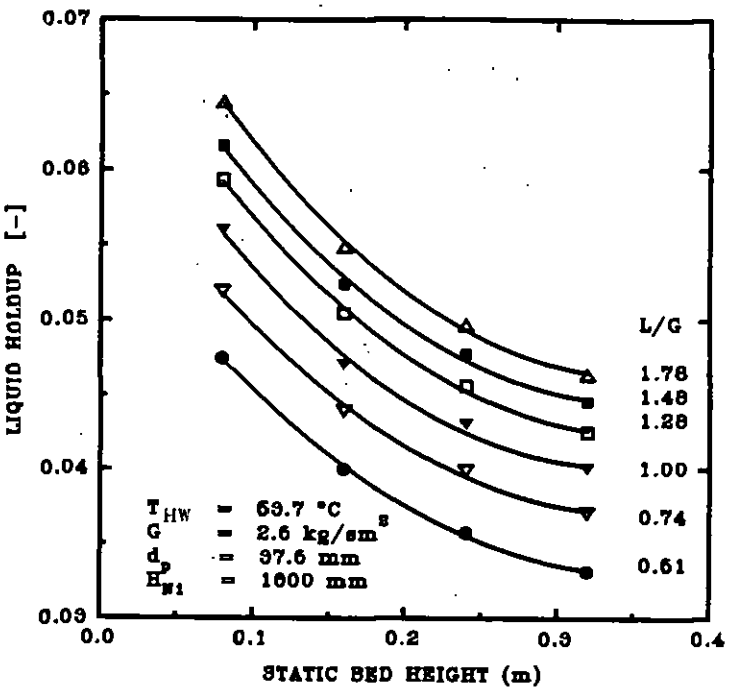

Figure 5.29 A cross-plot of Figure 5.28.

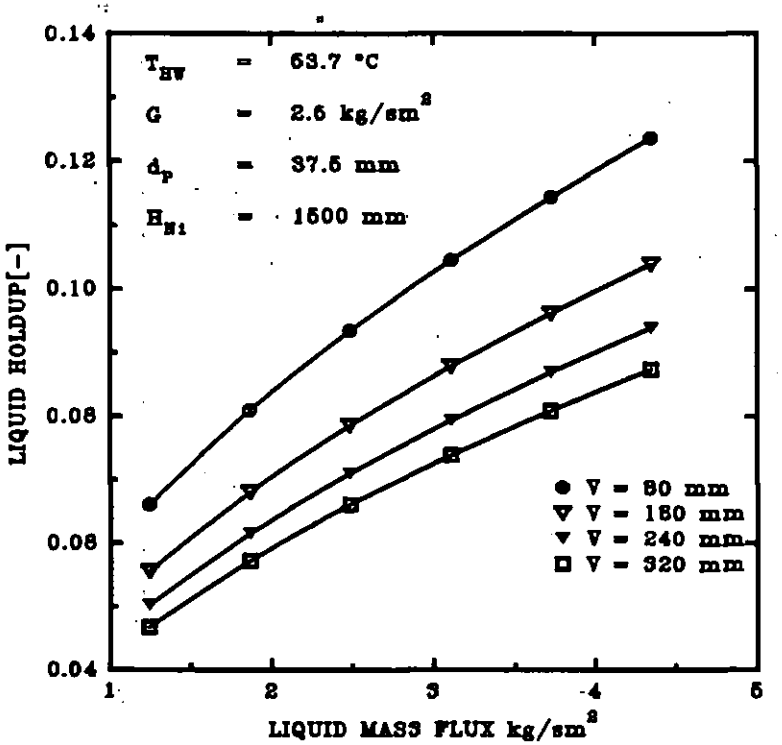

Figure 5.30 Effect of the liquid mass flux upon the volume of liquid holdup per unit volume of static bed as calculated the Equation of Gel'perin *et al.* (1968) using the experimental data of Figure 5.8.

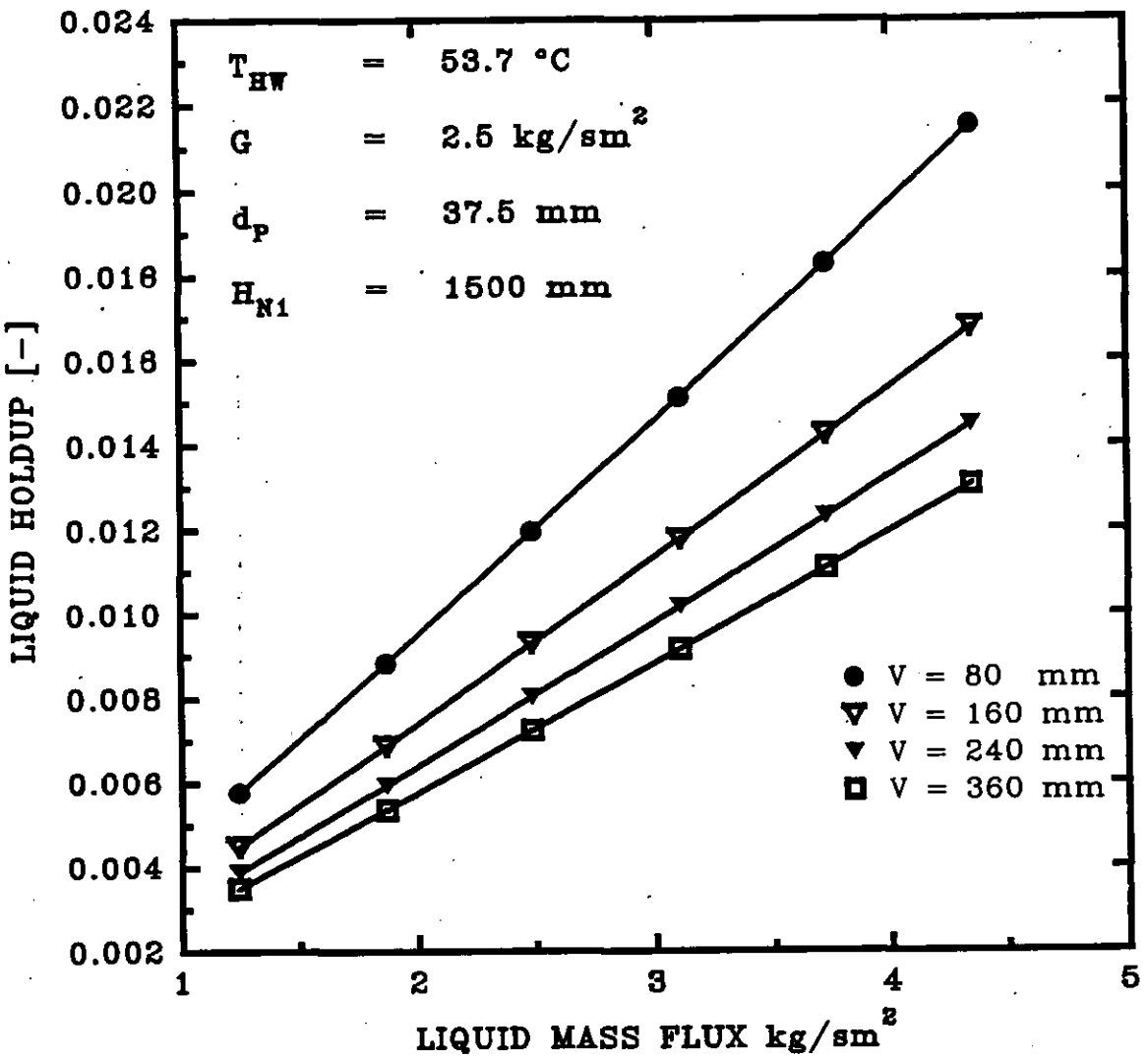

Figure 5.31 Effect of the liquid mass flux and the static bed height upon the volume of liquid holdup per unit volume of static bed calculated from the Equation of Barile *et al.* (1971) using experimental data of Figure 5.8.

L	V	V/d_p	h_L(Calculated) m^3/m^3				
kg/sm^2	(m)	[-]	Present Work	Chen *et al.* (1968)	Gelperin *et al.* (1968)	Barile *et al.* (1971)	Vunjak *et al.* (1987)
1.24	0.08	2.33	0.04627	0.03395	0.06607	0.00577	0.05608
1.24	0.16	4.67	0.03730	0.03395	0.05556	0.00450	0.04435
1.24	0.24	6.40	0.03254	0.03395	0.05020	0.00389	0.03935
1.24	0.32	8.53	0.02936	0.03395	0.04672	0.00350	0.03644
2.50	0.08	2.33	0.05837	0.04115	0.09343	0.01195	0.07938
2.50	0.16	4.67	0.04798	0.04115	0.07857	0.00931	0.06008
2.50	0.24	6.40	0.04248	0.04115	0.07099	0.00804	0.05184
2.50	0.32	8.53	0.03881	0.04115	0.06607	0.00725	0.04705
3.72	0.08	2.33	0.06630	0.04695	0.11436	0.01826	0.10877
3.72	0.16	4.67	0.05497	0.04695	0.09617	0.01423	0.07359
3.72	0.24	6.40	0.04898	0.04695	0.08690	0.01230	0.06258
3.72	0.32	4.67	0.04499	0.04695	0.08087	0.01109	0.05617
4.35	0.08	2.33	0.06953	0.04958	0.12360	0.02150	0.10877
4.35	0.16	4.67	0.05782	0.04958	0.10393	0.01675	0.07992
4.35	0.24	6.40	0.05163	0.04958	0.09391	0.01448	0.06761
4.35	0.32	8.53	0.04750	0.04958	0.08740	0.01305	0.06044

Table 5.1 A comparison of present data and those of other investigators on the calculated liquid holdup using the data of Figure 5.8.

5.9 Gas Holdup

Figure 5.32 and its corresponding crossplot displayed in Figure 5.33 indicates the dependence of the gas holdup, calculated from Equation 2.20 in chapter II using the liquid holdup data of Figure 5.28, upon the liquid mass flux and the static packing height. The gas holdup increases as the liquid mass flux is increased. This peciuliar behaviour may be explained in terms of the size of the droplets. Since the droplets are relatively large, droplets may be assumed to be in fluidized suspension within and above the bed. Since the number of liquid droplets increase as the liquid flow rate is increased, increasing turbulence levels, a quasi-three-phase flow develops above the bed with the droplets acting as spheres and creating the possibilty of air pockets being trapped within the droplet sphere voids causing the residence time of the gas in the tower to increase. The effect is an increase in the gas holdup in the entire tower at a constant gas mass velocity. This finding is however in conflict with that of Balabekov *et al.* (1969); Kito *et al.* (1978). The discrepancies may be attributed to differences in experimental conditions. They used rather relatively heavy particles with densities greater than the threshold value of 300 kg/m^3. It follows that their regime of operation was "fluidisation with incipient flooding" (type II) as compared to fluidisation before incipient flooding (type I) of the low density particle of 69 kg/m^3 of the present study as illustrated in Figures 5.32 and 5.33. It was discussed in section 5.1 that the type II regime is characterised by excessive liquid holdup in and above the bed. Therefore, the build up of gas as the liquid flow rate is increased at a constant gas rate is counteracted by the increased liquid holdup so as to maintain and conserve stability and matter in the system. Moreover, while the present study is based on air-water system, the findings of Kito *et al.* (1978) is in addition to water, based on other liquids with radically different properties.

The liquid holdup/static bed volume decreases almost exponentially as the static bed height is increased. The solid holdup is dependent upon the expanded bed height which in turn determines the free board volume. The expanded bed height

has been shown to increase with an increase in the static bed height (Guerriere *et al,* 1995). The result is a decrease in the free board volume of the fluidised bed. Since the gas holdup is dependent upon the free board volume, a decrease in the latter, reduces the interstitial spaces of the droplets for air entrapment.

Figure 5.33 shows that as the static bed height is increased for a particular liquid/gas mass flux ratio, the gas holdup decreases, passes through a minimum, and then increases sharply. This behaviour may be attributed to the fact that there is an optimum expanded bed volume after which the capacity of air being trapped within the voids of the large liquid droplet suspended in the freeboard is minimized. Nevertheless, the gas holdup then increases after the minimum value is reached so as to counteract the decrease in the liquid holdup per unit volume of static bed as the static bed height is increased.

Comparison of the present study with those of other investigators is displayed in Figure 5.34. This shows the variation of the gas holdup with the superficial gas velocity at contrastingly different conditions. It shows that the gas holdup increases exponentially as the superficial gas velocity is increased in excellent agreement with the other investigators [Kito *et al.* (1976); Kito *et al.* (1978); Balabekov *et al.* (1969); Gel'perin *et al.* (1966)]. The exponential increase of the gas holdup with increases in the superficial gas velocity is expected as the amount of gas in the tower increases. Yet, there is a limit of the proportion of gas that can be contained in the tower because the sum total of the three-phase gas-liquid-solid ratio is always constant and equal to unity.

The effect of simultaneously increasing the liquid and gas mass fluxes upon the gas holdup, calculated from the liquid holup values of Figure 5.28, is shown in Figure 5.34. It shows that relatively large light particles have a higher gas holdup than relatively small heavy particles. This is because the light larger particles have a higher static and expanded bed porosity with the effect that, for the same hydrodynamic and experimental conditions, the free flowing area created during

fluidisation is higher. These increases in the gas holdup values are further enhanced by the low density of the particles which can fluidise much more readily than relatively dense particles. Additionally, the low liquid holdup associated with type I regime means that the interstitial spaces of the particles are predominantly filled with the gas. Notwithstanding, in type II fluidisation, the interstitial spaces are predominantly filled with the gas but this is partly counteracted by the excessive liquid holdup. The trend of increase of the gas holdup as the gas and liquid mass fluxes are simultaneously increased is in agreement with Figures 5.32 and 5.33. However, the gas holdup increases, reaches a maximum value and then falls as the liquid and gas mass fluxes are increased. This behaviour of the relatively large and light density particles may also be attributed to the high liquid holdups at high liquid mass fluxes and a corresponding increase in the expanded bed height as the gas mass flux is simultaneously increased. Since relatively dense particles do not readily fluidise, the trend is similar to Figs 5.32 and 5.33.

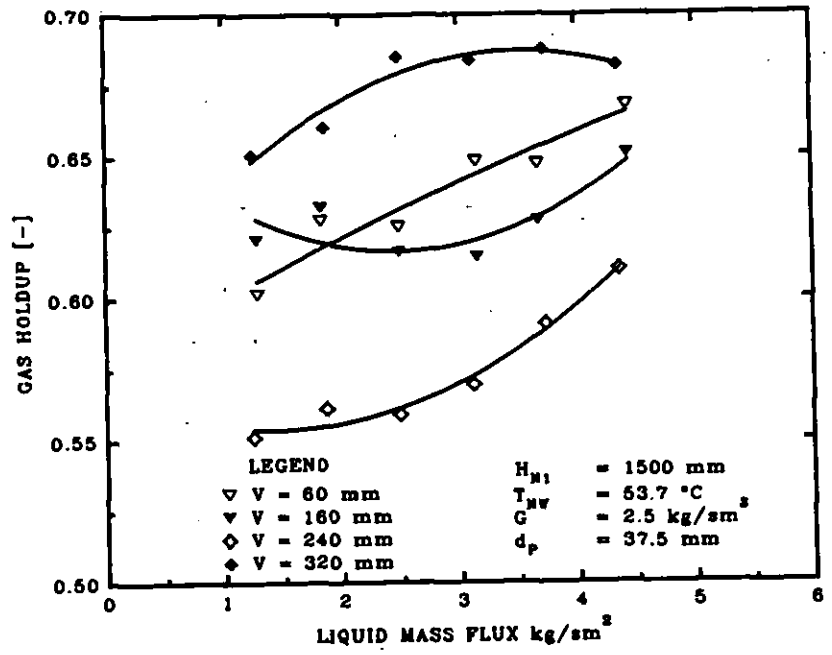

Figure 5.32 Effect of the liquid mass flux and the static bed height upon the gas holdup calculated from the Equation of Gel'perin *et al.* (1968). ρ_p = 69 kg/m^3. Coarse droplet spray nozzle.

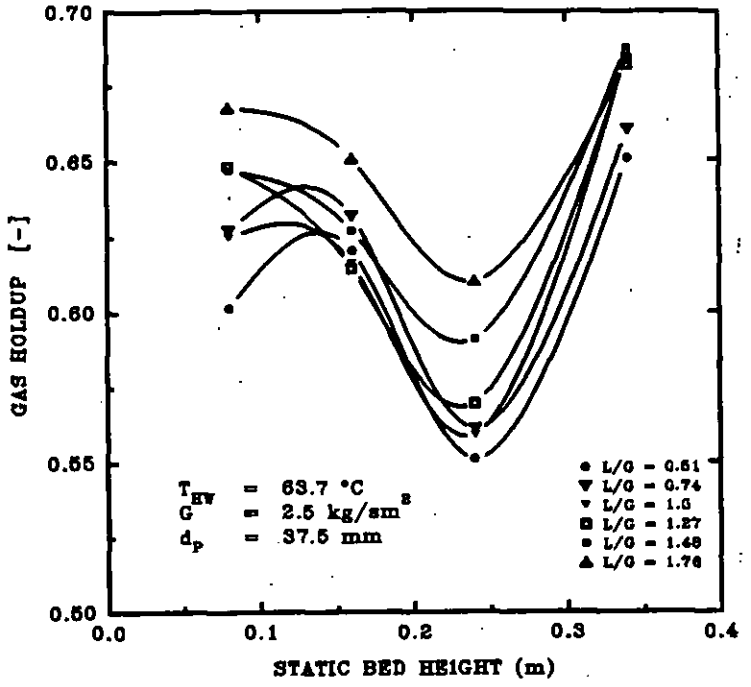

Figure 5.33 A cross-plot of Figure 5.22.

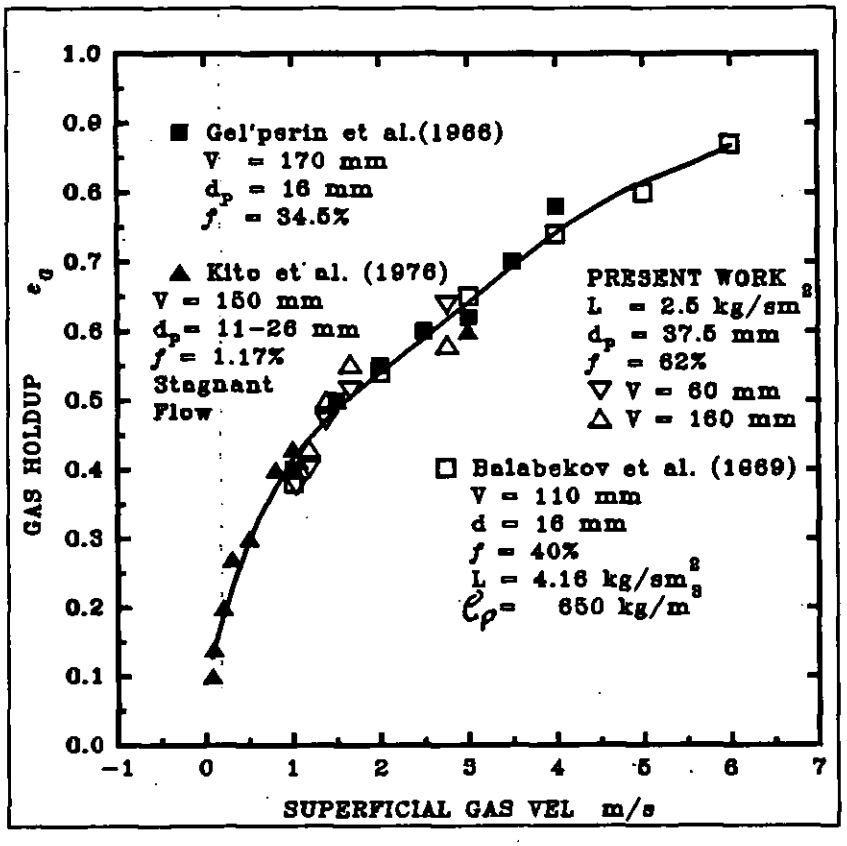

Figure 5.34 Variation of the gas holdup with the superficial gas velocity. A comparison of the present data with the work of other investigators.

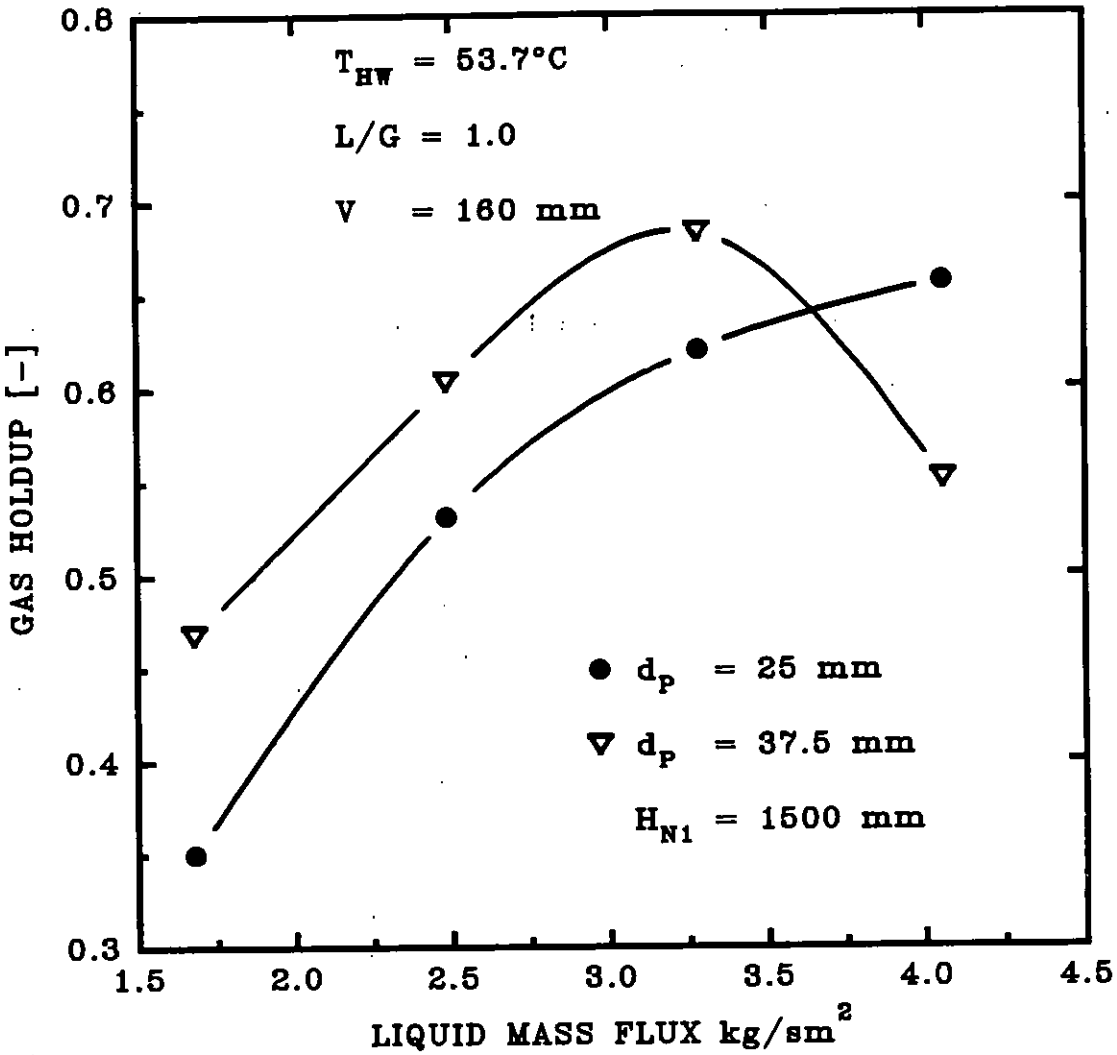

Figure 5.35 Simultaneous effect of the gas and liquid mass fluxes upon the gas holdup for the coarse droplet spray nozzle. ρ_p = 69 kg/m^3.

CHAPTER VI

EXPERIMENTAL RESULTS: BED EXPANSION AND LIMITING FLUIDISATION VELOCITIES

6.1 Introduction

The expanded bed height was studied because it is essential to the design of FBCTs. The liquid and gas holdups, the minimum fluidisation velocity, the heat transfer coefficient, and the distance between the distributor and the upper retaining grids are all evaluated using the expanded bed height. Thus, the aim of this work is to establish the response to the dependent expanded bed height as the independent hydrodynamic process factors and levels are varied.

6.2 Effect of the Gas Mass Flux

Figures 6.1 to 6.4 show the effect of the gas flow rate upon the bed expansion. Figure 6.1 corresponding to Figure 5.1 in section 5.1 shows that the expanded bed height increases as the gas flow rate is increased keeeping the liquid mass flux constant and that for the same gas mass flux, the expanded bed height increases as the liquid mass flux is increased.

As the gas mass flux is increased from about 0.5 to 1.5 kg/sm^2, the expanded bed height remains independent of the gas mass flux because the minimum fluidisation velocity has not been attained. After the minimum fluidisation gas mass flux has been surpassed, and the gas mass flux is increased further, the bed expansion increases slowly from about 1.5 to 2.5 kg/s m^2 and then sharply after because of the increase in gas-liquid interfacial stresses as a result of increased air power.

Figure 6.2, corresponding to Figure 5.3 in section 5.1, shows the effect of the the gas mass flux and the inlet water temperature on the expanded bed height for type II

FBCT. The expanded bed height is independent of the inlet water temperature with a similar trend of increase of the bed expansion at the two temperatures studied. A close examination of Figure 6.2 shows two break points resulting in three regions similar to the findings of Vunjak-Novakovic *et al.* (1987). The first break point is due to the transition from the stationary to fluidised state at the minimum fluidisation gas mass flux.

Before the minimum fluidisation gas mass flux is reached, the air power transmitted to the bed through the supporting grid is relatively small due to the relatively low gas flow rate while keeping the liquid mass flux constant. After the transition point to developed fluidisation, the bed begins to expand slowly and then rapidly as the gas flow rate is increased. This behaviour may be attributed to increases in the free flowing area of the bed as the gas flow rate is increased after the state of minimum fluidisation gas mass flux has been surpassed.

It has been shown experimentally, that the liquid holdup is independent of the gas flow rate after the minimum fluidisation velocity has been attained in both type I and II FBCT operations with relatively large free opening fraction of the supporting grid [Vunjak-Novakovic *et al.* (1987); Chen and Douglas (1968)] in agreement with my findings in section 5.1.

Thus, as the gas flow rate is increased for a particular liquid flow rate, the gas holdup in the bed increases resulting in increases in turbulence levels and a subsequent increase in the gas liquid interfacial tension. This action combined with the increased air power transmitted through the supporting grid, causes the bed height to rapidly increase.

The second break point occurs at the gas mass flux of about 2 kg/s m^2. Although the bed expansion continues to increase as the gas flow rate is increased, the rate of increase is slower. One of the reasons may be due to the fact that the expanded bed height equals and then surpasses the spray nozzle height resulting in the reduction of

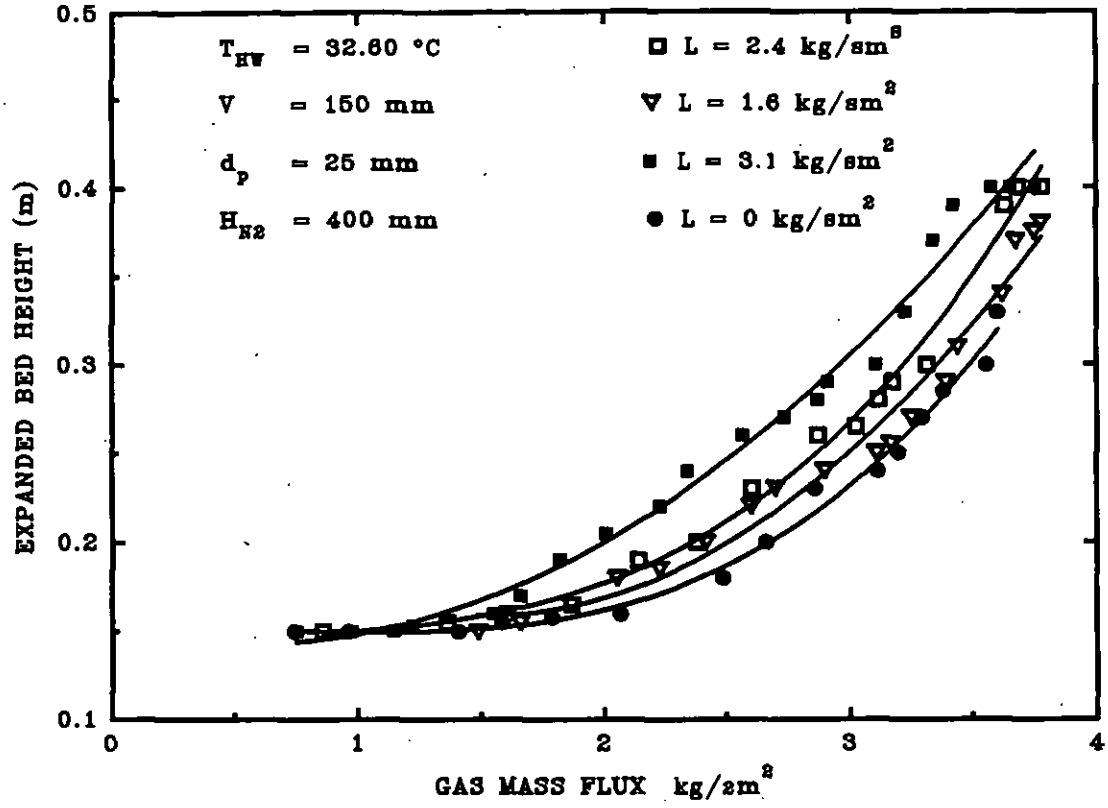

Figure 6.1 Effect of the gas and liquid mass fluxes upon the expanded bed height for fine droplet spray nozzle. ρ_P = 245 kg/m^3.

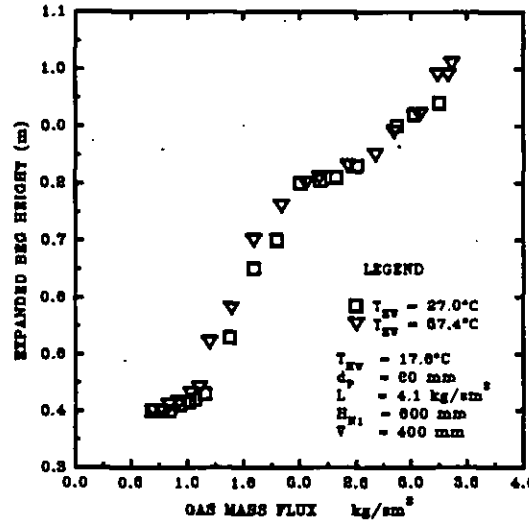

Figure 6.2 Effect of the gas mass flux and the inlet hot water temperature on the bed expansion. ρ_P = 239 kg/m^3. Coarse droplet spray nozzle.

the proportion of particles that directly makes contact with the liquid and, causing the interfacial activity to decrease as the gas mass flux is increased. This condition is unfortunate and unavoidable since the expanded bed height could not be predicted before experimental runs. Another reason for the second break point may be due to evaporation and entrainment of water as the gas mass flux is increased causing the actual liquid flow rate to decrease for a type II FBCT regime and, resulting in a decrease in the liquid holdup at a constant liquid flow rate.

Figure 6.3 and 6.4 show that for a constant liquid/gas mass flux ratio, in effect an increase in the gas mass flux, the bed expansion increases as the static bed height is increased in conformity with the findings of Strumillo *et al.* (1974). They reported that the ratio of the expanded bed height to the static bed height V_E/V is independent of the static bed height in agreement with Rama *et al.* (1983) and Tichy *et al.* (1972). Figure 6.5 shows that this is not the case in this study. Nevertheless, Figure 6.5 shows that the ratio of the expanded bed height/static bed height V_E/V, decreases as the static bed height is increased. The reason for this phenomenon may be that, the liquid holdup per unit volume of static bed decreases as the static bed height increases [Barile *et al.* (1971); Vunjak-Novakovic *et al.* (1987)], although the actual volume of liquid in the bed increases. Since the rate of interfacial activity per unit volume of static bed increases as the liquid holdup per unit static bed volume increases, the effect of decreases in the liquid holdup would be a fall in the operational bed volume per unit volume of the static bed causing ratio of the expanded bed height to static bed height V_E/V, to decrease as the static bed height is increased.

Figure 6.6 corresponding to Figure 5.5 in section 5.2, shows the effect of the static bed height and the liquid mass flux upon the expanded bed height at a constant gas mass flux of about four times the average minimum fluidisation gas mass flux. For the same liquid mass flux, the bed expansion increases almost proportionally as the static packing height is increased thus confirming our findings of Figure 6.3. Similarly, the expanded bed height increases as the liquid mass flux is increased for

the same static packing height. However, the expanded bed height is independent of the liquid mass flux at a static bed height of 0.32 m. The reason for this behaviour may be that, there is a limiting value of bed expansion after which the fluidised bed ceases to exist. As the actual amount of liquid holdup in the bed increases as the static bed height is increased, so does the tendency for the bed to reach "true" flooding point at the relatively high constant gas mass flux of 3.0 kg/s m^2. As the density of the particles is lower than the threshhold value of 300 kg/m^3, the bed reaches the flooding point after the minimum fluidisation state as in type I operation. The "true" flooding or maximum fluidisation point is characterised by the particles and droplets being blown out of the contacting zone, and congregating at the upper retaining grid. Thus the independence of the expanded bed height of the liquid flow rate for deep beds.

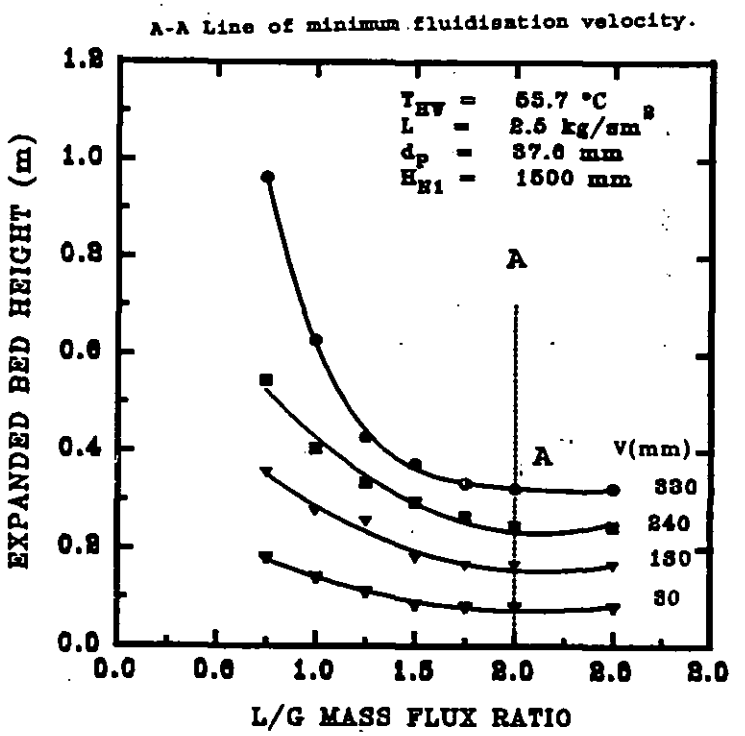

Figure 6.3 Effect of the liquid/gas mass flux ratio and the static bed height on the bed expansion. ρ_p = 69 kg/m^3. Coarse droplet spray nozzle.

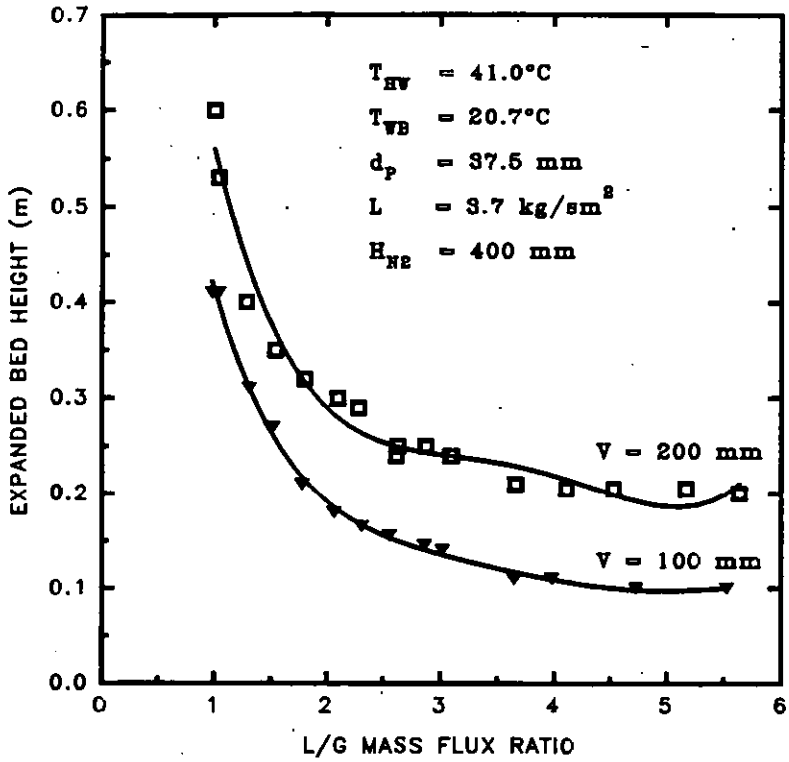

Figure 6.4 Variation of the expanded bed height and the liquid/gas mass flux ratio for fine droplet spray nozzle. ρ_P = 69 kg/s m^3.

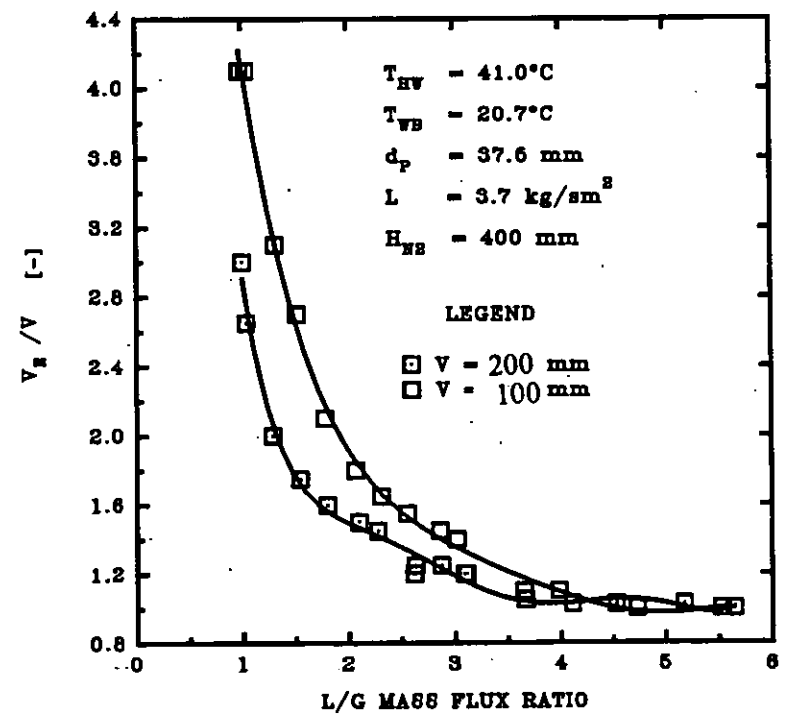

Figure 6.5 Variation of the expanded bed height/static bed height ratio with the liquid/gas mass flux ratio. ρ_P = 69 kg/m^3. Fine droplet spray nozzle.

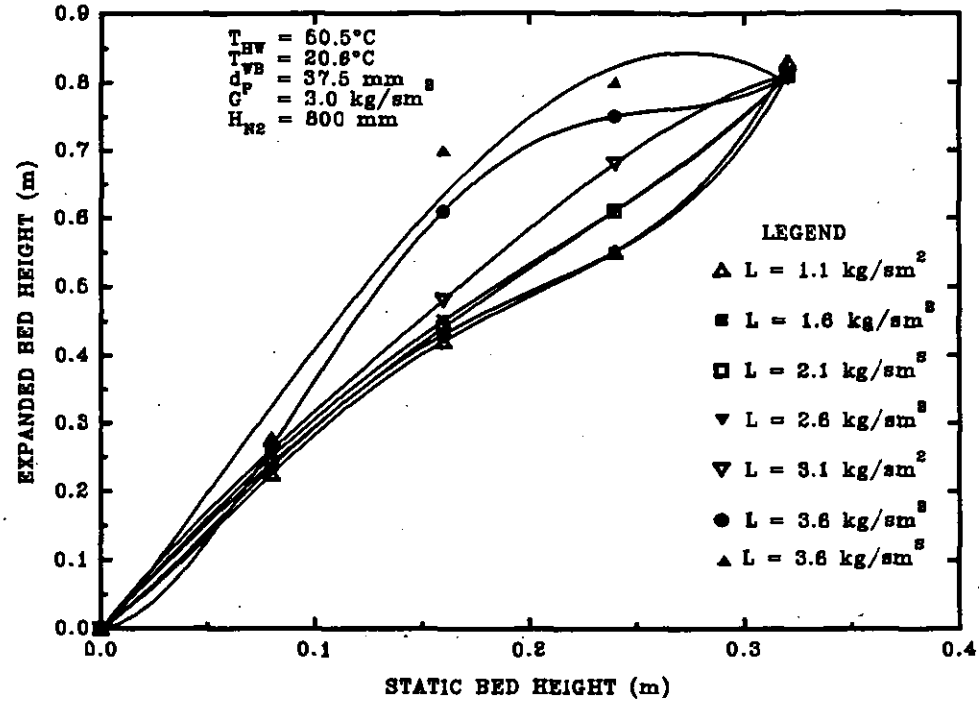

Figure 6.6 Effect of the static bed height and the liquid mass flux upon the Bed expansion. ρ_P = 69 kg/m^3. Fine droplet spray nozzle.

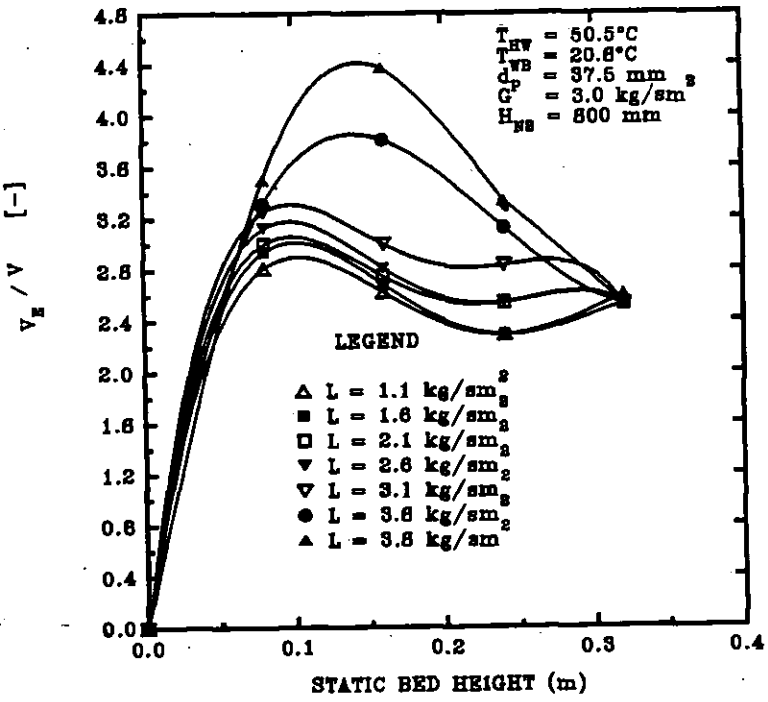

Figure 6.7 Dimensionless bed expansion vs the static bed height. Cross-plot of Figure 6.6.

Figure 6.6 above shows the effect of the static bed height upon the dimesionless ratio V_E/V derived from the data of Figure 6.6. The increase in the ratio V_E/V, in the range of static bed height from 0 to 80 mm is in line with expectations of increased V_E. For liquid flow rates under 3.1 kg/s m^2, the ratio V_E/V decreases as the static bed height is increased in agreement with the findings illustrated in Figure 6.5. However, Figure 6.7 shows that for this range of liquid mass flux, the ratio V_E/V, tends to increase exponentially and then decreases meaning that there is an optimum level after which the rate of decrease becomes constant due to the tendency for the bed to flood as the static bed height is increased in good agreement with the findings of Strumillo *et al.* (1974); Tichy *et al.* (1972); Rama *et al.* (1983).

The reason for this apparent conformity is not clear. Yet one premise may be attributed to the similarly low density of packings used by Rama *et al.* (1983) and Tichy *et al.* (1972) and that, most of the static bed height to column diameter ratios V/D_C were approximately less than 1, a condition for uniform and pure counter-current fluidisation. In addition, Strumillo *et al.* (1974) showed that the ratio V_E/V, decreases as V/D_C is increased for different diameter columns and that, V_E/V decreases as the column diameter is increased.

Figure 6.7 also shows that at liquid mass fluxes above 3.1 kg/s m^2, the ratio V_E/V increases, passes through a maximum value and the decreases sharply as the static bed height is increased. The explanation for this behaviour may be that, at shallow static bed heights, the dry weight of the spheres is relatively low compared to deep beds. Thus at relatively high liquid mass fluxes, the expected increase in interfacial activity per unit static bed volume and hence bed expansion that accompanies an increase in the liquid holdup per unit volume of static packing volume as the static packing height is decreased is counteracted by the weight of the liquid flowing downwards and causing the bed to become restrained. As this liquid holdup decreases as the static bed height is increased, a minimum value is reached whereby the operational liquid holdup per unit volume of static bed volume becomes the controlling factor for bed expansion. The maximum value of the the ratio V_E/V is

surpassed and starts to fall sharply in agreement with the work of Vunjak-Novakovic *et al.* (1987). In their experimental tests, using a similarly high liquid mass fluxes, they concluded that there is an optimum level at which the liquid holdup per unit bed volume varies with the static bed height.

6.3 Effect of the Liquid Flow Rate

The effect of the liquid flow rate upon the bed expansion was widely studied because it is the fluid of interest. Figures 6.8 to 6.15 show its effect upon the expanded bed height. Figures 6.8 and 6.9 correspond to Figures 5.7 and 5.8 respectively for the relatively low density particles of 69 kg/m^3 type I regime. They show the effect of the liquid mass flux and the static bed height upon the bed expansion keeping the gas mass flux constant. Despite differences in nozzle configurations, droplet size, gas velocities, spray nozzle height to static bed height ratio *H/V*, the expanded bed height is weakly dependent upon the liquid mass flux in agreement with the findings of Dengler (1977). In addition, it increases as the static bed height is increased. The almost independence of the bed expansion of the liquid mass flux may be attributed to the relatively moderate fluidising gas velocity that is about twice the minimum fluidisation velocity. It has been previously discussed in section 5.2 that low density particles experience fluidisation inconsistencies, especially in the development of a mono-layer at the column wall at velocities close to the minimum fluidisation velocity for type I operations. The congregation of the particles at the column wall is much more severe when $V/D_C < 1$ and $H/V \geq 4$ due to wall effect upon the water flow. Bearing these conditions in fluidisation inconsistensies in mind in these cases, the bed expansion was thus restrained keeping the expanded bed height relatively constant as the liquid mass flux is increased. In addition, the moderate fluidising gas velocity does not induce high enough interfacial activity that may have aided bed expansion.

The low turbulence levels that were observed in Figures 6.8 and 6.9 may also have been caused by the fact that fluidisation started before the flooding point is reached.

Thus, although the weight of the bed is relatively low and may have aided bed expansion, this advantage is counteracted by the downward flow of water; the surface tension between the liquid film on the particles and the column wall and the lack of effective interfacial activity within the fluidised bed. Figure 6.9 shows that when $V/D_C \geq 1$ (V = 320 mm) and $H/V \leq 4$ (H = 800 mm and V = 320), the bed expansion increases as the liquid mass flux is increased. This is because of increased interfacial activity due to increased actual liquid hold up and increased bed weight

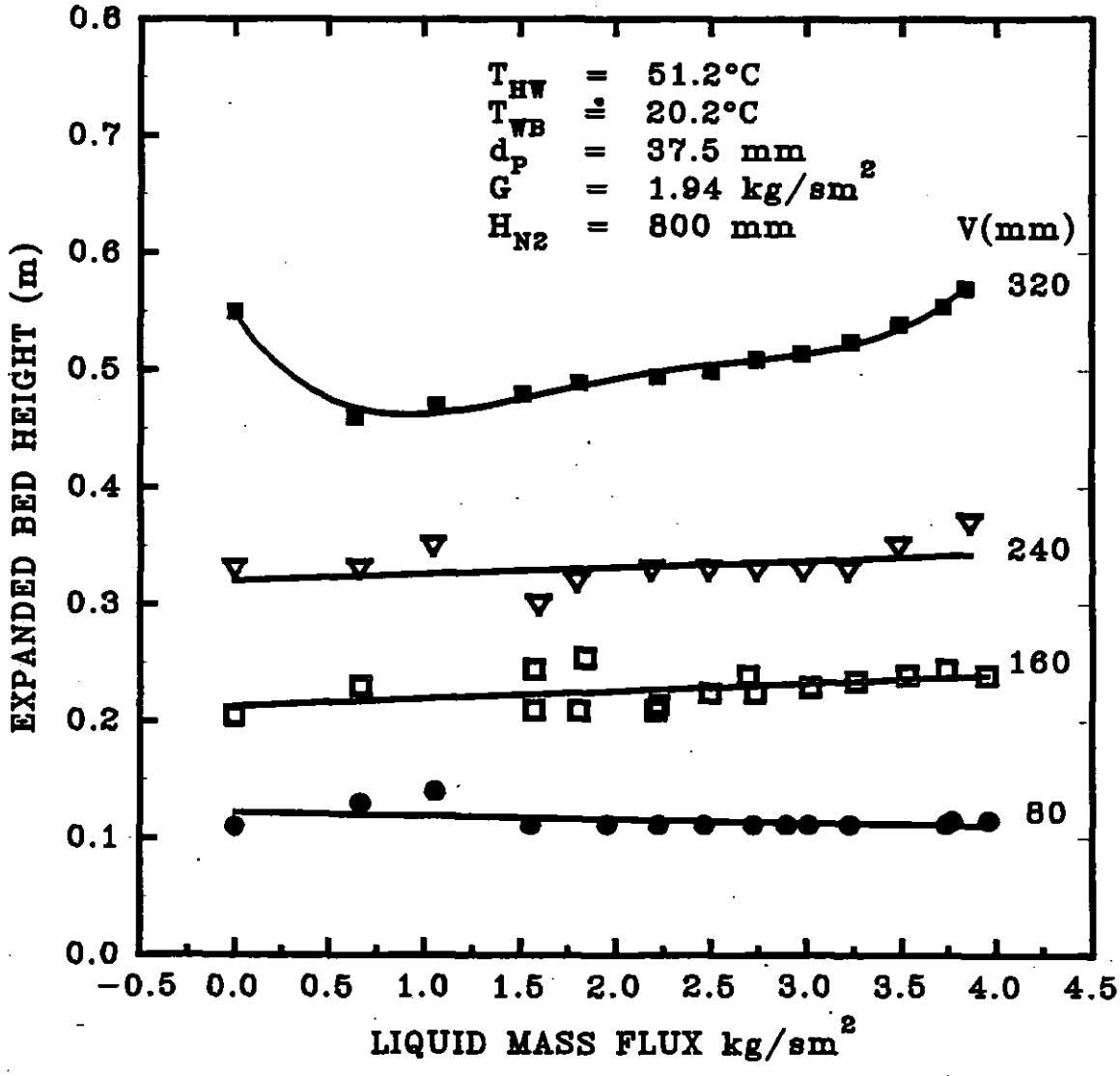

Figure 6.8 Effect of the liquid mass flux and the static bed height on the bed expansion at low fluidisation gas velocity. $\rho_p = 69$ kg/m^3. Fine droplet spray nozzle.

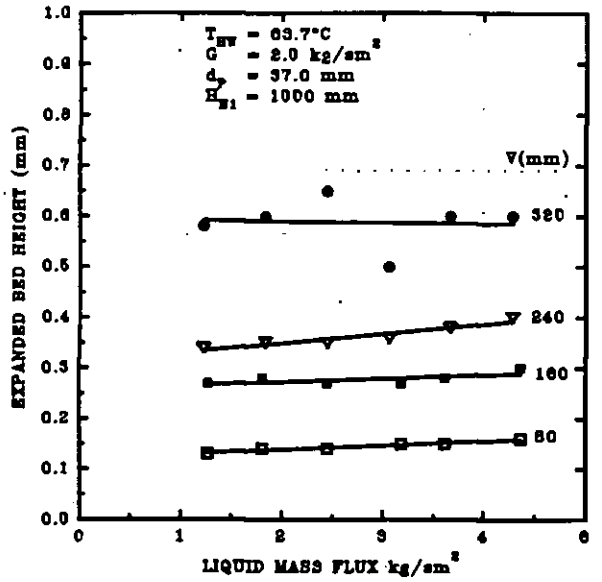

Figure 6.9 Effect of the liquid mass flux and the static bed height on the bed expansion. ρ_P = 69 kg/m^3. Coarse droplet spray nozzle.

that may have counteracted fluidisation inconsistencies. The initial decrease in the expanded bed height as the liquid mass flux is increased from about 0 to 1.0 kg/s m^2 occurs because of the initial high free area for air to flow for the two-phase gas-solid flow. As the liquid mass flux is increased further, the particle voids are filled with resulting in low liquid holdup at relatively low liquid mass flux. The free flow area then decreases and the expanded bed height decreases because the pressure drop increases. At a threshold value of liquid holdup as the liqid flow rate is increased further, the decrease in effectiveness of the available air power by the liquid in the voids of the bed is counteracted by an increase in the interfacial activity in the bed. The expanded bed height therefore begins to increase. The same phenomenon does not occur in Figure 6.9 because the *H/V* ratio is greater than 4 giving rise to mal-distribution of water in the bed as some of the liquid flows down the side of the column thus reducing the liquid holdup and therefore the turbulence level. Thus the expanded bed height remains almost constant even though the gas mass flux is higher. Another cause of differences between Figure 6.8 and 6.9 may be due to differences in fluid properties that may arise as a result of differences in the inlet hot water and ambient air temperatures.

Figure 6.10 shows the effect of the liquid flow rate and the inlet hot water temperature upon the bed expansion keeping the gas mass flux constant and similar to Figures 6.8 and 6.9. Figure 6.10 shows that the expanded bed height is independent of the inlet hot water temperature and that it increases linearly with increasing liquid mass flux. As the liquid rate is increased, the liquid holdup and the interfacial activity increase. This gives rise to high turbulence levels and hence the bed expands. Since the spray cone angle is small, and the *H/V* ratio is less than 4, the droplets are concentrated in the centre of the bed with negligible wall effect causing an increase in the bed inertia. Therefore the bed expansion increases. Moreover, the density of the particles is relatively high with the effect that no congregation of the particles occur at the column wall. This enhances the bed expansion as the liquid mass flux is increased. The inlet water temperature has no effect possibly due to the visual nature of bed expansion measurements.

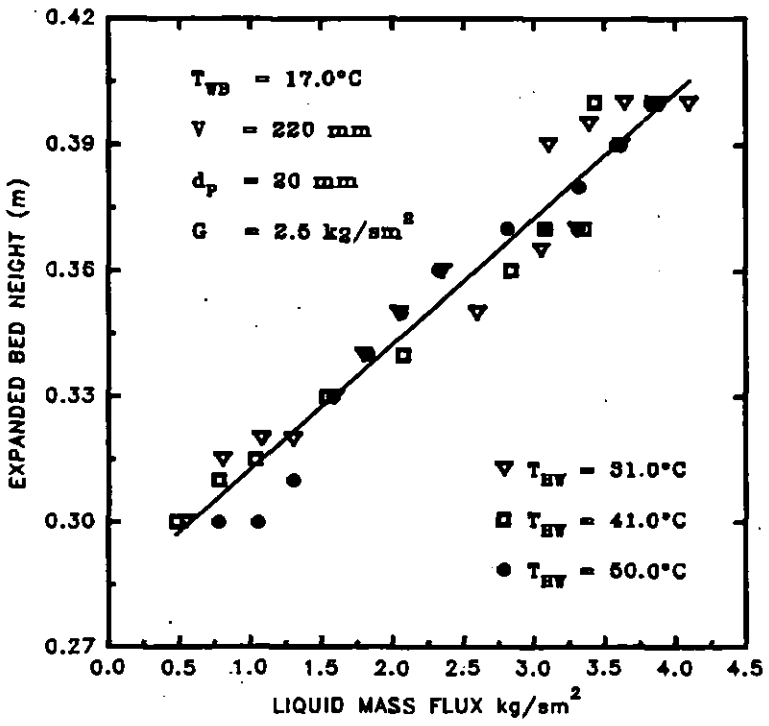

Figure 6.10 Effect of the liquid mass flux and the inlet liquid temperature on the expanded bed height. ρ_p = 239 kg/m^3. Fine droplet spray nozzle.

Figure 6.11 below corresponding to Figure 5.10, shows the effect of the liquid flow rate and the particle density upon the expanded bed height. It shows that the expanded bed height increases as the density of the particles is decreased for the same liquid mass flux, norminal sphere diameter and static bed height keeping the gas mass flux constant. This is due to increased weight of the bed. For similar experimental conditions, the amount of energy transmitted by the air on to the bed is higher for the particles with a lower density since the resistance to motion of the air is lower. Therefore, the bed exhibits a higher expanded bed height. This is not in agreement with the work of Tichy *et al.* (1972) who reported an independence of the bed expansion of the particle density. This discrepancy may be attributed to their very high *H/V* ratio with the effect the most of the liquid flows on the side of the wall causing only a limited effect of the density upon the bed expansion. Moreover, their gas mass velocities of about 1 to 3 kg/s m^2 were relatively low as compared to their liquid mass fluxes of between 5 to 33 kg/s m^2. This may have counteracted the effect of the particle density upon the expanded bed height. Additionally, methods of measurement of the expanded bed heights were different. This may have caused differences in response of the bed expansion to changes in the particle density.

Figure 6.11 also shows that the bed expansion increases as the liquid mass flux is increased and that the trend of increase is similar in both cases of particle densities. The increase is initially proportional but increases rapidly at the higher bands of the liquid mass flux. The linear increase is expected as the liquid holdup and hence the interfacial activity increases as the liquid mass flux is increased. Since the liquid distribution within the bed improves as the *H/V* ratio is decreased, the expanded bed height increases. The rapid increase in the expanded bed height may also be due to the high gas mass flux that approaches the "true" flooding or maximum velocity that is characterised by high interfacial activity of type I and II regimes. Strumillo *et al.* (1974) and Balabekov *et al.* (1969) using relatively large and heavy particles and relatively large liquid mass fluxes obtained similarly rapid bed expansion at velocities close to the flooding velocity of the bed.

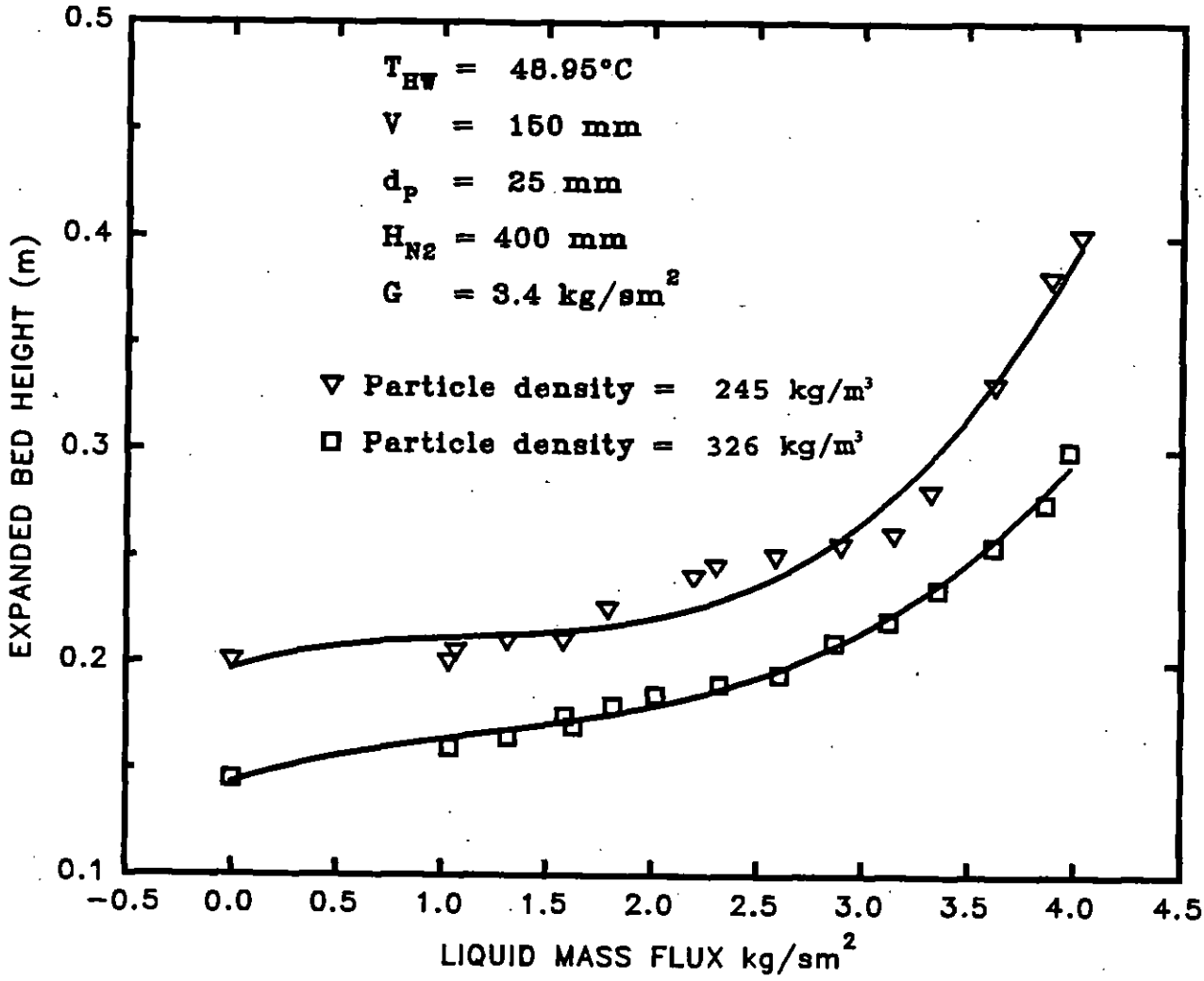

Figure 6.11 Effect of the liquid mass flux and the particle density on the bed expansion. Fine droplet spray nozzle.

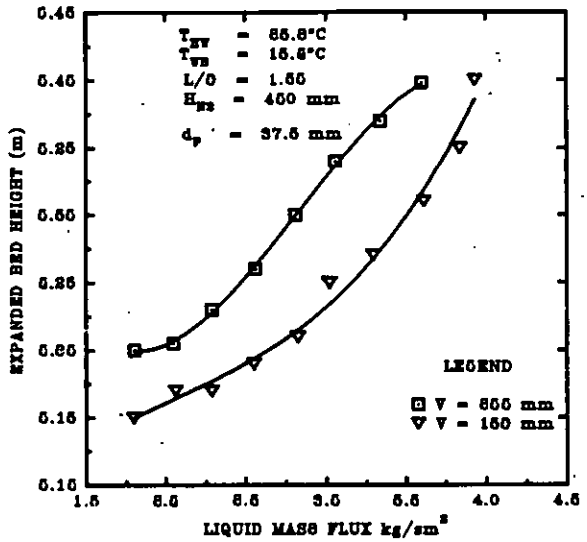

Figure 6.12a Variation of the bed expansion with the liquid and gas mass flux and the static bed height. ρ_p = 69 kg/m^3. Fine droplet spray nozzle.

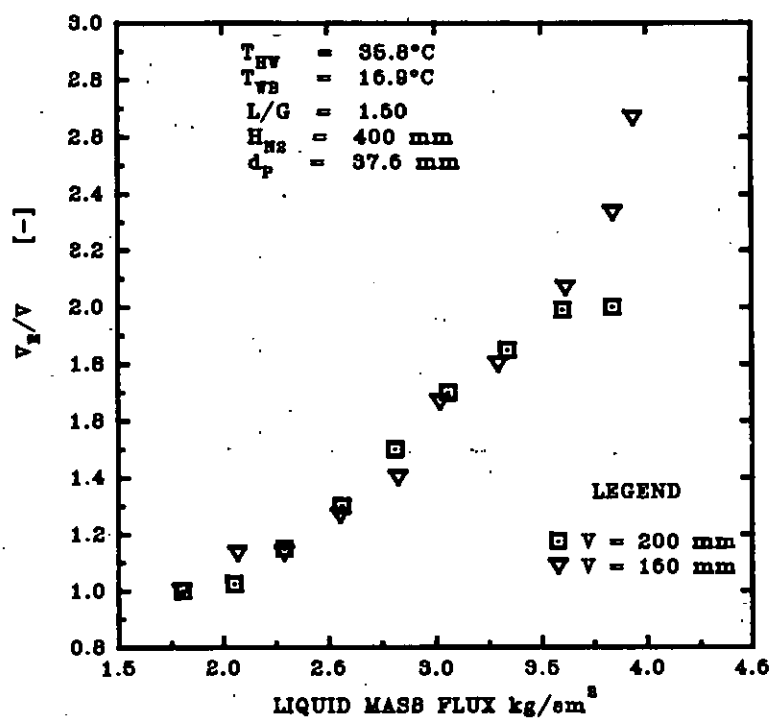

Figure 6.12b Dimensionless bed expansion vs the liquid mass flux corresponding to Figure 6.12a.

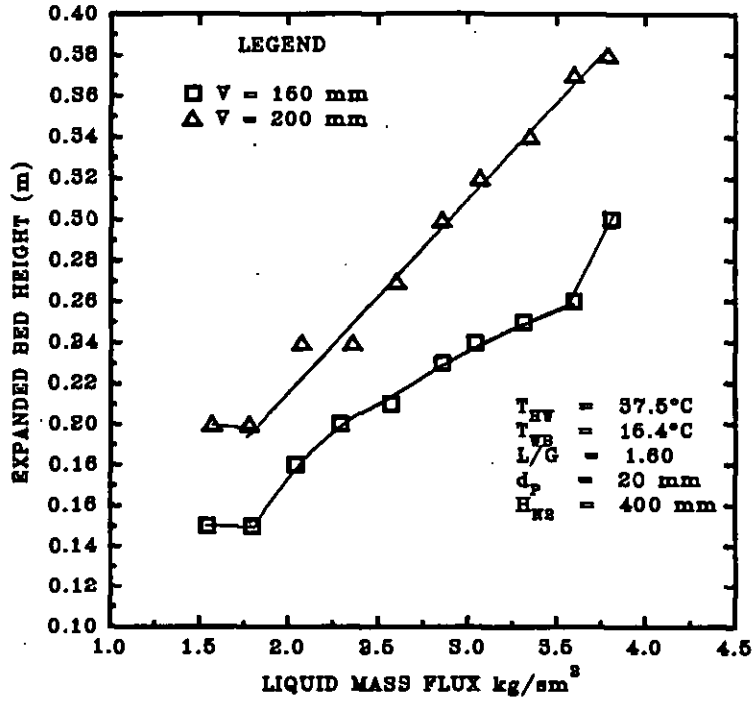

Figure 6.13a Variation of the bed expansion with the liquid and gas mass fluxes and the static bed height. ρ_p = 239 kg/m^3. Fine droplet spray nozzle.

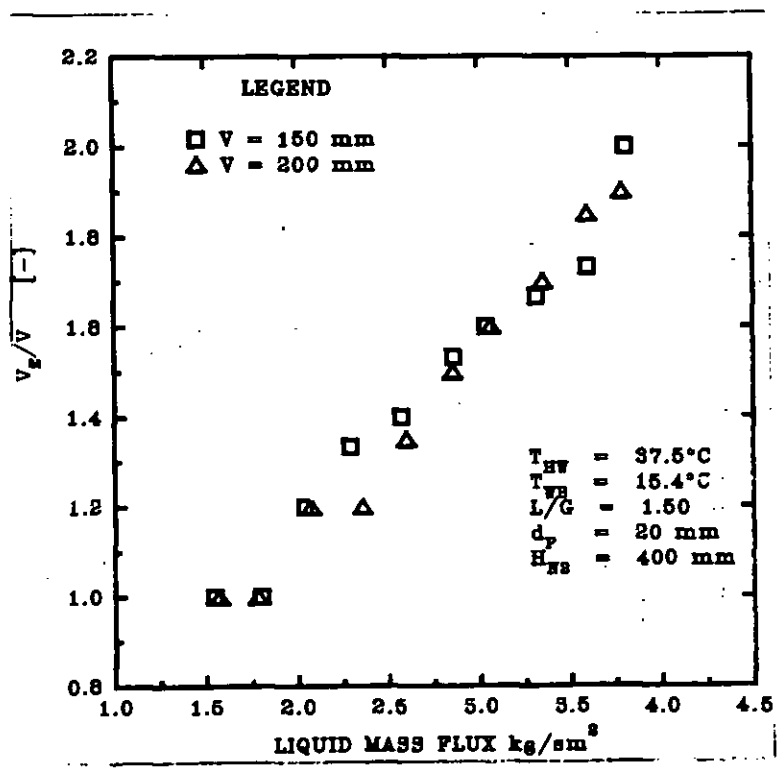

Figure 6.13b Dimensionless bed expansion vs the liquid mass flux corresponding to Figure 6.13a.

Figures 6.12a and 6.13a, corresponding to Figures 5.24 and 5.25, show the effect of both the liquid and gas mass fluxes and the static bed height upon the bed expansion. They show that the expanded bed height increases when the liquid and gas mass fluxes are simultaneously increased. This is expected as the power transmitted to the bed increases as the gas mass flux is increased. At the same time, the degree of agitation increases as the liquid mass flux is increased due to increases in the liquid holdup. The combined effect is a sharp and linear increase in the bed expansion as the both parameters are simultaneously increased. The break point in Figure 6.12a is due to the absence of bed expansion before the minimum fluidisation velocity is reached. Figures 6.12a and 6.13a also confirm our earlier findings in section 6.2 that the bed expansion increases as the static bed height is increased. As discussed previously, this is due to the increase in the number of spheres in the column. Also the actual amount of fluid holdup in the bed increases as the static bed height is increased for the same liquid/gas mass flux ratio. This action increases the interfacial activity and hence the bed expansion. Figures 6.12b and 6.13b show that the dimensionless bed height is independent of the static bed height. This conforms to our earlier findings in section 5.2 that as the static bed height is increased, the dimensionless parameter V_E/V decreases until it becomes independent of the static bed height.

6.4 Effect of the Spray Nozzle Height

Figures 6.14 and 6.15 show the effect of the height of the spray nozzle from the supporting grid and the liquid mass flux upon the bed expansion for the coarse droplet spray and low density particles keeping the gas mass flux constant and at a relatively high value. The expanded bed height generally increases as the liquid mass flux is increased for the same spray nozzle height. At the relatively low liquid mass flux of 0.8 kg/sm^2, the bed expansion is independent of the spray nozzle height. This may be due to the fact that at a relatively low liquid mass flow rate, the dominant factor for bed expansion is the gas mass flux and therfore the expanded bed height remains unchanged and similar to the effect of the spray nozzle height on a dry bed.

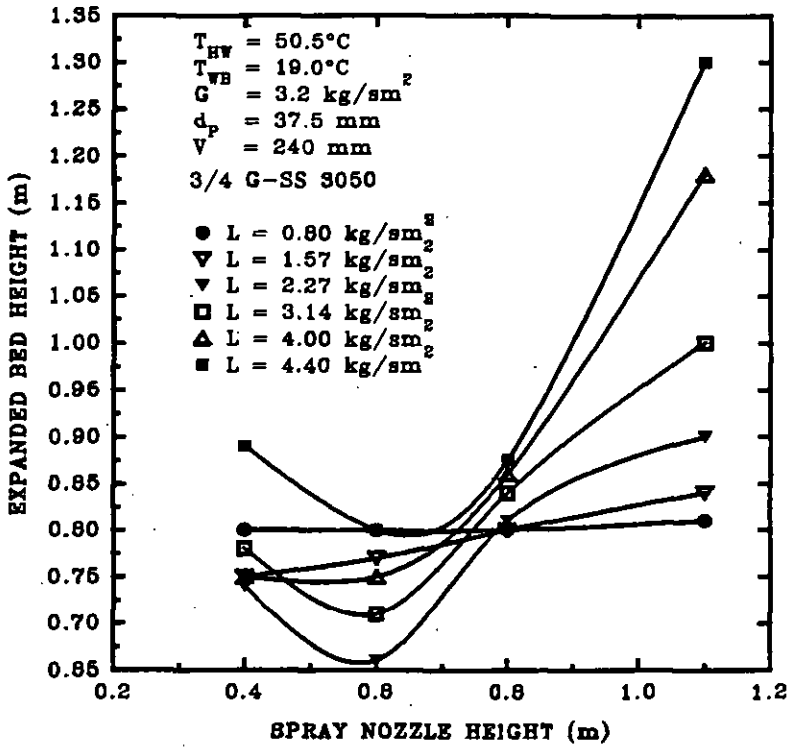

Figure 6.14 Variation of the bed expansion with the spray nozzle height and the liquid mass flux for Type I operation. ρ_p = 69 kg/m^3. Coarse droplet spray nozzle.

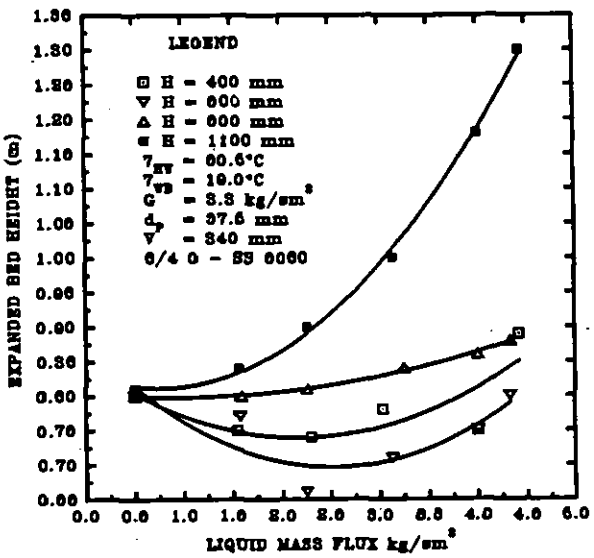

Figure 6.15 Cross plot of Figure 6.14.

As the liquid mass flux is increased to 1.57 kg/s m^2, the bed expansion increases slowly and linearly as the spray nozzle height is increased. As the spray nozzle height increases, the freeboard increases thus increasing the residence time of the

liquid in the bed. The effect is an increase in the liquid holdup in the bed for the same liquid mass flux. This is accompanied by an increase in bed agitation which in turn increases the interfacial activity and hence leads to increased bed expansion. As the liquid mass flux is increased further to 2.27 kg/s m^2, the bed initially expands slowly and then sharply as the spray nozzle height is increased.

Similarly, above the latter liquid mass flux, the expanded bed height decreases, passes through a minimum value and then increases sharply. As the spray nozzle height is increased, the spray cover area increases thereby increasing the probability of the liquid droplets coming into contact with the particles. However, the particle density is low so that an increased bed expansion, which normally follows an increased interfacial tension as a result of increased liquid holdup is counteracted by the downward momentum of the liquid spray. As the spray nozzle height is increased further a threshold value is reached whereby the upward flowing momentum of the air overcomes this resultant downward momentum of the liquid spray because the interfacial tension in the bed increases as a result of increased liquid holdup. The bed expansion therefore passes a minimum value and then starts to increase. The rapid increase of the expanded bed height at relatively high liquid mass flux may have been due to the increased tower working volume and hence increased possibility of gas-liquid-solid contact, the tendency for bed particles and liquid to be blown out of the contacting zone due to increased liquid holdup and the enhanced chances for the bed to reach its maximum fluidisation gas velocity and attaining "true" flooding state.

Figure 6.15 is a crossplot of Figure 6.14. It shows that in the range of the spray nozzle height of 400 to 800 mm, the bed expands slowly as the liquid mass flux is increased. This may have been due to limiting interfacial activity that may occured as the tower working volume is varied at a relatively high gas mass flux. However, at the spray nozzle height of almost 1100 mm, the bed expansion increases almost linearly at low liquid mass fluxes and then sharply as the liquid mass flux approaches high values. Since the gas mass velocity approaches the maximum value, droplets

and particles have the tendency to be blown out of the contacting zone as the liquid flow rate is increased. This effect becomes significant as the liquid mass flux becomes high for relatively low density particles since both the degree of agitation and the bed expansion increase.

Figures 6.16 below shows the effect of the spray nozzle and static bed heights upon the expanded bed height at a relatively high constant gas mass flux for a type II operation. Compared to Figures 5.14 and 5.15, the expanded bed height is generally smaller in value for similar static bed heights. This may have been due to the higher density of the particles since it has been shown in our earlier findings that the bed expansion increases as the density of the particles is decreased.

Figure 6.16 also shows that the expanded bed height increases as the static bed height is increased. In the range of static bed heights of 0 to 150 mm, the expanded bed height is almost independent of the spray nozzle height. As the spray nozzle height is increased, the residence time of liquid in the bed increases and hence the liquid holdup. Since the minimum fluidisation velocity is reached before the flooding point for a type II operation, an increased liquid holdup is would normally stimulate high interfacial activity at a gas velocity close to that of flooding. However, this may not be the case for shallow bed depths because the possibility of high interfacial activity is restrained due the small number of spheres per unit volume of the entire tower resulting in reduced turbulence levels. The expanded bed height therefore stays constant as the spray nozzle height is increased. Moreover, as the spray nozzle height is increased, the wall effect upon the liquid becomes significant at shallow bed heights. The effect is a reduction in the amount of liquid that makes contact with the particles and hence a decrease in the liquid holdup. The result is a reduction in turbulence levels and therefore a slow decrease in the expanded bed height. In the range of static bed heights of 200 and 250 mm, the bed height increases, passes through a maximum value and then decreases slowly as the spray nozzle height is increased. This effect may be attributed to an increased liquid holdup that accompanies an increase in the static bed height especially in relatively heavy

particles. Increased liquid holdup means increased turbulence levels and hence increased bed expansion. As the spray nozzle height is increased further, the wall effect becomes significant causing a fall bed expansion.

Figure 6.17 above, corresponding to Figure 6.16, shows a log-log plot of the dimensionless expanded height to static bed height ratio V_E/V, against the spray nozzle height to the static bed height ratio H/V. It confirms that the expanded bed height increases, reaches a maximum value and then decreases as the spray nozzle height is increased. In addition, it further confirms that the dimensionless ratio V_E/V decreases as the static bed height is increased. It is also in line with our earlier finding that the effect is much more significant at relatively shallow bed heights.

6.5 Effect of Spray Nozzle Configuration

The study of the spray nozzle configuration in relation the bed expansion is essential because it affects the liquid distribution in the bed and therefore the residence time of the liquid in the bed. The liquid residence time in turn affects the liquid holdup and hence the interfacial activity. Since the degree of interfacial activity affects the level of turbulence, the nozzle spray type may also affect the bed expansion.

Figures 6.18 to 6.21 show the effect of the spray nozzle type and the liquid mass flux upon the expanded bed height for both type I and II FBCT operations keeping the H/V ratio constant. Figure 6.18 is a type II regime and corresponds to Figure 5.15 in chapter V. It shows that, the expanded bed height increases as the spray droplet size and roughness increase. One of the reasons for this behaviour may be attributed to the increased liquid holdup as the droplet size is increased as discussed in section 5.4 in chapter V. Moreover, the increased rate of evaporation and entrainement at high gas mass fluxes associated with fine small droplet sprays means that only a proportion of the liquid reaches the fluidised bed. Therefore, the level of turbulence is lower for fine spray droplets as compared to coarse spray droplets. Another reason for this behaviour may be linked to the liquid distribution in the bed.

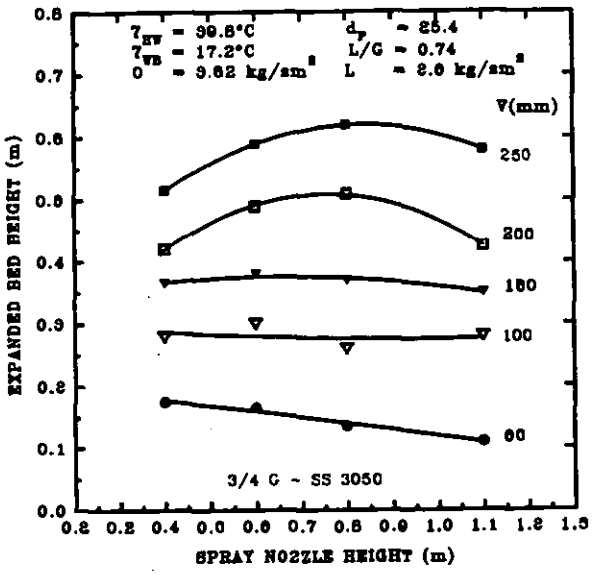

Figure 6.16 Effect of the spray nozzle height and the static bed height upon the expanded bed height for high density particles. $\rho_p = 326$ kg/m^3. Coarse droplet spray nozzle.

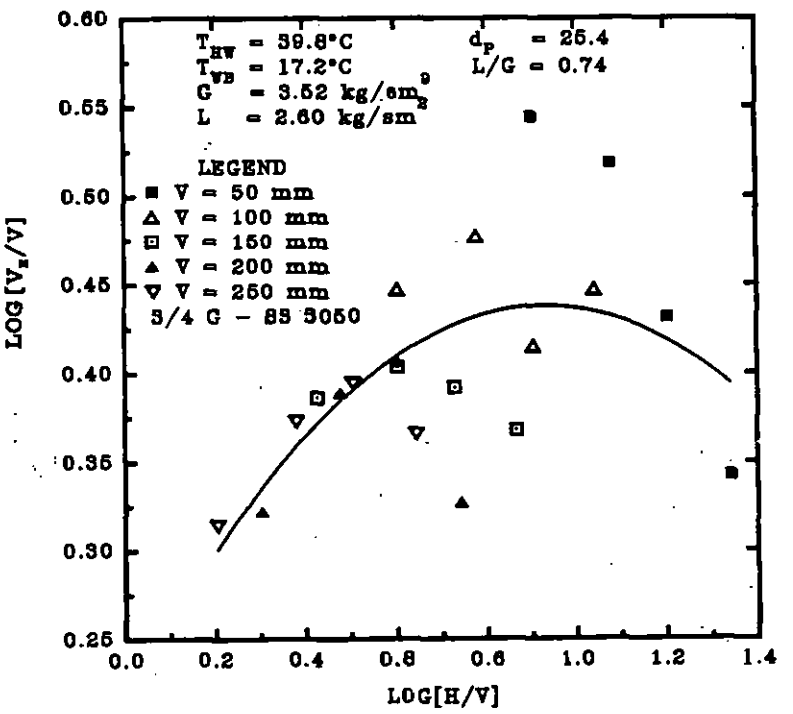

Figure 6.17 Dimensionless expanded bed height to static bed height ratio vs dimensionless spray nozzle height to static bed height ratio corresponding to Figure 6.16.

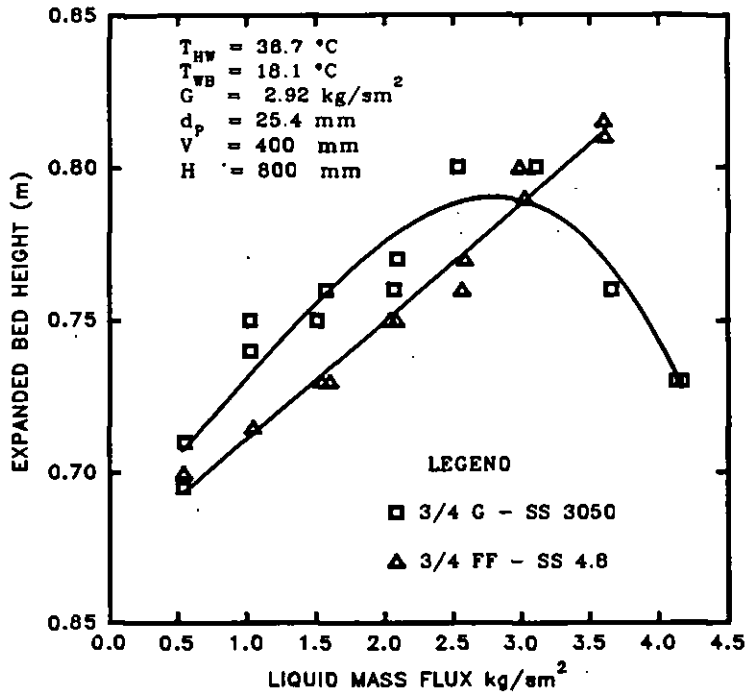

Figure 6.18 Effect of the liquid mass flux and the spray nozzle configuration upon the expanded bed height. ρ_p = 326 kg/m^3.

Since the nozzle producing the coarse spray has only one orifice, the spray is concentrated in the middle of the bed as compared to the fine spray nozzle which has twelve orifices and giving a much more uniform liquid distribution. The concentration of large coarse droplets in the middle means that the force of impact per unit area of the bed is higher than for fine small droplets for the same liquid mass flux. Therefore, the turbulence level is higher for coarse large droplets than for fine small spray droplet. The effect is a higher bed expansion for the coarse large droplets as compared to the fine spray.

For the fine spray, the expanded bed height linearly increases as the liquid mass flux is increased. For the coarse spray, the expanded bed height increases, passes through a maximum value and then decreases. As the liquid flow rate reaches an optimum value, increases in the liquid holdup, the gas-liquid interfacial tension and therefore the expanded bed height are counteracted by the downward force of the spray concentrated at the centre of the bed. This action causes the expanded bed height to decrease. This phenomenon does not occur when fine spray is in use because of the

much more even distribution of droplets within the bed. This accounts for differences in the expanded bed height for the two different spray configurations.

Figure 6.19 below shows the effect of the liquid mass flux and the spray nozzle configuration on the bed expansion for a type II FBCT regime keeping the gas mass flux constant but at a lower value than in Figure 5.58 to take into consideration the lower spray nozzle height. The ratio $H/V = 2$ remains the same. As in Figure 6.18, the expanded bed height increases almost linearly as the liquid mass flux is increased due to increases in the liquid holdup. In the range of liquid flow rates of about 0.5 to 2 kg/s m^2, the expanded bed height is higher for the large and coarse than for fine and small droplet spray for the same liquid mass flux. This may have been due to a higher concentration of coarse droplets in the centre of the bed as earlier explained. As the liquid mass flux is increased further, a limit is reached whereby the liquid residence time starts to decrease since the liquid passes through the middle of the bed without taking a significant part in the interfacial activity. On the contrary, the

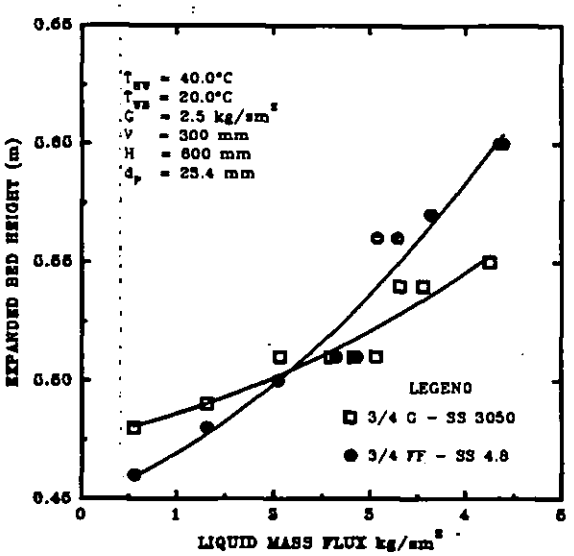

Figure 6.19 Effect of the liquid mass flux and the spray nozzle configuration upon the expanded bed height for type II FBCT operation at low spray nozzle height. ρ_p = 326 kg/m^3.

the good liquid distribution obtained for the fine small droplet spray ensures a higher residence time of the liquid in the bed thus higher liquid holdups and turbulence levels as compared to the coarse large droplet spray. After this point has been surpassed, therefore, the expanded bed height obtained for the fine small droplet spray is higher than for coarse large droplet spray. The band of liquid mass flux where this limit applies is longer in Figure 6.18 than for Figure 6.19. This may be due to the higher gas mass flux and the spray nozzle height of the latter as compared to the former. A higher gas mass flux and spray nozzle height ensures that the liquid residence time in the bed is higher since the expanded bed height increases as the spray nozzle height and the gas mass flux are increased. Moreover, as the spray nozzle height is increased, the base cover area of the coarse spray increases thus reducing the downward force per unit area of the spray upon the bed.

Figures 6.20 and 6.21 above show the effect of the liquid mass flux and the spray nozzle configuration upon the expanded bed height for type 1 FBCT operations. Several experimental conditions in these Figures were similar to those of Figure 5.58. In contrast to Figure 6.18 and 6.19. Figure 6.20 shows that the expanded bed height decreases as the liquid rate is increased, passes through a minimum value and then increases. At relatively low liquid mass fluxes, the total weight of the bed is low because of the low density of the particles. Therefore, the upward force transferred by the air to the bed overcomes the downward force of the bed. As the liquid rate is increased further, the expanded bed height decreases further as the weight of the bed increases and counteracting the upward flowing force of the air. Further increases in the liquid mass flux is accompanied by an increase in the liquid holdup and turbulence levels in the bed. Thus, the expanded bed height increases as the liquid mass flux is increased.

In contrast to Figure 6.18 and 6.19, the expanded bed height increases as the spray configuration is varied from coarse large droplet spray to fine small droplet spray for the same liquid mass flux. The concentration of the coarse large droplet spray in the middle of the bed creates a hollow region in the middle of the bed since the density

of the particles is low. This action results in a reduction in the liquid residence time in the bed thus reducing the liquid holdup and the interfacial activity causing the bed expansion to be lower than when fine small droplet spray is in use.

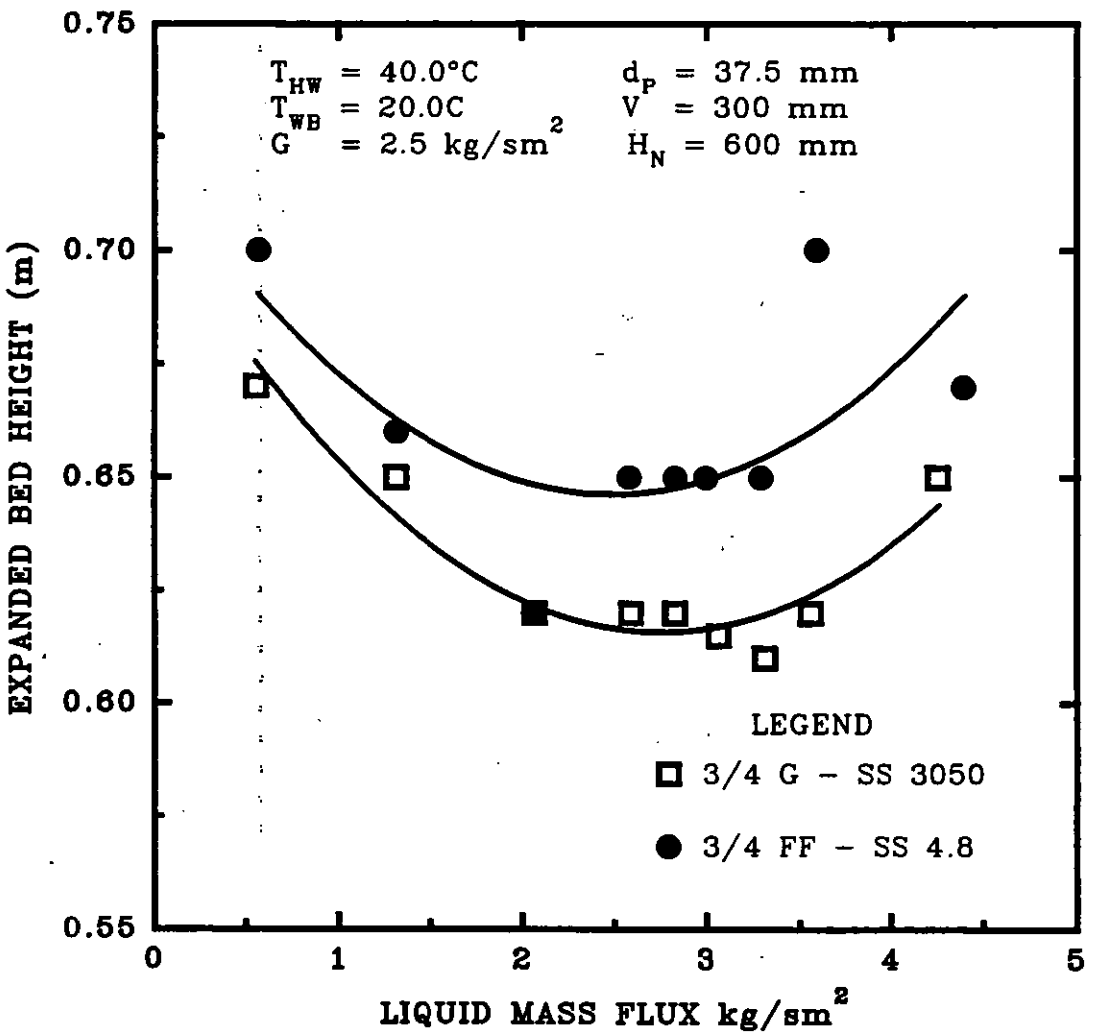

Figure 6.20 Effect of the liquid mass flux and the spray nozzle configuration upon the expanded bed height for type I operation. ρ_P = 69 kg/m^3.

Figure 6.21 is similar to Figure 6.20 in terms of the dependence of the expanded bed height upon the spray nozzle configuration. However, the difference in bed expansion is higher in the range of liquid mass flux of about 0.5 to 3.0 kg/s m^2. For the coarse

large droplet spray, the expanded bed height remains almost constant in this range and then it increases as the liquid mass flux is increased further. This behaviour may be attributed to fluidisation anomalies associated with low density particles as explained in sections 5.1 and 5.2 of chapter V. The congregation of some of the particles at the wall reduces the chances of the bed obtaining its full expansion potential. This situation is less significant in Figure 6.21 because the density of the particles is higher as compared that in Figure 6.20. The increase in the bed expansion as the liquid mass flux is increased beyond 3 kg/s m^2 may partly be due increased bed turbulence levels that are associated with increased liquid holdups as a result of the increase in the density of the particles. Slightly uniform fluidisation was attained because the fine droplets enhanced even liquid distribution and hence slightly uniform bed expansion. This may account for differences between the two spray types in relation to bed expansion at low and high liquid mass fluxes. Similar explanations may be applied to Figure 6.22 and 6.23 which illustrate the effects of the nozzle configuration upon the bed expansion for types I and II regimes. The reduction in the expanded bed height when the gravity spray is in use may be due to the fact that the liquid is prayed into the top of the tower almost purely by gravity at atmospheric pressure. Therefore, although the liquid distribution is best, the force per unit area of the spray is smallest because the number of orifices is highest. As a result, the decree of turbulence and interfacial activity is constrained causing a more restrained fluidised bed.

6.6 Comparison of the Present Work with other Data

It was necessary to compare the present data with the work of other investigators so as to substantiate our hypothesis in relation to bed expansion. Figure 6.24 shows the variation of the dimensionless expanded bed height/static bed height ratio V_E/V, with the superficial gas velocity for the present work and those of other investigators. It shows a similar trend in that the bed expansion increases as the superficial gas velocity is increased. In all cases, the expanded bed height increases sharply as the "true" flooding or maximum fluidisation gas velocity is approached agreement with

the findigs of this thesis. The data of Balabekov et al. (1969), Strumillo *et al.* (1974) and Vunjak-Novakovic *et al.* (1987b) show that for similar experimental conditions, the expanded bed height increases as the liquid mass flux is increased. This result is further substantiated by the results of Vunjak-Novakovik *et al.* (1987b). Despite some differences in experimental conditions, their values are similar to those in the present study for similar liquid mass flux values for a type I FBCT operation.

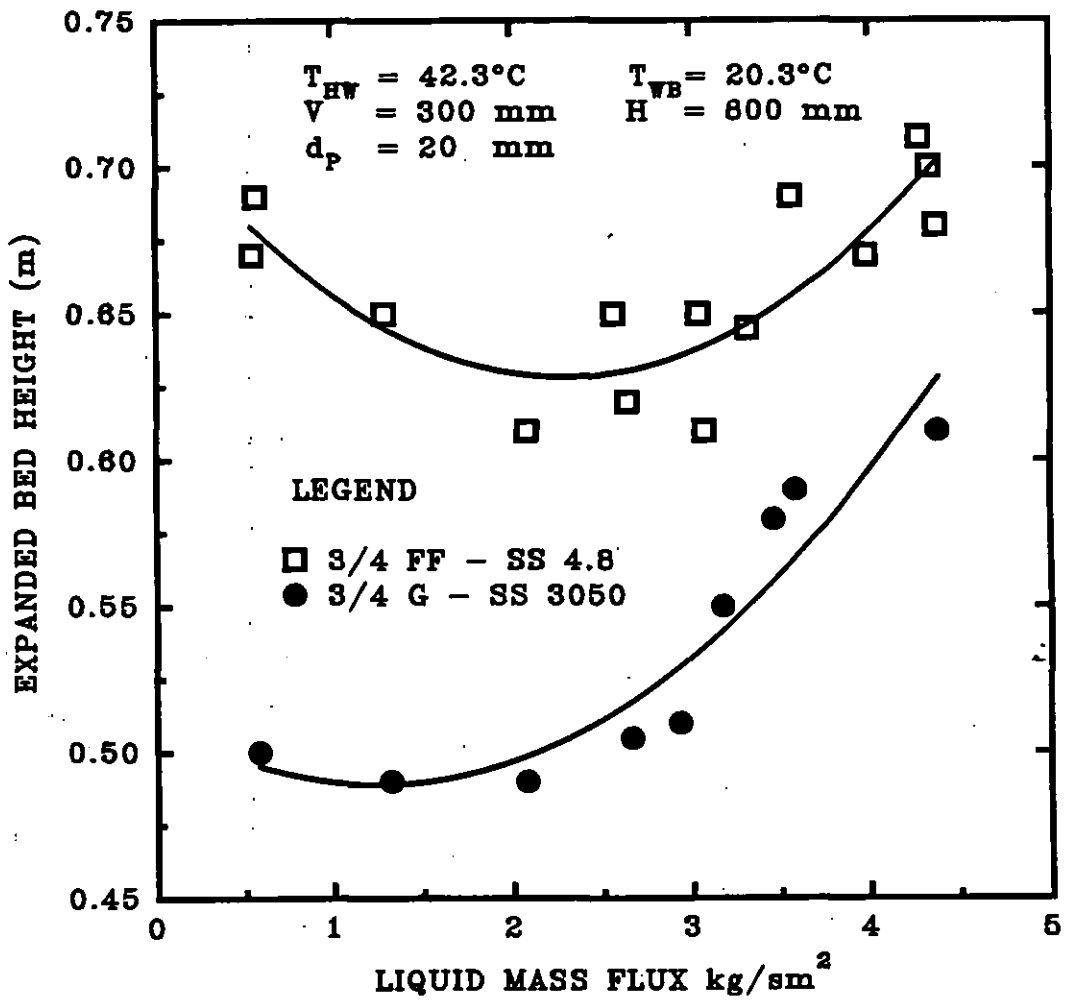

Figure 6.21 Effect of the liquid mass flux and the spray nozzle configuration upon the bed expansion for intermediate particle density. ρ_P = 239 kg/m^3.

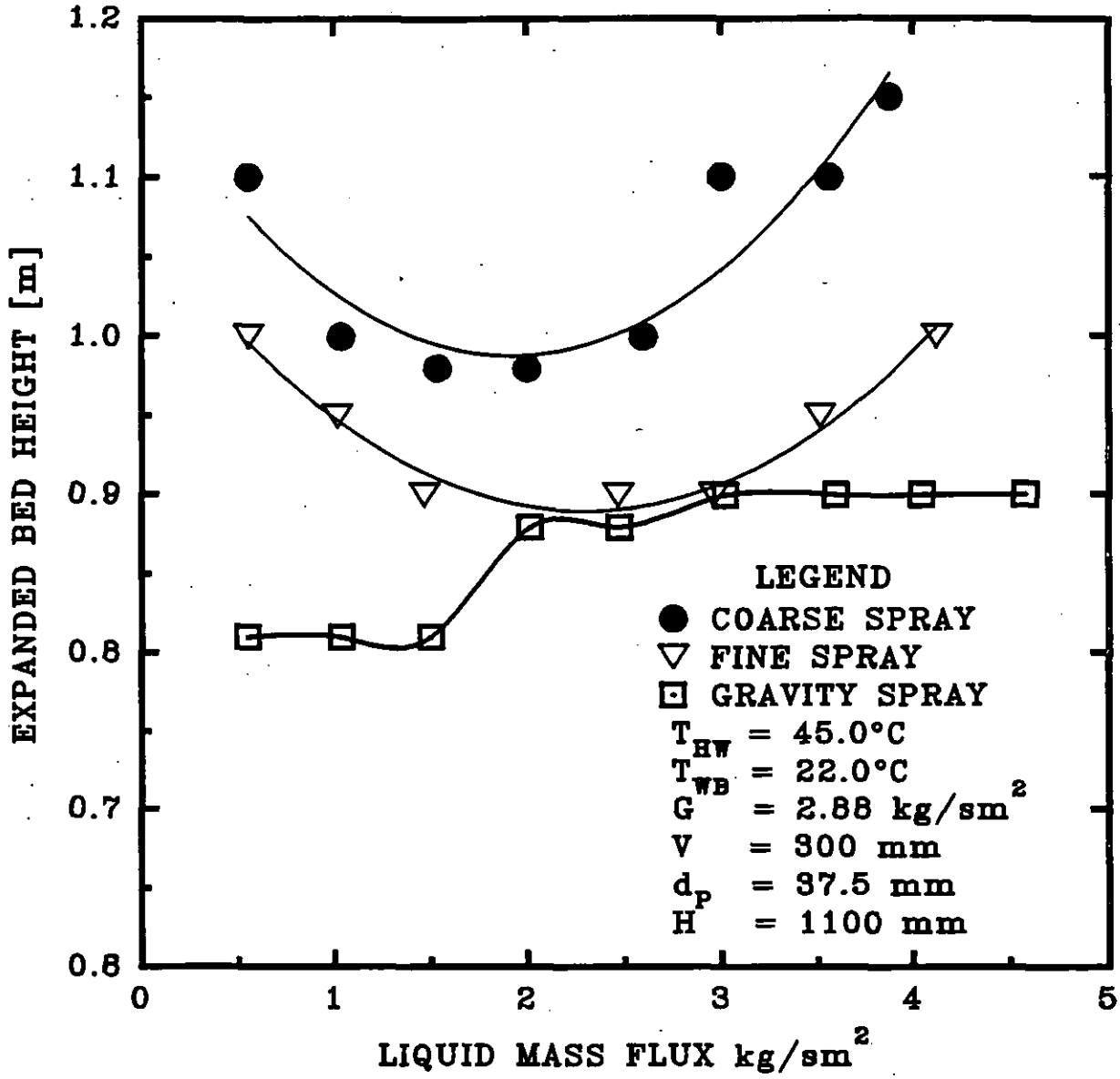

Figure 6.22 Effect of the spray nozzle configuration upon the bed expansion. A comparison of the coarse, fine and gravity spray nozzles for type I FBCT operation. ρ_P = 69 kg/m^3.

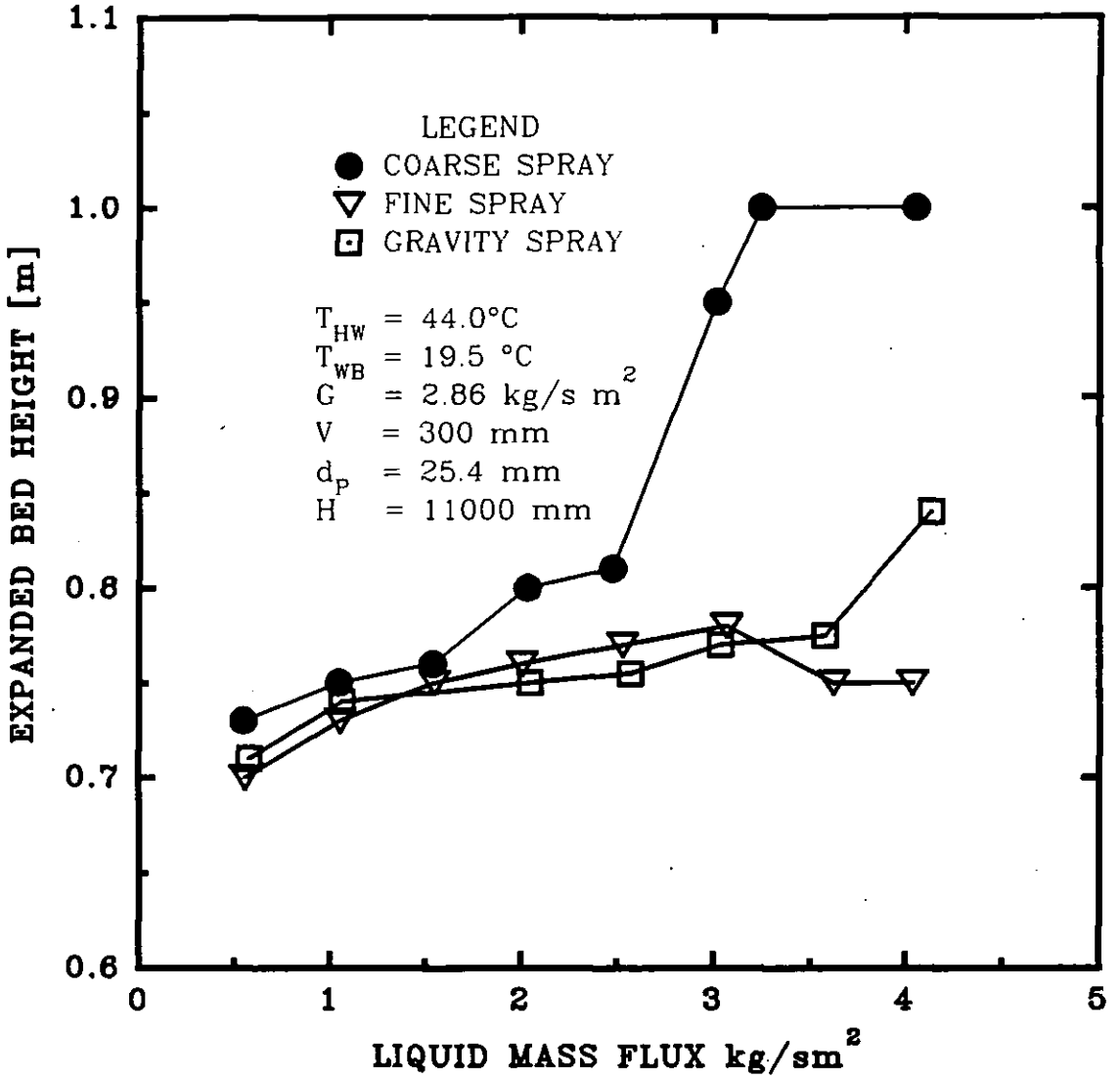

Figure 6.23 Effect of the spray nozzle configuration upon the expanded bed height. A comparison between the coarse, fine and gravity spray nozzles. ρ_p = 326 kg/m^3.

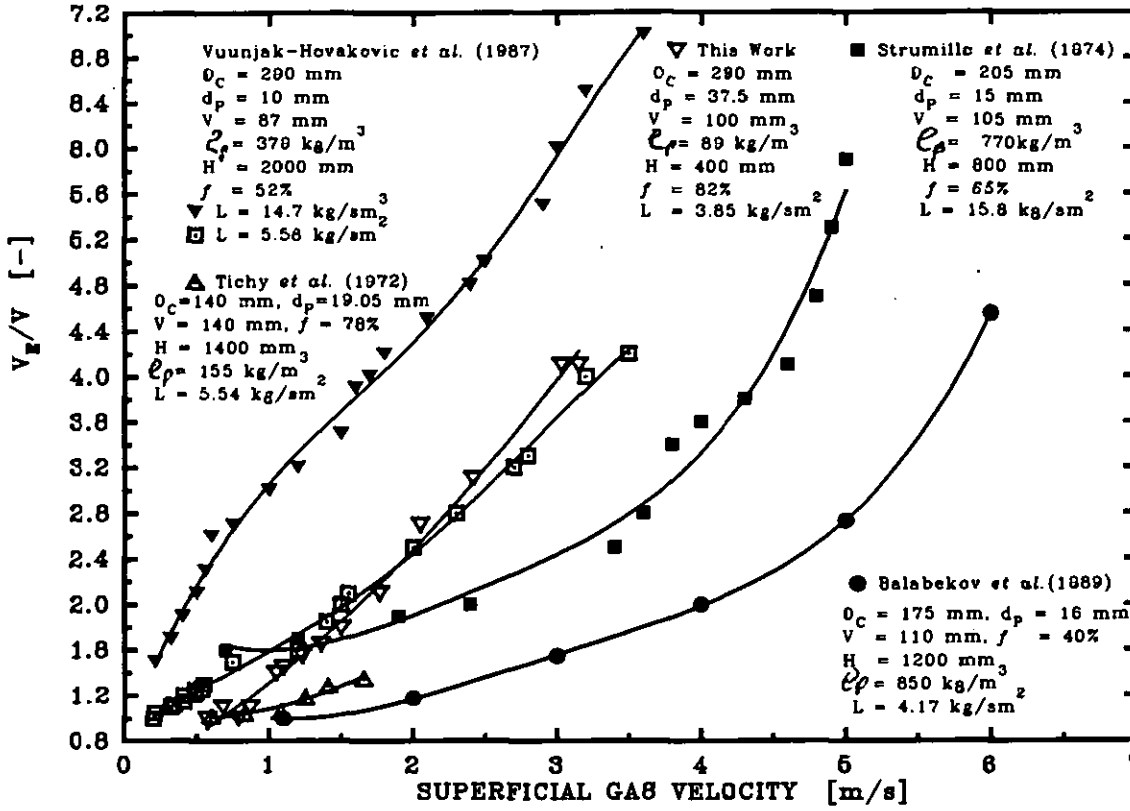

Figure 6.24 Comparison of the present data with those of other investigators.

These findings also add credence to the present work. A comparison of the data of Strumillo *et al.* (1974) with those of Balabekov *et al.* (1969) for similar liquid mass flux values shows that the expanded bed height increases as the particle density is decreased in agreement to our earlier findings.

Also, Vunjak-Novakovic *et al.* (1987b) obtained far higher expanded bed height values than those obtained by Balabekov *et al.* (1987) for similar experimental conditions using a lower density particles than those used by the former for a type

II regime. This may have been caused by differences in the *H/V* ratio. However, it has been shown in section 5.3.4 that the spray nozzle height has only a limiting effect upon the expanded bed height for a type II FBCT regime of relatively high density particles and for shallow bed heights.

A comparison of the data of Strumillo *et al.* (1974) with that of Vunjak-Novakovic *et al.* (1987) for a type II FBCT regime also showed that, for high liquid mass fluxes, the expanded bed height increases as the particle density is decreased. This further supports our result that showed that the expanded bed height increases as the density of the particle is decreased.

It was diificult to compare the present data on bed expansion with those of Tichy *et al.* (1968) because their superficial gas velocities were very close to the minimum fluidisation velocity. Nevertheless, a comparison of their data to the present data for type I operation, shows that the bed expansion increases as the density of the particles is decreased.

5.4 Minimum and Flooding Fluidisation Gas Velocities

The minimum and "true" flooding or maximum fluidisation gas velocities are the limiting parameters for the existence of three-phase gas-liquid-solid counter-current fliudisation.

Figures 6.25 to 6.27 and table 6.2 show the effect of the liquid mass flux upon the minimum fluidisation velocity. They all show that, the minimum fluidisation gas velocity decreases as the liquid flow rate is increased in good agreement with previous investigators.

This behaviour may be attributed to increases in the liquid holdup as the liquid mass flux is increased. Increases in liquid holdups increase the bed gas-liquid interfacial activity causing increased turbulence levels.

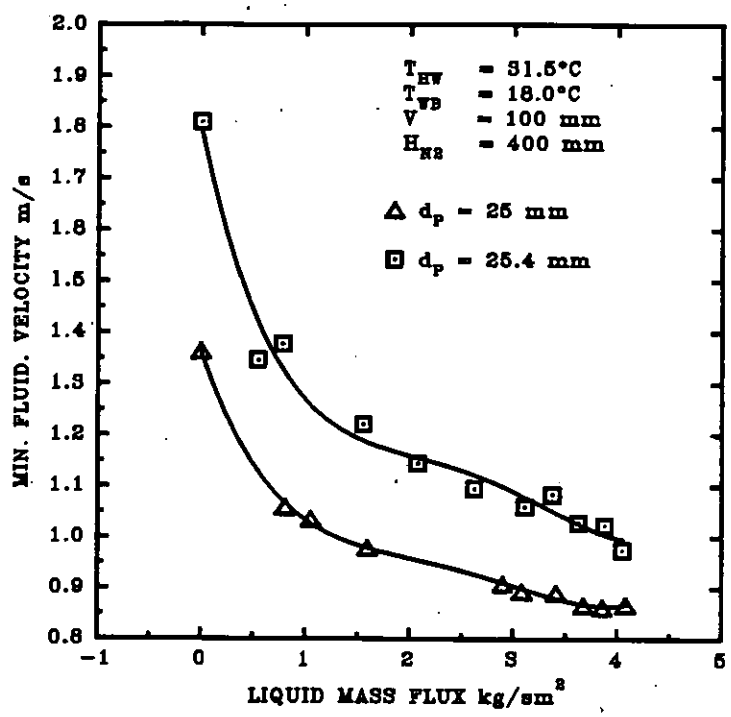

Figure 6.25 Effect of the liquid mass flux and the particle density upon the minimum fluidisation gas velocity. ρ_P = 245 kg/m^3, d_P = 25; ρ_P = 326 kg/m^3, d_P = 25.4 mm. Fine droplet spray nozzle.

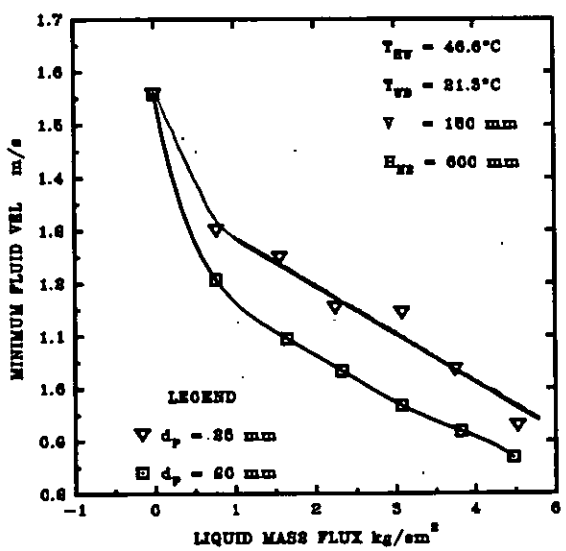

Figure 6.26 Effect of the liquid mass flux and the bed particle diameter upon the minimum fluidisation gas velocity. Nominal ρ_P = 242 kg/m^3. Fine droplet spray nozzle.

V [m]	L [kg/sm^2]	U_{mf} [m/s]	L/G [-]
0.08	0	1.07	0
0.16	0	1.10	0
0.24	0	1.04	0
0.32	0	1.10	0
0.08	1.46	1.04	1.30
0.16	1.54	1.08	1.25
0.24	1.56	1.04	1.31
0.32	1.49	1.07	1.20
0.08	2.05	1.03	1.76
0.16	2.36	1.08	1.93
0.24	2.31	1.04	1.95
0.32	2.31	1.05	1.90
0.16	3.10	1.05	2.60
0.24	3.11	1.04	2.62
0.32	3.02	1.00	2.60
0.08	3.77	1.02	3.26
0.16	3.76	1.00	3.28
0.24	3.83	1.02	3.26
0.32	3.88	0.99	3.39

Table 6.2 Effect of the static bed height upon the minimum fluidisation gas velocity. ρ_P = 69 kg/m^3, d_P = 37.5 mm. Fine droplet spray nozzle.

As the total weight of the bed reaches the total bed air pressure drop and hence the upward air force applied per unit bed area, the bed expands and the minimum fluidisation velocity is reached at a lower air velocity as the liquid mass flux is increased. The the minimum fluidisation gas velocity decreases sharply from 0 to 0.5 kg/s m^2 and then it decreases slowly and almost linearly as the liquid mass flux

is increased. This is because at a liquid mass flux of 0 kg/s m^2, the bed turbulence level is solely dependent upon the gas mass flux in a two-phase gas-solid fluidised bed. The bed turbulence level is therefore lower because of the reduced bed inertia and interfacial agitation than when liquid is present. Therefore, bed requires a higher gas power to expand causing the minimum fluidisation gas velocity to be higher. The linear decrease of the minimum fluidisation gas velocity as the liquid mass flux is increased may be due to the proportional increase of the liquid holdup since the liquid holdup is independent of the gas mass flux during and after the minimum fluidisation has been attained [Barile, 1971; Vunjak-Novakovic, 1987].

Figure 6.25 also shows the effect of the density of the particles upon the minimum fluidisation gas velocity. It shows that the minimum fluidisation gas velocity increases as the particle density is increased. This may be eplained on the basis that as the density of the particles is increased for a particular liquid mass flux, the holdup increases. However, the increased interfacial activity that accompanies an increased holdup is counter-balanced by the increased bed weight. Thus a bed with a lower particle density will expand at a lower superficial gas velocity because the total downward force of the bed is lower thus the bed pressure drop reaches the total weight per unit area of the bed at a lower air power reqirement and hence lower minimum fluidisation gas velocity.

Figure 6.26 shows the effect of the bed particle size upon the minimum fluidisation gas velocity. It shows that, for similar particle densities, the minimum fluidisation gas velocity increases as the particle size is increased. This may be attributed to the increase in initial static dry bed porosity as a result of the reduction of the number of particles per unit static volume as the particle diameter is increased. Therefore, for the same liquid mass flux, the liquid holdup increases as the particle diameter is decreased due to the increase in residence time of the liquid in the bed as a result of a decrease in the interstitial voids that increases path length of the liquid. The bed pressure drop increases due to a decrease in the free flowing area of the bed as the particle diameter is decreased. The higher bed agitation that is expected as the liquid

holdup is increased is therefore counteracted by the increase in the total bed weight. For the bed to reach initial expansion and hence minimum fluidization velocity, the total bed weight per unit bed area must equal the bed pressure drop. Therefore more air power is required to fluidize the bed with smaller particles at the same liquid mass flux causing a lower minimum fluidisation velocity than for beds with a higher particle size.

Table 6.2 above shows the effect of the static bed height and the liquid mass flux upon the minimum fluidisation gas velocity. It shows that the minimum fluidisation gas velocity is independent of the static bed height for the same liquid mass flux in agreement with the findings of EL-Dessouky Hisham (1995). The reason for this particular behaviour is unclear. However, this may be due to the fact that, the downward inertial force of the liquid spray counteracts the effect of increased liquid holdup as the static bed height is increased. Since this force per unit area stays constant irrespective of the static bed height for the same liquid mass flux, the minimum fluidisation gas velocity then remains constant as the static bed depth is varied.

The slow decrease with respect to increases in the liquid mass flux may be attributed the low density of the particles. Low density relatively large particles are susceptible to the effect of the surface tension between the column wall and the wetted particles. This therefore, inhibits initial fluidisation as the liquid flow rate is increased since the particles tend to congregate at the column wall. The relatively high average minimum fluidisation velocity of about 1 m/s is due to the fact that more air power is required to overcome the bed weight as well as surface tension stresses at the column wall.

Figure 6.27 shows a comparison of the present data with those of other investaigators in relation to the effect of the liquid mass flux upon the minimum fluidisation gas velocity. The present data on the minimum fluidisation gas velocity is similar in trend and values to those of other investigators. Figure 6.27 also confirms the present findings that the minimum fluidisation gas velocity is inversely proportional

to liquid mass flux values greater than zero. Differences in values of the minimum fluidisation gas velocity for the same liquid mass flux may have been caused by differences in experimental conditions and methods of measurement.

The relatively high minimum fluidisation velocity obtained by Kuroda *et al.* (1981) may have been caused by his measurement of the minimum fluidisation velocity when the bed pressure drops attains constancy. However, the minimum fluidisation velocity is a region and the beginning of the constancy of the bed pressure drop advances in the transition region as discussed in section 5.1 in chapter V. Therefore, the minimum fluidisation velocity based on the initial bed expansion would be less than that based on total axial pressure variation. The relatively low minimum fluidisation velocity obtained by EL-Dessouky (1993) may have been caused by the very high *H/V* ratio. Assuming that the spray nozzle cone angle is similar to the present study, the wall effect upon the hydrodynamics would be severe and, thus only a fraction of the liquid would reach the bed. The result would be a decrease in the actual liquid holdup in the bed and hence a reduction in the bed weight and the balancing bed air pressure drop. This could have caused the minimum fluidisation gas velocity to be relatively lower than those of other investigators.

Figure 6.28 shows the effect of the liquid mass flux upon the "true" flooding or maximum gas velocty for a type I operation. It shows that the flooding velocity decreases as the liquid mass flux is increased. The most likely explanation for this behaviour may be attributed the increase in the expanded bed height as the liquid mass flux is increased. An increase in the liquid mass flux causes an increase in the turbulence bed level and an increase in the amount of liquid that is transported to the mist eliminator. When the total upward force due to the air is greater than the downward force of the liquid and particles, the droplets and particles congregate at the top of the tower. The "true" flooding or maximum fluidisation gas velocity of high density type II regime was not extensively studied due to limitations of available power for experimental tests.

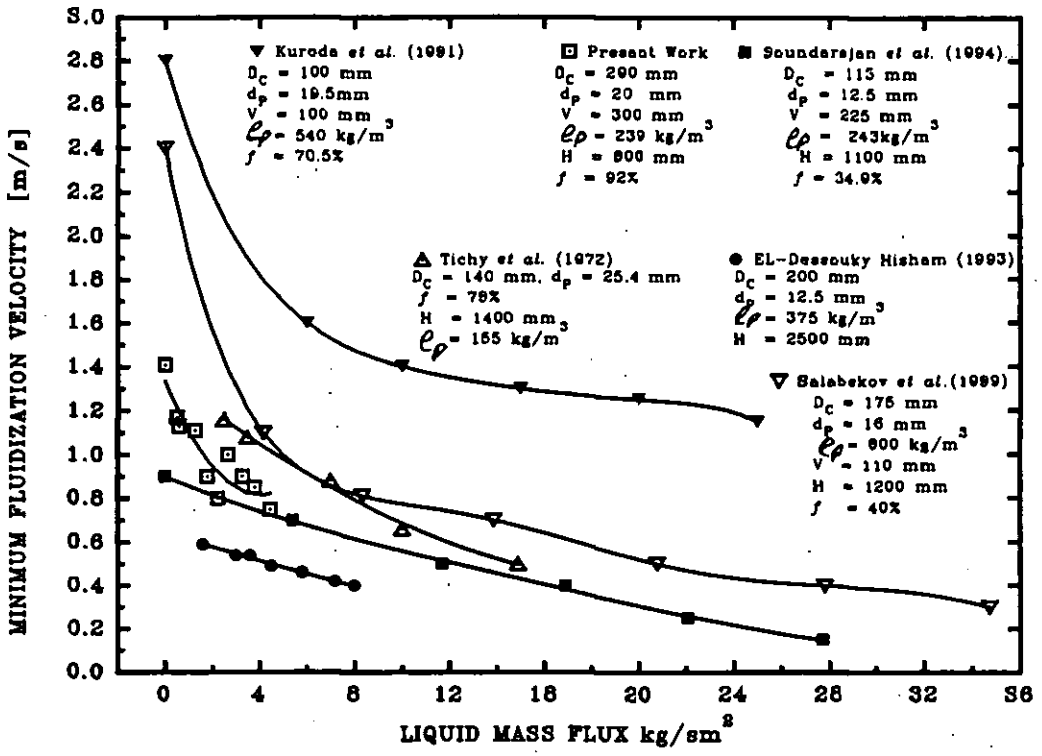

Figure 6.27 Comparison of the present data with those of other investigators for the minimum fluidisation gas velocity.

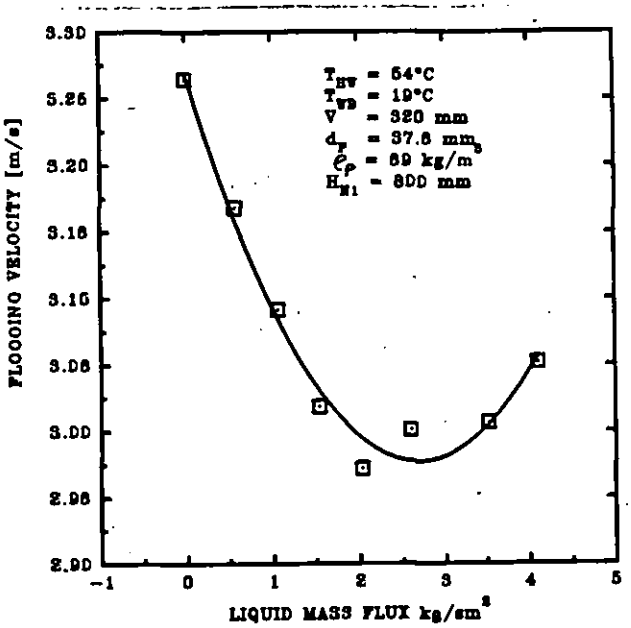

Figure 6.28 Effect of the liquid mass flux upon the flooding gas velocity. Coarse droplet spray nozzle.

CHAPTER VII

EXPERIMENTAL RESULTS: THE EFFECTS OF FLUID FLOW RATES AND INLET WATER TEMPERATURE UPON THE THERMAL PERFORMANCE

7.1 Introduction

The amount of heat and mass transferred in a cooling or heating process partially determines the size of an equipment. Four different methods that were based on three different outlet cooled water temperatures were used to indicate the FBCT thermal performance using nine different independent variables. The present work was then compared with the data of other investigators for both the fluidised bed and conventional fixed cooling towers. The position of the outlet cooled water sensor and end effects significantly affect FBCT thermal performance.

7.2 Effect of the Liquid/Gas Mass Flux Ratio, *L/G*

Figures 7.1 to 7.3 indicate the effect of the variable *L/G* upon the measured outlet cooled water temperature. The cooled water temperature at the grid and plenum increases exponentially as the liquid/gas mass flux ratio *L/G*, increases with both the liquid mass flux and the static bed height held constant as displayed in Figures 7.2 and 7.3. However, a lower cooled water temperature is recorded at the outlet plenum conditions since cooling continued to occur at the tower plenum chamber after leaving the fluidised bed itself. The cooled water temperature decreases as the static bed height is increased due to the higher level of agitation of the bed as a result of increases in the liquid holdup and bed weight.

Figure 7.4 is the temperature enthalpy diagram and corresponds to Figure 7.3 when *L/G* equals 0.75. This depicts the enthalpy potential concept of Merkel (1925). The line AB is the equilibrium or saturation line while CD is the air or operating line with gradient C_w*L/G* in accordance with the first law of

thermodynamics that establishes energy and mass balance. Line BC is the total available enthalpy potential. Numerical integration of the region ABCD results in the tower performance characteristic *KaV/L*. Figure 7.5 is a typical energy balance graph for simultaneous heat and mass transfer based on the outlet cooled water temperature from the tower plenum chamber and showing the rate of heat transfer from water to air. The average error of estimate is ±10%.

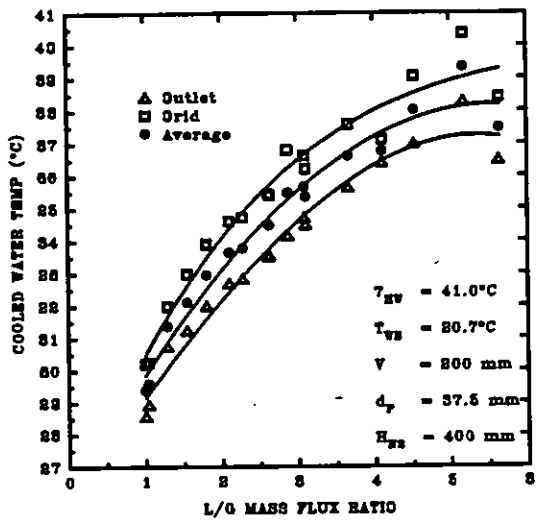

Figure 7.1 Effect of the liquid/gas mass flux ratio upon the outlet cooled water temperature for the fine droplet spray nozzle. ρ_p = 69 kg/m^3.

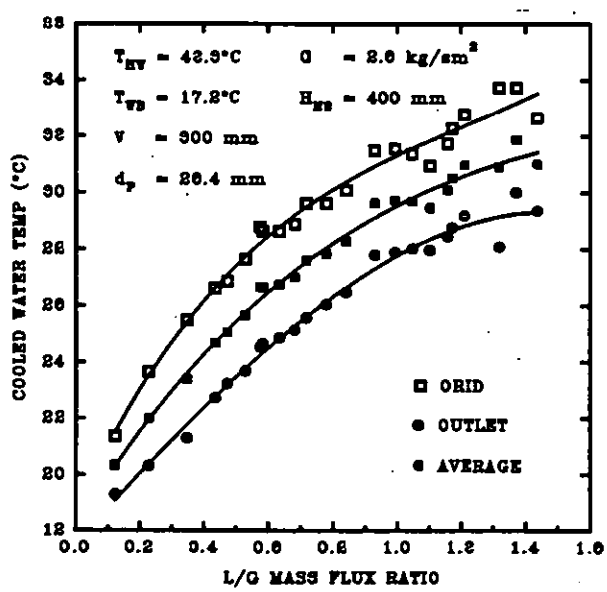

Figure 7.2 Effect of the liquid/gas mass flux ratio and the static bed height upon the supporting grid outlet cooled water temperature for the coarse droplet spray nozzle. ρ_p = 326 kg/m^3.

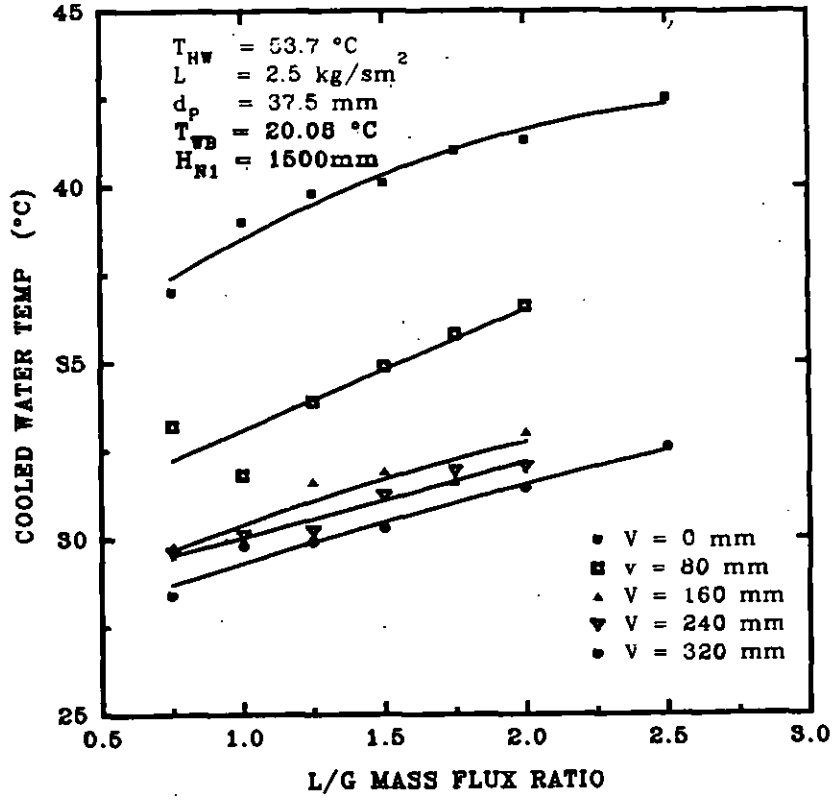

Figure 7.3 Effect of the liquid/gas mass flux ratio and the static bed height upon the supporting grid cooled water temperature for the coarse droplet spray nozzle. $\rho_P \doteq 69$ kg/m^3

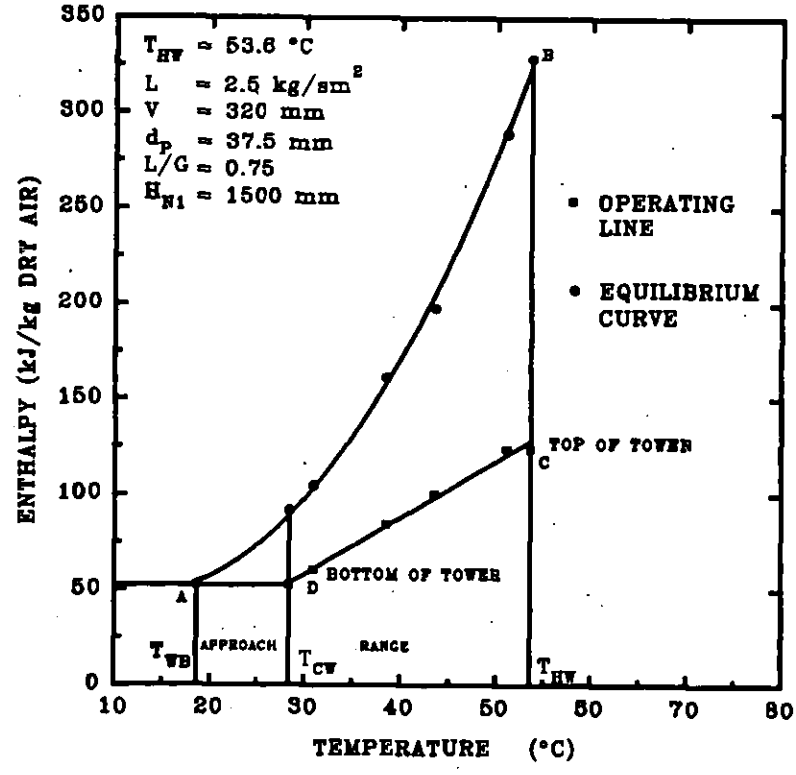

Figure 7.4 Temperature enthalpy diagram based on Figure 7.3 showing energy balance and enthalpy potential.

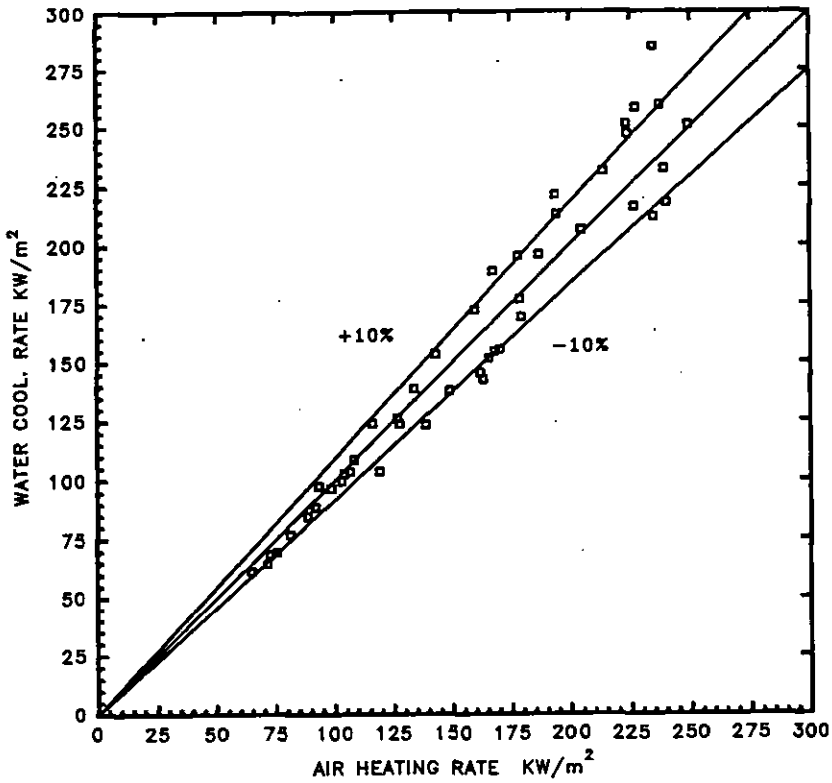

Figure 7.5 A typical Energy balance graph for a sample of 50 out of a total of about 1500 test runs.

7.2.1 Thermal Performance

Figures 7.6 to 7.14 show the effect of the liquid/gas mass flux ratio *L/G* upon the tower characteristic, cooling effectiveness, range and approach. Figures 6.6 to 6.10 show that the tower characteristic decreases as the liquid/gas mass flux ratio *L/G* is increased keeping either the liquid mass or gas flux constant while Figure 6.8 shows that the required tower characteristic increases as the liquid/gas mass flux ratio is increased. For a constant liquid mass flux run, a decrease in the gas mass flux tends the FBCT regime towards the minimum fluidisation state and, this is accompanied by a decrease in the degree of turbulence and intimate mixing of fluid and particles. The result is a decrease in interfacial activity and hence heat and mass transfer rate. When the gas flow rate is kept constant, the available tower charactristic also decreases as the liquid/gas mass flux ratio is increased. Figure 7.9 shows that data obtained from the present study is similar in trend and value as those of conventional towers. However, the FBCT is smaller in size than

conventional fixed bed cooling towers for the same liquid/gas mass flux ratio. This is because of the higher mass transfer coefficient generated by intense fluidisation that substantially increases the gas-liquid interfacial area of the FBCT. Figure 7.10 is the log-log plot of Figure 7.9. It also shows that the tower characteristic is directly proportional to the liquid/gas mass flux ratio and that it obeys the power law:

$$\frac{KaV}{L} = C\left(\frac{L}{G}\right)^{n} \qquad (6.1)$$

as stipulated by BS 4485 Part II (1988). Table 6.2 shows that the coeficient and exponents of the FBCT are similar in value to those of conventional fixed bed wet cooling towers. Figure 7.11 to 7.15 show the effect of the liquid mass flux upon the cooling effectiveness. The thermal performance is inversely proportional to the liquid/gas mass flux ratio when both the gas and liquid mass fluxes are held constant. Figure 7.11 shows that the cooling effectiveness increases as the static packing height is increased while Figure 7.12 shows that the cooling effectiveness increases as the inlet hot water temperature is increased.

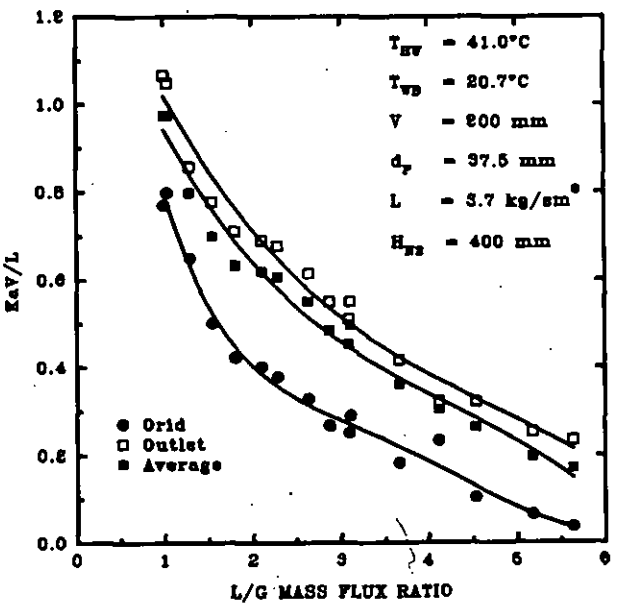

Figure 7.6 Effect of the liquid/gas mass flux ratio on the tower characteristic based on the grid, outlet (plenum) and average cooled water temperatures. The data was calculated from Figure 7.1.

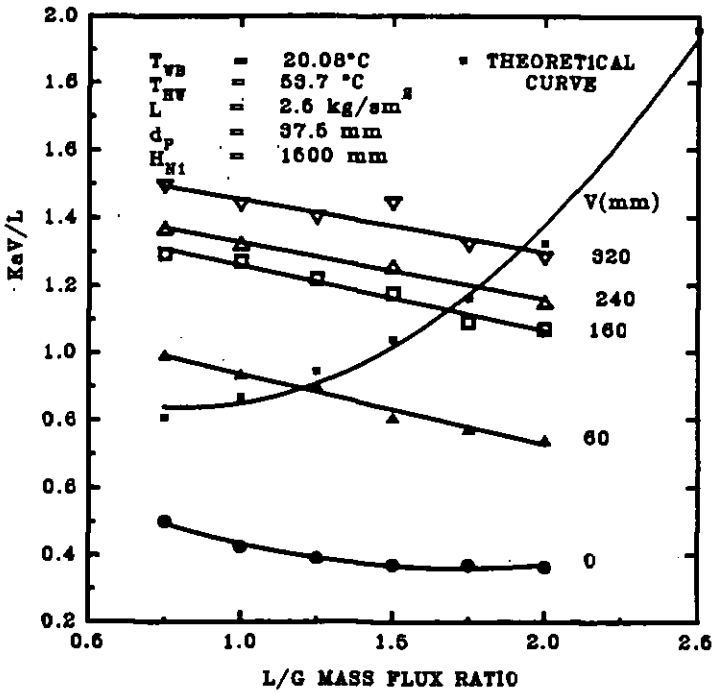

Figure 7.7 Effect of the static bed height and the liquid/gas mass flux ratio upon the available and required tower characteristics based on the supporting grid outlet cooled water temperature. The data was calculated from Figure 7.3.

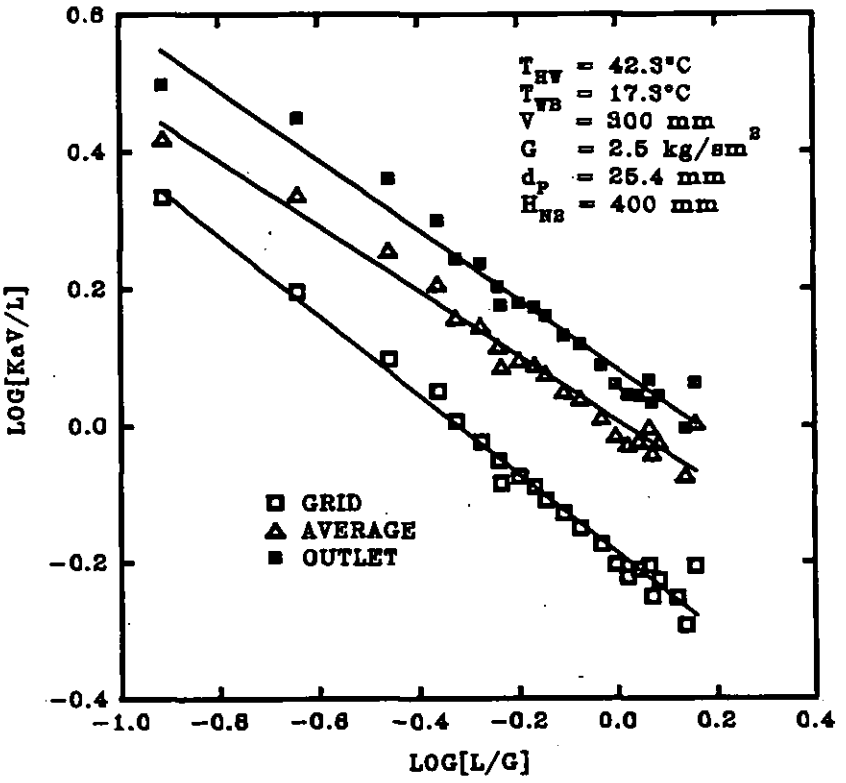

Figure 7.8 Effect of the logarithmic *L/G* upon the logarithmic *KaV/L*. The data was calculated from Figure 7.2.

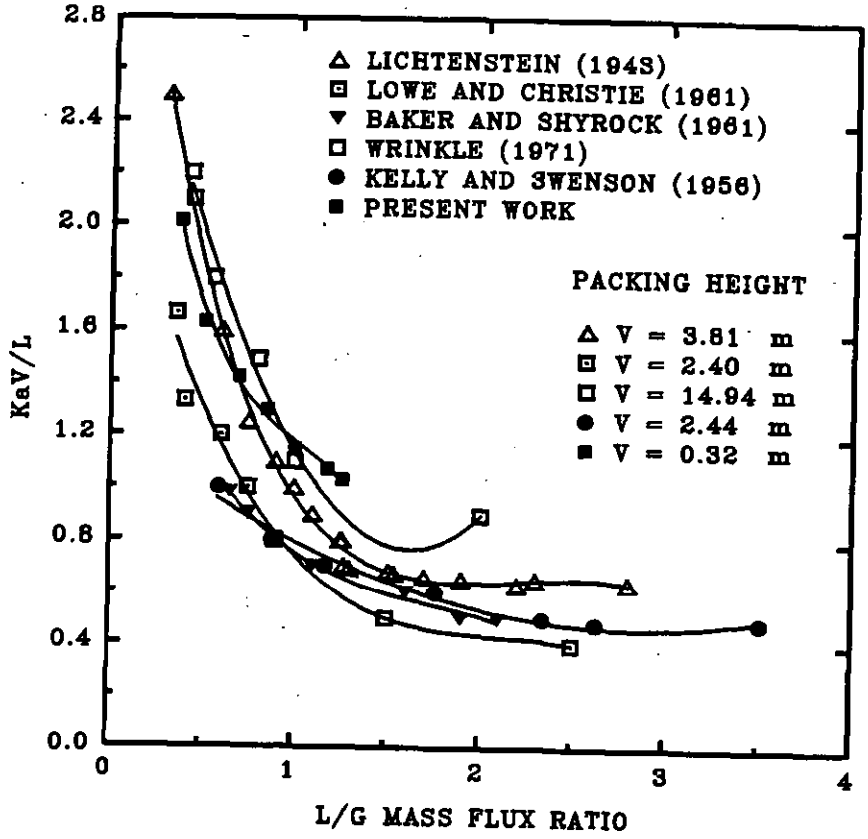

Figure 7.9 Effect of the liquid/gas mass flux ratio upon the tower characteristic. A comparison ofthe FBCT thermal performance with existing data on conventional fixed bed towers.

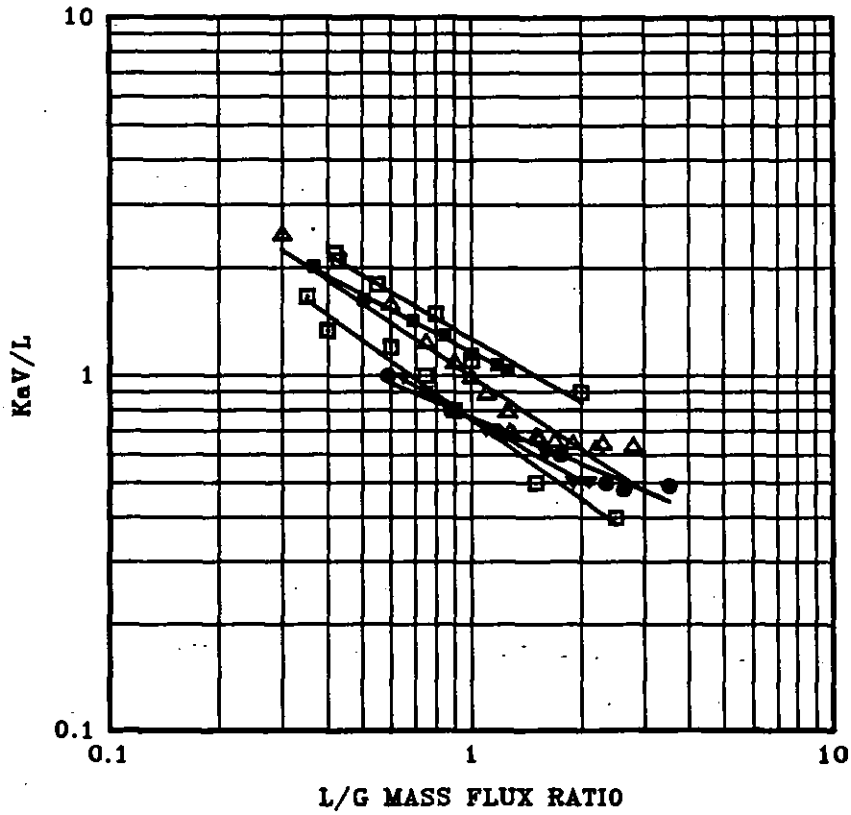

Figure 7.10 A log-log plot of Figure 7.9. All symbols as in Figure 7.9.

Investigator	Tower Type	C	n	r
Lichtenstein (1943)	Conventional Mechanical Draught	1.00	-0.68	0.95
Lowe and Christie (1961)	Conventional Natural Draught	0.75	-0.74	0.99
Baker and Shyrock (1961)	Conventional	0.76	-0.58	1.00
Wrinkle (1971)	Conventional Mechanical Draught	1.27	-0.60	0.99
Kelly and Swenson (1956)	Conventional Mechanical Draught	0.76	-0.43	0.98
Present Work	Fluidised Bed Mechanical Draught	1.17	-0.53	1.00

Table 7.1 Comparison of coefficients and exponents of the FBCT with those of conventional wet cooling towers to show the power law dependence.

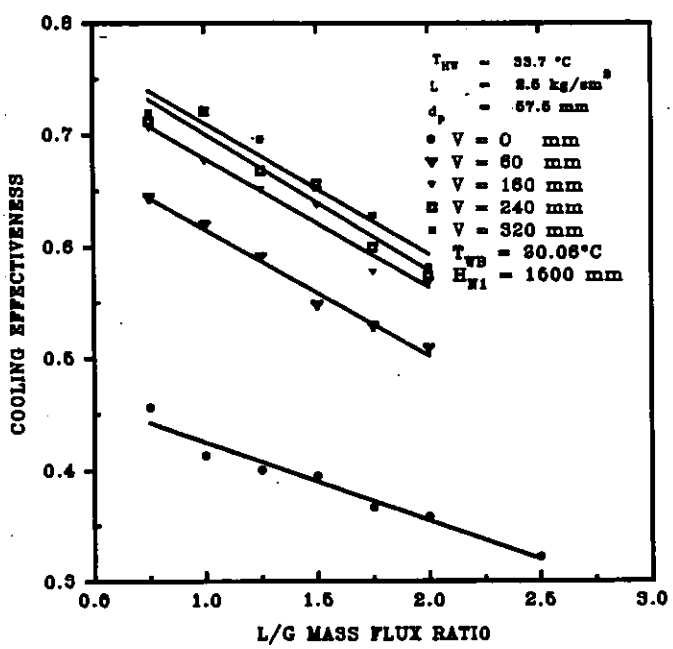

Figure 7.11 Effect of the liquid/gas mass flux ratio and the static bed height upon the cooling effectiveness. The data is calculated from Figure 7.3.

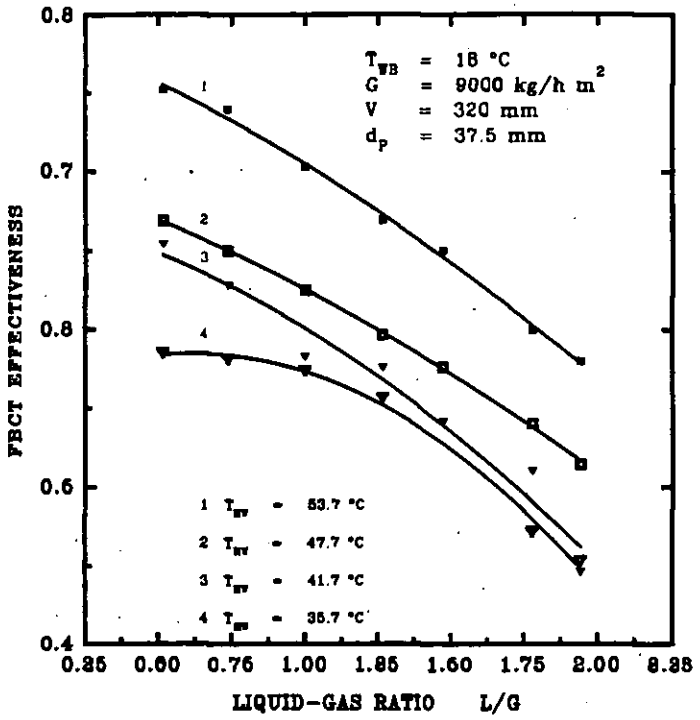

Figure 7.12 Effect of the liquid/gas mass flux ratio and the inlet hot water temperature upon the cooling effectiveness based on the cooled water temperature at the supporting grid. Coarse droplet spray nozzle, ρ_p = 69 kg/m^3.

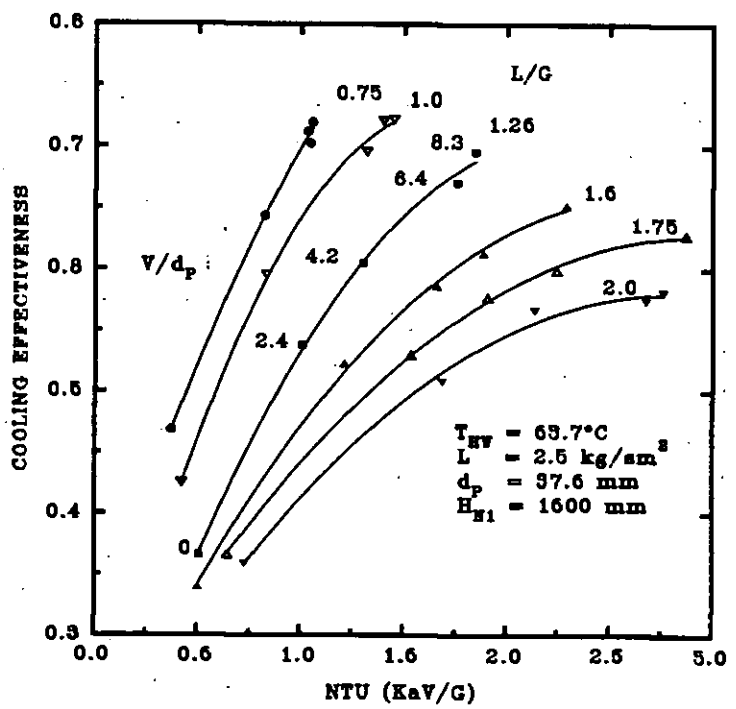

Figure 7.13 Dimensionless tower effectiveness vs dimensionless NTU based on the cooled water temperature at the distributor grid. The data was generated from Figures 7.3 and 7.7.

The increase in the cooling tower effectiveness as the inlet hot water temperature is increased may be due to the higher enthalpy potential difference between the inlet hot and cooled water temperatures. Figure 7.13 above also indicates that both the effectiveness and the NTU are interdependent and, thus summarises the effects of the different independent variables upon the two thermal response variables. Both the NTU and the effectiveness increase as the dimensionless static bed height to particle diameter ratio V/d_p, is increased from 0 to 8.53 (0 - 320 mm). Figure 7.13 also shows that for a particular bed height, the cooling effectiveness decreases as the liquid/gas mass flux ratio is increased but the number of transfer units (NTU) increase. This is because although the tower characteristics decreases as the tower L/G is increased, the actual heat and mass transfer rate per unit gas mass flux increases since the "potential" for cooling is very large at very low gas mass flux as well as high liquid mass flux.

Figure 7.14 shows the effect of the liquid/gas mass flux ratio L/G, upon the cooling range. It shows that the cooling range decreases as the liquid/gas mass flux ratio is increased in a similar manner to the response of the cooling effectiveness and the available tower characteristic. The decrease in range may be due to decreases in the gas mass flux. As the gas mass flux is decreased, the rate of heat transfer decreases since the degree of turbulence and hence liquid-gas-solid inter-mixing is approaches its minimum level. This action reduces the gas liquid interfacial area and therefore the outlet cooled water temperature increases at both the supporting grid and the plenum outlet.

Figure 7.14 also shows that cooling continues to occur in the plenum chamber after the water leaves the fluidised bed itself since the range obtained is higher at the plenum (outlet) than at the distributor grid. Observation of the plenum chamber as fluidisation occurred above the distributor grid indicated that water liquid droplets and particles were violently thrown in all directions as the air enters the tower plenum chamber while counter-currently making contact with the cooled water from the distributor grid. This action was very particularly intense

at high fluidisation gas velocities and may have significantly increased the interfacial activity of the entire tower and hence caused an increase in the FBCT heat and mass transfer due to enhanced evaporation rate. Athough the trend of decrease in the cooling range as the liquid/gas mass flux ratio *L/G,* is increased is similar at both the distributor grid and the plenum, the cooling range at both temperature sensor locations is closer at lower bands of the *L/G* ratio but diverges slowly as the *L/G* ratio is increased further. This may been caused by an increase in the cooling potential of the tower as the gas flow rate is decreased since there is a limited cooling potential at very high gas flow rate because infinite cooling can never be achieved in practice. Theoretically, the wet bulb temperature is the limit of water cooling that may be attained by a tower for a given heat duty.

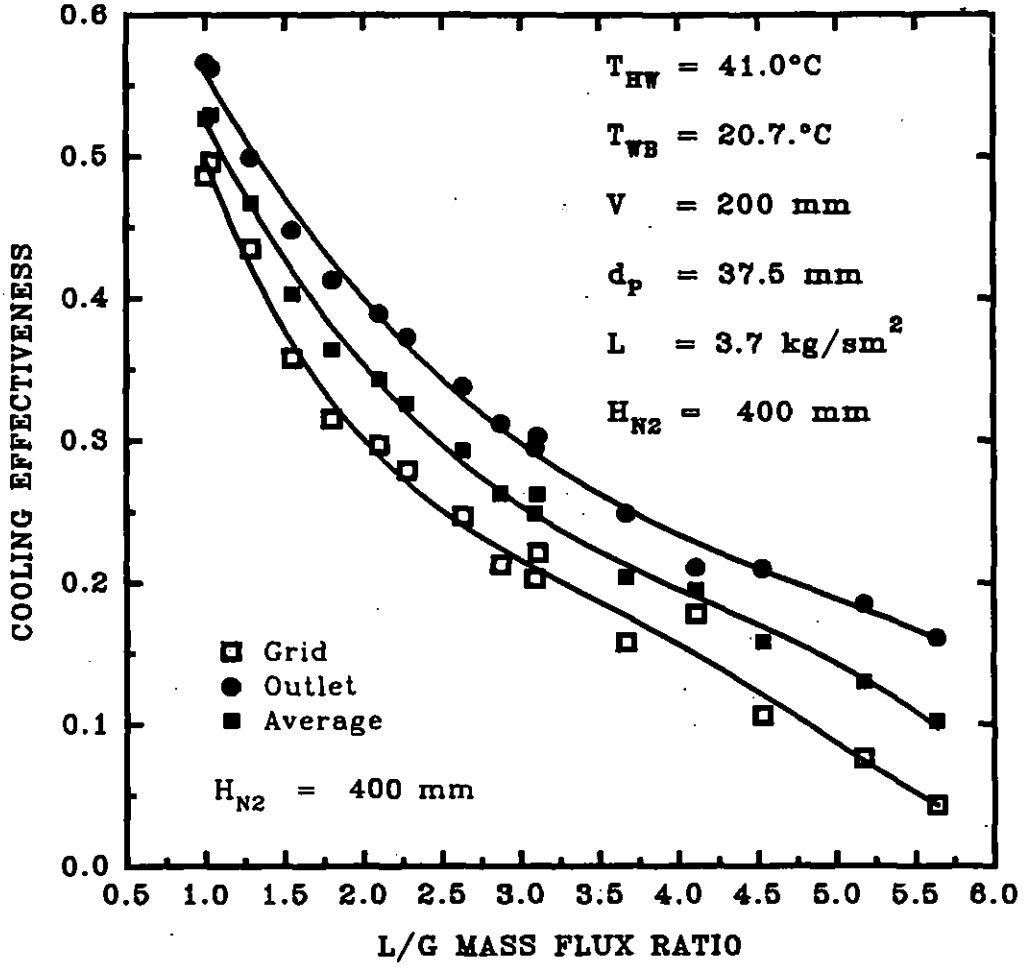

Figure 7.14 Comparison of the cooling effectiveness at the grid, outlet and average cooled water conditions. The data is generated from Figure 7.1

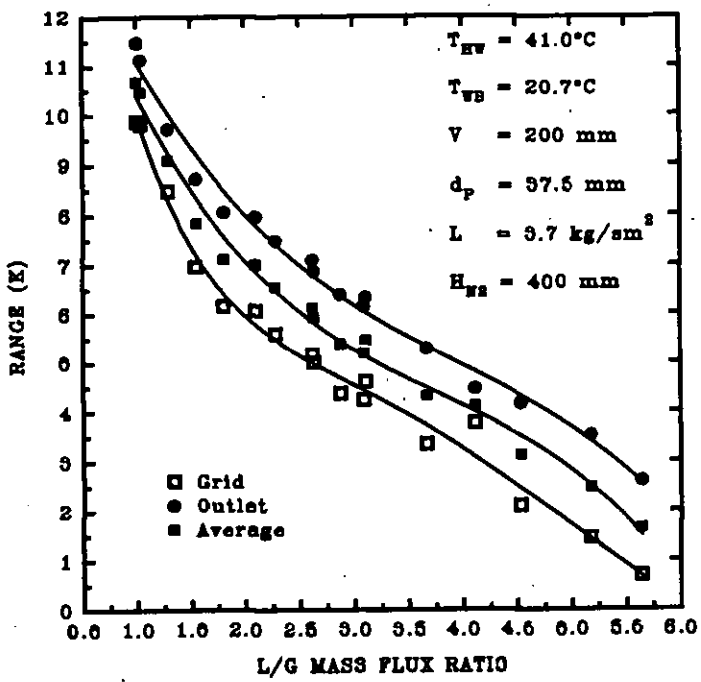

Figure 7.15 Effect of the liquid/gas mass flux ratio upon the range at the suporting and outlet plenum temperature sensors. The data was generated from Figure 7.1.

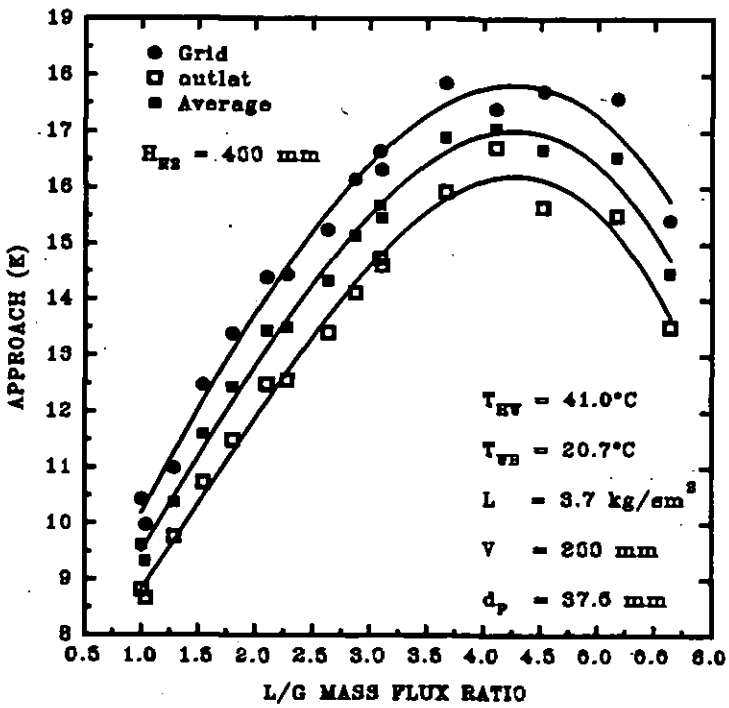

Figure 7.16 Effect of the liquid/gas mass flux ratio upon the cooling approach based on the grid, outlet and the average cooled water temperatures. The data was generated from Figure 7.1.

This occurs when the approach to the wet-bulb temperature is zero and may only happen in an infinitely long tower or zero liquid flow rate which is impractical and impossible.

Figure 7.16 above shows the effect of the *L/G* ratio upon the approach to the wet-bulb temperature. It shows that the approach increases, passes through a maximum and then decreases as the *L/G* ratio is increased. As the *L/G* ratio is increased - a decrease in the gas mass flux, the degree of interfacial activity decreases thus reducing the heat and mass transfer rate and initiating an increase in the cold water temperature. However, as the minimum fluidisation gas velocity is approached, the fluidised bed becomes unstable. It has been shown in Chapter V that the FBCT has an unstable transition point the minimum fluidisation to the fully fluidised bed. This may account for the optimum level of approach since the different outlet cooled water temperatures remains approximately constant for a particular average inlet air wet-bulb temperature. As the gas mass flux is decreased further, the fluidised bed starts to behave as a stable conventional fixed bed wet cooling tower and hence a decrease in the approach since colder outlet water temperatures are atained. Decreases in the wet-bulb temperature at the plenum outlet are due to decreases in the cooled water temperature as a result of the two-phase interfacial activity in the plenum.

7.2.2 Effect of the Gas Flow Rate

The effect of the gas mass flow rate upon the thermal performance of the FBCT was studied because it defines the maximum and minimum fluidisation velocities and hence the existence of a particular fluidised bed cooling tower. Moreover, the superficial gas velocity determines the size of the tower as well as the power required for the cooling process.

Figure 7.18 corresponds to Figure 5.2 in section 5.1 of type I FBCT regime. The tower characteristic generally increases as the gas mass flux is increased and

decreases as the liquid mass flux is increased. As the gas mass flux is increased, the amount of power transmitted to the bed increases and hence the level of turbulence and gas-liquid interfacial mixing. The increased mixing and turbulence increase the gas-liquid interfacial activity and, therefore enhances the heat and mass transfer rate due to increases in the gas-liquid interfacial area. In the range of the gas flow rate of between 0.7 to 2.0 kg/s m^2, the tower characteristic apparently increases as the liquid mass flux is increased. This may be due to the fact that the operation of the FBCT bordered between the static and the minimum fluidisation state. It has been discussed in chapter V that the minimum fluidisation velocity decreases as the liquid mass flow rate is increased, and that fluidisation is much more intense at low *H/V* ratios. Moreover, Koval *et al.* (Dec 1975) have experimentally shown that axial liquid mixing increases as the liquid flow rate is increased for a particular gas flow rate. An increase in the liquid flow rate and hence the liquid holdup also restricts the gas free flow passage through the bed and, therefore intensifies gas-liquid interaction at the interface causing an increase in the interfacial activity and the mass transfer coefficient. Figures 7.18 to 7.24 also characterises the FBCT thermal performance for a type I FBCT regime. Figure 6.19 shows that the tower characteristic also increases as the gas mass flux is increased and, that for the fine spray nozzle, the tower characteristic increases as the spray nozzle height is increased. As the gas mass flux is increased beyond the minimum fluidisation state, the bed expands and behaves like an aggregative fluidised bed stimulating bubble growth in accordance to the theoretical predictions of O'Neill *et al* (1972). The tower characteristic increases and then almost flattens out as the gas mass flux is increased. The increase may be due to enhanced bubble growth and increased bubble splitting especially at low bed expansion as reported by Epstein (1981). It has been shown in Chapter VI that the bed expands slowly and then rapidly as the gas flow rate is increased beyond the minimum fluidisation velocity. Epstein (1981) also reported that the gas holdup is reduced by bubble growth and increased by bubble splitting since the bubble rise velocity increases as the bubble size increases. Since the retension of gas in the three-phase bed increases in the interfacial activity and, it follows that the heat

and mass transfer rate and hence the thermal performance should increase. Kuroda, Hasatani and Tabei (1989) sucessfully correlated the interfacial area of a three-phase fluidised counter-current flow of gas liquid and solid to obtain the following Equation 2.55 in chapter II. This Equation was used to calculate the interfacial area of the FBCT for a type I operation as shown in Figure 7.25. It shows that the gas-liquid interfacial area increases as the gas holdup increases in agreement with our findings in chapter V that the gas holdup increases as the superficial gas velocity is increased.

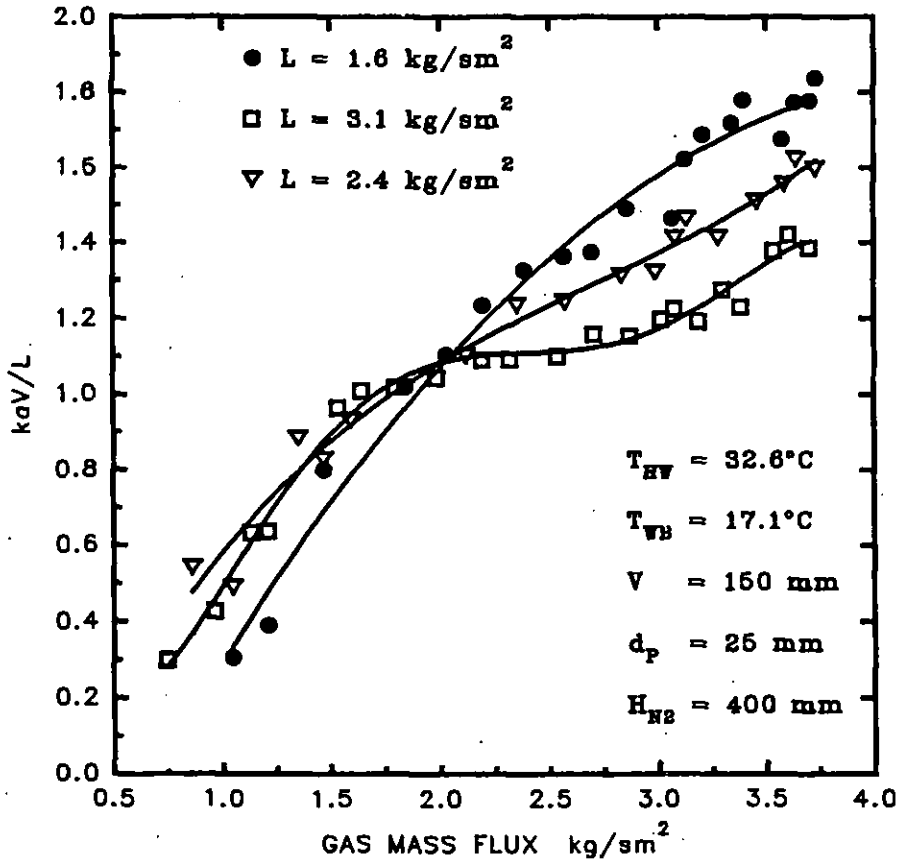

Figure 7.17 Effect of the gas and liquid mass fluxes upon the tower characteristic based on the plenum outlet cooled water temperature for the fine droplet spray nozzle. $\rho_p = 245$ kg/m^3.

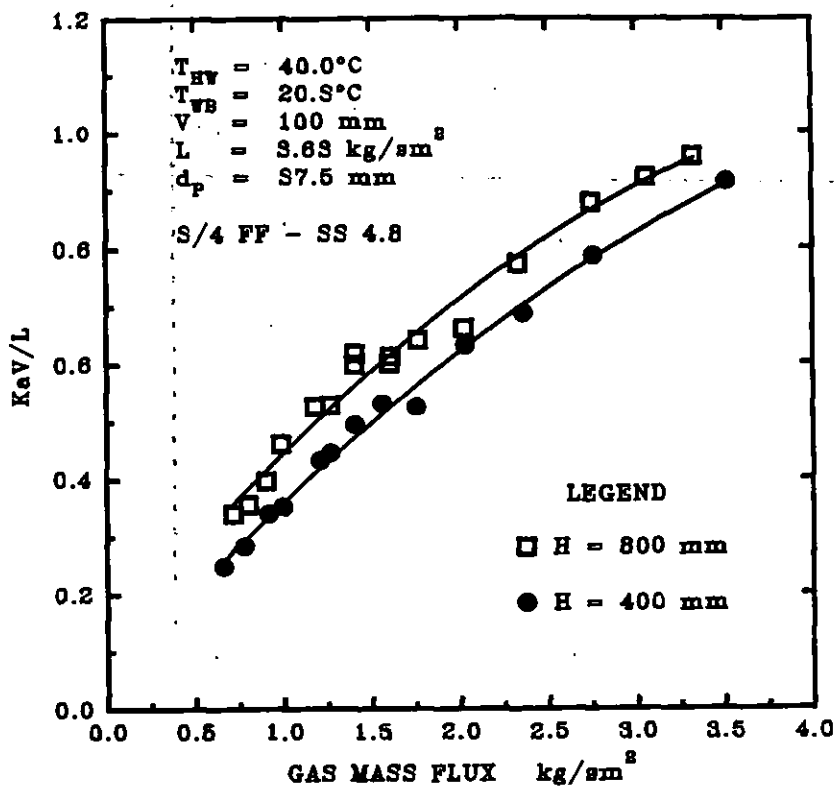

Figure 7.18 Effect of the gas mass flux and the tower characteristic based on the plenum outlet cooled water temperature. Fine droplet spray nozzle type 3/4 FF - SS 4.8. $\rho_P = 69$ kg/m^3.

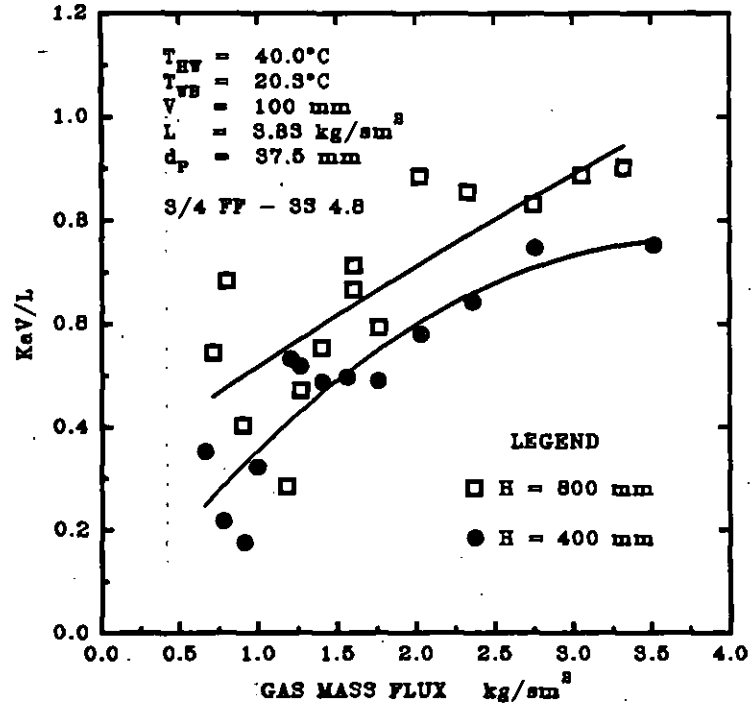

Figure 7.19 Effect of the gas mass flux and the spray nozzle height upon the tower characteristic based on the outlet cooled water temperature at the supporting grid. Notations correspond to Figure 7.18.

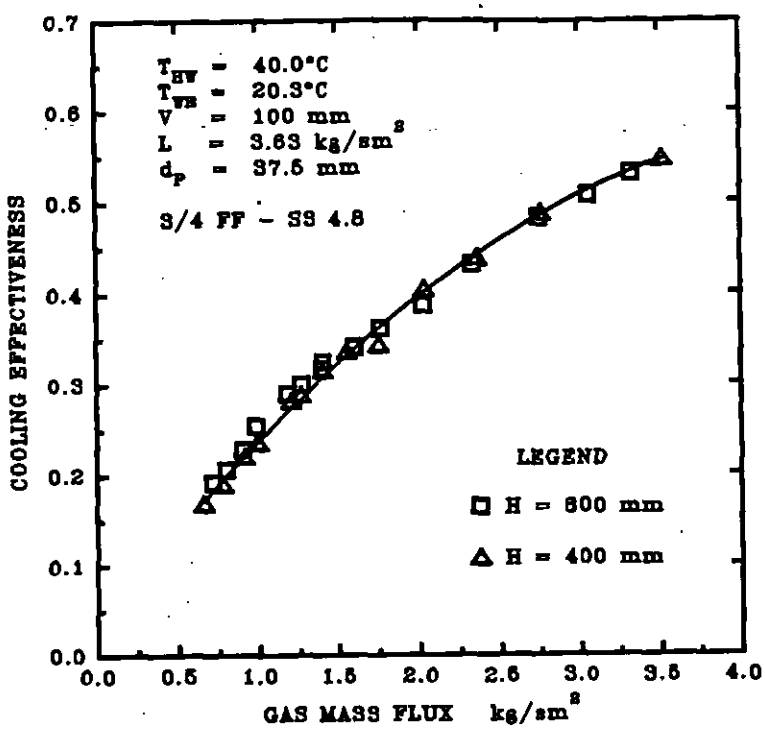

Figure 7.20 Effect of the gas mass flux upon the cooling effectiveness based on outlet cooled water temperature from the plenum chamber. Notations correspond to Figure 7.18.

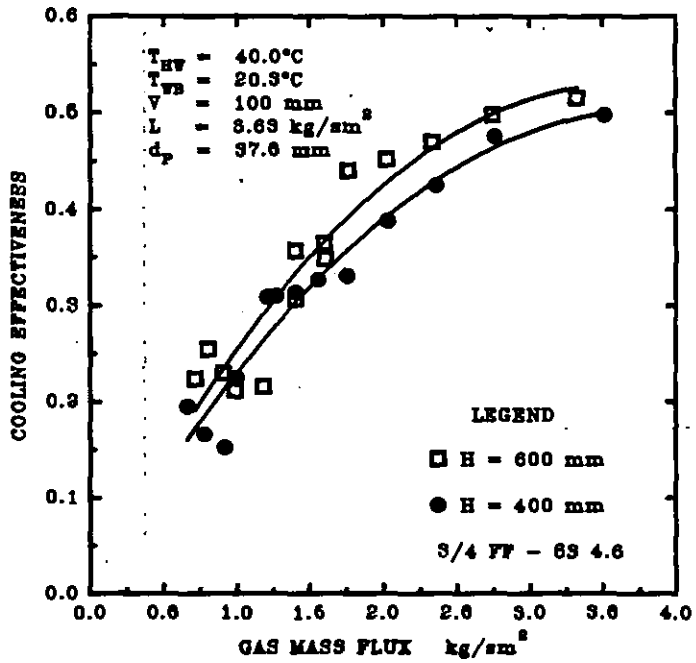

Figure 7.21 Effect of the gas mass flux and the spray nozzle height upon the cooling effectiveness based on the cooled water temperature from the distributor grid. Notations correspond to Figure 7.18.

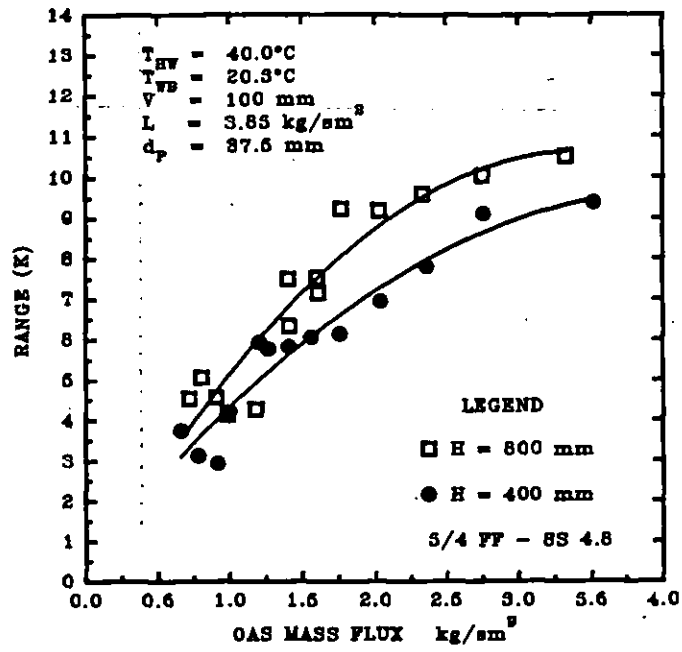

Figure 7.22 Effect of the gas mass flux and the spray nozzle height based upon the range based on the outlet cooled water temperature from the tower plenum chamber. Notations as in Figure 7.18.

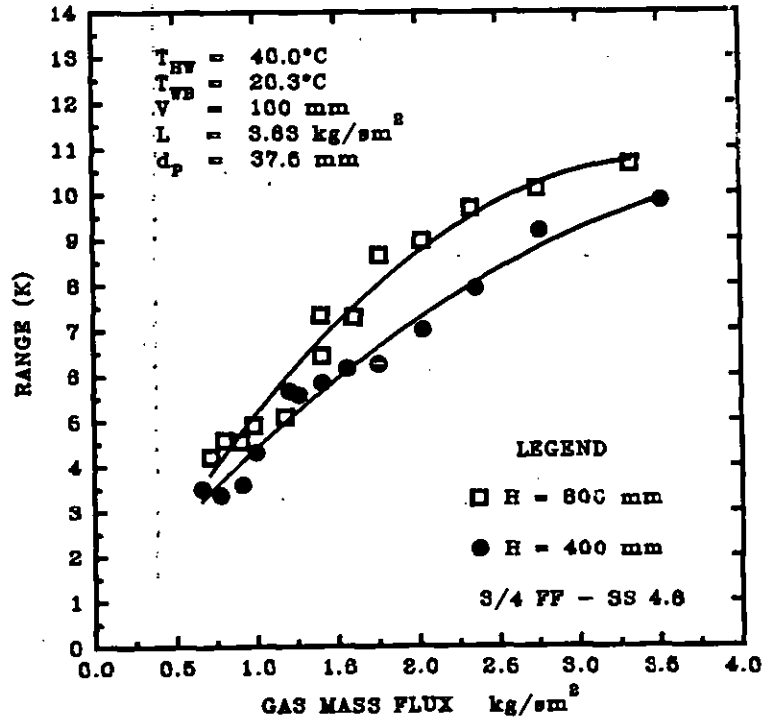

Figure 7.23 Effect of the gas mass flux and the spray nozzle height upon the range based on the outlet cooled water temperature from the supporting grid. Notations as in Figure 7.18.

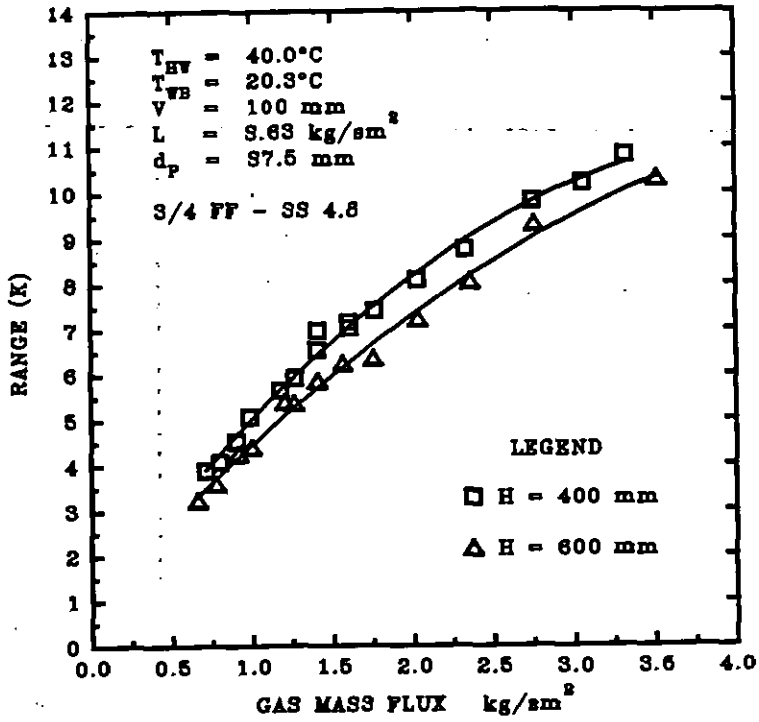

Figure 7.24 Effect of the gas mass flux and the spray nozzle height upon the range based on the average outlet cooled water temperature. Notations as in Figure 7.18.

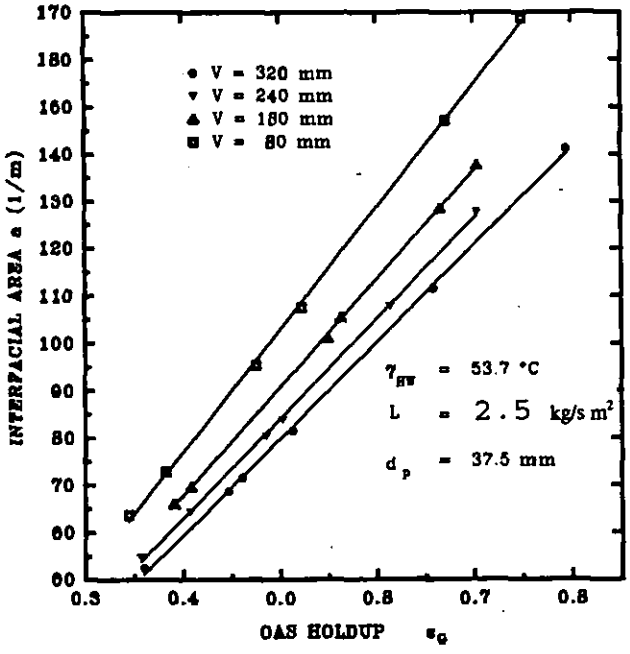

Figure 7.25 Effect of the gas holdup upon the gas-liquid interfacial area calculated from the Equation of Tabei *et al.* (1989). The data was generated from Figures 5.28 and 5.32 in chapter V. Notations correspond to Figure 5.28.

Figures 7.26 to 7.36, corresponding to Figures 5.3 and 6.1 of chapters V and VI repectively, show the effect of the gas flow rate upon the tower thermal performance for a type II FBCT regime. Figures 7.26 to 7.30 show the effect of the gas mass flux upon the tower thermal performance based on the supporting grid, plenum and average outlet cooled water temperatures. They further confirm the earlier findings that the tower characteristic increases as the cooling range and increases and that both dependent varaibles decrease as the approach decreases. This may be attributed to the high interfacial activity at the tower plenum chamber causing the water to undergo further cooling.

Figure 6.26 shows that, at lower gas mass flux band of about 0.6 to 1.5 kg/sm^2, there is little difference between the tower thermal performance based on the grid, average and plenum outlet cooled water temperatures. This may have been due to the lack of fluidisation at this liquid mass flux range. At the plenum outlet water conditions, the tower thermal performance increases sharply as the gas mass flux is increased and then flattens out as the gas mass flux approaches high fluidisation values. The rapid increase of the tower characteristics is due to increased density of the particle as opposed to the type I FBCT regime where particle densities are nominally less than 300 kg/m^3. Type II operation is characterised by excessive liquid holdups before the minimum fluidisation state is reached after which the liquid holdup stays constant. An increase in the liquid holdup is characterised by high interfacial stresses that causes an increase in the gas-liquid interfacial area. This enhances the heat and mass transfer rate. It has been shown that the minimum fluidisation velocity increases as the particle density is increased. The higher a minimum fluidisation greatly enhances the generation of turbulence in the bed and thereby increasing the probabilty of bubble break up into smaller sizes and hence an increase in gas holdup as reported by Epstein (1981). Increased gas holdup causes the interfacial area to increase and therefore initiating an increase in the heat and mass transfer coefficient. This may account for the initially rapid rise of the tower characteristic and cooling effectiveness as the gas mass flux is increased from the static to the minimum fluidisation states.

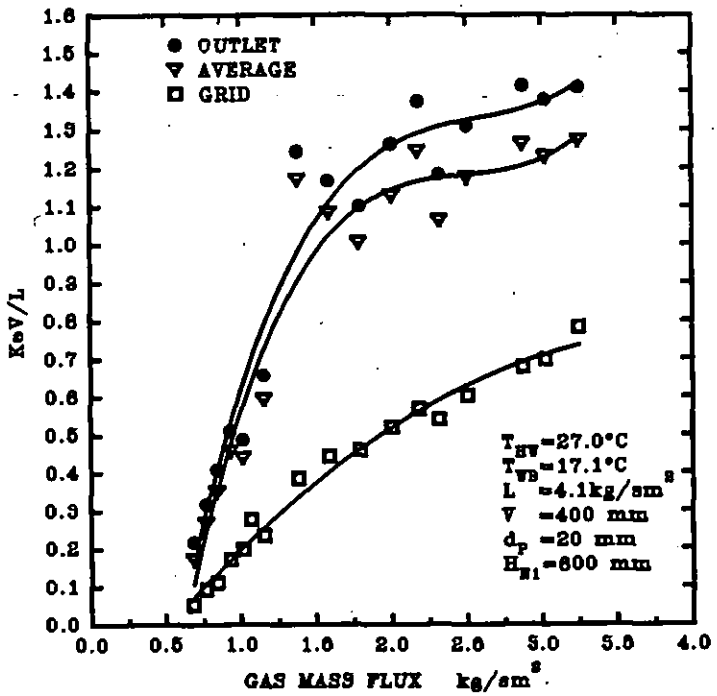

Figure 7.26 Effect of the gas mass flux upon the tower characteristic based on the supporting grid, average and the plenum outlet water temperatures.

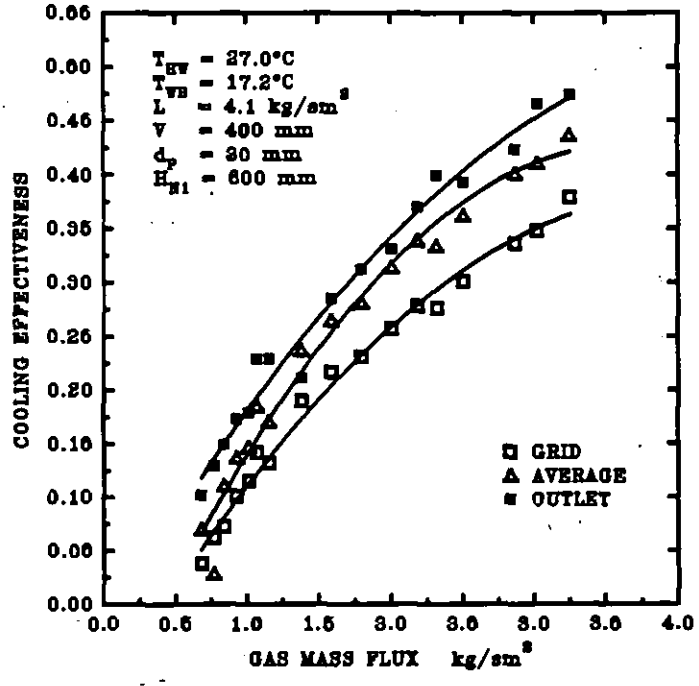

Figure 7.27 The effect of the gas mass flux upon the tower effectiveness. Notations as in Figure 7.26.

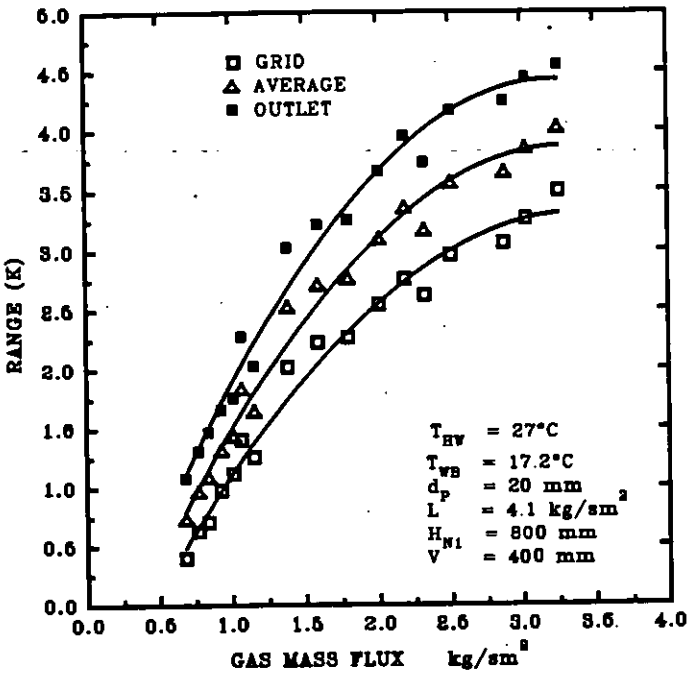

Figure 7.28 Effect of the gas mass flux upon the range. Notations as previously.

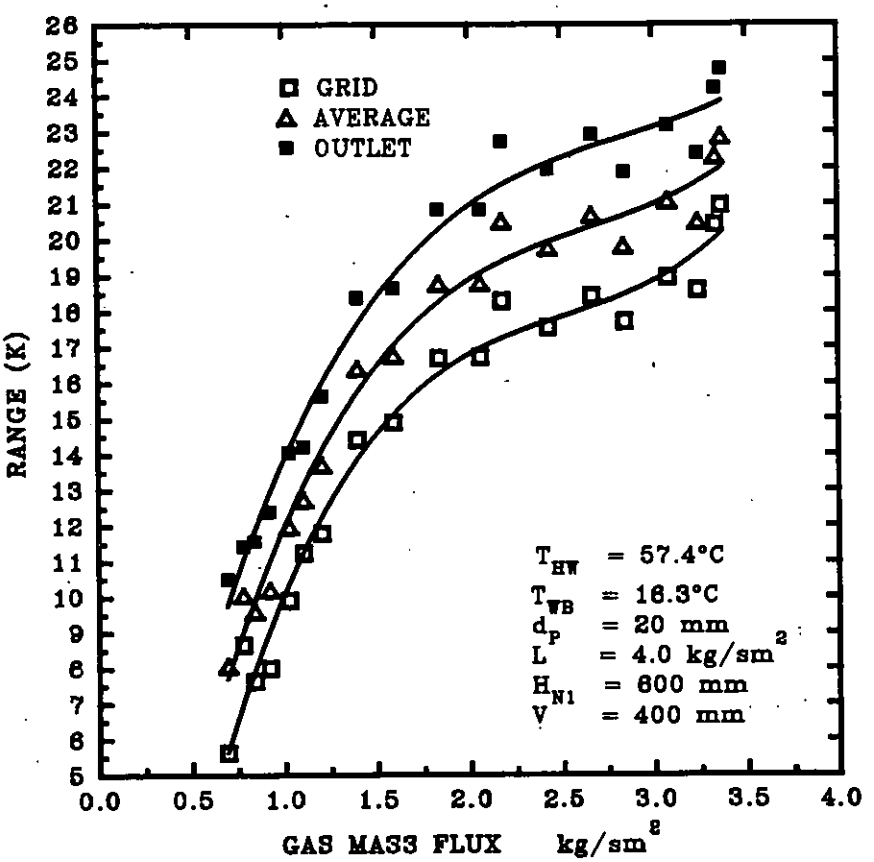

Figure 7.29 Effect of the gas mass flux upon the range based on the supporting grid, average and plenum outlet cooled water temperatures. Notations as in Figure 7.26.

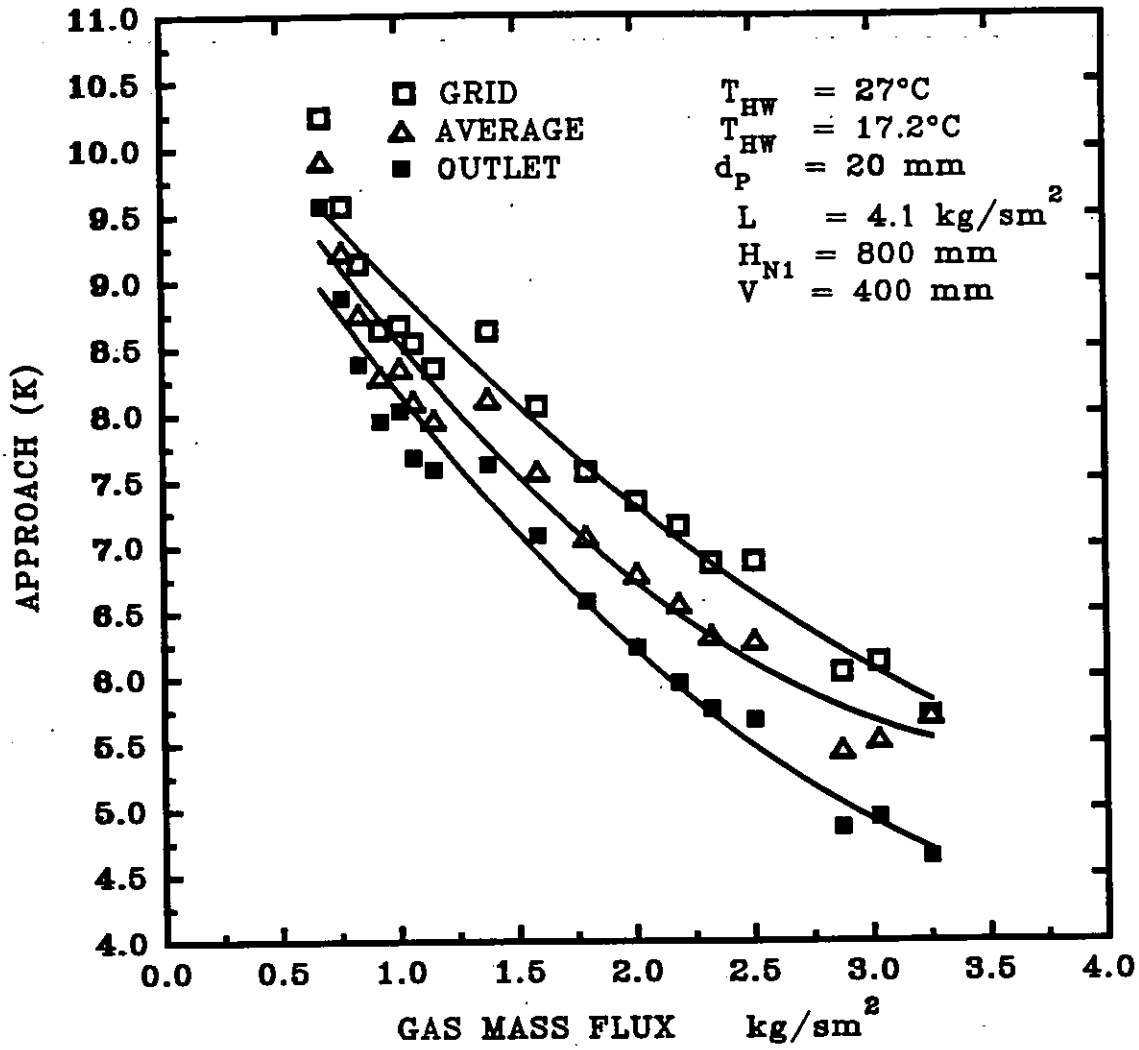

Figure 7.30 Effect of of the gas mass flux upon the approach. Caption as in Figure 7.29.

7.2.3 Effect of the Liquid Mass Flux

Figures 7.31 to 7.45 show the effect of the liquid mass flux upon the tower thermal performance. The tower characteristic, the cooling effectiveness and the cooling range generally decrease as the liquid mass flux is increased. However, the rate of decrease is not linear but it follows the power law. Initially, there is a sharp decrease and then the curve flattens out as the liquid mass flux is further increased.

This may be explained by the fact that for a particular gas mass flux, the total number of droplets that undergoes cooling by the ambient gas is smaller at a lower liquid flow rate. As a result, the possibility of a particular droplet coming into contact with the ambient air is higher. Therefore, tower characteristic per liquid mass flux increases as the liquid mass flux decreases resulting in the decrease in outlet cold water temperature as the liquid mass flow rate decreases for a particular set of experimental conditions and also causing the range and thus the cooling effectiveness to decrease. However, as the liquid mass flow rate is increased further, the range, effectiveness and the tower characteristic tend to become independent of the liquid mass flux. This is because as the liquid mass flux is increased above a threshold value, the degree of turbulence increases due to an increase in the liquid holdup. The increased agitation increases the chances of gas-liquid interfacial mixing thus counteracting the effect of a decrease in tower thermal performance due to increased number of droplets for a particular cooling effect. This explanation may be applied similarly to the exponential increase in the approach as the liquid mass flux is increased.

Figures 7.31 to 7.45 also show that the same trend is attained for both types I and II FBCT operation and that the tower thermal performance is higher when based upon the outlet cooled water temperature from the plenum than when it is based on the cooled water temperature from the distributor grid. This confirms earlier findings in section 7.1 and 7.2 that end effects are significant in the FBCT since cooling continues to occur in the plenum chamber.

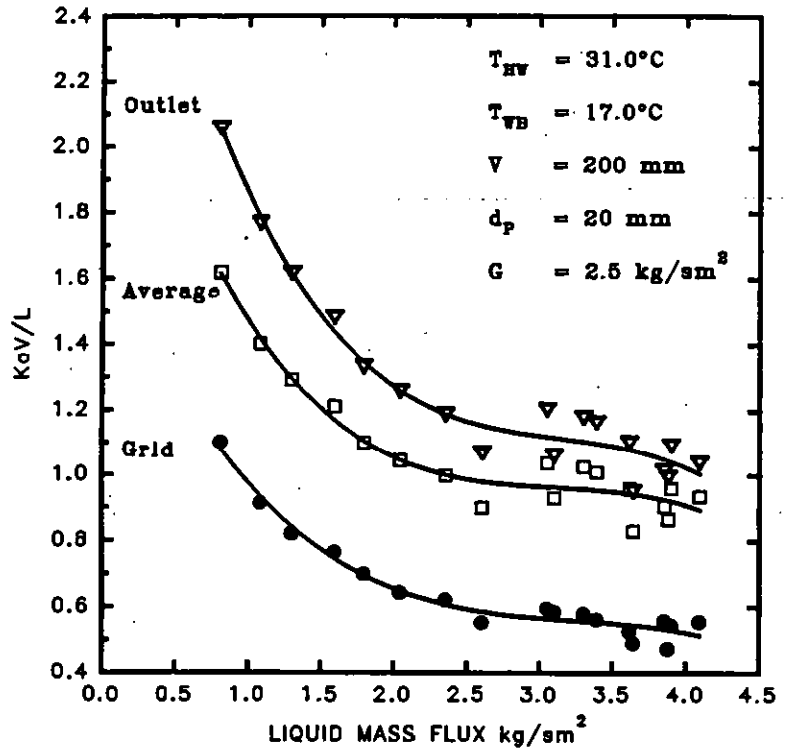

Figure 7.31 The effect of the liquid mass flux upon the tower characteristic. A comparison of the grid, outlet and the average outlet water conditions. H = 400 mm, ρ_p = 239 kg/m^3. Fine droplet spray nozzle type 3/4 SS - FF 4.8.

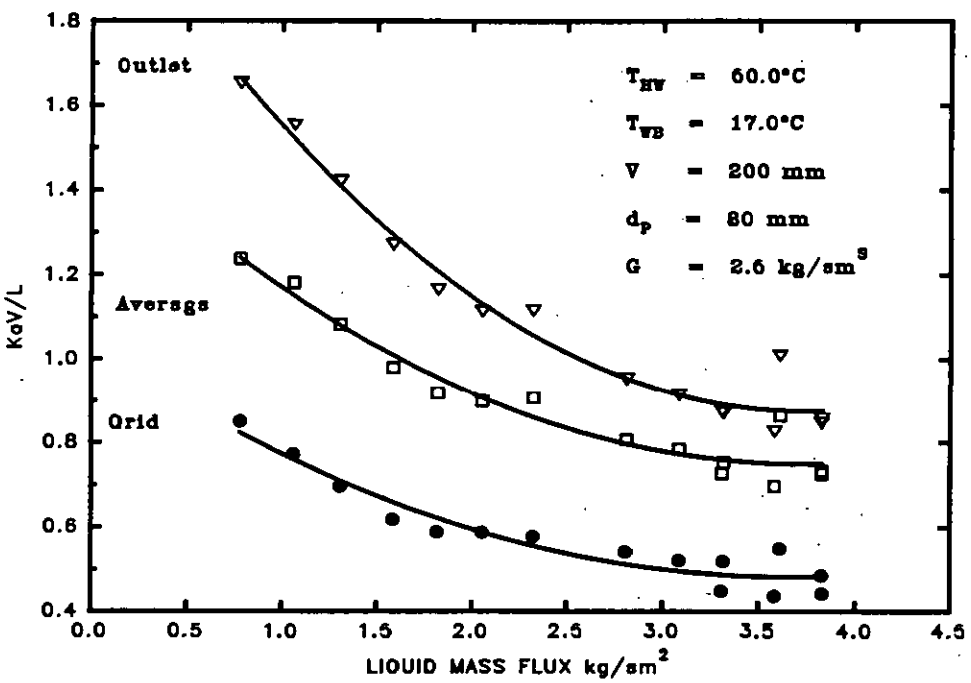

Figure 7.32 Effect of the liquid mass flux upon the tower characteristic at relatively high inlet water temperature. A comparison of the grid, outlet and average cooled water conditions. H = 400, ρ_p = 239 kg/m^3. Fine droplet nozzle type 3/4 SS - FF 4.8.

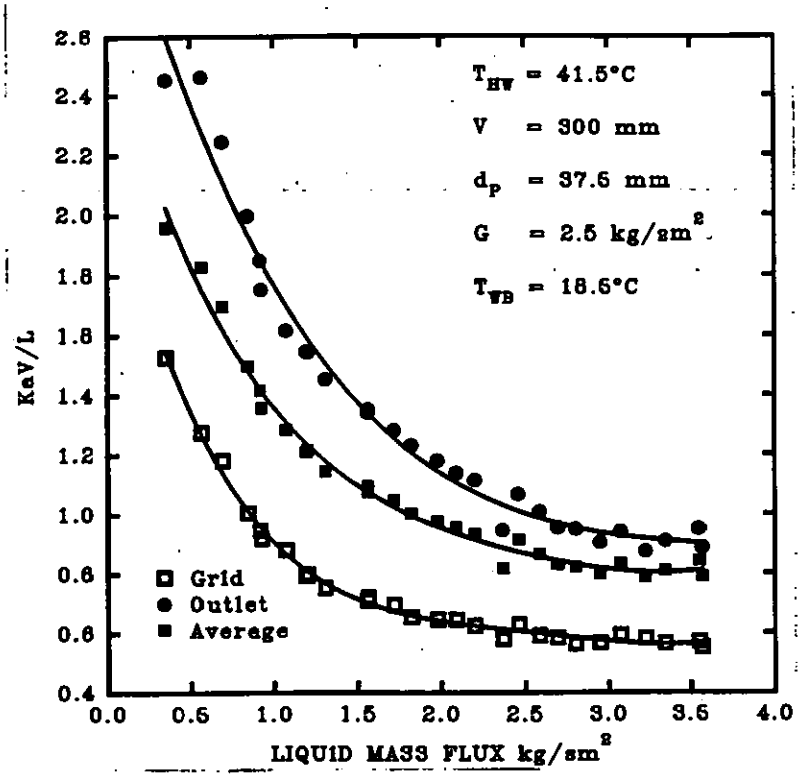

Figure 7.33 Effect of the liquid mass flux upon the tower characteristic for a typical type I operation. A comparison of the grid, outlet and average water conditions. H = 400 mm,ρ_r = 69 kg/m^3. Fine droplet spray nozzle type 3/4 SS - FF 4.8.

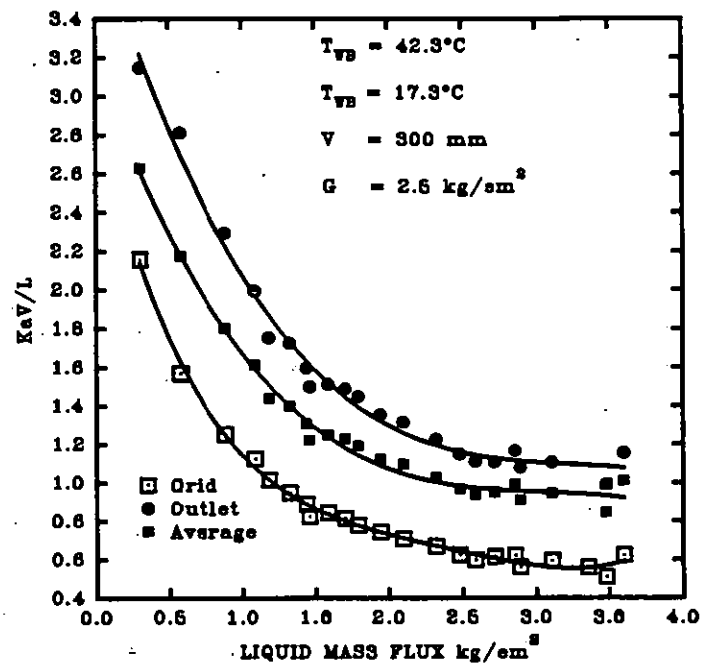

Figure 7.34 Effect of the liquid mass flux upon the tower characteristic for a typical FBCT type II operation. H = 400 mm, d_p = 25.4 mm, ρ_p = 326 kg/m^3. Fine spray droplet size nozzle type 3/4 SS - FF 4.8.

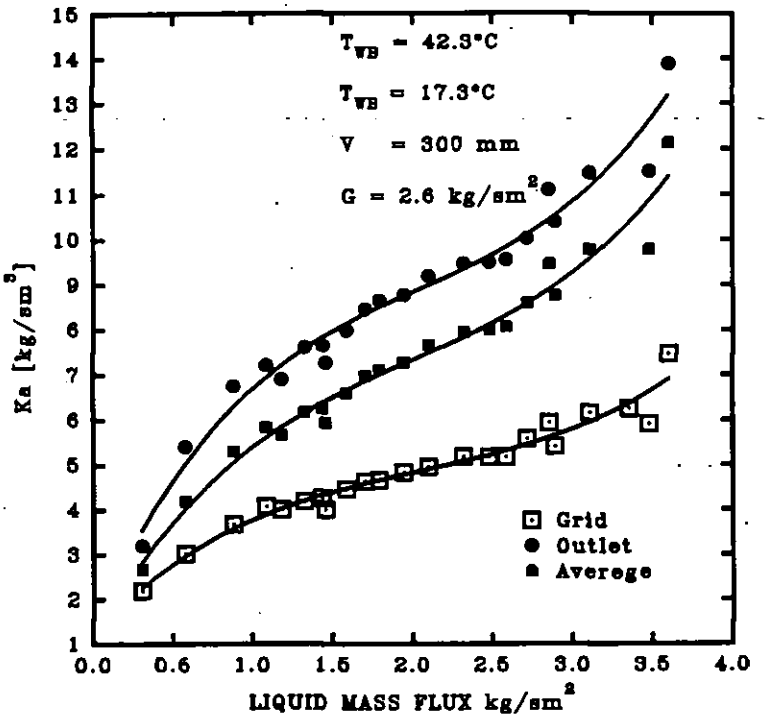

Figure 7.35 Effect of the liquid mass flux upon the overall mass transfer coefficient for a typical type II FBCT operation. A comparison of the grid, average and outlet cooled water temperatures. H = 400 mm, d_p = 25.4 mm, ρ_p = 328 kg/m^3. Fine spray nozzle type 3/4 SS - FF 4.8.

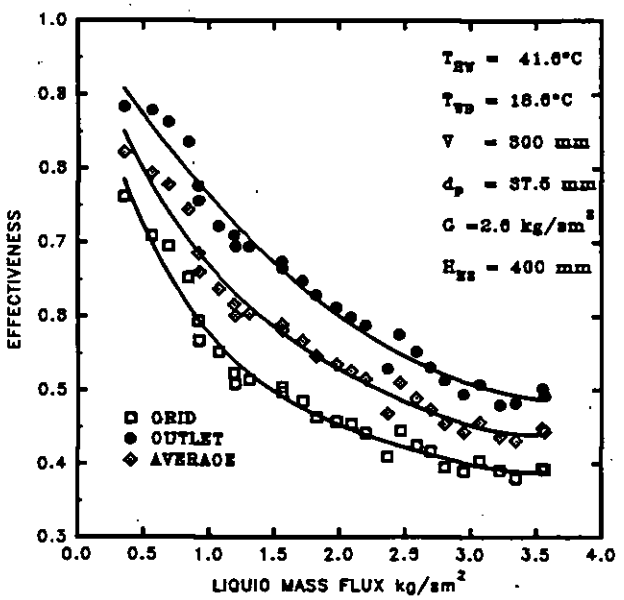

Figure 7.36 Effect of the liquid mass flux upon the cooling effectiveness for a typical type I FBCT operation. A comparison of the grid, average and the oulet cooled water condition. H = 400 mm, ρ_p = 69 kg/m^3. Fine droplet spray nozzle 3/4 SS - FF 4.8.

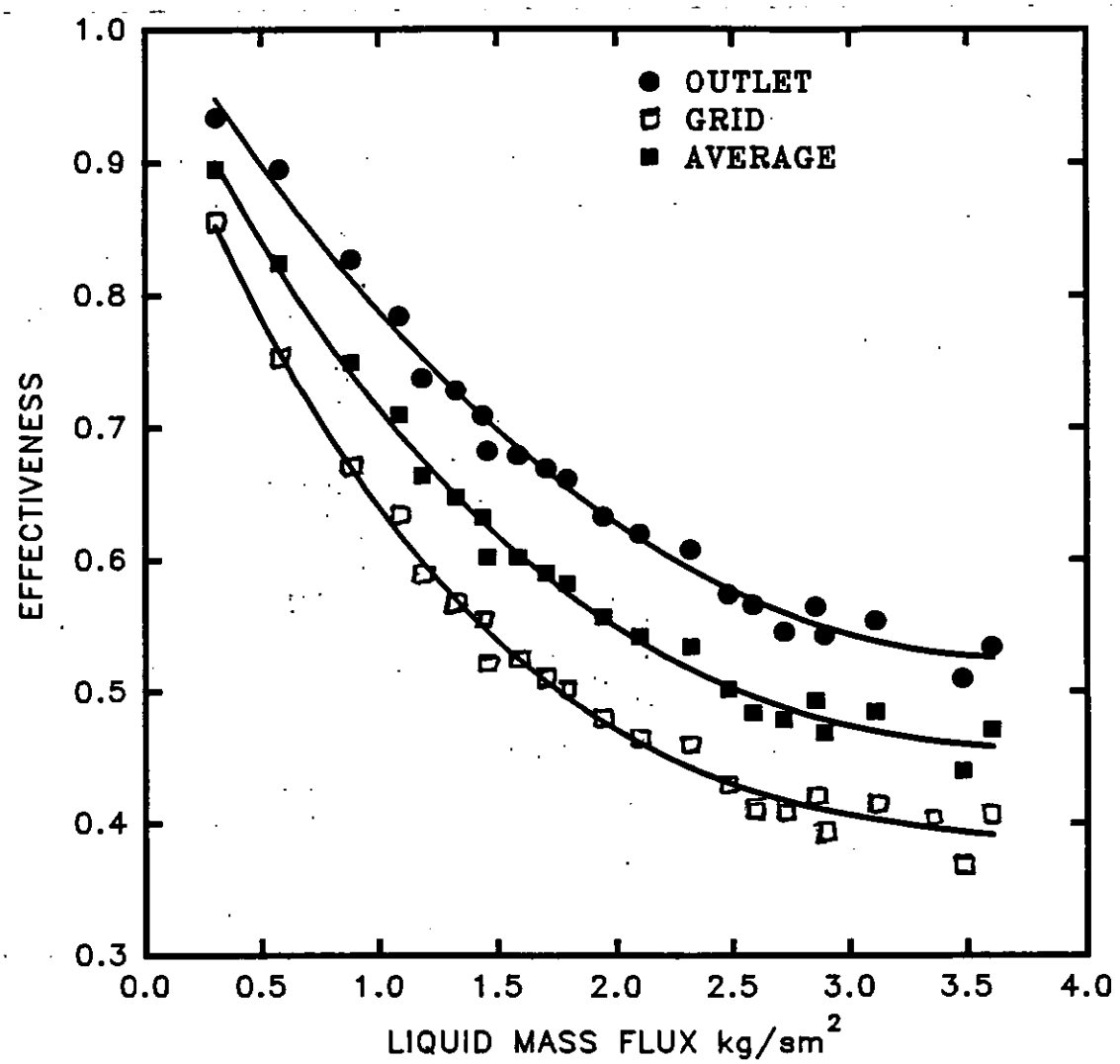

Figure 7.37 Effect of the liquid mass flux upon the cooling effectiveness for a typical type II FBCT operation. A comparison of the grid, average, and outlet cooled water conditions. H = 400 mm, d_p = 25.4 mm, ρ_p = 326 kg/m^3. Fine droplet spray type 3/4 SS - FF 4.8. Other notation as in Figure 7.34.

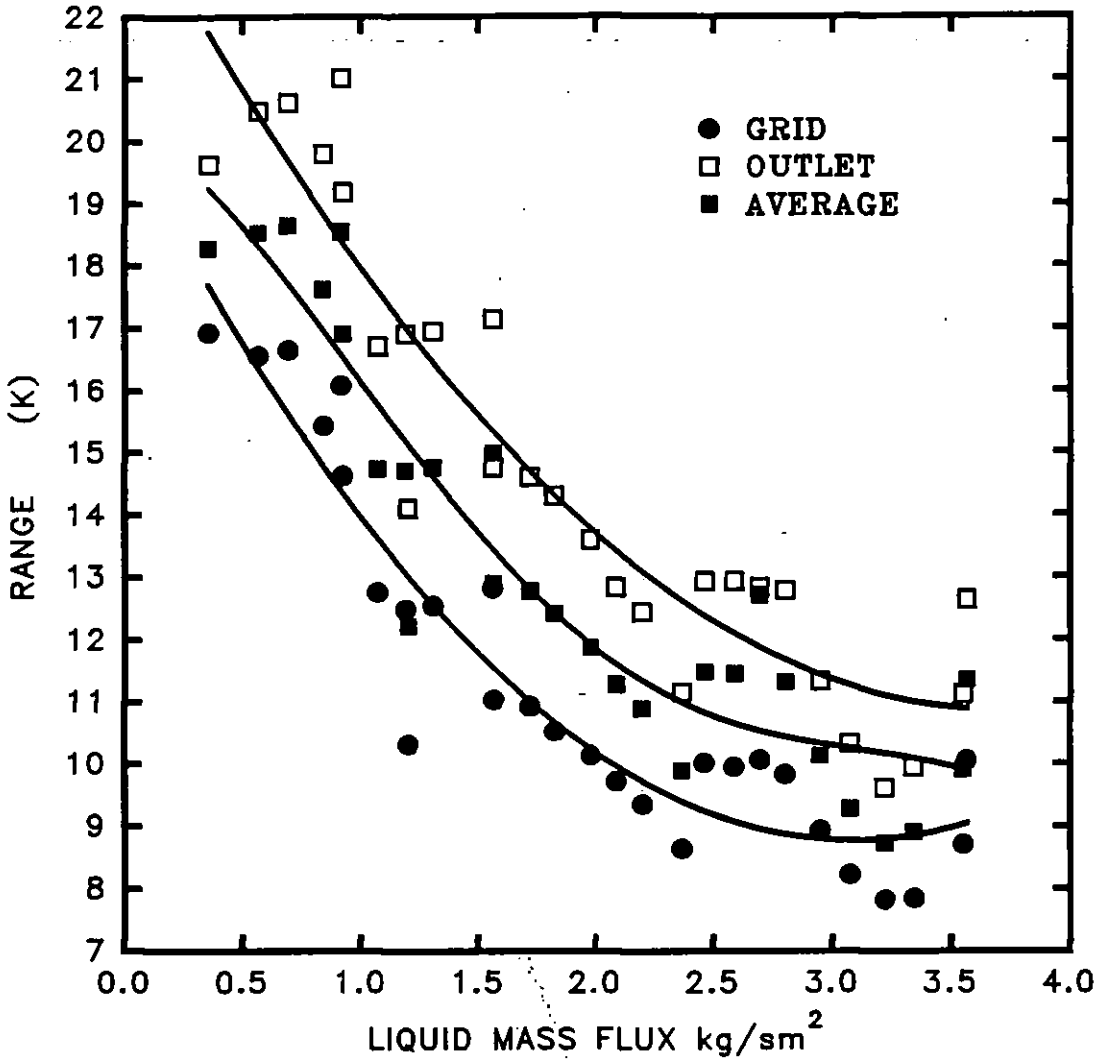

Figure 7.38 Effect of the liquid mass flux upon the cooling range for a typical type I FBCT operation. A comparison between the grid, average and outlet conditions. H = 400 mm, ρ_p = 69 kg/m^3. Fine droplet spray type 3/4 SS - FF 4.8. Other legend as in Figure 7.36.

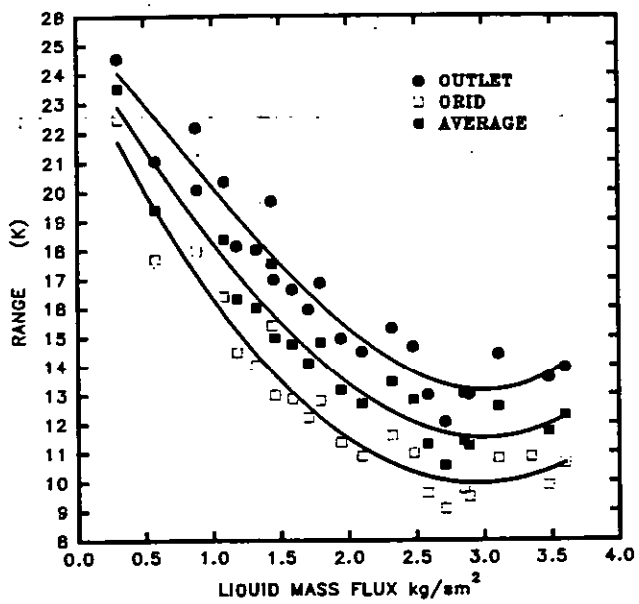

Figure 7.39 Effect of the liquid mass flux upon the cooling range for a typical type II FBCT operation. A comparison between the grid, average and outlet cooled water conditions. H = 400 mm, d_p = 25.4 mm, ρ_p = 326 kg/m^3. Other notations as in Figure 7.37.

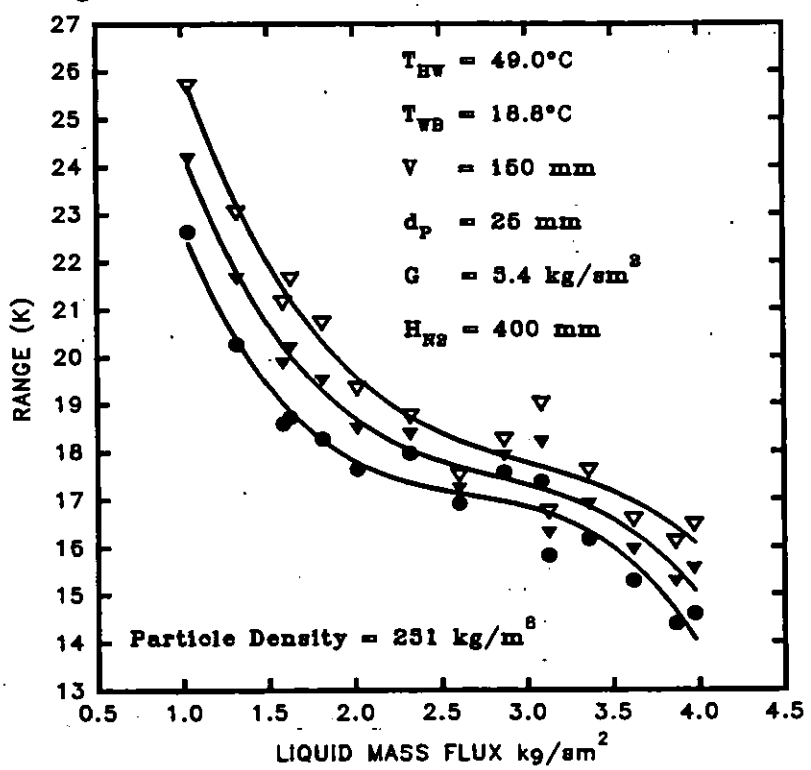

Figure 7.40 Effect of the liquid mass flux upon the range for a high gas mass flux type II FBCT operation. A comparison between the grid, average and outlet cooled water conditions for the fine droplet spray nozzle.

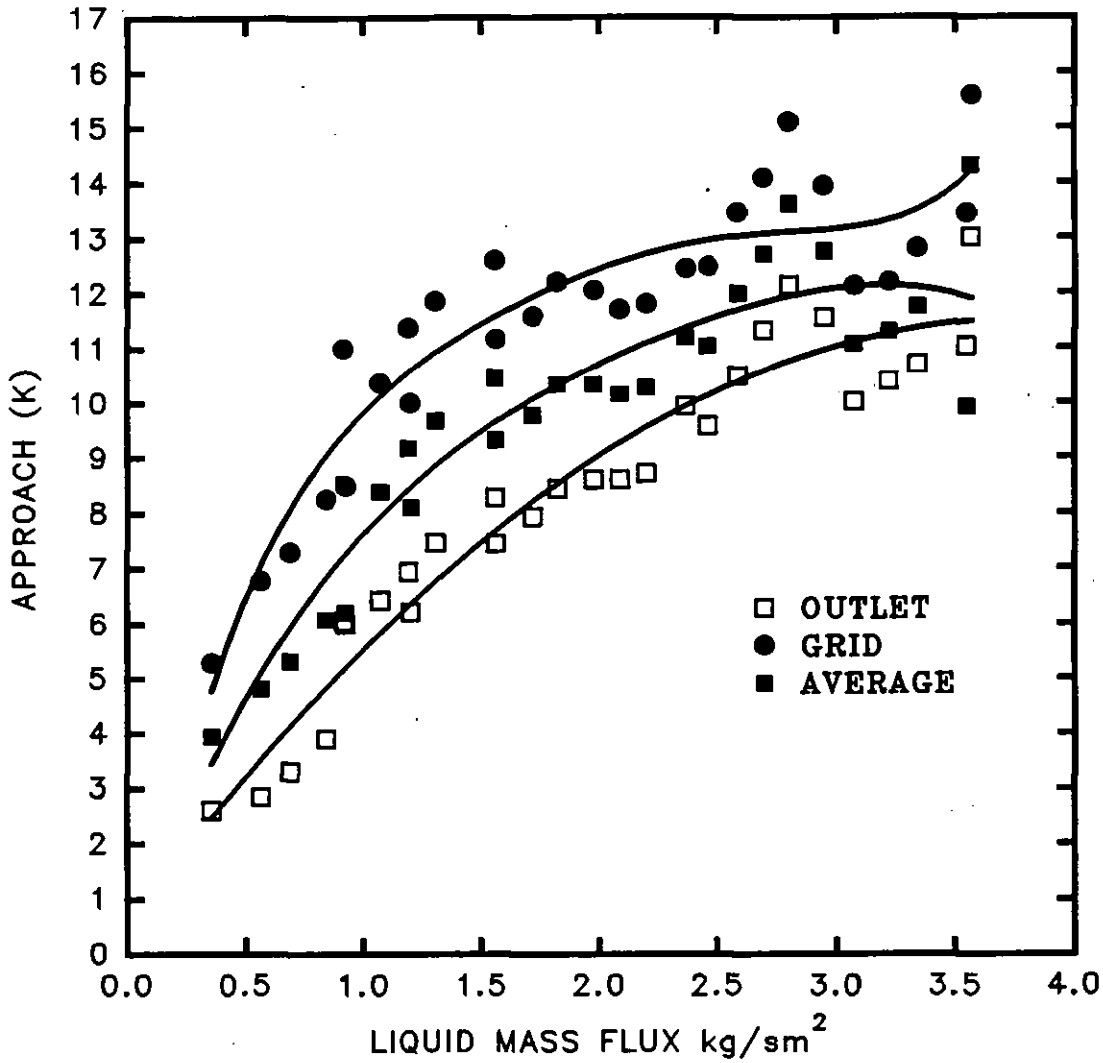

Figure 7.41 Effect of the liquid mass flux upon the approach for a typical type I FBCT operation. A comparison between the grid, average and outlet cooled water conditions. H = 400 mm, ρ_P = 69 kg/m^3. Fine droplet spray nozzle type 3/4 SS -FF 4.8. Other legend as in Figure 7.36.

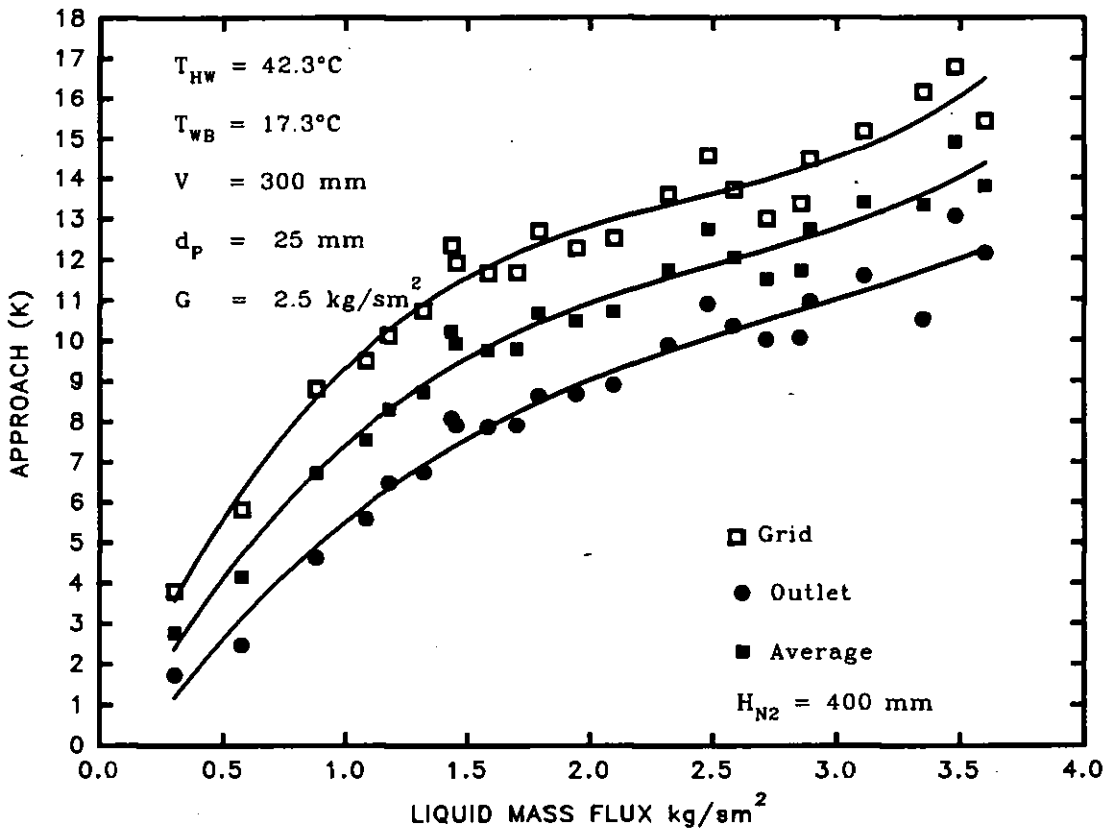

Figure 7.42 Effect of the liquid mass flux upon the approach for a typical type II FBCT operation. A comparison between the grid, average and outlet cooled water conditions. H = 400 mm, d_P = 25.4 mm, ρ_P = 326 kg/m^3. Fine droplet spray nozzle type 3/4 SS - FF 4.8.

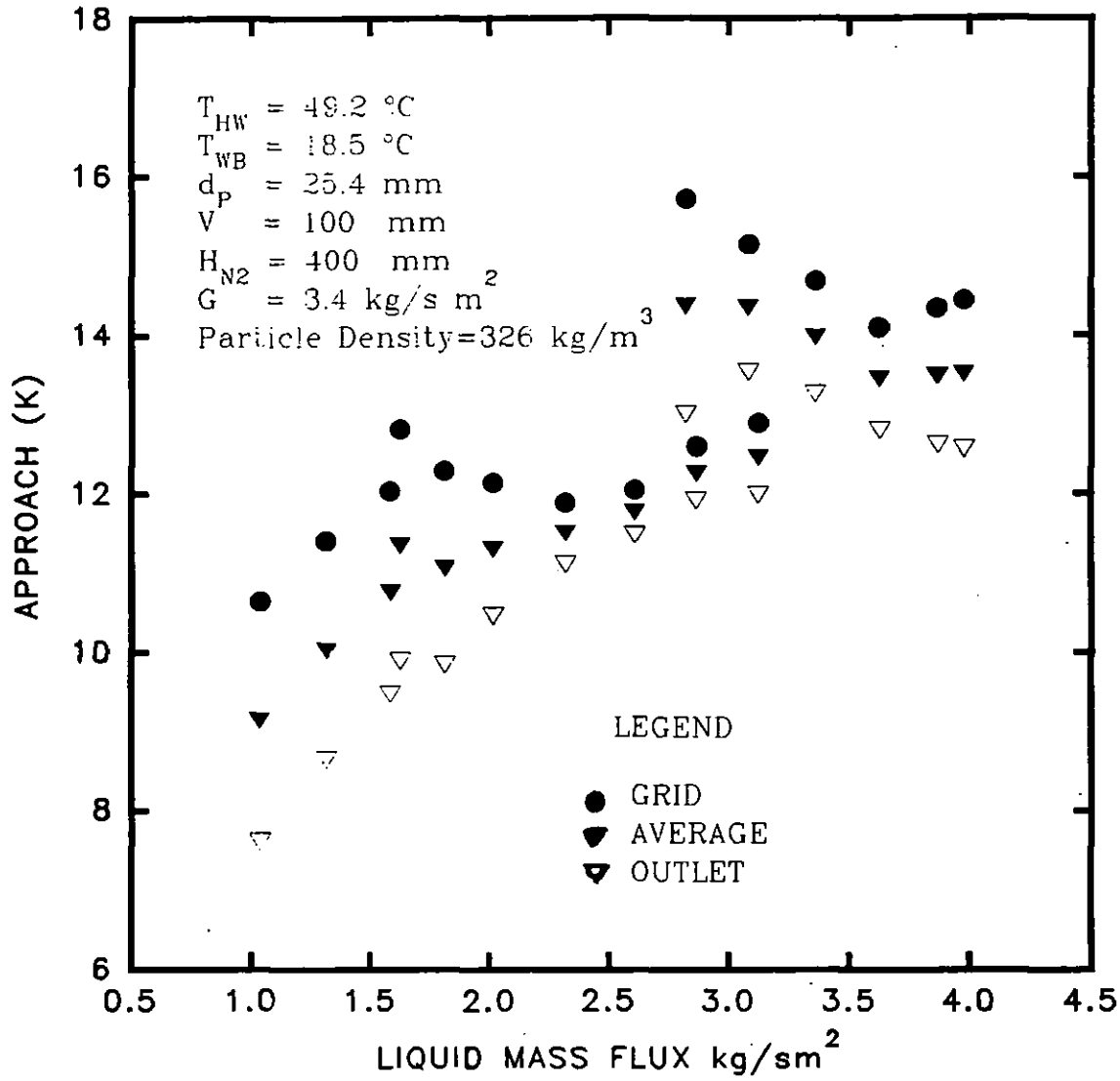

Figure 7.43 Effect of the liquid mass flux upon the approach for a typical type II FBCT operation at a high gas mass flux. A comparison of the grid, average and outlet cooled water conditions for the fine droplet spray nozzle.

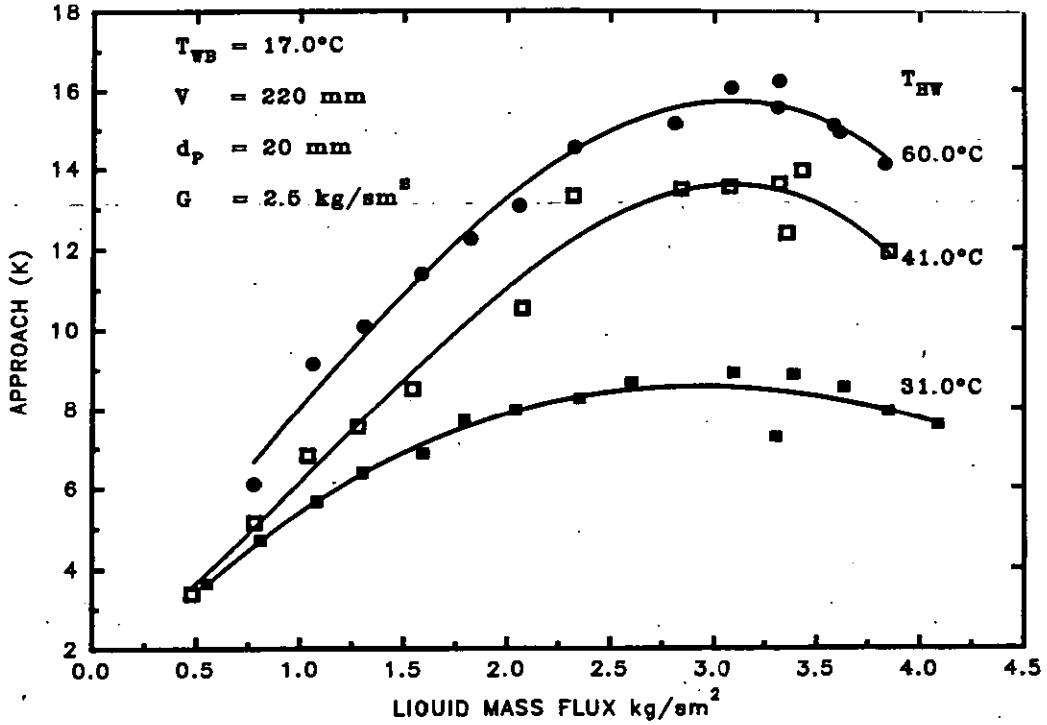

Figure 7.44 Effect of the liquid mass flux and the inlet water temperature upon the approach based on the outlet cooled water conditions. H = 400 mm, ρ_P = 239 kg/m^3. Fine droplet spray nozzle type 3/4 SS - FF 4.8.

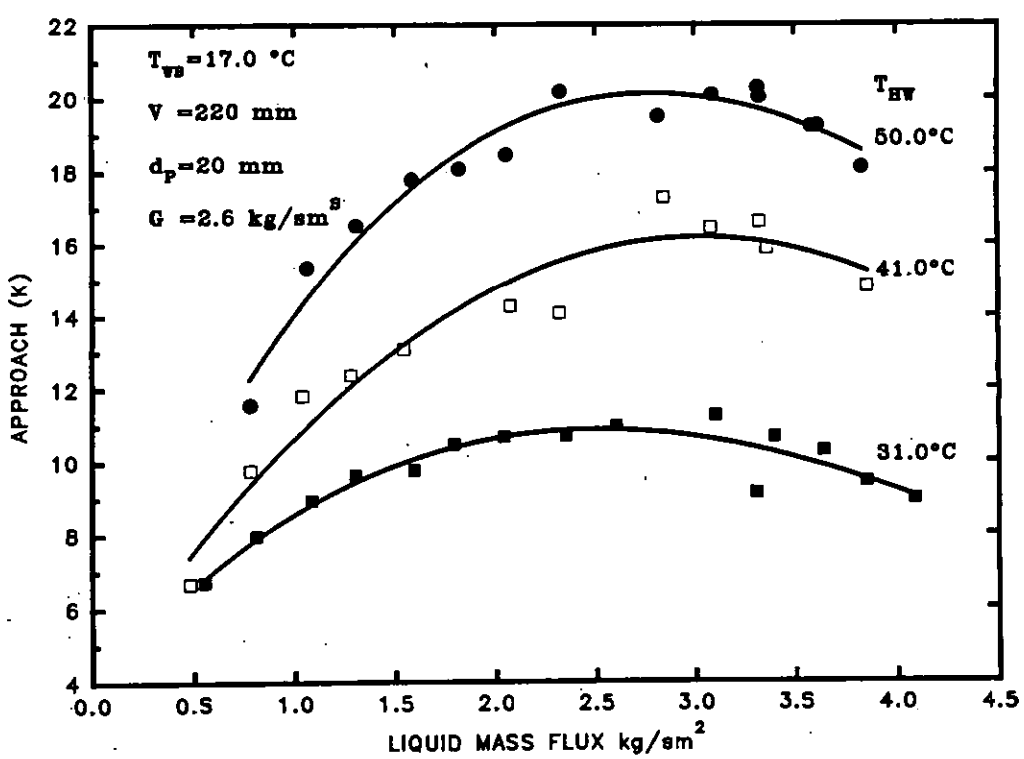

Figure 7.45 Effect of the liquid mass flux upon the approach based on the outlet cooled water conditions of the supporting grid. H = 400 mm, ρ_P = 239 kg/m^3. Fine spray nozzle type 3/4 SS - FF 4.8.

7.3 Effect of the Inlet Hot Water Temperature.

Figure 7.46 to 7.48 show the effect of the gas mass flux and the inlet hot water temperature upon the the tower performance. Irrespective of the position of the oulet cooled water temperature sensors, the tower characteristic decreases as the inlet hot water temperature is increased in good agreement with the findings of other investigators such as Kelly *et al.* (1956) who have researched conventional cooling towers.

For the FBCT, Dengler (1977) found that the tower characteristic deteriorated by about 10% for every degree rise in inlet hot water temperatures above 40°C which is in conflict with the findings of EL-Dessouky Hisham (1993). He reported an increase in the tower characteristic as the inlet hot water temperature is increased and attributing this peculiar behaviour to increases in the gas holdup as a result of decreases in the viscosity of water as the inlet hot water temperature increases. However, Marseille *et al.* (1991) carried out a theoretical analysis on the tower performance characteristic of conventional wet cooling towers and concluded that the tower characteristic decreases as the inlet hot water temperature is increased due to the assumptiom made by Merkel (1925) in his derivation of the enthalpy potential theory that neglected the liquid-side film resistance for heat and mass transfer and thus assuming that the temperature at the air water interface is that of the bulk water surrounding the air.

This assumption may be true at moderate inlet hot water temperatures below 40°C but the effects may be significant at relatively high inlet hot water temperatures when considerable sensible heat may be transferred from the hot water to the bulk air via the air/water interface. The result is that not all the heat transferred by the water to the air is accounted for by the enthalpy potential method of tower performance evaluation and thus an overprediction of tower performance at relatively low inlet hot water temperatures and an underprediction at relatively high inlet hot water temperatures.

Decreases in the tower characteristic as the inlet hot water temperature is increased may also be attributed to axial liquid mixing effects upon the FBCT operation. Koval *et al.* (1975a) have shown that the gas velocity exerts the greatest effect upon the axial liquid mixing in a FBCT and that the greater the difference in concentration of the liquid entering and leaving the bed, the greater the analytical error. These reasons may be applied to the cooling of water in the a bed with fluidised solids. Thus the increased difference in the tower characteristic as the gas mass flux is increased as shown in Figures 7.67 to 7.69. By analogy, an increase in differences in concentration of the liquid entering or leaving the tower may be considered as differences in the enthalpy potential relating to the differences in the inlet hot water and outlet cooled water temperatures. Barile *et al.* (1971) have shown that backmixing must be incorporated in the original equation of Merkel (1925). Therefore, the significant deterioration in the tower characteristic as the inlet hot water temperature is increased may also be attributed to the increase in backmixing with the operation tending towards a single equilibrium stage without true counter-current gas-liquid flow.

Figures 7.49 and 7.50 show that the cooling effectiveness increases as the inlet hot water temperature is increased for the same gas mass flux in contrast to the temperature effect upon the tower characteristic. This also shows that a given cooling tower can dissipate heat more efficiently and economically at a higher inlet hot water temperature. This is because the predominant process for the cooling of water is by the mass transfer of a fraction of the circulating water to the bulk moist air. The rate of mass transfer is a function of the difference between the partial pressure of the water vapour at the surface of the circulating water droplet and the partial pressure of the water vapour in the surrounding air. The larger the difference, the more quickly evaporation occurs and thus initiating a higher mass transfer rate as depicted in Figure 7.51 which shows that the rate of evaporation of water increases as the inlet hot water temperature is increased. It is known that the vapour partial pressure is proportional to the temperature for

a given fluid condition. Therefore, at a given inlet air condition, the vapour pressure driving force is increased by operating the FBCT at a higher inlet hot water temperature. This causes an increased water cooling rate and hence a larger cooling range and cooling effectiveness in Figures 7.73 to 7.74. Thus for a particular liquid mass flux, and assuming fluid properties remain unchanged, a higher power load may be handled at a higher inlet water temperature for the same FBCT dimensions.

The effects of the fluid flow rate and the inlet hot water temperature on *KaV/L* and *Ka* were discussed here. It was found that these variables significantly affect tower thermal performance. Other variables that can influence FBCT thermal performance will be discussed in the next chapter.

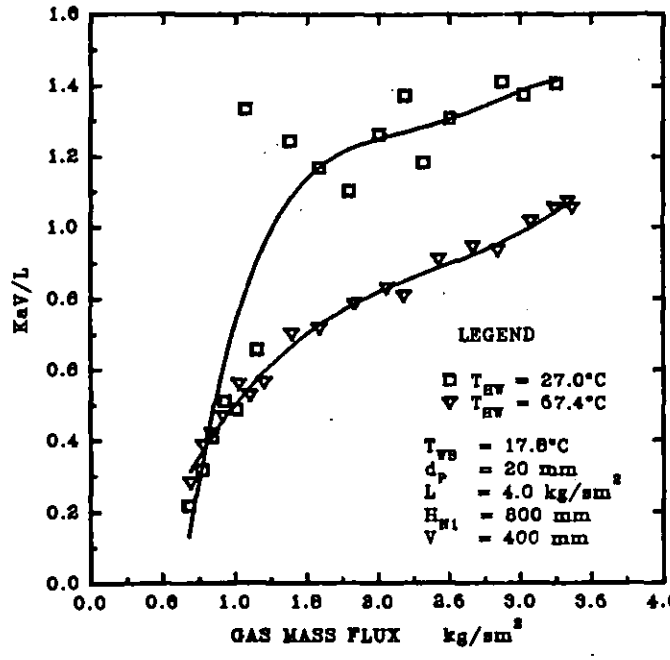

Figure 7.46 The effect of the gas mass flux and the inlet hot water temperature upon the tower characteristic based on the cooled water temperature from the plenum chamber for the coarse droplet spray nozzle. ρ_P = 245 kg/m^3.

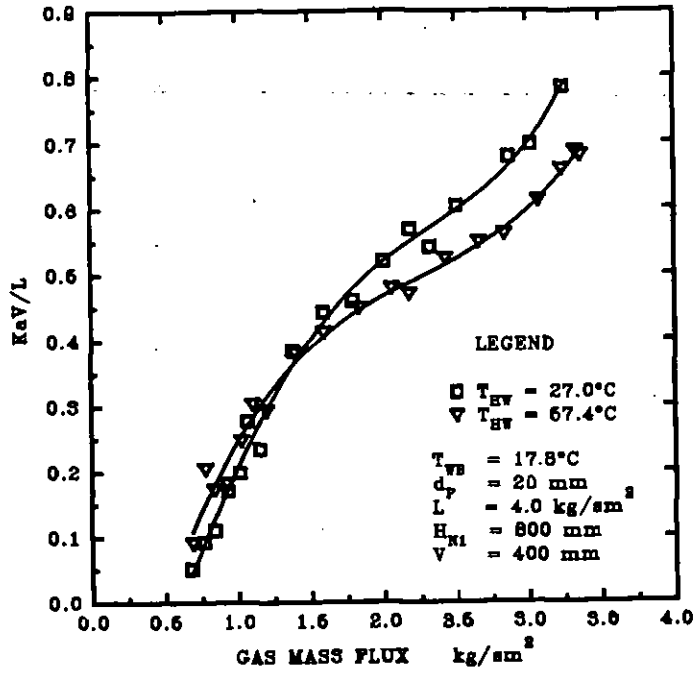

Figure 7.47 The Effect of the gas mass flux and the inlent hot water temperature upon the tower characteristic based on the outlet cooled water temperature from the distributor grid. Notations as in Figure 7.46.

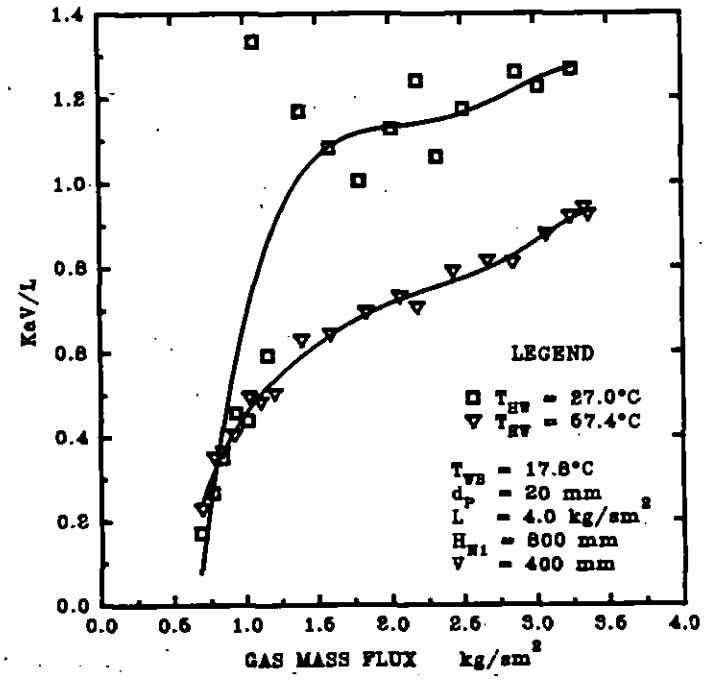

Figure 7.48 The effect of the gas mass flux and the inlet hot water temperature upon the tower characteristic based on the average outlet cooled water temperature. Notations as in Figure 7.46.

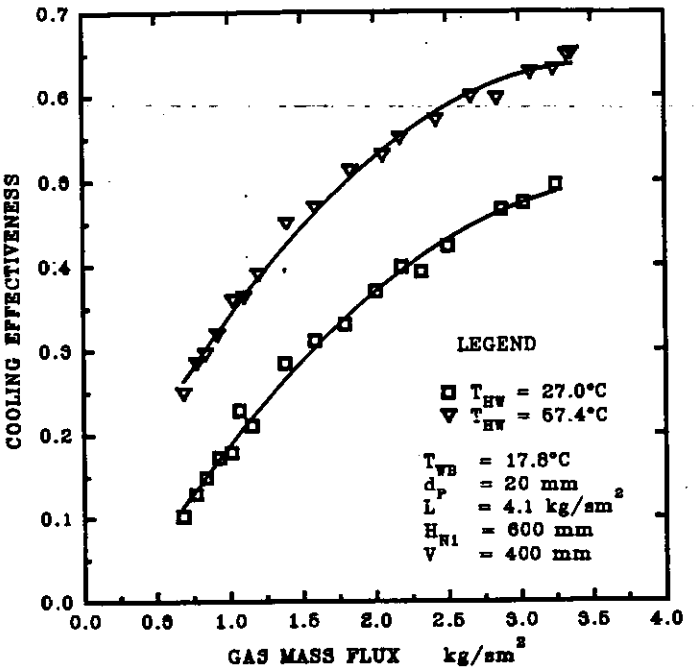

Figure 7.49 The effect of the gas mass flux and the inlet hot water temperature upon the cooling effectiveness base on the outlet cooled water temperature from the plenum chamber. Notations as in Figure 7.46.

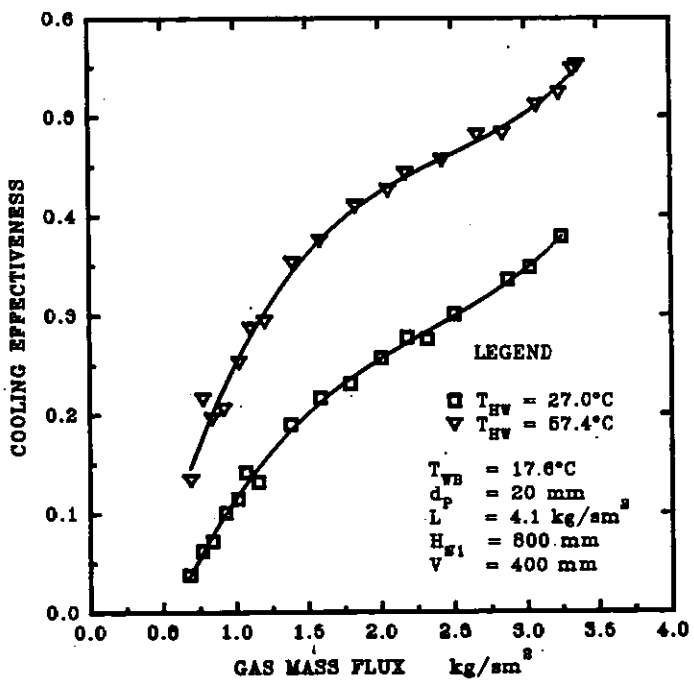

Figure 7.50 The effect of the gas mass flux and the inlet hot water temperature upon the cooling effectiveness based on the average outlet cooled water temperature. Notations as in Figure 7.46.

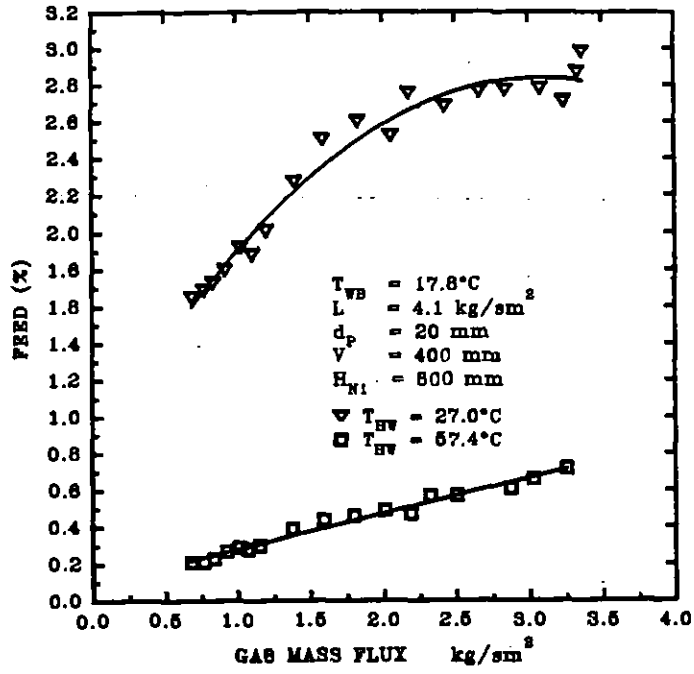

Figure 7.51 The effect of the gas mass flux and the inlet hot water temperature upon the percentage of liquid evaporated. Notations as in Figure 7.46.

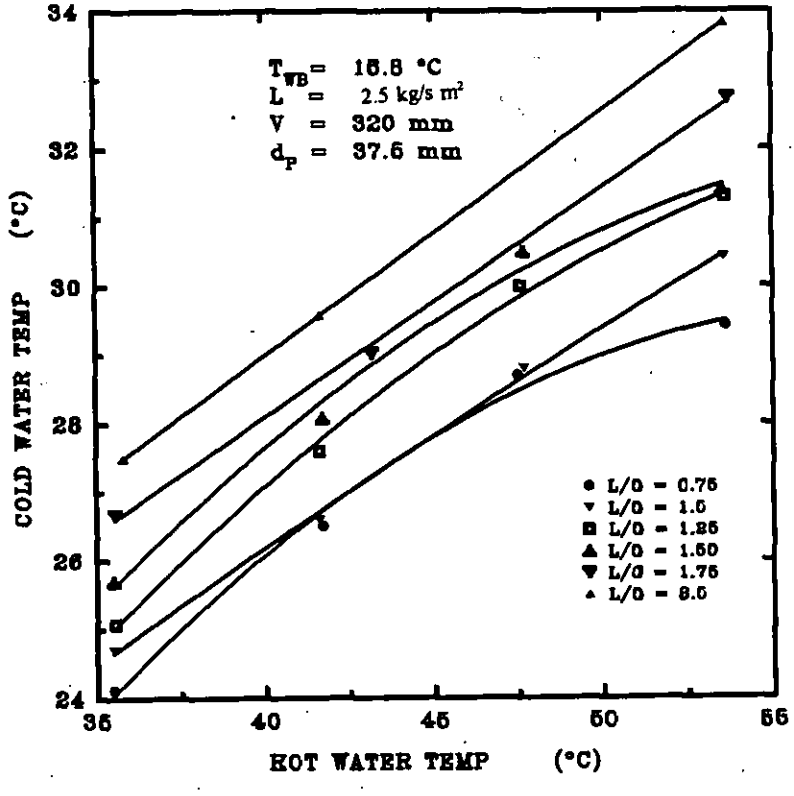

Figure 7.52 The effect of the inlet hot water temperature upon the outlet cooled water temperature from the distributor grid. Coarse droplet spray nozzle type 3/4 G - SS 3050. $\rho_P = 69$ kg/m^3.

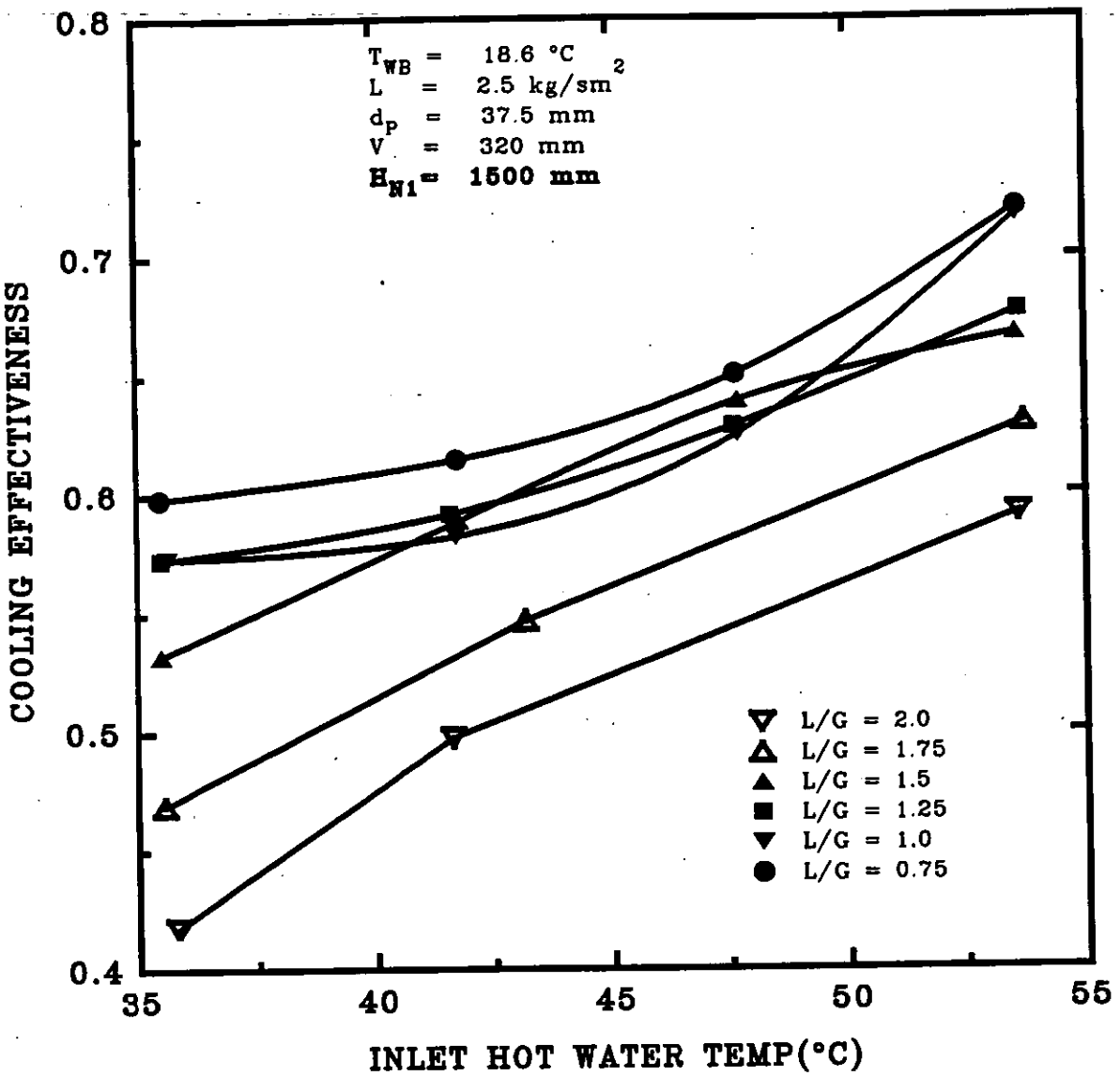

Figure 7.53 The effect of the inlet hot water temperature upon the cooling effectiveness. The data was generated from Figure 7.52 with the same notations.

CHAPTER VIII

EXPERIMENTAL RESULTS: THE EFFECT OF LINEAR DIMENSIONS AND PARTICLE PROPERTIES UPON THE THERMAL PERFORMANCE

8.1 Introduction

In this chapter, the experimental results relating to the design parameters that may constitute the physical characteristics of a full-size FBCT are discussed. Experiments were made so as to develop a clear picture of the most significant variables that may be used to develop design correlations relating to the tower thermal performance as well as verify the dimensional analysis carried out in chapter II. The linearly dimensioned variables were the spray nozzle height from the distributor grid, the spray nozzle type and the droplet size. The effect of the ρ_p and size were briefly described by Egbe *et al.* (1999) and in the appendix.

8.2 The Effect of the Static Bed Height

The effect of the static bed height upon the hydrodynamics of the FBCT has been studied in Chapter V. It was shown that the static bed height affects both the bed air pressure drop and the expanded bed height due to variations in the liquid and gas holdups. We have also shown in the previous chapter that the liquid and gas holdups affect the rate of heat and mass transfer. Although the effects of the static bed height upon the thermal performance have been mentioned in the preceeding sections, it is important that this parameter is studied in greater depth since it directly affects the size of the FBCT. Bearing this in mind, a series of experiments were designed and carried out so as to provide new insights on the fundamental workings of the FBCT in relation to heat and mass transfer.

Figures 8.1 to 8.14 below show the effect of the static bed height upon the FBCT thermal performance. In Figure 8.1, the effect of the static bed height and the

liquid/gas mass flux ratio, *L/G* upon the tower characteristic based on the outlet cooled water temperature from the plenum chamber for a constant gas mass flux is illustrated. For a particular *L/G* ratio, the tower characteristic increases as the static bed height is increased from 0 to 320 mm. It also shows that cooling does occur in an empty tower in the absence of packing.

The rate of increase in the tower characteristic with respect to increses in the static bed height decreases as the *L/G* mass flux ratio is increased. This may be attributed to the amount of liquid in the tower for the same gas mass flux. At a relatively small liquid/gas mass flux ratios, the predominant factor that affects the rate of heat and mass transfer in the FBCT is the gas-phase. Since the constant gas mass flux of 3.0 kg/s m^2 is relatively high (about three times that at the minimum fluidisation) the degree of turbulence is high. For a low liquid mass flux, therfore, a slight increase in the static bed height will result in a rapid increase in the interfacial activity and the bed heat transfer coefficient because of the high gas holdup. The increase in the gas-liquid interfacial area is also enhanced by the fine droplet spray. On the other hand, the tower characteristic decreases as the *L/G* mass flux ratio is increased for a particular static bed height since the liquid mass flux increases. As the liquid mass flux is increased and hence the *L/G* mass flux ratio at a constant gas mass flux of 3.0 kg/s m^2, the number of droplets in the bed increases. This decreases the rate of heat and mass transfer per unit mass flux of liquid as discussed in the previous chapter. Therefore, although the tower characteristic increases as the static bed height is increased, the rate of increase of the tower characteristic with respect to the static bed height decreases as the liquid/gas mass flux ratio is increased.

Figure 8.2 adds credence to the above explanation because a similar trend is observed as in Figure 8.1 for the same experimental condition. The former Figure shows that the percentage of liquid evaporated during for a given cooling duty generally increases as the static bed height is increased and decreases as the *L/G* mass flux ratio is increased for a constant gas mass flux. However, the rate of

increase of the percentage of liquid evaporated with respect increasing static bed height decreases as the liquid/gas mass flux ratio is increased. What is the cause of this phenomenon and what does it mean? A small liquid/gas mass flux ratio means that either the gas mass flux is high compared to the liquid mass flux or the liquid mass flux is small compared to the gas mass flux. In either case, this causes the water vapour partial pressure at the air-side of the gas-liquid interface to be greater than the water vapour partial pressure at the water-side of the interface thus creating a pressure gradient. Therefore at low liquid/gas mass flux ratio, the rate of diffusion of of water vapour into the bulk moist air stream increases.

At the same time, an increase in the static bed height causes an increased interfacial activity and hence intimate gas-liquid mixing resulting in an increase in heat and mass transfer rate. The combined effect is that the amount of liquid evaporated per unit liquid mass flux increases rapidly as the static bed height is increased. This phenomenon accounts for the rapid increase in the tower characteristic as the static bed height is increased for small liquid/gas mass flux ratios.

As the liquid/gas mass flux ratio is increased further, the number of droplets for a given gas mass flux and cooling duty increases. Although this may increase the FBCT enthalpy potential and hence driving force due to an increase in the gas-liquid interfacial area, the vapour partial pressure difference between the water vapour and the bulk moist air at the gas-liquid interface decreases because the increased water vapour in the bulk air causes the bulk air to approach saturation as the evaporation process proceeds. Therefore, the rate of increase of the proportion of evaporated water with respect to increases in the static bed height decreases as the static bed height is increased. At the same time, the proportion of liquid evaporated decreases as the liquid/gas mass flux ratio is increased.

Figures 8.3 and 8.4 show the effect of the static bed height upon the tower

characteristic based on the distributor grid and average outlet cooled water temperatures respectively at the same experimental conditions as in Figures 8.1 and 8.2. The tower characteristic increases as the static bed height is increased as expected. However, as opposed to Figure 8.1, the increase is not linear. The flattening of the curve as the static bed height is increased shows that there is a limit of cooling that may be attained for a particular type of packing arrangement and that, an infinite cooling range may not be possible by infinitely increasing the static bed height in line with the suggestion of Seetharamu *et al.* (1990). This may be accounted for by the fact that as the static bed height is increased, the rate of heat and mass transfer increases because the number of particles that makes contact with the liquid droplets increases and thus increasing the residence time of liquid in the bed. This coupled with increased turbulence, causes the effective gas-liquid interfacial contact to increase and with that the heat and mass transfer rate. However, the residence time of the liquid in the bed is not infinite.

An increased heat and mass transfer rate as a result of an increased static bed height causes the evaporation rate to increase. As the static bed height is increased further, the net partial pressure at the gas-liquid interface decreases as the bulk moist air tends towards saturation. Therefore, the tower characteristic flattens out as the static bed height is further increased.

This FBCT behaviour was further investigated by experimenting with large droplet spray nozzle as shown in Figures 8.5 to 8.7 which show similar results as in Figure 8.3 and 8.4 despite differences in experimental conditions and in good agreement with the findings of Barile *et al.* (1974) and Dengler (1977).

Figures 8.8 shows the effect of the satic bed height upon the mass transfer coefficient Ka. The Ka decreases as the static bed height is increased in line with earlier findings in chapter VII. This may be attributed to the decrease in the liquid holdup per unit static bed volume h_L, as the static bed height is increased as the static bed height is increased in agreement with findings in Chapter V.

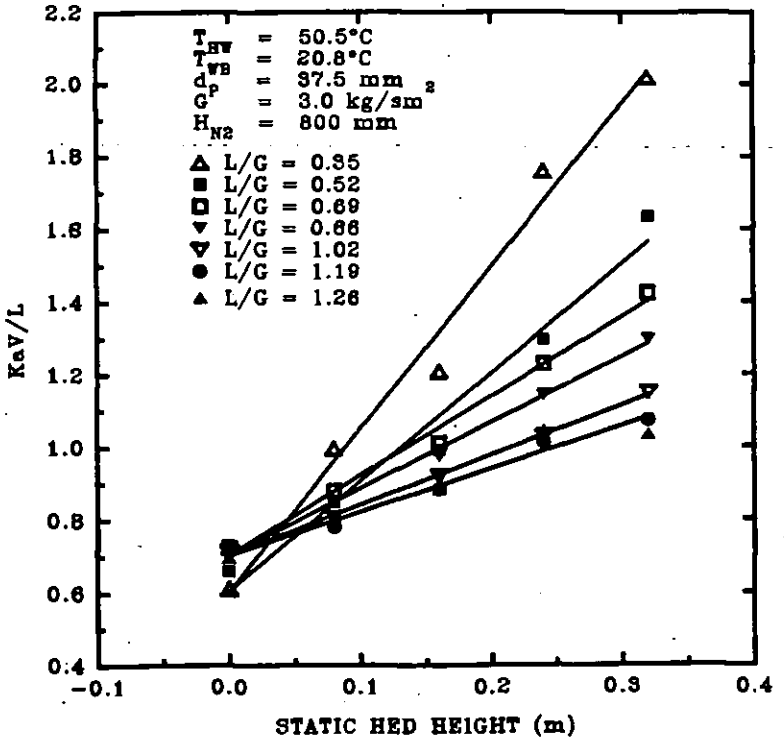

Figure 8.1 The effect of the static bed height and the liquid/gas mass flux ratio on the tower characteristic for a type I FBCT based on the outlet cooled water temperature from the plenum chamber. ρ_p = 69 kg/m^3. Fine droplet spray nozzle type 3/4FF - SS 4.8.

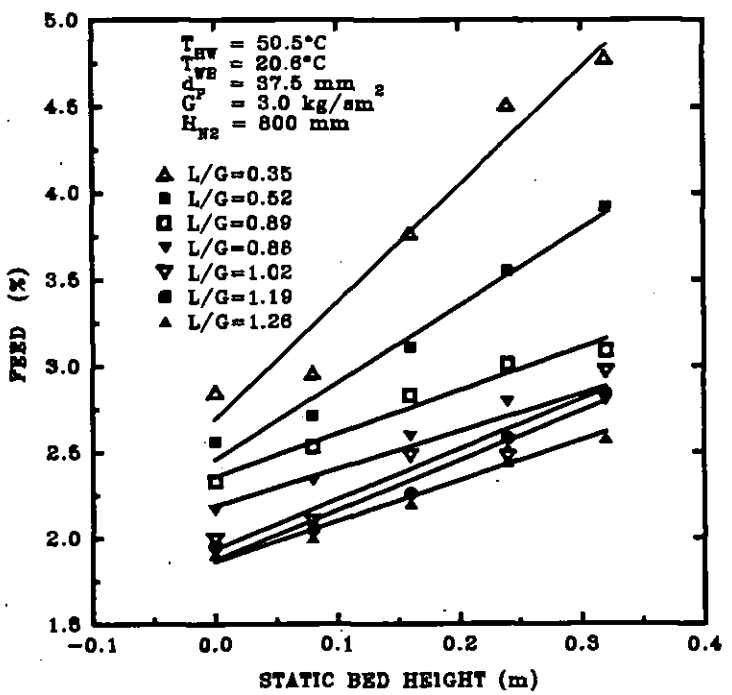

Figure 8.2 The effect of the static bed height and the liquid/gas mass flux ratio on the percentage of water evaporated for a type I FBCT operation. ρ_p = 69 kg/m^3. Fine droplet spray nozzle type 3/4 FF - SS 4.8.

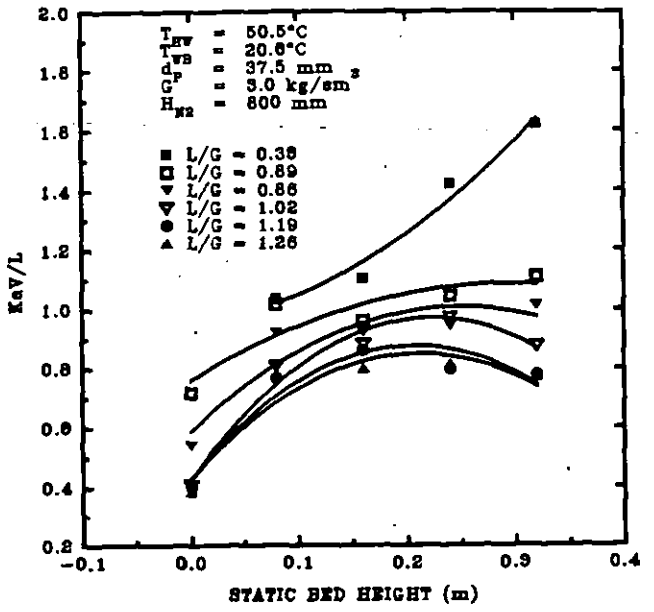

Figure 8.3 The effect of the static bed height upon the tower characteristic for a type I FBCT based on the outlet cooled water temperature from the distributor grid. ρ_P = 69 kg/m^3. Fine droplet spray nozzle type 3/4FF - SS 4.8.

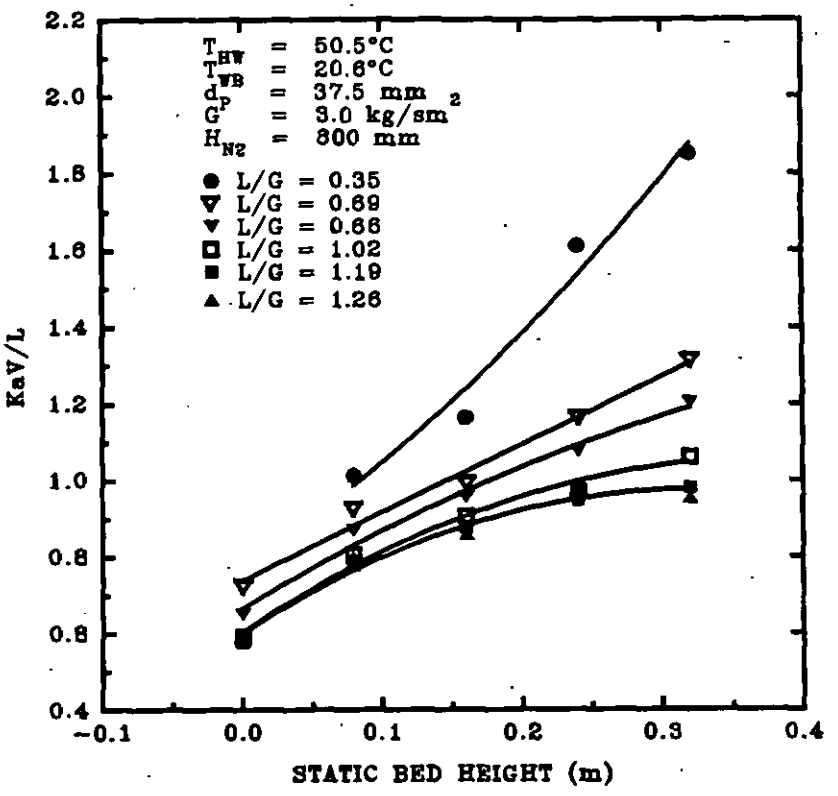

Figure 8.4 The effect of the static bed height and the liquid/gas mass flux ratio upon the tower characteristic based on the average outlet cooled water temperature for a type I FBCT operation. ρ_P = 69 kg/m^3. Fine droplet spray nozzle type 3/4 FF - SS 4.8.

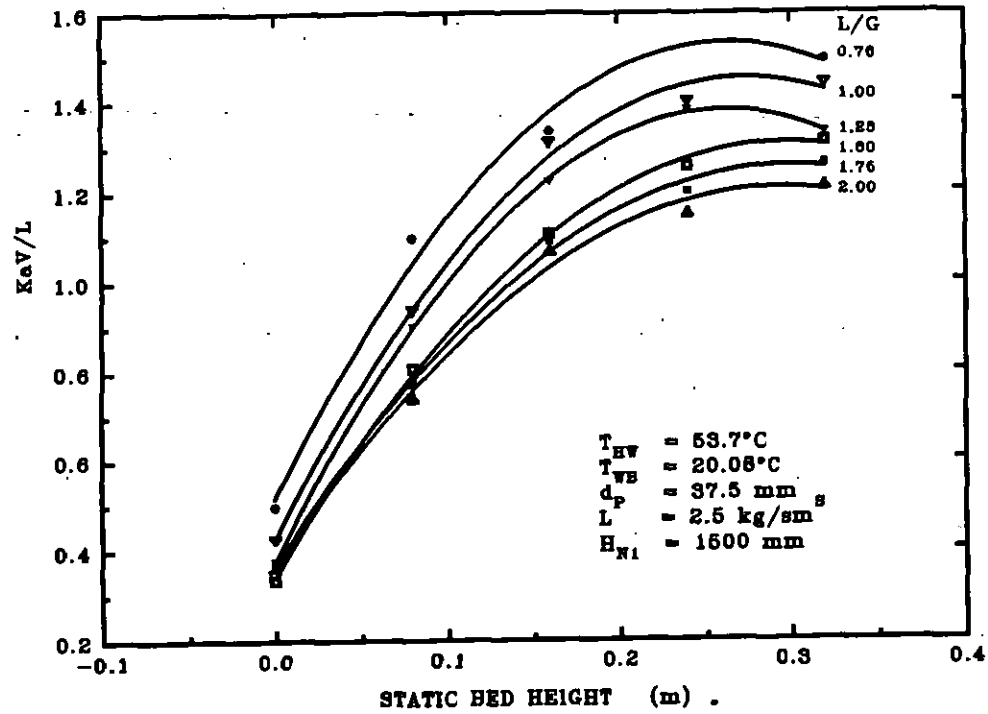

Figure 8.5 The effect of the static bed height and the liquid/gas mass flux ratio upon the tower characteristic for a type I FBCT operation based on the outlet cooled water temperature from the distributor grid. ρ_P = 69 kg/m^3. Coarse spray nozzle type 3/4 G - SS 3050. A cross-plot of Figure 7.7 in chapter VII.

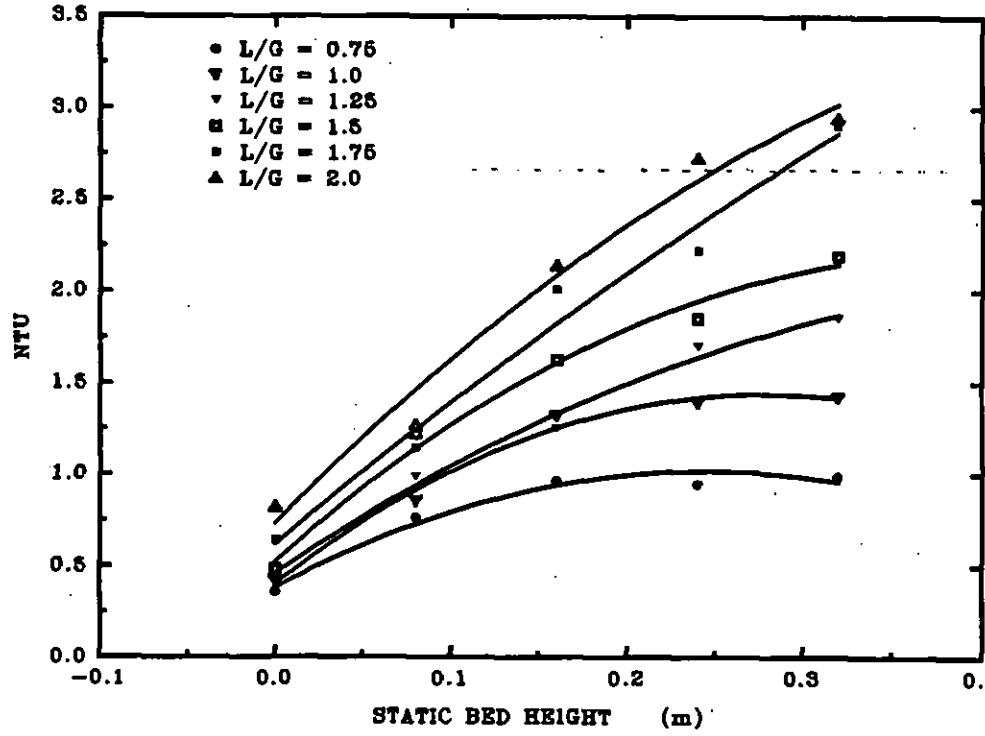

Figure 8.6 Effect of the static bed height and the liquid/gas mass flux ratio on the number of transfer unit calculated from the data of Figure 8.5.

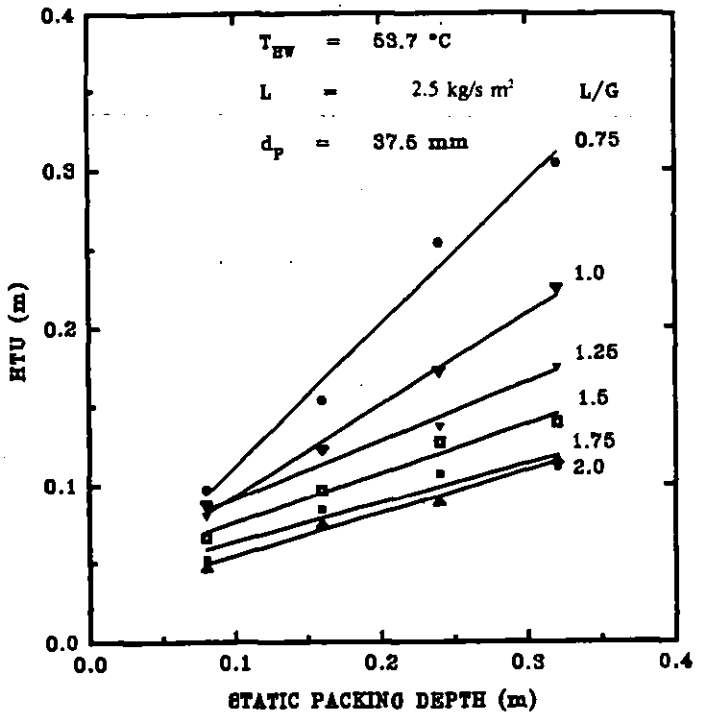

Figure 8.7 The effect of the static bed height and the liquid/gas mass flux rastio upon the height of a gas-phase transfer unit calculated from the data of Figure 8.5.

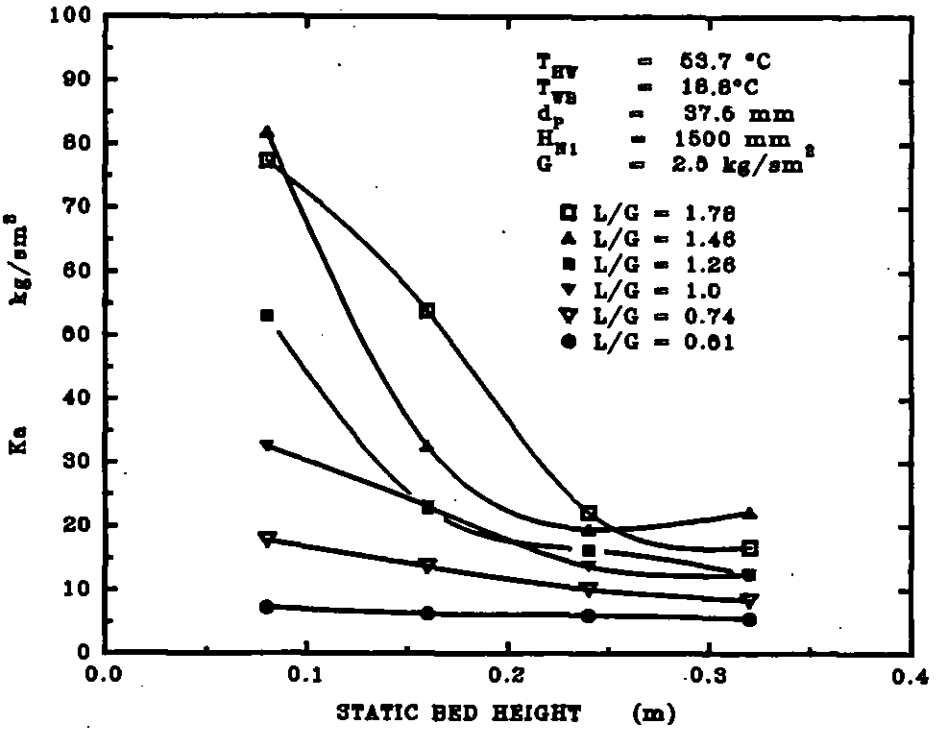

Figure 8.8 The effect of the static bed height and the liquid/gas mass flux ratio on the overall mass transfer coefficient for a type I FBCT operation based on the outlet cooled water temperature from the distributor grid. $\rho_p = 69$ kg/m^3. Coarse droplet spray nozzle type 3/4 G - SS 3050.

8.3 The Effect of the Spray Nozzle Configuration

It is important to study the effect of the spray nozzle configuration on the thermal performance because it is invaluable in the creation of fresh water surfaces for interfacial gas-liquid heat and mass exchange in evaporative counterflow cooling processes. Seven series of experiments were performed on all four different particles so as to establish the effect of the three spray nozzle types upon the FBCT thermal performance based on the grid, average and the plenum chamber outlet cooled water temperatures. In order to mimimize wall effects and ensure uniform fluidisation, care was taken so that the maximum *H/V* ratio was not greater than 4. Data analysis suggests that the FBCT thermal performance is significantly affected by the spray nozzle configuration and that end effects in the tower plays an important role in gas-liquid heat and mass exchange.

Figures 8.11 to 8.13 show the effect of the nozzle configuration upon the tower characteristic based on the plenum chamber, distributor grid and average cooled water temperatures respectively for a relatively low density type I FBCT regime. In all three cases, the fine droplet spray gave a better thermal performance than the coarse droplet spray for similar experimental conditions keeping the gas mass flux constant. The reason for this effect may be attributed to the increased amount of droplets generated by the fine spray nozzle as compared to that generated by the coarse spray nozzle for the same liquid/gas mass flux ratio. The increased number of droplets substantially increases the gas-liquid interfacial contact area and hence the heat and mass transfer coefficient.

Although the effect of the nozzle configuration is similar in all three cases of the outlet cooled water conditions, it is most significant when the tower characteristic is calculated based on the cooled water temperature from the supporting grid as seen in Figure 8.12. As the spray strikes the packing, it creates a free opening in the middle of the bed as fluidisation occurs because the coarse droplets are concentrated and individually heavier than the fine droplets. As a result, a higher

proportion of the coarse droplets pass through the tower without intimate contact with the upward flowing air due to the decrease in the liquid residence time in the bed.

As the droplets progress through the distributor grid and onto the plenum chamber, high gas-liquid interfacial activity continues to occur. Since the plenum chamber is now charged with only air and water, bubbles are formed with the droplets being blown around in different directions in a random manner. As each of the coarse large droplets have a high weight, the degree of two-phase gas-liquid mixing is much more intense than for fine droplets. This increased agitation enhances the rate of heat and mass transfer which may have partly counteracted the higher interfacial area of the small fine droplets within the fluidised bed itself. This causes a reduced effect of the spray nozzle configuration upon the tower characteristic as the water leaves the plenum chamber.

Figures 8.14 to 8.16 show the effect of the liquid/gas mass flux ratio and the spray nozzle configuration upon the tower charactristic for a type II FBCT operation based on the plenum chamber, distributor grid and average cooled water temperatures respectively. They indicate that a better thermal performance is achieved with small fine droplets than with large coarse droplets for the same liquid/gas mass flux ratio in conformity to the previous finding. However, the effect is more significant at the plenum chamber than at the supporting grid condition. This phenomenon may be attributed to both the increased particle density and the reduced particle size.

It was shown in chapter V that an FBCT operating with the 20 mm particles having a density of 239 kg/m^3 has high bed air pressure drops due to increased liquid holdups as a result of increases in residence times which is in turn caused by reduced static and dynamic porosities and increased particle surface area. Therefore, the amount of liquid holdup in the bed and hence the plenum chamber is higher than in a type I operation. In addition, we showed in chapter V that for

low density particles, fine spray droplets gave a higher pressure drop than coarse ones due to a better holdup of liquid. This causes the gas-liquid interfacial area to increase substantially at the outlet conditions and therefore an increase in the heat and mass transfer rate giving rise to a more significant effect of the spray nozzle configuration upon the tower characteristic at the plenum chamber than at the grid condition where interfacial activity is confined only to the fluidised bed itself. Since the density of the type II operation shown in Figures 8.14 to 8.16 is higher than the type I operation of Figure 8.11 to 8.13, the effect of concentration of spray in the middle of the bed and hence the creation of a hollow free flowing passage is minimal. This may be one of the causes of a low response of tower thermal performance as the spray droplet types are varied.

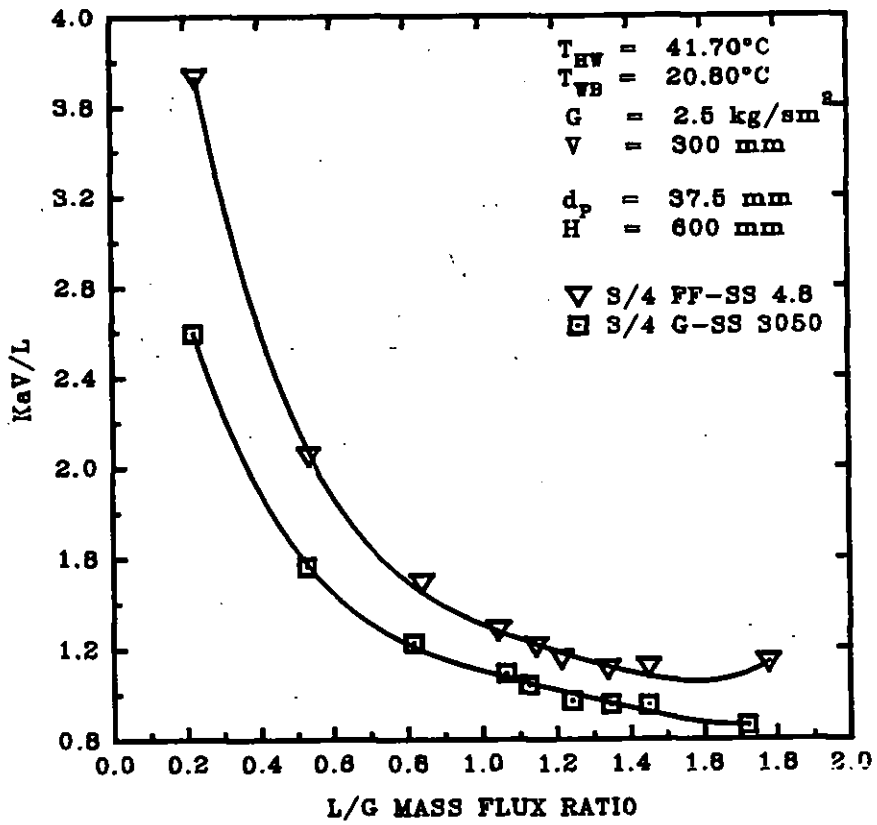

Figure 8.11 The effect of the liquid/gas mass flux ratio and the spray nozzle configuration upon the tower characteristic for a type I FBCT operation based on the plenum chamber cooled water temperature. ρ_P = 69 kg/m^3. 3/4 FF - SS 4.8 denotes fine droplet spray nozzle. 3/4 G - SS 3050 denotes coarse droplet spray nozzle.

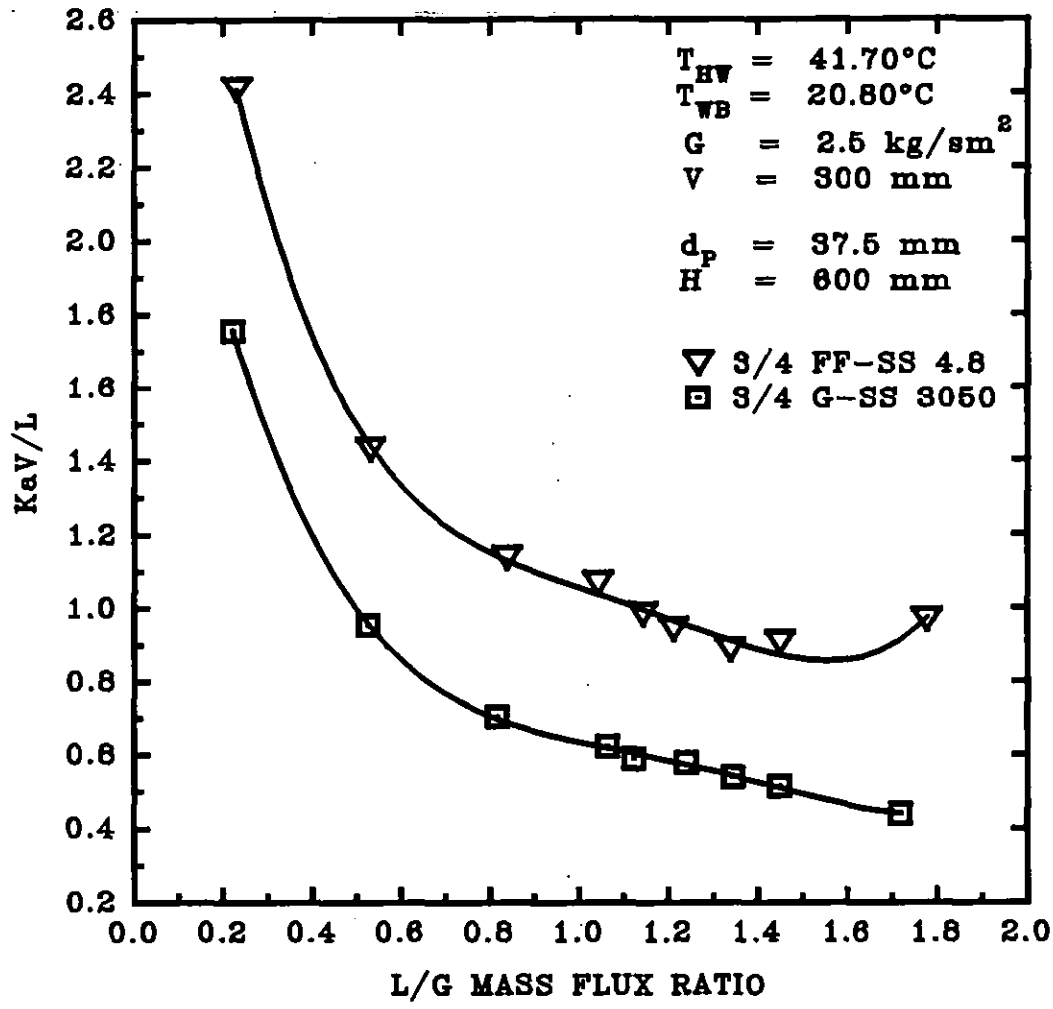

Figure 8.12 The effect of the liquid/gas mass flux ratio and the spray nozzle configuration upon the tower characteristic for a type I FBCT operation based on the cooled water temperature at the supporting grid. ρ_P = 69 kg/m^3. Nozzle codes as in Figure 8.11.

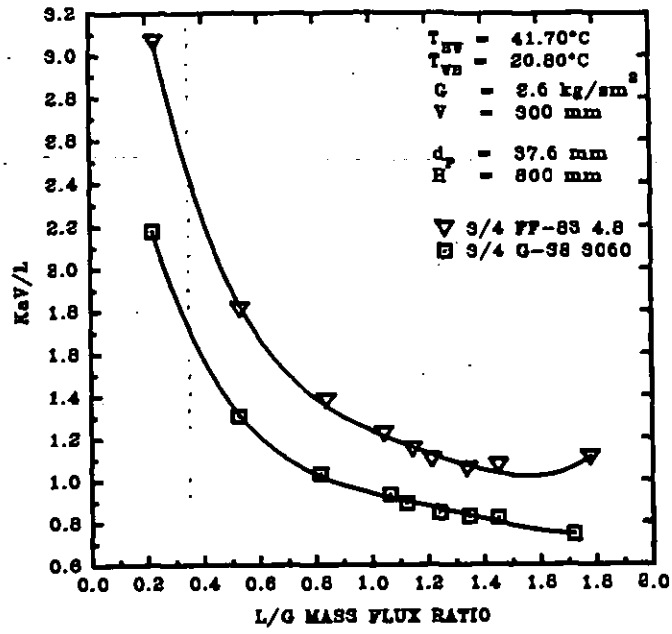

Figure 8.13 The effect of the liquid/gas mass flux ratio and the spray nozzle configuration upon the tower charateristic of a type I FBCT operation based on the average cooled water temperature. ρ_p = 69 kg/m^3. Nozzle codes as in Figure 8.11.

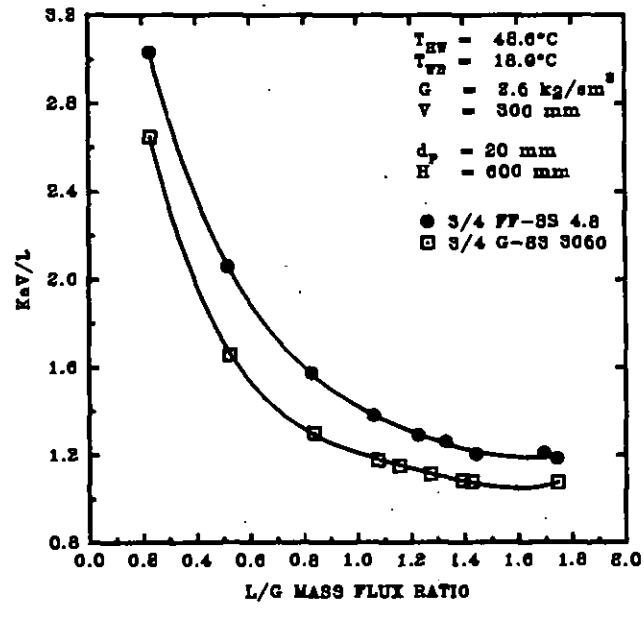

Figure 8.14 The effect of the liquid/gas mass flux ratio and the spray nozzle configuration upon the tower characteristic of a type II operation based on the outlet cooled water temperature. ρ_p = 239 kg/m^3. Nozzle codes as in Figure 8.11.

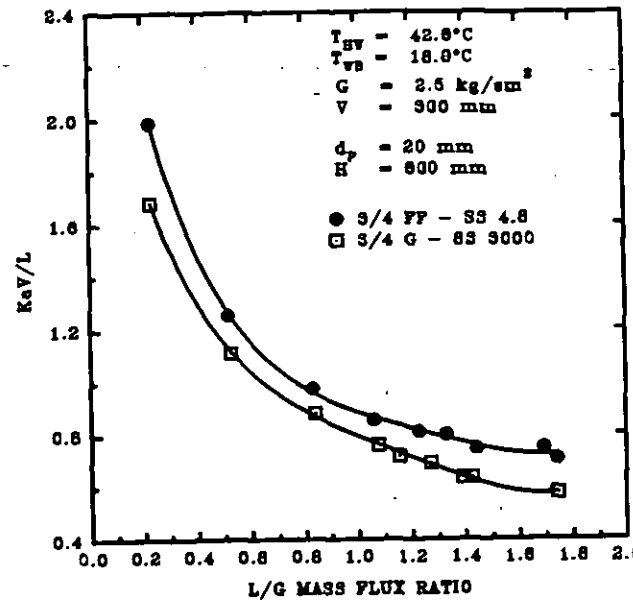

Figure 8.15 The effect of the liquid/gas mass flux ratio and the spray nozzle configuration upon the tower characteristic of a type II FBCT operation based on the cooled water temperature of the supporting grid. $\rho_p = 239$ kg/m^3. Nozzle codes as in Figure 8.15.

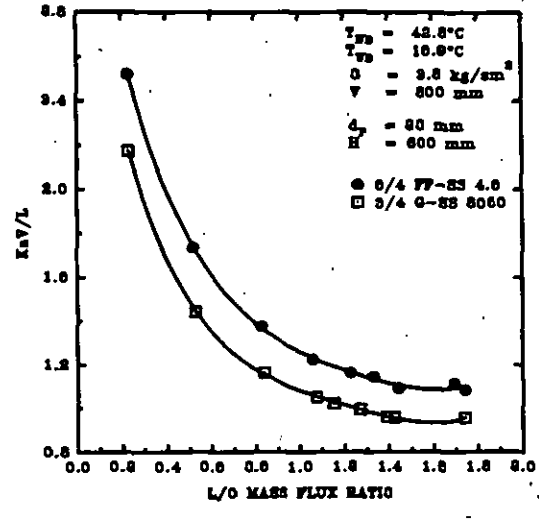

Figure 8.16 The effect of the liquid/gas mass flux ratio and the spray nozzle configuration upon the tower characteristic of a type II FBCT operation based on the average cooled water temperature. $\rho_p = 239$ kg/m^3. Nozzle codes as in Figure 8.11.

Figures 8.17 to 8.19 below illustrate the effect of the liquid/gas mass flux ratio *L/G*, and the spray nozzle configuration upon the tower characteristic for a type II FBCT operation under similar experimental conditions as in Figures 8.11 to 8.13. Although the effects of the liquid/gas mass flux ratio upon the tower characteristic are similar, the effect of the spray nozzle configuration is unexpected. As shown in Figure 8.17, the tower characteristic based on the plenum chamber outlet cooled water temperature is generally higher for the large coarse droplets than for the small ones for the same liquid/gas mass flux ratio *L/G*. However, at the distributor grid outlet cooled water conditions, the small droplet spray gave a slightly higher tower characteristic than the large ones shown in Figure 8.18. On the average, the coarse large droplet spray exhibit a better thermal performance than small fine droplets as seen in Figure 8.19.

This behaviour is peculiar to evaporative cooling. The most likely explanation may lie in the drop sizes, particle density and size. The high particle density of of 326 kg/m^3, means that flooding occurs in the tower before the minimum fluidisation state is reached. The effect is that droplets are entrained above the bed. Notage and Boelter (1940) have theoretically shown that deceleration of water droplets by an upward moving surrounding air has a more significant effect as regards the rate of heat transfer for small fine droplets that for large coarse ones. Therefore, small fine droplets are more likely to be carried out of the contacting zone because of their low individual weights as opposed to large coarse droplets having greater weights. In fact, Nottage and Boelter (1940) have estimated that a drop diameter of about 600 microns has a maximum velocity of about 2.5 m/s above which drift is likely to occur. Although the drift may be obviated by the drift eliminator, there is no evidence as to the maximum velocity at which this device is 100% effective for a FBCT. On this basis, it may be inferred that the fine droplets may have been blown out of the tower to be carried off as part of the exhaust air.

Nevertheless, the effect of a reduction in the number of droplets upon the heat and

mass transfer coefficient is not realised immediately after the water leaves the bed possibly because heat and mass exchange between the water droplets and the surrounding air continues to occur as the fine droplets are transported out of the working zone of the tower, and partly due to the fact that there is a threshold number of droplets that can be entrained at a specific instance beyond which the drift counteracts the increased rate of heat and mass transfer generated by the counter-current contact of air and water as reported by Nottage and Boelter (1940). This may account for the increase in KaV/L as the droplet size is decreased as shown in Figure 8.18 as opposed to that shown in Figure 8.19.

As the droplets enter the plenum chamber, drift continues to occur. However, this is limited since some of the droplets fall back to the chamber on impact upon the specially designed distributor that also acts as an air/water separator. Therefore, the main determinant in the heat and mass transfer process in the plenum chamber is the degree of turbulence and the total number of droplets present. Since many more fine small droplets are carried out of the tower into the exhaust than the large coarse droplets, there is a possibility of higher heat and mass transfer rate due to higher gas/liquid surface of contact for large coarse droplets than for small fine droplets. The conjecture by Nottage and Boelter (1940) that a certain optimum exists after which drift affects the tower characteristic, may therefore hold in this instance.

Another possible explanation for the higher tower characteristic of the coarse large droplets as compared to fine small droplets may be due to the degree of intimate mixing that occurs in the plenum chamber. A higher degree of turbulence is expected with the large droplets than the small droplets because of their greater individual weights, which give rise to a better degree of gas-liquid intimate mixing and hence a higher heat transfer coefficient in the plenum chamber. During experimental runs, many more bubbles were seen in the plenum chamber for the large droplets than the small fine ones. It has been shown that the gas-liquid interfacial area increases as the gas holdup increases, and that the gas

depended upon the number of bubbles generated in the tower [Epstein, 1981]. This may have contributed to the increased heat and mass transfer rate of the large spray nozzles as seen in Figure 8.17. As shown in Figure 8.18, the effect of the spray nozzle configuration upon the tower characteristic is small although the fine droplet spray exhibits a better cooling effect. Therefore, an increased interfacial activity in the plenum chamber above an optimum level may offset the increased heat and mass exchange experienced by the water immediately after it leaves the fluidised bed itself and enters the plenum chamber.

It was shown in Chapter V that the large coarse droplets gave a higher bed air pressure drop than the fine spray droplets for the same liquid mass flux keeping the gas mass flux constant for type II relatively high density particles. The reason for this behaviour was partly attributed to an increased liquid holdup due to increased residence time as the droplet size is increased. Increased liquid holdups may mean a higher interfacial activity in the bed. However, increased interfacial activity is not the only factor that affects the rate of heat and mass transfer. In this instance, especially in the fluidised bed itself, the drop size and hence its number is the predominant factor since similar experimental conditions are applied to both spray droplet types. Therefore, the increased tower characteristic shown in Figure 8.18 is expected. However, an increased residence time and hence increased liquid holdup for the coarse large droplets means that the coarse droplets spend more time in the plenum chamber than the small fine droplets. This may have increased the degree of two-phase gas-liquid mixing at steady state conditions and hence a better heat and mass transfer rate as seen in Figures 8.17 and 8.19. In type II FBCT operation, turbulence levels and hence interfacial activity in the bed increases as the particle density increases. An increase in turbulence in the bed is also reflected in the plenum chamber. Therefore, the heat and mass transfer rate may be higher in the plenum chamber for a type II FBCT than for a type I regime for experiments carried out at similar experimental conditions. Thus, although the reponse of the tower characteristic with changes in the droplet sizes and property may be similar at the grid conditions, it is

different in the two types of FBCT operation at the plenum chamber conditions.

The particle density and the liquid/gas mass flux ratio may not be the only factors that interacts with the spray nozzle configuration to affect the FBCT thermal performance. Therefore the effect of the nozzle configuration upon the tower characteristic studied so far may not be conclusive given the conflict of evidence as shown in Figures 8.11 to 8.19. Bearing this in mind, two different series of experiments were carried out so as to substantiate the argument adduced thus. The effect of the inlet water temperature upon the tower thermal performance, for

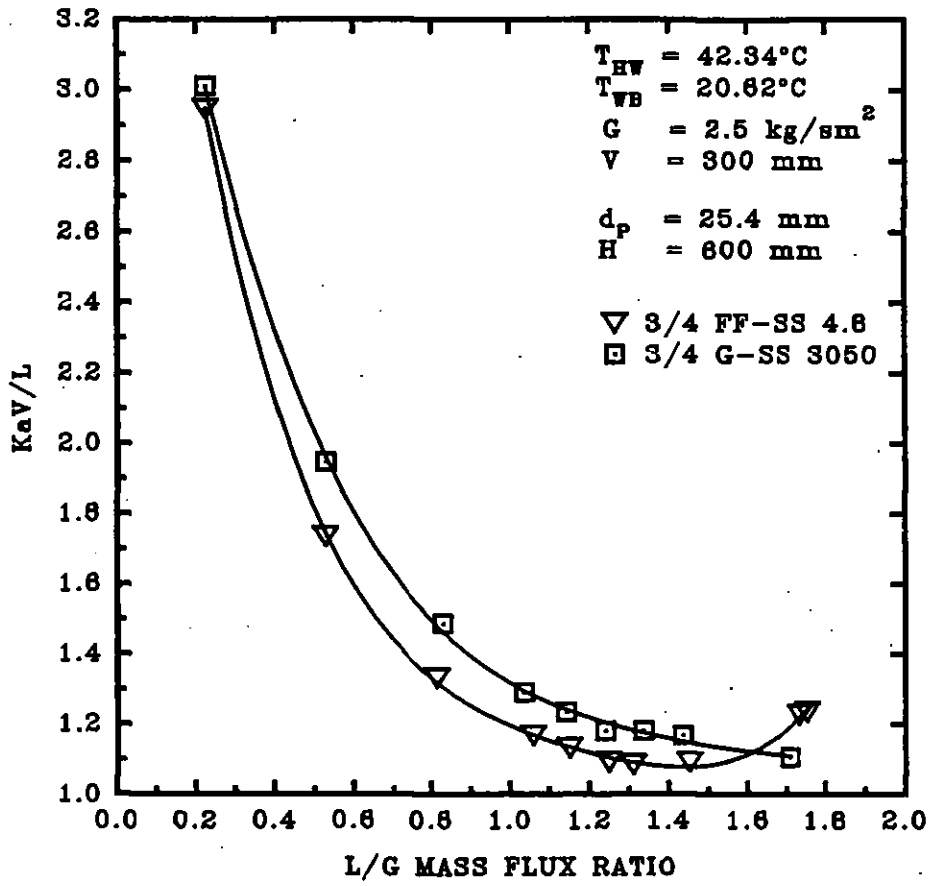

Figure 8.17 The effect of the liquid/gas mass flux ratio and the spray nozzle configuration upon the tower characteristic for a type II FBCT opertation based upon the outlet cooled water temperature of the supporting grid. $\rho_p = 326$ kg/m^3. Nozzle codes as in Figure 8.11.

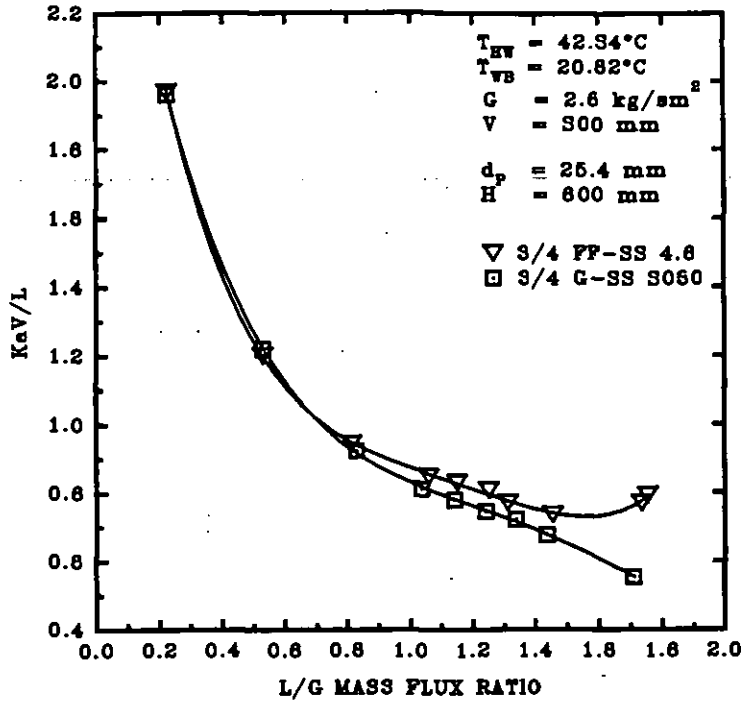

Figure 8.18 The effect of the liquid/gas mass flux ratio and the nozzle configuration upon the tower characteristic for a type II FBCT opertaion based on the cooled water temperature at the supporting grid. $\rho_P = 326$ kg/m^3. Spray nozzle codes as in Figure 8.11.

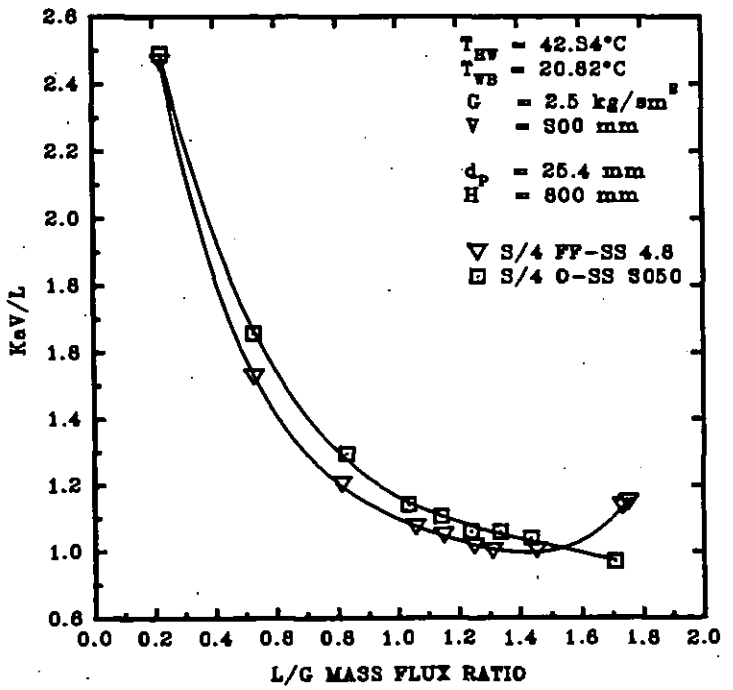

Figure 8.19 The effect of the liquid/gas mass flux ratio and the spray nozzle configuration upon the tower charateristic of a type II FBCT operation based on the average cooled water temperature. $\rho_P = 326$ kg/m^3. Spray nozzle code as in Figure 8.11.

example, have been shown to be important in Chapter VII. Figures 8.20 to 8.22 below shows the effect of the inlet water temperature and the spray nozzle configuration upon the tower characteristic for a shallow static bed depth situation and keeping the liquid/gas mass flux ratio *L/G*, constant at a typical value of 0.82.

For the same inlet water temperature, the large coarse droplet spray gave a better performance than the fine small droplet at the plenum outlet cooled water conditions. This may be due to the high gas mass flux that causes the small droplets to be entrained out of the working zone of the tower. The effect is therefore a reduced amount of droplets entering the plenum chamber and hence a reduction in gas-liquid interfacial contact. This results in a reduction in the heat and mass transfer coefficient. Another explanation may be found in the degree of vibration that occurs in the plenum chamber because of the very high gas flow rate. The high gas mass flux means that the interfacial activity in the plenum chamber is intense due to high turbulence levels. This action may serve to break the large droplets into smaller ones thus increasing the area of gas-liquid contact. This together with the increased bed agitation may have caused the large droplets to exhibit a better heat transfer rate than the small fine ones. Figure 8.20 also shows that the trend in tower characteristic response with respect to changes in spray nozzle configuration is similar in both types as the inlet water temperature is increased. The tower characteristic decreases as the inlet water temperature is increased thus confirming earlier findings in chapter VII. Figure 8.21 depicts the effect of the inlet hot water temperature and the spray nozzle configuration upon the tower characteristic based on the outlet cooled water temperature at the distributor. It confirms earlier finding that the small fine spray gives a better preformance at the grid conditions due to increased gas-liquid interfacial contact area. Although the small droplets may have been entrained out of the tower, heat and mass exchange continues to occur as the small droplets are transported out of

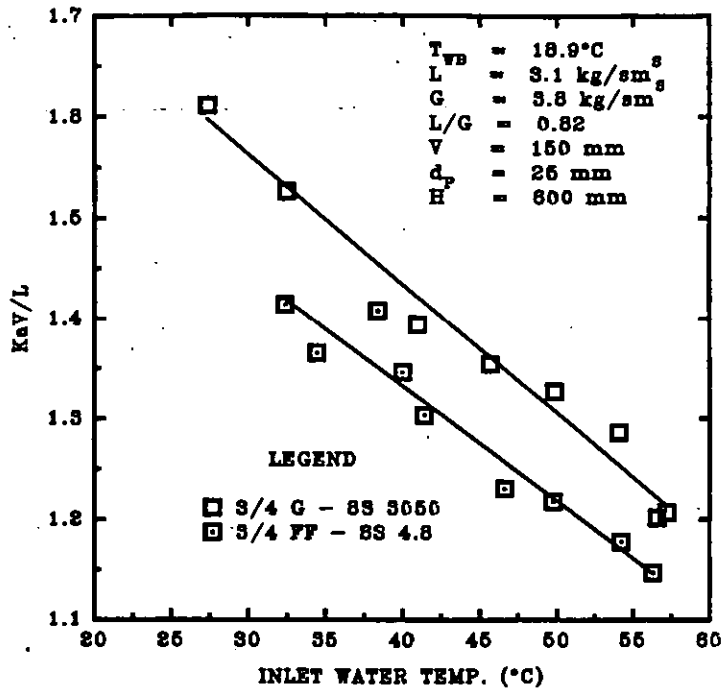

Figure 8.20 The effect of the inlet hot water temperature and the spray nozzle configuration upon the tower characteristic for a shallow bed model type I FBCT operation based on the final outlet cooled water temperature. ρ_P = 245 kg/m^3. Spray nozzle codes as in Figure 8.11.

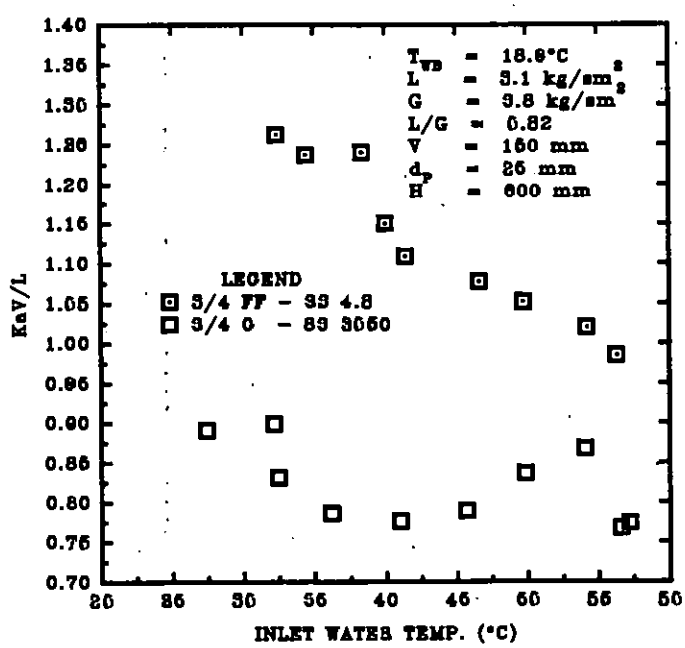

Figure 8.21 The effect of the inlet hot water temperature and the spray nozzle configuration upon the tower characteristic for a shallow bed model type I FBCT operation based on the cooled water temperature at the supporting grid. ρ_P = 245 kg/m^3. Spray nozzle codes as in Figure 8.11.

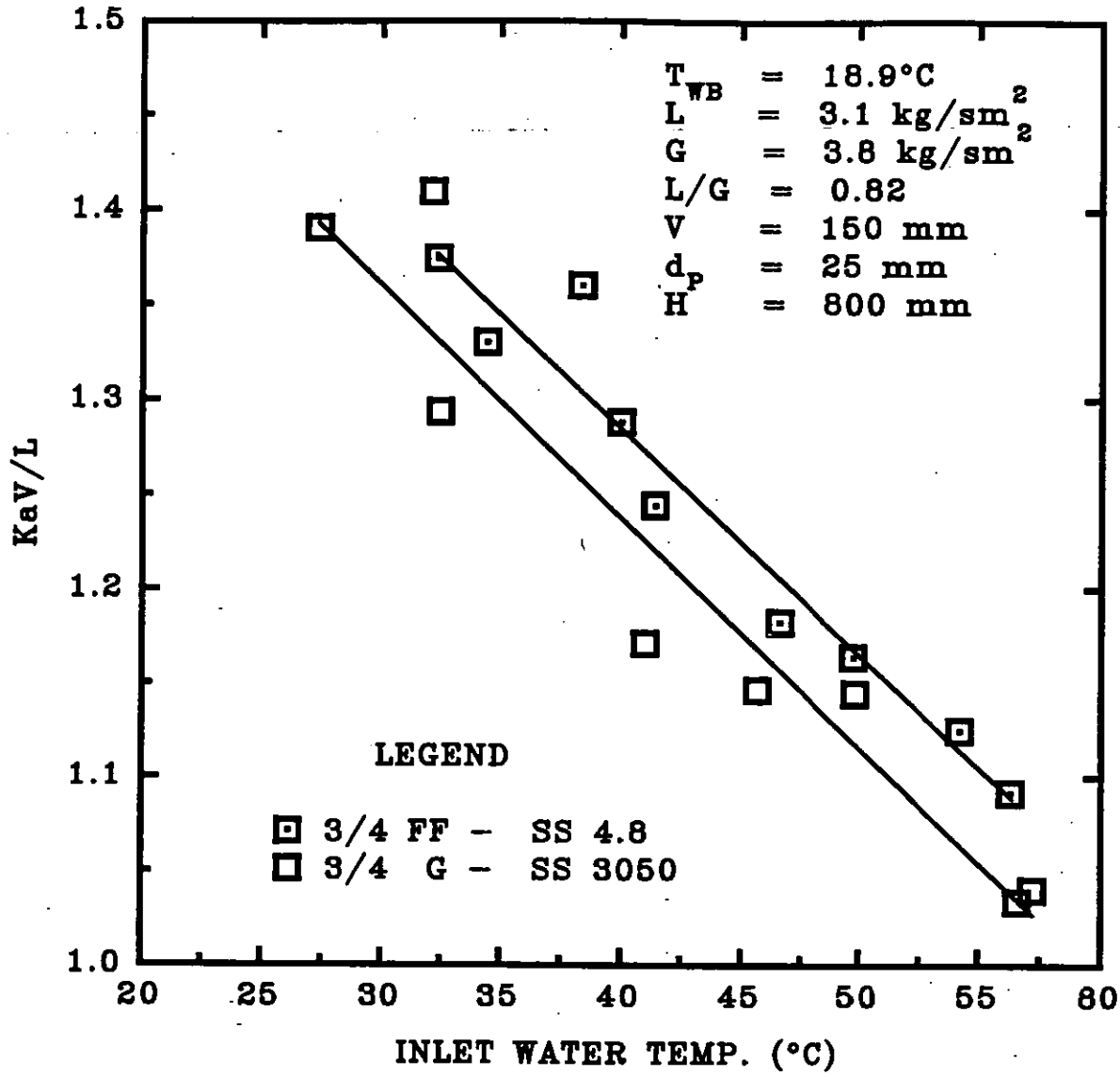

Figure 8.22 The effect of the inlet hot water temperature and the spray nozzle configuration upon the tower characteristic of a shallow bed model type I FBCT operation based on the average cooled water temperature. $\rho_P = 245$ kg/m^3. Spray nozzle codes as in Figure 8.11.

The increased effect upon the tower characteristic by the nozzle configuration at the grid cooled water conditions as compared to those at the plenum chamber may partly be attributed to the shallow static bed height. In chapter V it was shown that the expanded bed height increases as the static bed height is increased, and that the bed is restrained for shallow bed depths and relatively high *H/V* ratios for the fluid mass velocities studied in this work. The shallow depth of 150 mm (

V/D_C = 0.52) gave an average expanded bed height of 450 mm. Therefore, there was no complete contact between the droplets and the particles.

Intimate contact between liquid and the particles ensures that the role of the inert particle as a medium for heat and mass transfer is fully met. Also, the adhesive forces between the particle surface and the droplets ensures that most of the particles remain in the bed working section. Poor contact as in this instance means that a considerable proportion of the droplets may have been entrained as exhaust. This may have accounted for the large difference in heat and mass transfer rate at the grid conditions and an increased performance characteristic for the large droplets at the outlet conditions. On the average, the small fine droplets gave a higher tower characteristic than the large droplets. This may be attributed to the relatively high gas mass flux that enhances an already high gas-liquid interfacial area of the fine droplets as opposed to large droplets in the entire tower. The same response of the tower characteristic was not observed in Figure 8.19 possibly due to differences in particle density, static bed height, and the gas mass flux.

Having explored the effects of the nozzle configuration upon the tower thermal performance for a shallow bed height, it was necessary to investigate these effects on a deep and dense bed (type II) at a typical constant gas mass flux of 2.92 kg/s m^2 and keeping the H/V ratio as 2. The experimental results of such a model is shown in Figures 8.23 to 8.25. In all three cases, the fine droplet spray gave a better tower characteristic than the coarse one for the same liquid mass flux. Although a high particle density ensures that fine droplets are entrained out of the contacting zone, the deep bed means that the average expanded bed height was about 800 mm. This together with the fact that the expanded bed height increased as the liquid mass flux is increased enhanced the chances of a three-phase gas-liquid-solid contact. This must have reduced the amount of liquid entrained from the tower causing differences in the manner of response of the tower characteristic with respect to changes in the fluidisation regime.

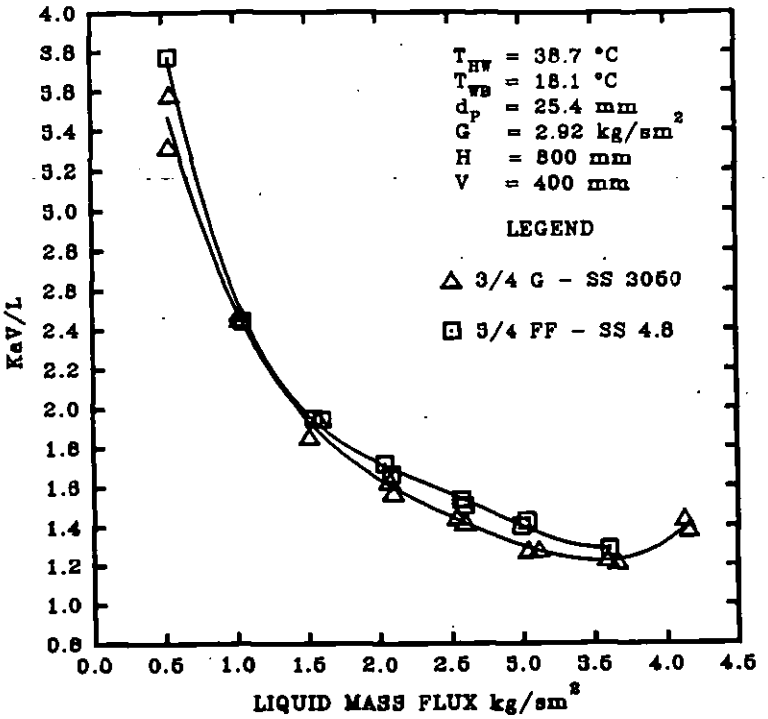

Figure 8.23 The effect of the liquid mass flux and the spray nozzle configuration upon the tower charateristic for a deep bed model type II FBCT operation based on the final outlet cooled water temperature. ρ_P = 326 kg/m^3. Spray nozzle codes as in Figure 8.11.

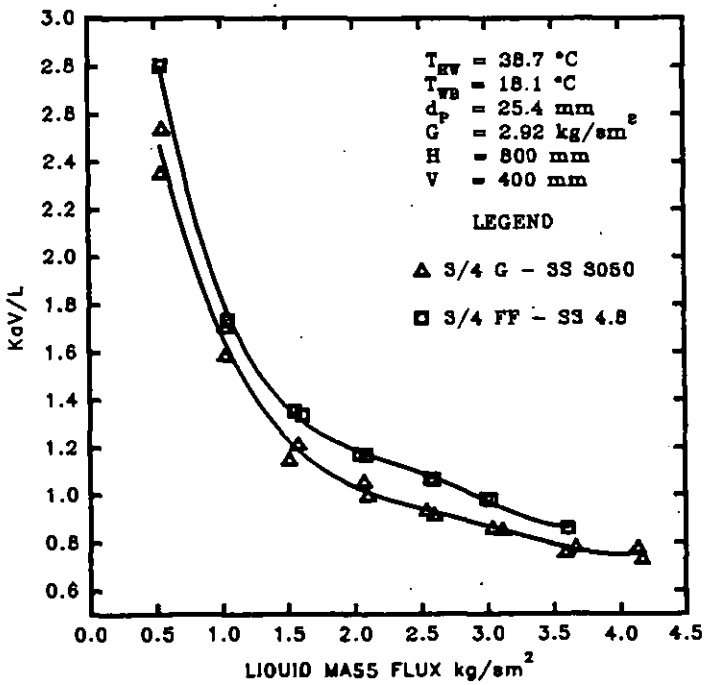

Figure 8.24 The effect of the liquid mass flux and the spray nozzle configuration upon the tower characteristic of a deep bed model type II FBCT operation based on the cooled water temperature at the supporting grid. ρ_P = 326 kg/m^3. Spray nozzle codes as in Figure 8.11.

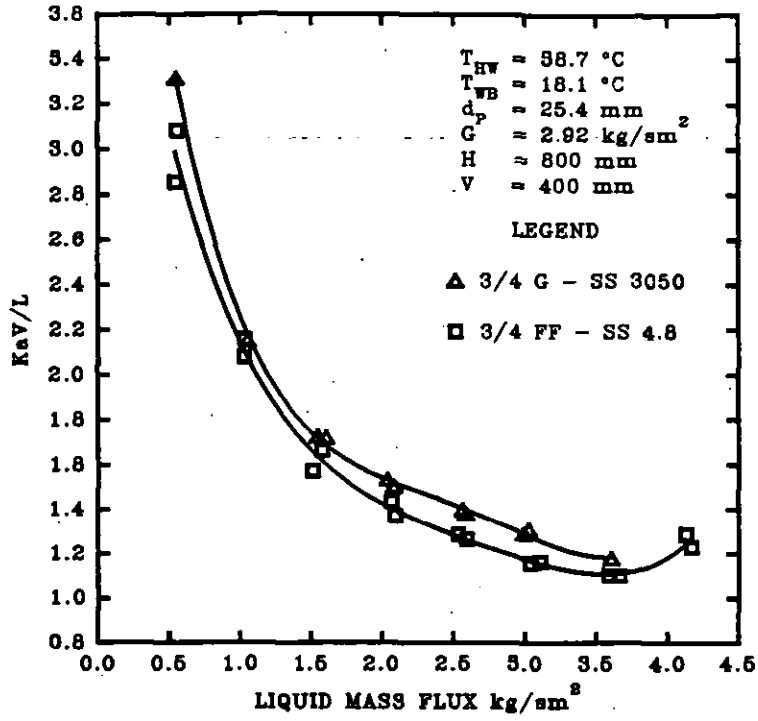

Figure 8.25 The effect othe liquid/mass flux and the spray nozzle configuration upon the tower characteristic for a deep bed model type II operation based on the average cooled water temperature. ρ_P = 326 kg/m^3. Spray nozzle codes as in Figure 8.15.

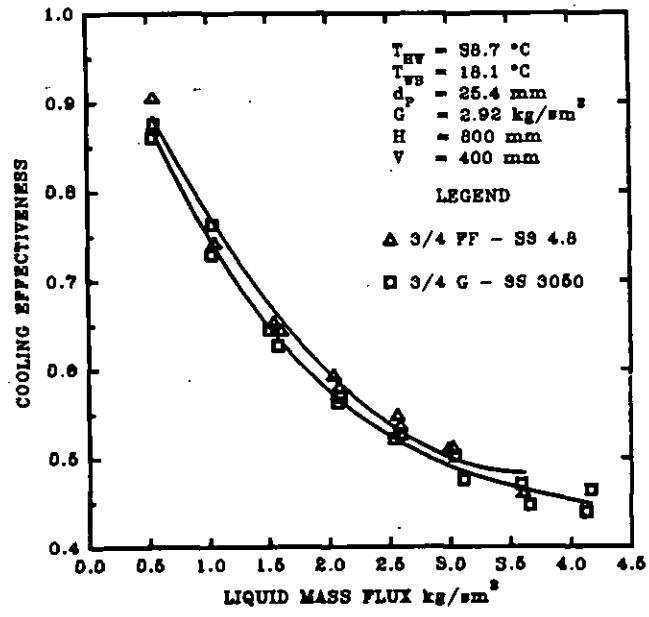

Figure 8.26 The effect of the liquid mass flux and spray nozzle configuration upon the cooling effectivess for a deep bed model type II FBCT operation based on the average cooled water temperature. ρ_P = 326 kg/m^3. Spray nozzle configuration as in Figure 8.11.

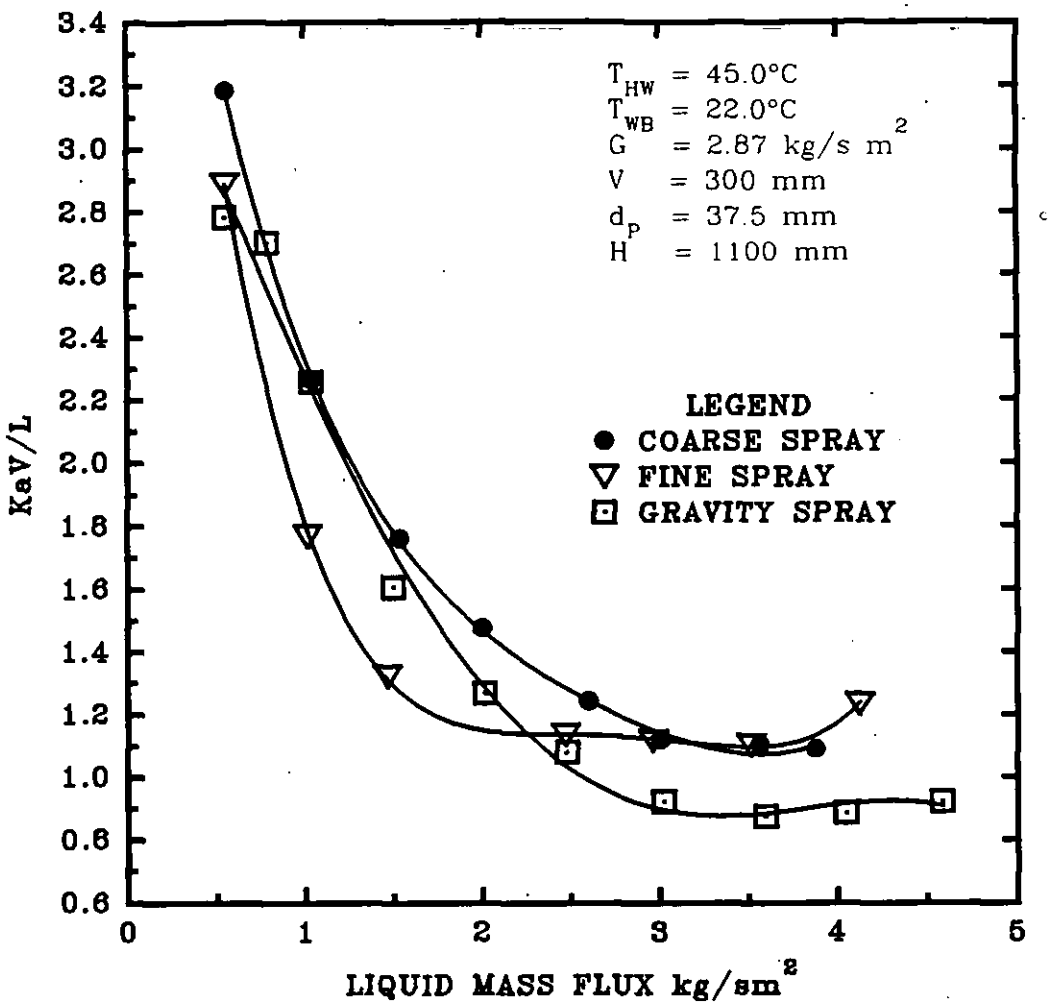

Figure 8.27 Dependence of the tower characteristic upon the spray nozzle configuration based on the temperature of the outlet cooled water from the plenum chamber. A comparison of the three different nozzles. ρ_p = 69 kg/m^3.

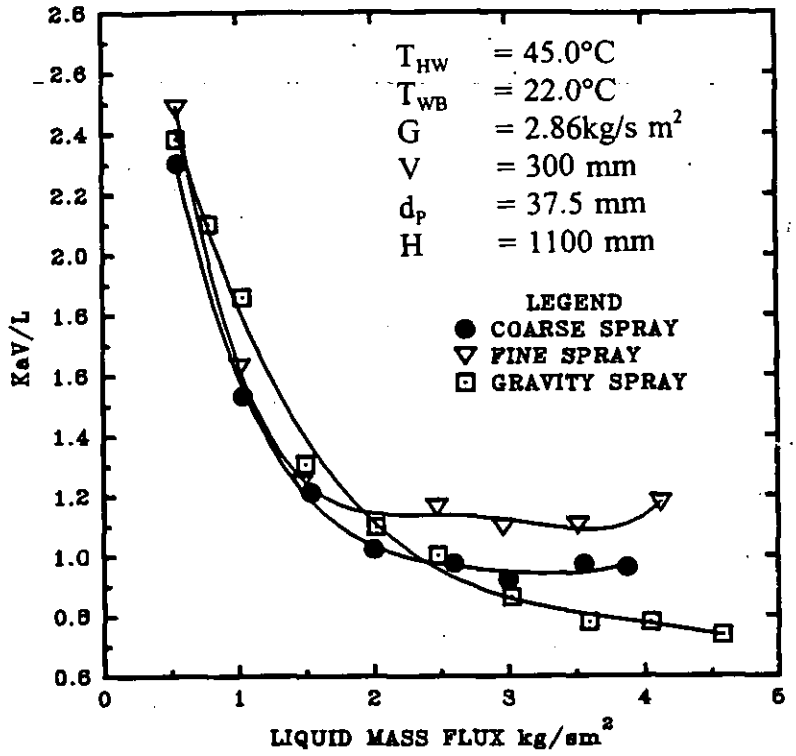

Figure 8.28 Dependence of the tower characteristic upon the spray nozzle configuration based on the outlet cooled water temperature of the distributor grid. Other notations as in Figure 8.27.

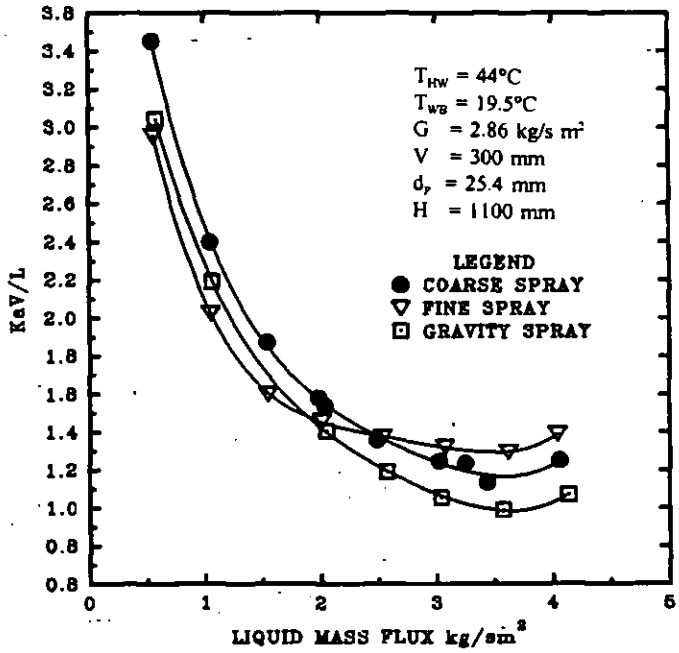

Figure 8.29 Dependence of the tower characteristic upon the spray nozzle configuration based on the temperature of the outlet cooled water from the plenum chamber. Type II, ρ_P = 326 kg/m³.

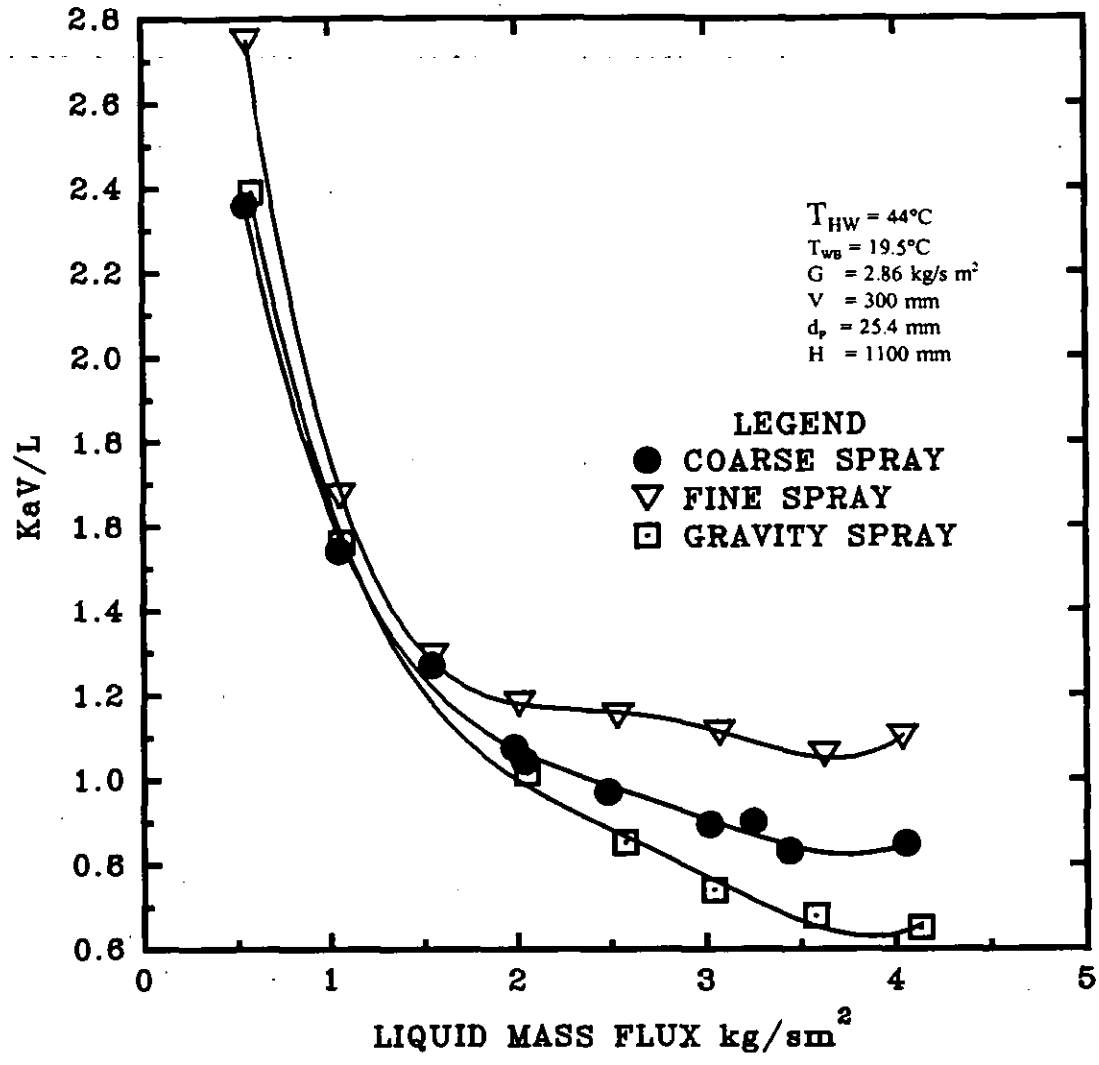

Figure 8.30 Dependence of the tower characteristic upon the spray nozzle configuration based on the temperature of the outlet cooled water temperature from the distributor grid. Type II. Particle density as in Figure 8.29.

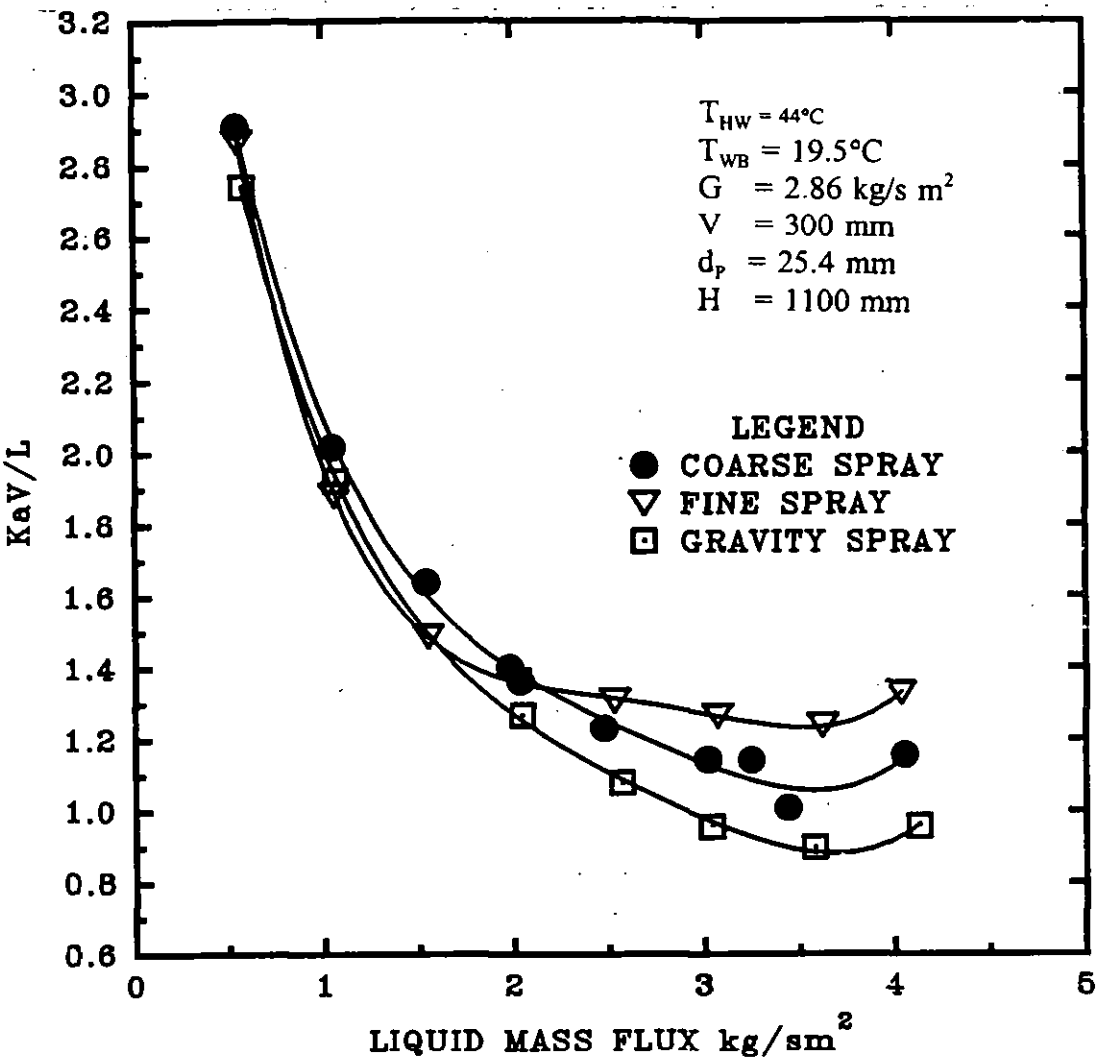

Figure 8.31 Dependence of the tower characteristic upon the spray nozzle configuration based on the average temperature of the outlet cooled water. Type II, $\rho_P = 326$ kg/m^3.

8.4 The Effect of the Spray Nozzle Height

It was briefly shown in chapter VII that the tower thermal performance increases as the spray nozzle height from the supporting grid *H*, is increased when the fine droplet spray was used. The spray nozzle orifice height above the distributor grid is an important parameter because it determines the height of the tower freeboard or disengagement section. This section in turn determines the total volume of the tower working section and therefore, bears a direct effect upon its capital outlay. Moreover, Albright (1984) has theoretically shown that the uniformity of spray is depended upon, amongst other factors, the height of the spray orifice from the packing surface of a counter-flow gas-solid-liquid bed.

In this light, it was important to conduct a detailed experimental investigation on the response of thermal dependence variables when they are subjected to changes in the spray nozzle height. Two different series of experiments were designed and carried out using the coarse droplet spray nozzle. This was used because of its suitability at relatively high spray nozzle heights - wall effects are reduced to a minimum because of the narrow spray angle and the single orifice. Both types I and II low density particles were subjected to a 6 x 4 factorial experiment. Experimental results indicate that the FBCT thermal performance is dependent upon the spray nozzle height and that, the plenum chamber plays an important role.

Figures 8.32 to 8.34 show the effect of the spray nozzle height and the *L/G ratio* upon the tower characteristic at a constant gas mass flux of 3.2 kg/s m^2 for a type I low density FBCT regime. In all three cases, the tower characteristic increases and then flattens out as the spray nozzle height above the distributor grid is increased. The initial increase may be due to increased residence times of the liquid in the tower as the droplet falling path is increased. Increased residence times mean that the amount of liquid retained in the tower increases and therefore the interfacial activity, the rate of heat and mass transfer increasing.

However, as the spray nozzle height is increased further, the tower characteristic flattens out because there is a limit of cooling that may be attained for a given cooling duty. An increased cooling rate as the spray nozzle height is increased is counteracted by a decrease in the net partial pressure beween the air and droplets at the air/water interface as the bulk air approaches saturation levels as seen in Figure 8.35 below. This finding is in good agreement with the theoretical findings of Nottage and Boelter (1940). Moreover, the minimum outlet cooled water temperature which may be attained by a specific cooling tower for a given cooling effect is the wet-bulb temperature. The achievement of the latter temperature may not be possible because the amount of droplets in the tower is limited as so does the enthalpy driving force. Also, it is impossible to design perfectly efficient equipment since some heat is usually lost to the surrounding.

A plausible cause of the increase and then flattening of the tower characteristic curves as the spray nozzle height is increased may be attributed to the wall effect. Albright (1984), using a computer to simulate liquid flow showed that the best single spray distributor in terms of tower perfomance, is one that is homogeneous in its spray characteristics and at the same time just reaches the column wall. At relatively low *H/V* ratios, say 1.66 as in Figures 8.32 to 8.36, the bed suffers from underspray when the spray diameter is less than the column wall. As a result, liquid distribution in the bed is poor since hydraulic wetability is confined to the middle of the bed giving rise to minimal gas-liquid-solid contact and hence reduced heat and mass transfer rate for a given cooling duty.

This finding is in agreement with experimental findings of Buyen and Kranc (1995). Using conventional fixed bed packings, they showed that conventional tower thermal performance is depended upon the liquid distribution in the packing with mal-distribution of water exhibiting poor thermal performance. It can therefore be concluded that the low tower characteristic obtained in Figures 8.32 to 8.34 at low *H/V* ratio may partly be attributed to underspray and hence poor liquid distribution in the bed.

On the other hand, the wall effect may become very significant at relatively high *H/V* ratios, say 4.58 in Figures 8.32 to 8.34, due to overspray. This usually occurs when the spray base diameter is greater than the column diameter. The effect is that, a proportion of the liquid runs down the column wall without coming into any significant contact with the upward flowing gas. Since this is bound to reduce the gas-liquid interfacial area, the expected increase in the heat and mass transfer coefficient as the spray nozzle height is increased is offsetted causing the tower characteritic to flatten out. This effect is further compounded by the relatively large particle diameter of 37.5 mm because Albright (1984), in his computer simulation of the liquid flow showed that the smaller the ratio of the column diameter to the particle diameter, D_C/d_P the more severe the wall effect and that, this effect may be increased at relatively large liquid mass fluxes as compared to small ones. This may therefore account for the slower increases in the tower characteristic with respect to the spray nozzle height as the liquid/gas mass flux ratio and hence the liquid mass flux is increased from 0.25 to 1.44 as seen in Figure 8.32.

Another possible explanation for the flattening of the tower characteristic as the spray nozzle height is increased from 0.4 to 1.1 m may be due to drifts of droplets out of the contacting zone. The increased residence time of the liquid in the bed as the spray nozzle height is increased increases the chances of many more droplets being entrained and since there is an optimum number of droplets that may be carried away for tower thermal performance to be affected, it is possible that such a level could be reached as to counteract the effects of increased heat and mass transfer in the tower. Further, observations made as the experiments progressed showed that the amount of liquid entrained out of the tower, for a particular *L/G* ratio, increased as the spray nozzle height was increased, adding credence to this conjecture. Moreover, it is clear from Figure 8.32 to 8.34 that the curves become steeper as the liquid/gas mass flux ratio is decreased from 1.44 to 0.25. This may be attributed to the fact that the drift effect becomes significant as the liquid mass flux is increased.

An increased tower volume also increases the possibility of air/droplet contact for a paricular liquid/gas mass flux ratio. An increased contact causes more intimate mixing and hence increased sensible heat transfer from the hot water to the air with a resultant increased tower characteristic. Kelly (1975) carried out a theoretical optimisation of conventional towers and found that larger towers gave a better cooling effect for a given duty. Nevertheless, his work was not supported by experimental data. This being the case, the present work may serve as an experimental verification of his theoretical findings since both works are in good agreement.

Figures 8.32 to 8.36 correspond to Figures 6.14 and 6.15 of chapter VI which illustrate the effects of both the spray nozzle height and the liquid mass flux respectively upon the bed expansion. In Chaper VI, it was shown that low density particles have a larger bed expansion than relatively heavy particles whe subjected to similar experimental conditions and that, the expanded bed height generally increases as the liquid mass flux is increased. In addition, the bed expansion increases, passes a minimum and then increases as the spray nozzle height is increased.

The increase in bed expansion as the spray nozzle height is increased from 0.4 to 1.1 m may account for the increase in the tower characteristic. This is because a higher bed expansion and hence increased turbulence increases the probability of intense liquid-gas-particle interaction which in turn enhances intimate interfacial mixing of air and water thereby causing the heat and mass transfer coefficient to increase for a particular *L/G* ratio as the spray nozzle height is increased.

Nevertheless, at relatively high spray nozzle heights of between 0.8 to 1.1 m, the expanded bed height becomes greater than the spray nozzle height. Therefore not all the particles take part in the fluidisation process at this stage. This unfortunate occurence has the counter-effect of decreasing the positive gradient of the tower characteristic with respect to the spray nozzle height therby causing the curves to

flatten. This effect is further exarcebated at relatively high liquid/gas mass flux ratios *L/G*, of between 1.0 to 1.44 because the the liquid flow rate is increased. Since the expanded height increases sharply as the spray nozzle height is increased from 0.8 to 1.1 m, considerably surpassing the spray nozzle height, it may be possible that the slow increase in the tower characteristic occur as a result of decreases in the gas-liquid-solid interfacial contact. Moreover, the relatively high gas mass flux gives velocities close to the flooding velocity of the bed causing more droplets to be entrained of the tower.

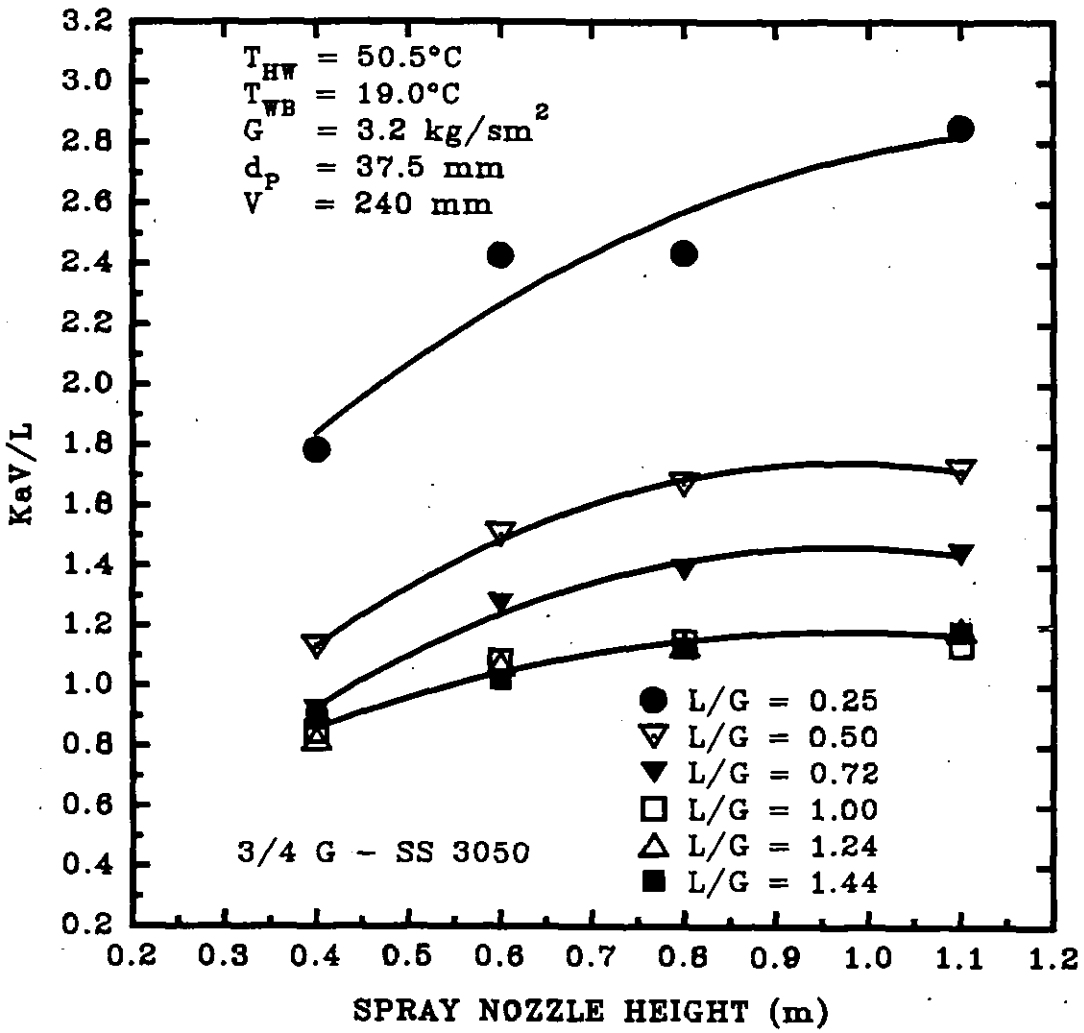

Figure 8.32 The effect of the spray nozzle height and the liquid/gas mass flux ratio upon the tower characteristic for a type 1 FBCT based on the temperaure of outlet cooled water from the plenum chamber for the coarse droplet spray nozzle. Type I, ρ_P = 69 kg/m^3.

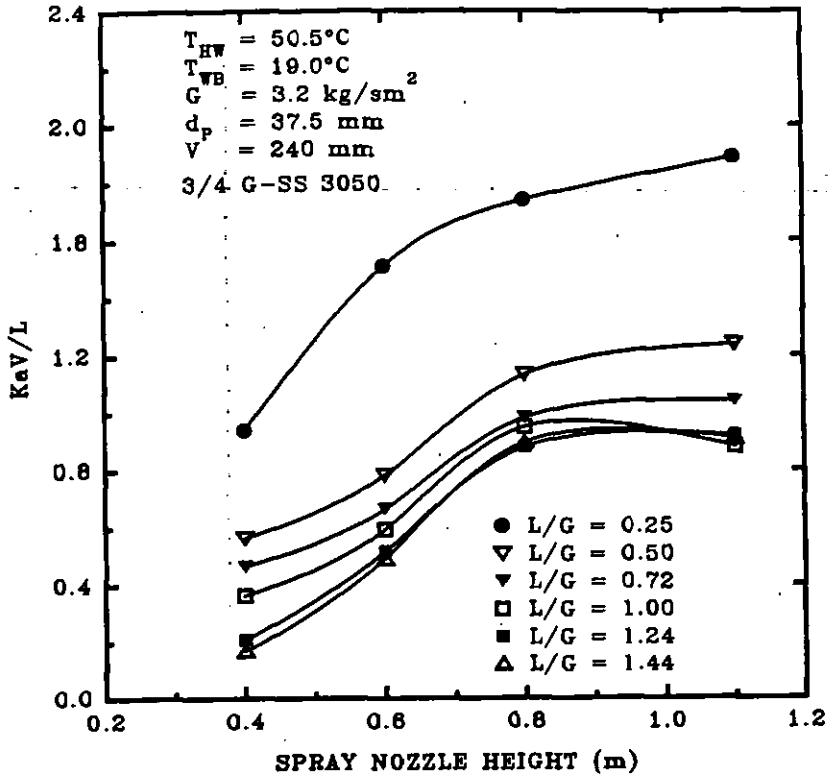

Figure 8.33 The effect of the spray nozzle height and the liquid/gas mass flux ratio upon the tower characteristic of a type I FBCT operation based on the cooled water temperature at the supporting grid for the coarse droplet spray nozzle. ρ_p =69 kg/m^3.

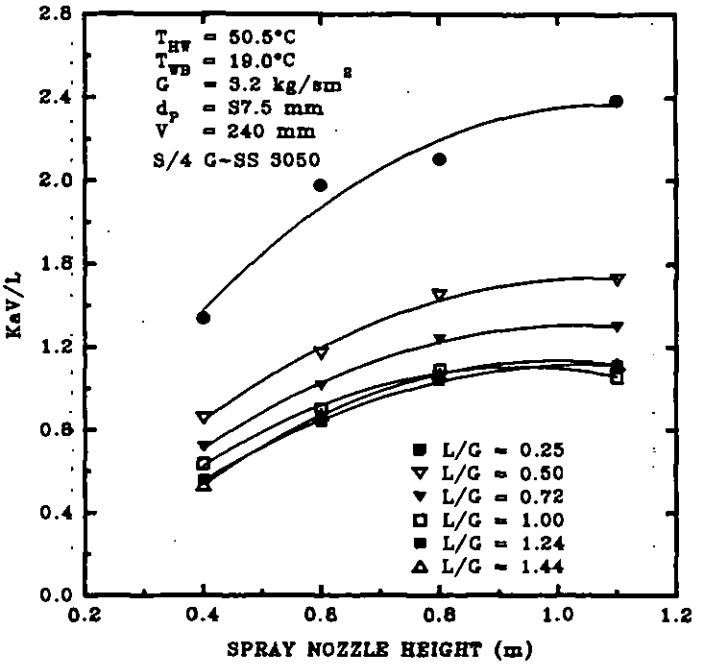

Figure 8.34 Effect of the spray nozzle height and the liquid/gas mass flux ratio upon the tower characteristic of a type I FBCT operation based on the average cooled water temperature for the coarse droplet spray nozzle. ρ_p = 69 kg/m^3.

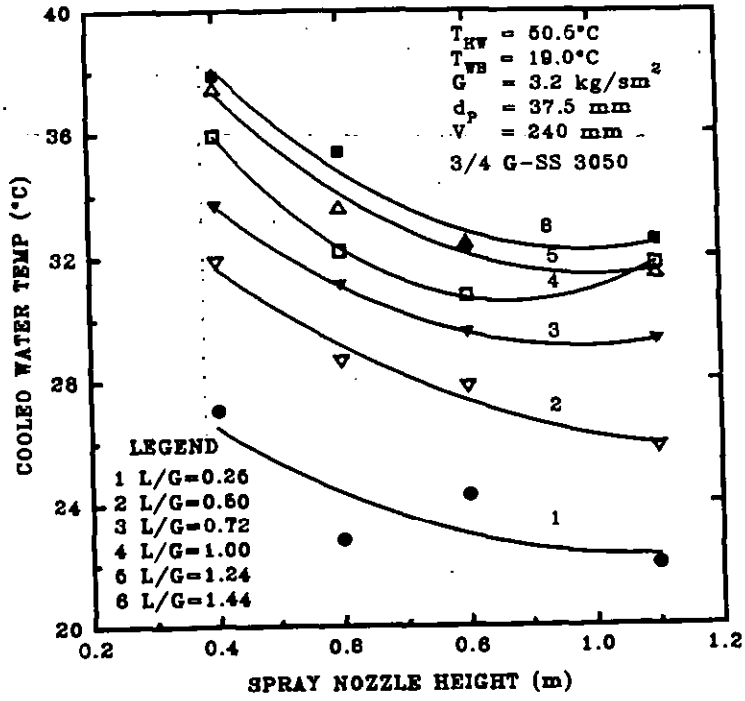

Figure 8.35 The effect of the spray nozzle height and the liquid/gas mass flux ratio upon the average cooled water temperature of a type I FBCT operation for the coarse droplet spray nozzle. ρ_p = 69 kg/m^3.

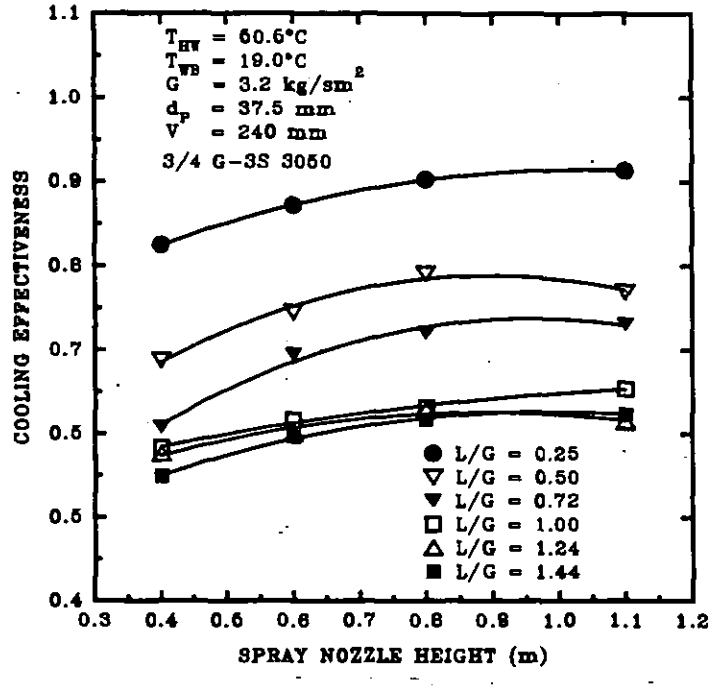

Figure 8.36 Effect of the spray nozzle height and the liquid/gas mass flux ratio upon the cooling effectiveness of a type I FBCT operation based on the average cooled water temperature for the coarse droplet spray. ρ_p = 69 kg/m^3.

Figures 8.39 to 8.43 show the effect of the spray nozzle and static bed heights upon the tower characteristic for a type II FBCT operation based on the outlet, grid and average cooled water temperatures at a typical liquid/gas mass flux ratio, *L/G* of 0.74. Figure 8.41 shows that for static bed heights ranging from 0 to 200 mm, the tower characteristic increases as the spray nozzle height is increased from 0.4 to 0.6 m and then decreases slightly as it is increased from 0.6 to 1.1 m. On the other hand, at the static bed height of 250 mm, the tower characteristic decreases as the spray nozzle height is increased from 0.4 to 0.6 m, and then stays almost unchanged as it is further increased from 0.6 to 1.1 m.

As the spray nozzle height is increased, the residence time of the liquid in the bed increases. The result is an increase in the degree of turbulence and interfacial activity giving rise to increased interfacial area. It follows that the heat and mass transfer coefficient increases. However, the high particle density means that fluidisation occurs after the flooding point is reached, in which case droplets accumulate above the particles. Therefore, the possibility of droplets being blown out of the tower working section increases. A further increase in the spray nozzle height thus further enhances the chances of the droplets coming into counter-current contact with the air because the tower volume increses and so does the residence time of the liquid in the tower as a result of an increased travelling distance. It follows that the amount of droplets that drifts out of the tower may have increased.

These hydrodynamic changes may have served to enhance the heat and mass transfer coefficient and therefore the tower characteristic but Figure 8.39 suggests otherwise. The decrease in the tower characteristic may have been due to an increased drift of droplets, especially at the relatively high fluidisation gas velocity of about 3.0 m/s. This action may have counteracted the expected increase in tower performance since there is an optimum level of drift after which tower performance is affected in accordance with the theoretical findings of Nottage and Boelter (1940). In addition, there is a limit of cooling that may be attained for

a particular duty as dicussed in type I operation. Also, Albright (1984), in his computer simulation, showed that the ratio of column diameter to spray base diameter is critical in tower performance as the ratio of column diameter to particle diameter D_C/d_P, is varied and that, the effects are adversely severe as this ratio increases. Although his findings were based on static packings, particle dimensions remain unchanged irrespective of the hydrodynamic conditions. Bearing this in mind, we may apply his theory on FBCT so as to provide an explanation for the bed behaviour as the spray nozzle height is changed.

Knowing that the spray base diameter varies from 0.19 to 0.5 m as the spray nozzle height is increased from 0.4 to 1.1 m, and that the particle diameter is relatively small giving rise to a relatively high $D_C/d_P > 10$ (11.6), it follows that an increase in the spray diameter as the spray nozzle height is increased will reduce the performance. Nevertheless, this may only occur if the spray base diameter is significantly greater than the column diameter. Therefore, there must exist an optimum spray nozzle height that provides an optimum column diameter to spray base diameter ratio. Figures 8.43 and 8.44 suggest that the best spray nozzle height for the best tower thermal performance is 0.6 m since it provides a spray base diameter to column diameter ratio of approximately unity. On this premise, the decrease in the tower characteristic as the spray nozzle height is increased after the 0.6 m threshold is passed is justified because the range of the the ratio spray base diameter to column diameter becomes greater than one causing severe wall effects. However, this model may only be applicable to an ideal situation when the tower is empty or at very low static bed height in a non-fluidising process of counter-current three-phase flow. The same arguments may not hold when a three-phase gas-liquid-particle bed is fluidised. This complication therefore demands a more comprehensive explanation, which takes into consideration the bed expansion.

Figure 8.42 also shows that the tower characteristic increases almost in proportion as the static bed height is increased in agreement with the findings in section 8.2.

However, the increase in the tower characteristic is sharper at the spray nozzle height of 0.4 in the range of static bed heights of 200 to 250 mm due to reasons relating the static and expanded bed heights. As the static bed height is increased from 0 to 250 mm, so does the expanded bed height in conformity with our discussions in chapter VI. Since the spray base diameter to column diameter ratio decreases as the bed expands, it follows that the wall effects are less severe and that thermal performance sould increase as the static bed height is increased. Moreover an increase in the expanded bed height as the static bed height is increased means that the gas-liquid interfacial contact is enhanced causing an increase in the tower characteristic at a particular bed height.

As the H/V ratio is increased, the possibility of the ratio of the spray nozzle height to the expanded bed height H/V_E, approaching unity diminishes because unlike the low particle density type I operation, type II FBCT operation with high density particles have a lower bed expansion and since the bed is restrained for a shallow bed height model, and in this instance $0.87 < V/D_C < 1$ ($V = 250$ mm, $D_C = 290$ mm). An $H/V_E = 1$ is a perfect spray condition because all the water is directly injected into the bed meaning that a perfect three-phase counter-current flow exists. The effect is that extremely high turbulence levels exist in the bed with the air transmitting the power that creates interfacial stresses and cause the interfacial activity and hence gas-liquid mixing to be very intense thereby enhancing heat and mass exchange. Since most of the particle voids of the bed is filled with liquid, and the particle density is high, the bed floods causing intense interfacial activity that stimulate heat and mass transfer and hence an increased tower characteristic.

An argument that may be put forward is that, flooding, especially at the velocity of about 3 m/s, is usually accompanied by droplets being blown out of the contacting zone and that an almost negligible spray base diameter may as well impair the FBCT thermal performance due to mal-distribution of liquid in the bed. However, these setbacks may be small as compared to the high degree of

turbulence that is generated as a result of the flooding which fully countercats them. Moreover, Levsh (1968) has theoretically shown that axial distribution of liquid in a type II FBCT operation is not uniform because a considerable proportion of the liquid in the bed stays at the distribitor grid and the lower sections of the bed. Since the spray angle is small, it follows that liquid mal-distibution due to underspray may occur at the top end of the bed. Interfacial activity may therefore, be much more intense at the lower sections of the bed. This hydrodynamic behaviour of type II FBCTs may have counteracted poor thermal performance that may be present at the top section of the bed.

The theoretical findings of Albright (1984) that, given enough bed height, mal-distribution will slowly improve to natural and that, other than perfect distribution, there is an initial distribution for each distributor that will minimize the bed depth needed to attain natural distribution, supports this argument. The variation of liquid distribution in the bed, as the spray nozzle and static bed height are increased from 0.4 to 0.6 may therefore account for the decrease in the tower thermal performance at the bed heights of 0 and 250 mm. This is explicitly illustrated in Figure 8.42 which shows the effect of the dimensionless *H/V* ratio upon the tower characteristic for non-zero static bed heights of 50 to 250 mm. It shows that the tower characteristic based on the outlet cooled water temperature, is dependent upon this ratio as derived from dimensional analysis in chapter II. In the static bed height range between 50 to 200 mm, the tower characteristic increases sharply as the *H/V* ratio is increased, passes through a maximum and then decreases in agreement with earlier argument that an optimum spray nozzle height exists for a particular static bed height after which mal-distribution begins to counteract the high thermal performance of the FBCT.

Yet, the rate of these increases and decreases as the static bed height is increased probably occurs because the possible operating range of the FBCT decreases as the static bed height is increased and possibly due to the fact that the FBCT quickly reaches limiting value as regards thermal performance. As the static bed

height is decreased, the effects of mal-distribution as a result of severe wall effects is counteracted by increased tower volume available for thermal performance and as such the effects of the *H/V* ratio is less pronounced. The shift of the curves to the right may be attributed to decreases in the tower characteristic as the static bed height is decreased and because the *H/V* ratio increases as the static bed height is decreased.

Figure 8.41, corresponding to Figure 8.39 shows the effect of the spray nozzle and static bed heights upon the tower characteristic based on the temperature opf the cooled water from distributor grid. In contrast to Figure 8.41, the tower characteristic decreases slightly in the range of spray nozzle heights of 0.4 to 0.6 m and then increases sharply from 0.6 to 0.8 m before increasing slowly from 0.8 to 1.1 m. Similarly as in Figure 8.41, this behaviour is different at the 0 and 250 mm static bed heights. At the 250 mm static bed height, the decrease in the tower characteristic is sharper, passes through a minimum at the spray nozzle height of 0.6 m, increases symetrically up to the spray nozzle height of 0.8 m and then remains almost independent upon the spray nozzle height from 0.8 to 1.1 m. At the static bed depth of 0 mm for an empty tower with no spheres, the increase is almost proportional to the spray nozzle height.

The reason for this complete contrast in FBCT behaviour at the grid and plenum chamber conditions is not clear. Higher tower performance is obtained at the plenum outlet cooled water conditions than at the cooled water conditions at the grid. This difference in the tower characteristic may be explained by the fact that cooling continues to occur at the plenum chamber. It follows that the cooled water at the grid continue to have a high "potential" for cooling which is enhanced due to the high gas velocity of 3.0 m/s. Therefore, the water leaving the plenum may have achieved its maximum range for each set of hydrodynamic conditions. This may have been one of the causes of the tower characteristic reaching a limiting value in Figure 8.41.

The increase in the tower characteristic as the spray nozzle height is increased in Figure 8.41 may therefore be attributed to the same reasons as put forward in Figure 8.39. The large difference in tower performance between an empty tower and a tower filled with packings shows that the high mass transfer coefficient *Ka*, is due to fluidisation of the particles with air and water at the high gas fluidization velocity.

Figure 8.41 also shows that the tower characteristic increases as the static bed height is increased for the same spray nozzle height. However, for the non-zero static bed heights from 50 to 250 mm, the gradient decreases and then becomes independent as the spray nozzle height is increased from 0.4 to 1.1 m. The reason for this behaviour may again be attributed to the theoretical findings of Albright (1984). According to him, a 1.25 % overspray may lead to significant decreases in tower performance for a packed bed with high D_C/d_p ratio. Although the fluidisation process may cast some doubt on this assertion, it may be generally true since overspray was observed in this case. This phenomenon may have caused a reduction in the gradient of the tower characteristic with respect to the spray nozzle height as the spray nozzle height is increased since such an effect would have counteracted an increase in tower characteristic that arises as the static bed height and the spray nozzle heights are increased in the case of a perfect spray. The effects of overspray is less significant at the outlet conditions beacuse of the high interfacial gas-liquid activity that occurs in the plenum which may have partly off-setted the effects of overspray or underspray.

The effect of the dimensionless *H/V* upon the tower characteristic at the grid cooled water conditions is depicted in Figure 8.42. Again the curves show that tower characteristic *KaV/L*, is dependent upon that ratio and that the tower characteristic generally increase as the ratio is increased for a particular static bed depth. Again the shift of the curves to the right occurs because the tower characteristic decreases as the static bed height is decreased and that the *H/V* ratio increases as the spray nozzle height is increased for a particular static bed height.

In addition, Figure 8.42 shows that the rate of change of tower characteristic with respect to the static bed height tends to zero as the spray nozzle height is increased. On the average, the tower thermal performance increases as the spray nozzle height is increased as seen in Figure 8.43. Also, Figures 8.44 to 8.46 show that the cooling range corresponds to the tower characteristic in relation to variations in the spray nozzle height in all three cases of cooled water temperatures, in line with previous explanations. Why are droplets not blown out of the contacting zone at such a relatively high velocity? The two-fold reason may be attributed to the great weight of the droplets and the short distance of the spray nozzle from the distributor grid. As the droplets receive energy as a result of gas-liquid interfacial tension, they are blown out of the contacting zone but they may not possess enough kinetic energy to travel the entire distance of about 1 m out of the tower.

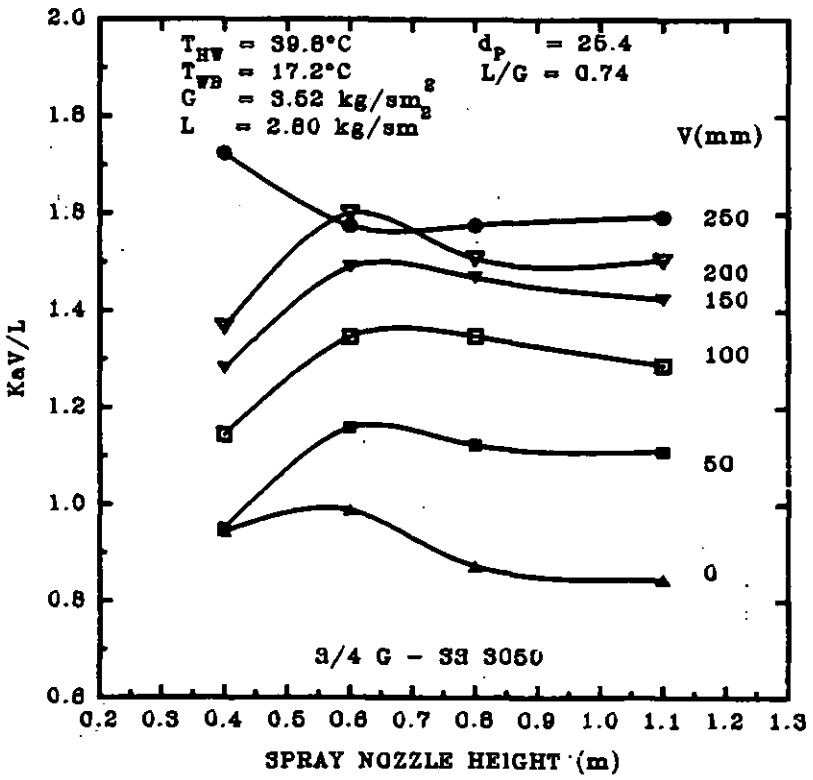

Figure 8.39 The effect of the spray nozzle height and the static bed height upon the tower characteristic of a type II FBCT operation based on the outlet cooled water temperature of the plenum chamber for the coarse droplet spray nozzle. ρ_p = 326 kg/m^3.

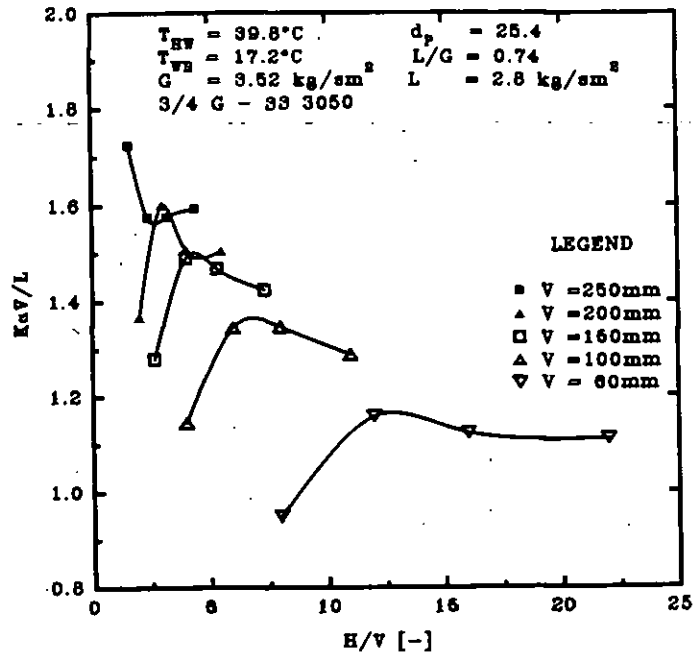

Figure 8.40 Dimensionless tower characteristic vs dimensionless spray nozzle height to static bed height ratio. This is based on the outlet cooled water temperature of the plenum chamber for a type II FBCT operation for a coarse nozzle. Particle density as in Figure 8.39.

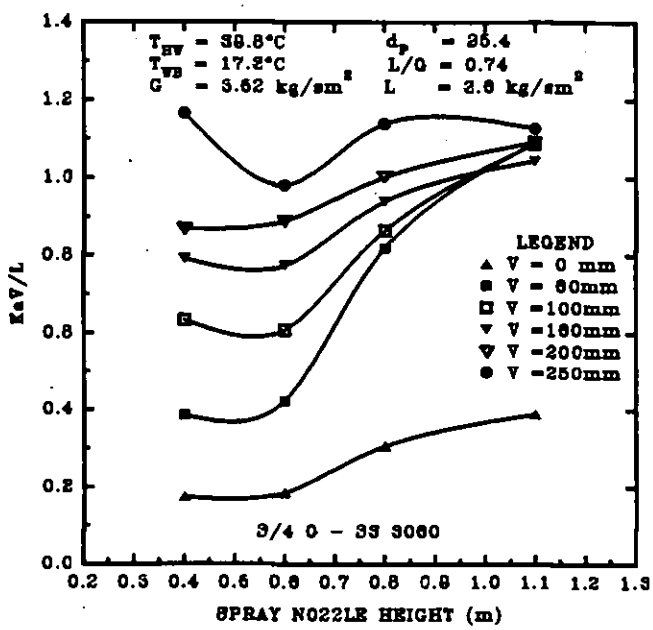

Figure 8.41 The effect of the spray nozzle height and the static bed height upon the tower characteristic based on the outlet cooled water temperature of the distributor grid of a type II FBCT operation for a coarse droplet spray nozzle. Particle density as in Figure 8.39.

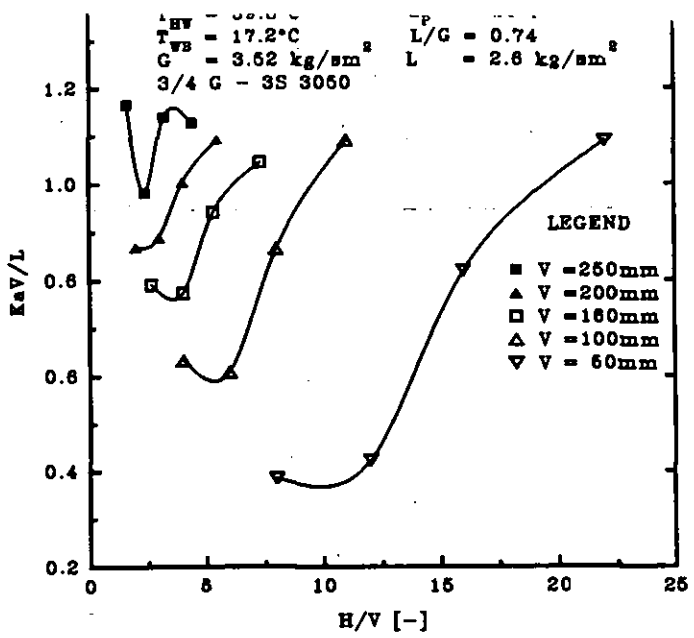

Figure 8.42 Dimensionless tower characteristic vs dimensionless spray nozzle height to static bed height ratio based upon the cooled water temperature of the distributor grid of a type II FBCT operation for a coarse droplet spray nozzle. Particle density as in Figure 8.39.

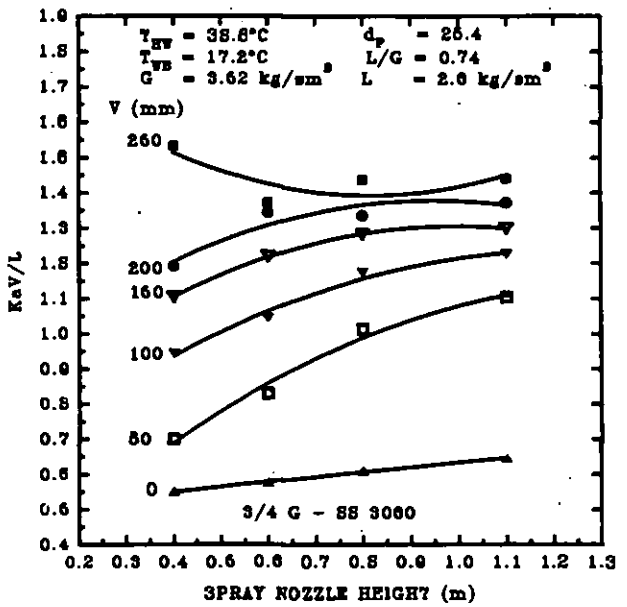

Figure 8.43 The effect of the spray nozzle height and the static bed height upon the tower characteristic of a type II FBCT operation based on the average cooled water temperature for a coarse droplet spray nozzle. Particle density as in Figure 8.39.

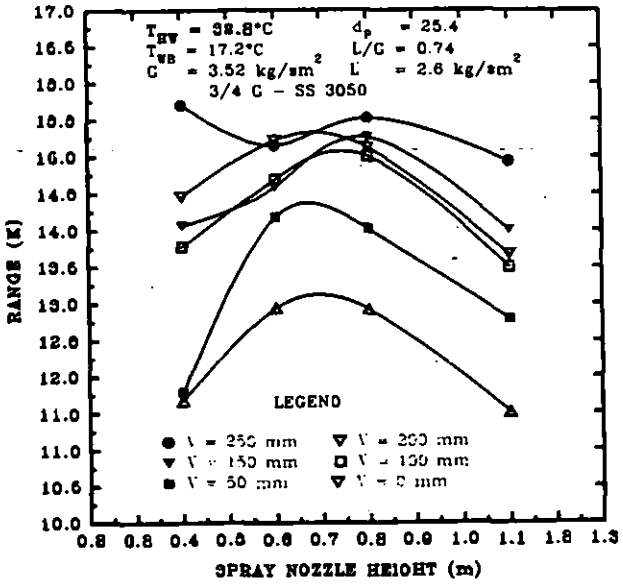

Figure 8.44 The effect of the spray nozzle height and the static bed height upon the cooling range of a type II FBCT operation based on the outlet cooled water temperature of the plenum chamber for a coarse droplet spray nozzle. Partcle density as in Figure 8.39.

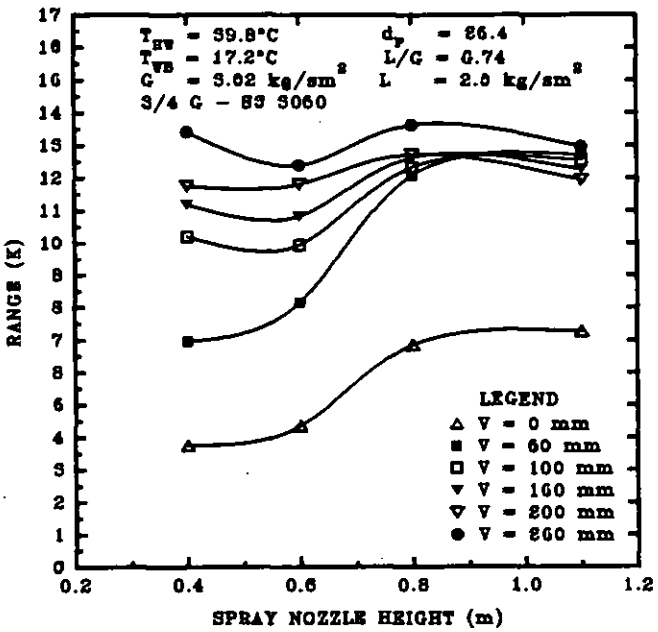

Figure 8.45 The effect of the spray nozzle height and the static bed height upon the cooling range of a type II operation based on the cooled water temperature of the distributor grid for the coarse droplet spray nozzle. Particle density as in Figure 8.45.

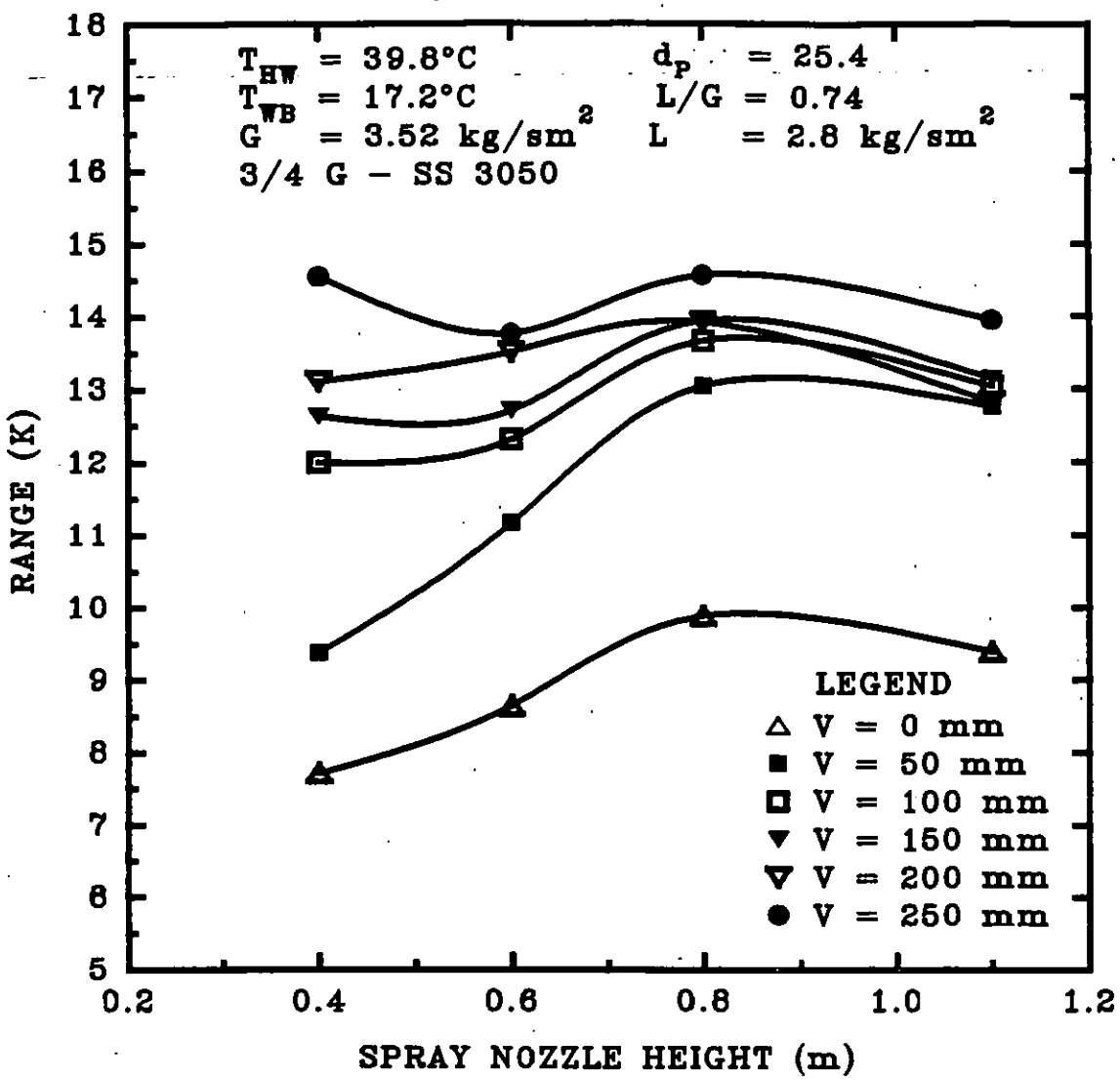

Figure 8.46 The effect of the spray nozzle height and the static bed height upon the cooling range of a type II FBCT operation based on the average cooled water temperature for the coarse droplet spray nozzle. Particle density as in Figure 8.39.

8.5 Local Temperature Distribution Measurement

Four different experiments were performed to investigate local axial and radial temperature distribution in the FBCT. The inlet water temperature was maintained at approximately 53°C while tests were conducted using the 37.5 mm low density spheres.

8.5.1 Axial Temperature Distribution

Figure 8.47 below shows the effect of the axial distance from the distributor grid upon the local average cooled water temperature at different axial positions. As expected, the water temperature increased as the axial distance is increased. However, the increase is not proportional in all sections of the tower. In the empty plenum lower section between the grid and the outlet, water temperature slowly decreases as the axial distance below the grid is increased. This is expected as the activity in the plenum is two-phase air/water flow with minimal interfacial agitation due to reduced interfacial area. Within the tower itself, the axial cooled water temperature decreases rapidly in all cases as the axial distance from the grid is decreased. It is expected that the cooled water temperature should decrease as the hot water descends in the tower in contact with the air since heat exchange of hot and ambient air is effected as a result of differences in temperature gradient. However, the reason for the rapid fall in axial water temperature between 0.2 to about 0.6 m of tower axial distance from the distributor is not clear. This is compounded by the fact that the expanded bed height at individual *L/G* does not seem to have affected these results. Therefore, this may be explained on the basis that at developed fluidisation, when the minimum fluidisation velocity has been surpassed, cooling is enhanced mainly in the region where spheres are in mobile three-phase contact with air/water and the the freeboard effect where there is only two-phase flow contribution to cooling is negligible. If this is the case, therefore, the hot water reaches the top of the spheres at a high potential since negligible cooling has occured at the freeboard. As a result, the temperature gradient and the

enthalpy potential between the upward flowing air and the hot water rapidly increases causing the rate of cooling of axial water to increase as the hot water axially traverses the tower from the inlet to the collecting device placed about 50 mm below the grid.

The local axial cooled water temperature decreases in the tower as the *L/G* is decreased due to increase in gas mass flux at constant liquid mass flux of 3.1 kg/s m^2. This confirms our earlier finding on bulk cooled water temperature measurements.

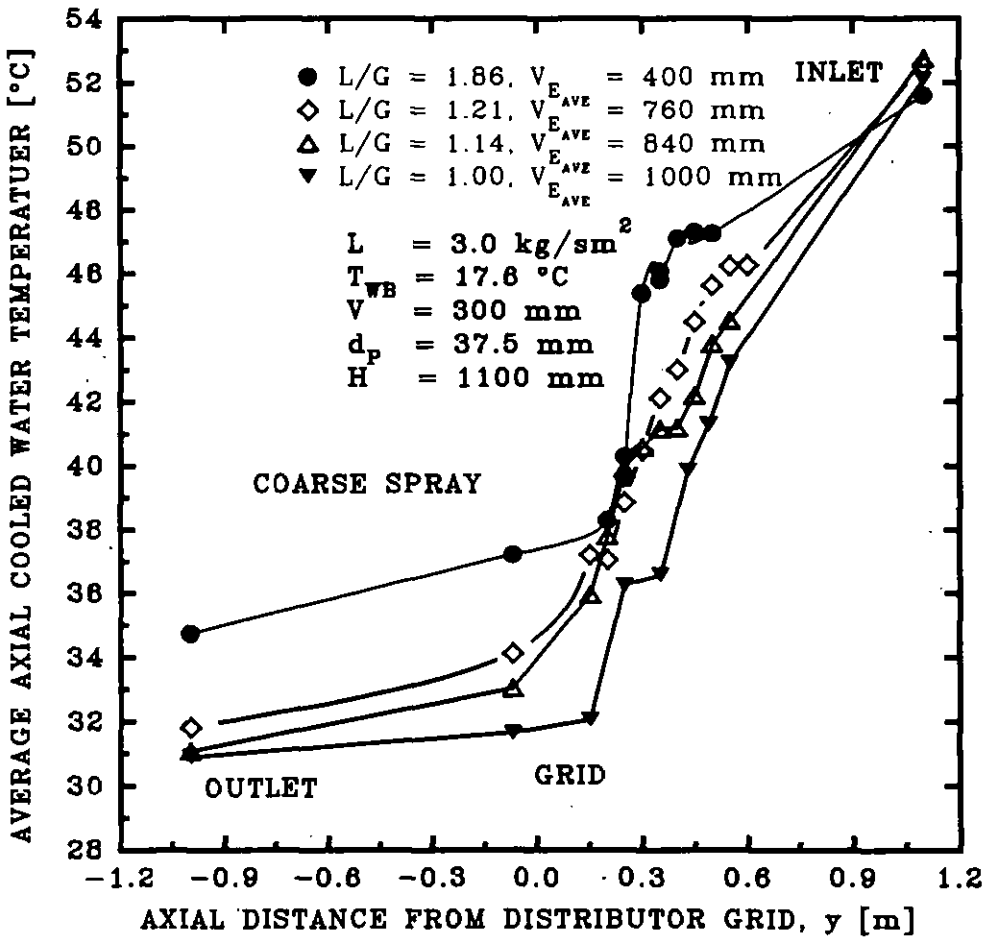

Figure 8.47 Variation of local axial water temperature with axial distance. ρ_p = 69 kg/m^3.

8.5.2 Radial Temperature Distribution

Three different series of tests were made so as to determine the radial temperature profile at the gas/liquid interface in a fully developed FBCT regime. The inlet water temperature was maintained at approximately 53°C. Using the same particle size as for the axial local water temperature measurement profile, Figures 8.48 to 8.50 show that the interfacial temperature is dependent upon air/water distance from the distributor grid for shallow bed FBCT of static bed height V of 130 mm. This is in agreement with our earlier findings on local axial conditions. Also, it can be seen that the radial temperature profile varies with both the distance from the distributor grid as well as the radial distance from the column wall.

In Figure 8.48, at 70 mm above the distributor grid, the local interfacial radial temperature decreases very slowly, remaining almost constant as the probe traverses the tower from left to right. On the other hand, at 570 mm above the distributor grid, the interfacial radial temperature remained relatively constant until the radius of the column is reached after which, the interfacial temperature decreases rapidly. This novel finding may be explained on the basis of and fluidisation non-uniformity at the top of the fluidised bed itself. We have shown in chapter VI that there is a reduction in solids concentration at the top of the fluidised bed in a fully developed fluidisation at high gas mass flux and low density particles acting as the fluidisation medium. It should be noted that the fall in interfacial temperature starts almost midway as the probe traverses the bed from the column wall. Normally, in fully developed velocity flow, the radial velocity profile generally shows maximum flow velocity at the centre of the duct, increasing and decreasing in an inverted U-shape. It is therefore likely that the high velocity in the middle of the bed may have contributed to a higher interfacial activity than at areas close to the column wall. As a result, heat exchange between the cold air and the hot water may have been enhanced causing the interfacial temperature to decrease.

The constancy of interfacial temperature at a height *y* of 70 mm validates average temperature that is obtained at 70 mm below the grid, T_{GCW}. Comparison with the temperature profile at a vertical height y, of 570 mm shows that at the liquid mass flux studied, the radial temperature distribution is relatively uniform and constant only at the bottom of the the bed. Another explanation for this may be due to the fact that as water and air flow downwards and upwards respectively, the enthalpy potential of the hot water decreases and tends towards a minimum and as a result, the temperature gradient between the water and the air decreases In which case, the rate of heat transfer and evaporation remains relatively constant. Similar arguments may be applied to Figure 8.49. In this case, conditions are similar to Figure 8.48. However, the liquid mass flux is reduced from 3.1 to 2.0 kg/s m^2 so as to study the effect of the liquid mass flux upon the radial temperature distribution within the bed. However, at a vertical height of 570 mm, the temperature seems to have stayed constant in the first 30% of the profile and then starts to gradually fall reaching a minimum at about 65% of the radial distance and then increases again to form a U-shaped distribution. This again may be attributed to the fact that the air velocity is highest at about the radial centre of the tower. However, the lower liquid mass flux may have meant that the effect of the gas mass flux upon the radial temperature distribution offsets that of the liquid mass flux. As a result, the temperature profile at this height is slightly different from that at Figure 8.48.

Another explanation relating to this behaviour may be found in the average expanded bed height V_E. We have shown in Chapter VI that the expanded bed height increases as the liquid mass flux is increased due to the higher interfacial activity in the tower. Applying this finding to Figures 8.48 and 8.49, it can be seen that the expanded bed height decreases from 600 to 560 mm as the liquid mass flux is decreased from 3.1 to 2.0 kg/s m^2 as expected. Since in situ temperature distribution were taken 10 mm just above the expanded fluidised bed itself in the case of Figure 8.49, it can be safely concluded that two-phase gas/liquid interfacial flow pre-dominated at the top of the solids. At a gas mass

flux of about 4.0 kg/s m^2, about twice that of the liquid mass flux, and considering that air is the continuous phase while water is the diapersed phase, it can be easily conclude that the gas mass flux offsets the effect of the liquid mass flux and the limited disturbance as a result of solid concentration in the vicinity of interfacial temperature measurement. Since interfacial activity is less vigorous the farther away from the centre of the tower or near the column wall for that matter, the interfacial temperatures are higher, almost remaining the same at the average inlet water temperature of 53.29°C on both sides of the radial symmetry. The highest interfacial temeperatures do not occur in the middle of the bed. This may be accounted for by fluidisation anomalies of recirculation of solids and poor water distribution, and gas/liquid mixing at the top of the tower where two-phase flow liquid/gas flow predominates but perturbed by the limited solids interference.

A similar test was carried out to take into account the entire working section of 1100 mm for a deep bed FBCT with static bed height V of 320 mm. All other experimental conditions that could be controlled were similar to those of Figure 8.49. Results of the radial temperature distribution is shown in Figure 8.50. Interfacial temperature distribution in this regime shows again that it is not radially symmetrical within the bed. At both vertical heights of 70 and 570 mm, the trend is similar in both cases. It is also similar to trends in Figures 8.48 and 8.49 at the vertical height of 70 mm although the rate of temperature change as the radial distance is varied from left to right is steeper that the latter case. This difference may be attributed to the fact that at deep beds, the change in temperature distribution is more pronounced as a result of the higher liquid holdup in the tower as the static bed and hence expanded height is increased. As to the decrease of temperature, this again may be attributed to changes in gas velocity distribution as the temperature probe moves from the vicinity of the wall to the centre of the fluidised bed. Also, it can be concluded that the behaviour of the FBCT is markedly different within the bottom half of the FBCT as compared to the top half of the bed. This may be due to poor liquid distribution as well as differences in the degree of mixing.

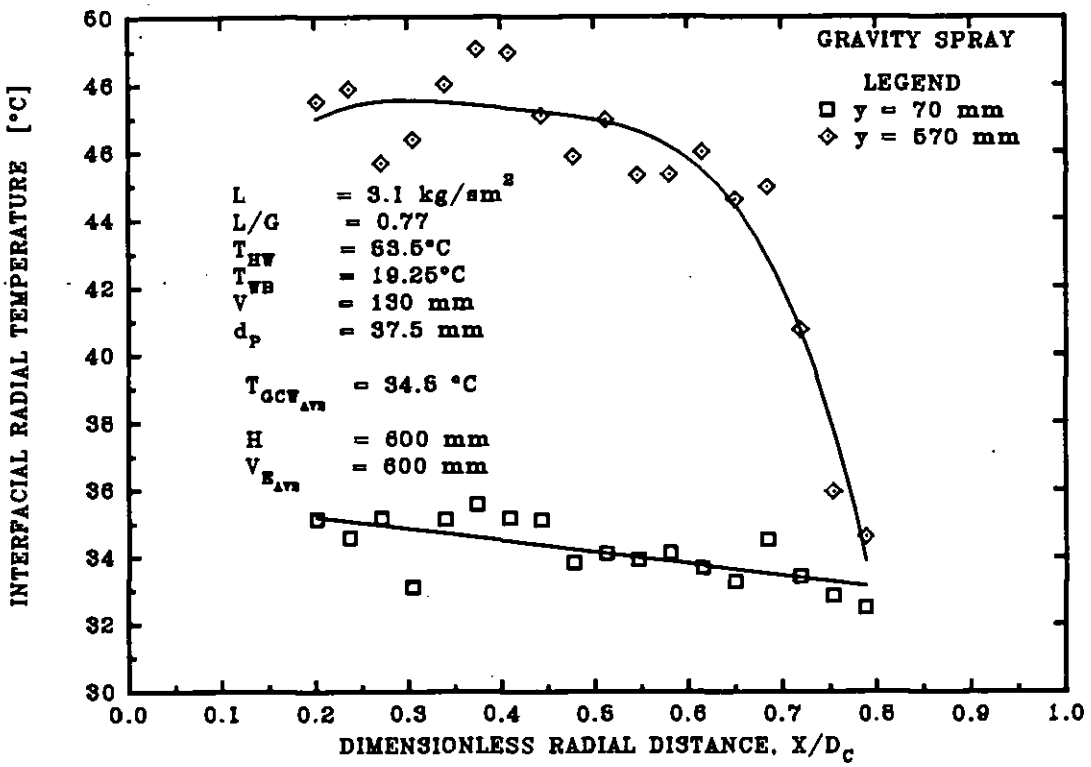

Figure 8.48 Radial temperature distribution in the tower for shallow bed at a high liquid mass flux. Measurements were taken as the probe radial distance was varied from left to right.

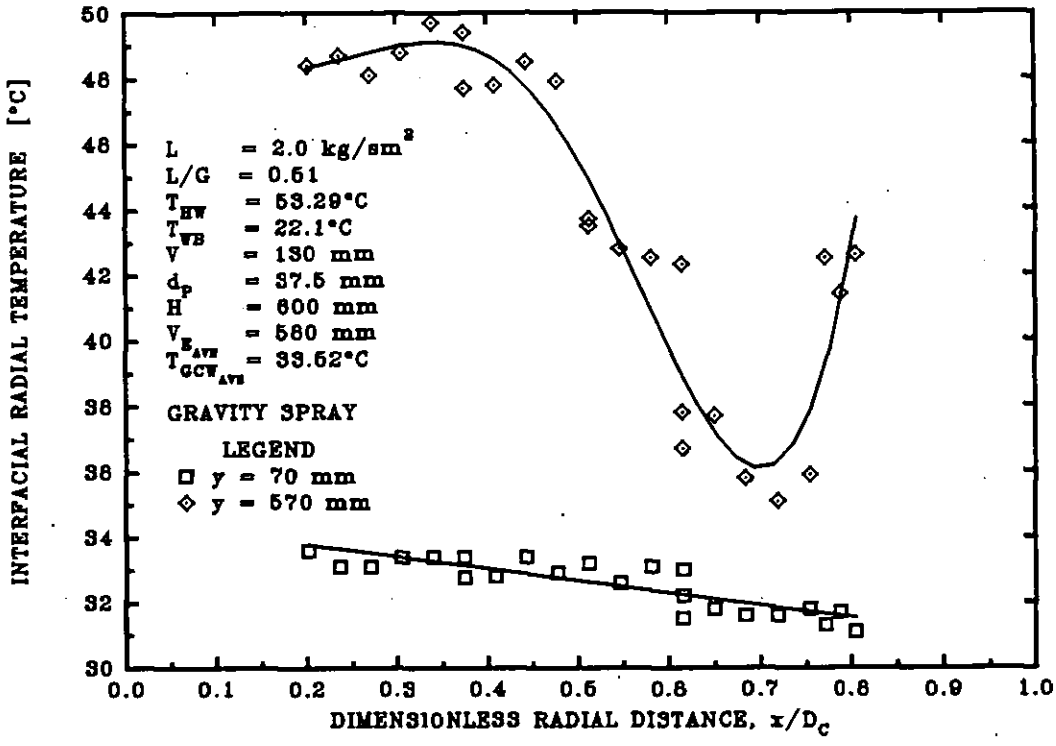

Figure 8.49. Radial Temperature distribution for shallow bed at a moderate liquid mass flux.

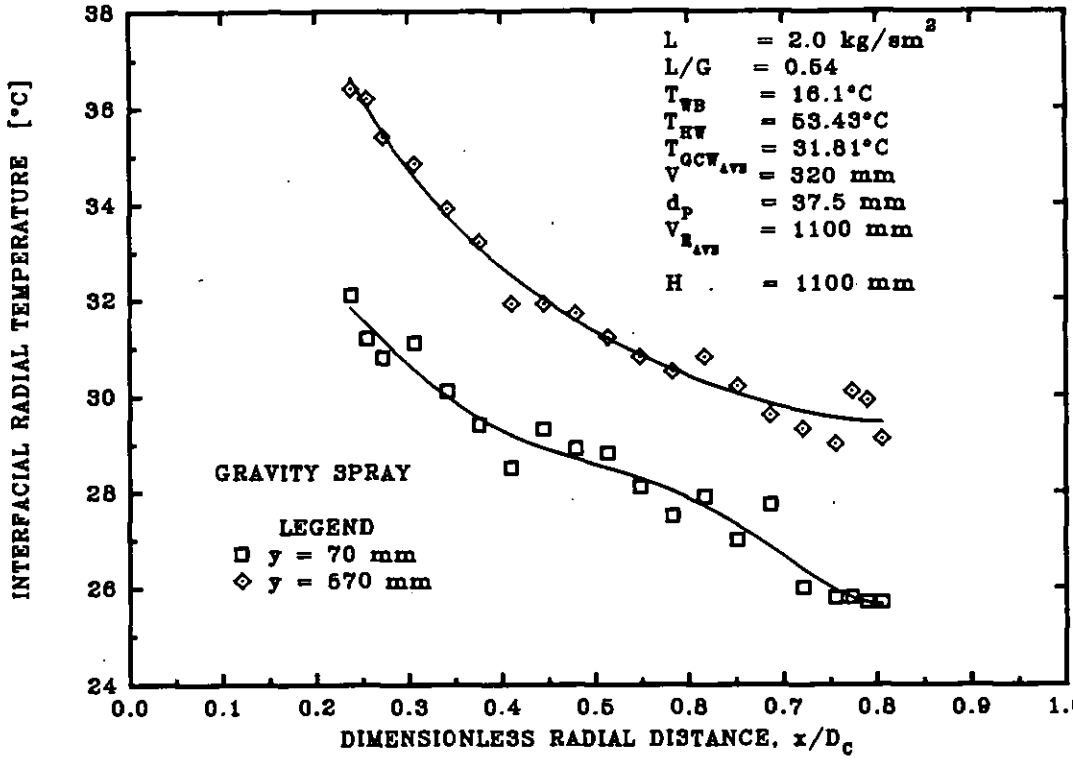

Figure 8.50 Radial Temperature distribution for a deep bed.

CHAPTER IX

REGRESSION ANALYSIS AND DESIGN CRITERIA

9.1 General Discussions

The main aim of any design process is to come up with a suitable and simple method that will enable the optimisation of the different dimensions involved. It has been shown in previous chapters that the FBCT is reliable, and that vast data can be accumulated so as to predict thermal-hydraulic performance. It has also been shown that the working of the FBCT allows for margins of errors. In this background, therefore, it is necessary to carry out a data reduction by correlating all the data into simple equations that can be used for the design of a full-scale FBCT. Correlations pertaining to the thermal and hydraulic performance have been presented here. Also derived were correlations for bed expansion, minimum and maximum fluidisation gas velocities. A design methology for the FBCT was developed and a computer programme relating to the design criteria was written.

The thermal-hydraulic performance and design of the FBCT is possible considering the large body of data that has been collected and discussed in the former chapters. The application of the method of Merkel (1925) in relation to heat and mass transfer has been shown to be effective and compares well with the findings of other investigators on fixed bed conventional cooling towers. The thermal performance of the FBCT is also dependent upon the rate of cooling in the plenum chamber because cooling continues to occur in this section as a result of two-phase gas-liquid heat and mass transfer. Generally, when the tower characteristic is calculated on the basis of the cooled water temperature from the plenum chamber, there is a marked increase in tower performance as compared to when it is based upon the outlet cooled water temperature from the fluidised bed itself. The trend of experimental results is also dependent upon the position

of the outlet cooled water sensor. On the average, the tower characteristic which indicates the thermal performance, decreases as the liquid flow rate is increased and decreases as the liquid/gas mass flux ratio *L/G* and as the inlet hot water temperature are increased. The reasons for the decrease in tower characteristic as the inlet water decreases may be attributable to assumptions in the derivation of the Merkel equation as discussed in Chapter VII. However, the cooling effectiveness increases as the inlet hot water temperature is increased due to increases in enthalpy potential with increases in the temperature range. The tower characteristic and effectiveness increase as the static bed height, spray nozzle height from the distributor grid, gas flow rate are increased as a result of increases in the liquid holdup in the interstitial voids of the bed which in turn results in increases in the gas-liquid interfacial area of the bed. Based on the droplet spray characteristics studied, the optimum spray nozzle height is when the ratio H/V_E is unity. The tower thermal performance increases as the particle density is increased due to increases in liquid holdup and hence bed agitation. On the other hand, it decreases as the particle size is increased due to decreases in contact area. However, there appears to be an optimum particle size for thermal performance.

The dependence of the tower thermal performance upon the spray nozzle characteristic is dependent upon the density and size of the spherical packing as well as the height of the spray nozzle from the distributor grid, and the position of the sensor. Relatively high density particles exhibited a better thermal performance when the coarse droplet spray is in use as compared to the fine droplet spray at the plenum cooled water temperature conditons and moderate spray nozzle heights from the distributor grid for reasons described in former chapters. On the basis of the fluidised bed itself, fine spray droplets indicated a better thermal performance than coarse droplet sprays due to increased gas-liquid interfacial area. On the average, fine droplet sprays gave a better performance that coarse droplet sprays. Both fine and coarse droplet sprays gave a higher thermal performance than the gravity spray which produced droplets at approximately atmospheric pressure. Dimensional analysis showed that the experimental results

were valid and the correlations that resulted numerically substantiated our experimental findings and will be well elaborated in the next section.

Experimental result showed that the design of the FBCT is possible in relation to the power requirements. Low density particles gave optimum bed air pressure drop but poor fluidisation characteristics while high density particles gave a higher bed air pressure drop as a result of their higher weights and hence a higher power requirement as well uniform fluidisation. The bed air pressure drop increases as the particle size is decreased again due to increased void tortuousity as the bed porosity decreases. The dependence of the bed air pressure drop upon the spray nozzle height from the distributor grid is affected by the density and size of the particles. However, it generally increases as the spray nozzle and the static bed heights are increased. Coarse large droplet sprays exhibited a higher bed pressure drop than the small fine ones which in turn gave a higher pressure drop than the gravity spray. The bed air pressure drop is almost independent of the inlet hot water temperature but increases as the the liquid flow rate is increased. In the case of the variation of the bed air pressure drop with the gas flow rate, it increases until the minimum fluidisation state is reached after which it remained constant, increasing sharply as the "true" flooding point is attained. Dimensional analysis suggests that correlations derived from the experimental data is valid. Correlations that can be used to calculate the bed air pressure drop and hence the power required for fluidisation will be given in the next section. Numerically, they are in accord with experimental findings.

The minimum fluidisation gas velocity increases as the density of the particle is increased, decreases with increasing liquid flow rate, and decreases as the particle size is increased but it is independent of the static bed height. The "true" flooding (maximum) gas velocity decreases as the liquid flow rate is increased. Correlations used to calculate the minimum fluidisation velocity were derived from those pertaining to the expanded bed height. The expanded bed height increases as the liquid and gas flow rates are increased, decreases as the density of the particles

are increased and increases with increasing static bed and the spray nozzle heights for reasons given in former chapters. The coarse droplet spray gave a higher bed expansion than the fine droplet spray which in turn gave a higher expansion than the atmospheric pressure gravity spray. The generalized correlation suggests that the bed expansion decreases as the particle diameter is increased. Overall, the correlations derived from experimental data indicate that experimental findings are valid and, therefore, they can be used to calculate the design dimensions of the FBCT.

A combined thermal-hydraulic correlation was also derived from the experimental data so that FBCT design dimensions can be optimized. The equation indicates that the least cost option for the FBCT design in terms of operational and capital cost is obtained when the liquid and gas mass fluxes are high while using low static and spray nozzle heights and relative low density large particles.

The design criteria developed shows that the FBCT may be about twenty-three times smaller than conventional fixed bed towers and they may operate at a similar or lower operational cost, as a result of low pressure drops, as the former.

9.2 Thermal Correlations

It was shown in chapter III that the thermal performance is dependent upon certain significant groups. All the groups were tried so as to correlate all data for thermal design. However, correlations were kept as simple as possible by including only the groups that contributed most to any given correlation. Since the Merkel approach could only be proved by dimensional analysis, correlations were done by the method of Raleigh using the sigma-plot linear iteration statistical package which was in the form of a constant multiplied by the product of all the significant dimensions or groups raised to their respective exponents. The coefficient and exponents were determined by multiple linear regression analysis upon the experimental data.

The multiple regression analysis using the Sigma-plot application package was applied initially upon the data of the individual spray droplet types and then generalized so that all the data could be included. For each of the cases, three sets of correlations were derived based on the grid, average and plenum cooled water conditions.

9.2.1 Coarse Droplet Spray

The regression equation based upon the outlet cooled water temperature at the distributor grid in accordance with the dimensioned experimental varaibles was found to be:

$$\frac{KaV}{L} = 1.076L^{-0.61}G^{0.85}V^{0.16}d_p^{0.06}H^{0.42}\rho_p^{0.09}T_{HW}^{-0.14} \qquad (9.1)$$

The average error of estimate of Equation 9.1 is 16%. The coefficient of correlation is 0.966 for 128 data points. Similarly, the linear regression equation based upon the outlet cooled water temperature at the plenum is given by:

$$\frac{KaV}{L} = 6.175L^{-0.53}G^{0.64}V^{0.16}d_p^{-0.02}H^{0.17}\rho_p^{0.03}T_{HW}^{-0.44} \qquad (9.2)$$

The average error of estimate of Equation 9.2 for the analysis of 128 data points is 9.76%. The coefficient of correlation 0.969. Multiple regression analysis based on the average outlet cooled water temperature yielded:

$$\frac{KaV}{L} = 6.331L^{-0.50}G^{0.62}V^{0.17}d_p^{-0.02}H^{0.27}\rho_p^{0.03}T_{HW}^{-0.48} \qquad (9.3)$$

The average error of estimate of Equation 9.3 is 11% at a coefficient of correlation of 0.958 for the analysis of 128 data points.

Dimensionless Equations for the FBCT thermal performance were also derived from experimental results for the coarse droplet spray. At the outlet cooled water from the distributor grid conditions, the multiple regression analysis gave:

$$\frac{KaV}{L} = 0.0070 \left(\frac{L}{G}\right)^{-0.62} \left[\frac{V}{d_p}\right]^{0.55} \left(\frac{H}{V}\right)^{0.38} \left[\frac{\rho_p}{\rho_L}\right]^{0.05} \left[\frac{Gd_p}{\mu_G}\right]^{0.38} \quad (9.4)$$

The average error of estimate of error of Equation 9.4 is 15 % for the 128 data points analyzed. The least square regression correlation coefficient is 0.962. Based upon the outlet cooled water temperature of the plenum chamber, the Equation was found to be:

$$\frac{KaV}{L} = 0.1451 \left(\frac{L}{G}\right)^{-0.52} \left[\frac{V}{d_p}\right]^{0.31} \left(\frac{H}{V}\right)^{0.14} \left[\frac{\rho_p}{\rho_L}\right]^{0.05} \left[\frac{Gd_p}{\mu_G}\right]^{0.17} \quad (9.5)$$

The average error of estimate of Equation 9.5 was found to be 11.32% for a correlation coefficient of 0.952. Multiple least-square regression analysis based on the average cooled water temperature of the plenum and the distributor grid yielded:

$$\frac{KaV}{L} = 0.0713 \left(\frac{L}{G}\right)^{-0.50} \left[\frac{V}{d_p}\right]^{0.40} \left(\frac{H}{V}\right)^{0.23} \left[\frac{\rho_p}{\rho_L}\right]^{0.05} \left[\frac{Gd_p}{\mu_G}\right]^{0.20} \quad (9.6)$$

The average error of estimate of the 128 data points analyzed is 13% and the coefficient of linear regression of the square of the errors is 0.934.

9.2.2 Fine Droplet Spray

The regression equation based on the outlet cooled water temperature of the plenum in terms of the experimentally dimensioned independent variables is given by the following correlation:

$$\frac{KaV}{L} = 5.697L^{-0.48}G^{0.69}V^{0.30}d_P^{-0.11}H^{0.074}\rho_P^{0.034}T_{HW}^{-0.50} \qquad (9.7)$$

The average error of estimate of Equation 9.7 is 8.7%. The least-square regression correlation coefficient is 0.958. Data analysis involved 379 points.

The linear regression correlation based on the outlet cooled water temperature of the distributor grid is given as:

$$\frac{KaV}{L} = 16.55L^{-0.44}G^{0.60}V^{0.013}d_P^{0.27}H^{0.44}\rho_P^{0.14}T_{HW}^{-0.70} \qquad (9.8)$$

The average error of estimate of Equation 9.8 is 19.9% and the coefficient of correlation is 0.859.

A least-square multiple regression analysis was also performed on the data based on based on the average cooled water temperature of the distributor grid and plenum chamber. It yielded:

$$\frac{KaV}{L} = 8.365L^{-0.43}G^{0.65}V^{0.21}d_P^{0.017}H^{0.20}\rho_P^{0.074}T_{HW}^{-0.59} \qquad (9.9)$$

The average error of estimate of Equation 9.9 is 10% at a correlation coefficient of 0.934.

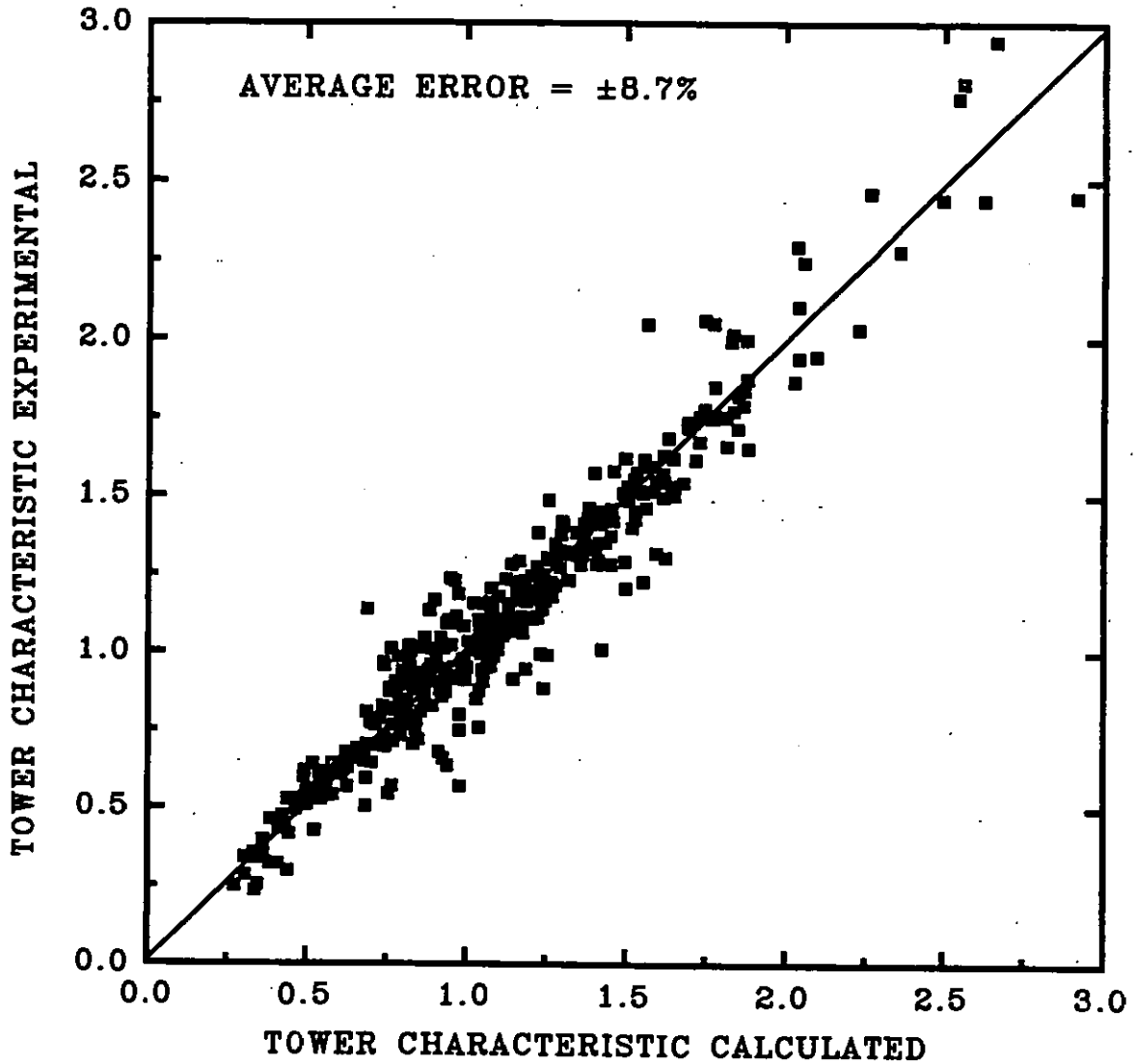

Figure 9.1 Comparison of the calculated and experimental tower characteristic based on Equation 9.7.

The dimensionless equation for the fine droplet spray was also derived from least-square regression analysis. In terms of the outlet cooled water temperature of the plenum chamber, the correlation is given by:

$$\frac{KaV}{L} = 0.0722\left(\frac{L}{G}\right)^{-0.45}\left[\frac{V}{d_p}\right]^{0.31}\left(\frac{H}{V}\right)^{-0.023}\left[\frac{\rho_p}{\rho_L}\right]^{0.078}\left[\frac{Gd_p}{\mu_G}\right]^{0.28} \qquad (9.10)$$

The average error of estimate is 11%. The linear regression correlation coefficient is 0.939.

Based on the outlet cooled water temperature of the distibutor grid, the regression analysis gave:

$$\frac{KaV}{L} = 0.02084\left(\frac{L}{G}\right)^{-0.39}\left[\frac{V}{d_p}\right]^{0.33}\left(\frac{H}{V}\right)^{0.29}\left[\frac{\rho_p}{\rho_L}\right]^{0.074}\left[\frac{Gd_p}{\mu_G}\right]^{0.35} \qquad (9.11)$$

The average error of estimate is 21.7% and a correlation coefficient of 0.808.

A least-square regression correlation based on the average cooled water temperature of the grid and plenum chamber may be written as:

$$\frac{KaV}{L} = 0.04411\left(\frac{L}{G}\right)^{-0.39}\left[\frac{V}{d_p}\right]^{0.32}\left(\frac{H}{V}\right)^{0.08}\left[\frac{\rho_p}{\rho_L}\right]^{0.091}\left[\frac{Gd_p}{\mu_G}\right]^{0.32} \qquad (9.12)$$

The average error of estimate is 12.6% as shown in Figure 9.12 and the coefficient of correlation is 0.904.

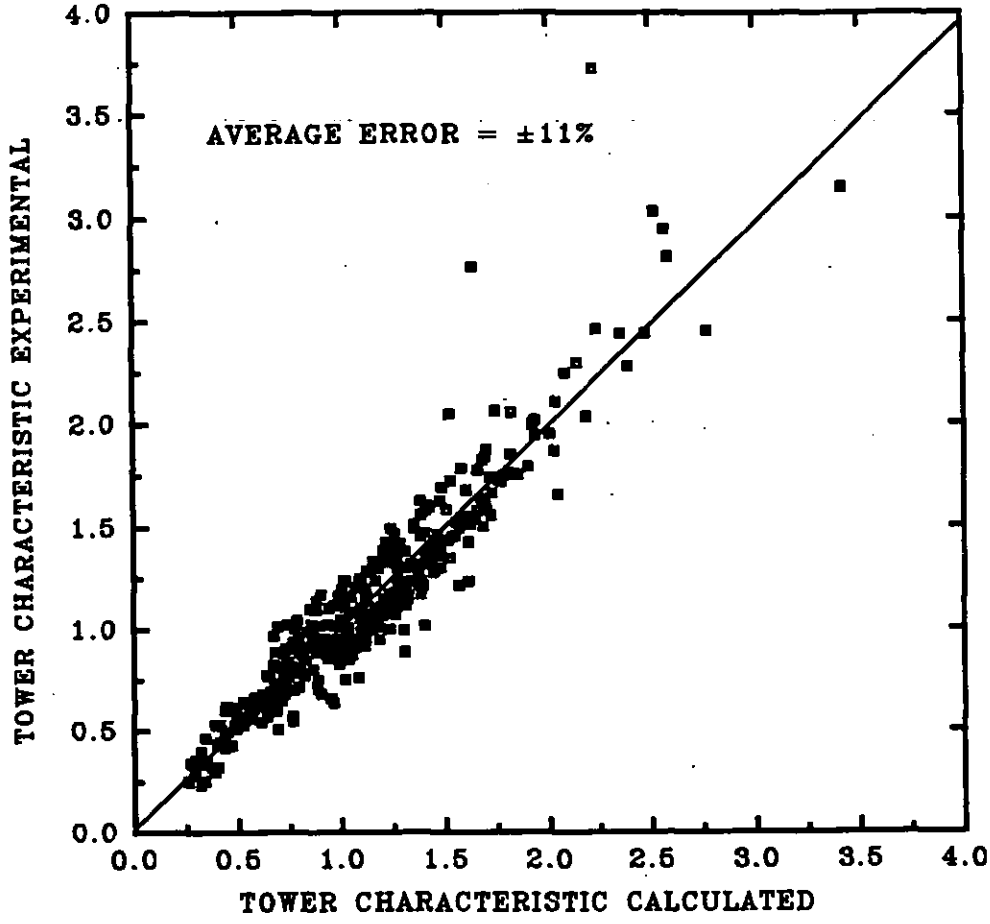

Figure 9.2 Comparison of the calculated and the experimental tower characteristic based on Equation 9.10.

9.2.3 Generalised Correlation for Fine and Coarse Drople Sprays

In order to make a numerical comparison between the coarse and the fine droplet sprays, it was necessary to carry out a multiple linear regression analysis that includes the FBCT thermal performance of both droplet sprays. Since both spray types were similar in design, only the most fundamental difference between the two spray types was used to characterize an all-encompassing correlation. Although one of the most important design features of the two nozzles is the total number and size of the nozzle orifice, it is the spray droplet median diameter that influences the heat transfer coefficient. As a result, this was the only variable that was included in the analysis. All other measured dimensions were similar to those of Equations 9.1 to 9.3.

The correlation obtained based on the outlet cooled water temperature of the plenum chamber may be wirtten as:

$$\frac{KaV}{L} = 6.434 L^{-0.50} G^{0.71} V^{0.26} d_p^{-0.02} d_s^{0.02} H^{0.09} \rho_p^{0.07} T_{HW}^{-0.46} \quad (9.13)$$

A total of 505 data points were analyzed. Equation 9.13 has an average error of 9.1%. The correlation coefficient is 0.960.

At the distributor grid outlet cooled water conditions, a regression analysis applied upon the 505 experimental data points gave:

$$\frac{KaV}{L} = 2.893 L^{-0.50} G^{0.69} V^{0.05} d_p^{0.22} d_s^{-0.16} H^{0.42} \rho_p^{0.11} T_{HW}^{-0.55} \quad (9.14)$$

The average error of estimate is 19.9% as seen in Figure 9.14. The correlation coefficient is 0.880.

Based on the average outlet cooled water conditions of the distributor grid and the plenum chamber, multiple regression analysis applied on all the data yielded:

$$\frac{KaV}{L} = 6.106 L^{-0.50} G^{0.67} V^{0.20} d_p^{0.03} d_s^{-0.03} H^{0.21} \rho_p^{0.08} T_{HW}^{-0.55} \quad (9.15)$$

The average error of estimate was 10.4%. Equation 9.15 has a correlation coefficient of 0.941. The least square regression analysis applied upon a total of 505 experimental data points.

Dimensionless correlations relating to the FBCT thermal performance were also derived to include both fine and coarse droplet spray types. The same method of analysis were applied upon the 505 data points that included both spray types. At

conditions based on the outlet cooled water temperature from the plenum chamber, the multiple regression equation was found to be:

$$\frac{KaV}{L} = 0.8070 \left(\frac{L}{G}\right)^{-0.51} \left[\frac{V}{d_p}\right]^{0.24} \left(\frac{H}{V}\right)^{0.025} \left[\frac{d_p}{d_s}\right]^{-0.06} \qquad (9.16)$$

The average error of estimate was found to be 13.6% and the coefficient of linear regression is 0.926. At the conditions of the outlet cooled water temperature of the distributor grid, the least square regression analysis of the 505 data points may be written as:

$$\frac{KaV}{L} = 0.1906 \left(\frac{L}{G}\right)^{-0.51} \left[\frac{V}{d_p}\right]^{0.34} \left(\frac{H}{V}\right)^{0.34} \left[\frac{d_p}{d_s}\right]^{0.12} \qquad (9.17)$$

The average error of estimate of Equation 9.17 is 24%. The coefficient of linear regression is 0.828. Based on the average outlet cooled water from the distributor grid and the plenum chamber a least square regression analysis yielded:

$$\frac{KaV}{L} = 0.5084 \left(\frac{L}{G}\right)^{-0.47} \left[\frac{V}{d_p}\right]^{0.29} \left(\frac{H}{V}\right)^{0.14} \left[\frac{d_p}{d_s}\right]^{-0.01} \qquad (9.18)$$

The average error of estimate is 15.5%. The coefficient of linear regression was 0.890. A least square regression analysis was also performed to obtain a generalized and simplified heat transfer Equation that includes the data of other investigators. The derived Equation is:

$$\frac{KaV}{L} = 0.53 \left(\frac{L}{G}\right)^{-0.54} \left[\frac{V}{d_p}\right]^{0.32} \left(\frac{H}{V}\right)^{0.08} \qquad (9.19)$$

The average error of estimate was 16%. The correlation coefficient was 0.923 for 615 data points. Present data agrees well with the data of other investigators as seen in Figure 9.3.

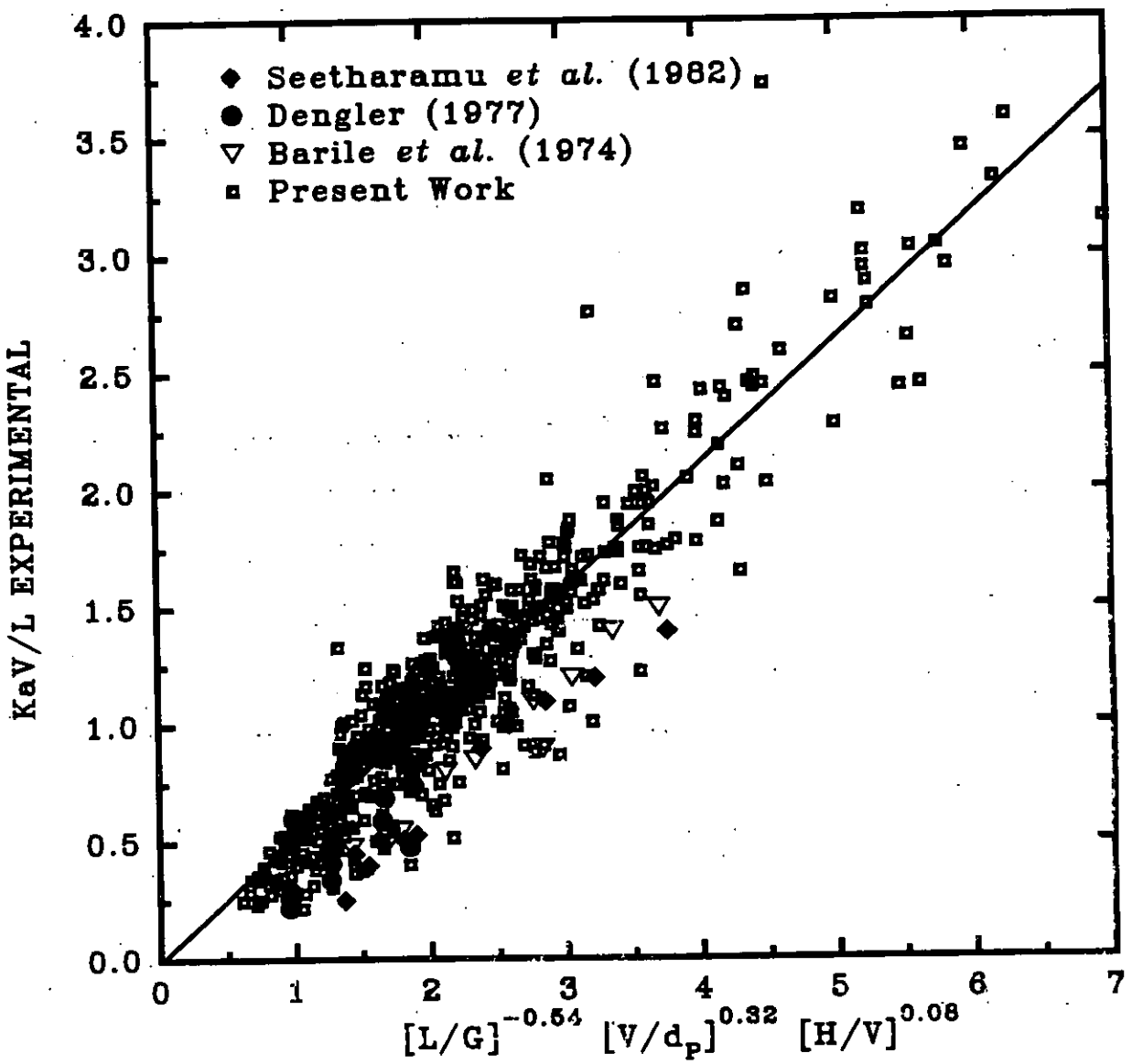

Figure 9.3 Comparison of the present data with those of other investigators.

9.3 Hydraulic Equations on the Bed Air Pressure Drop

A similar method of analysis as was carried out for the thermal performance was carried so as to determine the FBCT hydraulic performance. Separate analysis is done for both the coarse and the fine droplet spray types. A generalised correlation was also derived that included all three nozzle types.

9.3.1 Coarse Droplet Spray Nozzle

Using our experimental data and the dimensionless groups derived in chapter II a least square regression analysis for the large droplet spray gave:

$$\frac{\Delta P \rho_G^{0.5} \rho_L^{0.5}}{LG} = 0.186 \left(\frac{L}{G}\right)^{0.78} \left[\frac{V}{d_p}\right]^{0.94} \left(\frac{H}{V}\right)^{-0.1} \left[\frac{\rho_p}{\rho_L}\right]^{0.77} Fr_L^{-0.82} \quad (9.20)$$

The average error of analysis is 16 % and the coefficient of linear correlation 0.98 for the 128 data points analysed.

9.3.2 Fine Droplet Spray Nozzle

The correlation Equation based on similar dimensionless groups as in Equation 9.20 was found to be:

$$\frac{\Delta P \rho_G^{0.5} \rho_L^{0.5}}{LG} = 0.764 \left(\frac{L}{G}\right)^{0.35} \left[\frac{V}{d_p}\right]^{1.0} \left(\frac{H}{V}\right)^{0.22} \left[\frac{\rho_p}{\rho_L}\right]^{0.55} Fr_L^{-0.61} \quad (9.21)$$

The average error of estimate is ±27% for a total of 379 data points.

9.3.3 Generalised Correlation

A correlation was also developed so as to include the median droplet diameter. The Equation is:

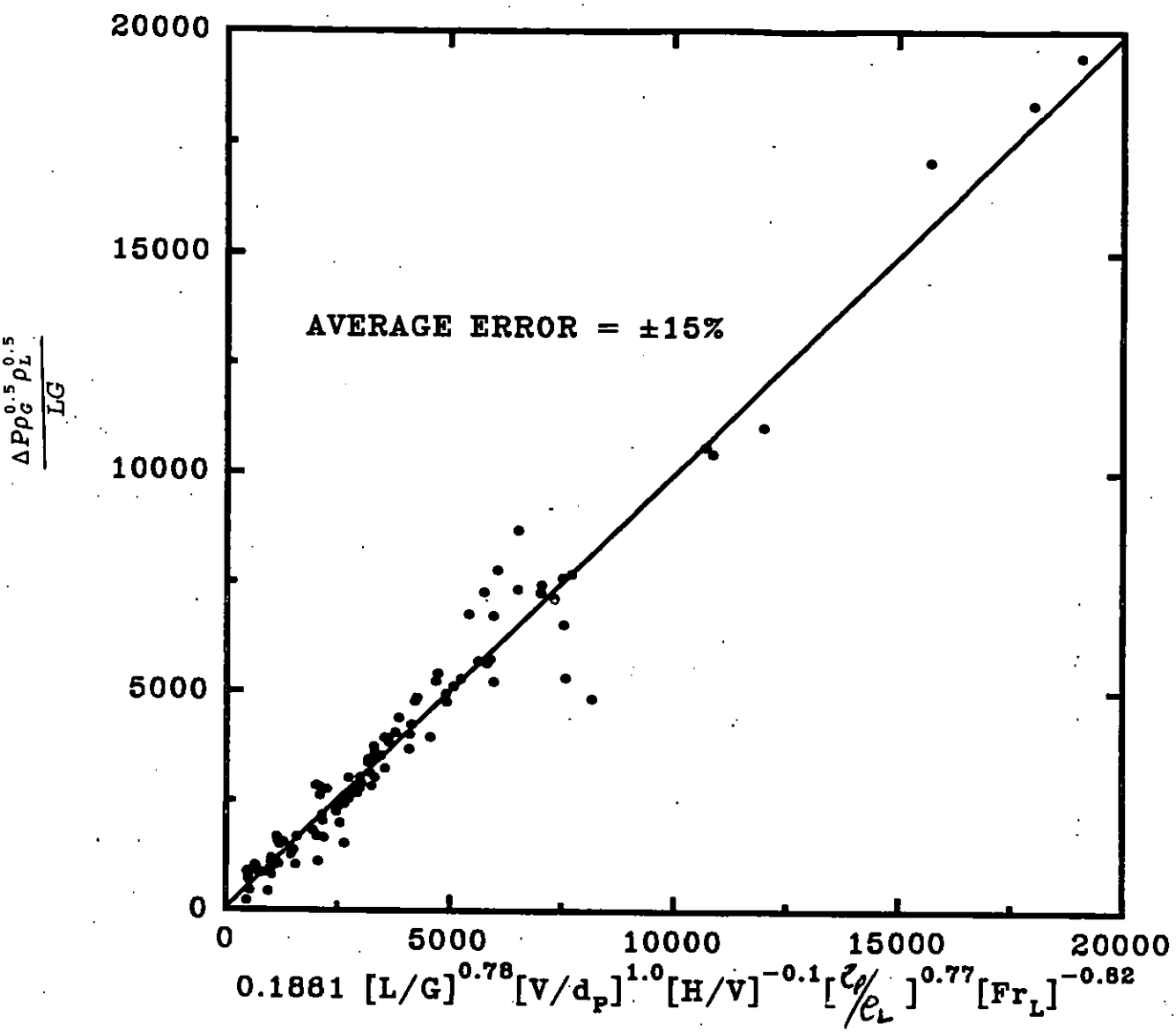

Figure 9.4 Comparison between measured and calculated bed air pressure term based on Equation 9.20.

$$\frac{\Delta P \rho_G^{0.5} \rho_L^{0.5}}{LG} = 2.2\left(\frac{L}{G}\right)^{0.38}\left[\frac{V}{d_p}\right]^{1.1}\left[\frac{d_p}{d_s}\right]^{-0.03}\left(\frac{H}{V}\right)^{0.36}\left[\frac{\rho_p}{\rho_L}\right]^{0.54} Fr_L^{-0.63} Re_G^{-0.2} \quad (9.22)$$

The average error of estimate is 23%. The coefficient of correlation is 0.965 for a total of 568 data points.

In terms of the dimensionally measured experimental variables, linear regression analysis yielded:

$$\frac{\Delta P \rho_G^{0.5} \rho_L^{0.5}}{LG} = 801\ L^{-0.88} G^{-0.70} d_p^{-0.23} d_s^{0.042} H^{0.30} \rho_p^{0.64} V^{0.88} \quad (9.23)$$

The average error of estimate was 24% for the 568 data points analyzed. The coefficient of linear regression is 0.97.

9.4 Bed Expansion

The same type of analysis was performed on the experimental data as regards the bed expansion. These correlations were initially based upon the type of nozzle and then developed into a generalzed equation that includes the droplet size.

9.4.1 Coarse Droplet Spray

The least-square regression analysis performed upon the dimensionless variables based on the dimensioal analysis in chapter II gave the following correlation:

$$\frac{V_E}{V} = 0.0254\left(\frac{L}{G}\right)^{-0.21}\left[\frac{V}{d_p}\right]^{0.01}\left(\frac{H}{V}\right)^{0.15}\left[\frac{\rho_p}{\rho_L}\right]^{-0.04} Re_L^{0.32} Re_G^{0.33} \quad (9.24)$$

The average error of estimate is 12% and the correlation coefficient is 0.88.

In terms of the dimensionally measured variables the least square analysis yielded:

$$\left[\frac{V_E}{V}\right] = 1.564\ L^{0.10}G^{0.90}d_p^{-0.29}H^{0.09}\rho_B^{-0.37}V^{-0.18} \qquad (9.25)$$

The average error of estimate is 11% and the correlation coefficient is 0.92 for a total of 128 data points.

9.4.2 Fine Droplet Spray Nozzle

The correlation representing the expanded bed height in terms of fine droplets was found to be given as:

$$\frac{V_E}{V} = 3.62*10^{-5}\left(\frac{L}{G}\right)^{0.28}\left[\frac{V}{d_p}\right]^{0.21}\left(\frac{H}{V}\right)^{0.34}\left[\frac{\rho_P}{\rho_L}\right]^{0.23} Re_L^{-0.10}Re_G^{1.33} \qquad (9.26)$$

The average error of estimate is 19% for the 379 data points analyzed. The coefficient of correlation is 0.861.

In terms of experimentally dimensioned variable, the correlation obtained is:

$$\left[\frac{V_E}{V}\right] = 0.40\ L^{0.22}G^{1.22}d_p^{-0.35}H^{0.31}\rho_p^{-0.23}V^{-0.18} \qquad (9.27)$$

The average error of estimate was 16% and the coefficient of correlation was 0.91 for 379 data points.

9.4.3 Generalised Bed Expansion Correlation

The generalised dimensionless Equation that characterises the fine and coarse droplet sprays may be written as:

The average error of estimate is 16% and the correlation coefficient is 0.85 for

$$\frac{V_E}{V} = 0.0023\left(\frac{L}{G}\right)^{-0.04}\left[\frac{d_P}{d_S}\right]^{-0.20}\left(\frac{H}{V}\right)^{0.12}\left[\frac{\rho_P}{\rho_L}\right]^{0.09} Re_G^{0.80} Re_L^{0.18} \quad (9.28)$$

a total of 561 data points analysed as shown in Figure 9.5. At $V_E/V = 1$, the minimum fluidisation velocity is reached in all cases. This accounts for the scatter of result at the lower end of results shown in Figure 9.5.

Similarly, the correlation in terms of experimentally dimensioned variables may be written as:

$$\left[\frac{V_E}{V}\right] = 1.516\ L^{0.17} G^{1.10} d_P^{-0.30} d_S^{0.13} H^{0.18} \rho_P^{-0.32} V^{-0.16} \quad (9.29)$$

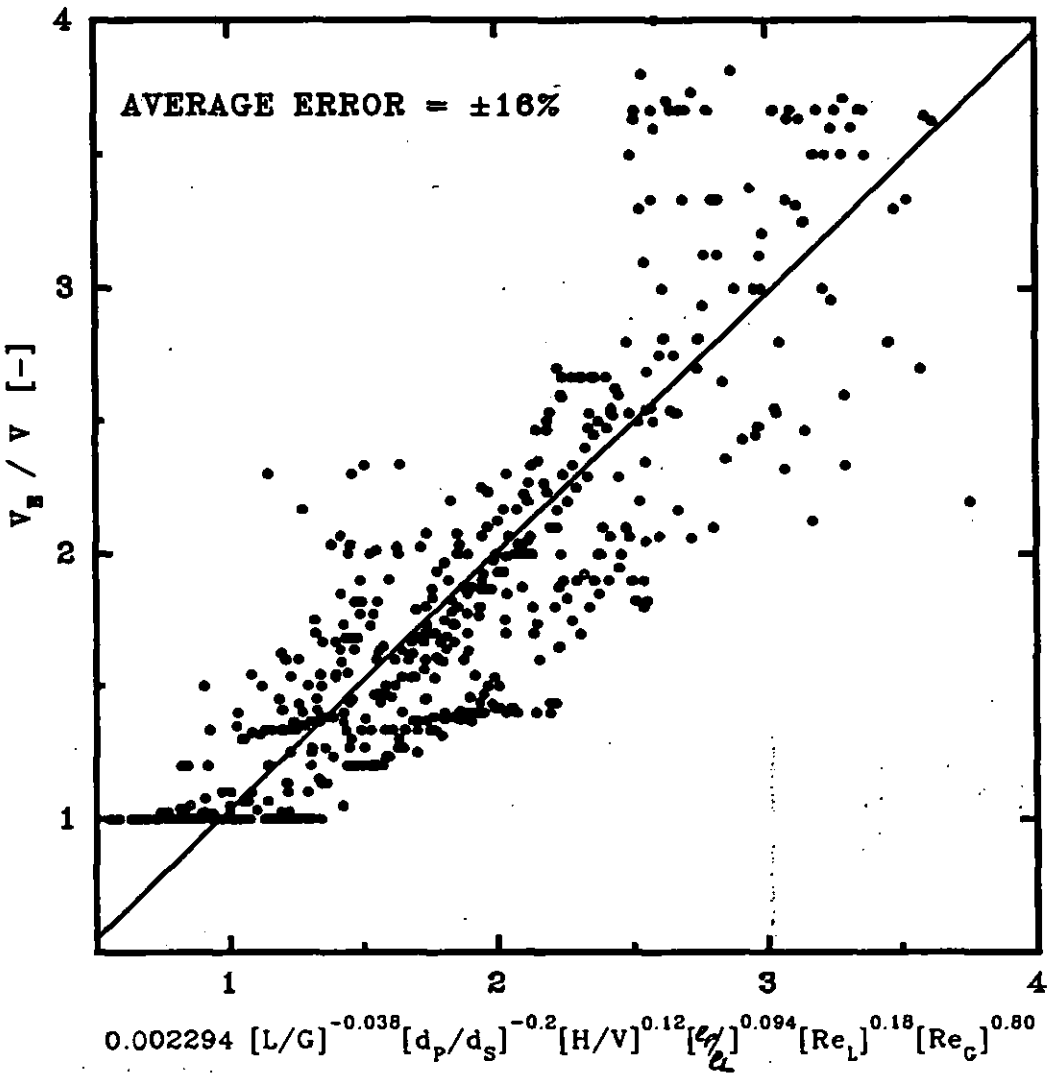

Figure 9.5 A comparison between calculated and measured V_E/V.

The average error of estimate was found to be less than 15% for a total of 568 data points. The coefficient of correlation is 0.901.

Having established and justified the expanded bed height, it is important that we develop design correlations that can be used to calculate the minimum and maximum fluidisation velocities.

9.5 The Minimum Fluidisation Velocity

In chapter II, it was shown that the minimum fluidisation gas mass flux or velocity may be determined by equating the dimensionless ratio V_E/V, to unity. Any of the above correlations can be used for this purpose depending upon the type of spray droplet. However, the generalised expanded bed height correlation was used for this purpose to take account of the droplet size. The correlation obtained thus may be written as:

$$435\left[\frac{L}{G_{mf}}\right]^{0.04}\left[\frac{G_{mf}d_p}{\mu_G}\right]^{-0.80}=\left[\frac{d_p}{d_s}\right]^{-0.20}\left(\frac{H}{V}\right)^{0.12}\left[\frac{\rho_p}{\rho_L}\right]^{0.08}Re_L^{0.18} \quad (9.30)$$

In order to make a comparison of our numerical and experimental findings on the minimum fluidisation gas mass flux, it was important to use Equation 9.29 because it directly relates the dependent V_E/V ratio to the independent experimental variables. Bearing this in mind, Equations 9.29 and 9.24 were respectively equated to unity resulting in the following dimensional and simple correlations for the minimum fluidisation gas mass flux:

$$G_{mf} = 0.6847\ L^{-0.67}d_p^{0.27}d_s^{-0.12}H^{-0.16}\rho_p^{0.32}V^{0.15} \quad (9.31)$$

$$42\left[\frac{L}{G_{mf}}\right]^{0.21}\left[\frac{G_{mf}d_p}{\mu_G}\right]^{-0.32}=\left(\frac{H}{V}\right)^{0.15}\left[\frac{\rho_p}{\rho_L}\right]^{-0.04}(Re_L)^{0.33} \quad (9.32)$$

9.6 Generalised Correlation for Tower Optimum Thermal-Hydraulic Performance

In the final analysis, an equation that can be used for the optimization of the thermal-hydraulic performance of a FBCT was developed by means of multiple regression analysis. In terms of the experimentally dimensioned variables, the correlation may be written as:

$$\frac{KaVG}{\Delta P \rho_G^{0.5} \rho_L^{0.5}} = 0.00214 L^{0.34} G^{0.1.11} V^{-0.56} H^{-0.08} d_p^{0.75} d_s^{0.021} \rho_P^{-0.10} \quad (9.33)$$

The average error of estimate was 28% and 85% of the data is accounted for by Equation 9.33. Only 505 data points of the fine and coarse droplet spray types were used. The relatively large error may have been caused by fluidisation anomalies that affect bed air pressure measurements. In dimensionless terms, the least square regression analysis gave:

$$\frac{KaVG}{\Delta P \rho_G^{0.5} \rho_L^{0.5}} = 0.0037 \left(\frac{L}{G}\right)^{-0.64} \left[\frac{V}{d_P}\right]^{-0.64} \left[\frac{d_P}{d_S}\right]^{-0.04} \left(\frac{H}{V}\right)^{-0.09} \left[\frac{\rho_P}{\rho_L}\right]^{-0.16} Fr_L^{0.50} Re_G^{0.58} \quad (9.34)$$

The average error of estimate was similar to Equation 9.34 for a total of 568 data points as seen in Figure 9.6 below.

Similarly, a least square regression analysis carried out on all the experimental data of 615 points including the gravity spray for the dimensioned variables that excluded the spray droplet size yielded:

$$\frac{KaVG}{\Delta P \rho_G^{0.5} \rho_L^{0.5}} = 0.0011 L^{0.33} G^{1.26} V^{-0.57} H^{-0.12} d_p^{0.46} \rho_P^{-0.24} \quad (9.35)$$

This was done so as to obtain a simple equation that does not include the droplet size since this parameter is normally not known. Equation 9.35 has a similar error

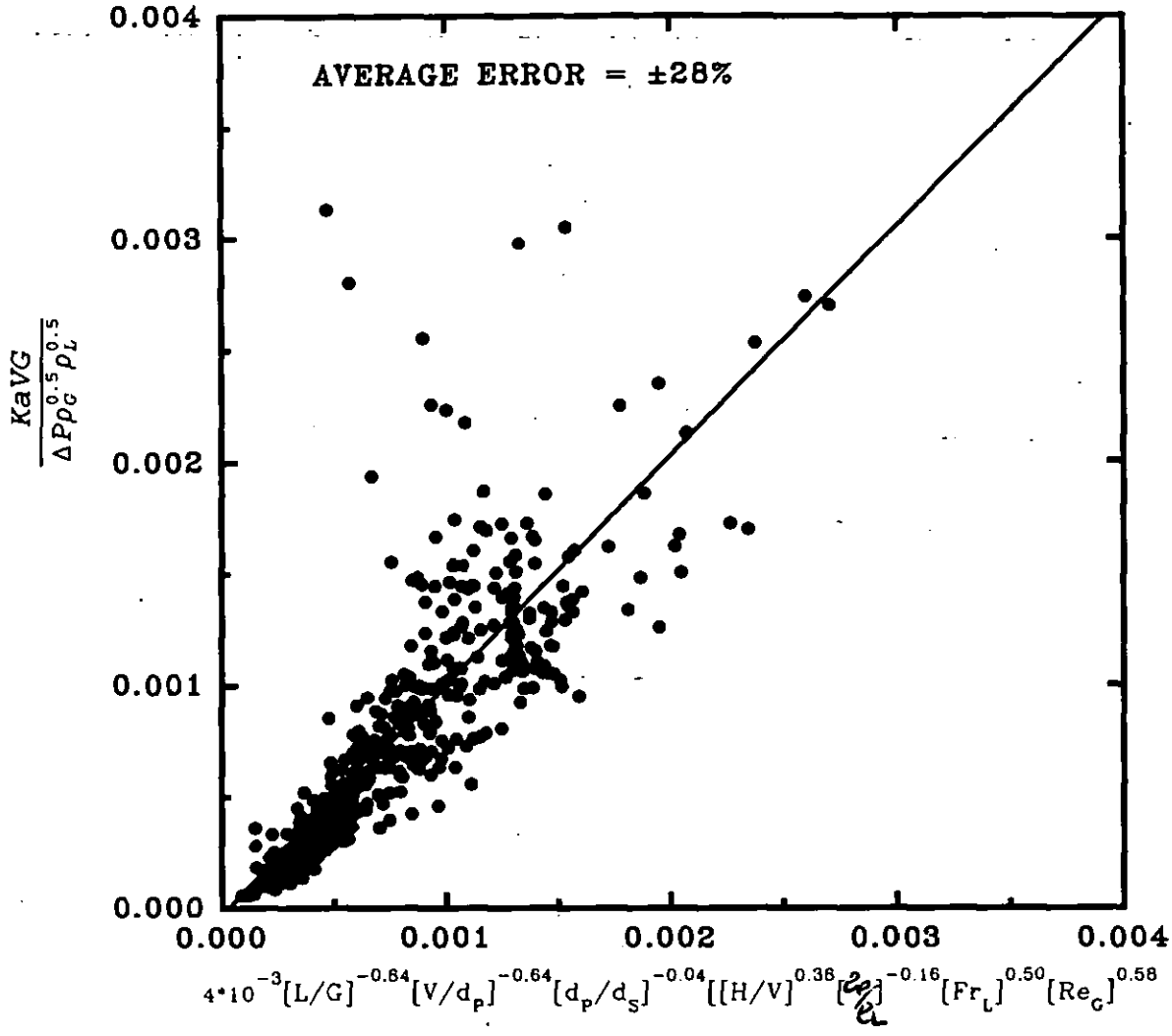

Figure 9.6 Optimization graph based on Equation 9.34.

to Equation 9.34. However, only about 75% of the data is accounted for by this Equation.

Equations 9.33 to 9.35 show that for a paricular gas flow rate, the best thermal-hydraulic performance of the FBCT may be obtained with relatively large low density particles in a small compact tower and high liquid flow rate. This quantitative finding is in good agreement with our experimental observation of chpaters V to VIII. The theoretical and empirical design of the FBCT is now complete. Equations have now been developed to calculate the thermal and hydraulic performance. The minimum and maximum fluidisation gas velocities

calculated. The expanded bed height can also be estimated. Equations that can help in the optimization of the FBCT performance have been developed. We can therefore proceed to establish the design criteria.

9.7 Design Criteria

In this section, the systematic method that can be used in the design of an FBCT will be elucidated. All equations that have been developed so far will be logically applied for this purpose and two full-scale models will be designed to illustrate the novelty of the present work. A sample design calculation will be given together with comparisons of conventional and fluidised bed cooling towers in terms of size and and operating power. A computer program is also written to facilitate design optimization.

9.7.1 Design Problem Formulation

In the design of a full scale FBCT, the following parameters are given.

1 The water flow rate is specified.

2 The wet-bulb, dry-bulb, inlet hot water temperatures are specified.

3 The range is calculated.

4 The maximum allowable power requirement is specified.

5 The size and density of the particles are chosen.

6 The liquid/gas mass flux ratio *L/G*.

7 The height of tower or the static bed height is specified together with the total available capital expenditure.

8 The spray droplet type and the median diameter is specified.

The design methodology is required to calculate and specify the following using the appropriate Equations.

1 The mode of operation is specified

2 The cooling range is calculated.

3 The required tower characteristic for a given liquid/gas mass flux ratio is calculated.

4 The gas mass flux and fluidisation velocity are calculated

5 The diameter and the total number of cells of the tower is estimated.

These are the preliminary steps and they are discussed in a greater depth below.

9.7.2 Flow Regime Selection

In chapter III, the different modes of operation that can be attained in a FBCT were discussed. This was extensively discussed in Chapters V to VIII. In the type II regime, the high density particles, spray nozzle height from the distributor grid, static bed height, the type of spray and the particle size are all important factor. However, the bed pressure drop attained is the most significant indicator of the mode of operation. In chapter III, Figure 3.3 indicates the classification of modes of operation. Low density particles less than 300 kg/m^3, generally operate in the type I regime which signifies fluidisation without incipient flooding and this is accompanied by low bed air pressure drops and hence lower power meaning a low operational cost, while particle densities greater than 300 kg/m^3 signify the type II regime and this is characterised by high bed air pressure drops indicating a high power requirement. It follows that the operational cost is higher although the thermal performance is higher than a type I operation as a result of athe high liquid holdup of the former as compred to the latter. Therefore, a type II FBCT operation will theoretically yield a smaller FBCT at a lower capital cost than a type 1 FBCT. In view of these factors, the mode of operation should be chosen so that the allowable power requirement and hence operational cost is not exceeded. Similarly, the selection must reflect the capital expenditure that is avalaible. In the quantitative analysis, selection of the different design variables may be obtained by refering to the flow regime diagram of Vunjak-Novakovic *et al.* (1980) shown in Figure 3.4 in chapter III. However, this must be treated with care because findings in this thesis suggest that there are no steadfast rules that govern the classification of FBCT flow regimes. Having specified the mode of

operation, it is therefore important that we choose the particle size and density as depicted Figure 3.4 in chapter III. Particle densities may range from 0 (an empty tower) to about 1300 kg/m^3. he size and density should be chosen so as to reflect the maximum and minimum fluidisation velocities.

9.7.3 Outline of Design Calculation Procedure

1 The range is calculated from Equation 2.28 in chapter II.

2 The required tower characteristic for a given *L/G* ratio is calculated from the left hand side of 2.43 or 2.45 in chapter II. For correct design, this value must be equal to the available tower characteristic of Equations 9.1 to 9.19 depending upon the specifications in section 9.2 above. The static bed or the spray nozzle height is then calculated.

3 The gas mass flux is calculated from the *L/G* ratio and the mass transfer coefficient KaV is calculated.

4 The expanded bed height is calculated from Equations 9.24 to 9.29. If this is higher lower than the spray nozzle height from the distributor grid H, then choose an arbitrary value about 1.2 times the expanded bed height and repeat the calculations from step 1.

5 The minimum liquid gas/mass flux ratio L/G_{mf} is calculated from Equations 9.30 to 9.32. If the chosen L/G ratio is less than the L/G_{mf} then choose another liquid/gas mass flux ratio about twice that at the minimum fluidisation velocity and go back to step 1.

6 The bed air pressure drop is then calculated from Equations 9.20 to 9.23 depending upon the specifications in section 10.2.

7 The design is checked for optimization by substitution of the calculated and specified parameters into Equations 9.33 to 9.35. Different parameters are tried to maximise the left hand side of these Equations.

8 An arbitrary tower diameter is chosen from which the superficial gas velocity U_G and U_L is calculated.

9 The total power consumption and hence operating cost is calculated. The

pumping power requirement is calculated from the spray nozzle height from the distributor grid, whilst the fan power is calculated from the bed air pressure drop. The power consumption is the sum total of the pumping power and the fan power. If this is too high, then go to step 7 and repeat the calculations.

The calculation procedure is shown in the computer progamme written in BASIC with typical design outputs shown in the Appendix B. For thermal design calculations, Equation 9.16 is the best because of its dimensionless simplicity, and that it is in good agreement with the data of other investigators. Equations relating to the the grid conditions (see Equation 9.16) had larger errors than those concerning average and plenum conditions since inlet air temperature measurements were made at the air plenum entrance. To estimate design bed expansion, Equation 9.28 is the most appropriate because it embraced all relevant independent variables in a dimensionless form at the reasonable error of estimate of 16%. For similar reasons, Equation 9.22 is the best equation for design bed air pressure drop calculations. Equation 9.30 is the most appropriate for design minimum fluidisation velocity calculations as it is both dimensionless and at the same time includes the most relevant independent variables that affect this dependent variable. However, Equation 9.31 is most appropriate for the design minimum fluidisation gas velocity if simplicity is of importance. On the other hand, the dimensioned correlations are easier to use as raw values can easily be substituted into the equation. However, their validity, as opposed to a dimensionless equation, can only extend to the limits of the data used in this study. All equations, together with those not mentioned here, show that the FBCT is versatile, and that any independent variable can be manipulated so as to obtain the cheapest designs. A trade-off of the tower total volume capital cost with the operational power cost may also be done if the maximum cost and return of the tower over its entire life-cycle is known. Design comparison of full-scale FBCTs and conventional towers are shown in Tables 9.1 and 9.2. It is clear from the computer output and the latter Tables that the FBCT can provide real estate

savings as a result of their lower base area, capital savings and environmental advantage due to their lower heights and huge savings in power requirement.

50 MWe	Conventional	FBCT
KaV/L	1.58	1.49
L/G	0.57	0.5
L, kg/s m^2	1.6	2.75
Total Number of Cells	8	8
Minimum Fluidisation Velocity U_{gmf}, m/s	[-]	0.6
Superficial Air Velocity, m/s	2.5	4.4
Cell Air Mass Flow Rate, m^3/s	493	537
Bed Air Bed Pressure Drop, Pa	250	263
Total Fan Power, MW	1	1.1
Total Pumping Power, MW	0.25	0.045
Total Power, MW	1.25	1.15
Static Packing Height V, m	10	0.19
Expanded Bed Height V_E, m	10	1.0
Total Tower Height HTOTAL, m	18.2	1.7
Cell Base Area, m^2	200	122
Cell Volume, m^3	3640	207

Table 9.1 Comparison between a full-scale FBCT and conventional fixed bed towers based on the data of Table 1.1 for a 50 MW electrical power plant. Total Heat Load = 173 MW, T_{HW} = 34.4°C, T_{DB} = 9.6°C, T_{WB} = 7.9°C, Range = 15.4 K, d_P = 37.5 mm, d_S = 2000 microns, ρ_P = 69 kg/m^3.

500 MWe	Conventional	FBCT
KaV/L	1.6	1.54
L/G	0.57	0.50
L, kg/s m^2	1.6	2.9
Total Number of Cells	14	14
Minimum Fluidisation Velocity U_{gmf}, m/s	[-]	0.6
Superficial Air Velocity, m/s	2.3	4.7
Cell Air Volume Flow Rate, m^3/s	693	761
Bed Air Pressure Drop, Pa	190	328
Total Fan Power, MW	1.8	3.5
Total Pumping Power, MW	0.6	0.1
Total Power, MW	2.4	3.6
Static Packing Height V, m	9.5	0.22
Expanded Bed Height V_E, m	9.5	1.28
Total Tower Height HTOTAL, m	15.9	2
Cell Base Area, m^2	298	162
Cell Volume, m^3	4738	324

Table 9.2 Comparison between a full-scale FBCT and conventional cooling towers based on the data of Table 1.1 for a 500 MW electrical power plant. Total Heat Load = 332 MW, T_{HW} = 30.55°C, T_{DB} = 9.6°C, T_{WB} = 8.8°C, Range = 12.55 K, d_P = 37.5 mm, d_S = 2000 microns, ρ_P = 69 kg/m^3.

CHAPTER X

CONCLUSIONS AND RECOMMENDATIONS

10.1 Conclusions

A model FBCT was specified and found to be technically feasible. Experimental test runs were performed and a large body of data was collected and analysed. The following conclusions relating to the design and characterisation of FBCTs were reached.

- Thermal and hydraulic correlations were developed using the Merkel approach to basic hydrodynamics and dimensional analysis.

- Thermal performance decreased with increases in the inlet hot water temperature meaning a larger tower size while hydraulic performance as regards the bed air pressure drop was independent of the inlet hot water temperature.

- Both tower size and power requirements increased with increases in liquid flow rate with a consequent increase in capital cost. Conversely, tower size decreased as the gas mass flow rate is increased while the power requirement increases for the same experimental variable.

- Generally, small low density particles gave a better thermal performance and hence a smaller tower size than large low density particles but gave a higher power requirement. High density particles yielded a relatively smaller tower size at the minimum fluidisation velocity but high power requirements.

- Small droplet sprays mean a smaller tower size while coarse droplet spray mean a larger tower size. An increase in the height of the spray nozzle from the distributor

grid increases the tower size and power requirements.

- The best possible thermal-hydraulic design may be attained by optimization of the independent variables so as to obtain the smallest and cheapest possible tower size and power requirements respectively.

- In general, expanded bed height increased as the liquid and the gas and liquid mass flux are increased but decreased as the particle density is increased.

- The minimum and flooding fluidisation gas velocities decreased from about 0.5 - 1.5 m/s and 2.8 - 3.3 m/s respectively as the liquid mass flux is increased from approximately 0.5 - 5 kg/s m^3. Similar range applies to the design equations.

- The plenum chamber contributes significantly to the thermal performance of the FBCT. According to Egbe (2000), this contribution lies in the region of up to 40% of the tower characteristic for the experimental conditions studied.

10.2 Recommendations

Experimental investigation of the FBCT has been concentrated purely on the bulk properties of the fluidised bed. Although limited investigation was carried out so as to study the local heat transfer properties, a more detailed experimental study within the fluidised bed itself excluding the plenum chamber may improve the understanding of the subject. Moreover, design has been based solely on the Merkel approach whose analysis and equation neglected the water-side heat transfer resistance at the air-water interface. An analysis that takes this assumption into consideration would be of permanent interest in FBCT design since this will account for the reduction in the tower characteristic as the inlet hot water temperature is increased.

Alternatively, a new method of modelling could be developed to utilize

Computational Fluid Dynamics (CFD). Only one size of the plenum chamber was studied. A much more detailed study of the effect of the plenum chamber size and design upon the thermal performance should be done by using different chamber sizes and shapes since the high thermal performance at the outlet cooled water temperature from the plenum chamber may be due to the air and grid distributor designs. More work has to be done so as to experimentally investigate the effects of the different design types upon the FBCT thermal-hydraulic performance. In addition, bed air pressure drop measurements are based solely on the fluidised bed alone without taking into consideration pressure losses in the plenum chamber. This problem needs to be addressed. Theoretical work needs to be done as concerns the maximum or "true" flooding velocity as the theory developed in this thesis needs further experimental study and verification.

Independent variables studied so far have not been fully exhausted in terms of breadth and depth. For example, more detailed experimental investigation needs to be carried out in order to study the effects of the spray nozzle characteristics on the thermal-hydraulic performance using a wide variety of spray nozzle configurations. The effect of the spray nozzle height from the distributor grid requires much more detailed experimental and theoretical investigation. In this context, the test rig needs to be modified so that a larger body of data that relates to this parameter may be obtained. A motorised axial and radial variation of the nozzle height can be used for easy, quick and more frequent nozzle height measurements. The degree of axial and radial bed turbulence can also be locally studied in greater experimental and theoretical depth as this will provide an insight as to the mechanism responsible for the high heat and mass transfer coefficient. The equipment and instrumentation may also be adapted so that it can be used as an air-conditioning equipment to cool or heat air for industrial purposes and a full-scale FBCT may be built so as to commercially verify the present work.

REFERENCES

Abdullah K Z, "Fluidised Bed Evaporative Cooling", *B.Eng(Hons) Project*, Middlesex Polytechnic, London, England (1989).

Aksel'rod L S And Yakovenko M M, "Certain Hydrodynamic Aspects of Mass Transfer Equipment with Mobile Spherical Packing", *Theor. Found. Chem. Eng.*, **3**, pp 124-126 (1969)

Albright M A, "Packed Tower Distributors Tested", *Hydrocarbon Proc.*, **63**, pp 173-177 (1984).

Allman W B, "Optimization Of Plant Cooling Tower Systems", *Power Division Of The ASME*, Industrial Power Conference, Pittsburgh, Pennslyvania (1975).

Anonymous, "Acceptance Test Procedure for Industrial Cooling Towers, Mechanical Draft Type", *CTI Bulletin ATP-105*, Houston, Texas (1975).

Anonymous, *ASHRAE Handbook of Fundamentals*, Chapter 5 (1981).

Baker C G J, Armstrong E R, Bergougnou M A, "Heat Transfer in Three-Phase Fluidised beds", *Powder Technology*, **21**, pp 195-204 (1978).

Baker D R, Shyrock, H A, "A Comprehensive Approach to the Analysis of Cooling Tower Performance", *ASME J. Heat and Mass Trans.*, **83**(3), pp 339-350 (1961).

Balabekov O S, Romanov E Ya Tarat, Mikhalev M F, "Operating Conditions of Columns with Wetted Spherical Packing", *Trans. from Zhurnal Prikladnoi Khimii*, **42** (7), pp 540-1547 (1969).

Barile R G, Meyer D W, "Turbulent Bed Cooling Tower", *Chem. Eng. Symposium Series*, **67** (119), pp 134-143 (1971).

Barile R G, Dengler J L, Hertwig T A, "Performance and Design of a Turbulent Bed Cooling Tower", *AIChE Symposium Series*, **70** (138), pp 154-62 (1974).

Bennet C O, Myers J E, "Momentum, Heat and Mass Transfer", McGraw-Hill, Japan, 3rd Edition (1969).

Blyakher I G, L Ya Zhivaikin, Yurovskaya N A, "Investigation of Hydrodynamics and Mass Transfer in Equipment with Movable Packing", *Khimic Trans. from heskoe i Neftyanoe Mashinostroenenie*, **2**, pp 18-21 (1967).

British Standard 4485,"Specification for Water Cooling Towers", **Part 1**: "Glossary Of Terms" (1969); **Part 2**: "Methods of Test and Acceptance Testing" (1988); **Part 3**:

"Thermal and Functional Design of Cooling Towers" (1977): **Part 4**: "Structural Design of Cooling Towers", 1975, *British Standards Institution*, London.

British Standard 1042, "Measurement of Fluid Flow in Closed Conduits", **Part 1**: "Orifice Plates, Nozzles and Venturi Tubes Inserted in Circular Cross-Section Conduits Running full", Section 1.1: *British Standard Institution*, London (1992).

Buyens D J, Kranc S C, "Testing and Evaluation of Spray Nozzles for Counterflow Cooling Towers", *Proc. ASME Heat Trans. Fluids. Eng. Divisions*, 1995 IMECE, HTD-Vol.321/FED-Vol.233, ASME (1995).

Hammond R P, "Calibration and Validation of on-line Measurements: Analysis of Results", *Trans. Inst. Measurement and Control*, **15** (1) (1993).

Chatfield D L, Streeton D F, "Cost Analysis of Large Evaporative Type Cooling Towers", *Trans. from Kerntechnik*, **11** (11), pp 649-652 (1969).

Chen B H, Douglas W J M, "Axial Mixing of a Turbulent Bed Contactor", *Can J Chem Eng*, **47**, pp 113-118 (1969).

Chen B H, Douglas W J M, "Liquid Hold-up and Minimum Fluidization Velocity in a Turbulent Bed Contactor", *Can. J. Chem. Eng.*, **46**, pp 246-249 (1968).

Cheremisinoff N P, Cheremisinoff P N, " Cooling Towers: Selection and Practice", Ann Arbor Science, Collingwood, Michigan (1983).

Danckwerts P V, Gillham A J, "The Design of Gas Absorbers: I - Methods for Predicting Rates of Absorption with Chemical Reaction in Packed Columns, and Tests with 1.5 in Raschig Rings, *Trans. Instn. Chem. Engrs.*, **44**, (1966).

Davidson J F, Harrisson D, "Fluidization", Academic Press, New York, (1971).

Dengler J L, "Turbulent Bed Contactor as Fluidised Cooling Tower", *PhD Thesis,* Purdue University, USA (1977).

Douglas H R, Snider I W A, Tomlison II G H, "The Turbulent Contact Absorber", *Chem. Eng Prog.*, **59** (12), pp 85-89 (1963).

Douglas W J M, "Heat and Mass Transfer in a Turbulent Bed Contactor", *Chem. Eng. Prog.*, **60** (7), pp 66-71 (1964).

Dreyer A A, Kriel D E, Erens P J, "Analysis of Spray-Cooled Finned-Tube Heat Exchangers", *Heat Trans. Eng.*, **13** (4), pp 53-71 (1992).

Egbe L M, "Fluidised Bed Cooling Tower Studies", *National Power Plc Report*,

Contract Reference **LC/2/0210**, pp 1 - 18 (1996a).

Egbe L M, "Pressure Drop, Liquid Holdup, Gas Holdup, and Gas-Liquid Interfacial Area in Fluidised Bed Cooling Towers", *Proceedings of MUCORT'96*, ISSN 1 362 - 2285, pp 57 -63, London (1996b).

Egbe L M, Lewis J S, Barham P, Kubie J, "Thermal Performance of a Fluidised Bed Cooling Tower", *IMechE Transactions of the Sixth UK National Conference on Heat Transfer*, Edinburgh, Paper No. C565/071/99, pp 373 - 378, (1999).

Egbe L M, "Plenum Chamber Effects in the Cooling of Water by Means of Fluidized Spherical Particles and Air", *Recent Advances in Transport Phenomena*, Edited by Ibrahim Dincer and Ferhat Yardim, Elsevier, pp 695 - 699, (2000).

El-Dessouky Hisham, "Thermal and Hydraulic Performance of a Three-Phase Fluidised Bed Cooling Tower", *Experimental Fluid Science*, **6** (4) (1993).

Elenkov D, Kosev A, "Mass Transfer in the Liquid Phase in Apparatus with Mobile Packing", *Trans. from Teoreticheskie, Osnovy, Khimicheskoi, Technologii*, **4** (1), pp 100-105 (1970).

Elgin J C, Browning F B, "Extraction of Acetic Acid with Isoprupyl Ether in a Spray Column", *Trans. Am. Inst. Chem. Eng.*, **31**, pp 639-670 (1935).

Elliot L, "Drop Size Data", *Spraying Systems Limited*, Surrey, England, UK, Personal Communication (1995).

Epstein N, "Three Phase Fluidisation: Some Knowledge Gaps", *Can. J. Chem. Eng.*, **59**, pp 649-657 (1981).

Ergun S, "Fluid Flow Through Packed Columns", *Chem. Eng. Prog.*, **48** (2), pp 84-94 (1952).

Fan L-S, Muroyama K, "Fundamentals of Gas-Liquid-Solid Fluidization", *AIChE J.*, **31** (1) (1985).

Fan L-S, Muroyama K, "In Gas-Liquid-Solid Fluidisation Engineering", Fan L-S(ed), Butterworth Stonehan, Chapter 5 (1989).

Fand R M, Thinakaran R,"The Influence of the Wall on Flow Through Pipes Packed with Spheres", Trans. ASME, *J. Fluids Eng.*, **112**, pp 85-88 (1990).

Fand R M, Sundaram M, Varahasamy M, "Incompressible Fluid Flow Through Pipes Packed With Spheres at Low Dimension Ratios", *Trans. ASME, J. Fluids Eng.*, **115**, pp 169-172 (1993).

Flint L F, Eisenklam P, "Longitudinal Gas Dispersion in Transitional and Turbulent Flow through a Straight Tube", *Can. J. Chem. Eng*, **47**, pp 101-106, (1969).

Forrester S E, Evans G M, "Computational Modelling Study of the Hydrodynamics in a Sudden Expansion - Tapered Contraction Reactor Geometry", *Chem. Eng. Sci.*, **52**, (21/22), pp 3773 - 3785 (1997).

Fraas A P, Ozisik M N, "Heat Exchanger Design", John Wiley & Sons Inc, New York, London, Sidney, Chapter 15, pp 241-255 (1965).

Galloway T R, Sage B H, "A Model Of The Mechanism Of Transport In Packed, Distended, and Fluidized Beds", *Chem. Eng. Sci.*, **25**, pp 495-516 (1970).

Gel'perin N I, Savschenko V M, Grishko V Z, "Some Hydrodynamic laws of Absorption Apparatuses Packed with Fluidized Spheres", *Teoreticheskie Ondsnovy Khimicheskoi Technologii*, **2, 1**, pp 76-83 (1968).

Gel'perin N I, Bukharin E N, Grishko V Z, Tsysin M I, "Contact Heat And Mass Transfer In Fluidized Spherical Packing", *Trans. from Khimichchescoe i Neftyanoe Machinostroenie*, **1**, pp 15-16 (1973).

Gel'perin N I, Grishko V Z, Savchenko V I, Schedro V M, "Investigation of the operation, of Absorption Apparatus with a Refluxed Ball Packing Type of a Pseudo-Liquified layer, Translation from *Khimichescoe i Neftyanoe Machinostroenie*, **1**, pp 22-26 (1966).

Gosi P, "Method and Chart for the determination of Evaporation Loss of Wet Cooling Tower", *Heat Transfer Engineering*, **10** (4) (1989).

Grandov A, Droshenko A, Yatskar I, Cooling Towers With Fluidized Beds For Contaminated Environment, *Int. J. Refrig.*, **18**(8), pp 512-517 (1995).

Guerriere R A, Fayed M E, Matchett A, "Pressure Drop Measurements in Turbulent Bed Contactor", *Proc. of the 18th Powder and Bulk Conf.*, Chicago (1993).

Guerriere R A, Fayed M E, Matchett A J, "Mass Transfer in Turbulent Bed Contactor", *Chem. Eng. Res & Des, Part A: Trans. of The Instn. of Chem. Engrs.*, **73**, No A3, pp 246-252 (1995).

Hollands K J T, "An Analysis of Counterflow Spray Cooling Towers", *Int. J. Heat and Mass Transfer*, **17**, pp 1227-1239 (1974).

Jackson J, "Cooling Towers with Special Reference to Mechanical-draught Systems",

Butterworths Publications Ltd, London (1951).

Jones W G, "Cooling Water for Power Stations", *Proc. Instn Civ. Engrs.*, Part 1, **62**, pp 373-298 (1977).

Kelly N W, Swenson L K, "Comparative Performance of Cooling Tower Packing Arrangements", *Chem. Eng. Prog.*, **52** (7), 2, pp 63-268 (1956).

Kielback A W, "The Development of a Floating Bed Scrubber", *Chem. Eng. Prog. Symposium Series*, **57** (35), pp 51-54 (1959).

Kim S D, Baker C G J, Bergougnou M A, "Bubble Characteristics in Three Phase Fluidised Beds", *Chem. Eng. Sci.*, **32**, pp 1299-1306 (1976).

Kito M, Shimada M, Sakai T, Sugiyama S, Wen C Y, "Performance of Turbulent Bed Contactor: Gas Holdup and Interfacial Area under Liquid Stagnant Flow" : in Keairns D L (ED), pp 411-429 (1976).

Kito M, Tabei M, Murata K, "Gas and Liquid Holdups in Mobile Beds under the Countercurrent Flow of Air and Liquid", *Ind. Eng. Chem. Process Des. Dev.*, **17** (4) (1978).

Kossev A, Elenkov D, Mass Transfer in the Gas Phase in Apparatus With A Mobile Packing, *Theor. Found. Chem. Eng.*, **7**, pp 795-798 (1973).

Koval' Zh A, Bespalov A V, Kuleshov O G, Zhukov A P, "Experimental Study of Lengthwise Liquid Mixing in a Column Having a Mobile Bed Packing", *Theor. Found. Chem. Eng.*, **Vol 9 B**, pp 837-843 (1975).

Koval' Zh A, Bespalov A V, Kuleshov O G, "Axial Mixing of a Liquid in a Vessel With Mobile Spherical Packing", *Theor. Found. Chem. Eng.*, **Vol 9 A**, pp 289-290 (1975).

Kranc S C, "Performance of Counterflow Cooling Towers With Structured Packings and maldistributed Water flow", *Numerical Heat Transfer*, **Part A**, **23**, pp 115-117 (1993).

Kuroda M, Tabei K, "Theoretical Discussion of the Minimum Fluidizing Velocity in a Mobile Bed", *Int. Chem. Eng.*, **21** (2), pp 219-223 (1981).

Kunesch T, "Keep Your Cool When Selecting the Right Tower", *Process Eng. Chem. & Process Eng.*, pp 164-167 (1978)

Kunesch T, "Environmental Aspects of Cooling Tower Selection", *Process Eng. Ind. Chem. & Process Eng.*, pp 86-91 (1978)

Lees Mike, "The Economics of Wet versus Dry Cooling for Combined Cycle", *IMechE Seminar on Condensers and Cooling Towers for CCGTs* (1994).

Lee M M, Hanratty, Adrian R J, "An Axial Viewing Photographic Technique to Study Turbulence Characteristics of Particles", *Int. J. Multiphase Flow*, **15**(5), pp 787-802 (1989).

Letan R, "On Vertical Dispersed Two-phase Flow", *Chem. Eng. Sci.*, **29**, pp 621-624 (1974).

Levsh I P, Krainev N I, Niyazov M I, Ganikhanova F F, "Mass Transfer in Absorbers with Fluidized Packed Beds", *Int. Chem. Eng.*, **Vol 8**, Part B (1968).

Levsh I P, Krainev N I, Niyazov M I, "The Calculation of Hydraulic Resistances and Height of a Three-phase Fluidized Bed", Translation from *Uzbeskii Khmicheskii Zhurnal*, **5** (72), pp 72-74 (1971).

Levsh I P, Krainev N I, Niyazov M I, "Hydrodynamic Calculations of Absorbers with Fluidised Beds, *Int. Chem. Eng.*, **8** (4), 619-622 (1968).

Lewis E W, Bowerman E W, "Fluidisation of Solid Particles in Liquid", *Chem. Eng. Prog.*, **48** (12) (1952).

Lewis J S, "An experimental and computational study of laminar combined natural and forced convection in vertical ducts", *PhD thesis*, The City University, London (1992).

Lichtenstein J, "Performance and Selection of Mechanical-draft Cooling Towers", *Trans. ASME*, **65**, pp 779-787, (1943).

Lichtenstein J, "Recirculation in Cooling Towers", *Trans. of ASME*, pp 1037-1042, (1951).

Lobo W E, Friend L, Hashmall F, Zenz F, "Limiting Capacity of Dumped Tower Packings", *Trans. AIChE*, **41**, pp 693-710 (1945).

Lowe H J, Christie D G, " Heat Transfer and Pressure Drop Data on Cooling Tower Packings, and Model Studies of the Resistance of Natural-Draught Towers to Airflow": *Proc. 1961 Int. Heat Transfer Conf.*, **Part V**, Colorado, pp 933-950 (1961).

Marseille T J, Schlisieng J S, Bell D M, Johnson B M, "Extending Cooling Tower Performance Prediction Using a Liquid-side Heat Resistance Model", *Heat Transfer Engineering*, **12** (3) (1991).

Massey T, Mechanical Induced Draught Cooling Towers Design and Technical Data,

National Power PLc, Windmill Hill Business Park, Whitehill Way, Swindon, Whiltshire, SN5 9NX, England (1994).

Mayak V 1, Matrozov V I, "Hydraulic Resitance of Plate Columns With Fluidized Packing", *Theor. Found. Chem. Eng.*, **3**, pp 64-67 (1969).

Merkel F, Verdunstungskuehlung, *Ver Deut Ing Forschungsarbeiten*, **No 275**, Berlin, (1925).

Michelsen M L, Ostergaard K, " Hold-Up and Fluid Mixing in Gas-Liquid Fluidised Beds", *The Chem. Eng. J.*, **1**, pp 37-45 (1970) .

Mickley H S, "Design of Forced-draft Air Conditioning Equipment", *Chem. Eng. Prog.*,45 (12), pp 739-745 (1949).

Miconnet M P, Guigon P, Large J F, "The Scrubbing of Acid Gases in Columns with Fixed or Mobile Packings", *Int. Chem. Eng.*, **22** (1) (1982).

O'Neill B K, Nicklin D J, Morgan N J, Leung L S, "The Hydrodynamics of Gas-Liquid Contacting in Towers with Fluidised Packings", *Can J Chem Eng*, **50**, pp 595-601 (1972)

Ostergaard K, Michelsen M L, "On the Use of Imperfect-Tracer Pulse Method for determination of Hold-up and Axial Mixing", *Can. J. Chem. Eng.*, **47**, pp 107-112, April (1969).

Ostergaard K, Michelson ML, "Holdup And Fluid Mixing In Gas-Liquid Fluidised Beds", *Chem. Eng.J.* , **1**, pp 37-46 (1970).

Paige P M, "Costlier Cooling Towers Require a New Approach to Water-Systems Design", *Chem. Eng.*, pp 93-98 (1967).

Paterson A H J, Clift R, "Liquid Holdup Measurements in a Turbulent Bed Contactor", *Can. J. Chem. Eng.*, 65, pp 10-17, (1987).

Perez-Blanco H, Bird W A, " Study of Heat and Mass Transfer in a Vertical-Tube Evaporative Cooler", *Trans. ASME, J. Heat Trans.* ,**106**, pp 210-215 (1984).

"*Perry's* Chemical Engineers' Handbook", Sixth Edition: Edited by Green D W, Perry R H, Maloney, J O (1984).

Rama O P, Rao D P, Subba Rao V, "Hydrodynamics of a Mobile Bed Contactor With Low Density Packing Particles of Different Shapes", *Can. J. Chem. Eng.*, **61**, pp 863-868, (1983).

Rama O P, Rao D P, Subba Rao V, "Liquid-Phase Axial Mixing Study in a Mobile Bed Contactor with Low Density Particles", *Can. J. Chem. Eng.*, **63**, (1985).

Ramamurthy K, Subbaraju K, "Bed Expansion Characteristics of Annular Liquid-Fluidised Beds", *Ind. Eng. Chem. Process. Des. Dev.*, **12** (2), (1973).

Richardson J F, Zaki W N, "Sedimentation and Fluidisation": **Part I**, *Transactions Int. Chem. Engrs.*, **32**, (1954).

Rish R F, "The Design of a Natural-Draught Tower", *Proc. 1961 Int. Heat Transfer Conf.*, **Part V,** Colorado, pp 951-958 (1961-1962).

Schiesser N E And Leon Lapidus, "Further Studies Of Fluid Flow and Mass Transfer in Trickle Beds", *AIChE*, **7** (1), pp 163-71 (1961).

Seetharamu K N, Swaroop S, "The Effect Of Size on The Performance of a Fluidised Bed Cooling Tower", *Warmw-und Soffubertragung*, **26** (17) (1990).

Sherwood T K, Shipley G H, Holloway F A L, "Flooding Velocities in Packed Columns", *Ind. Eng. Chem.*, **30**, pp 765-769, (1938).

Shih T-M, Ohadi M M, "Literature Survey on Numerical Heat Transfer (1990-1991)", *Numerical Heat Transfer*, **Part A, 23**, pp 129-169 (1993).

Simpson W M, Sherwood T K, "Performance of Small Mechanical Draft Cooling Towers", *Refrigerating Engineering*, **56**, pp 535-543 (1946).

Singham J R, Cooling Towers (Section 3.12) in Schlunder, E (ed): Heat Exchanger Design Handbook, **Vol 3**, Hemisphere Publishing Corporation, Washington, USA (1983).

Skold O J, "Energy Savings in Cooling Tower Packings", *Chem. Eng. Prog.*, **77**, pp 48-43 (1981).

Soundarajan K, Krishnaian K, "Hydrodynamics of Turbulent Bed Contactor: Flooding Aspects", *Can. J. Chem. Eng*, **72**(4), pp 569-575 (1994).

Strumillo C, Adamiec J, Kudra T, "Packed Columns with Expanding Beds", *Int. Chem. Eng.*, **14** (4), pp 652-657, (1974).

Strumillo C, Kudra T, "Interfacial Area in Three-Phase Fluidised Beds", *Chem. Eng.Sci*, **32**, pp 229-232 (1977).

Swaroop S, Seetharamu K N, "Experimental Investigation of the Performance of a Fluidised Bed Cooling Tower with Different Parameters", *Proc. of the 11TH National*

Conf. on Fluid Power, BHEL (R&D), Hyderabad, Paper HE 11 (1982).

Tabei K, Hasatani M, Kuroda M, "Effective Gas-Liquid Interfacial Area in A Mobile Bed Contactor", *Int. Chem. Eng.*, **29** (4), pp 679-698 (1989).

Teekaram A J H, "The Design, Construction and Testing of a Model Demonstration Cooling Tower", *BSc (Hons) Thesis*, Middlesex Polytechnic, England (1984).

Tichy J, Wong A, Douglas W J M, "Pressure Drop in a Mobile Bed Contactor", *Can. J. Chem. Eng.*, **50**, pp 215-220, (1972).

Toshio Aihara, "Augmentation of Convective Heat Transfer by Gas-Liquid Mist", *Proc. of The Ninth International Heat Transfer Conference*, Jerusalem, Israel (1990).

Uchida S, Chang C S, Wen C Y, "Mechanics of Turbulent Bed Contact Absorber", *Can. J. Chem. Eng.*, **55**, pp 392-396, (1977).

Uchida S, Suzuki T, Maejima H, "The Flooding Condition of a Turbulent Contact Absorber", *Can. J. Chem. Eng.*, **58**, pp 406-408 (1980).

Van Der Walt N T, West L A, Sheer T J, Kuball D, "The Design and Operation of a Dry Cooling System for a 200 MW Turbo-generator at Grootvlei Power Station, South Africa". *The South African Mechanical Engineer*, **26**, pp 498-507 (1976).

Visvanathan C, Leung L S, "Design of a Fluidised Bed Scrubber", *J. Ind. Eng. Chem. Process. Des. Dev*, **24** (9) (1985).

Vunjak-Novakovic' G V, Vukovic' D V, Obermayer A, Vogelpohl A, "Hydrodynamic and Mass Transfer Performance of a Turbulent Contact Absorber" in: Fluidisation, Edited by Grace J R, Matsen J M, Plenum Press (1980).

Vunjak-Novakovic' G V, Vukovic' D V, Littman H, "Hydrodynamics of Turbulent Bed Contactors", 1. Operating Regimes and Liquid Holdup, *Ind. Eng. Chem. Res.*, **26**, pp 958-966 (1987a).

Vunjak-Novakovic' G V, Vukovic' D V, Littman H, "Hydrodynamics of Turbulent Bed Contactors". 2. Pressure Drop, Bed Expansion, and Minimum Fluidisation Velocity, *Ind. Eng. Chem. Res.*, **26**, pp 967-972 (1987b).

Webb R L,"A Unified Theoretical Treatment for Thermal Analysis of Cooling Towers, Evaporative Condensers, And Fluid Coolers", *ASHRAE Trans.*, **90, Part 2B**, pp 398-415 (1984).

Webb R L, Villacres A, "Algorithm for the Performance Simulation of Cooling Towers, Evaporative Condensers, and Fluid Coolers, *ASHRAE Trans*, **90, Part 2B**, pp

416-458 (1984).

Wood B, Betts P, "A Temperature-Total Heat Diagram For Cooling Tower Calculations", *The Engineer (London)*, **189**, pp 337-342 (1950).

Wozniak M, Ostergaard K, "An Investigation of Mass Transfer in a Countercurrent Three-phase Fluidised Bed", *Chem. Eng. Sci.*, **28**, pp 167-171 (1973).
Wozniak M: Pressure Drop and Effective Interfacial Area in a Column With a Nozzle Bed, *Int. Chem. Eng.*, **8**, pp 553-559 (1977).

Wrinkle R B, "Performance Of Counterflow Cooling Tower Cells", *Chem Eng Prog*, **7**, pp 45-48 (1971).

Xukun Luo, Jian Z, Katsumi T, Liang-Shih Fan, "On the Rise Velocity of Bubbles in Liquid-Solid Suspensions at Elevated Pressure and Temperature", *Chem. Eng. Sci.*, **52** (21/22), pp 3693 - 3699 (1997).

Zabrodsky S S, "Hydrodynamics and Heat Transfer in Fluidised Beds", Translated by Scripta Technica, Inc. Edited by Zenz F A. MIT Press: Cambridge, Massasuchetts (1966).

APPENDIX A: CALCULATION OF AIR AND WATER PROPERTIES

All properties concerning psychometry was calculated from the ASHRAE Fundamentals Handbook (1981). The most important property, the partial saturation pressure of water vapour was calculated by the following Equation:

$$P_{ws} = Exp\left[\frac{C_8}{T} + C_9 + C_{10}T + C_{11}T^2 + C_{12}T^3 + C_{13}\ln[T]\right] \qquad \textbf{(A1)}$$

constants:-

C_8 = -5800.2206

C_9 = 1.3914993

C_{10} = -0.048640239

C_{11} = 0.41764768E-04

C_{12} = -0.14452093E-07

C_{13} = 6.5459673

P_{WS} = The Saturation Pressure, Pa

T = Absolute Temperature, K

The specific humidity ω is given by:

$$\omega = 0.62198\left[\frac{P_\omega}{P - P_\omega}\right] \qquad \textbf{(A2)}$$

and

$$\omega = \left[\frac{[2501 - 2.381T^*]\omega_S^* - [T - T^*]}{[2501 + 1.805T - 4.186T^*]}\right] \qquad \textbf{(A3)}$$

Where T and T^* are the dry bulb and wet-bulb temperatures respectively in °C. The value ω^* corresponds to the saturation specific humidity ratio at T^* and the specific humidity at saturation, ω_S, is given by:

$$\omega_s = 0.62198\left[\frac{P_{ws}}{P-P_{ws}}\right] \quad \textbf{(A4)}$$

Where P is the total pressure in Pa.

Air Dynamic Viscosity

Sutherland's Law:

$$\mu_G = \mu_0 + \left[\frac{T}{T_0}\right]^{1.5}\left[\frac{(T_0+S1)}{(T+S1)}\right] \quad \textbf{(A5)}$$

Reference Temperature (=T_0) = 275.00 K

Reference Dynamic Viscosity (= μ_0) = 1.725 * 10^{-5} kg/m s

S1 = Constant for Air = 110.00 K

Water Dynamic Viscosity

The dynamic viscosity of water can be calculated from the sixth order equations:

$$\mu_L = (AT^6+BT^5+CT^4+DT^3+ET^2+FT+c)*10^{-6} \quad \textbf{(A6)}$$

Constants:

A	=	3.2704E-10
B	=	-2.3593E-7
C	=	6.9089E-5
D	=	-1.6081E-2
E	=	9.5951E-1
F	=	-5.2589E1
c	=	1.7456E3

Density of Air

The density of air is calculated from the ideal gas Equations making use of psychometric properties as given in the ASHRAE Handbook of Fundamentals

(1981).

Density of Water

This was calculated from the fifth order polynomial developed by Lewis (1992):

$$\rho_L = BT^5 + CT^4 + DT^3 + ET^2 + FT + A \qquad \textbf{(A7)}$$

Where T is the water tempearture in °C.

Constants:

B	=	1.702156E-09
C	=	-5.311156E-07
D	=	7.463283E-05
E	=	-0.008642677
F	=	0.06522775
A	=	999.8429

Evaluation of the Air Flow Rate

Orifice Pipe Diameter	=	150.0 mm
Orifice Plate Diameter	=	108.0 mm
Diameter Ratio (β)	=	0.720
Upstream Tapping Distance	=	140.0 mm
Downstream Tapping Distance	=	72.0 mm
Manometer Fluid Relative Density (Paraffin)	=	0.784
Upstream Air Temperature	=	26.96 °C
Upstream Air Density	=	1.186 kg / m^3
Expansibility Factor	=	0.998
Dynamic Viscosity (Calculated from Eqn. A1)	=	1.846E-05 kg/m s

No. of Iterations	Coefficient of Discharge, C_D	Mass Flow Rate kg/s	Reynolds Number Re
1	0.5959	0.2432	1.119E05
2	0.6132	0.2504	1.151E05
3	0.6130	0.2504	1.151E05
4	0.6130	0.2504	1.151E05

Table A1 Calculation of the Air Mass Flow Rate from the Orifice Pressure Drop Measurement.

T_{HW} °C	H_{Water} kJ/kg	P_{WS} Pa	W_S kg/kg	H_W kJ/kg	H_A kJ/kg
54.38	227.58	**INLET**			
51.91	217.24	13571	0.09604	301.10	121.39
44.52	186.36	9359	0.06321	207.68	96.53
39.59	165.79	7225	0.04769	162.27	79.97
32.20	134.85	4813	0.03098	111.47	55.06
29.74	124.6	**PLENUM OUTLET**			
SUM ($1/[H_W - H_A]$)			**0.0444**		
KaV/L			**1.1440**		

Table A2 Evaluation of Tower Characteristic using the Merkel - Tchebycheff Method based on the water enthalpy change from the inlet to the plenum outlet.

APPENDIX B: COMPUTER PROGRAM AND OUTPUT

```
10 REM THIS PROGRAMME ESTIMATES THE OPTIMUM DESIGN DIMENSIONS OF FULL-SCALE
20 REM FLUIDIZED BED COOLING TOWERS BASED ON THE THERMAL-HYDRAULIC EQUATIONS
22 REM DEVELOPED BY LOUIS EGBE AND USING THE DATA SUPPLIED BY NATIONAL POWER
24 REM PLC FOR A COMBINED CYCLE GAS TURBINE ELECTRICITY PLANT. A PLENUM CHAMBER
26 REM HEIGHT OF 0.7 m IS ADDED TO THE SPRAY NOZZLE HEIGHT TO OBTAIN THE TOTAL
27 REM FBCT HEIGHT (HTOTAL) FROM GROUND LEVEL
28 PRINT
30 PRINT "MECHANICAL DRAUGHT COOLING TOWERS FOR A 50 MWe PLANT"
32 PRINT
36 PRINT "THERMAL-HYDRAULIC PARAMETERS"
38 PRINT
42 PRINT "DESIGN","L/G","L","G"
44 PRINT "No","[-]","kg/s m^2","kg/s m^2"
45 REM INPUT OF SPECIFIED PARAMETERS AND FLUID PROPERTIES
46 READ VSG,VSL,DENG,DENL
47 READ PRESSMAX
48 READ N
49 FOR I = 1 TO N
50 READ H(I)
51 NEXT I
52 FOR I = 1 TO N
53 READ DS(I)
54 NEXT I
55 FOR I = 1 TO N
56 READ dP(I)
57 NEXT I
58 FOR I = 1 TO N
59 READ DENS(I)
60 NEXT I
61 FOR I = 1 TO N
62 READ F(I)
63 NEXT I
90 REM CALCULATION OF THE GAS MASS FLUX
120 FOR I = 1 TO N
130 READ L(I)
170 NEXT I
180 FOR I = 1 TO N
185 LET G(I)=L(I)/F(I)
190 NEXT I
200 FOR I = 1 TO N
210 READ K(I)
220 NEXT I
320 FOR I = 1 TO N
330 READ LTOT(I)
340 NEXT I
350 FOR I = 1 TO N
360 READ CELL(I)
400 NEXT I
410 REM V/d RATIO IS CALCULATED FROM REGRESSION EQUATION 9.16
420 REM DEVELOPED BY EGBE OF MIDDLESEX UNIVERSITY.
430 FOR I = 1 TO N
450 LET RG(I)= G(I)*dP(I)/VSG
455 LET RL(I)= L(I)*dP(I)/VSL
460 LET FRL(I)=(L(I)^2)/(DENL^2*9.81*dP(I))
465 LET FRG(I)=(G(I)^2)/(DENG^2*9.81*dP(I))
470 LET F1(I)= F(I)^(-0.51)
480 LET K1(I)=0.8070* dP(I)^(-0.24)*H(I)^0.025*F1(I)*(dP(I)/DS(I))^(-0.06)
490 LET V(I)= (K(I)/K1(I))^4.651
500 LET VOD(I)=V(I)/dP(I)
505 LET KaV(I)=K(I)*L(I)
507 LET KAVG(I)=(KaV(I)*G(I))/(PRESSMAX*DENL^0.5*DENS(I)^0.5)
510 NEXT I
511 FOR I=1 TO N
512 PRINT I,INT(F(I)*100+0.5)/100,INT(L(I)*10+0.5)/10,INT(G(I)*10+0.5)/10
514 NEXT I
515 REM THE EXPANDED BED HEIGHT IS CALCULATED FROM EQUATION 9.28
516 FOR I= 1 TO N
517 LET Z(I)=(dP(I)/DS(I))
519 LET S(I)=H(I)/V(I)
521 LET DN(I)=DENS(I)/DENL
```

```
523 LET VZ(I)=2.294E-3*F(I)^-0.038*Z(I)^-0.2*S(I)^0.12*DN(I)^0.094*RL(I)^0.18
525 LET VE(I)=V(I)*VZ(I)*RG(I)^0.8
530 NEXT I
531 REM PRINT SPECIFIED DESIGN VARIABLES
532 PRINT
534 PRINT "DESIGN","V","H","VE"
535 PRINT "No","m","m","m"
536 FOR I = 1 TO N
538 PRINT I,INT(V(I)*100+0.5)/100,INT(H(I)*10+0.5)/10,INT(VE(I)*100+0.5)/100
540 NEXT I
584 REM THE MINIMUM FLIDIZATION VELOCITY IS CALCULATED FROM EQUATION 9.29
588 FOR I = 1 TO N
590 LET GMF1(I)=Z(I)^-0.2*S(I)^0.12*DN(I)^0.094*RL(I)^0.18
592 LET GM(I)= ((GMF1(I))/(436*(L(I)^0.038)*(dP(I)/VSG)^-0.8))^-1.1905
594 LET UM(I)=GM(I)/DENG
598 NEXT I
602 REM THE BED AIR PRESSURE DROP IS CALCULATED FROM EQUATION 9.22
610 FOR I = 1 TO N
620 LET R2(I)= RG(I)^-0.19
630 LET FR2(I)= FRL(I)^(-0.63)
640 LET DN1(I)=DN(I)^0.54
642 LET S1(I)=S(I)^0.36
643 LET Z1(I)=Z(I)^-0.028
644 LET LG(I)=L(I)*G(I)
645 LET PS(I)=2.18*F(I)^0.38*VOD(I)^1.108*R2(I)*FR2(I)*DN1(I)*S1(I)*Z1(I)
646 LET PV(I)=PS(I)*LG(I)
650 LET PS(I)=PV(I)/(DENG^0.5*DENL^0.5)
652 NEXT I
654 REM CHECK FOR MAXIMUM EFFICIENCY
656 FOR I = 1 TO N
658 LET PRESS2(I)=KaV(I)*G(I)/(PRESS(I)*DENL^0.5*DENG^0.5)
660 NEXT I
661 PRINT
662 PRINT "DESIGN","HTOTAL","dP","dS"
664 PRINT "No","m","m","m"
670 FOR I = 1 TO N
690 PRINT I,H(I)+0.7,dP(I),DS(I)
700 NEXT I
810 PRINT
820 PRINT "DESIGN","GMF","UMF","PRESSDROP"
840 PRINT "No","kg/s m^2","m/s","Pa"
842 FOR I = 1 TO N
844 PRINT I,INT(GM(I)*100+0.5)/100,INT(UM(I)*100+0.5)/100,INT(PS(I)*100+0.5)/100
846 NEXT I
847 PRINT
848 PRINT "FULL-SCALE FBCT DESIGN DIMENSIONS AT THE REQUIRED AIR VELOCITY"
850 PRINT
852 PRINT "DESIGN","UG","CELLAREA","CELLDIAMETER"
854 PRINT "No","m/s","m^2","m"
856 FOR I = 1 TO N
860 LET GL(I)=LTOT(I)*DENL
870 LET F(I)=L(I)/G(I)
880 LET GG(I)=GL(I)/ F(I)
890 LET A(I)=GL(I)/L(I)
900 LET UG(I)=(GG(I)/DENG)/A(I)
905 LET UL(I)=L(I)/DENL
910 LET ACELL(I)=A(I)/CELL(I)
920 LET DC(I)= (ACELL(I)*4/3.142)^0.5
930 PRINT I,UG(I),ACELL(I),DC(I)
940 NEXT I
950 PRINT
952 PRINT "FBCT CELL VOLUME, PUMPING AND FAN POWER REQUIREMENT"
954 PRINT
960 PRINT "DESIGN","CELLVOL","PUMPPOWER","FANPOWER"
962 PRINT "No","m^3","KW","KW"
964 REM THE FBCT CELL AND TOTAL VOLUME, PUMP AND FAN POWER ARE CALCULATED
970 FOR I = 1 TO N
980 LET VOL(I)=ACELL(I)*(H(I)+0.7)
984 LET VL(I)=A(I)*(H(I)+0.7)
990 LET PP(I)=DENL*9.81*LTOT(I)*(H(I)+0.7)
```

```
1000 LET FAN(I)= PS(I)*GG(I)/DENG
1020 PRINT I,VOL(I),INT(PP(I)*1E3+0.5)/1E6,INT(FAN(I)*1E3+0.5)/1E6
1030 NEXT I
1040 PRINT
1042 PRINT "FBCT TOTAL POWER, TOTAL BASE AREA AND TOTAL VOLUME"
1044 PRINT
1050 PRINT "DESIGN","TOTALPOWER","TOTALAREA","TOTALVOL"
1052 PRINT "No","KW","m^2","m^3"
1054 REM THE TOTAL FBCT POWER REQUIREMENT IS CALCULATED
1060 FOR I = 1 TO N
1070 LET TP(I)=FAN(I)+PP(I)
1072 PRINT I,INT(TP(I)*1E3+0.5)/1E6,INT(A(I)*10+0.5)/10,INT(VL(I)*100+0.5)/100
1074 NEXT I
1076 PRINT
1077 REM CALCULATE THE ("TRUE" FLOODING) MAX LIQUID VEL GIVEN THE GAS VELOCITY
1078 PRINT "FBCT MAXIMUM WATER VELOCITY AT THE GIVEN AIR VELOCITY"
1079 PRINT
1080 PRINT "DESIGN","LHOLDUP","UL","ULMAX"
1084 PRINT "No","[-]","m/s","m/s"
1088 REM THE LIQUID HOLDUP IS CALCULATED FROM THE EQUATION OF BARILE ET AL(1971)
1089 FOR I = 1 TO N
1090 LET C(I)=1160*FRL(I)^0.78*RL(I)^(-0.51)*VOD(I)^-0.36
1092 LET J1(I)= (DENL/(DENL-DENG))^0.25
1094 LET J2(I)= (DENG/(DENL-DENG))^0.25
1096 LET J3(I)=UG(I)^0.5
1098 LET J4(I)=(9.81*DC(I))^-0.25
1100 LET J5(I)=((1-(0.38*UG(I)^0.5))/(9.81*V(I)*((1-0.4)+C(I))))^0.25
1102 LET J6(I)=(9.81*dP(I))^-0.25
1104 LET J7(I)=J4(I)+J5(I)+J6(I)
1105 LET J8(I)=J2(I)*J3(I)*J7(I)
1106 LET UM(I)= ((1-J8(I))/(J1(I)*J7(I)))^2
1107 PRINT I,INT(C(I)*1E7+0.5)/1E7,INT(UL(I)*1E7+0.5)/1E7,INT(UM(I)*1E8+0.5)/1E8
1108 NEXT I
1110 REM INPUT FLUID PROPERTIES
1120 DATA 1.763E-5,780E-6,1.2439,994.255
1122 REM INPUT MAXIMUM BED PRESSURE DROP
1130 DATA 250
1170 REM INPUT DESIGN NUMBER
1180 DATA 9
1182 REM INPUT SPRAY NOZZLE HEIGHT
1184 DATA 0.4,0.6,0.8,1.0,1,1.2,1.5
1186 DATA 2,2.2
1188 REM INPUT DROPLET MEDIAN VOLUME DIAMETER
1190 DATA 20E-4,20E-4,20E-4,20E-4,20E-4,20E-4,20E-4
1192 DATA 20E-4,20E-4
1198 REM INPUT PARTICLE DIAMETER
1200 DATA 37.5E-3,37.5E-3,37.5E-3,37.5E-3,37.5E-3,37.5E-3,20E-3
1202 DATA 25E-3,25E-3
1204 REM INPUT PARTICLE DENSITY
1206 DATA 69,69,69,69,69,69,69
1208 DATA 69,69
1210 REM INPUT LIQUID/GAS MASS FLUX RATIO
1212 DATA 0.5,0.5,0.5,0.5,0.5,0.5
1214 DATA 0.75,0.75,0.75
1240 REM INPUT WATER FLUX
1250 DATA 1.0,1.75,2.0,2.5,2.75,2.90,3.5
1300 DATA 3.75,4.0
1360 REM INPUT THE REQUIRED TOWER CHARACTERISTIC KaV/L
1370 DATA 1.49,1.49,1.49
1380 DATA 1.49,1.49,1.49
1390 DATA 1.76,1.76,1.76
5000 REM INPUT TOTAL WATER LOAD
5010 DATA 2.69,2.69,2.69,2.69,2.69,2.69,2.69
5020 DATA 2.69,2.69
6000 REM INPUT TOTAL CELL NUMBER
6010 DATA 8,8,8,8,8,8,8
6020 DATA 8,8
6040 REM INPUT FIRST APPROXIMATION FOR MAXIMUM ("TRUE" FLOODING) GAS VELOCITY
6050 REM IN INTERVAL BISECTION
6070 END
```

THERMAL-HYDRAULIC PARAMETERS

DESIGN No	L/G [-]	L kg/s m^2	G kg/s m^2
1	.5	1	2
2	.5	1.8	3.5
3	.5	2	4
4	.5	2.5	5
5	.5	2.8	5.5
6	.5	2.9	5.8
7	.75	3.5	4.7
8	.75	3.8	5
9	.75	4	5.3

DESIGN No	V m	H m	VE m
1	.22	.4	.38
2	.21	.6	.66
3	.2	.8	.76
4	.19	1	.95
5	.19	1	1.04
6	.19	1.2	1.1
7	.44	1.5	1.24
8	.58	2	2.08
9	.57	2.2	2.22

DESIGN No	HTOTAL m	dP m	dS m
1	1.1	.0375	.002
2	1.3	.0375	.002
3	1.5	.0375	.002
4	1.7	.0375	.002
5	1.7	.0375	.002
6	1.9	.0375	.002
7	2.2	.02	.002
8	2.7	.025	.002
9	2.9	.025	.002

DESIGN No	GMF kg/s m^2	UMF m/s	PRESSDROP Pa
1	1.02	.82	117.55
2	.87	.7	178.64
3	.81	.65	207.96
4	.75	.6	249.88
5	.74	.59	263.33
6	.71	.57	284.98
7	1.35	1.09	831
8	1.08	.87	1008.99
9	1.06	.85	1073.01

FULL-SCALE FBCT DESIGN DIMENSIONS AT THE REQUIRED AIR VELOCITY

DESIGN No	UG m/s	CELLAREA m^2	CELLDIAMETER m
1	1.60785	334.318	20.6304
2	2.81373	191.039	15.5951
3	3.21569	167.159	14.5879
4	4.01962	133.727	13.0478
5	4.42158	121.57	12.4406
6	4.66275	115.282	12.1146

7	3.75164	95.5195	11.0274
8	4.01962	89.1515	10.6535
9	4.28759	83.5796	10.3152

FBCT CELL VOLUME, PUMPING AND FAN POWER REQUIREMENT

DESIGN No	CELLVOL m^3	PUMPPOWER KW	FANPOWER KW
1	367.75	28.861	505.497
2	248.351	34.1085	768.187
3	250.739	39.3559	894.281
4	227.336	44.6034	1074.57
5	206.669	44.6034	1132.4
6	219.036	49.8509	1225.47
7	210.143	57.7221	2382.35
8	240.709	70.8407	2892.61
9	242.381	76.0882	3076.15

FBCT TOTAL POWER, TOTAL BASE AREA AND TOTAL VOLUME

DESIGN No	TOTALPOWER KW	TOTALAREA m^2	TOTALVOL m^3
1	534.358	2674.5	2942
2	802.296	1528.3	1986.81
3	933.637	1337.3	2005.91
4	1119.17	1069.8	1818.69
5	1177	972.6	1653.36
6	1275.33	922.3	1752.29
7	2440.07	764.2	1681.14
8	2963.46	713.2	1925.67
9	3152.24	668.6	1939.05

FBCT MAXIMUM WATER VELOCITY AT THE GIVEN AIR VELOCITY

DESIGN No	LHOLDUP [-]	UL m/s	ULMAX m/s
1	.003941	.10058E-02	.351512E-01
2	.72139E-02	.17601E-02	.01395
3	.84002E-02	.20116E-02	.976038E-02
4	.107177E-01	.25144E-02	.441587E-02
5	.118458E-01	.27659E-02	.280473E-02
6	.126211E-01	.29168E-02	.201744E-02
7	.020439	.35202E-02	.323279E-02
8	.161565E-01	.37717E-02	.465926E-02
9	.173584E-01	.40231E-02	.335764E-02

```
Alpha1:SESSIONEXIT
  Process LOUIS1_1 logged out at 10-FEB-1999 15:11:47.72
```

MECHANICAL DRAUGHT COOLING TOWERS FOR A 500 MWe PLANT

THERMAL-HYDRAULIC PARAMETERS

DESIGN No	L/G [-]	L kg/s m^2	G kg/s m^2
1	.5	1	2
2	.5	1.8	3.5
3	.5	2	4
4	.5	2.5	5
5	.5	2.8	5.5
6	.5	2.9	5.8
7	.75	3.5	4.7
8	.75	3.8	5
9	.75	4	5.3

DESIGN No	V m	H m	VE m
1	.14	.4	.2
2	.14	.5	.34
3	.17	.9	.56
4	.16	1.2	.7
5	.22	1.3	1.21
6	.22	1.3	1.28
7	.53	1.6	1.5
8	.53	1.7	1.61
9	.53	1.7	1.71

DESIGN No	HTOTAL m	dP m	dS m
1	1.1	.025	.002
2	1.2	.025	.002
3	1.6	.03	.002
4	1.9	.03	.002
5	2	.0375	.002
6	2	.0375	.002
7	2.3	.02	.002
8	2.4	.02	.002
9	2.4	.02	.002

DESIGN No	GMF kg/s m^2	UMF m/s	PRESSDROP Pa
1	1.38	1.11	114.98
2	1.21	.98	166.25
3	.94	.76	223.81
4	.87	.7	273.71
5	.72	.58	318.59
6	.71	.57	328.04
7	1.36	1.1	991.21
8	1.33	1.08	1046.73
9	1.32	1.06	1084.56

FULL-SCALE FBCT DESIGN DIMENSIONS AT THE REQUIRED AIR VELOCITY

DESIGN No	UG m/s	CELLAREA m^2	CELLDIAMETER m
1	1.61721	469.297	24.4428
2	2.83011	268.17	18.477
3	3.23441	234.648	17.2837
4	4.04302	187.719	15.459
5	4.44732	170.653	14.7396
6	4.6899	161.826	14.3533

7	3.77348	134.085	13.0652
8	4.04302	125.146	12.6222
9	4.31255	117.324	12.2214

FBCT CELL VOLUME, PUMPING AND FAN POWER REQUIREMENT

DESIGN No	CELLVOL m^3	PUMPPOWER KW	FANPOWER KW
1	516.227	70.8985	1221.69
2	321.804	77.3439	1766.41
3	375.437	103.125	2378.01
4	356.666	122.461	2908.21
5	341.307	128.906	3385.14
6	323.653	128.906	3485.48
7	308.395	148.242	7021.3
8	300.35	154.688	7414.57
9	281.578	154.688	7682.48

FBCT TOTAL POWER, TOTAL BASE AREA AND TOTAL VOLUME

DESIGN No	TOTALPOWER KW	TOTALAREA m^2	TOTALVOL m^3
1	1292.59	6570.2	7227.17
2	1843.75	3754.4	4505.25
3	2481.13	3285.1	5256.12
4	3030.67	2628.1	4993.32
5	3514.04	2389.1	4778.29
6	3614.38	2265.6	4531.14
7	7169.55	1877.2	4317.53
8	7569.25	1752	4204.9
9	7837.17	1642.5	3942.09

FBCT MAXIMUM WATER VELOCITY AT THE GIVEN AIR VELOCITY

DESIGN No	LHOLDUP [-]	UL m/s	ULMAX m/s
1	.63865E-02	.10045E-02	.231234E-01
2	.116013E-01	.17579E-02	.69551E-02
3	.105359E-01	.20091E-02	.66746E-02
4	.013479	.25114E-02	.24058E-02
5	.108585E-01	.27625E-02	.35239E-02
6	.114813E-01	.29132E-02	.27068E-02
7	.182284E-01	.35159E-02	.00407
8	.196477E-01	.003767	.28024E-02
9	.210253E-01	.40182E-02	.18353E-02

Alpha1:SESSIONEXIT
  Process LOUIS1_1 logged out at 10-FEB-1999 17:01:46.90

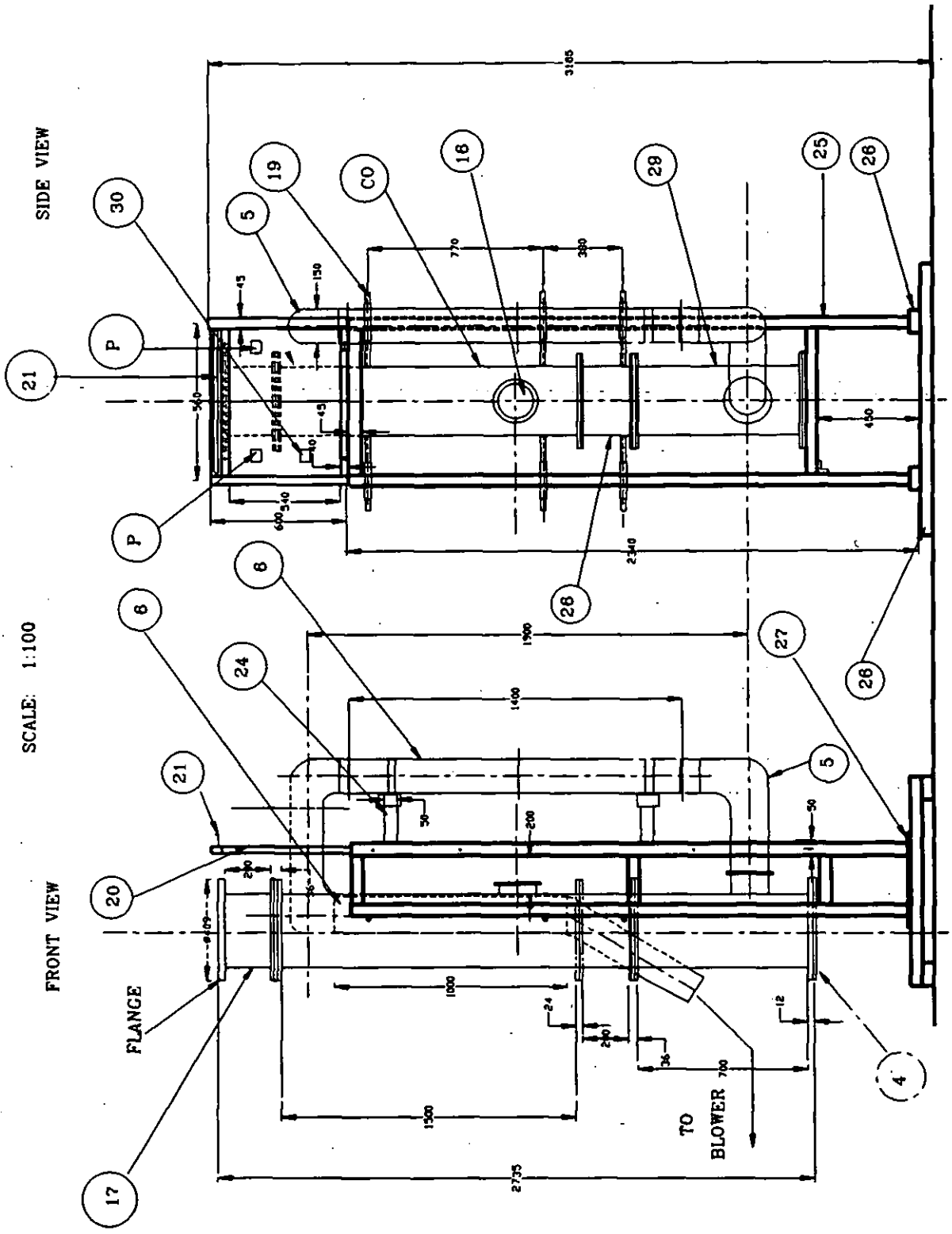

Figure C1 Technical details of the FBCT. See Chapter IV for Parts list.

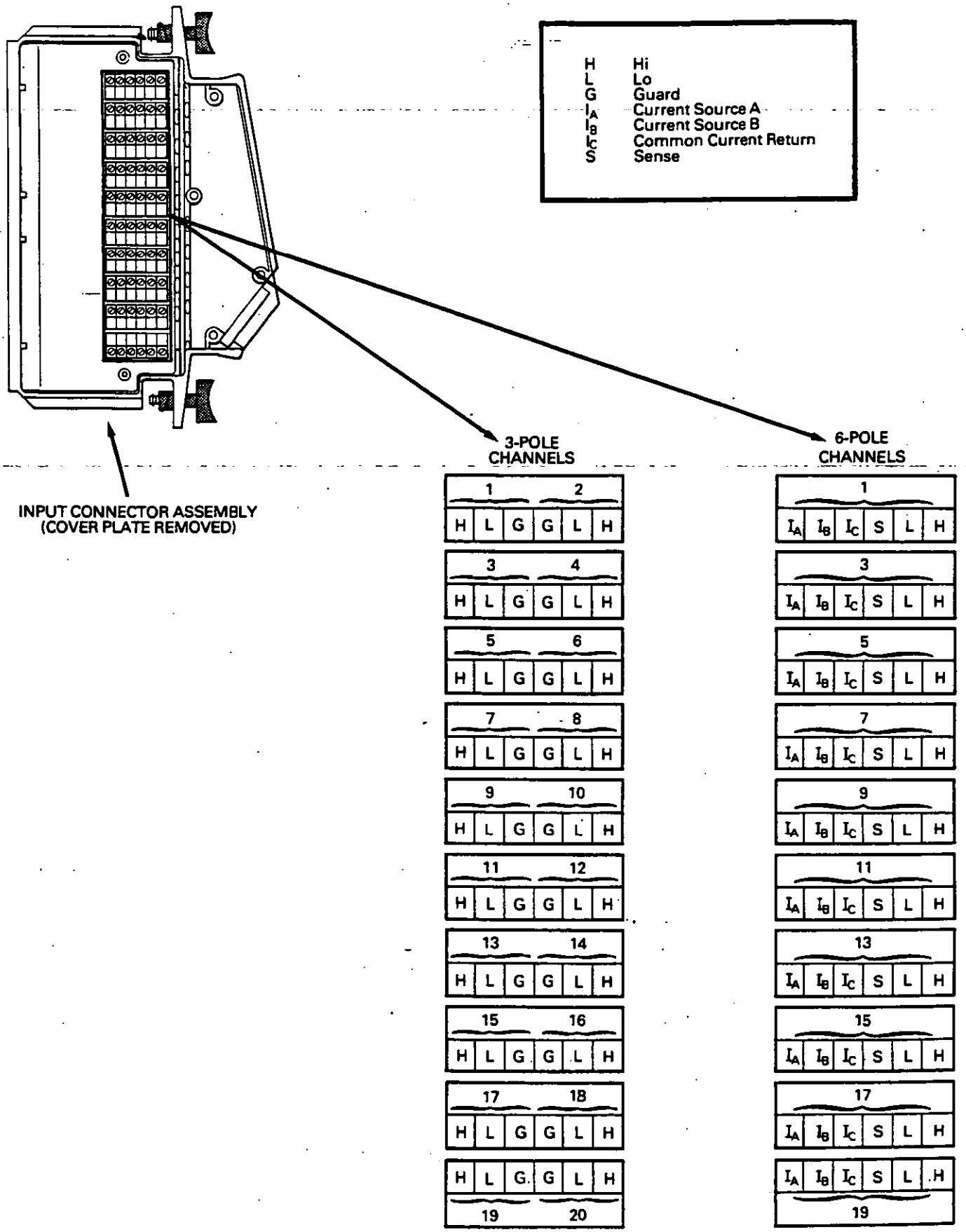

Figure C2 Channel Numbering and Assignment of Terminals on the Input Connectors.

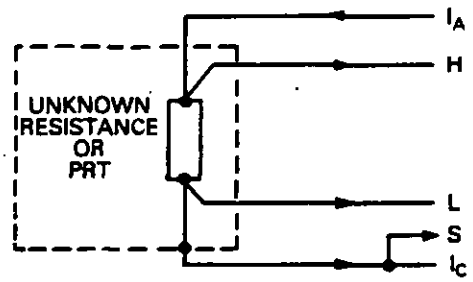

(a)

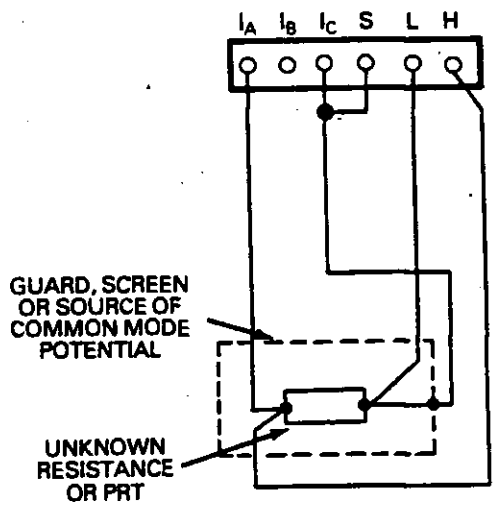

(b)

Figure C3 4-Terminal Resistance for PRT measurement. (a) Theoretical diagram. (b) Practical Connection diagram.

Transducer No:34B2895 Serial No:9701152 for air mass flow measurement			
Pressure	Instrument output	Deviation	%FSD
1000.500	4.996	-0.007	-0.13
599.9	3.011	0.011	0.23
200.1	1.008	0.007	0.15
0.000	0.003	0.003	0.06
Transducer No:34B2896 Serial No:971153 for the bed pressure drop measurement			
1000.800	4.994	-0.010	-0.20
600.3	3.011	0.009	0.19
199.5	1.004	0.006	0.13
0.000	0.001	0.001	0.02

Table C1 Calibration of differential pressure transducers (Furness Controls Limited, 1997).

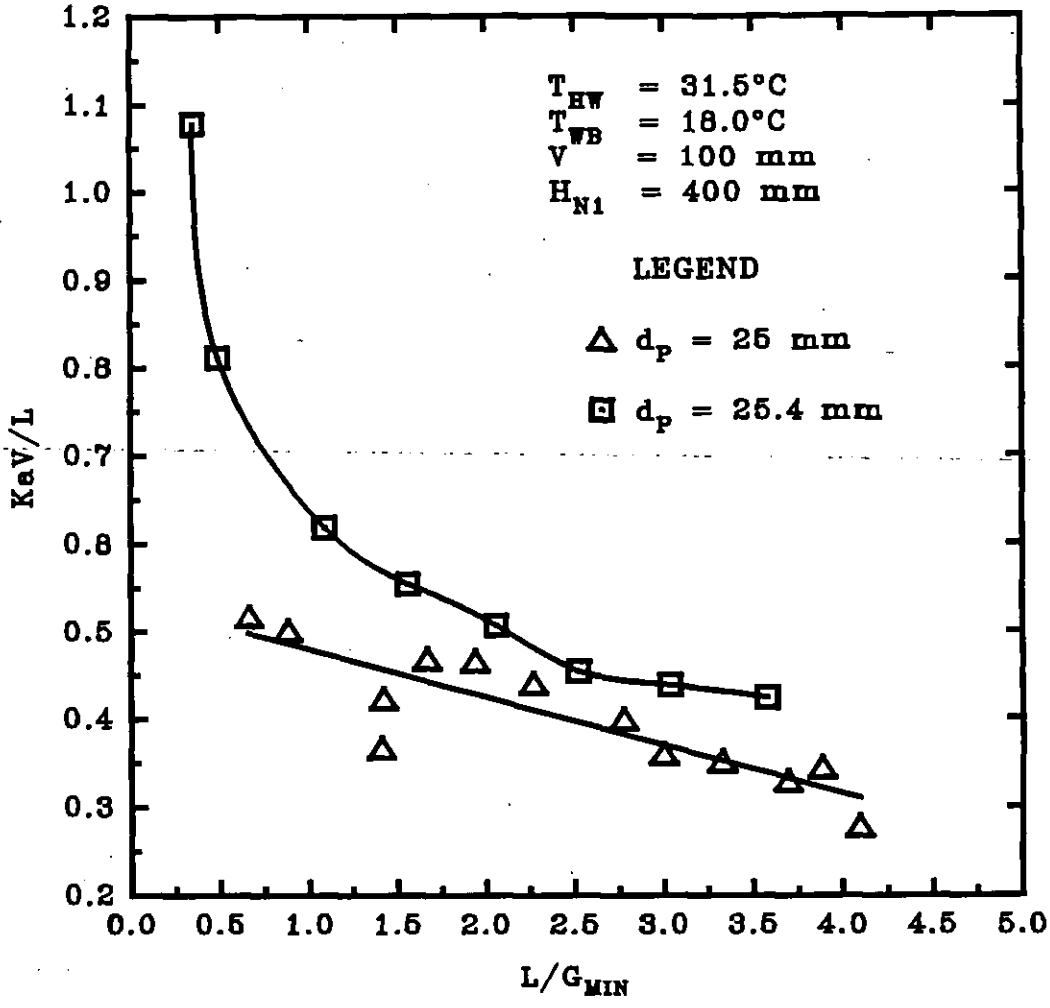

Figure C4 Effect of the liquid gas mass flux ratio and the density of the paticle upon the tower characteristic based on the outlet cooled water temperature at the minimum fluidisation state for a nominal size particle diameter of 25 mm. Fine droplet spray nozzle type. The 25.4 mm particle has a density of 326 kg/m^3. The 25 mm particle has a density of 245 kg/m^3.

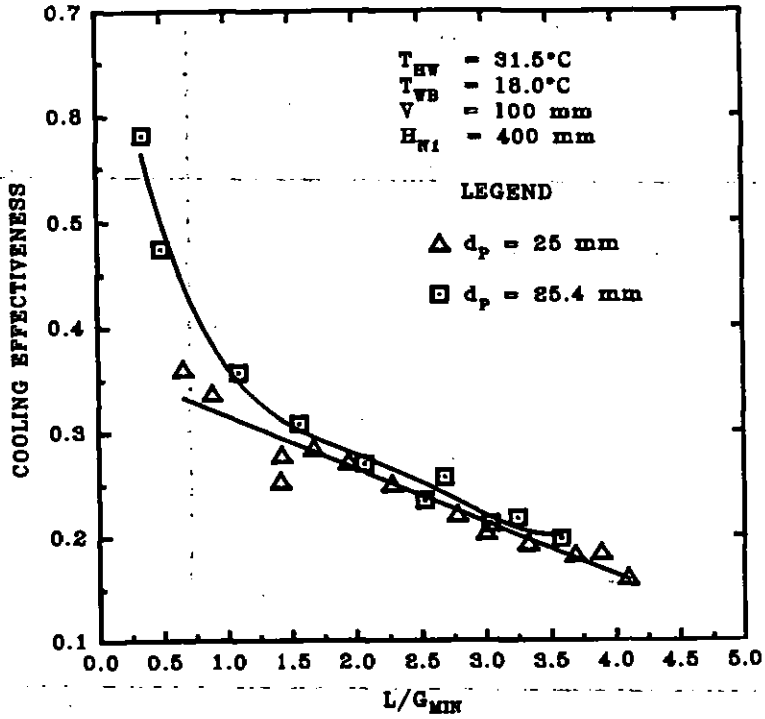

Figure C5 Effect of the liquid/gas mass flux ratio and the density of the particles upon the cooling effectiveness based on the outlet cooled water temperature at the minimum fluidisation state for a nominal particle size diameter of 25 mm. Fine droplet spray nozzle. The 25.4 mm particle has density of 326 kg/m^3. The 25 mm particle has density of 245 kg/m^3.

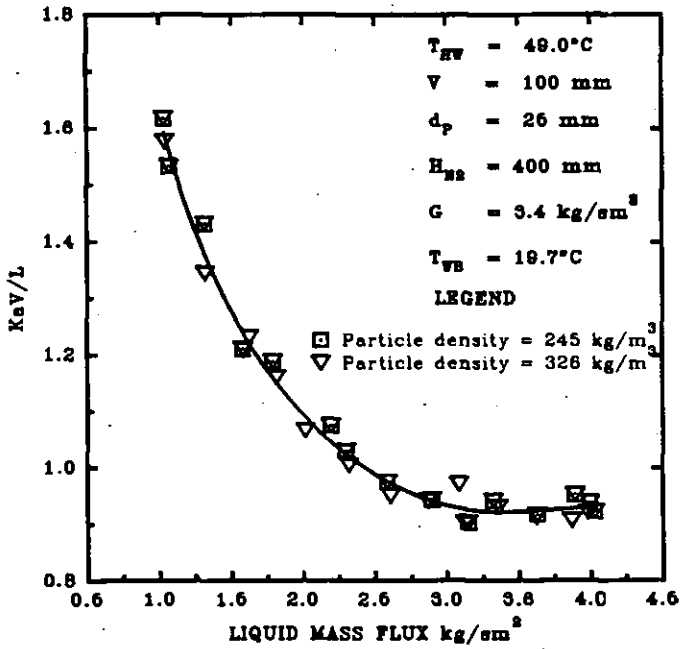

Figure C6 Effect of the liquid mass flux and the density of the particles upon the tower characteristic based on the outlet cooled water temperature of the plenum chamber for a high fluidisation velocity state and a nominal particle diameter of 25 mm. Fine droplet spray nozzle.

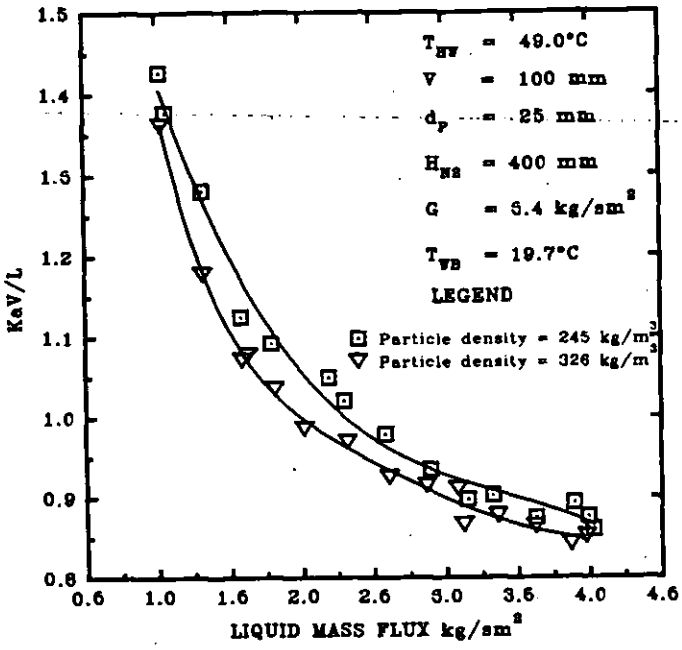

Figure C7 The effect of the liquid mass flux and the density of the particles upon the tower characteristic based on the average cooled water temperature at high fluidisation gas mass flux. Fine spray nozzle.

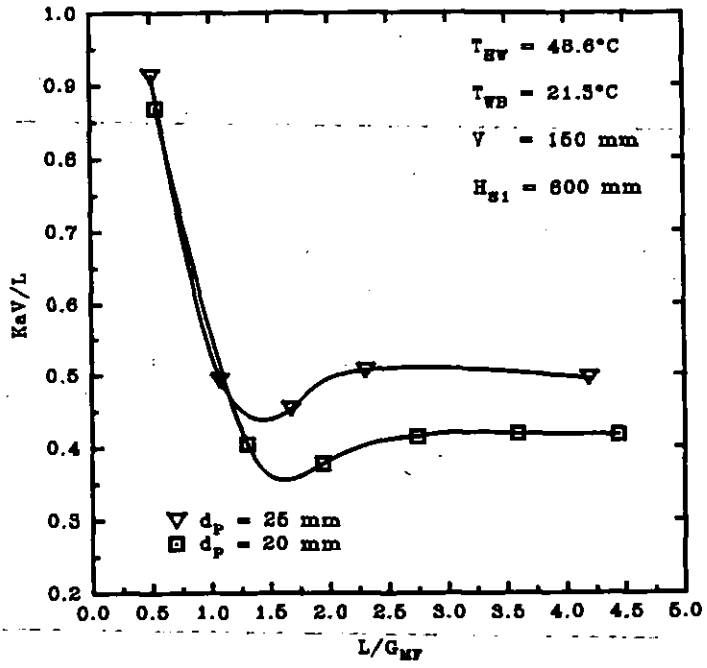

Figure C8 The effect of the liquid/gas mass flux ratio at the minimum fluidisation state and the particle size with nominal density of 242 kg/m^3 upon the tower characteristic based on the outlet cooled water temperature for the coarse droplet spray.

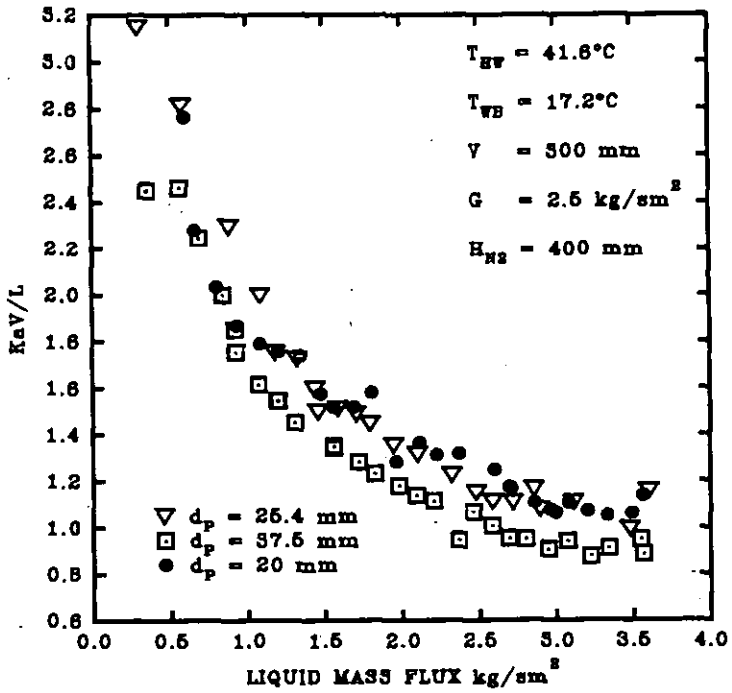

Figure C9 The effect of the liquid mass flux and the particle size upon the tower characteristic based on the plenum chamber outlet cooled water temperature. d_P = 25.4, ρ_P = 326 kg/m^3; d_P = 20.0 mm, ρ_P = 239 kg/m^3; d_P = 37.5 mm, ρ_P = 69 kg/m^3. Fine droplet spray nozzle code 3/4 FF - SS 4.8.

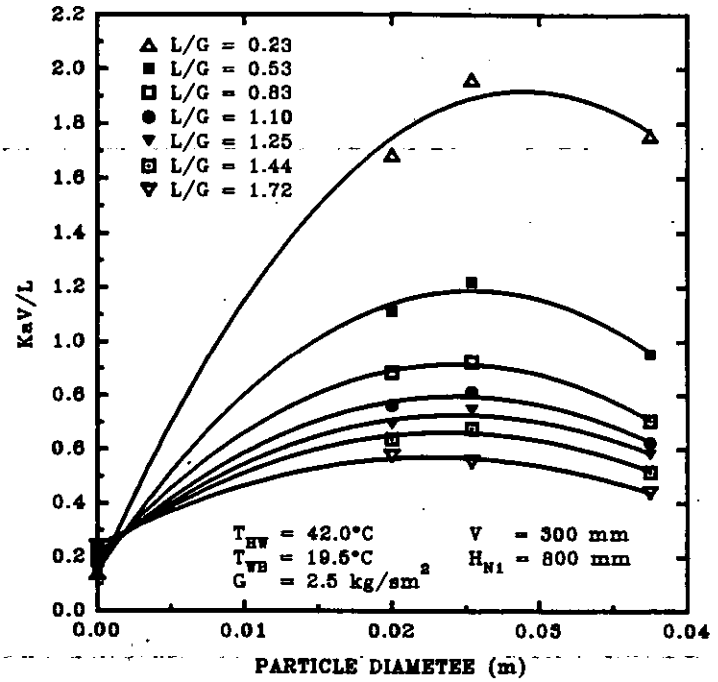

Figure C10 The effect of the particle size and the liquid/gas mass flux ratio upon the tower characteristic based on the cooled water temperature at the distributor grid.

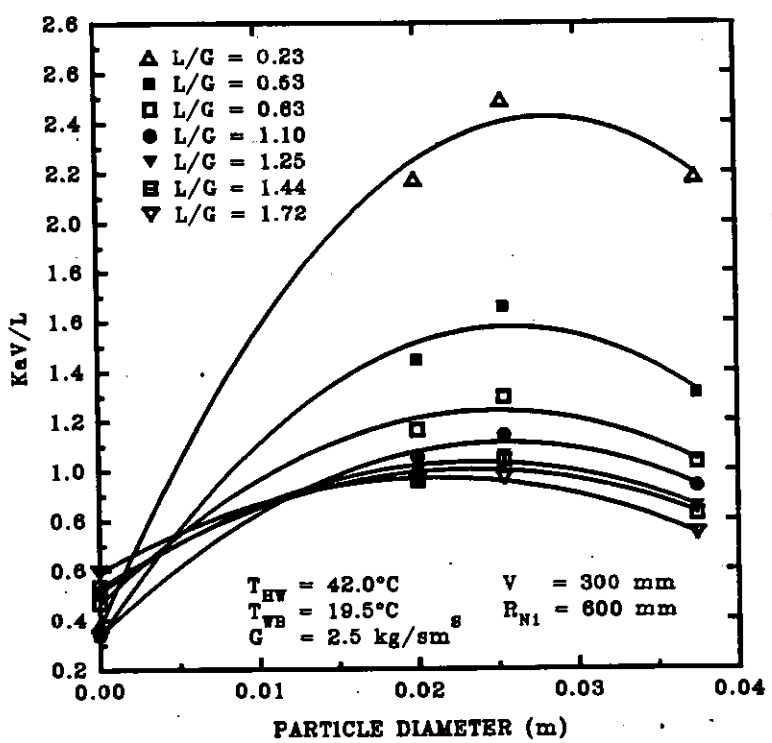

Figure C11 The effect of the particle size and the liquid/gas mass flux ratio upon the tower characteristic based on the average cooled water temperature.

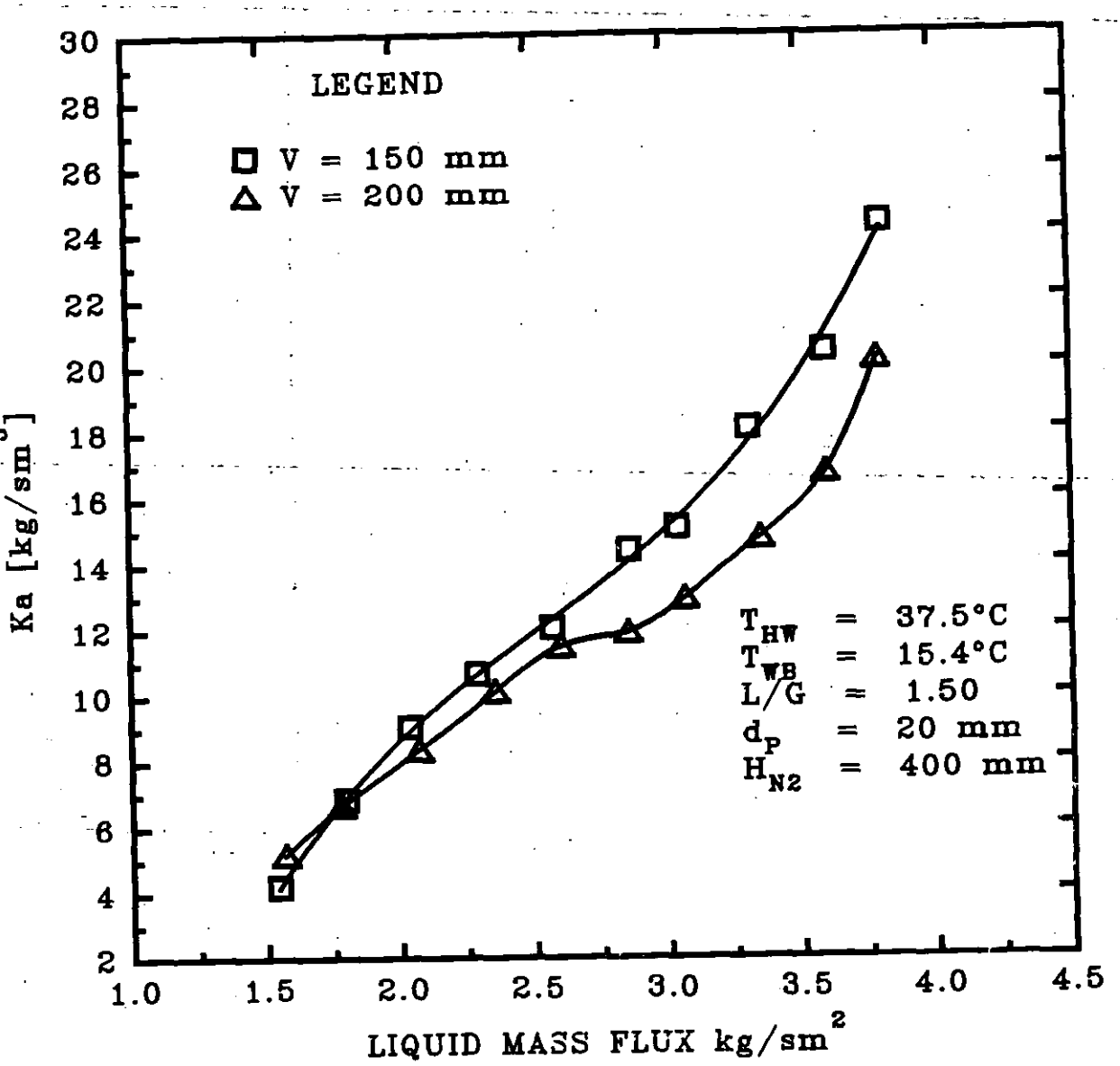

Figure C12 Effect of the simultaneous variation of the liquid and the gas mass fluxes upon the overall mass transfer coefficient, *Ka* of a type II FBCT operation based on the average outlet cooled water temperature. ρ_P = 239 kg/m^3. Fine droplet spray nozzle type 3/4 FF - SS 4.8.

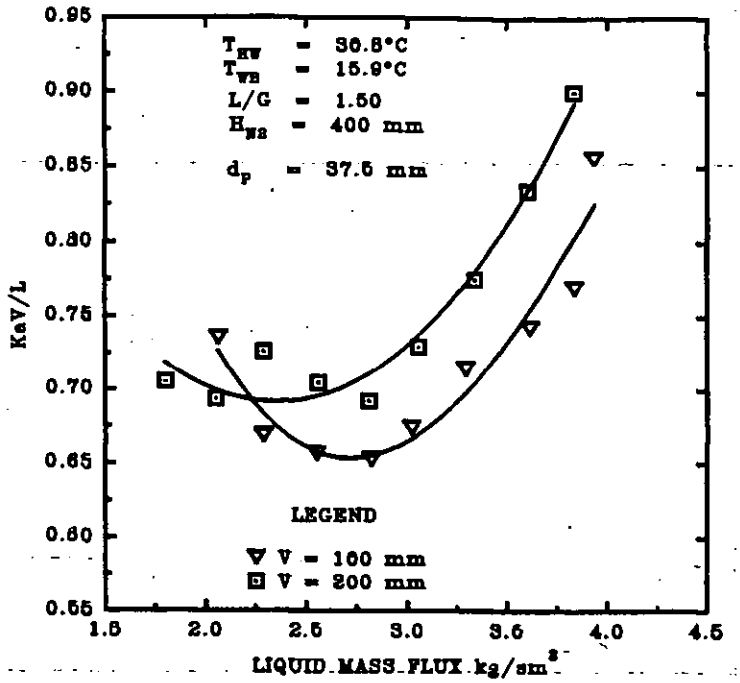

Figure C13 Effect of the simultaneous variation of the liquid and the gas mass flux upon the tower characteristic based on the average outlet cooled water temperature. ρ_p = 69 kg/m^3. Fine droplet spray type 3/4 FF - SS 4.8.

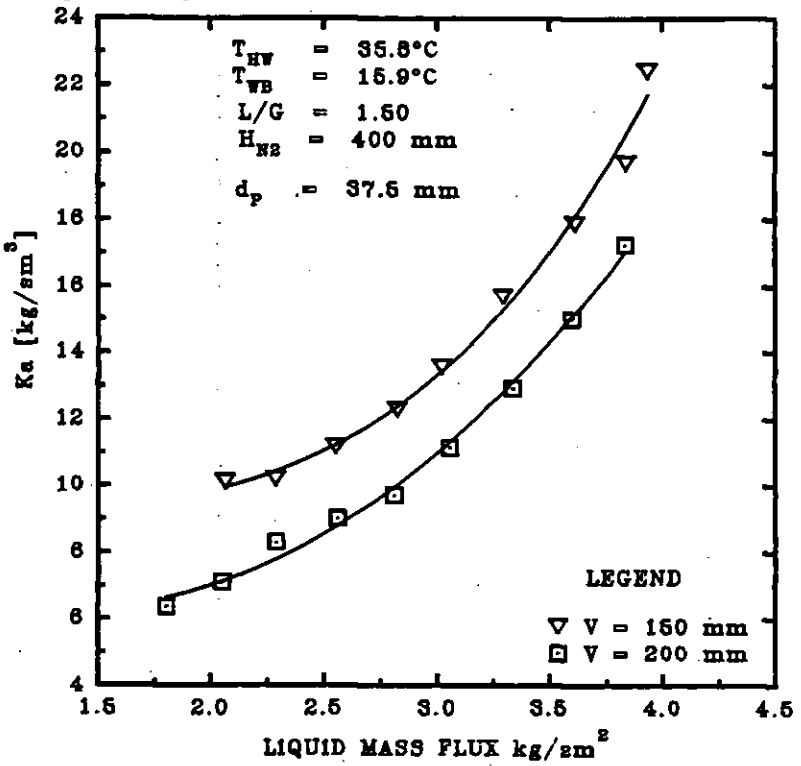

Figure C14 Effect of the simultaneous variation of the liquid and the gas mass fluxes upon the overall mass transfer coefficient, *Ka* of a typical type I FBCT operation based on the average cooled water temperature. ρ_p = 69 kg/m^3. Fine droplet spray nozzle type 3/4 FF - SS 4.8.

APPENDIX D: PUBLISHED WORKS

C565/071/99

Thermal performance of a fluidized bed cooling tower

L M EGBE, J S LEWIS, and **P BARHAM**
School of Engineering Systems, Middlesex University, London, UK
J KUBIE
School of Engineering, Napier University, Edinburgh, UK

SYNOPSIS

Experiments have been performed to measure the thermal performance of a fluidized bed cooling tower of 290 mm diameter. Hollow plastic spheres of three different sizes, with diameters of 20, 25.4 and 37.5 mm and particle densities ranging from 69 to 326 kg/m^3 were investigated as packing materials, and results for static bed heights of 100 mm and 300 mm are reported. Measurements were obtained at an approximately constant inlet hot water temperature of around 42°C and cover a range of water mass flux from 0.3 to 3.6 kg/s m^2. Liquid/gas ratios varied between 0.1 and 5.5. Results for thermal performance are presented showing the effects on the cooling tower characteristic, *KaV/L*, of the different packing elements and of varying water flow rate, air flow rate and the height of the hot water distributor above the bed.

1 INTRODUCTION

Cooling towers are used in many power, process and refrigeration plants to transfer large amounts of rejected heat from recirculated cooling water streams to the atmosphere. In addition to achieving a high cooling effectiveness, a cooling tower must also be economic to construct, operate and maintain. The thermal performance of a cooling tower packing is often expressed by the dimensionless quantity, *KaV/L*, known as the tower characteristic, where the composite quantity *Ka* is the overall volumetric mass transfer coefficient, *V* is the volume of the packing per unit plan area and *L* is the liquid (water) mass flux. An alternative measure is the number of transfer units, *NTU*, which is simply related to the tower characteristic by $NTU = (KaV/L)(L/G)$, where *G* is the gas (air) mass flux (1).

Previous work has demonstrated the potential of the fluidized bed cooling tower (FBCT) that utilises a mobile bed of low density non-permeable spheres in place of a conventional fixed packing. In the FBCT hot water is sprayed downward on to the bed of spherical packing elements in counterflow to an upward flowing unsaturated air stream that fluidizes the bed, thus creating a three-phase turbulent bed contactor characterized by large interfacial area, vigorous

mixing and high heat and mass transfer coefficients. Douglas (2) reported excellent performance for the cooling and dehumidification of a hot wet air stream in a floating bed contactor with a packing consisting of hollow polypropylene spheres of diameter 38.1 mm and a static bed height, V, of 254 mm. Over the ranges tested, NTU was found to decrease with increasing water or air mass flow rate. Experiments for water cooling in a FBCT, by Barile *et al* (3), covered static bed heights up to 457.2 mm and spherical packing diameters of 19.05 mm and 38.1 mm. The tower characteristic KaV/L was found to increase, albeit at a diminishing rate, with increased static bed height, and was slightly lower for the larger spheres. The measurements exhibited values of Ka an order of magnitude higher than those for fixed packing towers. Furthermore, the data indicated that Ka decreases as V increases, and increases with increase in either G or L. Seetharamu and Swaroop (4) tested two different sizes of FBCT, with tower cross-sections 250 mm square and 1100 mm square. Extended polystyrene spheres of diameter 25.4 mm were used as the packing material and static bed heights up to 310 mm were investigated. They concluded that in comparison with conventional cooling towers, with either splash or film type fills, the FBCT requires a much lower packing height, has a comparable pressure drop and can handle higher liquid throughputs. El-Dessouky (5) experimented with a FBCT packing of 12.7 mm diameter spongy rubber balls and static bed heights of 300 to 500 mm, and found that increasing the hot water inlet temperature produced a marked improvement in KaV/L. This was attributed to the increased interfacial area and gas holdup associated with the smaller air bubble mean diameter formed at higher water temperatures due to the reduction in surface tension and viscosity.

This paper reports on work in progress to extend the range of experimental data available for use in the design of fluidized bed cooling towers. The FBCT tests conducted cover a larger number of spherical packing element sizes than previously considered in a single study.

2 EXPERIMENTAL WORK

A schematic of the FBCT apparatus developed for this work, including the air and water supply systems, is shown in Figure 1. The experimental tower consists of a vertical 290 mm internal diameter transparent perspex column having working and inlet plenum sections 1500 mm and 700 mm long respectively. The bed, comprising hollow plastic spheres, is supported on a wire grid with a free flow area exceeding 80% of the tower cross-sectional area. Hot water is introduced through a single spray nozzle mounted centrally above the bed. The nozzle height can be adjusted to vary the extent of the freeboard region. Instrumentation includes platinum resistance thermometers for measurement of the hot and cooled water temperatures, and the dry bulb and wet bulb air temperatures at inlet and outlet. The air and hot water flow rates are measured using an orifice plate and a turbine flow meter respectively. Pressure transducers are provided to measure the bed pressure drop and the orifice plate differential pressure. All measurement outputs are connected to a data-logger linked to a personal computer for rapid data acquisition and analysis. Barometric pressure and the static pressure at the orifice plate are recorded separately. A backup system of mercury-in-glass thermometers, rotameters and U-tube manometers is also provided.

The uncertainty associated with the PRT measurements is estimated to be less than ±0.5°C. Calibration data and manufacturers' specifications indicate that, apart from at the lowest end of

the test ranges, the air flow rate and water flow rate measurements are accurate to ±5%. The average energy balance error for all the tests included in this paper is 11%.

Thermal performance testing of the FBCT apparatus described above has been conducted for both the fixed bed and the fluidized bed regimes. Test data have been obtained for the following approximate ranges of operating variables: water mass flux, L = 0.3 to 3.6 kg/s m^2, water/air mass flux ratio, L/G = 0.1 to 5.5 and hot water inlet temperature, $T_{w,i}$ = 25 to 55°C.

Three different sizes of spherical packings were employed, with diameters of 37.5, 25.4 and 20 mm and respective particle densities of 69, 326 and 239 kg/m^3. The two smaller sizes are hollow polypropylene spheres and the largest size resemble table tennis balls. Tests were also made with the column empty. The static bed height was varied over the range 50 to 400 mm. In addition, two different commercial spray nozzles (Spraying Systems) were used; one with a 4 mm diameter single orifice that produces relatively coarse droplets of 2000 micron average median volume diameter, and a multi-orifice nozzle that produces finer droplets of 800 micron average median volume diameter. The height of the spray nozzle above the bed support grid, H, was varied from 400 to 1100 mm. A sample of results is presented in the following section.

3 TYPICAL RESULTS AND DISCUSSION

Typical results showing the response of the FBCT performance characteristic to changes in different test variables are presented in Figures 2 to 4. In each figure, the caption shows the average values of other quantities that were held reasonably constant in the tests represented.

Values of KaV/L were calculated from the test measurements using Merkel's equation (1):

$$\frac{KaV}{L} = \int_{h_{w,o}}^{h_{w,i}} \frac{dh_w}{h_s - h_g} \qquad (1)$$

where V is taken as the static bed height, h_w is the specific enthalpy of the water stream, h_s is the specific enthalpy of saturated air at the water temperature, h_g is the specific enthalpy of the bulk air-water vapour mixture, given by $h_g = h_{g,i} + (L/G)(h_w - h_{w,o})$, and the subscripts i and o denote inlet and outlet respectively. The integral in equation (1) was evaluated using the 4-point Tchebycheff approximation given in BS4485 (6).

In Figure 2, KaV/L is plotted versus the particle diameter, d_P, of the spherical packings for seven different values of L/G. The air flow rate, static bed height and the hot water inlet temperature are fixed. At all water/air mass flux ratios other than L/G = 0.23, KaV/L is consistently lower for the 37.5 mm spheres than for the 20 mm spheres. This appears to confirm the finding of Barile *et al* (3) who noted a similar trend using two spherical packing element diameters, 19.05 and 38.1 mm, approximating to the smallest and largest sizes used in this work. Figure 2 also shows that, for all but the highest value of L/G, the value of KaV/L is higher for the 25.4 mm spheres. This at first may seem to suggest an optimum diameter for the spherical packings. It should be noted, however, that the particle densities of the three sizes of spheres do not vary monotonically with sphere diameter (see Section 2). Therefore, it is unclear if the trends seen in Figure 2 are due to variation of the sphere diameter, the particle density or a combination of both. Further work, using lower density 25.4 mm diameter spheres, is to be carried out to clarify this matter.

A strong dependence of *KaV/L* on *L/G* is also evident in Figure 2, and it can easily be established that this is not a simple inverse relationship as suggested by the appearance of L in the denominator of *KaV/L*. Factoring *KaV/L* by *L/G*, noting that V and G are fixed, reveals that the more fundamental quantity *Ka*, the product of the mass transfer coefficient and the interfacial area per unit volume, increases with water mass flux as found by previous workers (3, 5).

A much larger amount of test data showing the effects of water mass flux and the different size spherical packings on the tower characteristic is presented in Figure 3 . With the exception of the change in the type of spray nozzle used and its height above the bed support grid, the other fixed parameters are the same as for Figure 2. Furthermore, the results confirm the relatively weak dependence of *KaV/L* on d_P and the much stronger dependence of *KaV/L* (and *Ka*) on L.

Figure 4 shows the effect of the air mass flux on *KaV/L* for a fixed water mass flux, and two different heights of the hot water spray nozzle. The packing used consisted of 37.5 mm diameter spheres and the static bed depth was 100 mm. As V and L are fixed, it can be deduced that the volumetric mass transfer coefficient, *Ka*, also increases with G in the same manner as *KaV/L*.

Raising the height of the spray nozzle above the packing introduces a spray zone that increases the interfacial area available for gas-liquid contact in the tower, and would be expected to lead to an increase in *KaV/L* for the tower. This is confirmed in Figure 4, where the lowest and highest air flow rates correspond to fixed bed operation, at a static bed height of 100 mm, and full fluidization with an expanded bed height of approximately 400 mm respectively. Consequently, with the nozzle set at H = 400 mm the spray zone height reduces from 300 mm to zero as the bed expands, and for H = 800 mm the corresponding reduction is from 700 mm to 400 mm. As the vertical separation of the two curves in Figure 4 remains reasonably constant, the percentage contribution to *KaV/L* of the additional spray zone height of 400 mm decreases as the bed expands with increasing gas flow rate.

4 CONCLUDING REMARKS

Thermal performance tests have been carried out on a fluidized bed cooling tower. The experimental results presented show the effects of the water and air mass fluxes on the tower characteristic, *KaV/L*, and the volumetric mass transfer coefficient, *Ka*, and confirm the findings of previous researchers. Further work is required to distinguish the effects of the diameter and the density of the spherical packing elements. The influence of the height of the hot water spray nozzle has been demonstrated.

REFERENCES

(1) Singham, J.R., Cooling towers, in *Heat Exchanger Design Handbook*, (eds. E.U.Schlünder *et al*), Section 3.12, Hemisphere, 1983.

(2) Douglas, W.J.M., Heat and mass transfer in a turbulent bed contactor, *Chemical Engineering Progress*, 60, (7), 66-71, 1964.

(3) Barile, R.G., Dengler, J.L. and Hertwig, T.A., Performance and design of a turbulent bed cooling tower, *AIChemE Symposium Series*, 70, (138), 154-162, 1974.

(4) Seetharamu, K.N. and Swaroop, S., The effect of size on the performance of a fluidized bed cooling tower, *Wärme- und Stoffübertragung*, 26, 17-21, 1990.
(5) El-Dessouky, H., Thermal and hydraulic performance of a three-phase fluidized bed cooling tower, *Experimental Fluid and Thermal Science*, 6, (4), 1993.
(6) British Standard 4485, *Water Cooling Towers*, Part 2. Methods for Performance Testing, British Standards Institution, London, 1988.

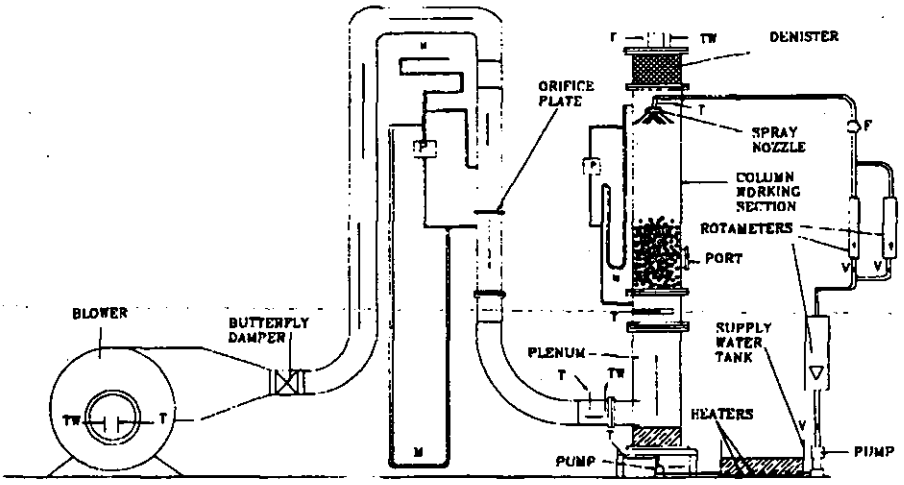

Figure 1. Schematic of the FBCT apparatus.

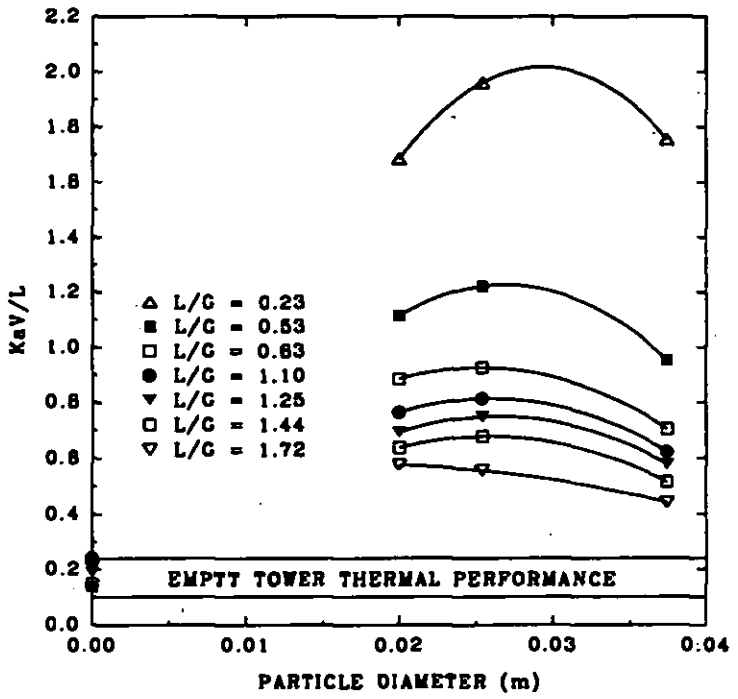

Figure 2. Effect of *L/G* and particle size on *KaV/L* (G = 2.5 kg/s m^2, V = 300 mm, H = 600 mm (coarse spray), $T_{w,i}$ = 42.0°C and T_{wb} = 19.5°C).

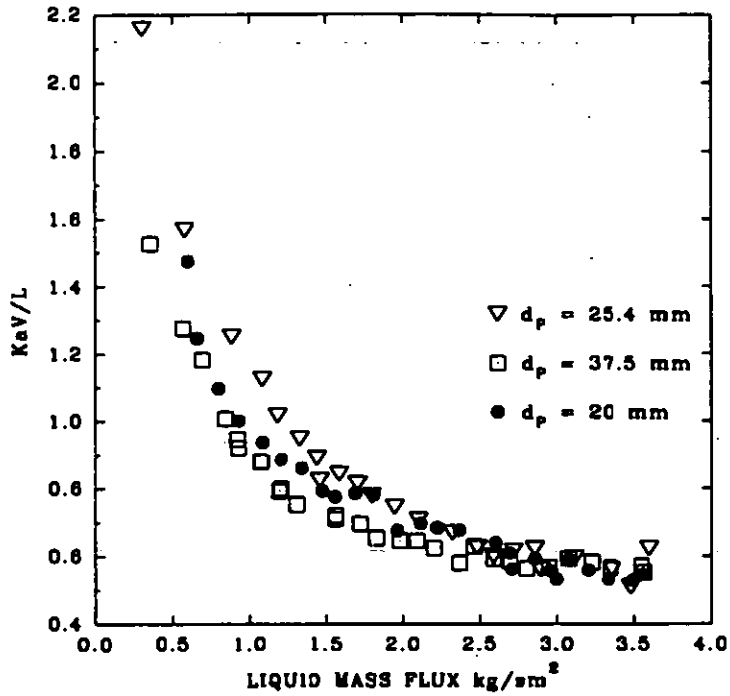

Figure 3. Effect of L and particle size on KaV/L (G = 2.5 kg/s m^2, V = 300 mm, H = 400 mm (fine spray), $T_{w,i}$ = 41.8°C and T_{wb} = 17.2°C).

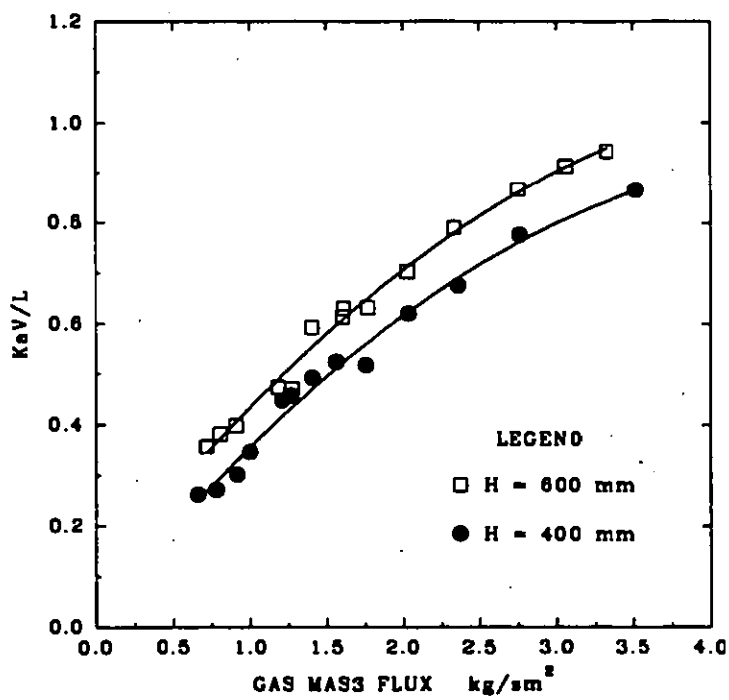

Figure 4. Effect of G and height of nozzle (fine spray) on KaV/L (L = 3.63 kg/s m^2, V = 100 mm, d_p = 37.5 mm, $T_{w,i}$ = 40.0°C and T_{wb} = 20.3°C).

PLENUM CHAMBER EFFECTS IN THE COOLING OF WATER BY MEANS OF FLUIDIZED SPHERICAL PARTICLES AND AIR

L.M. Egbe

School of Engineering Systems, Middlesex University, London, N11 2NQ.

ABSTRACT

We report here a new type of Fluidized Bed Cooling Tower (FBCT) designed with a view of experimentally investigating the dependence of the thermal performance upon plenum chamber design in the cooling of hot water. This equipment uses air and fluidized spherical packing as contacting medium. Experimental results indicate that hot water can be evaporatively cooled in this way, and that end effects due to plenum design play a significant part in its thermal performance.

INTRODUCTION

Cooling towers are essential in the energy industry, process and refrigeration plants to reject heat from recirculated cooling water streams to the environment. Moreover, the cooling tower must be cheap to constuct, maintain and operate. In this particular FBCT, the conventional fixed packing is replaced with a fluidized bed of light non-permeable spheres which undergo fluidization due to upward flowing ambient air and downward flowing hot water in order to achieve evaporative water cooling. Barile *al* (1) experimentally investigated the usefulness of this FBCT as a cooling device and they showed that this technology produces heat and mass transfer rates much higher than those in conventional cooling towers. More recently, El-Dessouky (2) performed experiments on an FBCT using 12.7 mm diameter spongy rubber spheres and found that the tower thermal performance increased as the inlet hot water temperature is increased attributing this finding to increases in interfacial area as a result of decreases in gas bubble diameter as the inlet water temperature is increased causing a reduction in surface tention and viscosity. Despite their encouraging findings, paucity of experimental data persists as regards the thermal performance of the FBCT. Moreover, no experimental data exists concerning the effects of the non-packing regions for cooling towers in general. Kelly *et al* (3) first attempted to quantify end effects in connection to their contribution to conventional cooling towers by extrapolating experimental data so as to account for the absence of packing. However, this method is unreliable since no experiments were performed to substantiate their analysis. Egbe *et al* (4) also carried out tests with the tower empty to account for the contribution of the non-packing regions in fully fluidized states as well as the plenum chamber, to the thermal performance. They found that cooling occurred in an empty tower but no systematically generalized method was evolved by them to account for the contribution of the plenum alone as well as the spray zone just above a fully fluidized packing region. No experimental investigation is in existence that soley accounts for the intluence of the plenum chamber on either the FBCT or conventional cooling towers.

This paper reports on the experimental investigation and preliminary analysis in relation to the contribution of the plenum chamber to the thermal performance of this novel device since we believe that it significantly contributes to the cooling of water in the FBCT.

EXPERIMENTAL APPARATUS

The experimental equipment is shown in Fig.1. It comprises a 290 mm ID transparent acrylic column having working and inlet air plenum sections of 1500 mm and 700 mm long respectively. The bed which consisted of polypropylene spheres, is supported on a wire grid with 80% open area and located between these two sections. Hot water is introduced through two different types of nozzles or a perforated tube distributor mounted centrally above the bed. The height of the spray head can be varied by using different pipe lengths so as to eliminate the effect of the spray zone above the bed during fluidization expansion. Instrumentation includes nine different platinum resistance thermometers for the measurement of the cold and hot water temperatures, the ambient, inlet, outlet wet and dry-bulb temperatures. One of the PRTs was located about 50 mm below the wire grid so as to measure the temperature just leaving the bed while another one was located just below the plenum in order to measure the final cooled water temperature. In this way, the net effect of the plenum chamber contribution to the FBCT thermal

performance could be assessed. The air and water volume flow rates were measured using an orifice plate and an electronic turbine flow meter respectively. Two differential pressure transducers were used to measure the orifice differential pressure and the bed air pressure drop. The fan static and the atmospheric pressures were measured by a differential fluid manometer and a mercury barometer respectively. All electronic measurement outputs were connected to a data logger linked to a personal computer for rapid data acquisition and analysis. A manual back-up system of mercury-in-glass thermometers, rotameters and U-tube manometers is provided. Instrumental uncertainties are the same in a more recent paper (4). The average error for energy balance for all tests included in this paper is 11%. Thermal performance experimental tests were conducted for the fluidized bed in the range of liquid rates of approximately 0.3 to 3.6 kg/s m^2, liquid/gas mass flux ratio *L/G* in the approximate range of 0.1 to 1.5. The gas mass flux was maintained at about 2.5 kg/s m^2 while the inlet hot water temperature was held approximately constant at about 42°C. Two different sizes of hollow spherical polypropylene packing were used as the packing material. They had diameters of 37.5 and 25.4 mm and respective particle densities of 69 and 326 kg/m^3. The static bed height was maintained at 300 mm. The spray nozzle used was a multi-orifice one that produces fine droplets of 800 micron median volume diameter. The height of the spray nozzle above the bed was maintained at 400 mm so as to eliminate the effect of any empty spraying zone. Typical results displaying the contribution of the plenum to the thermal performance are shown in the following section.

RESULTS AND DISCUSSION

Sample results showing the effect of different variables and their significance in relation to end effects of the plenum are shown in Figures 2 to 5. Analysis of results was made by means of the Merkel Equation (5). The general form can be written as:

$$\frac{KaV}{L} = \int_{h_{w,0}}^{h_{wi}} \frac{dh_w}{h_s - h_g} \quad (1)$$

The right hand side of equation 1 is termed the required tower characteristic normally obtained by the mathematical calculation of the left hand side for a specific design *L/G*, inlet hot water temperature, cold water temperature and average wet and dry bulb temperatures. The integral of equation (1) was evaluated using the 4-point Tchebycheff approximation given in BS4485 (6). The left hand side of the equation, known as the available tower characteristic, must be determined by experiment and it is dependent only on the nature of the packing. The design point of a particular tower is the intersection of both sides of the equation. Figure 2 below shows the effect of the liquid mass flux upon the cooled water temperature at the grid, average and plenum outlet conditions. In all three cases, the cooled water temperature increases exponentially as the liquid mass flux is increased. For a given gas mass flux, the rate of evaporation decreases as the liquid mass flux is increased due to the fact that the moist air in the tower tends towards saturation as more vapour is being latently and sensibly removed from the bulk water stream. As a result, the pressure gradient between the air and water decreases. As the liquid flow rate is increased further upwards from 2.5 kg/s m^2, the curve tends to flatten out. There seems to be a threshold of liquid mass flux after which the degree of bed agitation increases due to increases in the liquid holdup in the interstitial voids of the spheres. This ection has the two-fold effect of increasing the gas-liquid interfacial area and at the same time enhancing the effectiveness of air/water mixing for sensible heat exchange, thus counteracting the effect of an increased water temperature as the liquid mass flux is increased. Figure 2 also shows that the plenum chamber significantly contributes to the cooling of the hot water despite the fact that it contains no packing. This is because a lower cooled water temperature is achieved at plenum conditions than when measurements are taken just below the grid where the outlet water temperature of the fluidized bed itself is measured. An enhanced cooling of about 5°C may be achieved as a result of the plenum contribution at a temperature range of between 10 and 25 K. This may be attributed to the fact that two-phase gas-liquid heat exchange continues to occur in the plenum as a result of turbulence and mixing after the water leaves the fluidized bed itself and enters the plenum. Fig.3. was generated from Fig.2. *KaV/L* is shown to decrease exponentially as the liquid mass flux is increased as expected and in concomitance with Fig.2. with the thermal performance being higher at the plenum condition than at the grid condition. Again, this confirms our earlier findings that the plenum chamber contributes to the thermal performance of the FBCT. Data analysis for fixed bed conventional counter-current cooling towers have consistently followed the power law equation given in (2):

$$\frac{KaV}{L} = C\left(\frac{L}{G}\right)^{n} \quad (2)$$

$$\frac{KaV}{L} = C\left(\frac{L}{G}\right)^{-0.6} \quad (3)$$

Fig.3. is a plot of *KaV/L* against *L* showing that the FBCT is analytically similar to equation (2). Bearing this in mind, a log-log plot of Fig.3 was made as seen in Fig.4. All three cases of the grid, average and plenum tower characteristic gave reasonably straight lines thus validating our experimental findings. A similar plot was done for experimental data using the 37.5 mm particles as shown in Fig.5. Again, it shows a similar trend despite differences in particle size. In order to numerically establish the contribution of the empty plenum to the *KaV/L* of the FBCT, the exponent, *n* and its corresponding coefficient *C* in equation (2) were calculated by an iterative substitution. In all cases of fully developed fluidization with *KaV/L* based on the plenum outlet conditions, *C* ranged from about 1.0 to 1.2 while *n* averaged about -0.52. For the grid conditions, *n* ranged from approximately -0.45 to -0.6 while *C* ranged from 0.61 to 0.65. Based on the average water temperature of the plenum and grid outlet cooled water conditions, *n* ranged from -0.44 to -0.47 while *C* ranged from 0.9 to about 1.02. Given that *n* averaged about -0.5 for both the plenum and the grid conditions, it can be safely stated that for the conditions studied, the plenum contributes between 40 and 50% of the entire tower characteristic.

COMPARISON WITH CONVENTIONAL TOWERS

A comparison was also made between the FBCT and conventional fixed bed tower data by other investigators with *KaV/L* plotted against *L/G*. It indicates that the FBCT *KaV/L* is in good agreement in trend and values with those of other investigators in (3, 7) on conventional wet cooling towers making it the more educible that both types of technologies similarly follow the power law. Furthermore, the height of the static packing of the FACT is on average several times shorter than conventional fixed bed one. With effective design trade-off, this may imply that the FBCT is smaller in size in good agreement with the findings of Seetharamu *et al.* (7). A comparison of *C* and *n* between the present FBCT investigation and conventional fixed bed towers was also made. On this basis, the FBCT is in good agreement with conventional towers (3, 8) and, therefore, validates the well-known Equation:

where C is dependent only on the nature of the packing, in this case fluidized spherical packing.

CONCLUDING REMARKS

1. Water can be cooled using fluidized spherical packing in a model FBCT equipment with the view of designing a full-scale model.The tower plenum significantly contributes to the tower *KaV/L*. A better *KaV/L* is achieved at plenum conditions than at the grid conditions.FBCT thermal performance is dependent upon the spherical fluidized particle characteristcs.The FBCT is smaller in size than conventional fixed bed towers.

NOMENCLATURE

Ka overall mass transfer coefficient, kg/s m^3
d_p particle diameter, m
G gas mass flux, kg/s m^2
H spray height of nozzle, m
h_a specific enthalpy of bulk air, kJ/kg
h_s specific enthalpy of saturated air, kJ/kg
h_w specific enthelpy of the water, kJ/kg
L water mass flux, kg/s m^2
T_{wbi} inlet air wet bulb temperature, °C
$T_{w,o}$ cooled water temperature, °C
$T_{w,i}$ hot Water temperature, °C
V static bed Height, m

Subscripts

i inlet
o outlet
w water
N_2 fine droplet spray

REFERENCES

1. R.G. Barile, J.L. Dengler and T.A. Hertwig, Performance and design of a turbulent bed contactor, *AIChem Symposium Series*, 70, 138, 154 - 162 (1974)
2. H. El-Dessouky, Thermal and hydraulic performance of a three-phase fluidized bed cooling tower, *Experimental Fluid and Thermal Science*, 6, 4 (1993).
3. N.W. Kelly, L.K. Swenson, Comparative performance of cooling tower arrangements, *Chem. Eng. Prog.*, 52, 7, 263 - 268 (1956).
4. L.M. Egbe, J.S. Lewis, P. Barham, J. Kubie, Thermal performance of a fluidized bed cooling tower, *Transactions of the Sixth UK National Conference on Heat Transfer*, Edinburgh, IMechE Paper No C565/071/99 (1999).

5. J.R. Singham, Cooling Towers, in *Heat Exchanger Design Handbook*, (eds. E.U. Schlünder *et al.*), Section 3.12, Hemisphere (1983).
6. British Standard 4485, water cooling towers, Part 2. Methods of performance testing, *British Standard Institution*, London (1988).
7. K.N. Seetharamu, S. Swaroop, The effect of size on the performance of a fluidized bed cooling tower, *Wärme - und Stoffübertragung*, 26, 17 - 21 (1990).
8. R.B. Wrinkle, Performance of counter-flow cooling tower cells, *Chem. Eng. Prog.*, 7, 45 - 48 (1971).

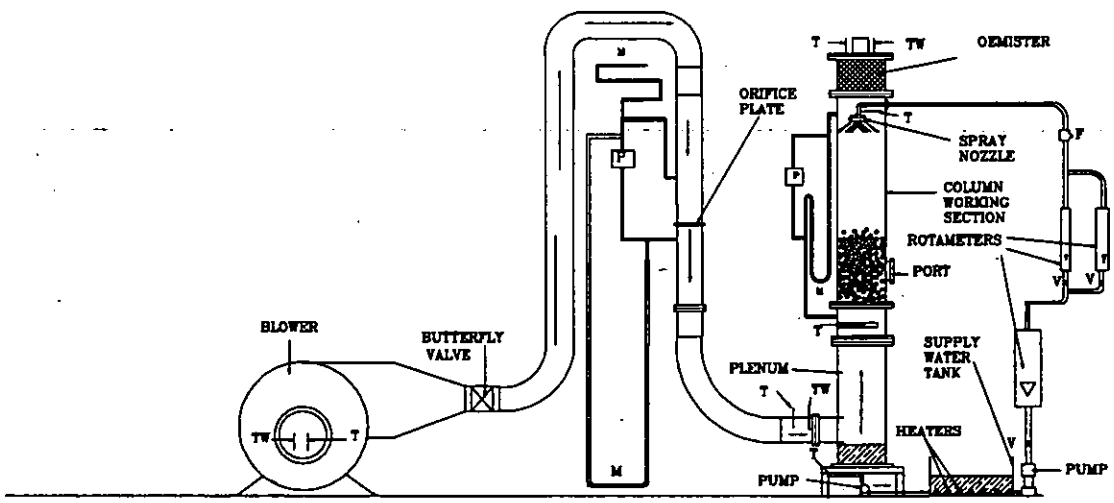

Fig.1. Schematic of the FBCT: M manometer P pressure transducer V valve T dry-bulb PRT TW wet-bulb PRT F electronic turbine water flow meter

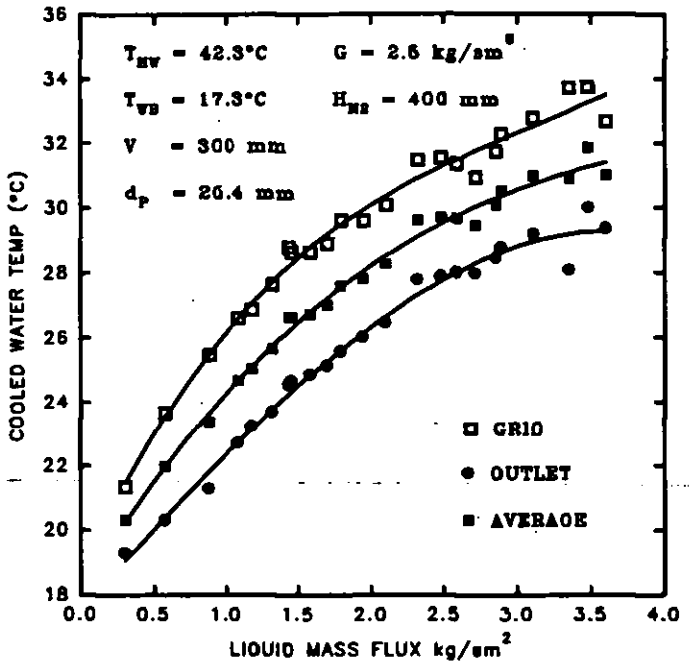

Fig.2. The effect of the liquid mass flux upon the cooled water temperature at various outlet water conditions

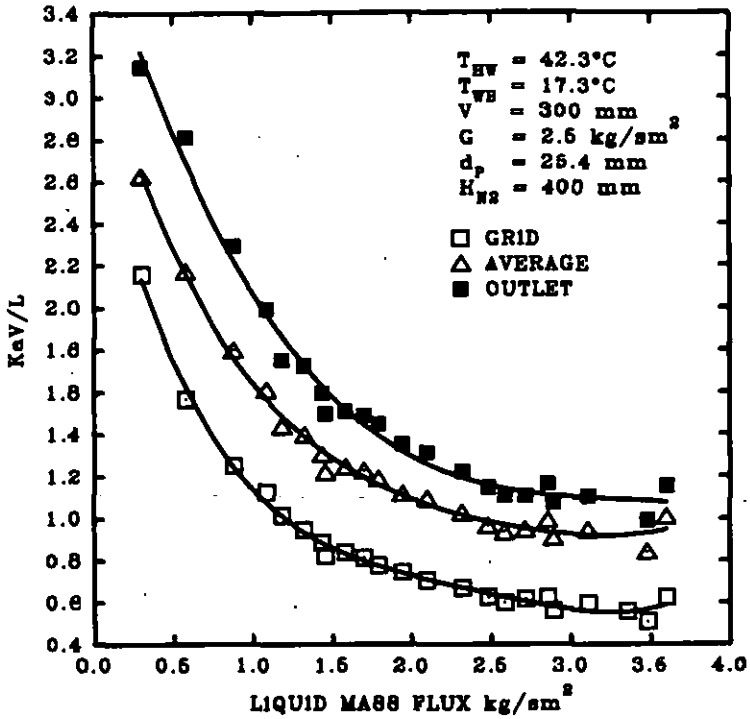

Fig.3. The effect of the liquid mass flux upon the tower characteristic

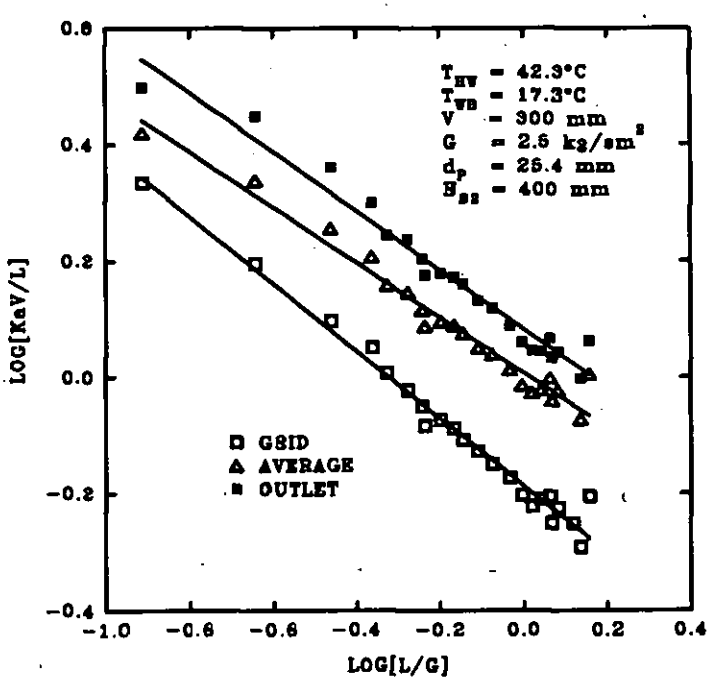

Fig.4. The effect of L/G on the tower characteristic. A log-log plot of Fig.3.

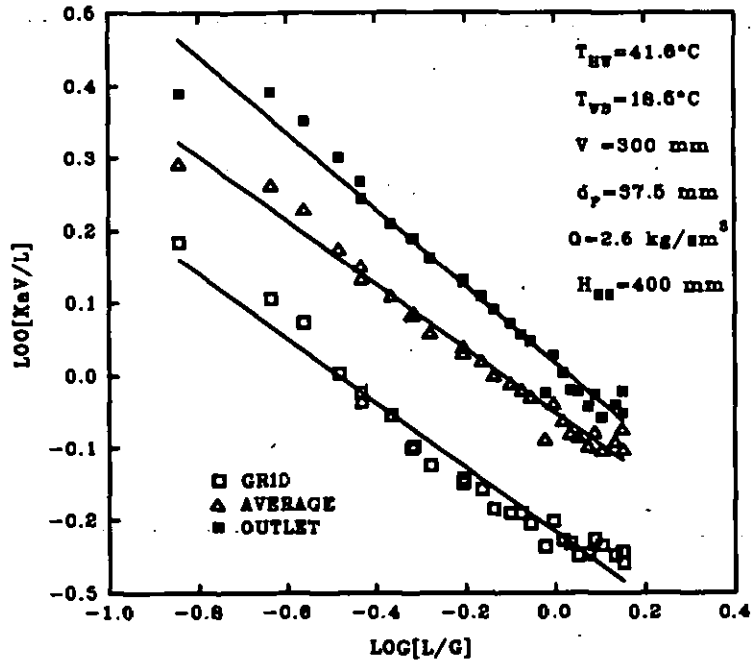

Fig.5. The effect of L/G upon the tower characteristic.A log-log plot for the 37.5 mm particle.